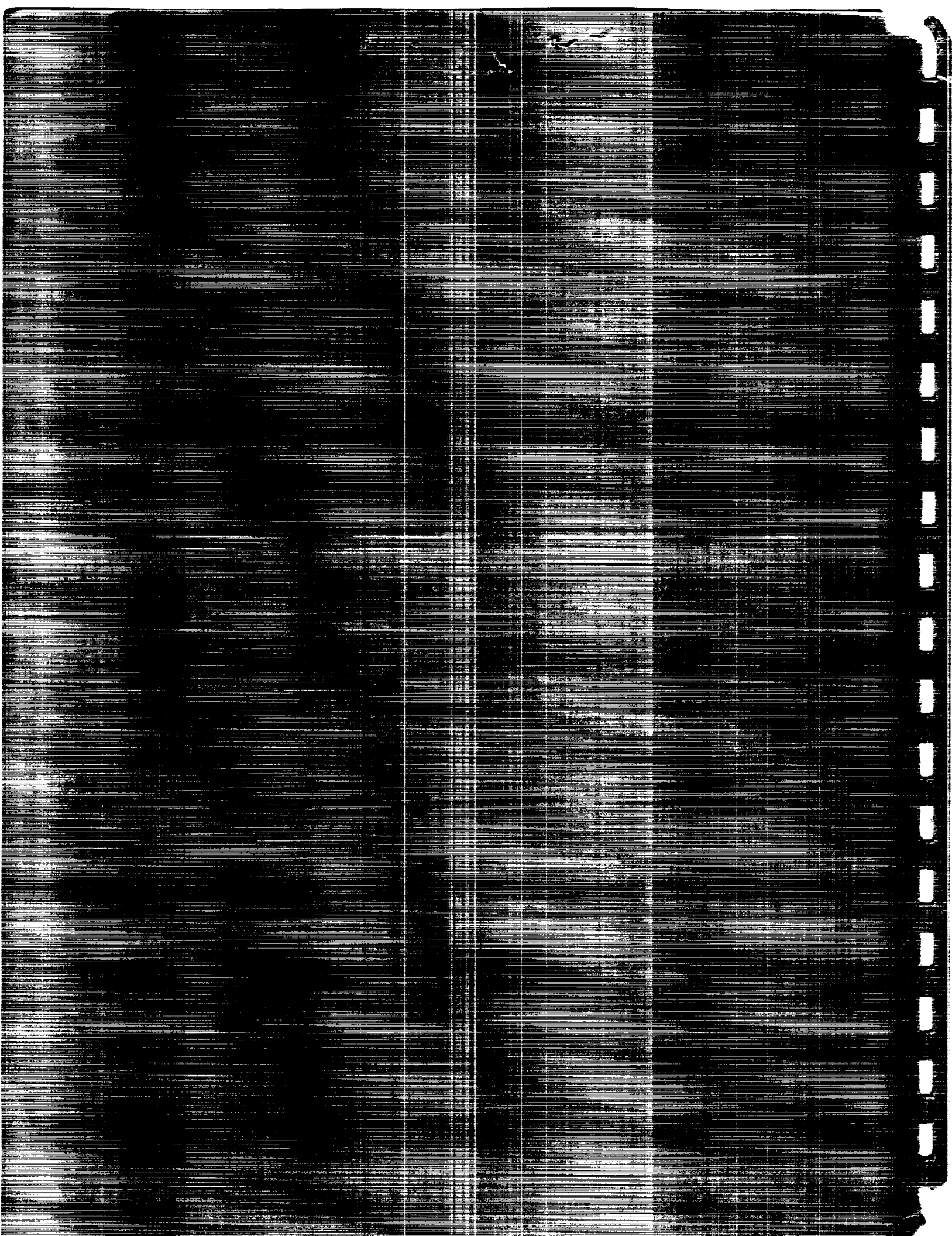


(NASA-CR-135109) VEHICLE ANTENNA FOR THE  
MOBILE SATELLITE EXPERIMENT Final Report  
(Teledyne Ryan Electronics) 332 000000 220

896-14271

Unclas

61/18 0252028

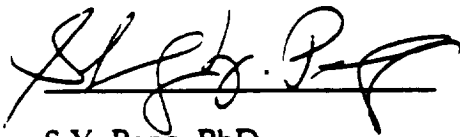


VEHICLE ANTENNA  
FOR THE  
MOBILE SATELLITE EXPERIMENT  
FINAL REPORT

Signatures on this page signifies approval of this document.



C.M. Sparks  
Program Manager



S.Y. Peng, PhD.  
Technical Monitor



H.L. Faller  
Project Engineer

This work was performed for the Jet Propulsion Laboratory, California Institute of Technology, sponsored by the National Aeronautics and Space Administration.

Reference herein to any specific commercial product, process, or service by trade name, trademark, manufacturer, or otherwise, does not constitute or imply its endorsement by the United States Government, Teledyne Ryan Electronics, or the Jet Propulsion Laboratory, California Institute of Technology.



## FOREWORD

This document is hereby presented to NASA/Jet Propulsion Laboratory under contract number 957468 in fulfillment of Article 1, Task 9 of the Statement of Work entitled, "Vehicle Antenna for the Mobile Satellite Equipment". Technical monitoring of this contract was done under the direction of Dr. John Huang of JPL and carried out at Teledyne Ryan Electronics, San Diego, California, under the technical and managerial direction of Dr. S.Y. Peng and Mr. C.M. Sparks respectively.

Contributors to this report and the section they authored are listed as follows.

<u>Section</u>	<u>Title</u>	<u>Author(s)</u>
1	Introduction	Dr. Sheng Y. Peng
2	Array Performance	Dr. H.H. Chung
3	Antenna/Element Feed Network	Dr. H.H. Chung, D. Leggiere and W. Foy
4	Beamformer Network	Dr. G. Schaffner
5	Antenna Beam Angle Steering Control	J. Nelson, W. Pagels, and M. Vayner
6	MSAT-X Mechanical Design	W. Hardin and D.C. Wells
7	MSAT-X Production Antenna Cost Analysis	H. L. Faller
8	Test Plan/Procedure	L. Messer, D. Leggiere and H. L. Faller
9	Conclusions and Recommendations	Dr. Sheng Y. Peng



## TABLE OF CONTENTS

SECTION	TITLE	PAGE
1	INTRODUCTION .....	1-1
1.1	PROGRAM BACKGROUND REVIEW .....	1-1
1.2	SUMMARY OF RESULTS .....	1-2
1.2.1	Antenna Pattern and Gain Performance .....	1-2
1.2.2	Pointing System Performance .....	1-4
1.2.3	Cost Analysis.....	1-5
2	ARRAY DESIGN AND PERFORMANCE .....	2-1
2.1	ANALYTICAL MODEL DEVELOPMENT .....	2-2
2.1.1	GTD Model .....	2-4
2.1.2	Mutual Coupling Model .....	2-6
2.1.3	Error Model.....	2-10
2.2	ARRAY DESIGN AND ANALYSIS.....	2-10
2.2.1	Array Aperture Design .....	2-11
2.2.2	Predicted Array Performance .....	2-13
2.3	ARRAY ASSEMBLY .....	2-33
2.4	MEASURED ARRAY PERFORMANCE.....	2-44
2.4.1	Measured Array Patterns.....	2-44
2.4.2	Measured Array Gain .....	2-59
2.4.3	Measured Intersatellite Isolation .....	2-65
2.5	CONCLUSIONS.....	2-71
2.6	RECOMMENDATIONS.....	2-71
2.7	REFERENCES.....	2-72
3	ANTENNA ELEMENT FEED NETWORK .....	3-1
3.1	SUBSTRATE MATERIAL SELECTION .....	3-1
3.2	CROSSED-SLOT DESIGN PARAMETERS .....	3-3
3.3	BREADBOARD DESIGN.....	3-7
3.3.1	Experimental Model Development .....	3-7
3.3.2	Breadboard Model Development .....	3-9
3.3.3	Measured Antenna Performance And Gain Analysis .....	3-19
3.3.4	Conclusions Derived from Breadboard Design Phase .....	3-32
3.4	BREADBOARD ARRAY ELEMENT DEVELOPMENT .....	3-32

## TABLE OF CONTENTS (CONTINUED)

SECTION	TITLE	PAGE
3.4.1	Optimization of Feed Network Design .....	3-35
3.4.2	Optimization of Hybrid Network .....	3-35
3.4.3	Modifications Required of Hybrid Network .....	3-39
3.5	CONCLUSIONS.....	3-41
3.6	RECOMMENDATIONS.....	3-41
4	BEAMFORMER NETWORK.....	4-1
4.1	SUMMARY OF THE DEVELOPMENT OF THE PHASE SHIFTER AND DIVIDER .....	4-1
4.2	DESCRIPTION OF THE BEAMFORMER ASSEMBLY .....	4-14
4.3	TEST RESULTS FOR THE FIRST TWO BEAMFORMERS .....	4-19
4.4	FEATURES .....	4-26
4.5	DEFICIENCIES AND WORK TO BE DONE IN THE NEXT PHASE .....	4-26
5	ANTENNA BEAM ANGLE STEERING CONTROL.....	5-1
5.1	STEERING CONTROL SYSTEM DESCRIPTION .....	5-1
5.2	POINTING ELECTRONICS.....	5-11
5.2.1	Hardware Description.....	5-11
5.2.2	Transceiver Interface .....	5-15
5.2.3	User Interface.....	5-15
5.2.4	Antenna Interface .....	5-20
5.2.5	Power Supply .....	5-20
5.3	POINTING SOFTWARE.....	5-21
5.3.1	MSAT-X Software Procedure Descriptions .....	5-23
6	MSAT-X MECHANICAL DESIGN .....	6-1
6.1	GENERAL DESCRIPTION.....	6-1
6.2	MECHANICAL DESIGN .....	6-1
6.2.1	Beamformer .....	6-5
6.2.2	Cover.....	6-5
6.2.3	Hybrid Layer.....	6-5
6.2.4	Feeders .....	6-5

## TABLE OF CONTENTS (CONTINUED)

SECTION	TITLE	PAGE
6.2.5	Radiator Layer .....	6-6
6.2.6	Radome .....	6-6
6.2.7	Back Cover.....	6-6
6.2.8	Connectors .....	6-6
6.3	FABRICATION .....	6-7
6.4	MECHANICAL TECHNIQUES ASSOCIATED WITH MSAT-X.....	6-9
6.4.1	Bonding.....	6-9
6.4.2	Connectors .....	6-9
6.4.3	Plating.....	6-10
6.4.4	Soldering Techniques.....	6-10
6.4.5	Intra-Antenna Interconnects.....	6-10
6.4.6	Sealing.....	6-11
6.5	CONCLUSION.....	6-11
7	MSAT-X PRODUCTION ANTENNA COST ANALYSIS.....	7-1
7.1	COST ANALYSIS.....	7-2
7.1.1	Material and Parts .....	7-2
7.1.2	Assembly/Labor.....	7-3
7.1.3	Manufacturer's Cost (MC).....	7-3
7.1.4	Manufacturer's Selling Price (MSP).....	7-4
7.1.5	Wholesale Price and Retail Price.....	7-4
7.2	RESULTS .....	7-5
7.3	CONCLUSIONS AND RECOMMENDATIONS .....	7-5
8	TEST PLAN/PROCEDURE.....	8-1
8.1	TEST PLAN .....	8-1
8.1.1	Introduction .....	8-1
8.1.2	Scope.....	8-1
8.1.3	Differences Between Breadboard and Production Tests .....	8-1
8.1.4	Location of Tests and Witnessing .....	8-3
8.1.5	Description of the Test Range.....	8-3
8.1.6	Test Plan Details.....	8-5

## TABLE OF CONTENTS (CONTINUED)

SECTION	TITLE	PAGE
8.2	ENGINEERING TEST PROCEDURE.....	8-14
8.2.1	Introduction .....	8-14
8.2.2	Applicable Documents.....	8-14
8.2.3	Test Requirements .....	8-14
8.2.4	List of ETP Tests .....	8-15
8.3	SYNOPSIS OF ACCEPTANCE TESTS.....	8-16
8.3.1	VSWR Tests .....	8-16
8.3.2	Antenna Patterns .....	8-16
8.3.3	Cross-Polarization.....	8-22
8.3.4	Intersatellite Isolation .....	8-22
8.3.5	System Acquisition/Track/Steering .....	8-23
9	CONCLUSIONS AND RECOMMENDATIONS.....	9-1
9.1	CONCLUSIONS.....	9-1
9.2	RECOMMENDATIONS.....	9-2

### APPENDICES

A	TEST PATTERNS: MSAT-X ANTENNA SYSTEMS #1 AND #2.....	A-1
B	TABLES OF BEAMFORMER CALCULATIONS.....	B-1
C	THEORY OF THE ANTENNA AZIMUTH BEAM ANGLE STEERING CONTROL.....	C-1
D	SCHEMATICS AND DIAGRAMS OF MSAT-X SYSTEM.....	D-1
E	MSAT SYSTEM TEST DATA SUMMARY (RF SIGNAL).....	E-1
F	OPERATING INSTRUCTION MANUAL FOR MSAT-X ANTENNA SYSTEM.....	F-1

## LIST OF ILLUSTRATIONS

FIGURE	TITLE	PAGE
1-1	Photo to Show the Developed Breadboard Vehicle Antenna for MSAT-X Program .....	1-3
1-2	Photo to Show the Breadboard Antenna Mounted on the Top of a Vehicle .....	1-3
2-1	Coordinate System .....	2-3
2-2	Field Computation for the j-th Element on Top of Finite Ground Plane.....	2-5
2-3	Computed Element Radiation Patterns at 1545 MHz (Sheet 1 of 2) .....	2-7
2-4	Comparison Between Calculated and Measured Radiation Pattern .....	2-9
2-5	Array Geometry .....	2-12
2-6	Computed Elevation Pattern at 1545 MHz (Sheet 1 of 3).....	2-15
2-7	Computed Azimuth Array Pattern at 1545 MHz (Sheet 1 of 3) .....	2-18
2-8	Random Errors Effect on the Array Performance.....	2-21
2-9	Photo of Seven Element Array (Top View) .....	2-22
2-10	Photo of Seven Element Array (Bottom View).....	2-23
2-11	Measure Coupling Value of the Seven Element Array .....	2-24
2-12	Computed Scanning Active Return Loss at Center Element of the Seven Element Array .....	2-25
2-13	Six Critical Locations in the United States.....	2-29
2-14	RHCP Array Pattern: Scan to Theta = 30 and phi = 182 degs.....	2-30
2-15	LHCP Array Pattern: Scan to Theta = 30 and phi = 182 degs. ....	2-31
2-16	Beam Pointing Study, $\theta_s = 60^\circ$ , $\theta = 70^\circ$ .....	2-34
2-17	Beam Pointing Study, $\theta_s = 30^\circ$ , $\theta = 30^\circ$ .....	2-35
2-18	Top Layer (Crossed-Slot Radiators) of the Array.....	2-37
2-19	Second Layer (Feeder Arrangement) of the Array.....	2-38
2-20	Third Layer (90° Hybrids/180° Corporate) of the Array .....	2-39
2-21	Fourth Layer (Ground Plane) of the Array.....	2-40
2-22	19 Element Fabrication Experimental Model .....	2-41
2-23	Fifth Layer (Beamformer Board) of the Array.....	2-42
2-24	Final Assembled MSAT-X Phased Array.....	2-43
2-25	19-Element Array Mounting Geometry.....	2-46

## LIST OF ILLUSTRATIONS (CONTINUED)

FIGURE	TITLE	PAGE
2-26	Measured RHCP Array Pattern in the Elevation Plane at 1545 MHz, SLL = -21 dB (Broadside) .....	2-47
2-27	Measured RHCP Array Pattern in the Elevation Plane at 1660 MHz, SLL = -23 dB (Broadside) .....	2-48
2-28	Measured Spinning Linear Pattern in the Elevation Plane at 1545 MHz ( $\theta_s = 40^\circ$ , $\phi_s = 0^\circ$ ; $\theta = \text{VAR}$ , $\phi = 0^\circ$ ) .....	2-49
2-29	Measured Spinning Linear Pattern in the Elevation Plane at 1660 MHz ( $\theta_s = 40^\circ$ , $\phi_s = 0^\circ$ ; $\theta = \text{VAR}$ , $\phi = 0^\circ$ ) .....	2-50
2-30	Measured RHCP Azimuth Array Pattern at 1545 MHz, Gain = 10.9 dBic, SLL = -18 dB, BL = -17 dB, ( $\theta_s = 40^\circ$ , $\phi_s = 0^\circ$ ; $\theta = 40^\circ$ , $\phi = \text{VAR}$ ) ...	2-51
2-31	Measured RHCP Azimuth Array Pattern at 1660 MHz, Gain = 11.2 dBic, SLL = -18 dB, ( $\theta_s = 40^\circ$ , $\phi_s = 0^\circ$ ; $\theta = 40^\circ$ , $\phi = \text{VAR}$ ) .....	2-52
2-32	Measured Spinning Linear Elevation Array Pattern at 1545 MHz, ( $\theta_s = 60^\circ$ , $\phi_s = 0^\circ$ ; $\theta = \text{VAR}$ , $\phi = 0^\circ$ ) .....	2-53
2-33	Measured Spinning Linear Elevation Array Pattern at 1660 MHz, $60^\circ$ , $\phi_s = 0^\circ$ ; $\theta = \text{VAR}$ , $\phi = 0^\circ$ ) .....	2-54
2-34	Measured Spinning Linear Azimuth Pattern at 1545 MHz, ( $\theta_s = 60^\circ$ , $\phi_s = 0^\circ$ ; $\theta = 60^\circ$ , $\phi = \text{VAR}$ ) .....	2-55
2-35	Measured Spinning Linear Azimuth Pattern at 1660 MHz, ( $\theta_s = 60^\circ$ , $\phi_s = 0^\circ$ ; $\theta = 60^\circ$ , $\phi = \text{VAR}$ ) .....	2-56
2-36	Measured RHCP and LHCP Azimuth Pattern at 1660 MHz, ( $\theta_s = 70^\circ$ , $\phi_s = 0^\circ$ ; $\theta = 70^\circ$ , $\phi = \text{VAR}$ ) .....	2-57
2-37	Measured RHCP and LHCP Elevation Pattern at 1660 MHz, ( $\theta_s = 70^\circ$ , $\phi_s = 0^\circ$ ; $\theta = \text{VAR}$ , $\phi = 70^\circ$ ) .....	2-58
2-38	Measured Array Gain at 20 Degrees Elevation Angle (Above Horizon), Frequency = 1545 MHz, Average Gain = 9.25 dBic ( $\theta_s = 70^\circ$ , $\phi_s = 0^\circ$ , $45^\circ$ , $90^\circ$ , $135^\circ$ , $180^\circ$ , $225^\circ$ , $270^\circ$ , $315^\circ$ ; $\theta = 70^\circ$ , $\phi = \text{VAR}$ ) .....	2-61
2-39	Measured Array Gain at 20 Degrees Elevation Angle, Frequency = 1660 MHz, Average Gain = 9.9 dBic ( $\theta_s = 70^\circ$ , $\phi_s = 0^\circ$ , $45^\circ$ , $90^\circ$ , $135^\circ$ , $180^\circ$ , $225^\circ$ , $270^\circ$ , $315^\circ$ ; $\theta = 70^\circ$ , $\phi = \text{VAR}$ ) .....	2-62

## LIST OF ILLUSTRATIONS (CONTINUED)

FIGURE	TITLE	PAGE
2-40	Measured Array Gain at 20 Degrees Elevation Angle, Frequency = 1660 MHz, Average Gain = 8.3 dBic ( $\theta_s = 70^\circ, \phi_s = 0^\circ,$ $45^\circ, 90^\circ, 135^\circ, 180^\circ, 225^\circ, 270^\circ, 315^\circ; \theta = 70^\circ, \phi = \text{VAR}$ ).....	2-63
2-41	Elevation Plane Patterns at Various Scan Angles ( $\theta_s = 30^\circ, 40^\circ,$ $50^\circ, 60^\circ, 70^\circ$ ).....	2-66
2-42	Measured Aperture Distribution of the Beamformer at 1660 MHz for $\theta_s = 60^\circ$ and $\phi_s = 0^\circ$ Scan.....	2-67
2-43	Computed Array Pattern for the Realized and Ideal Design Beamformer ( $\theta_s = 60^\circ, \phi_s = 0^\circ$ ) Frequency = 1660 MHz.....	2-68
2-44	Pictorial/Block Diagram Depicting Equipment Hook-up for MSAT-X• System Tests on Outdoor Antenna Range.....	2-69
3-1	Crossed-Slot Design Parameters.....	3-4
3-2	Field Distribution with #2 & #4 Port Excited.....	3-5
3-3	Earlier Model of the Element.....	3-7
3-4	Experimental Model of the Crossed-Slot.....	3-8
3-5	Isolation Between Ports of Crossed-Slot Model-P.....	3-10
3-6	Measured Impedance Plot for Crossed-Slot Model-P.....	3-11
3-7	Spinning Linear Pattern at 1545 MHz.....	3-12
3-8	Spinning Linear Pattern at 1602 MHz.....	3-13
3-9	Spinning Linear Pattern at 1660 MHz.....	3-14
3-10	Breadboard Crossed-Slot Element.....	3-15
3-11	Hybrid Feed Network for Circular Polarization.....	3-16
3-12	90 Degree Branch Line Hybrid with Two 180 Degree Corporate Feed Circuit.....	3-18
3-13	90 Degree Branch Line Hybrid with Two 180 Degree Wilkinson Power Divider Feed Circuits.....	3-19
3-14	Measured Return Loss of Unit #1 Crossed-slot Element.....	3-20
3-15	Measured Return Loss of the Unit #2 Crossed-slot Element.....	3-21

## LIST OF ILLUSTRATIONS (CONTINUED)

FIGURE	TITLE	PAGE
3-16	Measured Isolation between the Input and the Load Port of the Unit #1 Crossed-slot Element.....	3-22
3-17	Measured Isolation Between the Input and the Load Port of the Unit #2 Crossed-slot Element.....	3-23
3-18	Element Gain Reduction Versus Load Port Isolation.....	3-24
3-19	Measured RHCP Elevation Pattern of the Unit #2 Crossed-slot Along the 40" Ground Plane Cut at 1545 MHz. Note: Antenna was mounted on the center of a 40" x 50" finite ground plane.....	3-25
3-20	Measured RHCP Elevation Pattern of the Unit #2 Crossed-slot Along the 40" Ground Plane Cut at 1660 MHz. Note: Antenna was mounted on the center of a 40" x 50" finite ground plane.....	3-26
3-21	Measured RHCP Elevation Pattern of the Unit #2 Crossed-slot Along the 50" Ground Plane Cut at 1545 MHz. Note: Antenna was mounted on the center of a 40" x 50" finite ground plane.....	3-27
3-22	Measured RHCP Elevation Pattern of the Unit #2 Crossed-slot Along the 50" Ground Plane Cut at 1660 MHz. Note: Antenna was mounted on the center of a 40" x 50" finite ground plane.....	3-28
3-23	Measured RHCP Azimuth Pattern at 20 Degrees Elevation Angle (Above Horizon), at frequency of 1545 MHz .....	3-29
3-24	Measured RHCP Azimuth Pattern at 20 Degrees Elevation Angle (Above Horizon), at frequency of 1660 MHz .....	3-30
3-25	Measured VSWR of the Crossed-Slot.....	3-33
3-26	Embedded Element Pattern of the Center Element of the Seven Element Array at 1660 MHz.....	3-34
3-27	Feed Line Characteristics.....	3-36
3-28	Measured VSWR and S21 Characteristics on a Typical Element in an Array with the Feed Circuit Optimized.....	3-37
3-29	Axial Ratio versus Feed Amplitude/Phase Unbalance.....	3-38
3-30	Element Feed Configuration .....	3-40

## LIST OF ILLUSTRATIONS (CONTINUED)

FIGURE	TITLE	PAGE
4-1	Sketch of Phase Shifter #1 .....	4-3
4-2	First Design of Array Phase Shifter .....	4-4
4-3	Revised Array Phase Shifter Design.....	4-5
4-4	Theoretical phase shifter loss in the 315° condition .....	4-7
4-5	Photograph of the self-biased PIN Diode Phase Shifter .....	4-9
4-6	Schematic Diagram of MSAT-X 1:19 Unequal Power Divider .....	4-10
4-7	Layout of the Test 19-Way Divider.....	4-11
4-8	Comparison of Microwave Performance of IMS and Component General 50 Ohm Chip Resistors. ....	4-15
4-9	Schematic Representation of Power/Combiner and 3-Bit Phase Shifter...	4-16
4-10	Photograph of Prototype #1 .....	4-17
4-11	Layout of the Beamformer .....	4-18
4-12	Beamformer Loss vs. Pointing Angle or Phase Shifter Setting .....	4-24
4-13	Beamformer Phase Delta from Desired vs. Pointing Angle of Phase Shifter Setting.....	4-25
5-1	MSAT-X Antenna Steering Control.....	5-2
5-2	A Front Panel View of the Electronics Box .....	5-12
5-3	View of the Electronics Box with the Top Cover Removed.....	5-13
5-4	Block Diagram/Cable Interconnect of MSAT-X Antenna System.....	5-14
5-5	Block Diagram of Transceiver Interface.....	5-16
5-6	Block Diagram of MSAT-X User Interface .....	5-18
5-7	Test Equipment Parallel Bus Definition.....	5-19
5-8	MSAT-X Processor Block Diagram.....	5-22
5-9	MSAT-X Executive Flowchart (Sheet 1 of 2) .....	5-24
5-10	MSAT-X Position Scan Flowchart.....	5-27
5-11	MSAT-X Track Dither Flowchart.....	5-28
5-12	MSAT-X Azimuth Update Flowchart (Sheet 1 of 2).....	5-30
5-13	Hybrid Loop Procedure Flowchart (Sheet 1 of 2).....	5-32
5-14	MSAT-X Elevation Dither Procedure Flowchart .....	5-34
5-15	External Interrupt Flowchart .....	5-35

## LIST OF ILLUSTRATIONS (CONTINUED)

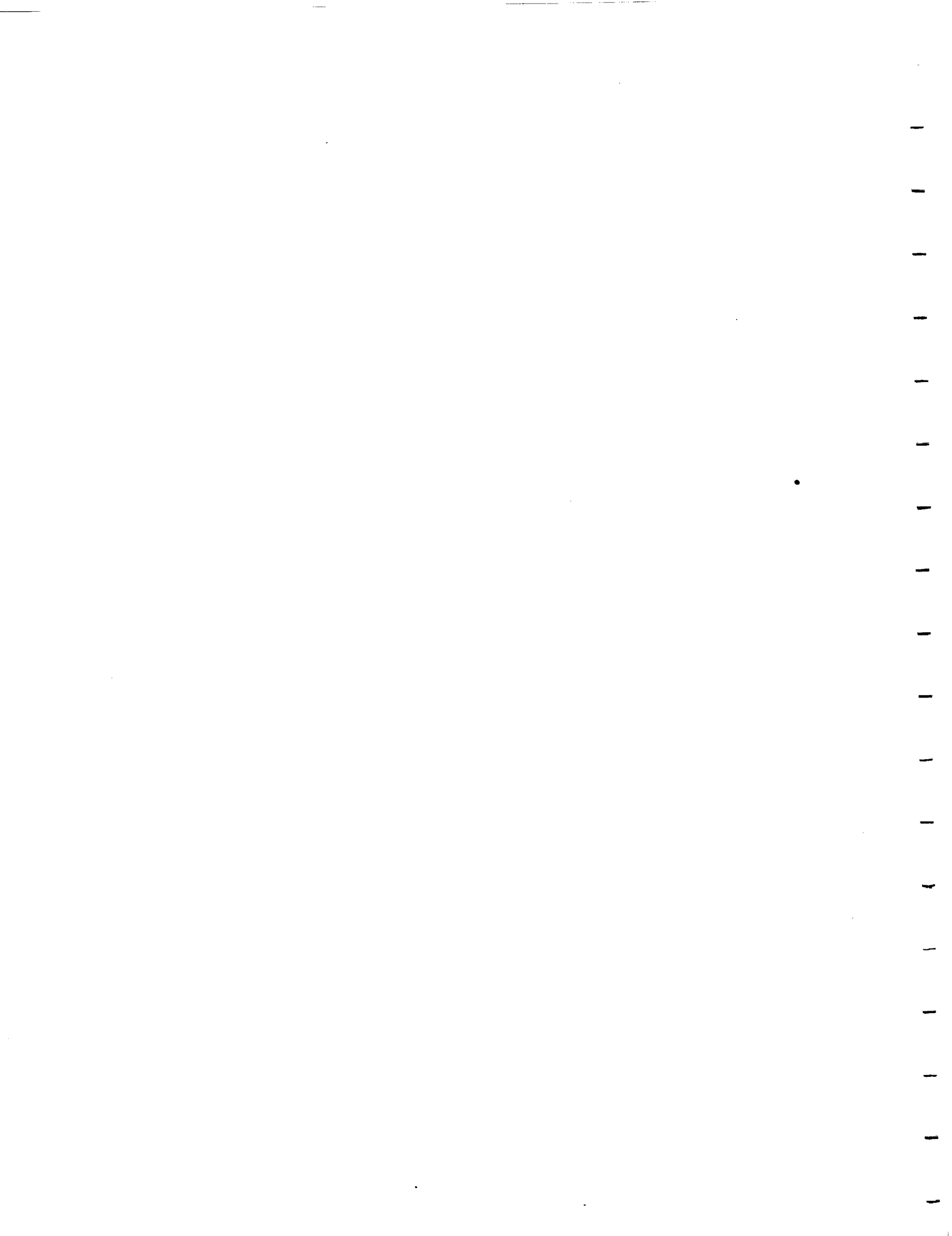
FIGURE	TITLE	PAGE
5-16	Pointing Error Sample Flowchart .....	5-36
6-1	Planar Views of MSAT-X Vehicle Antenna .....	6-2
6-2	Exploded View of MSAT-X Vehicle Antenna.....	6-3
6-3	MSAT-X Vehicle Antenna System .....	6-4
6-4	19-Element Fabrication Experimental Model .....	6-9
8-1	Antenna Test Range.....	8-4
8-2	MSAT-X Antenna Steering Control.....	8-8
8-3	ICOM Reference Antenna Receiver.....	8-12
8-4	Block Diagram Depicting how MSAT-X Equipment is Interconnected for Functional Tests.....	8-17
8-5	Pictorial/Block Diagram Depicting Equipment Hook-up for MSAT-X Systems Tests on Outdoor Antenna Range .....	8-18
8-6	19-Element Array, Top View.....	8-20
8-7	Block Diagram Depicting Equipment Hook-up for Antenna Pattern Tests .....	8-21
8-8	Intersatellite Isolation Spectrum Analyzer Display .....	8-24

## LIST OF TABLES

TABLE	TITLE	PAGE
1-1	Summary of Antenna Performance .....	1-4
1-2	Summary of Pointing System Performance .....	1-6
1-3	Cost Analysis Summary.....	1-7
1-4	High Cost Driver Items for 10,000 Units Per Year.....	1-7
2-1	Summary of Array Performance.....	2-14
2-2	Loss Budget.....	2-27
2-3	Predicted Gain and Backlobe .....	2-27
2-4	Colored Symbol Versus Power Level .....	2-32

## LIST OF TABLES (CONTINUED)

TABLE	TITLE	PAGE
2-5	Summary of Results: Beam Angle vs. Pattern Roll-off .....	2-33
2-6	Summary of Measured Array Performance.....	2-45
2-7	Summary of Measured Gain of the Array .....	2-60
2-8	Gain Analysis of Array Unit #2.....	2-64
2-9	Measured Intersatellite Isolation .....	2-70
3-1	Price of Cu-Clad Substrate, One Ounce Copper Two Sides, Per 100 Sheets or More Per Sq. Ft. ....	3-2
3-2	Performance versus Cost Comparison for Several Different Types of Substrate Material .....	3-3
3-3	Measured Hybrid Network Performance.....	3-17
3-5	Performance Summary of Typical Hybrid Network.....	3-39
4-1	Summary of Mid Frequency Phase Shifter Data for Three Designs .....	4-6
4-2	7-Way Divider Data (No Resistors).....	4-12
4-3	19-Way Divider Data (No Resistors) .....	4-13
4-4	Beamformer #1 Performance Summary.....	4-21
4-5	Summary of Beamformer Losses for Various Beamformer Configurations .....	4-22
4-6	Summary of Beamformer Mean Phase Errors for Various Beamformer Configurations .....	4-23
5-1	LED Reading versus Elevation Angle .....	5-20
5-2	Output versus Input Voltage (Efficiency at VIN = 12V is 68%) .....	5-21
5-3	List of Electronics Box Drawings and Context Matter .....	5-23
7-1	Cost Analysis Summary.....	7-1
7-2	High Cost Driver Items for 10,000 Units per Year .....	7-2
7-3	TRE Fab. and Assy. Complete, 11 Units .....	7-6
7-4	TRE Fab. and Assy. Complete, 1000 Units/Yr - over a 5-year period.....	7-7
7-5	TRE Fab. and Assy. Complete, 5000 Units/Yr - over a 5-year period.....	7-8
7-6	TRE Fab. and Assy. Complete, 10,000 Units/Yr - over a 5-year period.....	7-9
7-7	TRE Decated Offsite Operation, 10,000 Units/Yr - over a 5-year period.....	7-10
9-1	Array Gain Performance .....	9-2



**NASA  
FORMAL  
REPORT**

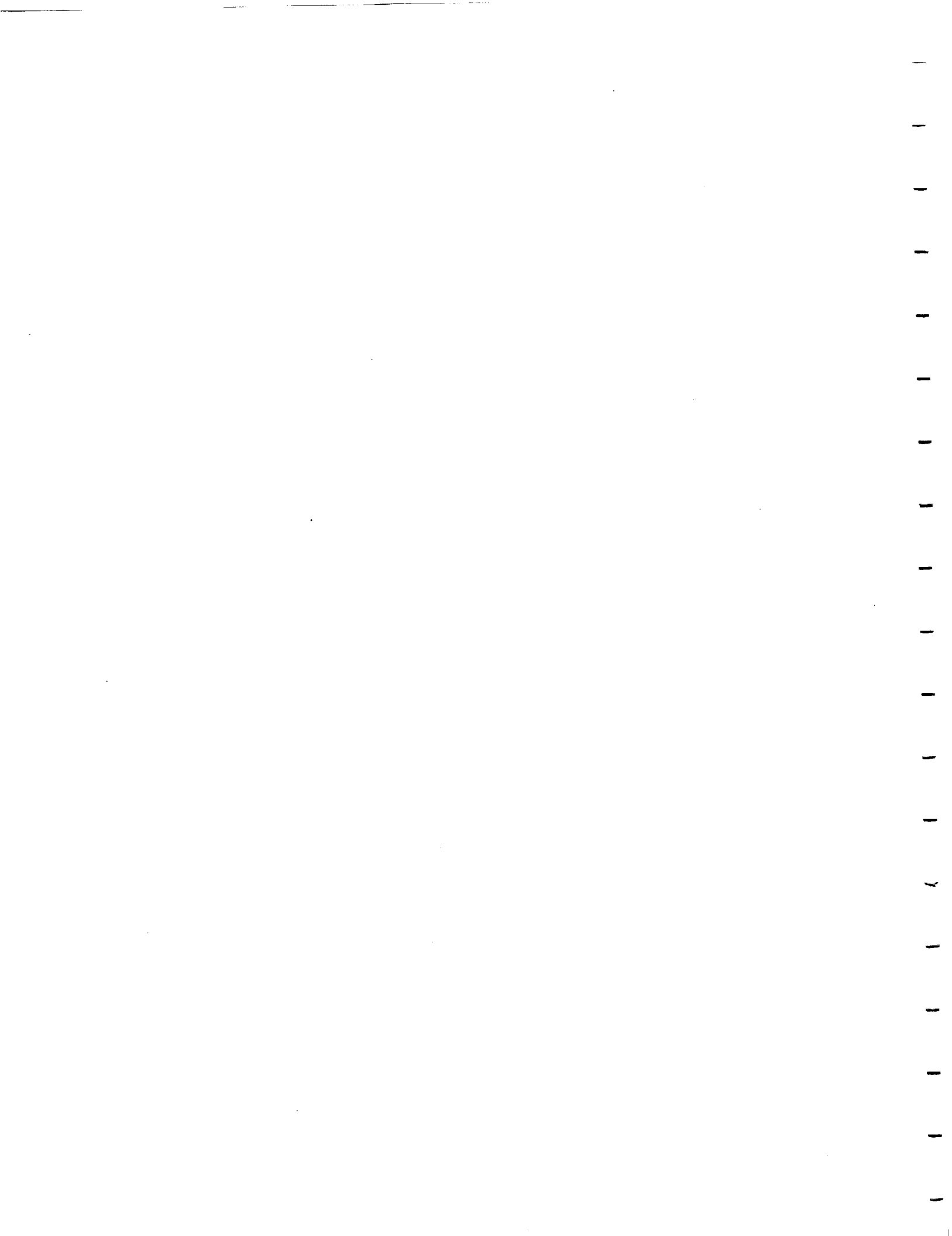


## ABSTRACT

A low profile, low cost, printed circuit, electronically steered, right hand circularly polarized phased array antenna system has been developed for the Mobile Satellite Experiment (MSAT-X) Program. This work was conducted under contract with the Jet Propulsion Laboratory (JPL), of Pasadena, California. The success of this antenna is based upon the development of a crossed-slot element array and detailed trade-off analyses for both the phased array and pointing system design. The optimized system provides higher gain at low elevation angles (20 degrees above the horizon) and broader frequency coverage (approximately 8 1/2% bandwidth) than is possible with a patch array. Detailed analysis showed that optimum performance could be achieved with a 19 element array of a triangular lattice geometry of 3.9 inch element spacing. This configuration has the effect of minimizing grating lobes at large scan angles plus it improves the intersatellite isolation. The array has an aperture 20 inches in diameter and is 0.75 inch thick overall, exclusive of the RF and power connector.

The pointing system employs a hybrid approach that operates with both an external rate sensor and an internal error signal as a means of fine tuning the beam acquisition and track. Steering the beam is done electronically via 18, 3-bit diode phase shifters. A nineteenth phase shifter is not required as the center element serves as a reference only.

Measured patterns and gain show that the array meets the stipulated performance specifications everywhere except at some low elevation angles. The measured acquisition and track performance has met the required specifications including operation under weak signal conditions and in the presence of high power interfering signals. Intersatellite isolation, as measured, is well above the 20 dB level required by the spec. With respect to price, the goal of \$1500.00 per unit at manufacturer's cost can be realized on a basis of 10,000 units per year over five consecutive years through a dedicated production plant located outside the United States.



## SECTION 1 INTRODUCTION

Research and development performed under Contract No. 957468, "Vehicle Antenna for MSAT-X," by Teledyne Ryan Electronics (TRE) with Jet Propulsion Laboratory (JPL), Pasadena, California, is summarized and analyzed in this final report. This section will briefly review the program background and present a summary of the results achieved.

### 1.1 PROGRAM BACKGROUND REVIEW

The "Vehicle for MSAT-X" program is a two-phase program. The work performed and reported here in only for Phase I - Breadboard Development. The major tasks for this phase are:

- Antenna performance analysis
- Breadboard design
- Breadboard test plan and procedures
- Cost analysis
- Breadboard antenna development

The goal of this phase of the program is to develop a low cost, low profile, electronically steered phased array antenna system. In addition, a pointing system will be developed which uses an external rate sensor and an internal error signal to search and track satellite locations.

After a detailed antenna performance analysis, a 19-element crossed-slot phased array was designed and fabricated. This antenna was tested according to the prepared breadboard test plan and procedures (Reference 1). The measured data showed good results. In addition, an extensive cost analysis was performed which showed the low cost goal can be achieved. All results are summarized in the next subsection.

---

1 TRE Report, "Breadboard Test Plan/Procedure for MSAT-X Satellite Communications Antenna," Report No. TRE/SD105662-1B (September 2, 1987).

1.2

## SUMMARY OF RESULTS

1.2.1

### Antenna Pattern and Gain Performance

Based on the results of an extensive trade-off analysis, a 19-element crossed-slot phased-array with a triangular lattice element spacing at 3.9 inches was designed. The major feature of this design is to minimize grating lobes and back lobes at large scan angles over the entire frequency bandwidth. The choice of the crossed-slot over the patch for the array element is mainly due to the following merits:

- A crossed-slot has broader frequency coverage and is thinner in thickness, and
- a crossed-slot has better gain coverage at low elevation angles (20 degrees above horizon).

In the beamforming network, there are 18 3-bit diode phase shifters that electronically steer the array beam positions. The center element is used as the reference, hence it does not need a phase shifter.

A total of two antenna systems were built, tested and delivered to JPL to fulfill the contract requirement. The total array thickness was 0.68 and 0.75 inches for units #1 and #2, respectively, exclusive of the input RF connector and beam control DC connector. For the final production array, holes can be planned by the car manufacturers to accommodate these connectors, so the array can be flush-mounted right on the car top. The actual thickness above the car roof should be less than one inch (0.75 inch). Figure 1-1 shows a photo of the developed breadboard vehicle antenna delivered to JPL, and Figure 1-2 shows the breadboard antenna mounted on the top of a car.

The measured antenna performance for both units #1 and #2 is summarized in Table 1-1. It should be noted that the measured performance has met or is better than the design specification in most areas, except for the gain coverage and backlobes. It is felt, however, that the gain can be improved by minimizing the loss from the beamforming circuits and from the isolation between the right hand and left hand circular polarization ports of a crossed-slot element. In addition, the optimization in beam scan positions through calibration will provide further gain improvement.

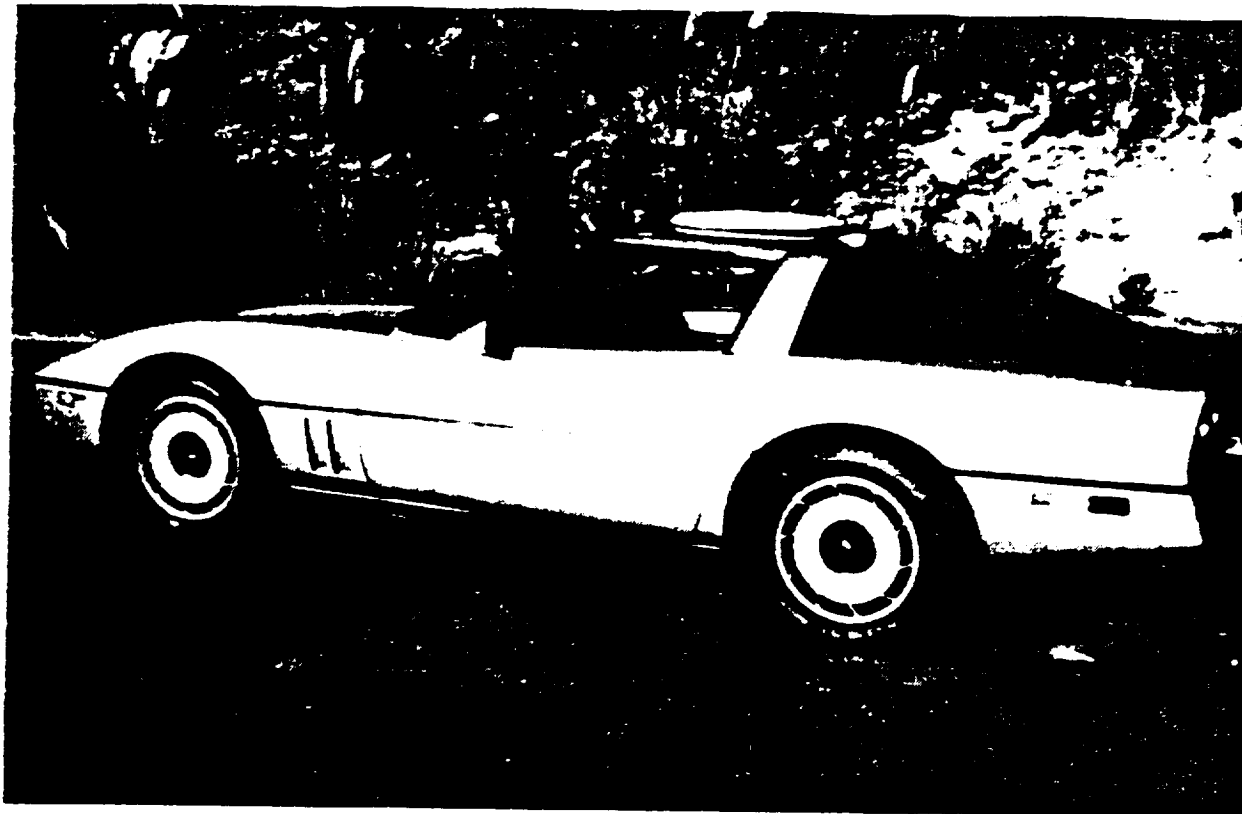


Figure 1-1. Photo to Show the Breadboard Antenna Mounted on the Top of a Vehicle

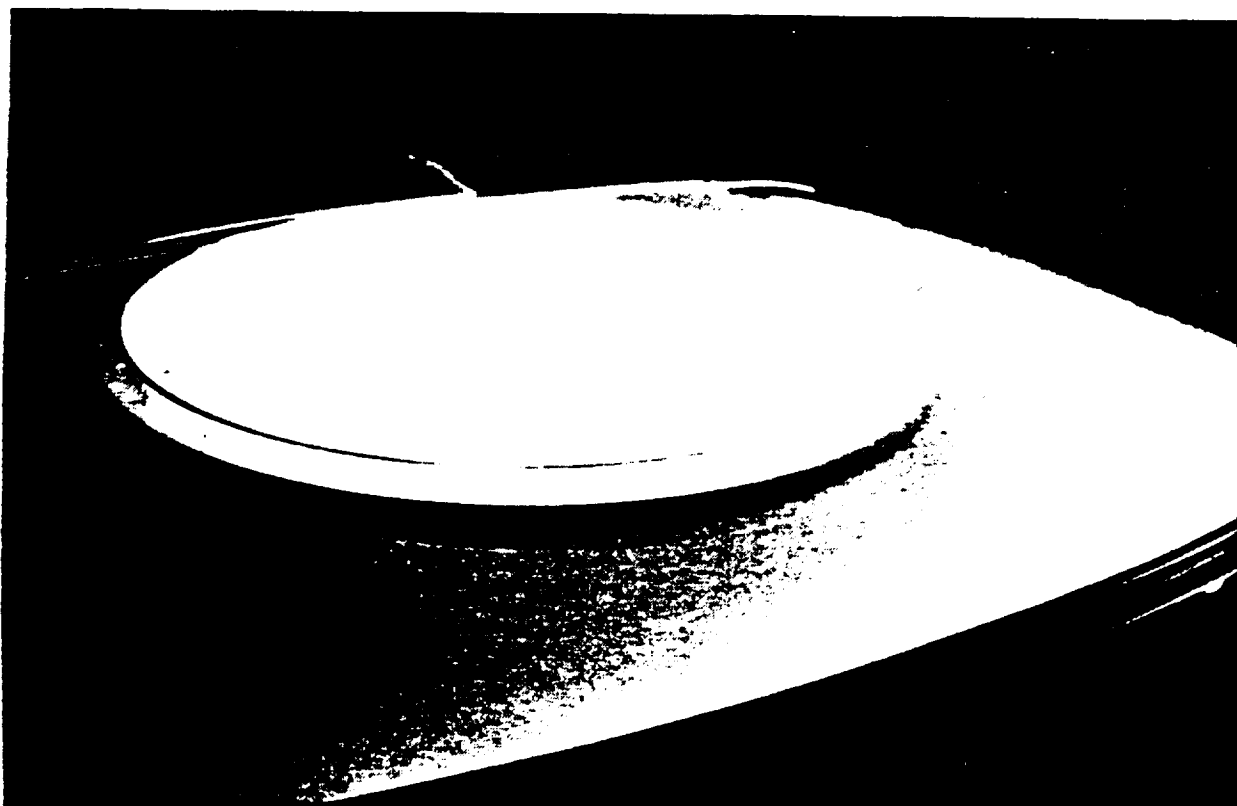


Figure 1-2. Photo to Show the Developed Breadboard Vehicle Antenna for MSAT-X Program

Table 1-1. Summary of Antenna Performance

Performance	Design Spec.	Designed Value	Measured Unit #1 Data	Measured Unit #2 Data	Remarks
Antenna Gain (dBic)					
$F_L$ at 20° elev. ( $F_L = 1545$ MHz)	10.0	10.0	9.2* (avg.)	9.3 (avg.)	Unit #2 $F_L$ : 9.9 highest 8.2 lowest
$F_H$ at 20° elev. ( $F_L = 1660$ MHz)	10	10	7.7** (avg.)	8.3 (avg.)	$F_H$ : 8.8 highest 7.2 lowest
Antenna Height (inches) maximum	1.0	1.0	0.68***	0.75***	Unit #2 used thicker array substrates
Antenna Size (inches) maximum diameter	24	22	22	22	Array aperture size plus mounting area
Multipath Rejection (dB) minimum	6	>6	>6	>6	
Backlobe (dB) highest at 20° elev.	12	12	$\geq 12$ <12	$\geq 12$ <12	95% 5%
Sidelobe highest at broadside	none	19	>18	>18	

\* 9.2 is averaged over 360 degrees in azimuth. the worst value is 8.3; the highest value is 9.9.

\*\* 7.7 is averaged over 360 degrees in azimuth. The worst value is 6.7 dB; the highest is 8.3.

\*\*\* Exclusive of connectors underneath the antenna.

### 1.2.2 Pointing System Performance

The development of the pointing system has been completed. The major tasks in the development were generating the pointing algorithm, building pointing hardware, and

coding the pointing software. The system uses an external rate sensor and internal error signal to search and track satellite locations. The major features of the system are summarized below.

- Beam pointing accuracy <2 degrees
- Probability of signal detection for C/N > 40 dB-Hz is 99%
- Azimuth tracking - sequential lobing
- Elevation tracking - maximum signal level
- Angular rate sensor is used in aiding azimuth tracking
- Tracking speed - 45 degrees/second

The system performance was measured during the acceptance test, results of which are summarized in Table 1-2. Note that all requirements have been met, except the peak amplitude and phase variations. There were cases, only about 5% of the time, that the amplitude and phase variations were worse than the specified values. The measured search and track performance, however, was very good, even under the fading and high power conditions. It should be pointed out that the problem of peak amplitude and phase variations was corrected before the delivery of the complete antenna system to JPL. Note that the measured minimum intersatellite isolation level was 26 dB.

### 1.2.3 Cost Analysis

The cost analysis for a phased array antenna system including the angular rate sensor cost, has been completed. The results are summarized in Table 1-3. The goal of the cost analysis is to determine how the \$1500 or less per unit price for the manufacturer's cost can be achieved, and to identify high cost driver items.

It should be noted that two different manufacturing conditions were assumed in our cost analysis for the 10,000 units per year for 5 year's production. The first one is to use a dedicated off-site operation (outside U.S.A.). The estimated TRE's manufacturing unit cost is \$1363 which meets the ultimate goal of \$1500. The second condition is using a local plant (in U.S.A.). The estimated TRE's manufacturer's unit cost is \$1848 which is higher than the targeted unit price of \$1500. For yearly production quantities of 5000 and 1000

Table 1-2. Summary of Pointing System Performance

Performance	Design Spec.	Designed Value	Measured Data	Remarks
Peak Amplitude Variation (in dB)	1	1	< 1 1.5*	95% time 5%
Peak Phase Variation (in degrees)	10	10	< 10 15*	95% time 5%
Acquisition Time (in seconds) for 4 pilot frequencies	10	10	10	Search time per pilot frequency is 2.5 seconds
Fading Test, using amplitude modulation to simulate a 5 dB fade at 40 Hz rate	No impairment of tracking or acquisition	No impairment of tracking or acquisition	No impairment of tracking or acquisition	Tested at 10 degrees per second to simulate vehicle turn speed
High Power Test (10 watts transmitted from the array)	No impairment in system operation	No impairment in system operation	No impairment in system operation	Tested with 20 watts power transmitted into the diplexer with 3 dB cable loss
C/N Range (dB)	from 55 to 38 (threshold)	from 55 to 38	from 55 to 38	Two sources
Intersatellite Isolation (dB) minimum	20	22	26	Two sources were separated by 30 degrees in azimuth and 10 degrees in elevation

\* The peak-to-peak anomalies for both amplitude and phase variations were corrected before the delivery of hardware.

Table 1-3. Cost Analysis Summary

Quantity per year	Manufacturer's Cost (\$)	Manufacturer's Selling Price (\$)	Wholesale Price (\$)	Retail Price (\$)
10,000(A)	1363	1800	2215	2770
10,000(B)	1848	2595	3195	3995
5000	2060	2890	3560	4450
1000	2589	3635	4480	5595
11	4461	6260	7710	9640

**NOTE:** 10,000(A): Dedicated Offsite Operation (outside of U.S.A.); 10,000(B): Local Plant (in U.S.A.).

units, the corresponding manufacturer's unit cost is \$2060 and \$2589, respectively. For the first 11 units, the manufacturer's unit cost is \$4461. For completeness, the estimated manufacturer's selling price, wholesale price, and retail price is also included in the table.

High cost driver items are identified and summarized in Table 1-4. It is noted that the most costly item is the teflon fiberglass dielectric circuit board material.

Table 1-4. High Cost Driver Items for 10,000 Units Per Year

Items	Cost	Percent of Total Cost
Dielectric Circuit Boards	\$293	25.7%
Phase Shifters	\$259	22.7%
Electronics	\$250	21.9%
Angular Rate Sensor	\$180	15.8%

In conclusion, the targeted manufacturer's unit cost \$1500 can be met, using a local plant (outside the U.S.A.). The method of achieving the low cost goal is to lower circuit board material cost, the overhead cost, and to advance the manufacturing technology.



## SECTION 2

### ARRAY DESIGN AND PERFORMANCE

The development of a low cost vehicular phased array for mobile satellite communications has been a challenging task for the antenna designer. A broad spectrum of considerations must be taken into account in the design phase so that the final product can meet the challenging requirements listed below:

- Intersatellite Isolation: > 20 dB
- Gain: minimum 10 dBic
- Thickness : within 1 inch
- Manufacturing Cost: \$1500.00
- Multipath Rejection Capability: > 6 dB (Pattern drop off from 20 to 0 degree above the horizon)
- Backlobe Level : > 12 dB
- Frequency : (1545 to 1660) MHz
- Scan Coverage:
  - Azimuth: 360 degrees
  - Elevation: 20 to 60 degrees above the horizon
- Polarization: right hand circular polarization
- Size: within 24 inches in diameter

In order to ensure the success of the program, a sophisticated computer program was developed for the purpose of the antenna element selection and array design. A brief analytical development model is introduced in Section 2.1. The array design and analysis will be discussed in Section 2.2 with the array assembly and the measured array performance presented in Sections 2.3 and 2.4, respectively. Conclusions and recommendations for future study will be discussed in Sections 2.5 and 2.6, respectively.

In order to predict an array performance close to the final realization, it is important to include the following major factors in the analytical model:

- scattering effect from the antenna mounting structure
- mutual coupling between array elements
- predictable component design errors
- random manufacture errors

Consider an  $N$  element array situated in an  $x$ - $y$  plane as shown in Figure 2-1. The total field of the array (which is scanning to the angle  $(\theta, \phi)$  at a distant point  $P(r, \theta, \phi)$  in free space) is given by

$$\bar{E}(\theta, \phi) = \sum_{i=1}^N I_i^t(\theta_s, \phi_s) e^{-j\Phi_i^t(\theta_s, \phi_s)} \bar{E}_i(\theta, \phi) e^{jk\bar{P}_i^s \cdot \hat{R}} \quad (2-1)$$

where

$I_i^t(\theta_s, \phi_s)$  and  $\Phi_i^t(\theta_s, \phi_s)$  = final total amplitude and phase excitations of the  $i$ -th element as the array scans to the angle  $(\theta_s, \phi_s)$ ,

$\bar{E}_i(\theta, \phi)$  =  $i$ -th element's radiating field which includes the finite ground plane effect,

$k$  = wavenumber

$\bar{P}_i^s$  = position vector of the  $i$ -th element

$$\hat{R} = \hat{x} \sin(\theta) \cos(\phi) + \hat{y} \sin(\theta) \sin(\phi) + \hat{z} \cos(\theta)$$

Note that the antenna array will be mounted on the center of the car top, with the latter serving as a conducting ground plane. Hence, in order to account for the finite ground plane effect on the array performance, the Uniform Geometrical Theory of Diffraction (GTD) was applied to compute the radiating field  $\bar{E}_i(\theta, \phi)$  of each element. The GTD

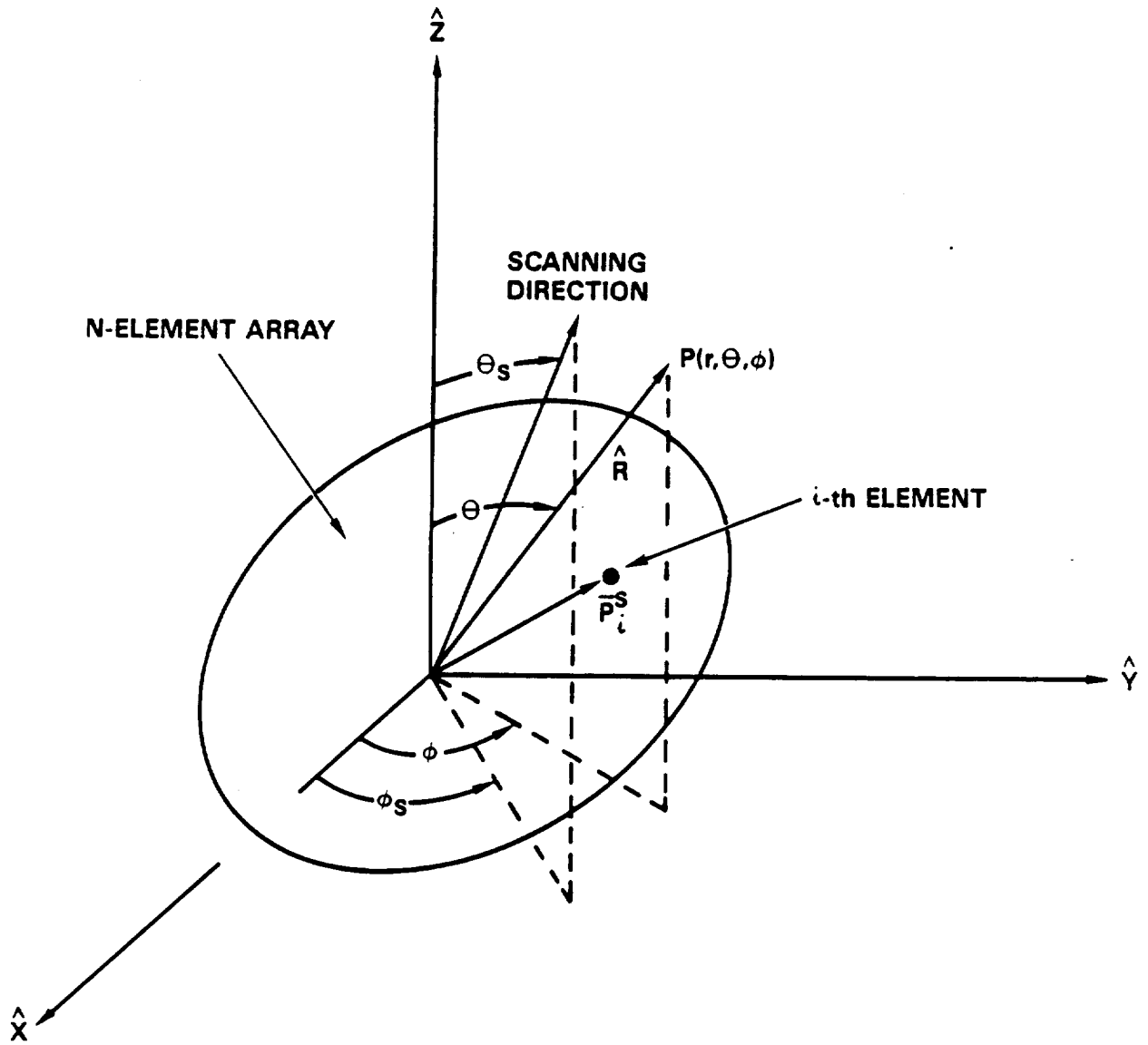


Figure 2-1. Coordinate System

model will be presented in Section 2.1.1. Mutual coupling between elements, the potential component errors and the phase shifter quantization error will affect the final total amplitude ( $I_i^t(\theta_s, \phi_s)$ ) and phase ( $\Phi_i^t(\theta_s, \phi_s)$ ) excitation of each element, which in turn will impact the array performance. A hybrid technique based on the measured s-parameter and analytical circuit model, is used to investigate the mutual coupling effect on the active scanning impedance. The mutual coupling model will be discussed in Section 2.1.2. The error model will be introduced in Section 2.1.3.

### 2.1.1 GTD Model

The Uniform Geometrical Theory of Diffraction was applied to compute the radiation field of the antenna mounted on a finite ground plane. As shown in Figure 2.-2, the total far field at any observation point  $(\theta, \phi)$  is given by

$$\bar{E}_j^{TOT}(\theta, \phi) = \bar{E}_j^s(\theta, \phi) + \sum_{i=1}^4 (\bar{E}_{i,j}^{ed}(\theta, \phi) + \bar{E}_{i,j}^{sd}(\theta, \phi) + \bar{E}_{i,j}^{cd}(\theta, \phi)) \quad (2-2)$$

where

$\bar{E}_j^s(\theta, \phi)$  = j-th element source field,

$\bar{E}_{i,j}^{ed}(\theta, \phi)$  = j-th element edge diffracted field from the i-th edge of the ground plane and is calculated through GTD solution [1],

$\bar{E}_{i,j}^{sd}(\theta, \phi)$  = j-th element slope diffracted field from the i-th edge of the ground plane and is calculated through GTD solution [2],

$\bar{E}_{i,j}^{cd}(\theta, \phi)$  = j-th element corner diffracted field from the i-th corner of the ground plane and is calculated through GTD solution [3].

Then, the RHCP and LHCP field of the crossed-slot are given by

$$\bar{E}_{RHCP}(\theta, \phi) = \left[ \bar{E}_1^{TOT}(\theta, \phi) - j\bar{E}_2^{TOT}(\theta, \phi) \right] / \sqrt{2} \quad (2-3)$$

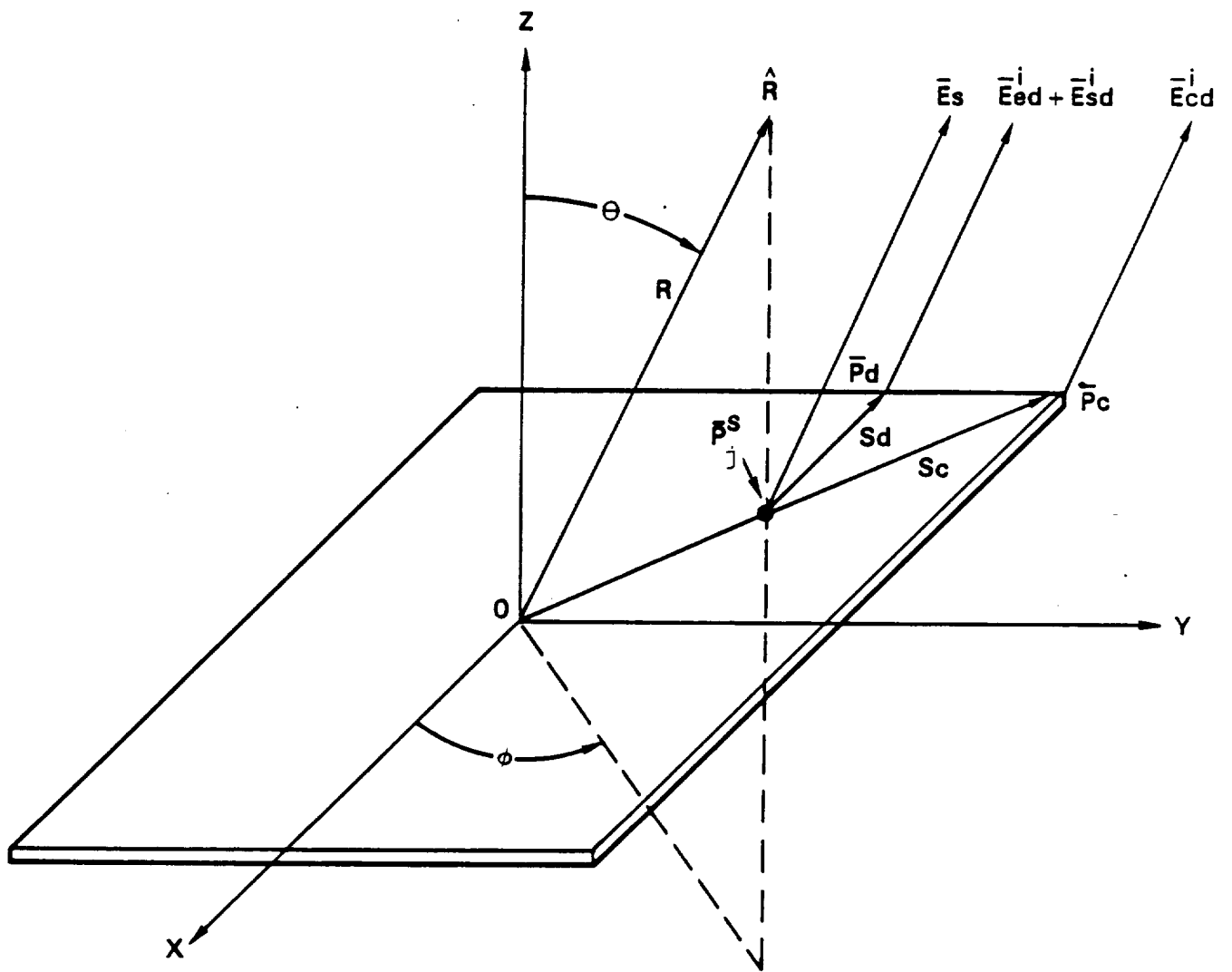


Figure 2-2. Field Computation for the  $j$ -th Element on Top of Finite Ground Plane

$$\bar{E}_{\text{LHCP}}(\theta, \phi) = \left[ \bar{E}_1^{\text{TOT}}(\theta, \phi) + j\bar{E}_2^{\text{TOT}}(\theta, \phi) \right] / \sqrt{2} \quad (2-4)$$

Based on the field solution presented above, a computer simulation program was developed. The computed radiation patterns (both RHCP and LHCP) for a single crossed-slot mounted on top of a 40" x 50" ground plane are shown Figure 2-3. Note that the  $\theta$  angle stands for the elevation angle from the zenith and the  $\phi$  angle is the azimuth angle from the x-axis as shown in Figure 2-2. As shown in Figure 2-4, good agreement between the computed and measured data was achieved.

### 2.1.2 Mutual Coupling Model

The hybrid technique is used to evaluate the mutual coupling effect on the array performance. The S-parameters of the array elements are measured and recorded by using the HP 8510 Network Analyzer. These data are then used to establish the impedance matrix [z].

The Kirchhoff's circuit relations are applied to the array and manipulated to obtain

$$\begin{bmatrix} I^t \end{bmatrix} = \begin{bmatrix} Z_{\text{NOR}} \end{bmatrix} \begin{bmatrix} I^d \end{bmatrix} \quad (2-5)$$

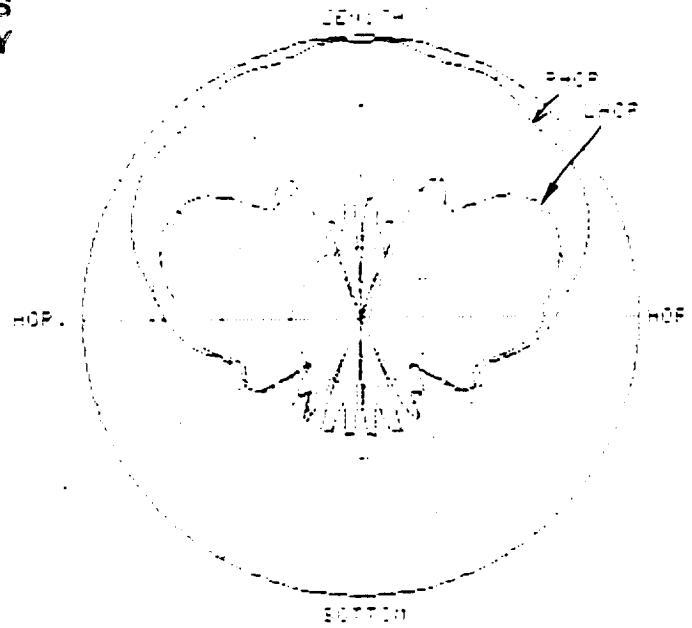
where

$I^t = I^d + I^c = \text{total current}$

$I^d = \text{driving current}$

$I^c = \text{coupling current}$

ORIGINAL PAGE IS  
OF POOR QUALITY



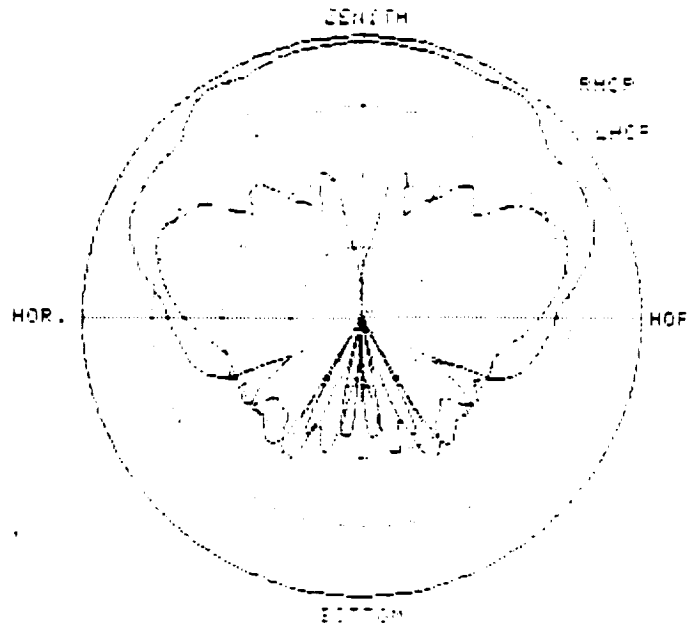
(a)  $\phi = 0$  deg.  
 $\theta = \text{Var}$



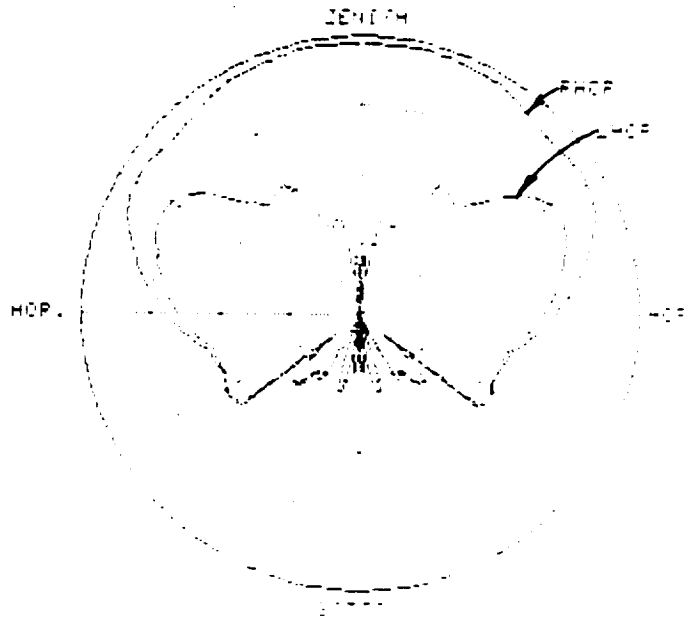
(b)  $\phi_s = 30$  deg.  
 $\theta = \text{Var}$

Figure 2-3. Computed Element Radiation Patterns at 1545 MHz (Sheet 1 of 2)

ORIGINAL PAGE IS  
OF POOR QUALITY

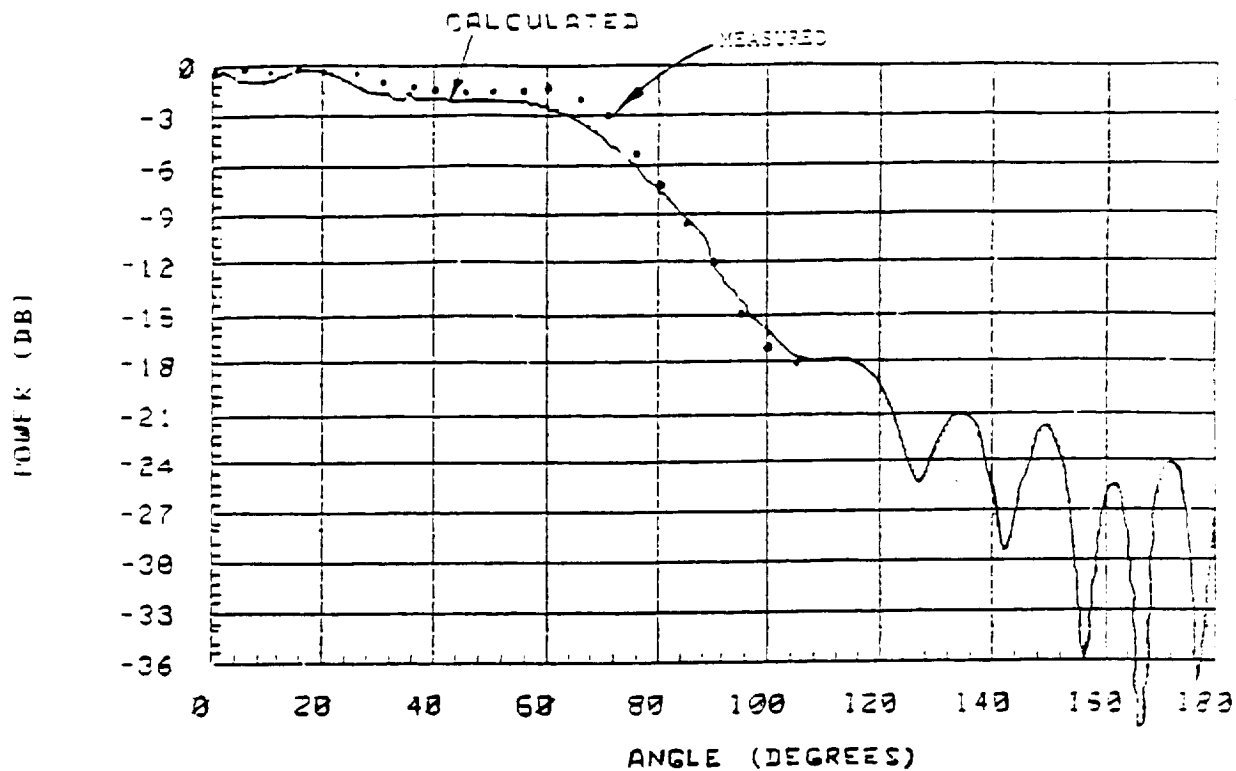


(c)  $\phi = 60$  deg.  
 $\theta = \text{Var}$

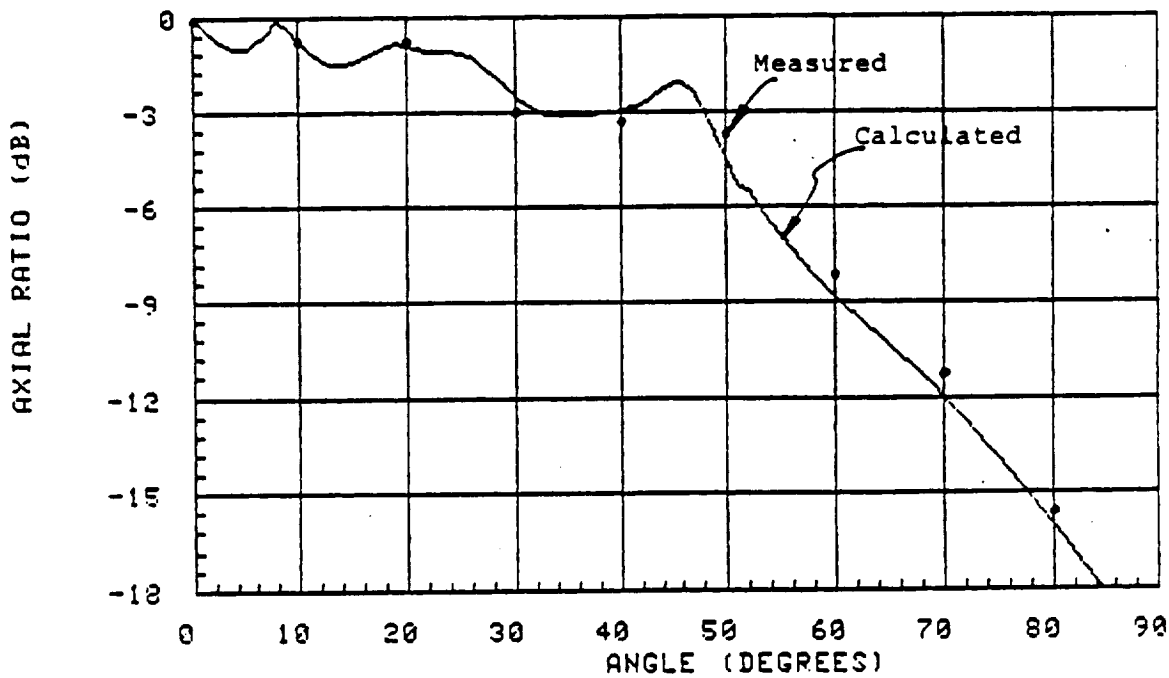


(d)  $\phi_s = 90$  deg.  
 $\theta = \text{Var}$

Figure 2-3. Computed Element Radiation Patterns at 1545 MHz (Sheet 2 of 2)



(a) Element Pattern



(b) Axial Ratio

Figure 2-4. Comparison Between Calculated and Measured Radiation Pattern

$Z_{\text{NOR}}$  = normalized impedance matrix

$$= \begin{bmatrix} 1 & \frac{z_{12}}{z_{11}} & \dots & \frac{z_{1N}}{z_{11}} \\ \frac{z_{21}}{z_{11}} & 1 & \dots & \dots \\ \frac{z_{22}}{z_{11}} & \dots & \ddots & \dots \\ \frac{z_{N1}}{z_{11}} & \dots & \dots & 1 \\ \frac{z_{NN}}{z_{11}} & \dots & \dots & \dots \end{bmatrix}$$

The active scanning impedance of the  $i$ -th element is given by

$$z_i^{\text{active}}(\theta, \phi) = \sum_{j=1}^N \frac{I_j^d(\theta, \phi)}{I_i^d(\theta, \phi)} z_{i,j}(\theta, \phi) \quad (2-6)$$

### 2.1.3 Error Model

In order to predict the array performance as close as possible to the final product, the potential errors which could exist in all component levels need to be incorporated into the model. The potential errors include the deterministic and random errors. The deterministic errors are the predictable ones such as phase shifter performance across the frequency band, unbalance in the antenna feed circuit and the power divider over the frequency band, a single phase shifter setting for both receiving and transmitting frequency, etc. Random errors will take into account the real world manufacturing capability and the nature of the material used in each component.

## 2.2 ARRAY DESIGN AND ANALYSIS

The major challenges of the vehicular phased array for Mobile Satellite Communications are the required gain (10 dBic) at low elevation angles, good intersatellite isolation (20 dB), low profile (within 1 inch), and low cost. To meet these challenges, a detailed array analysis and design was performed and discussed in Section 2.2.1. The predicted array performance is presented in Sections 2.2.2.

### 2.2.1 Array Aperature Design

The first task in the aperture design was to select a proper radiating element. Since a low profile was imperative to the antenna, the search was rapidly narrowed down to two candidates . . . , the crossed-slot and the patch element. Of these two, the printed cavity backed, stripline-fed crossed-slot was selected because of its superior features with respect to the patch antenna.

- Broader pattern coverage over the upper hemispherical space
- Better gain at low elevation angles
- Maintains a good axial ratio even at low elevation angles
- Thinner for the same frequency bandwidth

Following the element selection, the aperture design was performed to meet the required performance at the lowest cost. The major features of the design are listed below in the order of the importance of the requirements:

1. Intersatellite isolation - 20 db
2. Array gain - 10 dBic
3. Array thickness - 1 inch
4. Manufacturing cost - \$1500.00
5. Multipath rejection capability - > 6 dB pattern drop off from 20 to 0 degrees above the horizon
6. Backlobe level - 12 dB

The design approach used by TRE was to minimize the number of elements while making efficient use of the aperture and avoiding the grating lobe as much as possible. After a detailed trade off analysis, the following design characteristics were arrived at.

- a. A 19 element crossed-slot array with a triangular lattice arrangement and proper amplitude taper was chosen, as shown in Figure 2-5.
- b. The element spacing is 3.9 inches.
- c. Array size is 22 inches including the mounting space.
- d. A 3-bit diode phase shifter was selected.

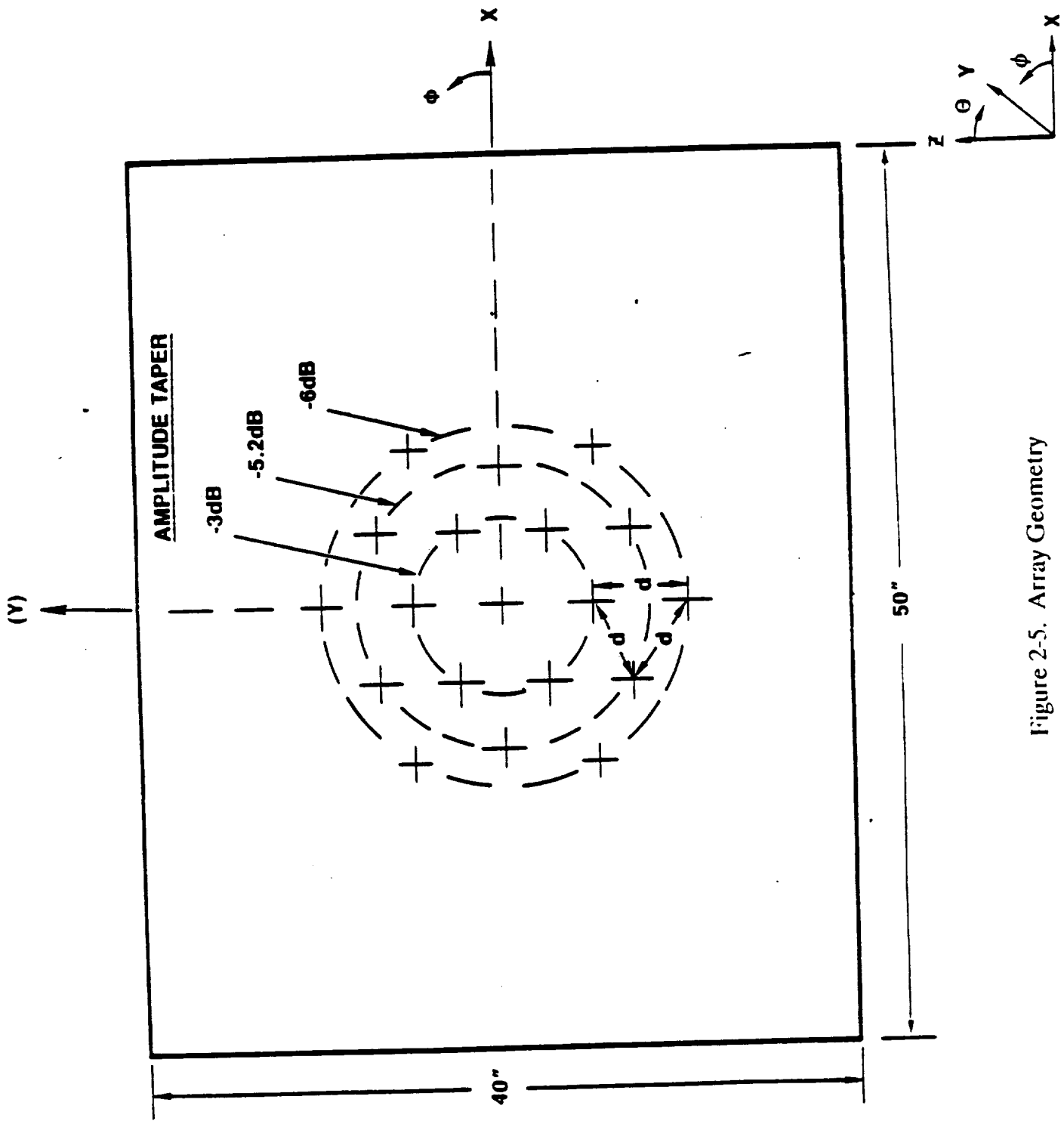


Figure 2-5. Array Geometry

Note that the amplitude taper was used to reduce the sidelobe level in order to achieve the required intersatellite isolation.

## 2.2.2 Predicted Array Performance

A brief discussion of the predicted array performance is given in the following subsections and summarized in Table 2-1.

### 2.2.2.1 Computed Array Patterns

Typical computed array patterns in the elevation and azimuth plane are shown in Figures 2-6 and 2-7 respectively. Note that  $\theta_s$  stands for the elevation scan angle from the array broadside and  $\phi_s$  is the azimuth scan angle from the x-axis.  $\theta$  and  $\phi$  are pattern cut angles. The random manufacturing errors of 0.5 dB and 10 degrees (standard deviation) are assumed in the calculations. As noted from Figure 2-8, the sidelobe is coming up due to the effects of the random errors. The finite ground plane effect is also included in the GTD model. The following observations are made through the calculated results:

- (1) Array scan patterns are well behaved.
- (2) Very good polarization characteristics are achieved. The cross-polarization level is maintained 10 dB below the co-polarization level up to 55 degrees from the array boresight.
- (3) 12 dB backlobe requirement is maintained until the array is scanned to very low elevation angles ( such as 70 degrees from the array boresight).
- (4) It is not recommended to scan the array to 70 degrees from the array broadside. Low elevation angle area (60 degrees) will be covered by the 60 degrees scan beam.
- (5) + 0.5 dB gain fluctuation in the azimuth plane at the same elevation angle was observed.

### 2.2.2.2 Mutual Coupling Effect Analysis

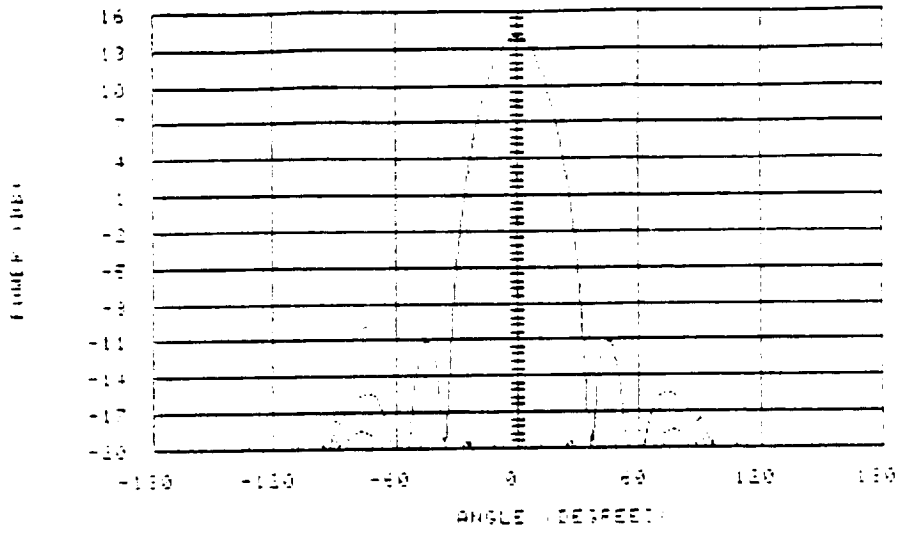
As shown in Figures 2-9 and 2-10, a seven element array, which is the central portion of the whole array, was built and used to evaluate the mutual coupling effect. The measured coupling between the element's input port (with the other port terminated in 50 ohms) is shown in Figure 2-11. Note that the true coupling value may be masked by the 90 degree hybrid feed circuit. However, the measured data still provides the qualitative information on whether or not there are blind spots. By applying equation (2-6), the computed active scanning return loss versus frequency is shown in Figure 2-12. It is observed that the input

Table 2-1. Summary of Array Performance

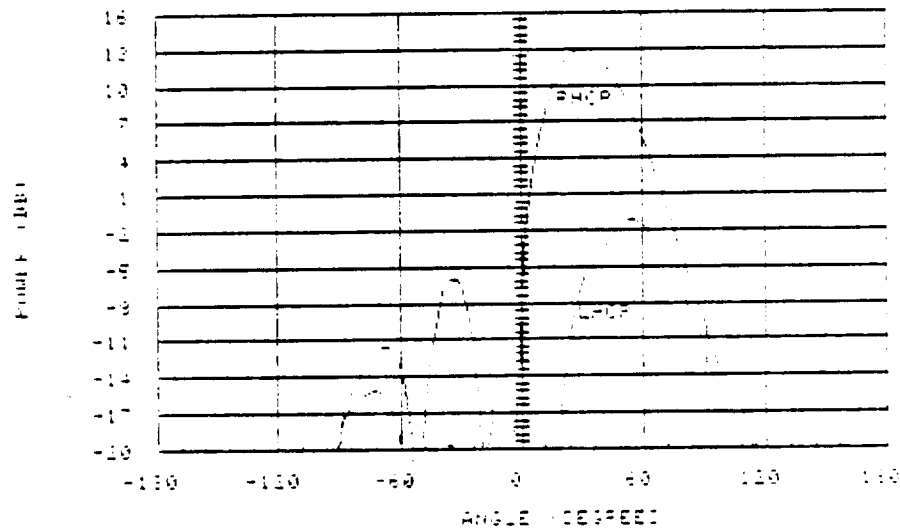
Array Geometry	<u>Design</u>	<u>Spec.</u>
	Triangular Lattice	None
Number of Elements	19	None
Element spacing (inch)	3.9	None
Gain at 20° above horizon (db): Average/Lowest	10.0/9.7	10
Intersatellite Isolation (dB)	22	20
Forward Sidelobe level, (dB)	19	None
Backlobe Level (dB) <relative to main beam >	12	12
Multipath Rejection (dB) (pattern drop off from 20° to 0° elevation)	>6	6
Azimuth Beamwidth		
at 30° above horizon	32	
at 40° above horizon	35	None
at 50° above horizon	41	
at 60° above horizon	52	
Elevation Beamwidth		
at 30° above horizon	44	
at 40° above horizon	38	None
at 50° above horizon	34	
at 60° above horizon	30	

match is slightly degraded at the higher frequencies as the array scans to  $\theta_s = 60$  degrees. The measured active element patterns, given in Section 3, are also well behaved. Hence, it is concluded that the effects of mutual coupling on the performance of the array is small.

EXAMPLES OF  
POOR QUALITY



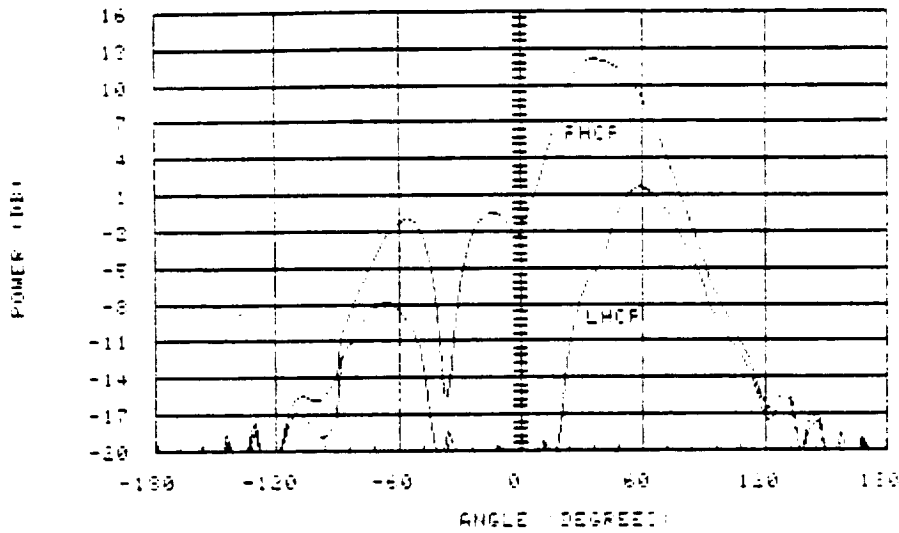
(a) Broadside (x cut)



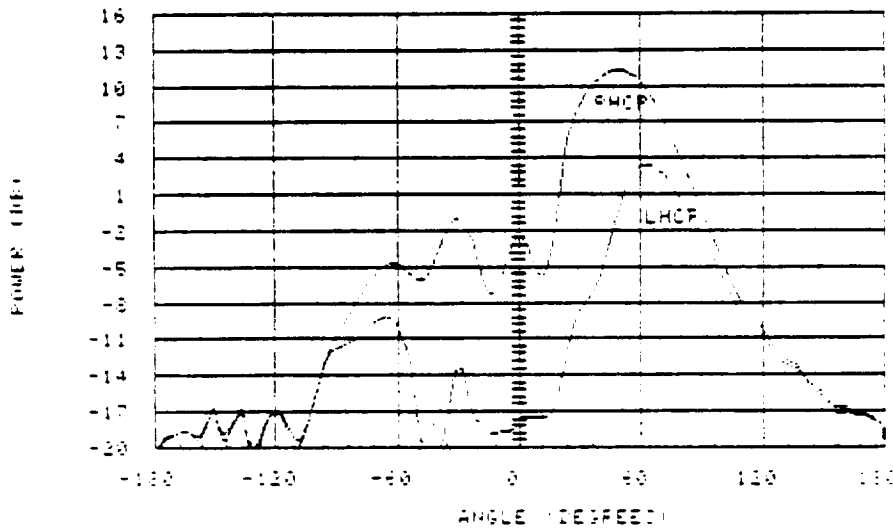
(b)  $\theta_s = 30^\circ$ ,  $\phi_s = 0^\circ$ ;  $\theta = \text{VAR}$ ,  $\phi = 0^\circ$

Figure 2-6. Computed Elevation Pattern at 1545 MHz (Sheet 1 of 3)

ORIGINAL PAGE IS  
OF POOR QUALITY



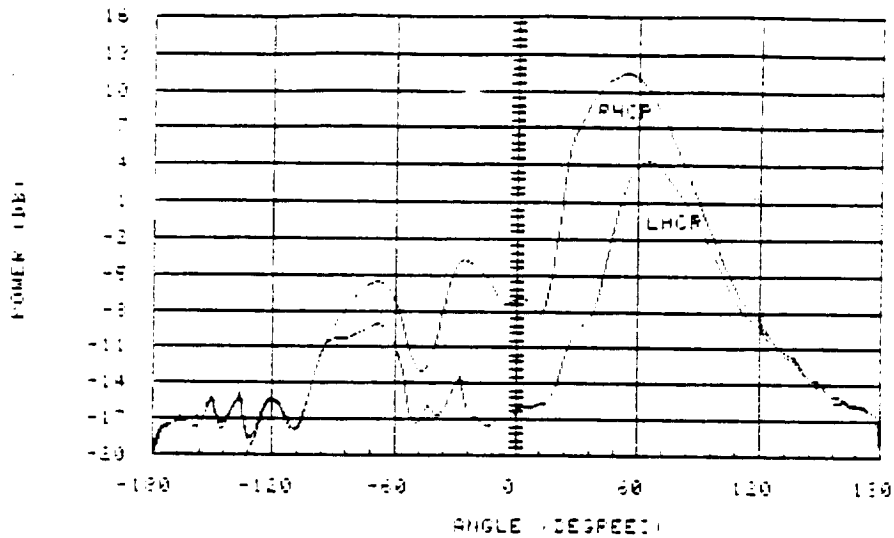
(c)  $\theta_s = 40^\circ$ ,  $\phi_s = 0^\circ$ ;  $\theta = \text{VAR}$ ,  $\phi = 0^\circ$



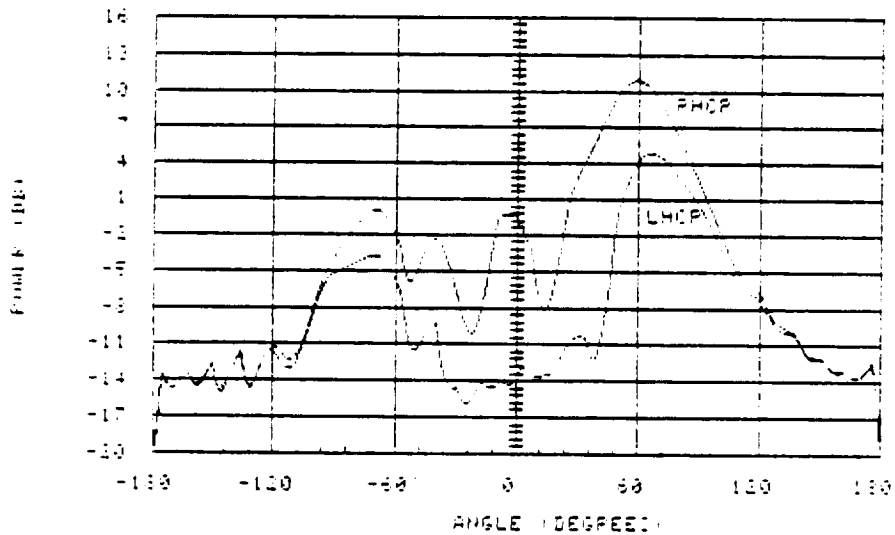
(d)  $\theta_s = 50^\circ$ ,  $\phi_s = 0^\circ$ ;  $\theta = \text{VAR}$ ,  $\phi = 0^\circ$

Figure 2-6. Computed Elevation Pattern at 1545 MHz (Sheet 2 of 3)

ORIGINAL PAGE IS  
OF POOR QUALITY

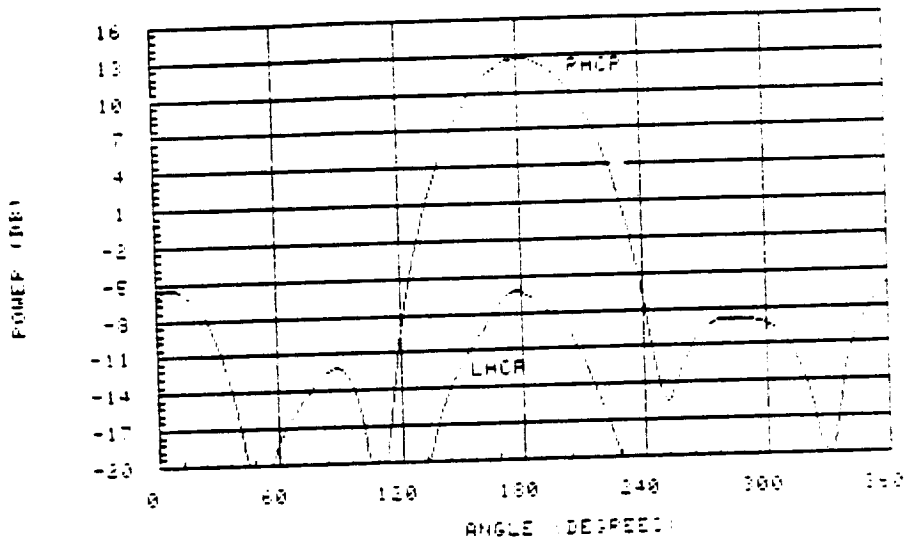


(e)  $\theta_s = 60^\circ$ ,  $\phi_s = 0^\circ$ ;  $\theta = \text{VAR}$ ,  $\phi = 0^\circ$

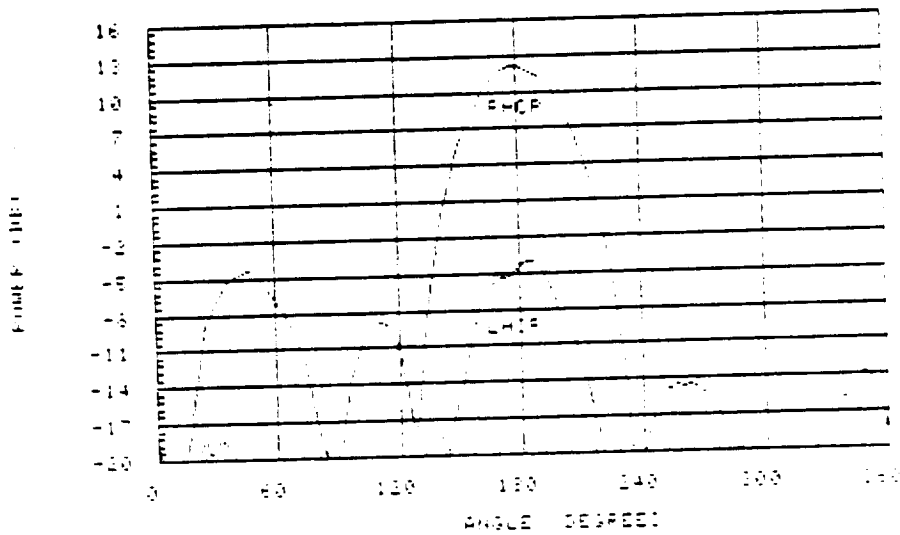


(f)  $\theta_s = 70^\circ$ ,  $\phi_s = 0^\circ$ ;  $\theta = \text{VAR}$ ,  $\phi = 0^\circ$

Figure 2-6. Computed Elevation Pattern at 1545 MHz (Sheet 3 of 3)



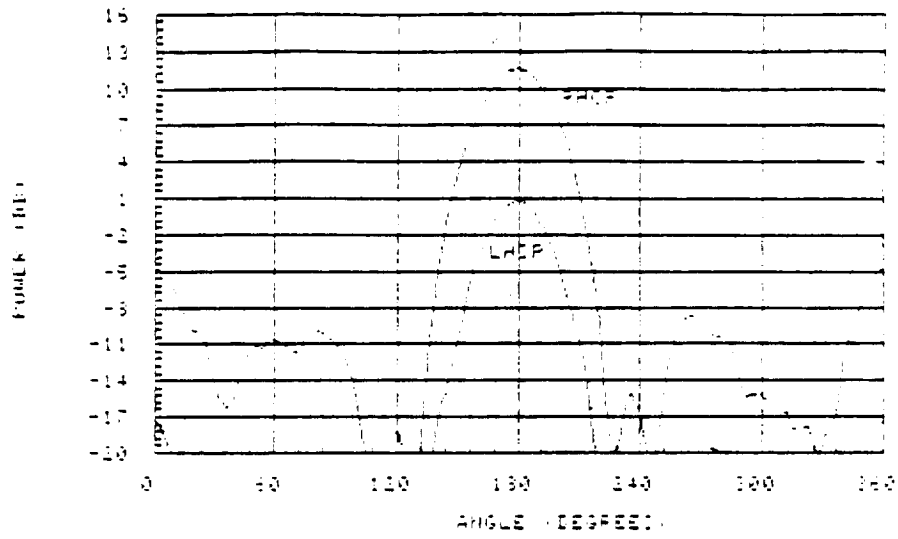
(a)  $\theta_s = 30^\circ$ ,  $\phi_s = 180^\circ$ ;  $\theta = 30^\circ$ ,  $\phi = \text{VAR}$



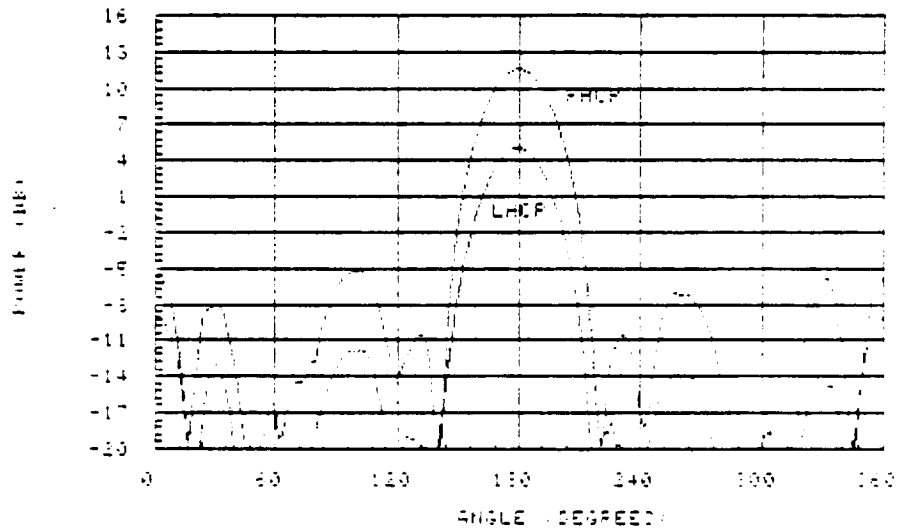
(b)  $\theta_s = 40^\circ$ ,  $\phi_s = 180^\circ$ ;  $\theta = 40^\circ$ ,  $\phi = \text{VAR}$

Figure 2-7. Computed Azimuth Array Pattern at 1545 MHz (Sheet 1 of 3)

ORIGINAL PAGE IS  
OF POOR QUALITY



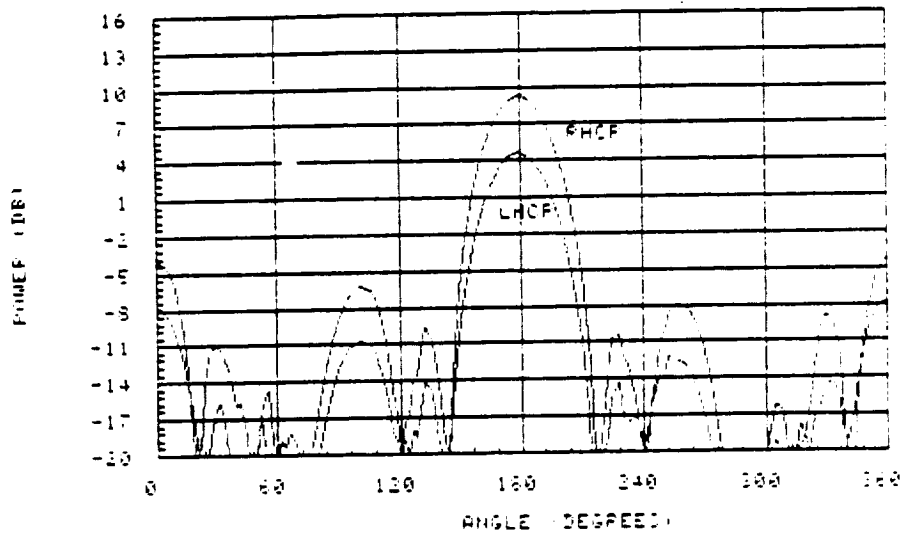
(c)  $\theta_s = 50^\circ$ ,  $\phi_s = 180^\circ$ ;  $\theta = 50^\circ$ ,  $\phi = \text{VAR}$



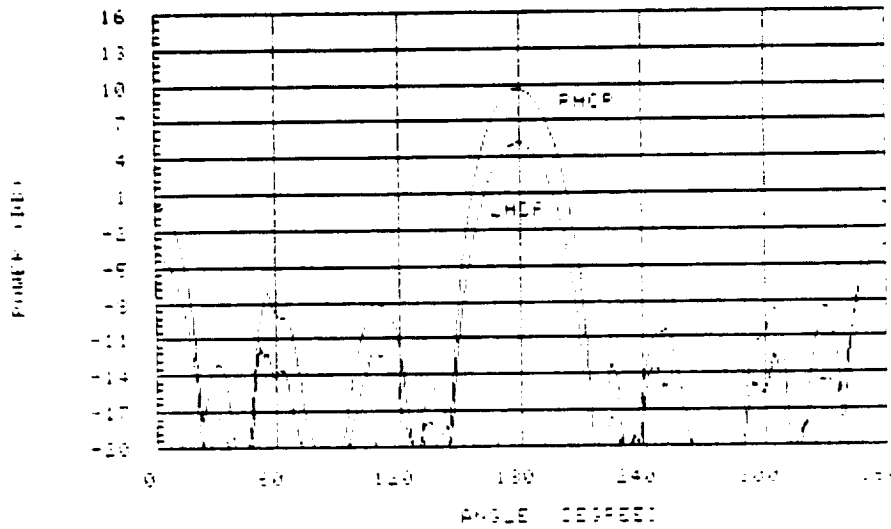
(d)  $\theta_s = 60^\circ$ ,  $\phi_s = 180^\circ$ ;  $\theta = 60^\circ$ ,  $\phi = \text{VAR}$

Figure 2-7. Computed Azimuth Array Pattern at 1545 MHz (Sheet 2 of 3)

ORIGINAL PAGE IS  
OF POOR QUALITY



(e)  $\theta_s = 60^\circ$ ,  $\phi_s = 180^\circ$ ;  $\theta = 70^\circ$ ,  $\phi = \text{VAR}$



(f)  $\theta_s = 70^\circ$ ,  $\phi_s = 180^\circ$ ;  $\theta = 70^\circ$ ,  $\phi = \text{VAR}$

Figure 2-7. Computed Azimuth Array Pattern at 1545 MHz (Sheet 3 of 3)

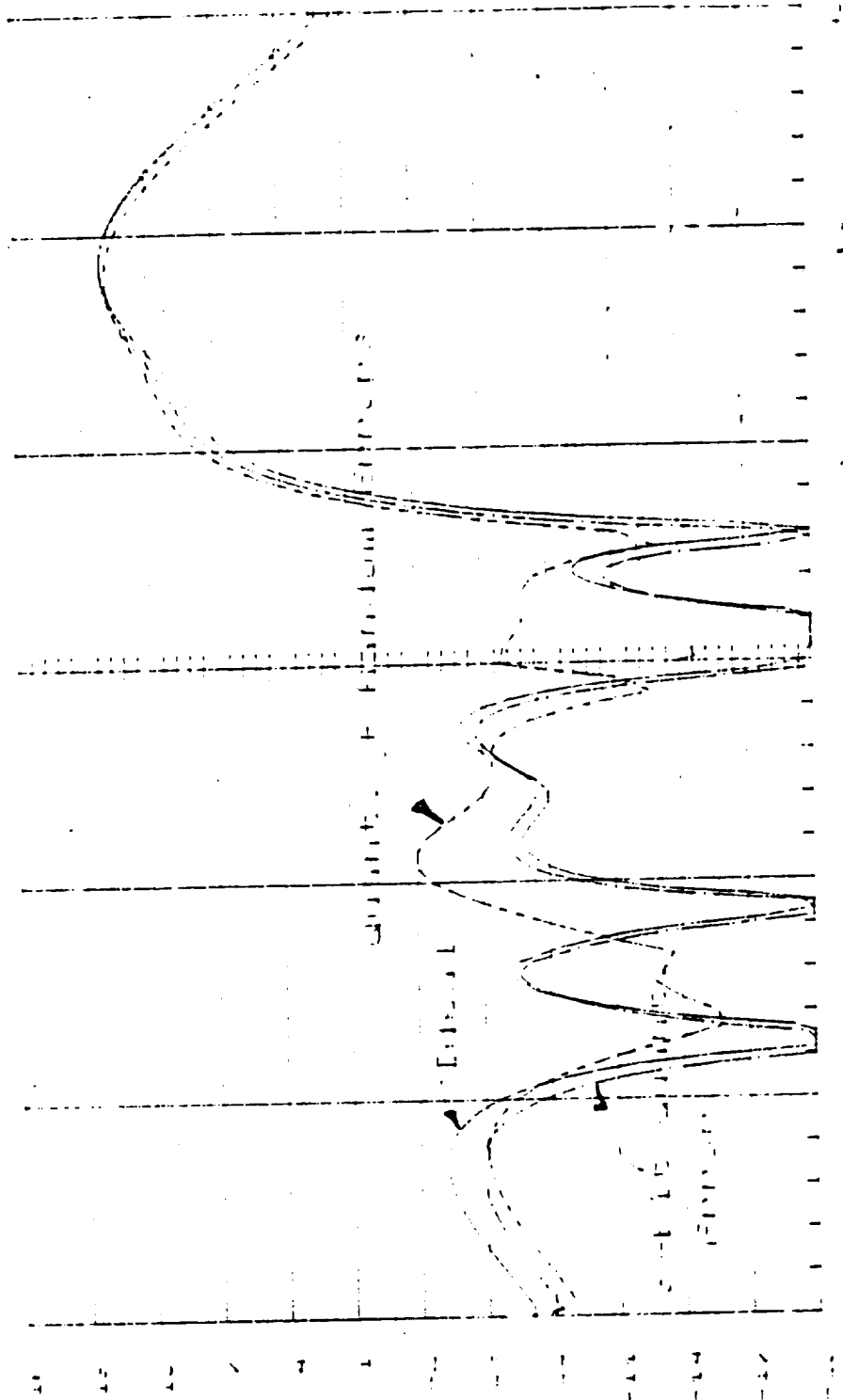


Figure 2-8. Random Errors Effect on the Array Performance

ORIGINAL PAGE  
BLACK AND WHITE PHOTOGRAPH

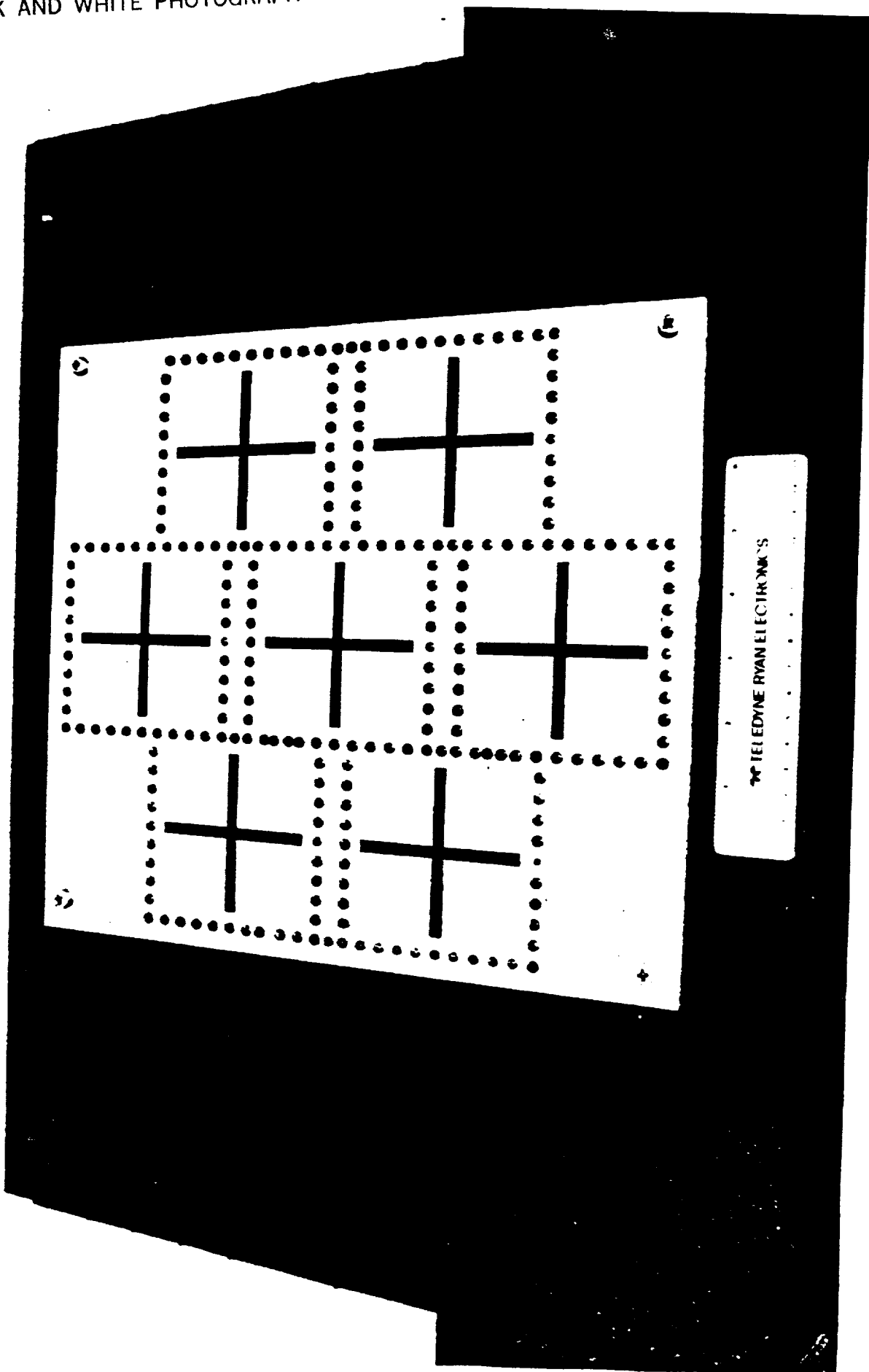
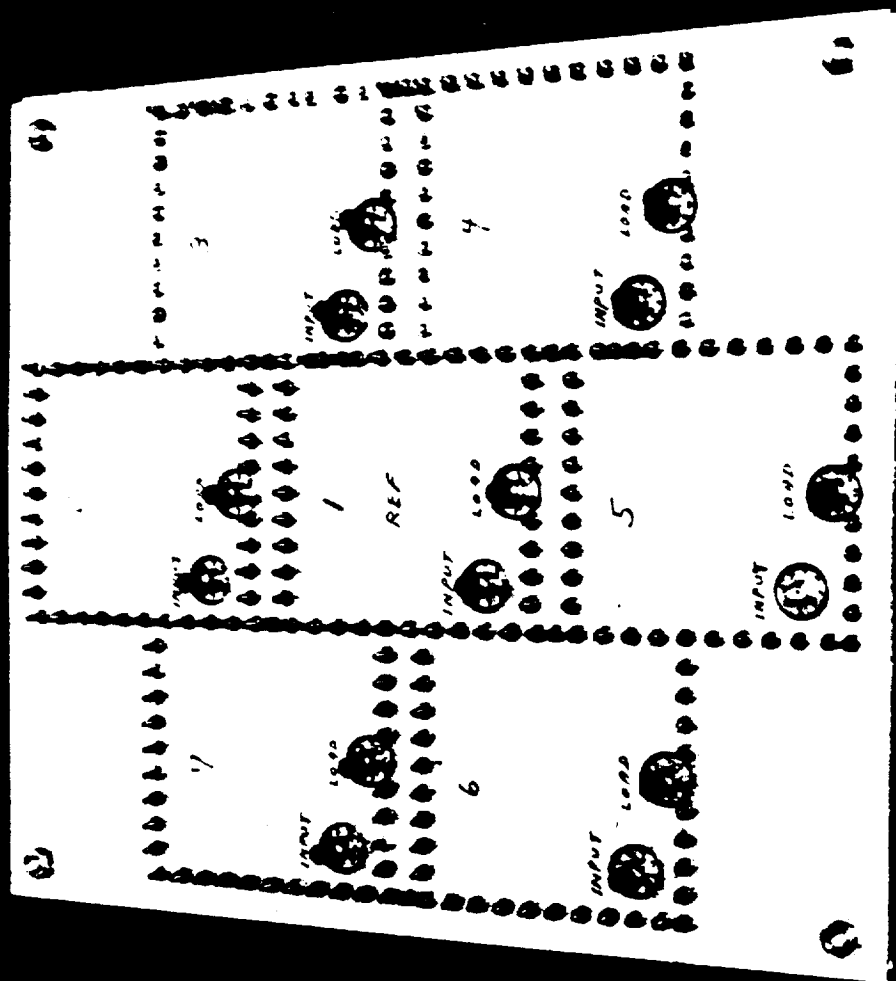


Figure 2-9. Photo of Seven Element Array (Top View)

ORIGINAL PAGE  
BLACK AND WHITE PHOTOGRAPH



TELEDYNE RYAN ELECTRONICS

Figure 2-10. Photo of Seven Element Array (Bottom View)

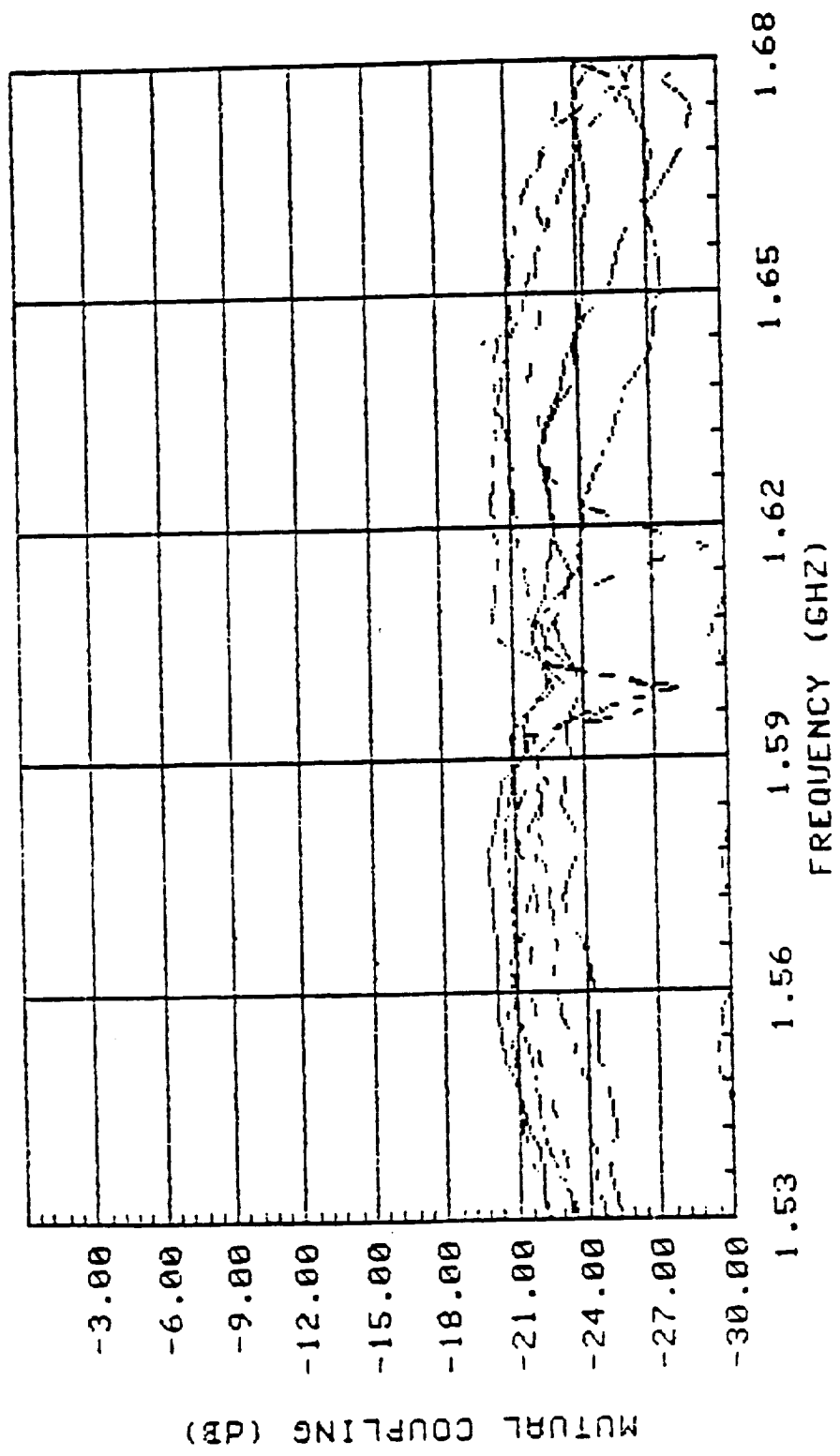


Figure 2-11. Measure Coupling Value of the Seven Element Array

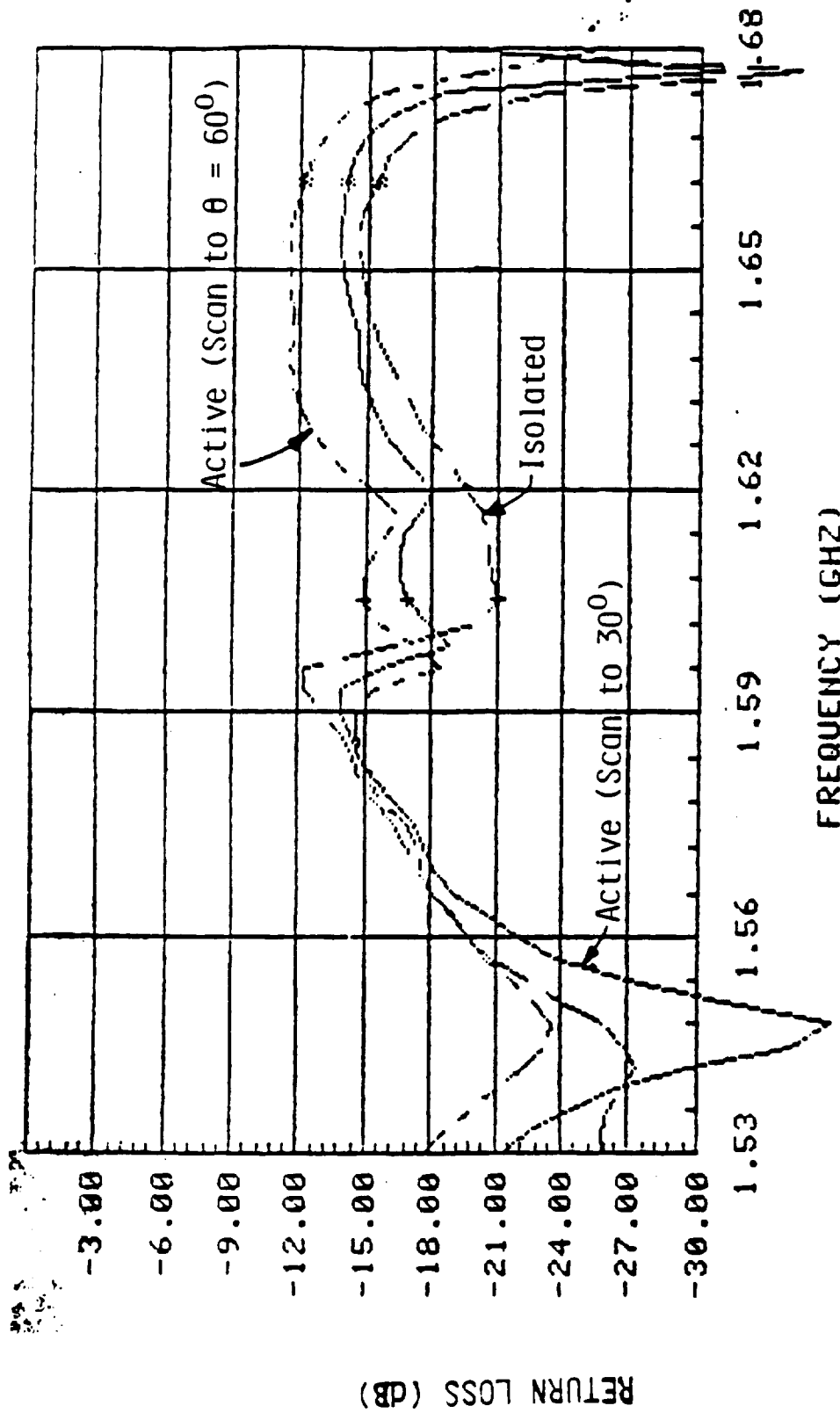


Figure 2-12. Computed Scanning Active Return Loss at Center Element of the Seven Element Array

### 2.2.2.3 Gain analysis

The computed gain is given by

$$G_{RHCP}(\theta_0, \phi_0) = D_{RHCP}(\theta_0, \phi_0) - \text{LOSS BUDGET} \quad (2-7)$$

where the directivity is given by

$$D_{RHCP}(\theta_0, \phi_0) = \frac{4\pi |E_{RHCP}(\theta_0, \phi_0)|^2}{\int_0^\pi \int_0^{2\pi} [ |E_{RHCP}(\theta, \phi)|^2 + |E_{LHCP}(\theta, \phi)|^2 ] \sin\theta d\theta d\phi} \quad (2-8)$$

The predicted loss budget and gain at an elevation angle of 20 degrees, when the array was scanned to  $\theta_s = 60$  degrees and various  $\phi_s$  angles, is summarized in Table 2-2 and 2-3, respectively. Note that a 2 degree increment in both  $\theta$  and  $\phi$  angles was used in the directivity calculation. The average gain over an azimuth angle of 360 degrees at an elevation angle of 20 degrees is 10 dBic.

### 2.2.2.4 Intersatellite Isolation Analysis

The analysis of intersatellite isolation involves the comparison of the power received by the array from two satellites when the array is tracking the desired one. The satellites are in geosynchronous orbit, one at 80 degrees west longitude and the other at 115 degrees west longitude with opposite senses of circular polarization. The azimuth angle  $\theta_0$  and elevation angle  $\phi_0$  of a satellite relative to the earth station is given by

$$\phi_0 = \tan^{-1} \left( \frac{\tan(\Delta\phi)}{\sin(\theta_e)} \right) - n\pi \quad (2-9)$$

$$\theta_0 = \tan^{-1} \left( \frac{\cos(\Delta\phi) \cos(\theta_e) - 0.151}{\sqrt{1 - \cos^2(\Delta\phi) \cos^2(\theta_e)}} \right) \quad (2-10)$$

Table 2-2. Loss Budget

Loss Budget Item	Loss (dB)
Power Divider	0.5
Phase Shifter	1.1
Antenna Feed	0.3
Antenna Mismatch	0.2
Junction	0.1
Radiation Efficiency	0.5
<b>Total</b>	<b>2.7</b>

Table 2-3. Predicted Gain and Backlobe

Scan Angle ( $\theta_s, \phi_s$ )	Gain (dBic)	Backlobe (dB)
(60°, 0°)	10.0	12.0
(60°, 10°)	9.7	12.5
(60°, 20°)	10.1	18.0
(60°, 30°)	10.0	14.8
(60°, 40°)	10.2	17.5
(60°, 50°)	10.0	15.5
(60°, 60°)	10.3	14.0
(60°, 70°)	9.8	14.2
(60°, 80°)	10.0	18.5
(60°, 90°)	9.8	15.5
<b>Average Gain = 10 dBic</b>		

NOTE: Gain at 70 degrees from the zenith at 1545 MHz.

where

$\Delta \phi$  = satellite longitude ( $\phi_s$ ) - earth station longitude ( $\phi_e$ )

$\theta_e$  = earth station latitude

$n = \begin{cases} 0 & \text{southern hemisphere} \\ 1 & \text{northern hemisphere} \end{cases}$

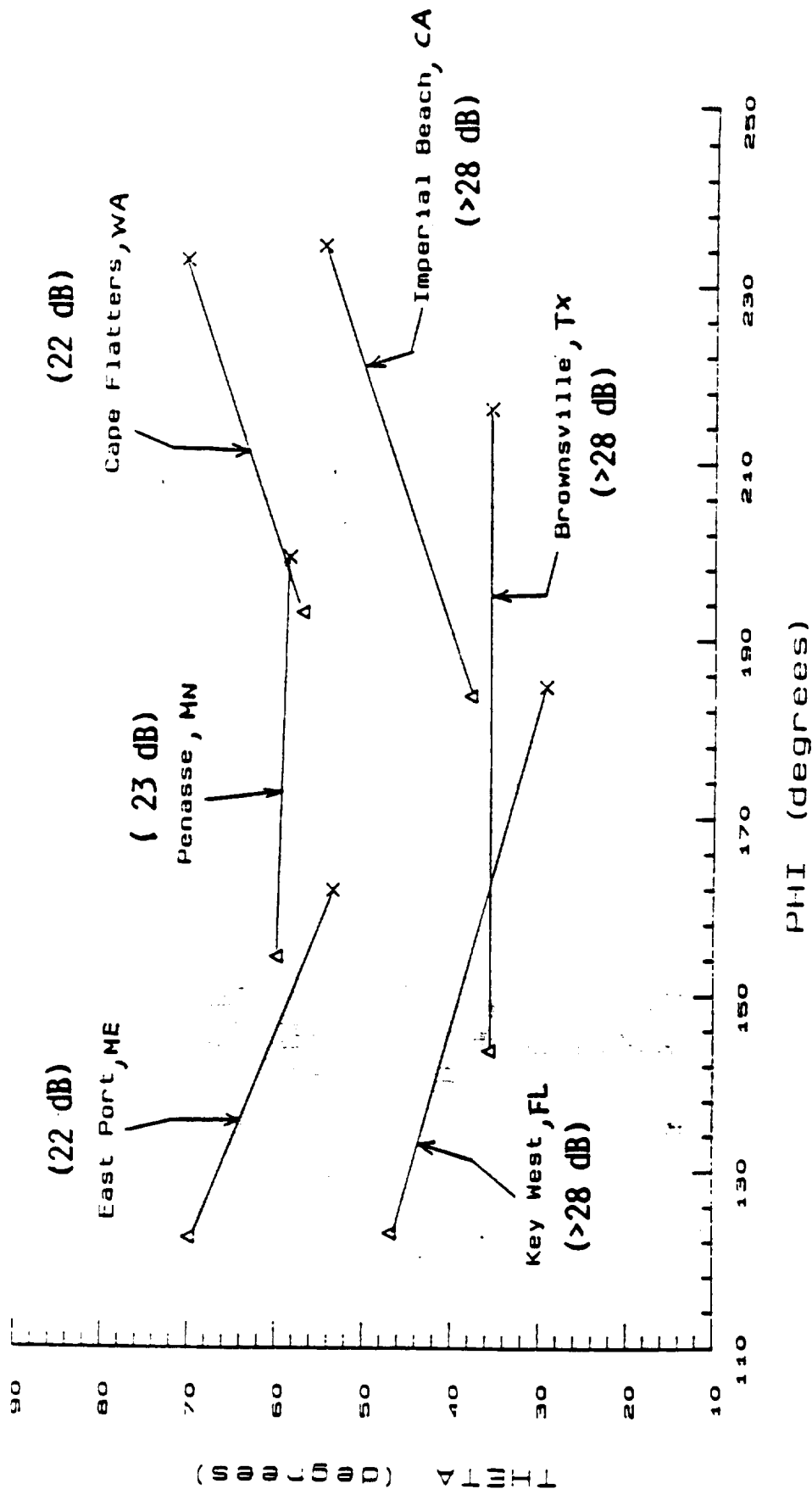
Intersatellite isolation for six critical locations in the United States was analyzed as shown in Figure 2-13. Note that the effects of beam pointing errors and beam lobing have been included in the analysis. It was assumed that the two satellites transmit equal power, with perfect but opposite sense of circular polarization. The array aperture amplitude tapering and excellent polarization characteristics of the crossed-slot element ensure a satisfactory intersatellite isolation level.

As an example, at Key West, Florida, the array was scanned to  $\theta = 30$  and  $\phi = 182$  degrees with satellite #1 assumed to be the desired satellite. The computed RHCP and LHCP radiation patterns are plotted in Figures 2-14 and 2-15 respectively. Table 2-4 lists the reference power level. By overlaying Figures 2-13 with Figure 2-14 and 2-15, it can be determined by comparing the relative power levels of the RHCP (-6 dB) and LHCP (< -34 dB) patterns that the intersatellite isolation at Key West was greater than 28 dB. From this type of detailed analysis, it is predicted that the required intersatellite isolation of 20 dB can be satisfied anywhere within the continental United States (CONUS).

#### 2.2.2.5 Multipath Rejection Analysis

The predicted elevation pattern drop off from an elevation angle of 20 to 0 degrees, is greater than 6 dB as summarized in Table 2-5. It is noted from the computed radiation patterns that all co-polarized and cross-polarized radiation fields below 0 degrees elevation angle is less than that of the co-polarized level at 0 degrees. The cross-polarized level is less than the co-polarized level between elevation angles of 0 to 20 degrees, hence, it is expected that the array can meet the required multipath rejection capability.

Satellite Coordinates



X - satellite #1  
 Δ - satellite #2

THETA/PHI = Elevation/Azimuth angle of a satellite relative to the earth station

Figure 2-13. Six Critical Locations in the United States

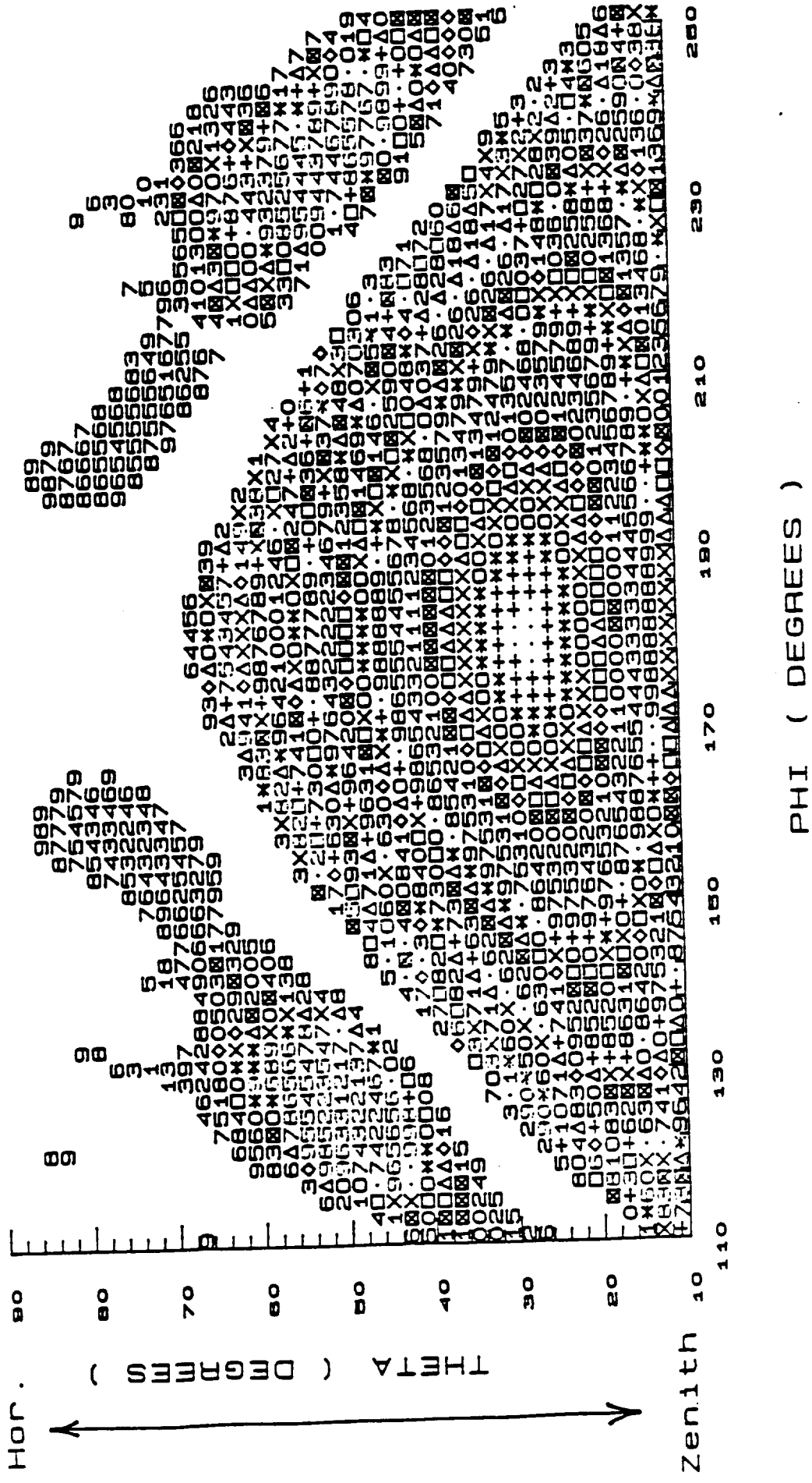


Figure 2-14. RHCP Array Pattern: Scan to Theta = 30 and phi = 182 degs.



Table 2-4. Colored Symbol Versus Power Level

Black		Red		Green		Gold		Blue		Brown	
0 ~ -5.7		-5.7 ~ 11.4		-11.4 ~ -17.1		-17.1 ~ -22.8		-22.8 ~ -28.5		-28.5 ~ -34.2	
...	0	...	-5.7	...	-11.4	...	-17.1	...	-22.8	...	-28.5
+++	-0.3	+++	-6.0	+++	-11.7	+++	-17.4	+++	-23.1	+++	-28.8
***	-0.6	***	-6.3	***	-12.0	***	-17.7	***	-23.4	***	-29.1
000	-0.9	000	-6.6	000	-12.3	000	-18.0	000	-23.7	000	-29.4
XXX	-1.2	XXX	-6.9	XXX	-12.6	XXX	-18.3	XXX	-24.0	XXX	-29.7
ΔΔΔ	-1.5	ΔΔΔ	-7.2	ΔΔΔ	-12.9	ΔΔΔ	-18.6	ΔΔΔ	-24.3	ΔΔΔ	-30.0
□□□	-1.8	□□□	-7.5	□□□	-13.3	□□□	-18.9	□□□	-24.6	□□□	-30.0
ΔΔΔ	-2.1	ΔΔΔ	-7.8	ΔΔΔ	-13.5	ΔΔΔ	-19.2	ΔΔΔ	-24.9	ΔΔΔ	-30.6
☒☒☒	-2.4	☒☒☒	-8.1	☒☒☒	-13.8	☒☒☒	-19.5	☒☒☒	-25.2	☒☒☒	-30.9
000	-2.7	000	-8.4	000	-14.1	000	-19.8	000	-25.5	000	-31.2
111	-3.0	111	-8.7	111	-14.4	111	-20.1	111	-25.8	111	-31.5
222	-3.3	222	-9.0	222	-14.7	222	-20.4	222	-26.1	222	-31.8
333	-3.6	333	-9.3	333	-15.0	333	-20.7	333	-26.4	333	-32.1
444	-3.9	444	-9.6	444	-15.3	444	-21.0	444	-26.7	444	-32.4
555	-4.2	555	-9.9	555	-15.6	555	-21.3	555	-27.0	555	-32.7
666	-4.5	666	-10.2	666	-15.9	666	-21.6	666	-27.3	666	-33.0
777	-4.8	777	-10.5	777	-16.2	777	-21.9	777	-27.6	777	-33.3
888	-5.1	888	-10.8	888	-16.5	888	-22.2	888	-27.9	888	-33.6
999	-5.4	999	-11.1	999	-16.8	999	-22.5	999	28.2	999	-33.9

Table 2-5. Summary of Results: Beam Angle vs. Pattern Roll-off

Scan Angle ( $\theta_s, \phi_s$ )	Pattern Roll-off (dB)
(60°, 0°)	6.5
(60°, 10°)	8
(60°, 20°)	8.4
(60°, 30°)	7.8
(60°, 40°)	8.1
(60°, 50°)	8.4
(60°, 60°)	8.4
(60°, 70°)	8.3
(60°, 80°)	8
(60°, 90°)	7.8

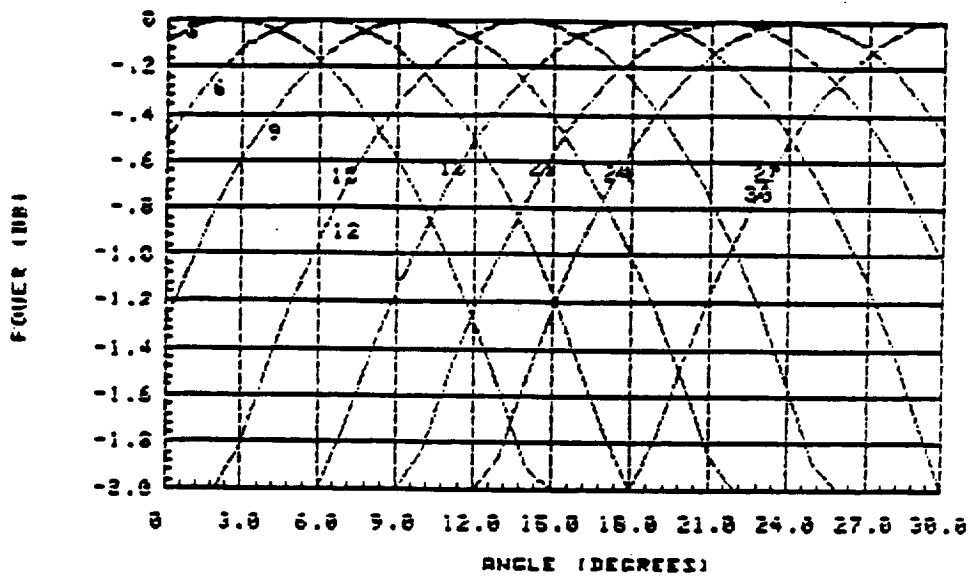
NOTE: Pattern roll-off = dB difference between 20° and 0° above horizon.

#### 2.2.2.6 Beam Pointing Accuracy Analysis

The effects of the phase shifter quantization errors on the beam pointing accuracy was analyzed. By using the systematic round off scheme for the phase shifter settings, a pointing error of more than 3 degrees was observed. This error could be improved by applying a random round off scheme which eliminates the accumulated bias error. The beam pointing accuracy can further be improved by using a hybrid scheme which always selects the best phase shifter setting at each angle from either a systematic or random round off scheme. Typical results are shown in Figures 2-16 and 2-17. Note that a beam pointing accuracy of two degrees is achieved through the random round off scheme.

### 2.3 ARRAY ASSEMBLY

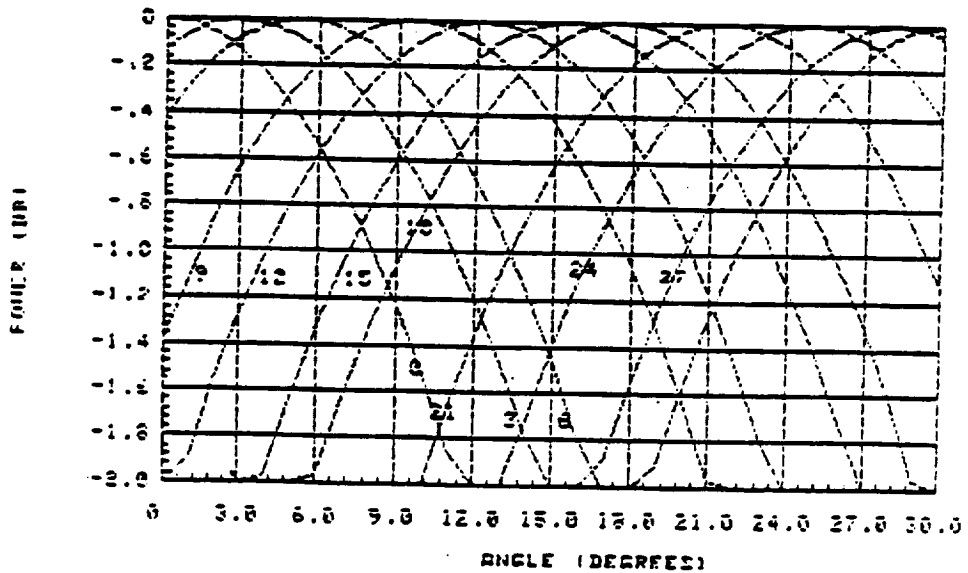
A total of five layers of teflon board material was used to construct the phased array which consists of an antenna module and a beamformer module. These two modules were assembled separately to facilitate intermediate testing and glean valuable information for further improvements to the antenna. Following is a brief description of the array assembly. Detail discussions on the fabrication and assembly of the array will be given in Section 6.



Analysis of pointing error due to the quantization error  
in the 3-bit phase shifter.

(Azimuth plane with  $\theta_{az} = 60^\circ$  degs. cut)

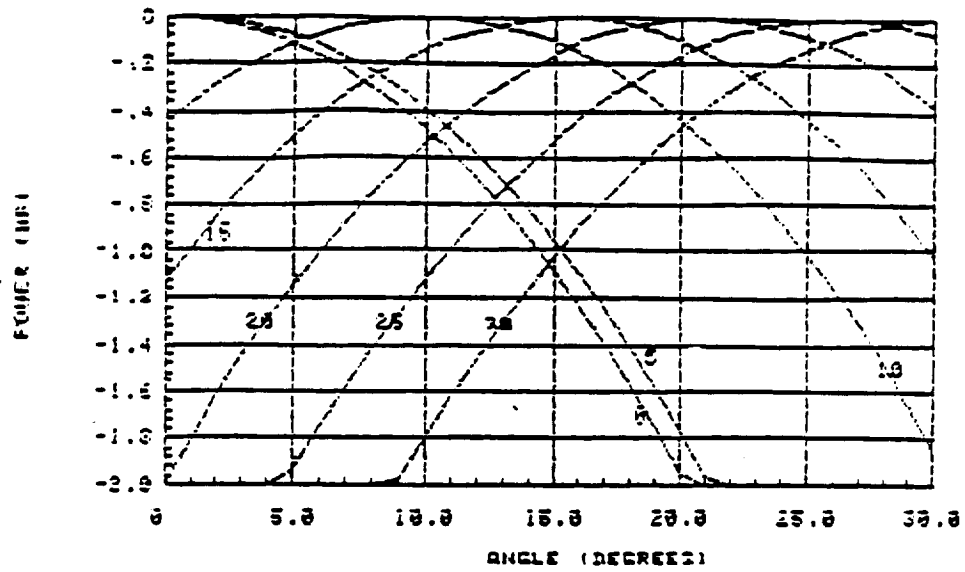
(a) Systematic Round-off



Analysis of pointing error due to the quantization error  
in the 3-bit phase shifter (deterministic errors included)  
Scan in azimuth plane ( $\theta_{az} = 70^\circ$  degs cut) with  $\theta_{az} = 60^\circ$  degs.

(b) Random Round-off

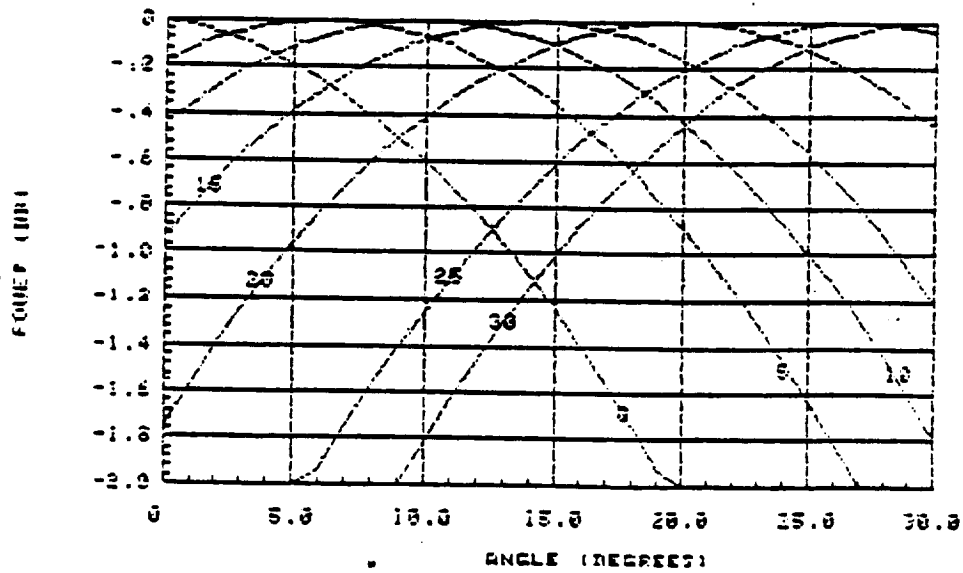
Figure 2-16. Beam Pointing Study,  $\theta_s = 60^\circ$ ,  $\theta = 70^\circ$



Azimuth scan with theta=30 degs.

(a) Systematic Round-off

ORIGINAL PAGE IS  
OF POOR QUALITY



Azimuth scan with theta=30 degs. and use random scheme.

(b) Random Round-off

Figure 2-17. Beam Pointing Study,  $\theta_s = 30^\circ$ ,  $\theta = 30^\circ$

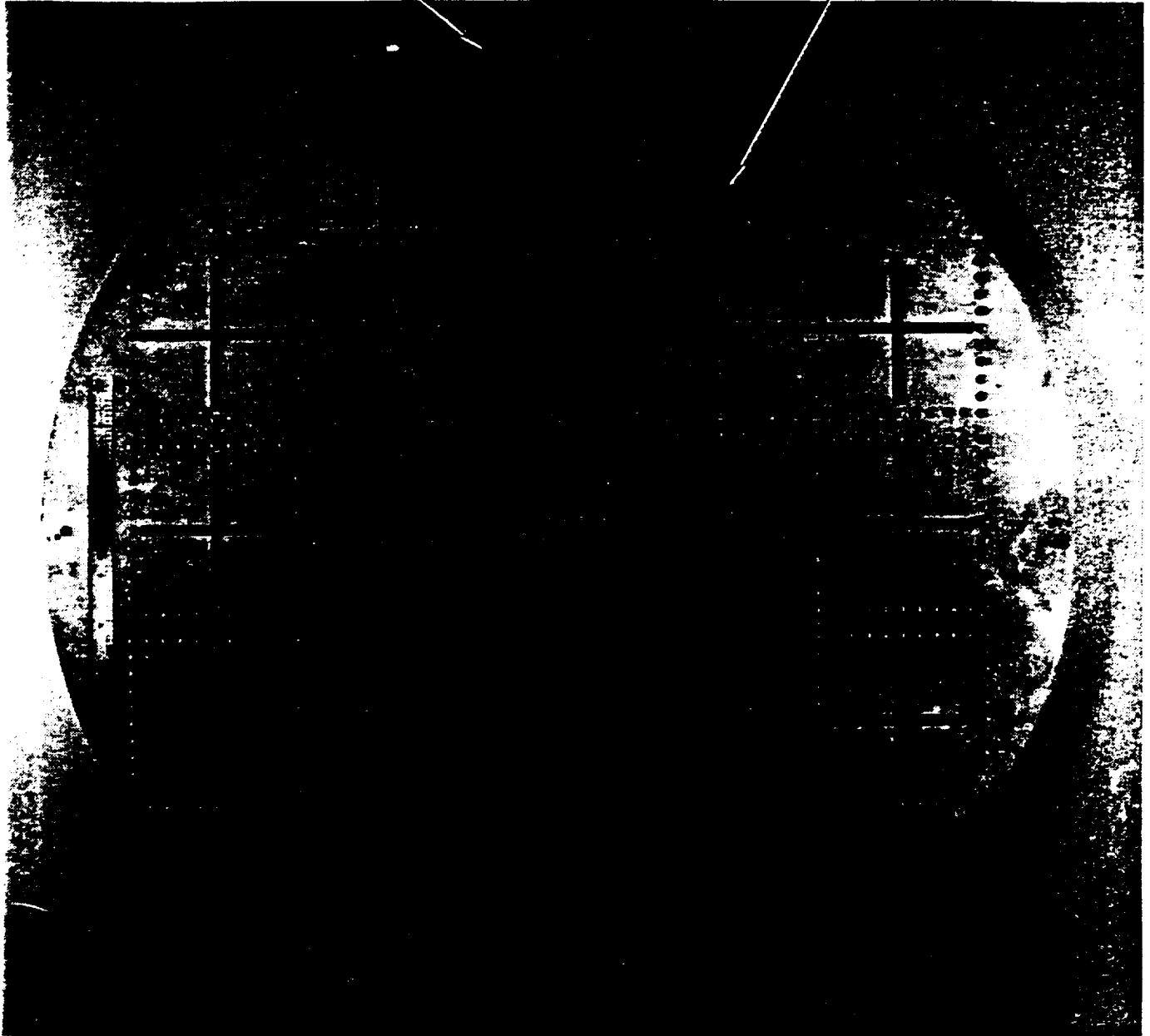
The antenna array module consists of four boards - a top crossed-slot board, a stripline excitation feeder board, a hybrid/corporate feed network board and a bottom ground plane board, as shown in Figures 2-18 thru 2-21. The top layer of the array (crossed-slot element matrix) was etched on a single sided, copper clad, teflon fiberglass board. The thicknesses of the boards are 0.09 inch and 0.125 inch for breadboard unit #1 and unit #2 arrays. The thicker board was selected for unit #2 in order to increase the antenna's bandwidth; this will be discussed in Section 3. The next layer is the crossed-slot excitation feeders which are etched on another copper clad teflon fiberglass board having the same thickness. A set of plated through holes around the crossed-slots are required to form the cavity wall for the crossed-slot element. The bottom two layers of the antenna array have thickness of 0.031 inches and constitute the stripline hybrid/corporate feed network boards used to form the required right hand circular polarization pattern. As shown in Figure 2-22, these four boards and a 0.125 inch stiffner plate of aluminum are held together by means of brass screws inserted through the plated cavity holes. RF connectors are attached to both the input and the isolated port of the hybrid circuit, via the bottom ground plane board.

As shown in Figure 2-23, the beamformer board consists of a radial nineteen way unequal power divider and eighteen three-bit phase shifters. The beamformer board and a 0.125 inch stiffner plate are bonded together, with silver-loaded epoxy, to form the beamformer test module. After independent, intermediate testing of these two modules, the 0.125 inch stiffner plate for the antenna array was removed and all four boards were keyed together with the beamformer module. As shown in Figure 2-24, they were bolted together with the back cover leaving an air gap of 0.2 inch between the beamformer circuit and the cover. A very thin (0.002 inch) painted polyurethane type radome (Laminar X-500 translucent gray radome coating - product of Midland Division of Dexter Corporation) was employed to provide protection against the enviroment. The total thickness of antenna array unit #1 and unit #2 are 0.68 inch and 0.75 inch, respectively. The thickness of the final production array will be reduced to 0.625 inch when the stiffner plate between the antenna boards and the beamformer board is removed.

**19 ELEMENT ARRAY**

**PLATED THRU CAVITY  
HOLES. 620 PLACES**

**CROSSED-SLOT  
RADIATOR.  
19 TOTAL**



**ORIGINAL PAGE  
BLACK AND WHITE PHOTOGRAPH**

**4 BRD ASSY HELD TOGETHER  
WITH 2 X 56 BRASS SCREWS  
& NUTS THRU CAVITY HOLES AND  
.125 ALUMINUM BASE PLATE.**

Figure 2-18. Top Layer (Crossed-Slot Radiators) of the Array

# FEED LINE BOARD

ORIGINAL PAGE  
BLACK AND WHITE PHOTOGRAPH

PLATED THRU FEED  
POINT HOLE. 76 PLACES

3 PLATED THRU GROUND  
HOLES. 76 PLACES

PLATED THRU  
CAVITY HOLE  
620 PLACES.

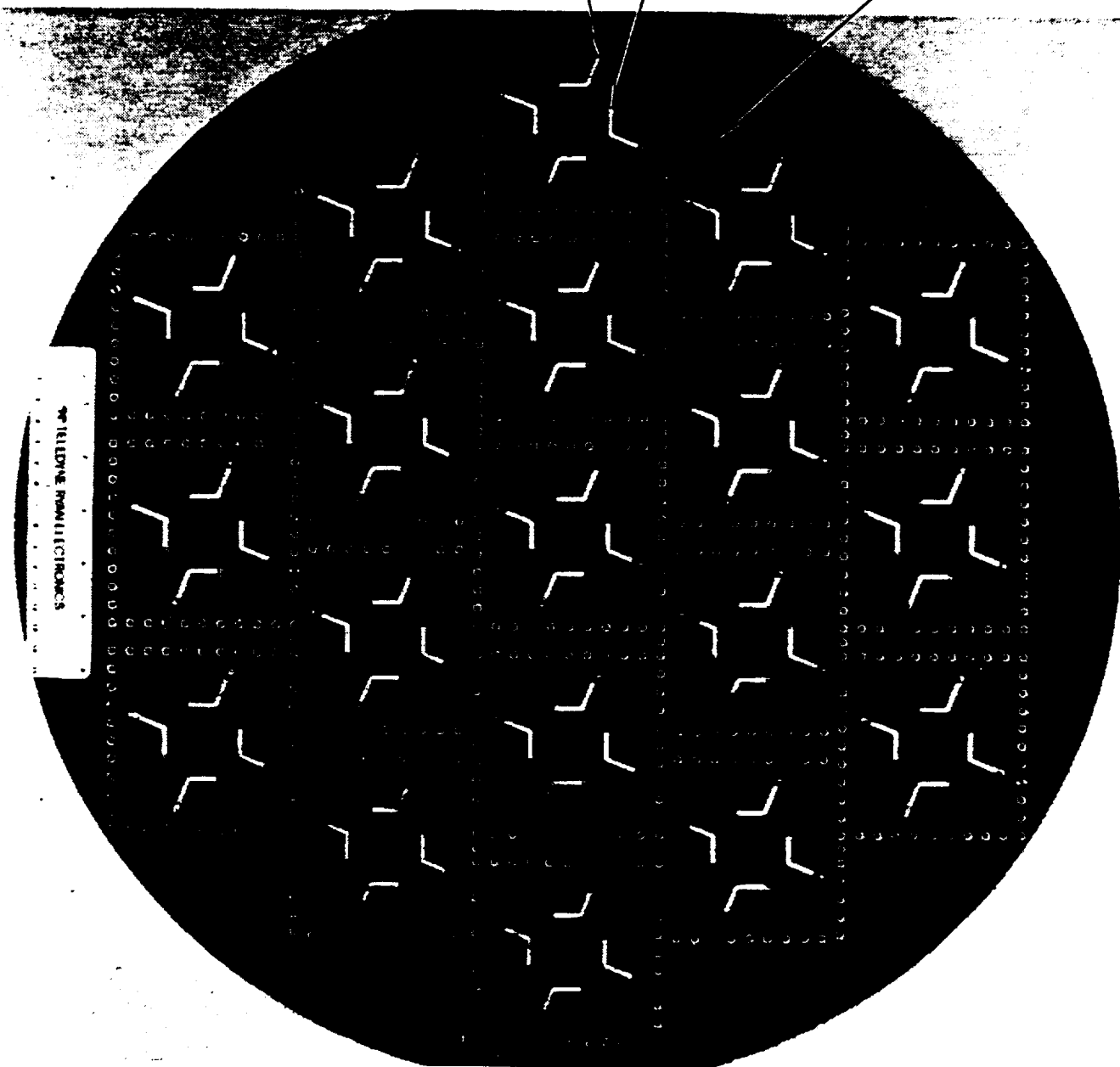


Figure 2-19. Second Layer (Feeder Arrangement) of the Array

# HYBRID BOARD

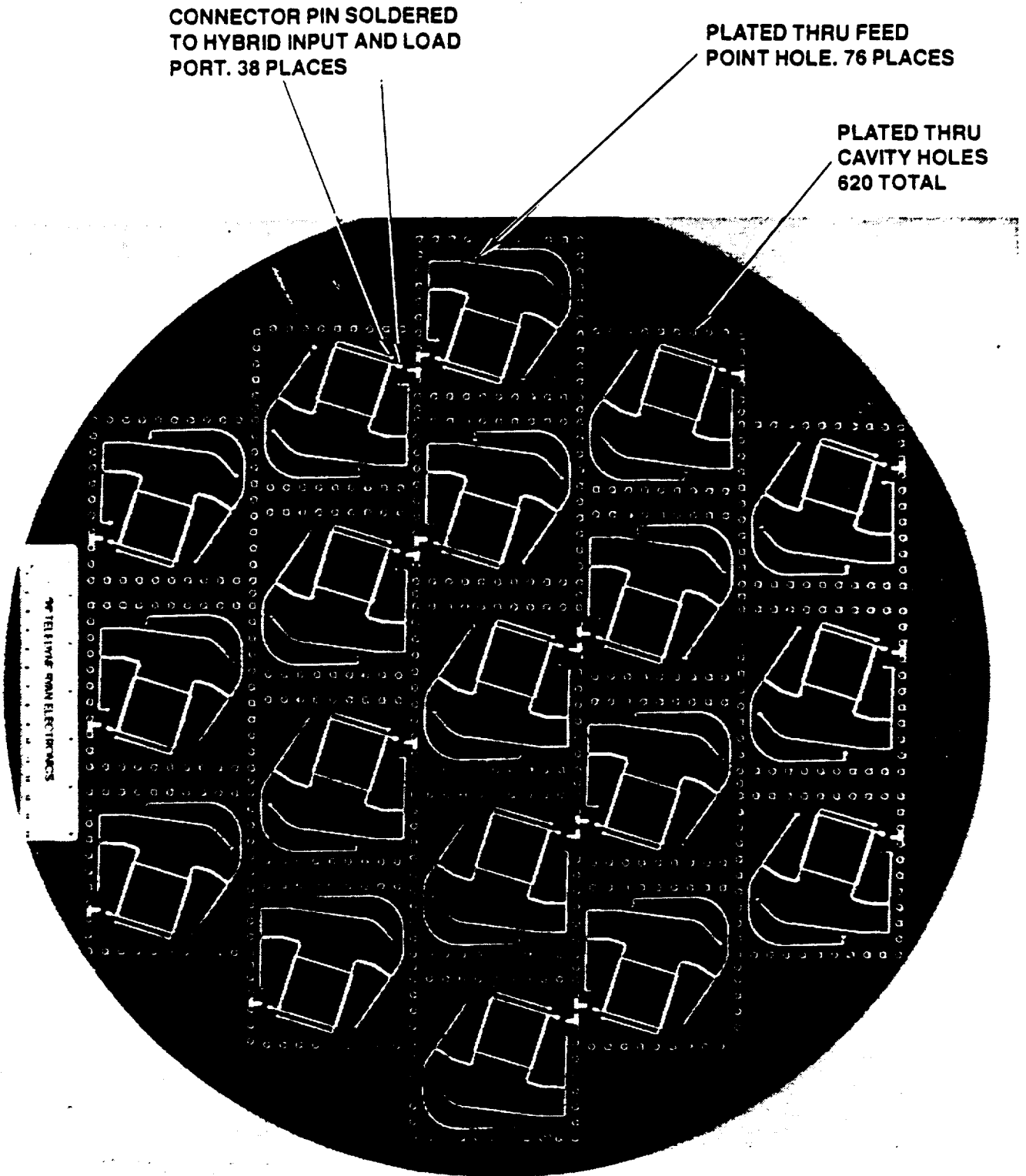


Figure 2-20. Third Layer (90° Hybrids/180° Corporate) of the Array

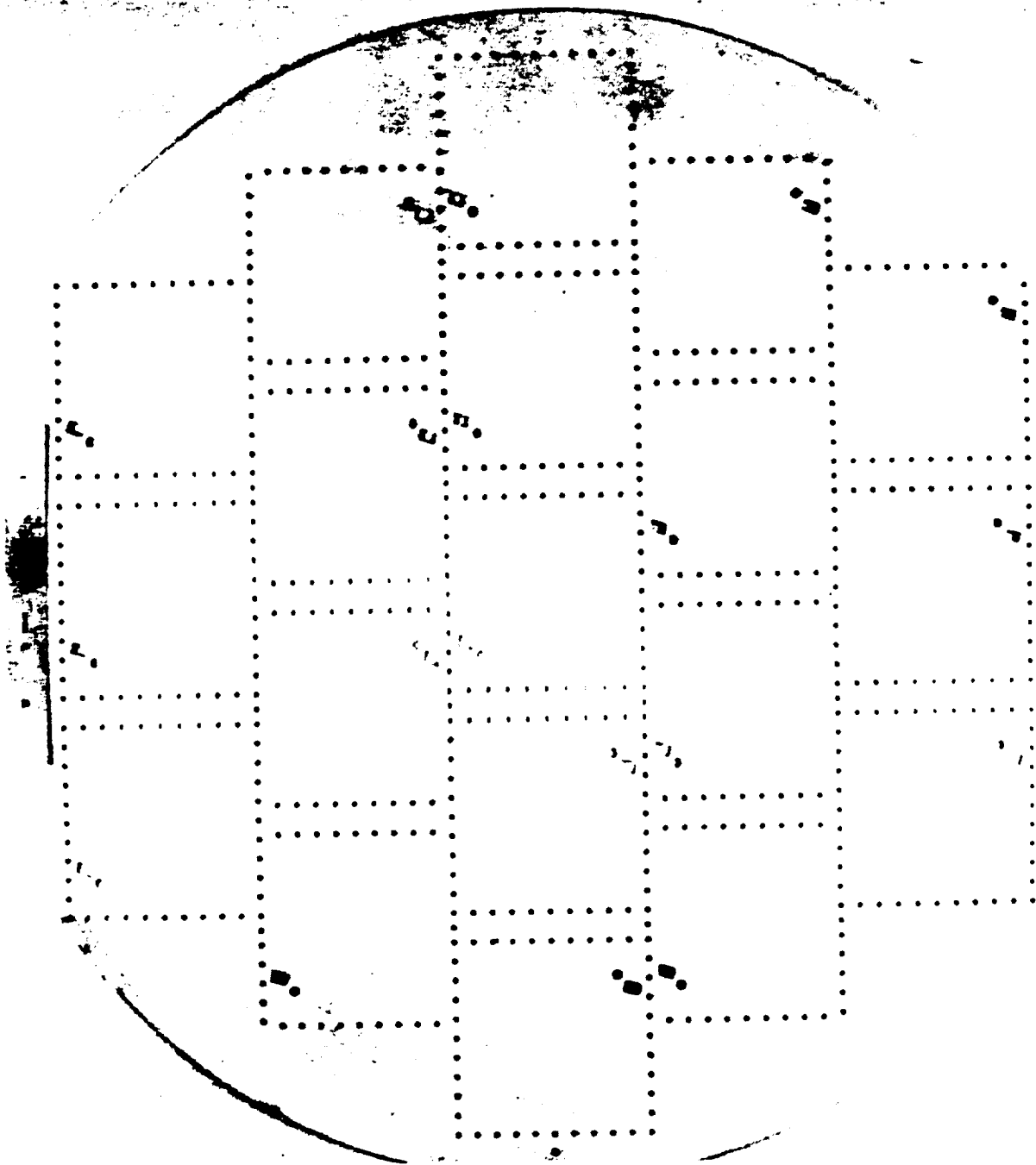


Figure 2-21. Fourth Layer (Ground Plane) of the Array

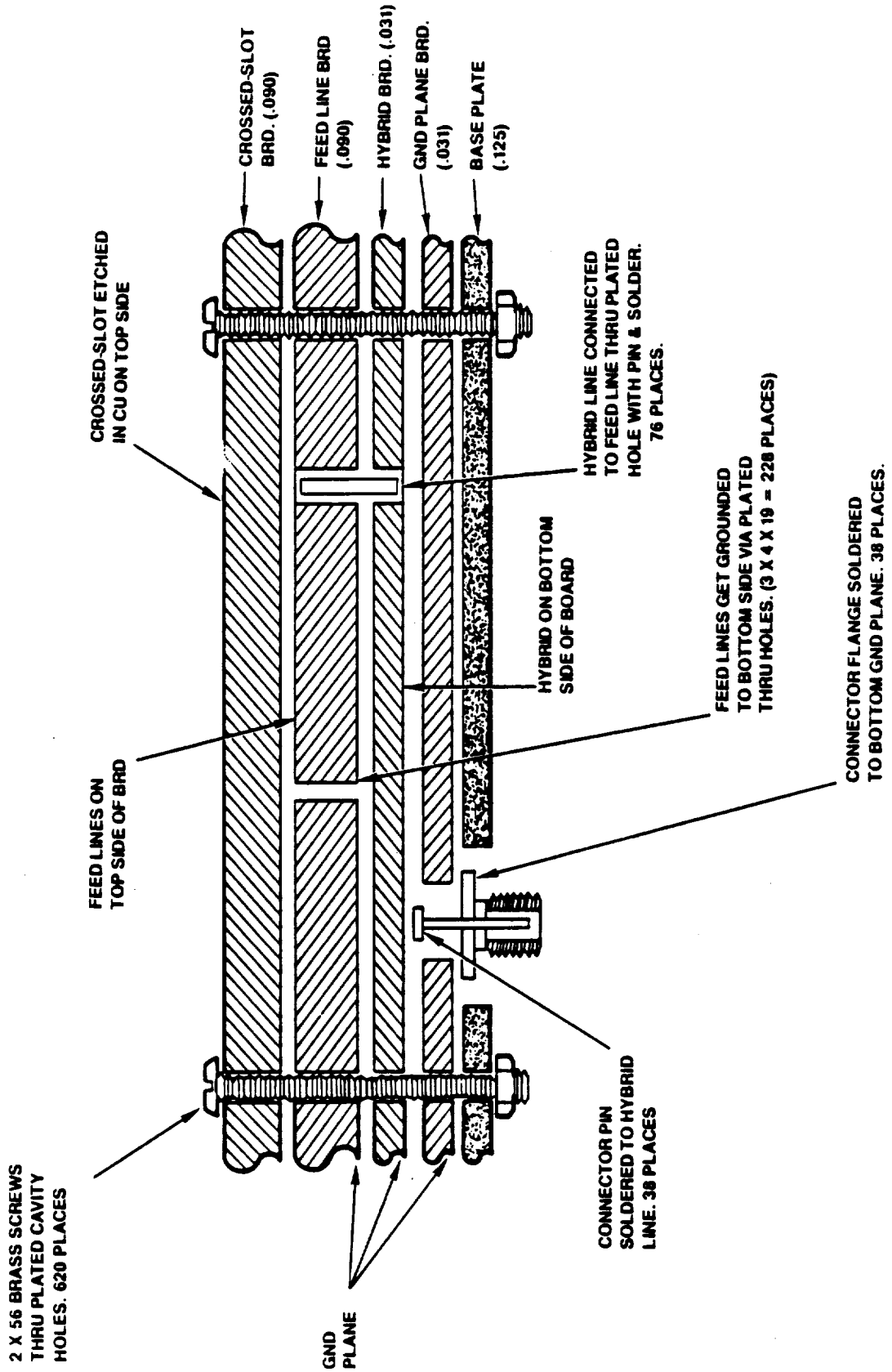


Figure 2-22. 19 Element Fabrication-Experimental Model

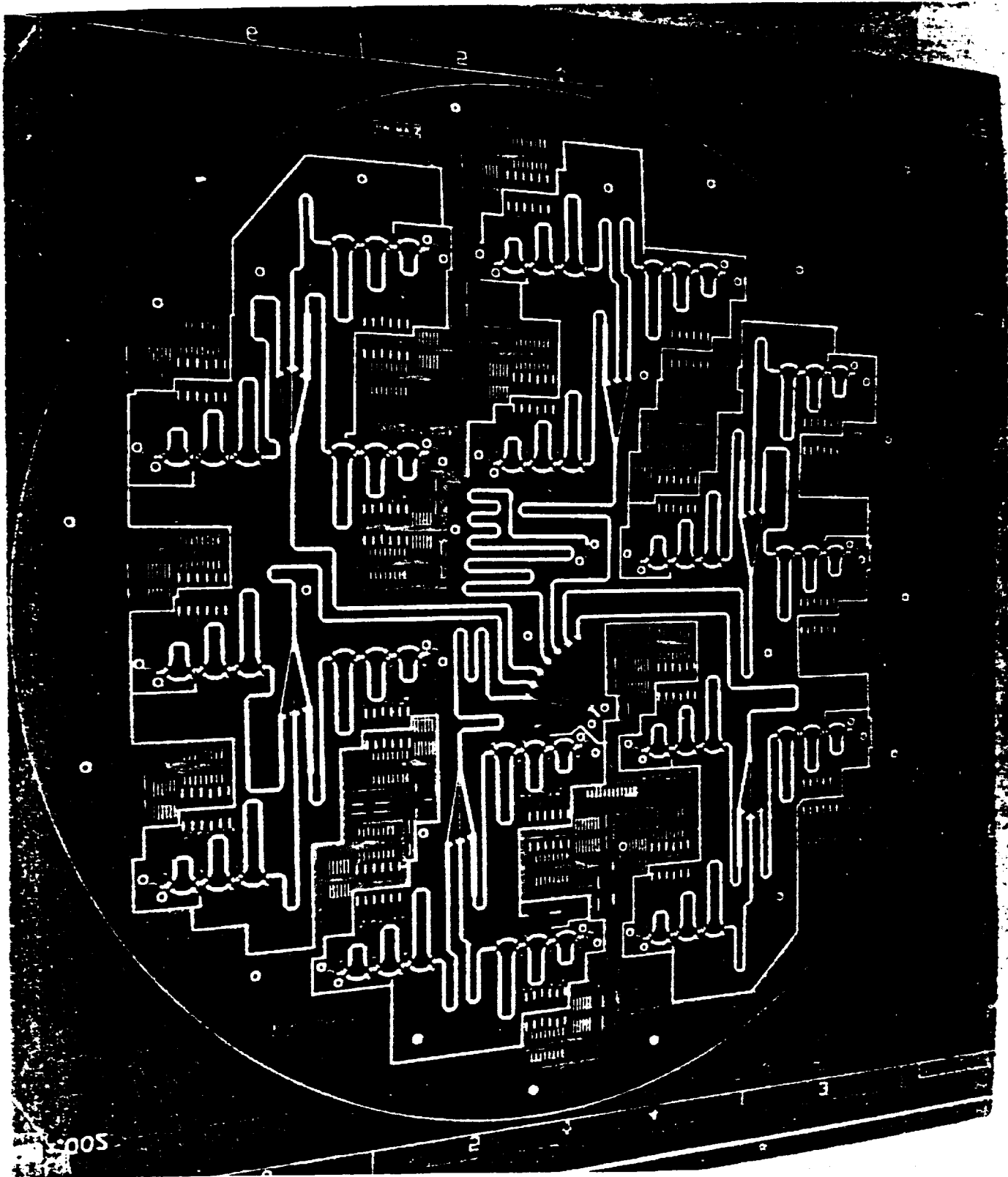


Figure 2-23. Fifth Layer (Beamformer Board) of the Array

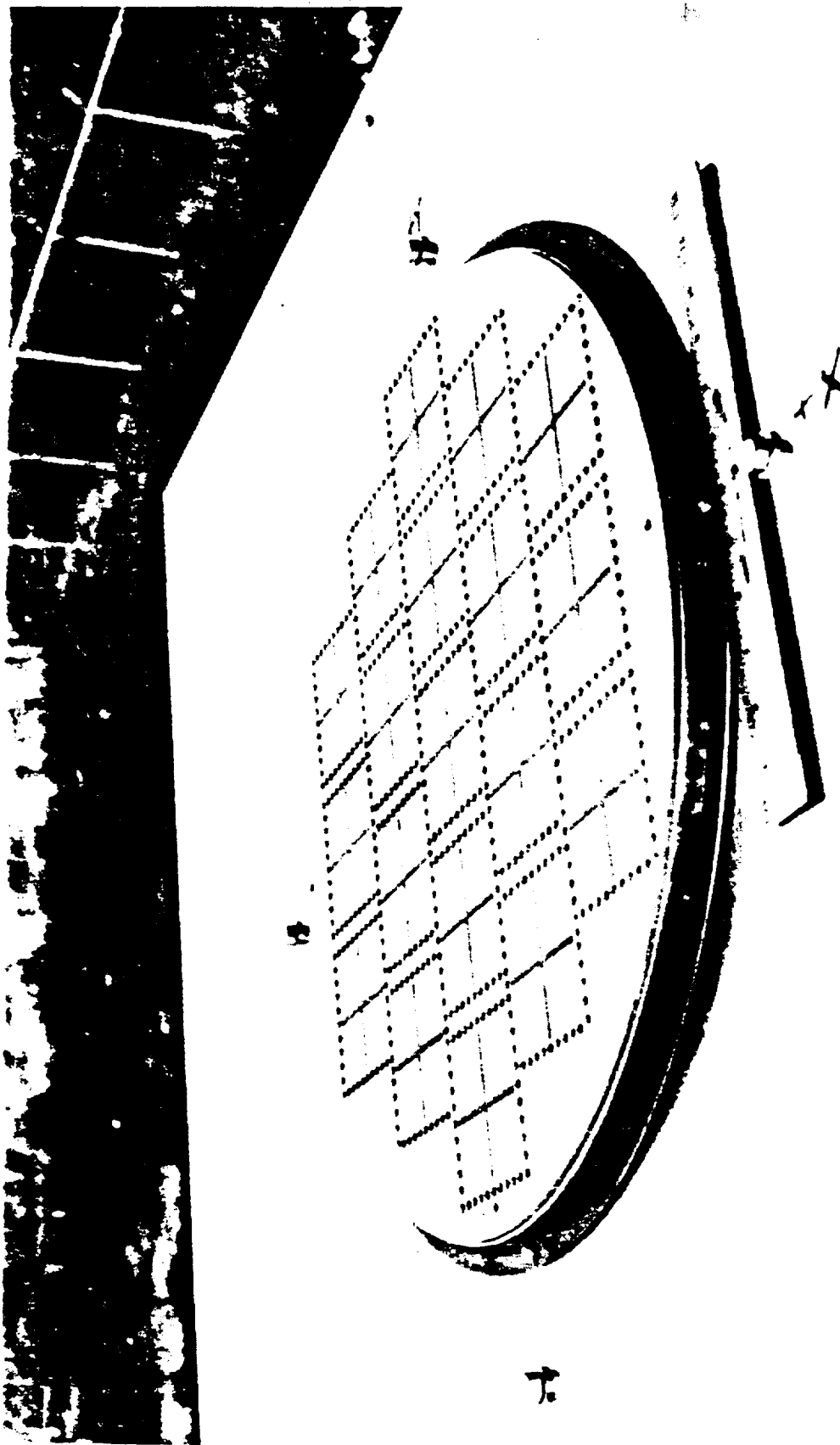


Figure 2-24. Final Assembled MSAT-X Phased Array

Extensive measurements were performed at Teledyne Ryan's outdoor antenna range during acceptance testing. Details of the test setup will be discussed in Section 8.3. The measured array performance is summarized in Table 2-6. Discussions on the measured array pattern performance, array gain and intersatellite isolation will be presented in the following subsections.

#### 2.4.1 Measured Array Patterns

The array was mounted on a 40" x 50" ground plane which in turn was affixed to the positioner using the orientation shown in Figure 2-25. Both spinning linear and circular polarization patterns were measured. Typical array patterns are shown in Figures 2-26 thru 2-37. Additional measured patterns are given in Appendix A.

As shown in Figures 2-26 and 2-27, excellent broadside RHCP patterns were realized. The sidelobe level reaches the design value which is 22 dB. Scanning patterns cut in both azimuth and elevation planes are shown in Figures 2-28 thru 2-33.  $\theta_s$  and  $\phi_s$  represent the elevation scan angle from the array broadside and the azimuth scan angle from the x-axis, respectively, as defined in Figure 2-1.  $\theta$  and  $\phi$  are the pattern cut angles. An excellent axial ratio (<5 dB) of the array patterns was achieved within 95% of the required space coverage across the frequency band. The sidelobe level of the azimuth plane patterns remains below -18 dB in most of the space except at very low elevation angle scans, as shown in Figures 2-34 thru 2-37. The backlobe level comes up as expected when the array scans to very low elevation angles. These high backlobe problems are mainly due to the selected element spacing which is optimal for the array's overall performance. Note that the array is designed to scan up to 60 degrees from the array broadside. This will provide sufficient gain at low elevation angle (>60 degrees) areas.

As noted from the measured patterns, the pattern drop off from 20 to 0 degree elevation angles is greater than 7 dB. All co-polarized and cross-polarized radiation fields below a 0 degree elevation angle is less than that of the co-polarized level at 0 degrees. The cross-polarized level is less than the co-polarized level between the 0 to 20 degree elevation angles as shown in Figure 2-37, hence the multipath rejection capability requirement was satisfied.

Table 2-6. Summary of Measured Array Performance

	<u>Measured Value</u>		
	Unit #1	Unit #2	Spec.
Gain at 20° elevation (dBic)	9.2 (average)	9.3 (average)	
1545 MHz	9.9 (highest)	9.9 (highest)	≥10
	8.3 (lowest)	8.2 (lowest)	
1600 MHz	7.7 (average)	8.3 (average)	
	8.3 (highest)	8.8 (average)	≥10
	6.7 (lowest)	7.2 (lowest)	
Intersatellite Isolation (dB)	26	26	≥20
Backlobe (dB)	≥12 (95%) < 12 ( 5%)	≥12 (95%) < 12 ( 5%)	≥12
Multipath Rejection (dB) (pattern drop off from 20° to 0° elevation)	>6	>6	≥6
Azimuth Beamwidth (degs.)			
at 20° above horizon	29	29	
30° above horizon	32	32	None
40° above horizon	35	35	
50° above horizon	44	44	
60° above horizon	52	52	
Elevation Beamwidth (degs.)			
at 20° above horizon	45	45	
30° above horizon	42	42	
40° above horizon	39	39	None
50° above horizon	35	35	
60° above horizon	31	31	
Broadside Beamwidth	26	26	None
Antenna Thickness (Exclusive of RF Connector)	0.68	0.75	< 1

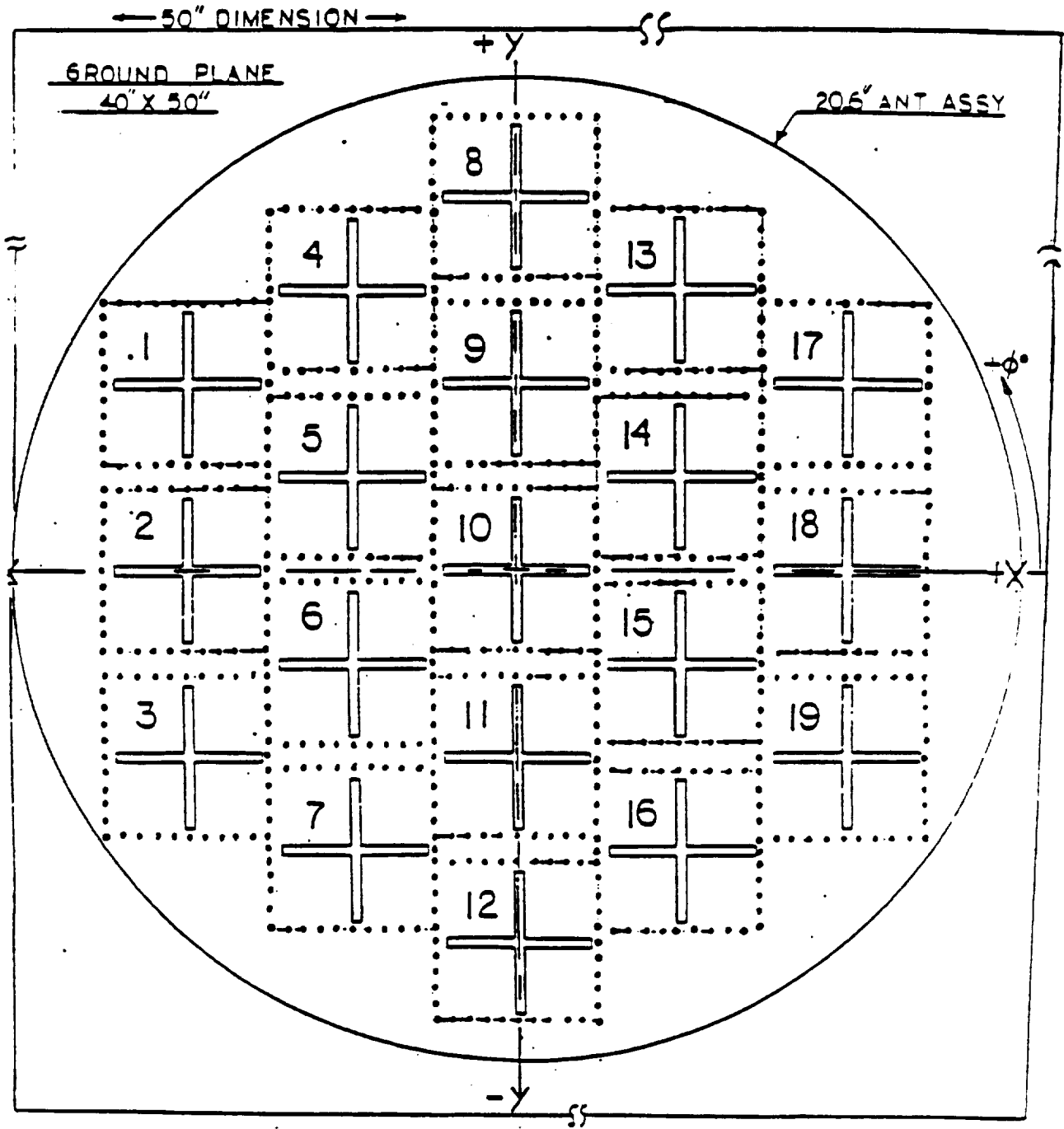


Figure 2-25. 19-Element Array Mounting Geometry



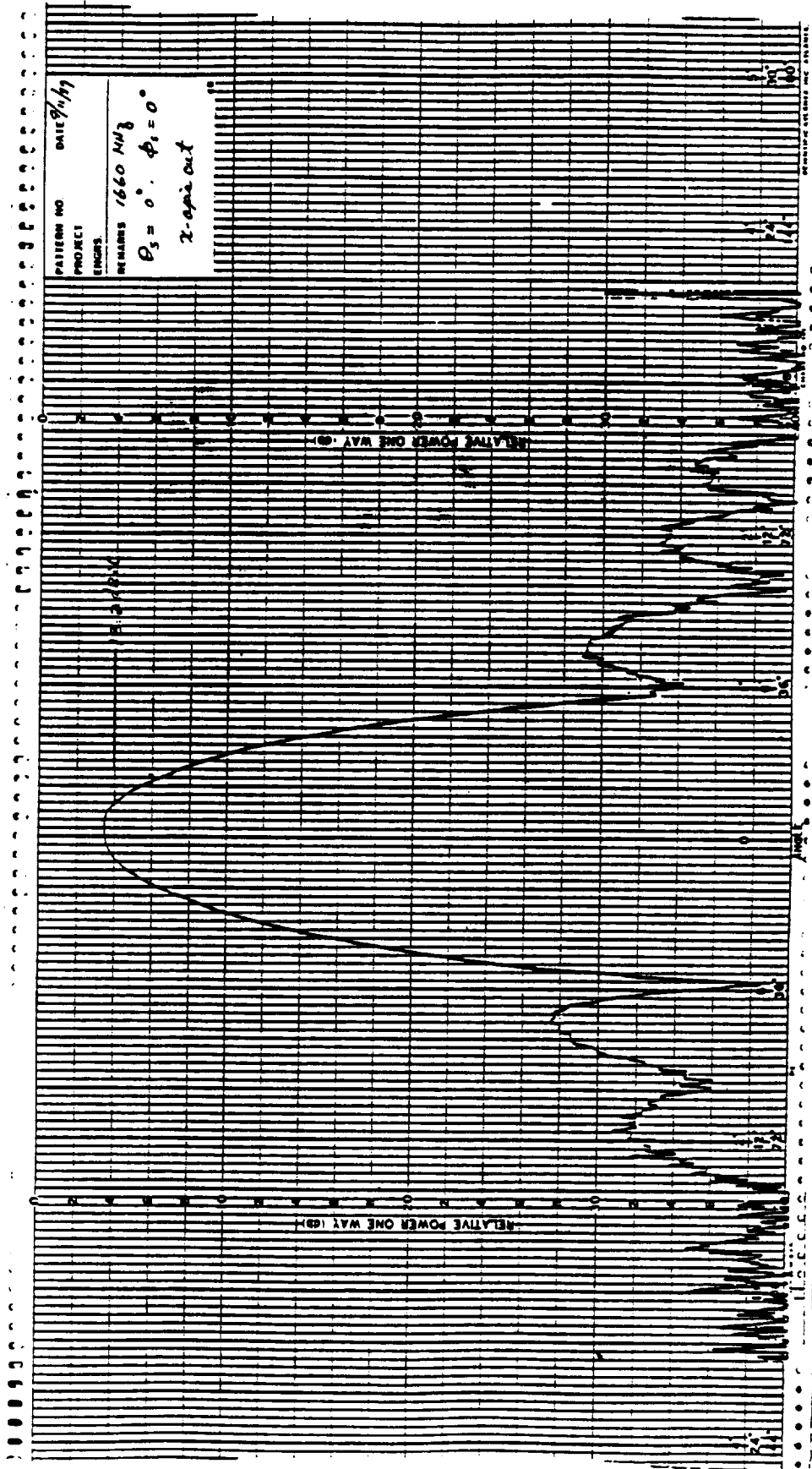


Figure 2-27. Measured RHCP Array Pattern in the Elevation Plane at 1660 MHz, SLL = -23 dB (Broadside)

ORIGINAL PAGE IS  
OF POOR QUALITY

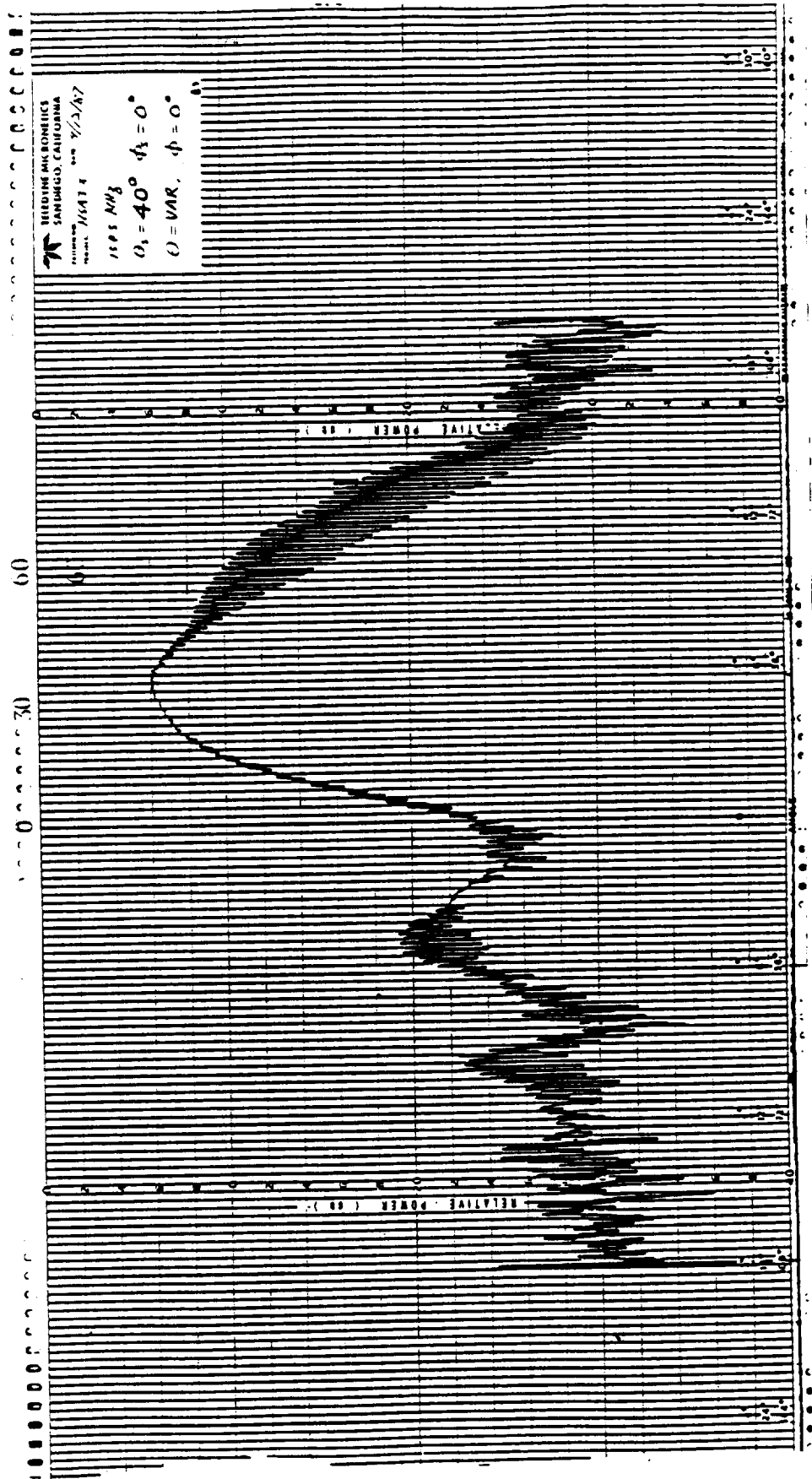


Figure 2-28. Measured Spinning Linear Pattern in the Elevation Plane at 1545 MHz ( $\theta_s = 40^\circ$ ,  $\phi_s = 0^\circ$ ;  $\theta = \text{VAR}$ ,  $\phi = 0^\circ$ )

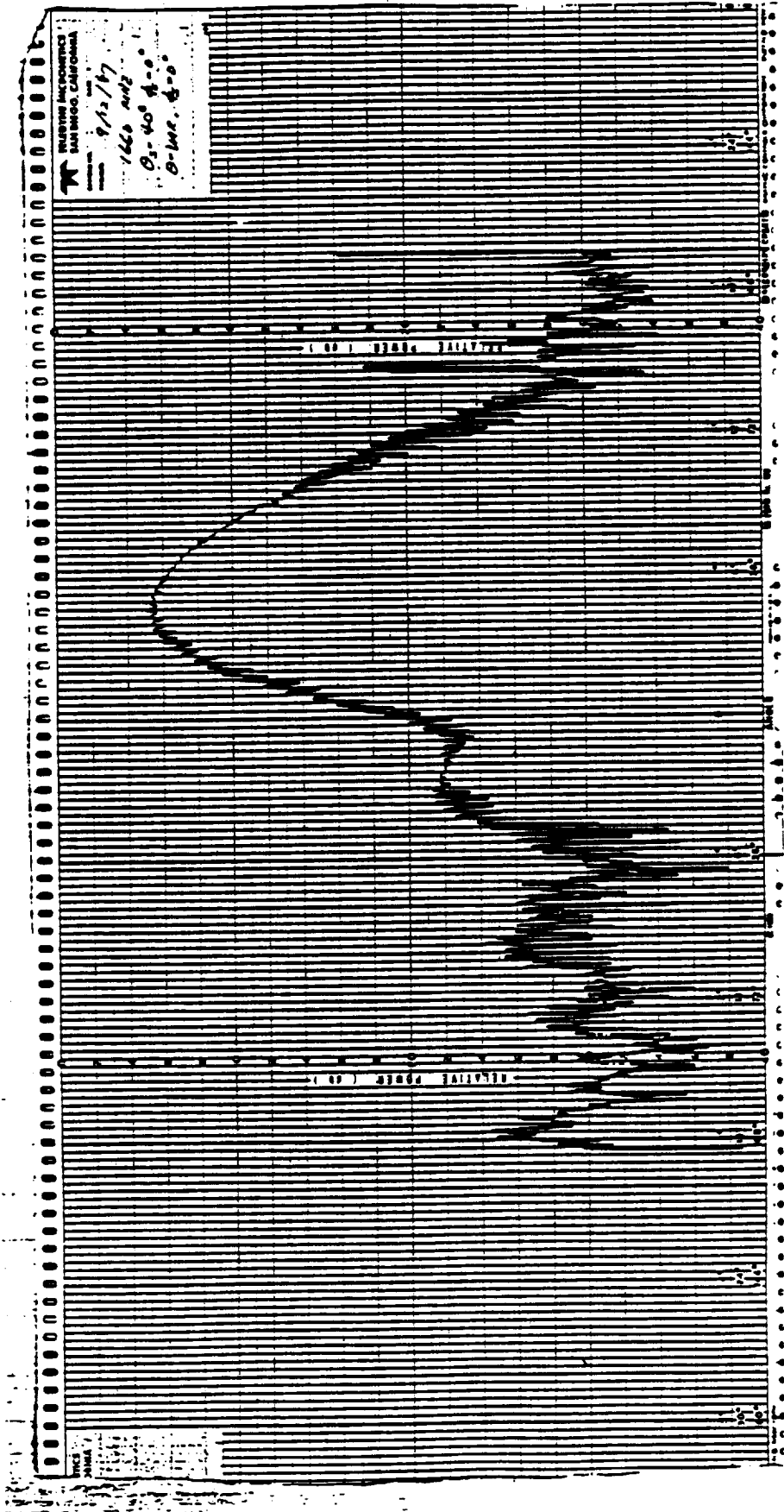


Figure 2-29. Measured Spinning Linear Pattern in the Elevation Plane at 1660 MHz ( $\theta_s = 40^\circ$ ,  $\phi_s = 0^\circ$ ;  $\theta = \text{VAR}$ ,  $\phi = 0^\circ$ )

ORIGINAL PAGE IS  
OF POOR QUALITY

ORIGINAL PAGES IS  
OF POOR QUALITY

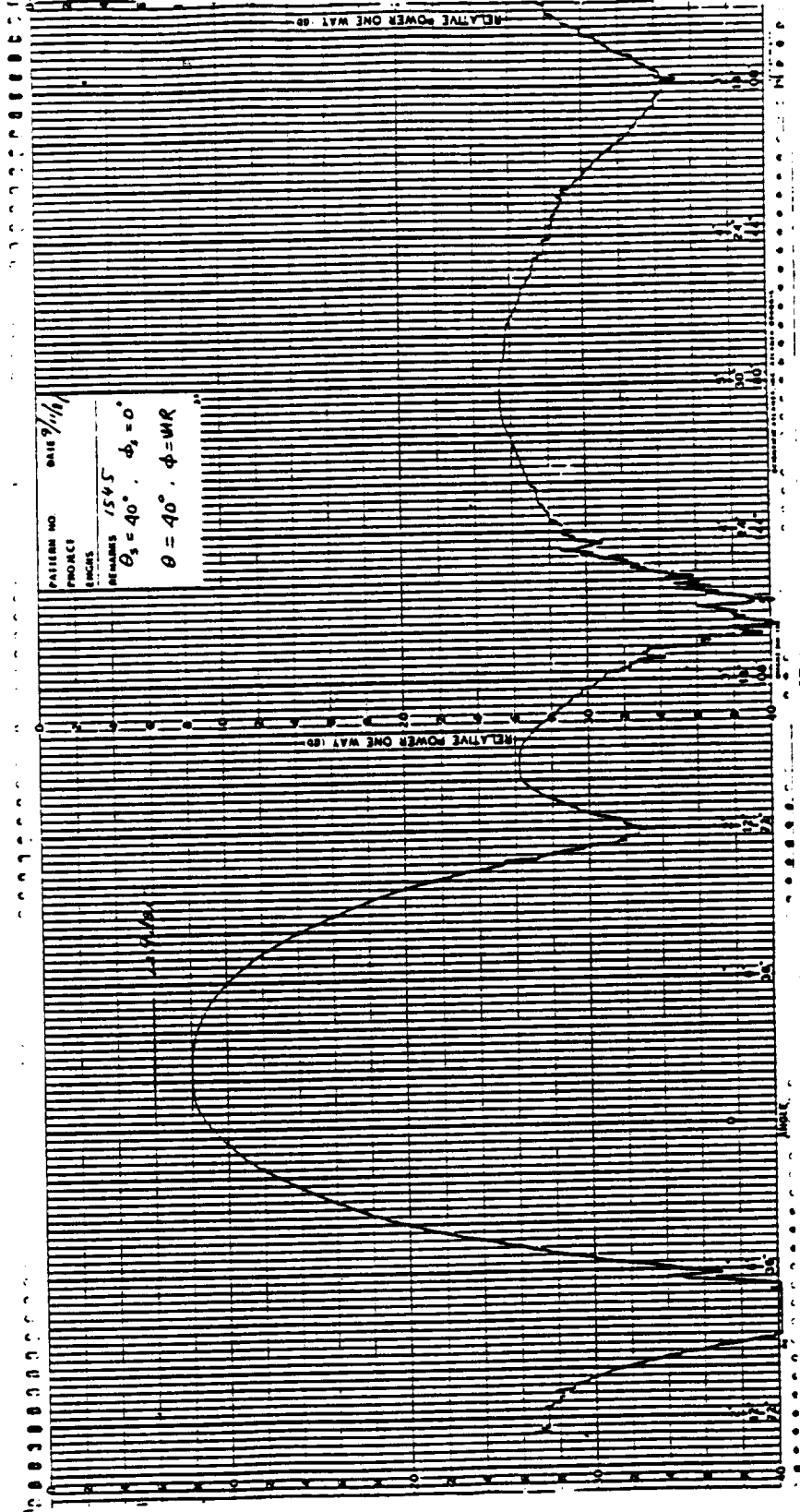


Figure 2-30. Measured RHCP Azimuth Array Pattern at 1545 MHz, Gain = 10.9 dBic, SLL = -18 dB, BL = -17 dB,  
( $\theta_s = 40^\circ$ ,  $\phi_s = 0^\circ$ ;  $\theta = 40^\circ$ ,  $\phi = VAR$ )

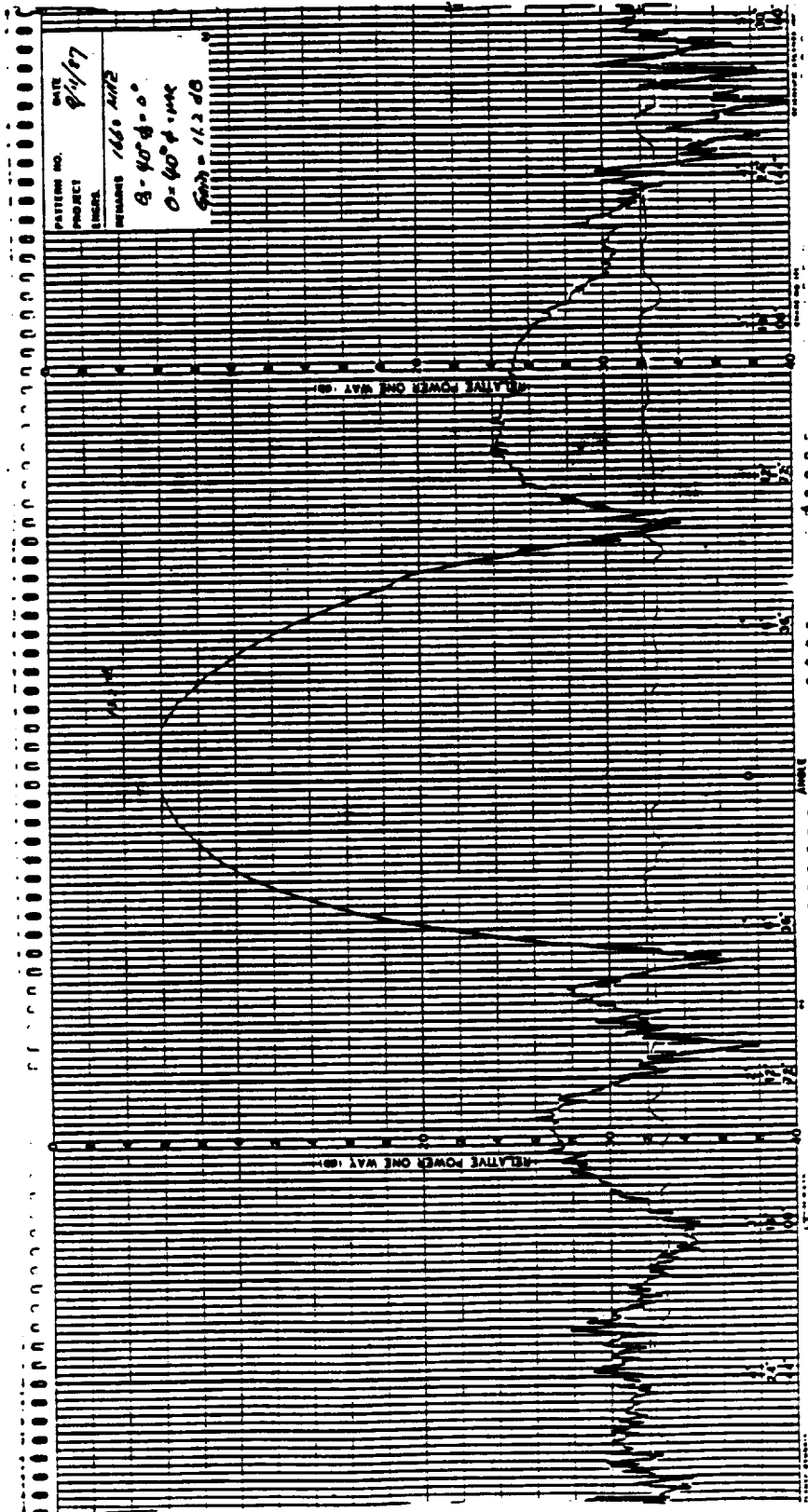


Figure 2-31. Measured RHCP Azimuth Array Pattern at 1660 MHz, Gain = 11.2 dBic, SLL = -18 dB, ( $\theta_s = 40^\circ$ ,  $\phi_s = 0^\circ$ ;  $\theta = 40^\circ$ ,  $\phi = \text{VAR}$ )

ORIGINAL PAGE IS  
OF POOR QUALITY

ORIGINAL PAGE IS  
OF POOR QUALITY

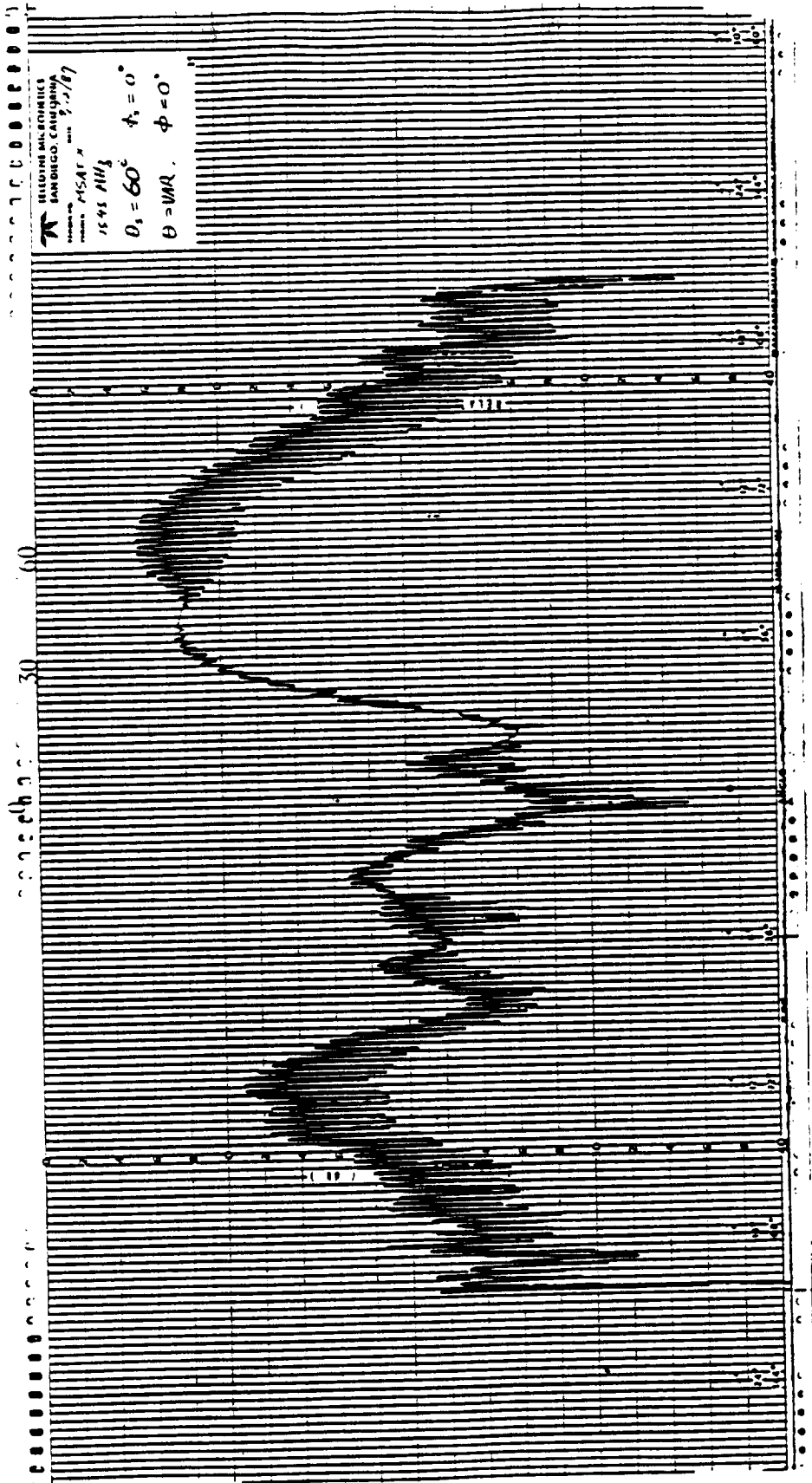


Figure 2-32. Measured Spinning Linear Elevation Array Pattern at 1545 MHz, ( $\theta_s = 60^\circ$ ,  $\phi_s = 0^\circ$ ;  $\theta = \text{VAR}$ ,  $\phi = 0^\circ$ )

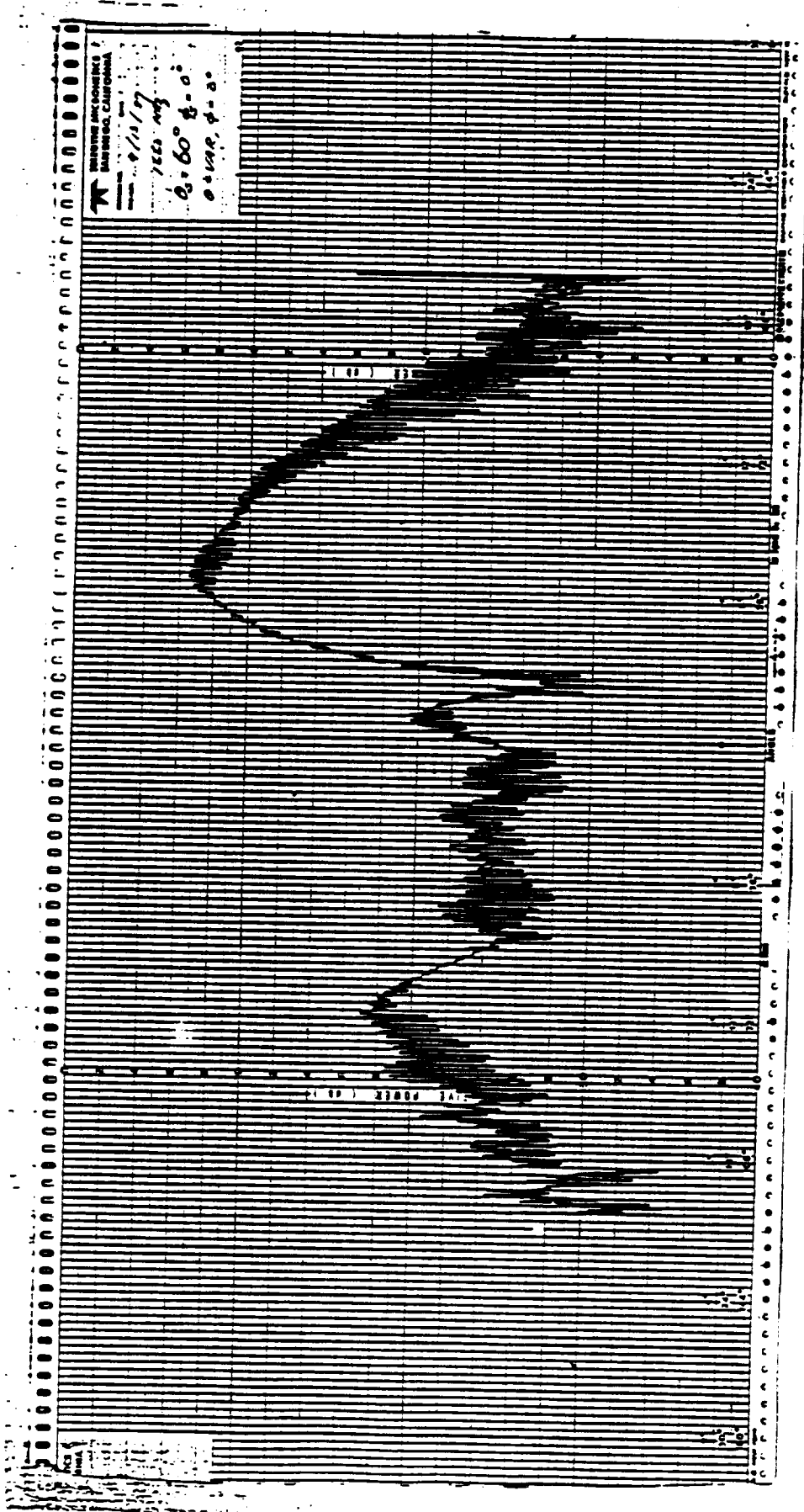


Figure 2-33. Measured Spinning Linear Elevation Array Pattern at 1660 MHz, ( $\theta_s = 60^\circ$ ,  $\phi_s = 0^\circ$ ;  $\theta = \text{VAR}$ ,  $\phi = 0^\circ$ )

ORIGINAL PAGE IS  
OF POOR QUALITY

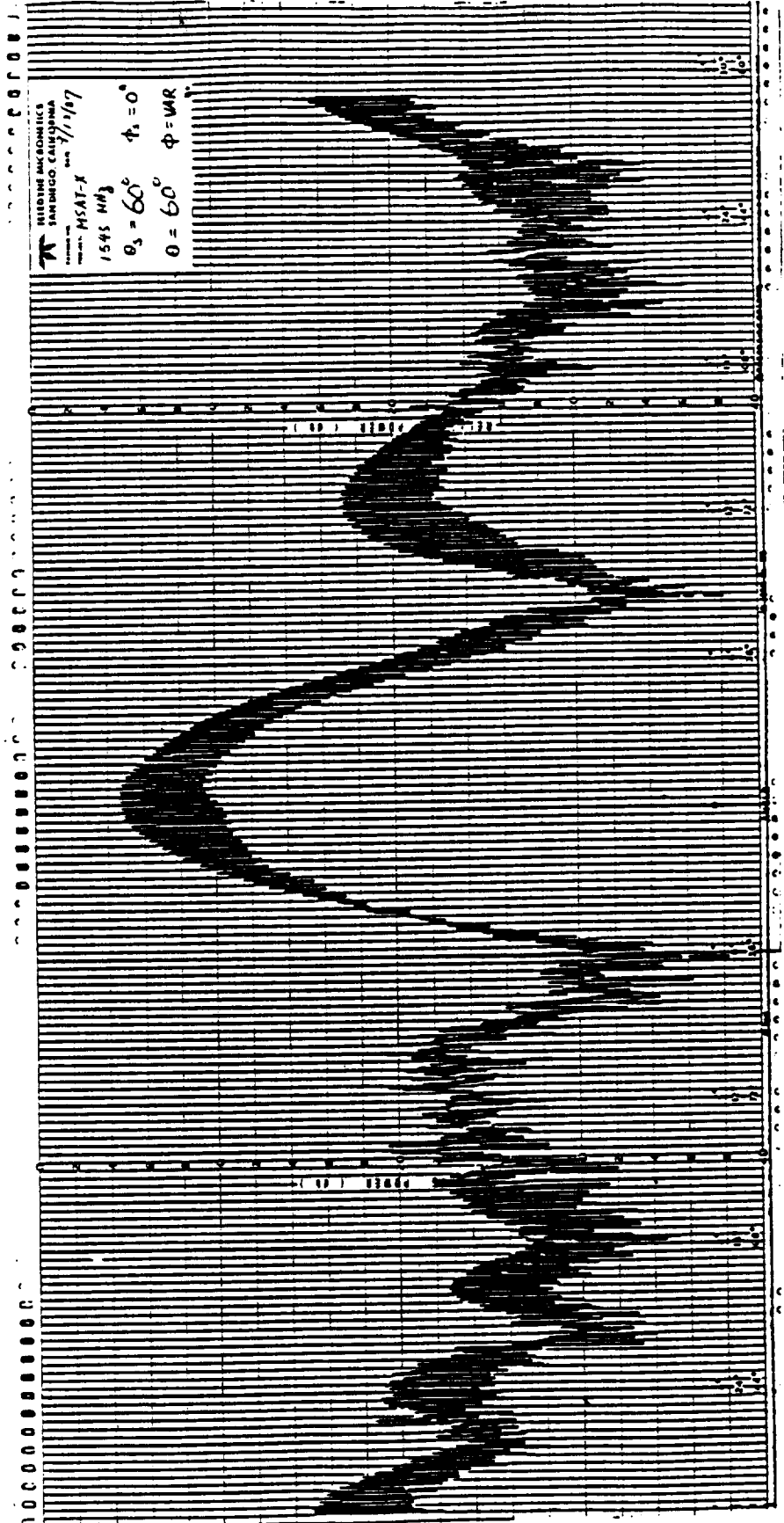


Figure 2-34. Measured Spinning Linear Azimuth Pattern at 1545 MHz, ( $\theta_s = 60^\circ$ ,  $\phi_s = 0^\circ$ ;  $\theta = 60^\circ$ ,  $\phi = \text{VAR}$ )

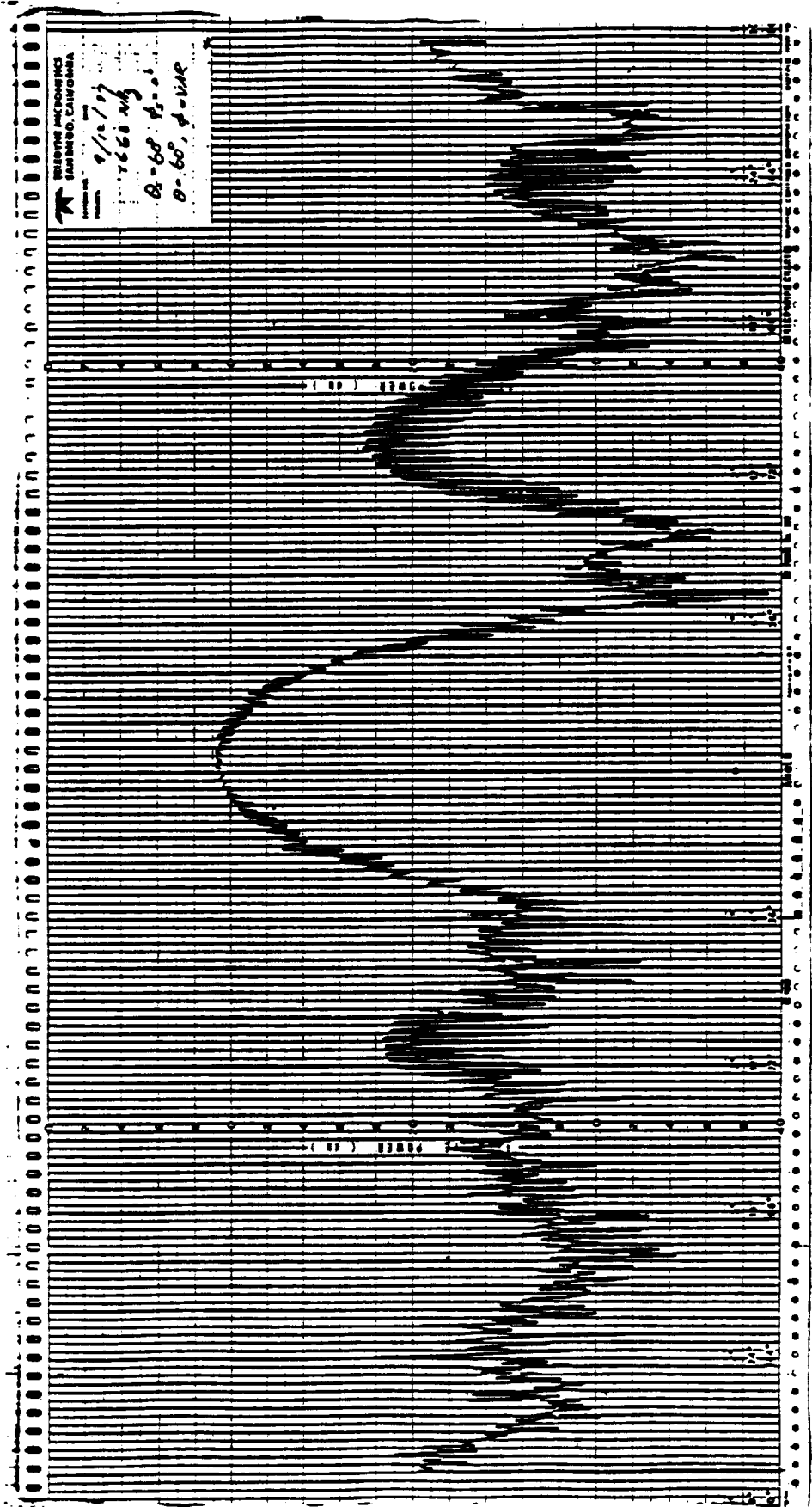


Figure 2-35. Measured Spinning Linear Azimuth Pattern at 1660 MHz, ( $\theta_s = 60^\circ$ ,  $\phi_s = 0^\circ$ ;  $\theta = 60^\circ$ ,  $\phi = \text{VAR}$ )

ORIGINAL PAGE IS  
OF POOR QUALITY

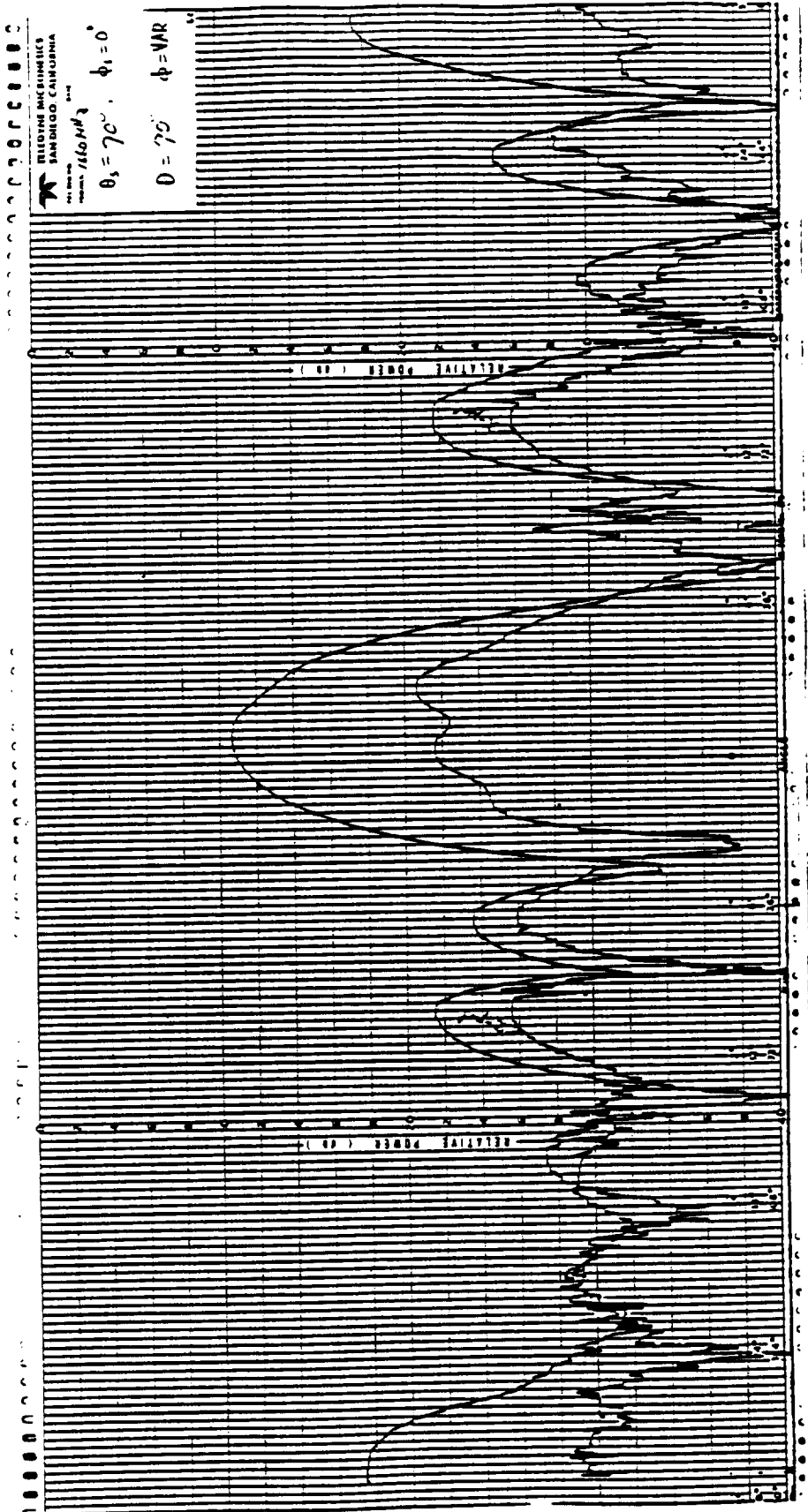


Figure 2-36. Measured RHCP and LHCP Azimuth Pattern at 1660 MHz, ( $\theta_s = 70^\circ$ ,  $\phi_s = 0^\circ$ ;  $\theta = 70^\circ$ ,  $\phi = \text{VAR}$ )

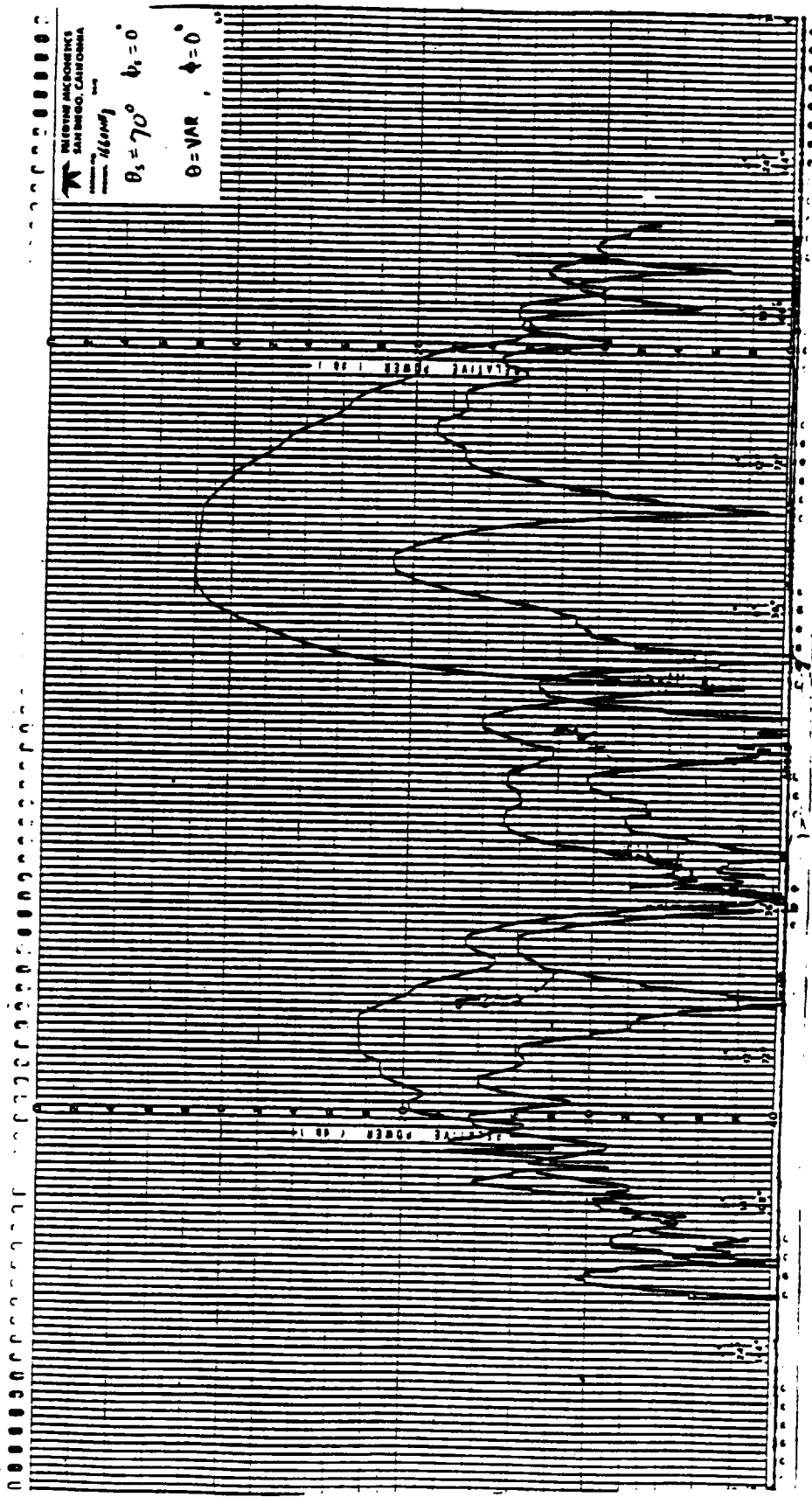


Figure 2-37. Measured RHCP and LHCP Elevation Pattern at 1660 MHz, ( $\theta_s = 70^\circ$ ,  $\phi_s = 0^\circ$ ;  $\theta = \text{VAR}$ ,  $\phi = 70^\circ$ )

One interesting observation from the measured array patterns is that the axial ratio of the array patterns at low elevation angles is better than expected. This could be attributed to the balanced four point feed in the crossed-slot design which eliminates potential higher order moding inside the crossed-slot cavity. The cross-polarized fields of each antenna element may cancel out each other at certain scan angles. In order to answer this polarization phenomena, however, further theoretical understanding and analysis of the crossed-slot array is needed, an area TRE is currently pursuing.

#### 2.4.2 Measured Array Gain

The measured array gain for both unit #1 and unit #2 is given in Table 2-7. Note that the array gain of the second antenna is improved by 0.6 dB at an elevation angle of 20 degrees at 1660 MHz. This is because it has better calibration of the beamformer (especially so with the phase shifter settings) and less dissipation loss at the isolation port of the hybrid. As shown in Figures 2-38 to 2-40, the average gain of unit #2 at an elevation angle of 20 degrees (above the horizon) is 9.3 dBic, 9.9 dBic and 8.3 dBic for frequencies of 1545 MHz, 1600 MHz and 1660 MHz, respectively.

In order to further improve the array gain (especially at 1660 MHz), the gain and loss budget of the array was analyzed and summarized in Table 2-8. It is observed from the gain analysis that (1) the dissipation loss at the isolation port of the hybrid, (2) the radiation efficiency loss, and (3) the aperture loss (due to the aperture bias distribution by the beamformer) must be reduced. Note that the array gain at the center frequency (1600 MHz) reached the design goal (10 dBic), because all the component designs are optimized to that frequency.

The dissipation loss at the isolation port of the hybrid is mainly due to mismatch at the four excitation feeders of the crossed-slot. The location of the plated through ground holes of the crossed-slot (Figure 2-19) is not right at the edge of the slot during the fabrication stage. This could possibly affect the antenna matching at two extreme ends of the optimizing frequency range, hence efforts to optimize the antenna matching is required for future work. A possible gain improvement on this loss is estimated to be 0.6 dB and 0.8 dB for frequencies of 1545 MHz and 1660 MHz respectively.

Proper design of the excitation feeder could be the key to improving the radiation efficiency of the crossed-slot. The dog leg shape (bent stripline) of the excitation feeder in the current design is not desirable because it can generate higher order moding inside the cavity which in turn will degrade the radiation efficiency. An effort to optimize the feed

Table 2-7. Summary of Measured Gain of the Array

Beam Position		Gain (dBic)			
		1545 MHz		1660 MHz	
AZ	EL (above horizon)	Unit 1	Unit 2	Unit 1	Unit 2
Broadside		12.6	12.5	13.7	13.7
0°	60°	11.4	10.8	11.7	12.1
0°	50°	10.9	10.4	11.2	11.4
0°	40°	10.0	9.8	9.6	10.2
0°	30°	9.4	9.3	8.2	8.7
0°	20°	9.2	9.1	6.7	7.7
45°	20°	8.3	8.2	7.7	7.9
90°	20°	9.1	9.3	8.3	8.7
135°	20°	9.9	9.9	8.2	8.6
180°	20°	9.7	9.0	6.8	7.2
225°	20°	8.7	9.1	7.7	8.7
270°	20°	8.6	9.6	7.8	8.4
315°	20°	9.9	9.8	8.2	8.8
Average gain at 20 degrees above horizon		9.2	9.3	7.7	8.3

point of the stripline is also required in the quest to improve the radiation efficiency. Note that balanced cavity excitation requires four perfectly symmetrical probe feeds located at the four quadrants and along the diagonal of the crossed-slot. In addition, the bandwidth of the crossed-slot must be increased. Thicker cavities and the use of a flared slot to broaden the bandwidth are being pursued. Another area that can improve the gain performance of array is to bond it together. As mentioned earlier in Section 2.3, the multilayer boards of the array were bolted together. The potential uneven tightness of each bolt could generate higher order modes inside the crossed-slot and also degrade the stripline hybrid circuit performance. A possible gain improvement to the radiation efficiency is estimated to be around 0.4 dBic and 0.8 dBic for frequencies of 1545 MHz and 1660 MHz respectively.

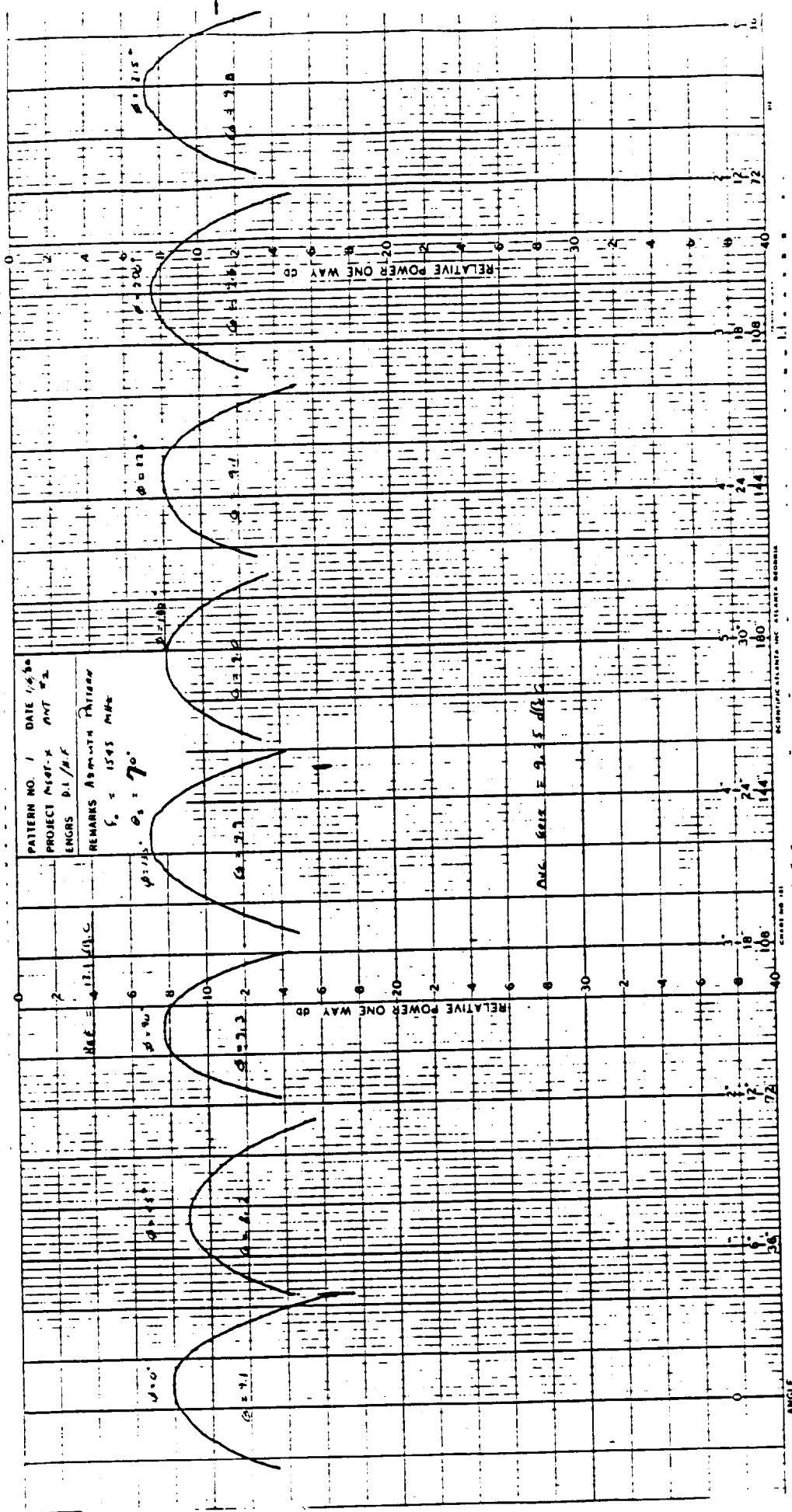


Figure 2-38. Measured Array Gain at 20 Degrees Elevation Angle (Above Horizon), Frequency = 1545 MHz, Average Gain = 9.25 dBic ( $\theta_s = 70^\circ$ ,  $\phi_s = 0^\circ$ ,  $45^\circ$ ,  $90^\circ$ ,  $135^\circ$ ,  $180^\circ$ ,  $225^\circ$ ,  $270^\circ$ ,  $315^\circ$ ;  $\theta = 70^\circ$ ,  $\phi = \text{VAR}$ )

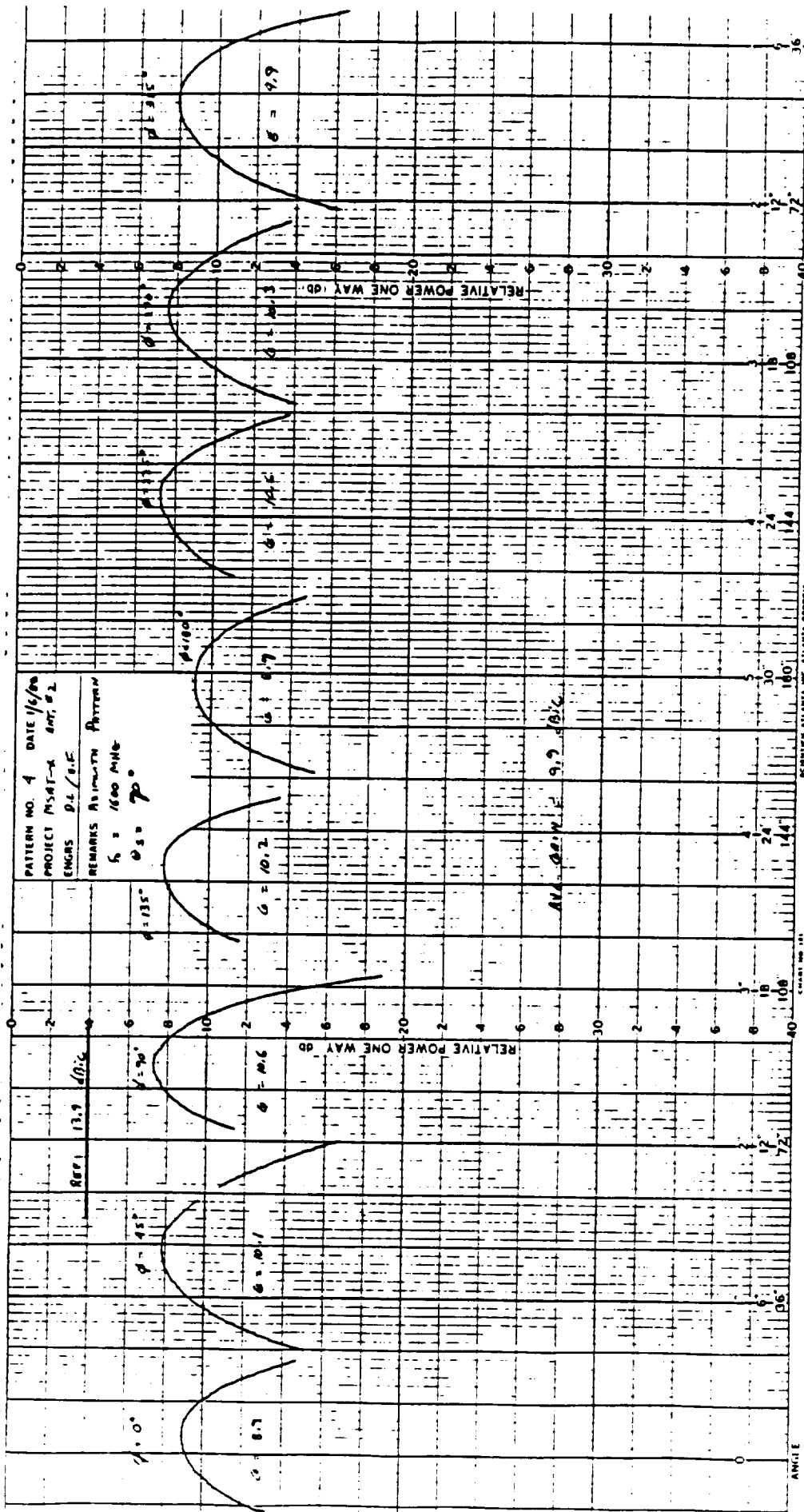


Figure 2-39. Measured Array Gain at 20 Degrees Elevation Angle, Frequency = 1660 MHz, Average Gain = 9.9 dBic ( $\theta_s = 70^\circ$ ,  $\phi_s = 0^\circ$ ,  $45^\circ$ ,  $90^\circ$ ,  $135^\circ$ ,  $180^\circ$ ,  $225^\circ$ ,  $270^\circ$ ,  $315^\circ$ ;  $\theta = 70^\circ$ ,  $\phi = \text{VAR}$ )

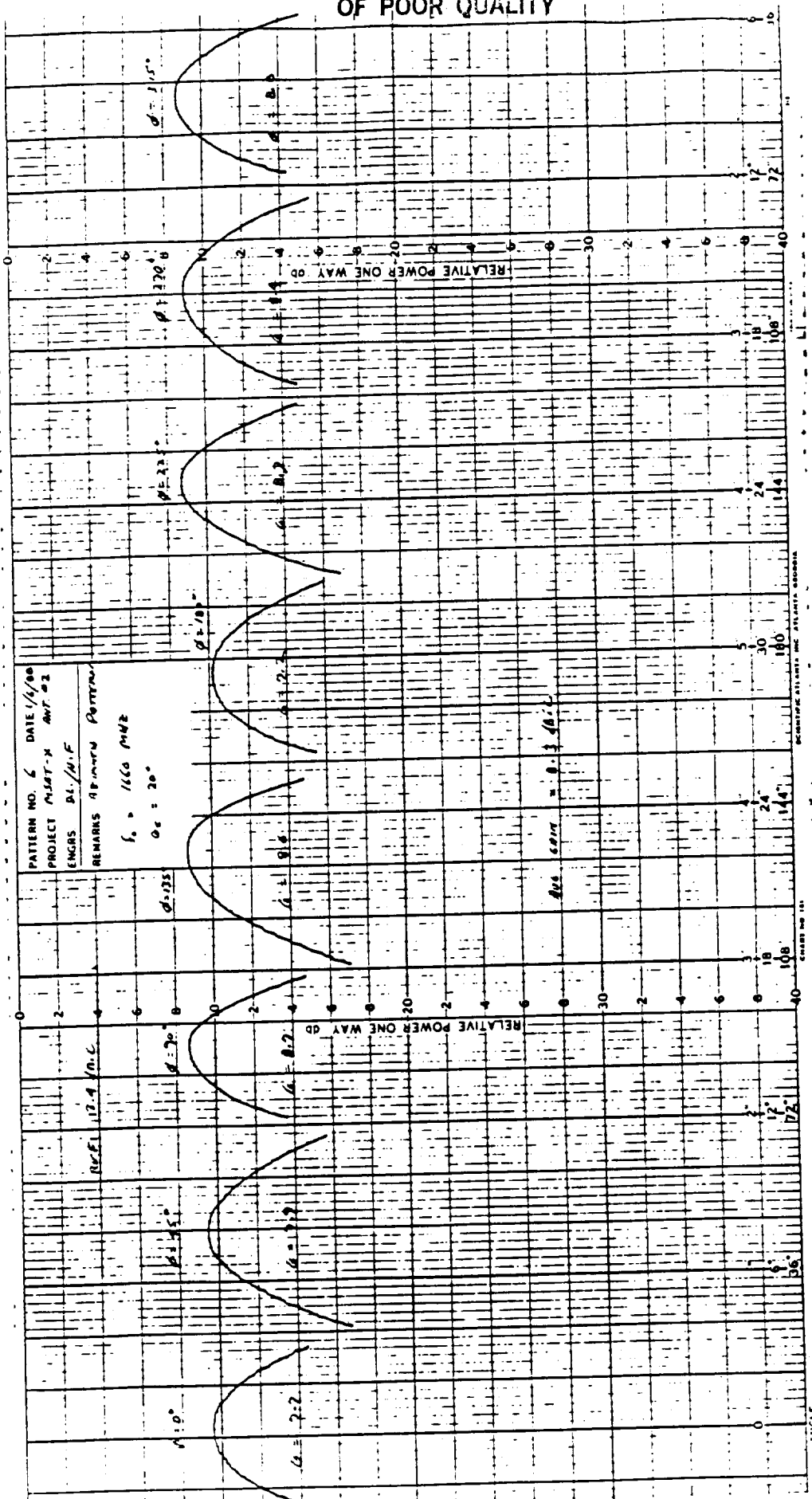


Figure 2-40. Measured Array Gain at 20 Degrees Elevation Angle, Frequency = 1660 MHz, Average Gain = 8.3 dBic ( $\theta_s = 70^\circ, \phi_s = 0^\circ, 45^\circ, 90^\circ, 135^\circ, 180^\circ, 225^\circ, 270^\circ, 315^\circ$ ;  $\theta = 70^\circ, \phi = \text{VAR}$ )

Table 2-8. Gain Analysis of Array Unit #2

	<u>Frequency (MHZ)</u>			Remarks
	1545	1600	1660	
Directivity (dBic)	17.8	18.0	18.2	
Loss Budget (dB):				
1. Hybrid Insertion Loss	-0.25	-0.25	-0.25	
2. Beamformer Insertion Loss	-1.85	-1.80	-1.75	
Total Resistive Loss (dB)	2.1	2.05	2.0	Important for G/T
S <sub>21</sub> between input and load port of hybrid	-6.64	-13.21	-6.04	Due to the mismatch at the four feeders
3. Dissipation loss at hybrid load port	-1.05	-0.2	-1.25	
4. Polarization loss	-0.5	-0.5	-0.6	
5. Mismatch at RF input port	-0.2	-0.2	-0.2	VSWR 1.5:1
6. Scan loss at 70 degree from the array broadside	-4.7	-4.7	-4.7	
Total Measurable Loss	-8.55	-7.65	-8.75	
Not Measurable Loss (dB): (Radiation Efficiency and Improper Scan Loss)	-4 ±.4	-4 ±.4	-1.2 ±1	Due to the improper excitation and bias phase distribution of the beamformer
Gain at 70° from the array broadside	8.85 ±.4	10 ±.4	8.25 ±1	

Aperture loss is due to a phase bias distribution across the antenna's aperture which does not allow the array to scan properly. The phase bias distribution could be due to the unequalized length of the meander line to each element. The effects of the meander line on the effective path length should be included in future designs. Since the coupling effect between the components of the beamformer could also impact the aperture distribution. As shown in Figure 2-41 (a) and (c), the measured and the calculated data showed that the array is scanned properly at 1545 MHz. However, for the frequency of 1660 MHz, the comparison between the measured and the calculated data (Figure 2-41(b) and 2-41(d)) showed that the array was not scanned properly. The measured aperture distribution of the array, for the beam angle scanned to  $\theta_s = 60$  degrees and  $\phi_s = 0$  degrees, at 1660 MHz is shown in Figure 2-42. Based on this set of measured values, the array pattern was computed and plotted in Figure 2-43. It is obvious from this figure that the realized array gain at 60 degrees is 0.8 dB less than the design value.

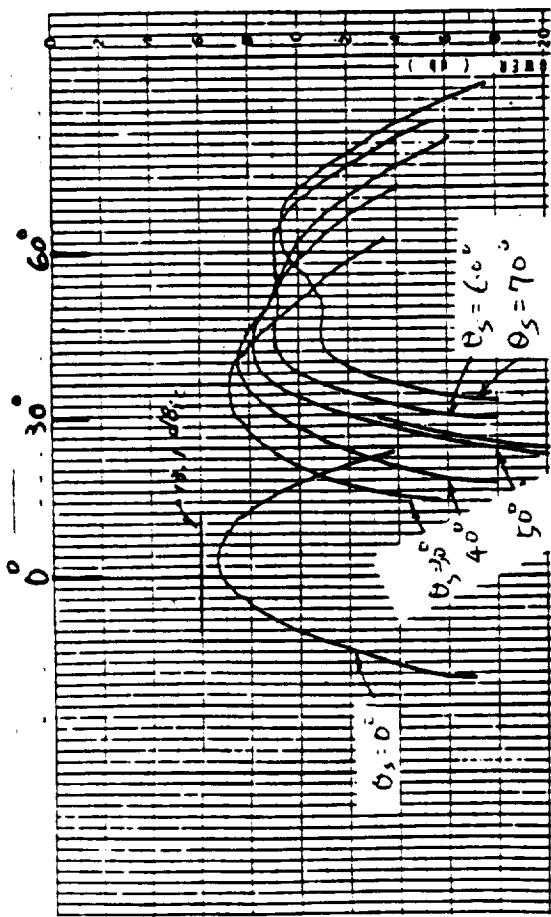
It is concluded from the gain data analysis that a 10 dBic array gain across the operating frequency band is achievable in the future. However, a 9.5 dBic array gain can be realized in the near future through the following improvements:

1. Improve the antenna matching at the four excitation feeders.
2. Optimize the crossed-slot excitation design.
3. Broaden the crossed-slot element bandwidth.
4. Bond the array assembly.
5. Optimize the beamformer aperture distribution.
6. Carefully calibrate the phase shifter settings.

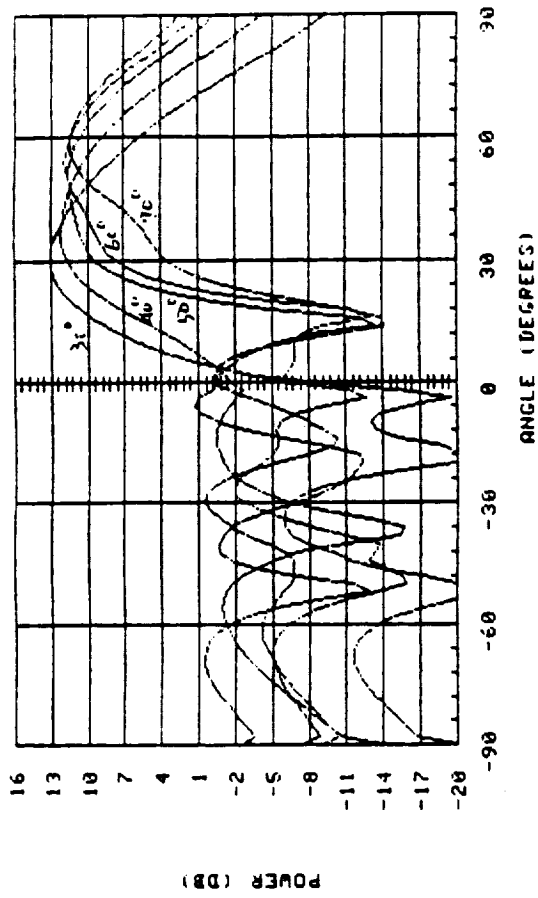
### 2.4.3 Measured Intersatellite Isolation

The outdoor antenna range used for intersatellite isolation measurements is shown in Figure 2-44. A twelve foot movable boom was rigged to the roof of the auxiliary tower on the range. An LHCP helical antenna was attached to the end of the boom to serve as the undesired signal source. An RHCP dish antenna was mounted on the secondary tower to simulate the desired signal. Refer to Section 8.3.4 for a detailed description of the test setup.

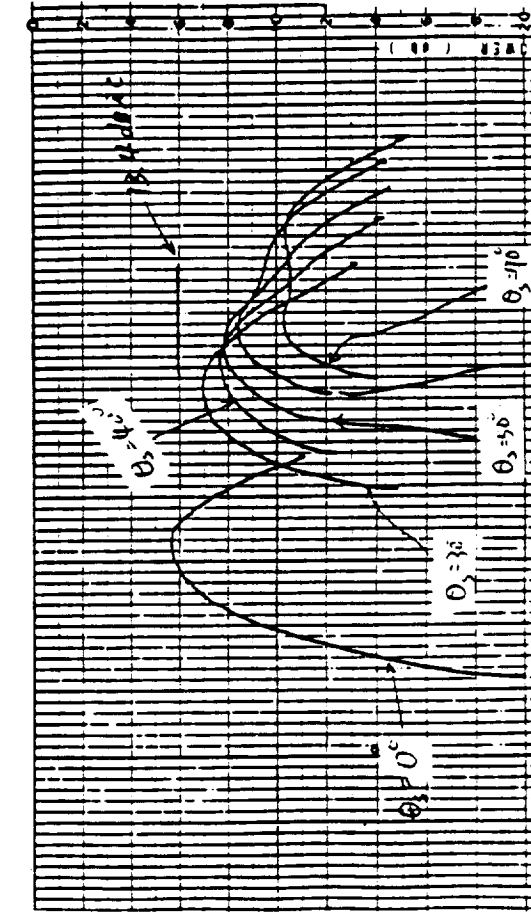
The measured results of four different cases are given in Table 2-9. Note that condition I is close to the location of the State of Washington . Condition IV is close to the location of



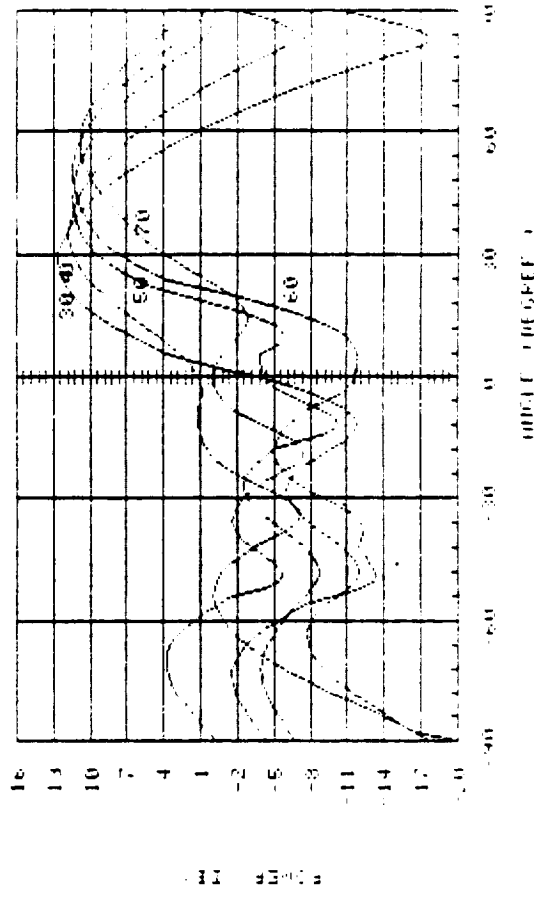
(a) Measured Patterns at 1545 MHz



(c) Computed Patterns at 1545 MHz



(b) Measured Patterns at 1660 MHz



(d) Computed Patterns at 1660 MHz

Figure 2-41. Elevation Plane Patterns at Various Scan Angles ( $\theta_s = 30^\circ, 40^\circ, 50^\circ, 60^\circ, 70^\circ$ )

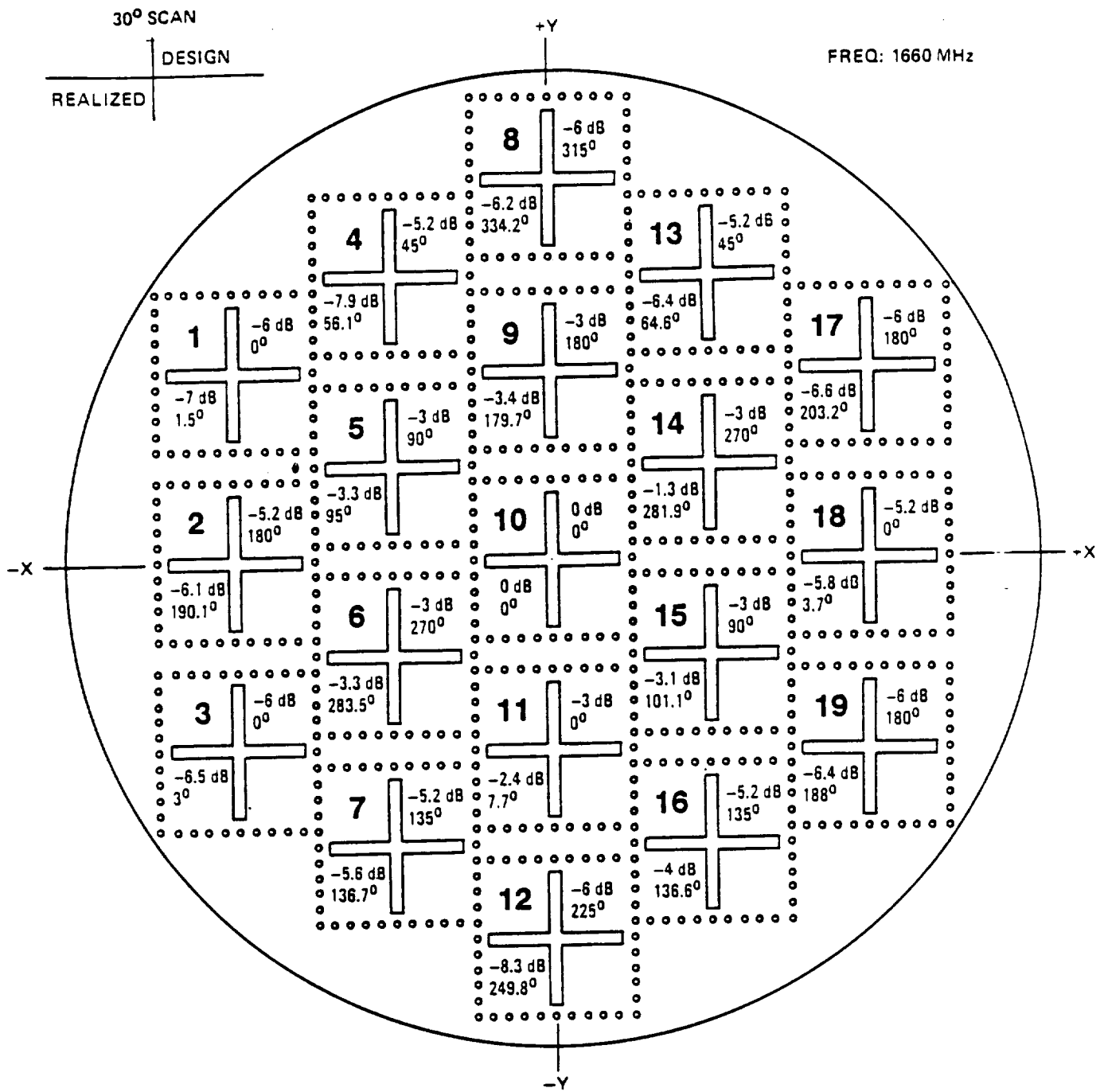


Figure 2-42. Measured Aperture Distribution of the Beamformer at 1660 MHz for  $\theta_s = 60^\circ$  and  $\phi_s = 0^\circ$  Scan

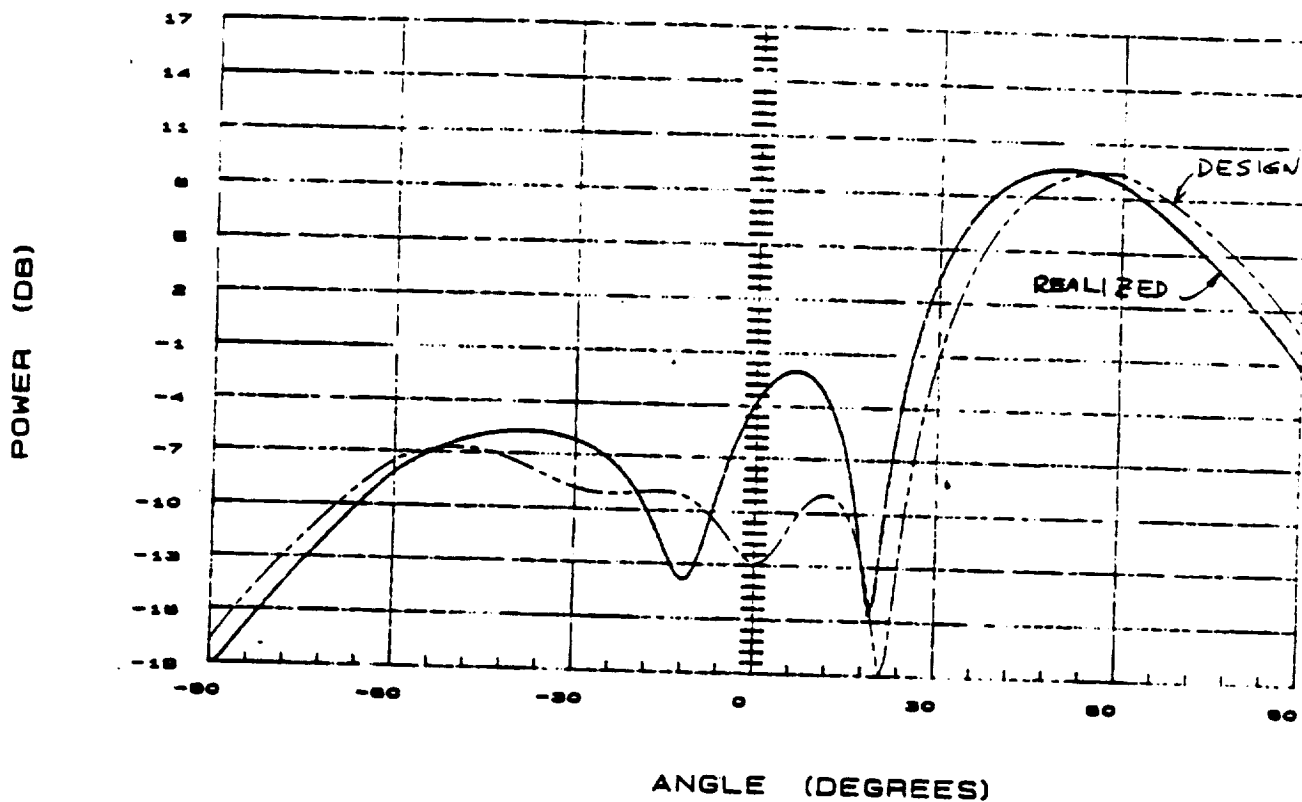


Figure 2-43. Computed Array Pattern for the Realized and Ideal Design Beamformer  
 $(\theta_s = 60^\circ, \phi_s = 0^\circ)$  Frequency = 1660 MHz

the State of Minnesota . Conditions II and III are used to simulate the location of Washington with beam pointing error factors. These results show that an isolation of 26 dB was achieved which is better than predicted (see Figure 2-13). The outstanding polarization purity and low sidelobe level of the array patterns could be the key to the excellent intersatellite isolation. It is noted from the measured array patterns that the developed array will provide 10 dB of polarization isolation in 90% of the space coverage. However, due to the importance of intersatellite isolation , more locations in the continental United States (CONUS) must be simulated on the range test to ensure the success of this program.

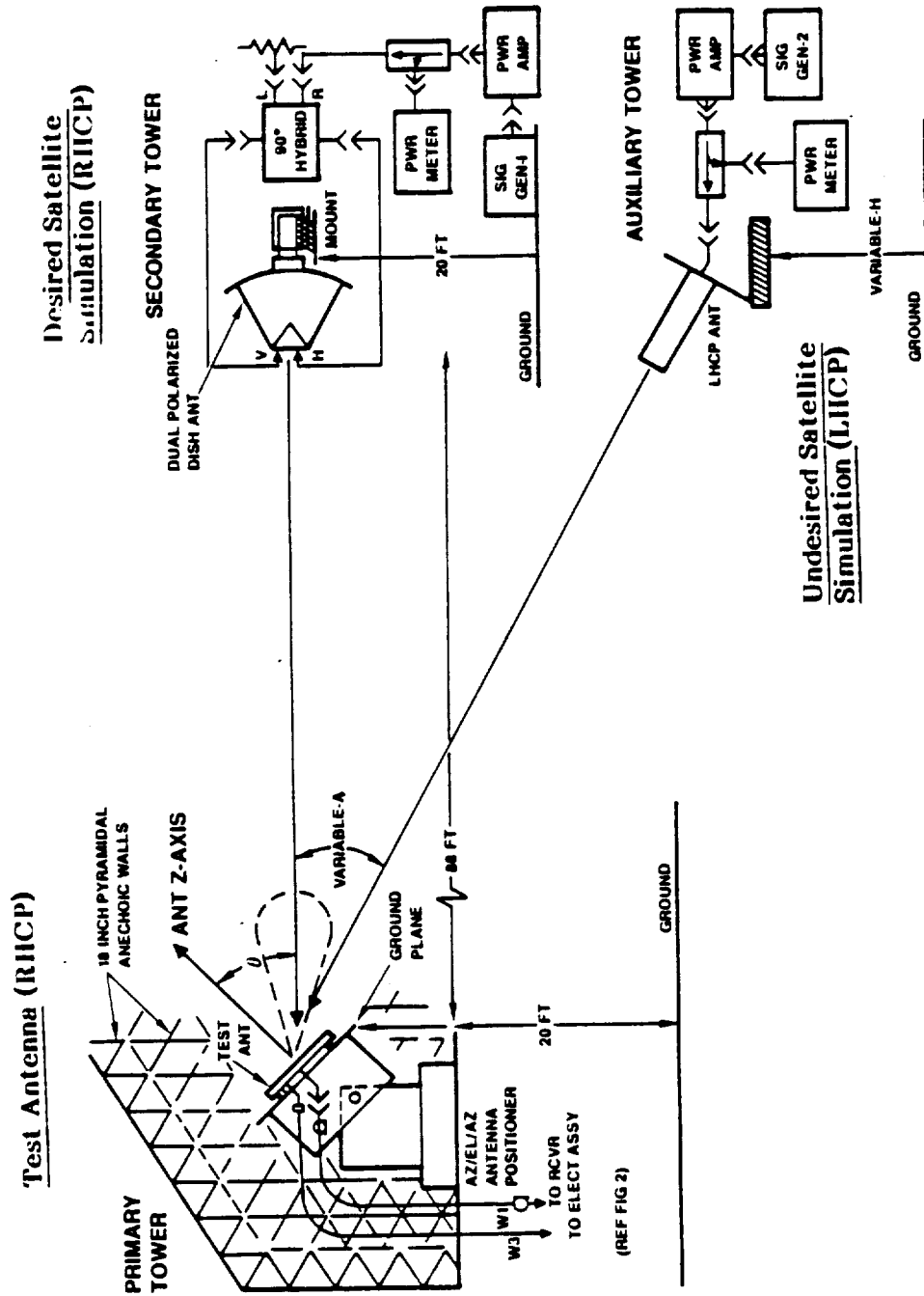


Figure 2-44. Pictorial/Block Diagram Depicting Equipment Hook-up for MSAT-X System Tests on Outdoor Antenna Range

Table 2-9. Measured Intersatellite Isolation

Condition	Desired Signal Location (RHCP)	Undesired Signal Location (LHCP)	Array Pointing Angle (degs)	Isolation (dB)	Remarks
I	$\theta_d = 30^\circ, \phi_d = 0^\circ$	$\theta_u = 20^\circ, \phi_u = 30^\circ$	$\theta_s = 30^\circ, \phi_s = 0^\circ$	35	Simulate Location of Washington State
II	$\theta_d = 30^\circ, \phi_d = 0^\circ$	$\theta_u = 20^\circ, \phi_u = 30^\circ$	$\theta_s = 30^\circ, \phi_s = 5^\circ$	30	Simulate Location of Washington State with pointing error
III	$\theta_d = 30^\circ, \phi_d = 0^\circ$	$\theta_u = 20^\circ, \phi_u = 30^\circ$	$\theta_s = 30^\circ, \phi_s = 10^\circ$	30	Simulate Location of Washington State with pointing error
IV	$\theta_d = 30^\circ, \phi_d = 0^\circ$	$\theta_u = 30^\circ, \phi_u = 30^\circ$	$\theta_s = 30^\circ, \phi_s = 0^\circ$	26	Simulate Location of Minnesota State

## CONCLUSIONS

An L-band car-top conformal phased array has been successfully developed for the Mobile Satellite Communications experiment. The array consists of nineteen crossed-slot elements in a triangular lattice arrangement. The element spacing is 3.9 inches. Proper amplitude taper (see Figure 2-5) provides the sidelobe control needed to satisfy the intersatellite isolation requirements. Eighteen three-bit diode phase shifters are used to steer the array. The array size is 22 inches in diameter including the mounting space. Based on the measured array performance, one can draw the following conclusions and achievements:

1. The printed, cavity backed, stripline fed crossed-slot element has been proved to be the superior radiating element for the MSAT phased array.
2. The measured array gain at 70 degrees from array broadside is 9.3 dBic and 8.3 dBic for frequencies of 1545 MHz and 1660 MHz, respectively. A gain of 10 dBic across the frequency band is achievable in the future. However, 9.5 dBic array gain can be realized in the near future.
3. The measured intersatellite isolation level is 26 dB which is better than the requirement (20 dB).
4. The total thickness of the developed array is 0.68 inch and 0.75 inch for units #1 and #2, respectively.
5. The multipath rejection requirement was satisfied.
6. The backlobe level is better than 12 dB in 95% of the space coverage. The worst backlobe level is 6 dB when the array was scanned to 70 degrees from the array broadside (at certain azimuth angles).

## RECOMMENDATIONS

In order to further improve the performance of the array, especially with respect to the antenna's gain at 1660 MHz, the following tasks are recommended for future development work:

1. Improve the matching of the four excitation feeders to the antenna. Improper location of the plated through ground holes of the crossed-slot (shown in Figure 2-19) must be corrected. Eliminate the dog leg shape of the feeder.
2. Theoretically and experimentally investigate and optimize the excitation mechanism. The four probe excitation method is recommended because it could reduce the unnecessary metal inside the cavity of the crossed-slot, which in turn can improve the antenna's radiation efficiency.
3. Investigate a broadbanding technique to improve the antenna's gain across the required frequency band. A slot with a flared shape is worth further study.

4. Bonding must be used to improve the radiation efficiency and the operating stability.
5. Additional optimization of the beamformer is required in order to further improve the aperture distribution. The meander lines in the beamformer must be tuned to eliminate the phase bias distribution.
6. The developed array must go through a calibration process. Optimizing the phase shifter settings is a very important task if the final array is to scan properly.

2.7

### REFERENCES

- [1] R. G. Kouyoumjian and P. H. Pathak, "A Uniform Theory of Diffraction for an Edge in a Perfectly Conducting Surface", pp 1448-1461, Proceedings of the IEEE, Nov. 1974.
- [2] C. A. Mentzer, L. Peters, Jr., and R. C. Ruduck, " Slope Diffraction and Its Applications to Horns", pp 153-159, IEEE Trans on AP-S, March, 1975.
- [3] W. D. Burnside, N. Wang and E. L. Pelton, "Near Field Pattern Analysis of Airborne Antennas", pp 318-327, May 1980.

## SECTION 3

### ANTENNA ELEMENT FEED NETWORK

Among the low profile antenna candidates, the crossed-slot and patch element were considered. The cavity-backed, printed, stripline fed crossed-slot was selected, however, because it has (1) wider beamwidth, (2) better gain and axial ratio at low elevation angles, and (3) is thinner for the same operating frequency band than that of a patch antenna. In this section, the substrate material selection, the crossed-slot design parameters, breadboard design and array element development will be presented. Conclusions and recommendations will be discussed at the end of this section.

#### 3.1 SUBSTRATE MATERIAL SELECTION

The choice of substrate material and its evaluation is an essential part of the antenna design. Major substrate properties include: 1) dielectric constant and loss tangent and their variation over frequency and temperature; 2) substrate thickness uniformity and; 3) dimensional stability with processing, temperature, humidity, and aging. Also, chemical resistance, bondability, machinability, etc., are quite important in fabrication. For the commercial market, the substrate unit price is also very important since it is a major cost item in the whole array. A list of major substrate manufacturers is given in Table 3-1. Based on the considerations of cost and performance, the substrate material of 3M-250 GX is recommended.

In an effort to reduce both manufacturing and raw material costs, further investigation was conducted on other substrate materials that could possibly be used. The evaluation was based on a performance/cost comparison, using Teflon-glass substrate as a reference. The performance characteristics were based on transmission line losses in a stripline configuration, where the total loss in db/inch is the combination of dielectric loss  $\alpha_d$  and conductor loss  $\alpha_c$ . The search rapidly narrowed to two substrate types, namely Polyimide, and Epoxy-Glass. Table 3-2 summarizes the performance versus cost comparison for the three types of materials that were evaluated.

As noted in Table 3-2, the cost reduction ratio of 8.5 for the type III material is very attractive. However the theoretical line loss is almost four times that of the Teflon-glass material. Therefore, an actual feed network was not fabricated with the epoxy-glass

Table 3-1. Price of Cu-Clad Substrate, One Ounce Copper Two Sides, Per 100 Sheets or More Per Sq. Ft.

Suppliers	0.062"	0.090"	0.125"	Dielectric Constant		Comments
				1 MHz	10 GHz	
3M 250 GX	34.00	43.33	56.97	2.45 ±0.04	2.55 ±0.04	Recommended 3M 250 GX
250 LX	39.83	49.49	66.35	2.40 ±0.04	2.55 ±0.04	
ROGERS				2.33	2.35	
RT/DUROID 5870	64.18		103.77	±0.02	±0.02	
RT/DUROID 5880	70.59		114.14	2.20 ±0.02	2.20 ±0.02	
OAK 602	31.67	44.17	59.58	2.45 ±0.05	2.65 ±0.04	
605	38.25	57.50	76.67	2.17 ±0.05	2.35 ±0.04	
KEENE 522	27.56	42.75	50.73			
527	29.63	45.96	54.53			
TACONIC						
TAC-LAM-X	28.32	40.68	53.23			

material. On the other hand, the Type II Polyimide Material does have potential. Although the cost reduction ratio of 3.1 is not as high as the Type III Material, the predicted network loss could possibly be tolerated. Due to schedule restraints, however, the use of Type II Material for further development of the feed network was not pursued.

Table 3-2. Performance versus Cost Comparison for Several Different Types of Substrate Material

Material	Dielectric Constant	Theoretical Line Loss $\alpha_C + \alpha_D$ dB/in	Predicted Network Loss dB	Measured Network Loss dB	Basic Material Cost \$/ft <sup>2</sup>	Cost Reduction Ratio
Type I Teflon-Glass	2.5	0.025	0.29 db	0.24 db	\$20.80	1.0
Type II Polyimide	3.8	0.065	0.60 db	NA	\$6.77	3.1
Type III Epoxy-Glass	4.8	0.195	1.13 db	NA	\$2.45	8.5

NOTES:

1. Measured at center freq. of 1603 MHz
2. Based on 1000 sheet quantity price 0.031 inch in thickness one ounce copper on both sides.

3.2 CROSSED-SLOT DESIGN PARAMETERS

The major design parameters involved in the design of the stripline fed, cavity backed crossed-slot, as shown in Figure 3-1, are delineated as follows.

1. Slot width, length and shape controls the resonant frequency. Flared shapes tend to have a wider frequency VSWR response.
2. Stripline feed location along the slot governs the impedance variation of the slot.
3. Stripline width, length and shape are key parameters in impedance matching.
4. Feed point for the strip-line controls impedance matching and internal moding; it will affect radiation efficiency.
5. Cavity thickness governs bandwidth and radiation efficiency.
6. Cavity size determines the resonant frequency.

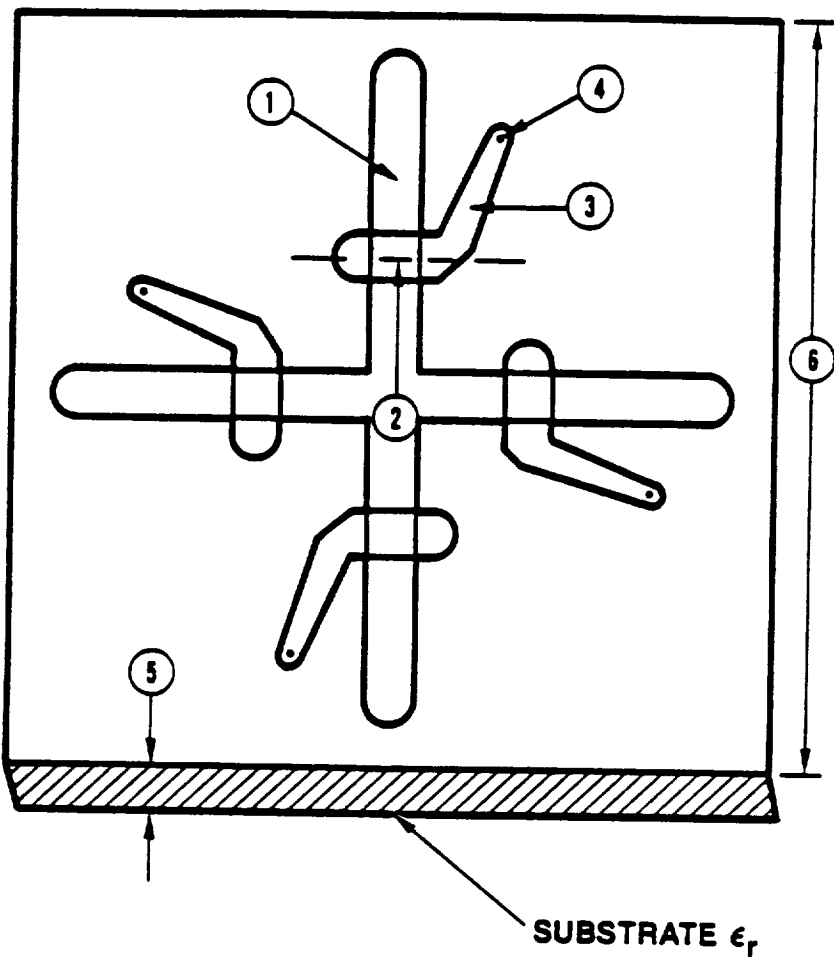


Figure 3-1. Crossed-Slot Design Parameters

Note that stripline was used to feed the printed, cavity-backed, crossed-slot because it provides additional degrees of freedom in terms of impedance matching. However, the presence of the metal of the stripline feeders inside the cavity could generate extra higher order modes which in turn may hurt the radiation efficiency.

There are two major excitation mechanisms involved in this kind of feeding configuration. One is the "coupling excitation" mode from the stripline across the slot and the other is the "cavity excitation" mode of the probe feed. The combination of these two excitation modes will determine the impedance characteristics of the crossed-slot at the probe feed point. The input impedance of the slot, measured at the feed point is a function of the length and

width of the slot and the location of the probe feed points. The optimal positions of the excitation feeder and the probe feed point will be determined empirically.

The stripline running across the slot will excite the slot due to displacement current caused by the interruption of the electric field by the slot. The coupling is controlled by the angle of the stripline. The coupling excitation mode should avoid the cross-talk problems between two orthogonal slots. This requires two symmetrical striplines feeding each of the orthogonal slots, as shown in Figure 3-2.

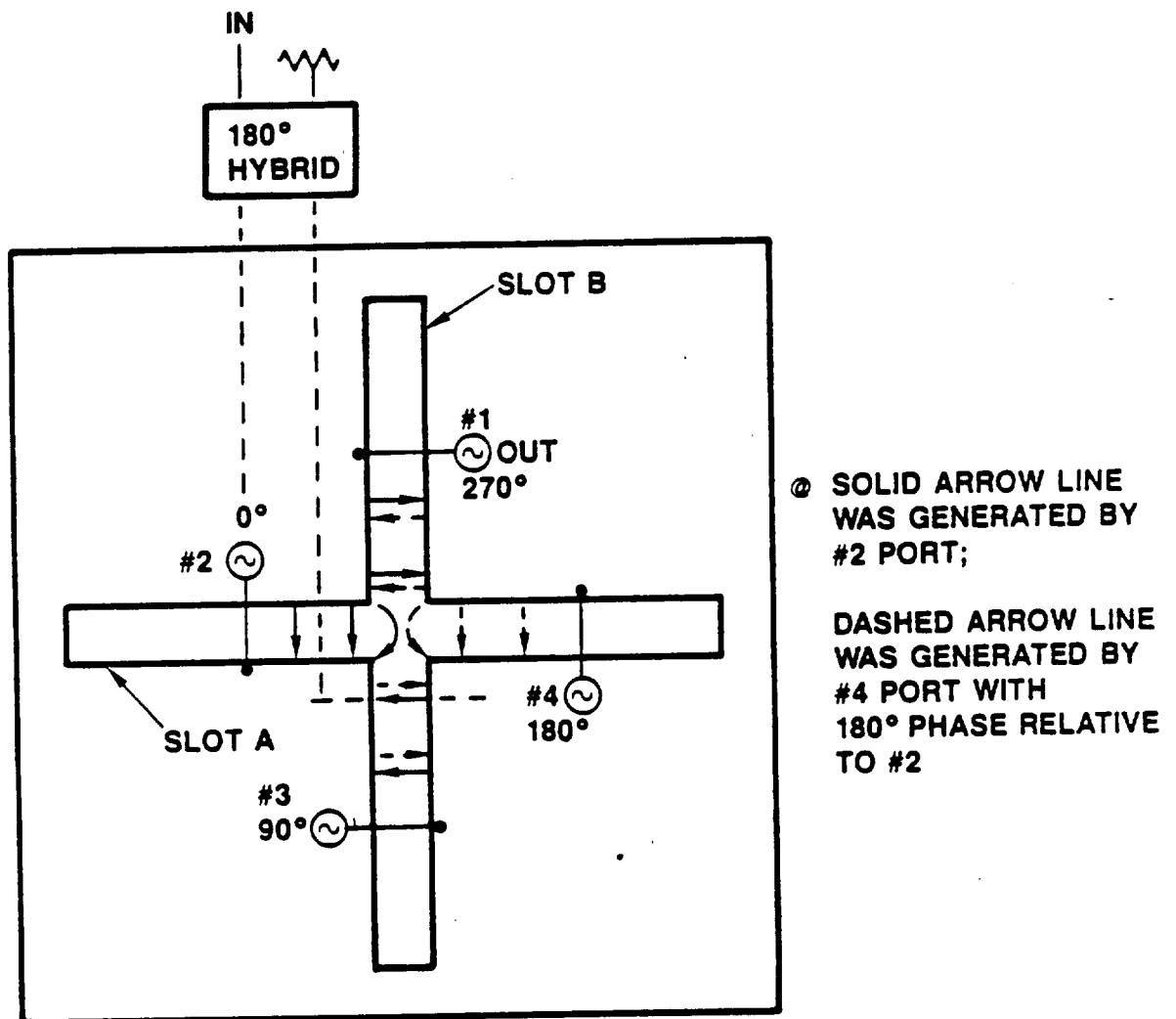


Figure 3-2. Field Distribution with #2 & #4 Port Excited

Port #2 and Port #4 are attached to feed lines that are positioned on opposite sides of the slot. The two ports are energized with voltages having a 180 degree phase difference. This will produce a field distribution across slot A as indicated by the solid and dashed lines. This is the desired condition for proper radiation from the slot. However, as noted in the figure, the solid and dashed lines representing the field distribution across Slot B, as a result of the excitation of Slot A, are of opposite sense. This produces a net field cancellation in Slot B, due to the excitation of Slot A, thereby effectively isolating Slot B from the effects of Slot A.

In a similar manner, by applying a voltage to Ports #1 and #3, Slot B is excited. These two ports also have a 180 degree phase difference between them. They are also in phase quadrature to the #2 and #4 port voltages. This quadrature relationship is necessary to produce the 0-90-180-270 degree phase sequence required to achieve circular polarization of the radiated wave. The phase sequence has no effect on the crossed-slot isolation; therefore, the same analogy may be used to explain the isolation of Slot A due to the effects of Slot B, as was used to explain the isolation of slot B relative to Slot A.

Excitation of the proper cavity mode requires additional design constraints, namely that these four probe feed points should be symmetrically located at the four quadrants of the crossed-slot cavity as shown in Figure 3-2. The optimal probe feed points are along the diagonal of the crossed-slot. Note that the field distributions of the  $TE_{011}$  mode in the cavity at these feed points are perfectly symmetrical with respect to each other. These four feed points must be excited in balanced amplitude and 0-90-180-270 degree phase rotation so that higher order modes inside the cavity can be suppressed, and also to achieve the required circular polarization.

In order to have good radiation efficiency of the crossed-slot, the antenna designer should accomplish the following tasks:

1. Good impedance matching at the four feed points.
2. Balance the excitation between two orthogonal slots.
3. Even excitation between two feeds at each of the two orthogonal slots.
4. Minimum metal inside the cavity.
5. Avoid any unnecessary bending of the stripline feed if possible.

### 3.3

## BREADBOARD DESIGN

The development of the newly invented, cavity-backed, printed crossed-slot element has been a very challenging task for the antenna designer. In this subsection, discussions on the experimental model and breadboard model developments are presented below.

### 3.3.1 Experimental Model Development

During the earlier phase of the breadboard design, a two feed point method (Figure 3-3) was used. The required bandwidth was achieved, but the element would not radiate efficiently. Through detailed analysis and measured results, it was observed that internal moding and mutual loading of the orthogonal slots were the two major factors. In other words, the two orthogonal slots were coupling to each other resulting in poor isolation between the feed ports. In view of this, an experimental mode utilizing a four point feed (as shown in Figure 3-4) was fabricated.

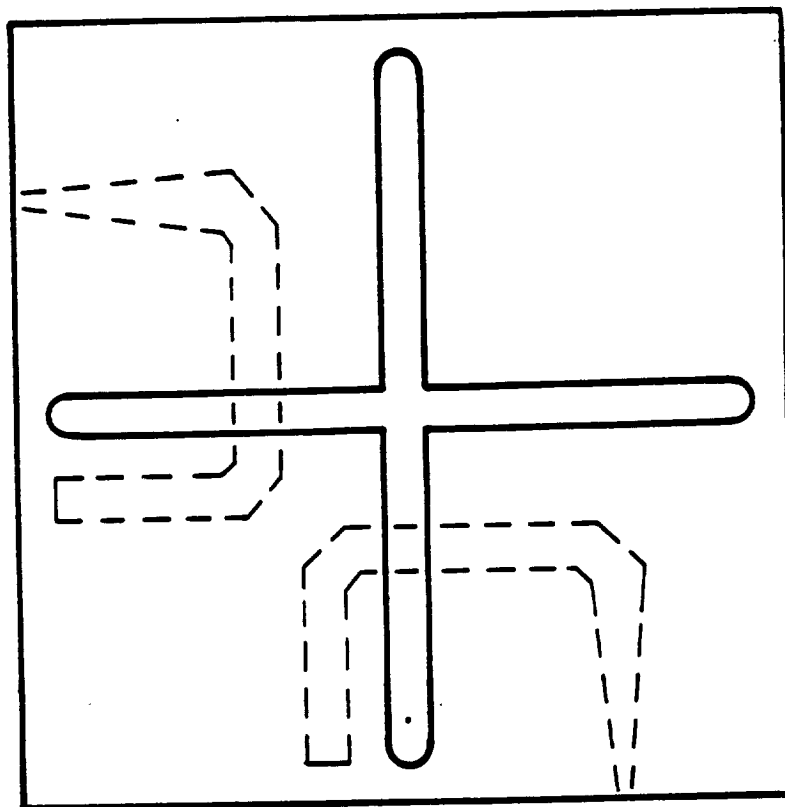


Figure 3-3. Earlier Model of the Element

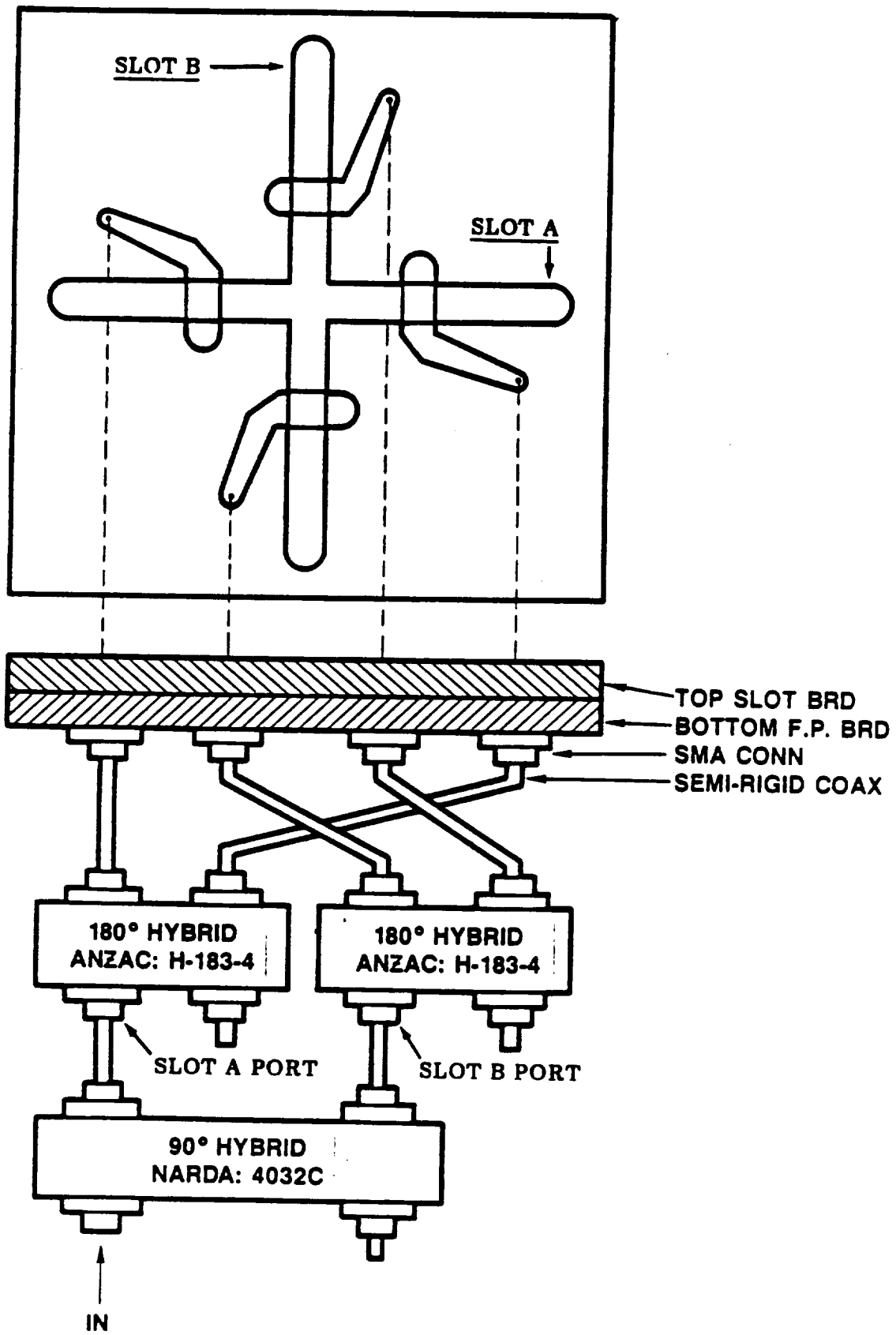


Figure 3-4. Experimental Model of the Crossed-Slot

A variety of tests were performed on the experimental element model to verify design objectives. For example, a plot of isolation measurement between the Slot A port and the Slot B port of the crossed-slot (Figure 3-4) as a function of frequency is shown in Figure 3-5. As indicated, more than 30 db of isolation is achieved over a major portion of the frequency band. This data proved the concept discussed previously regarding the method to overcome the cross-talk problems between the two orthogonal slots.

The input impedance of the element under different test conditions is shown in Figure 3-6. As noted, with the isolated port of the 90 degree hybrid terminated in 50 ohms, the input VSWR is within 1.5:1 over the frequency of interest.

Radiation patterns of the experimental model were taken both with and without a 40 X 50 inch ground plane. These patterns are shown in Figures 3-7 thru 3-9. For the experimental model, the patterns are considered to be reasonably good, with axial ratio and gain being within expected limits. The measured gain is approximately 3.8 db with no ground plane, and 2.2 db with a 40 X 50 inch ground plane. It should be noted that the losses of the feed network used for the gain test were around 1.2 db.

### 3.3.2 Breadboard Model Development

During the early stages of the breadboard design, the antenna element was fabricated in two separate sub-assemblies to facilitate testing. That is, the radiator consisting of a top crossed-slot board and a bottom feed line board (Figure 3-10) became one sub-assembly. The hybrid feed network board (Figure 3-11), and its associated ground plane board, was the other sub-assembly. Each sub-assembly had RF Connectors attached to its signal ports. The radiator sub-assembly had four connectors, and the hybrid feed sub-assembly had six connectors. With this arrangement, each sub-assembly could be tested individually and the data analyzed as a separate entity. In addition, the two sub-assemblies could be connected together by means of connector adapters or very short sections of semi-rigid coax. This allowed the element to be tested as an integrated unit. Typical test data of the hybrid feed network subassembly is shown in Table 3-3. The results showed that reasonable good performance was achieved; however, the unbalance in amplitude and phase between ports can be further improved.

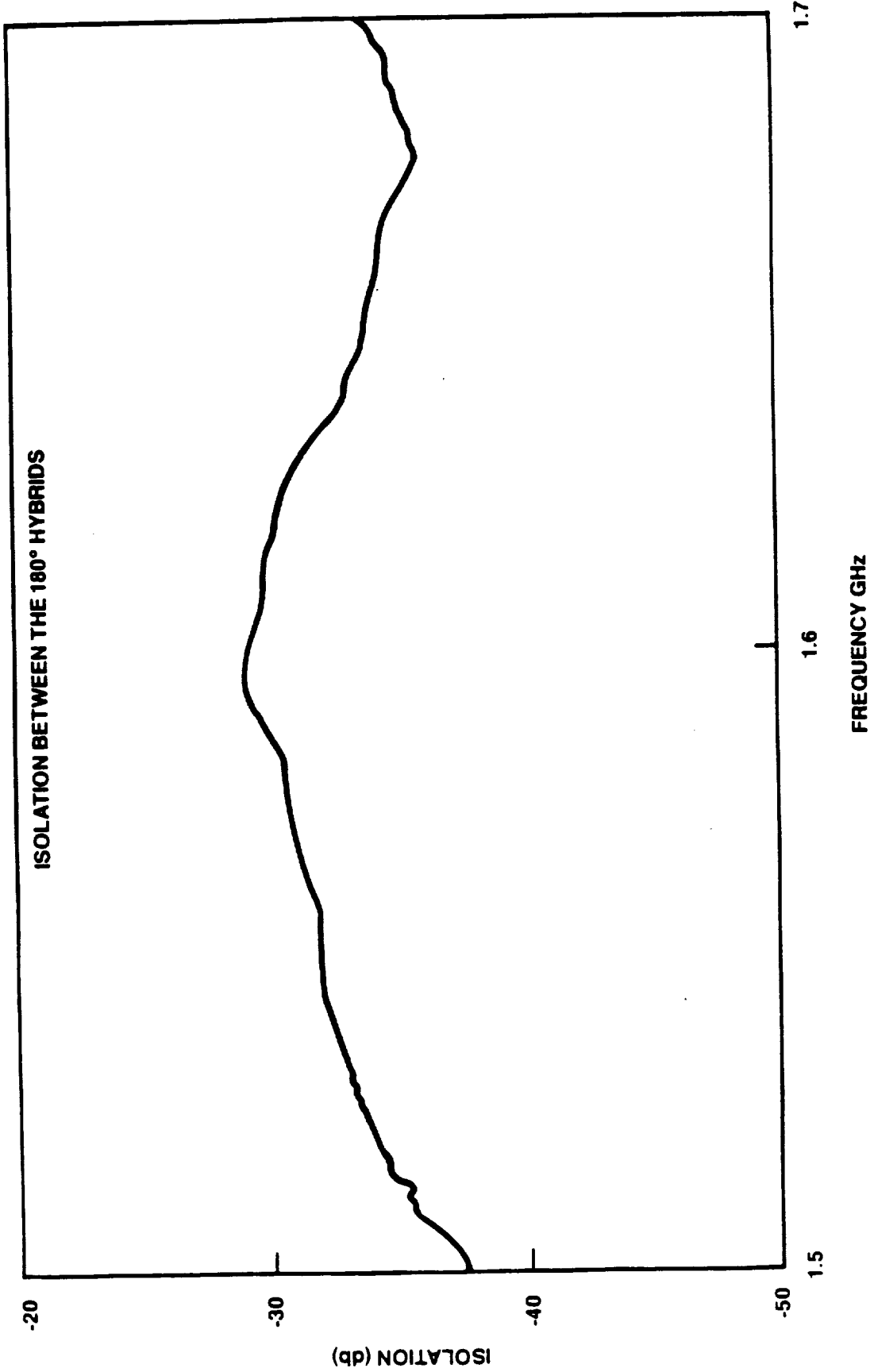
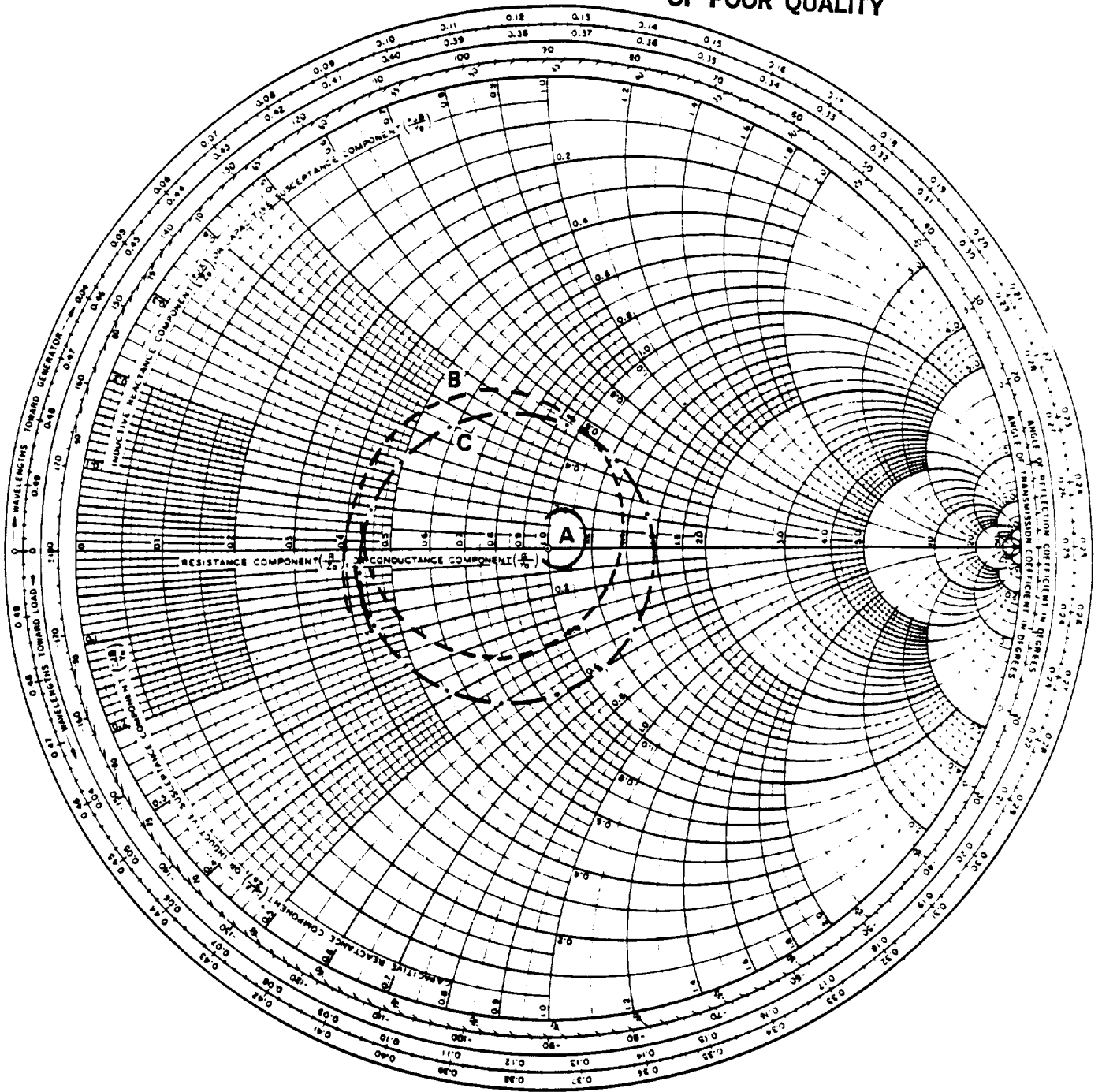


Figure 3-5. Isolation Between Ports of Crossed-Slot Model P

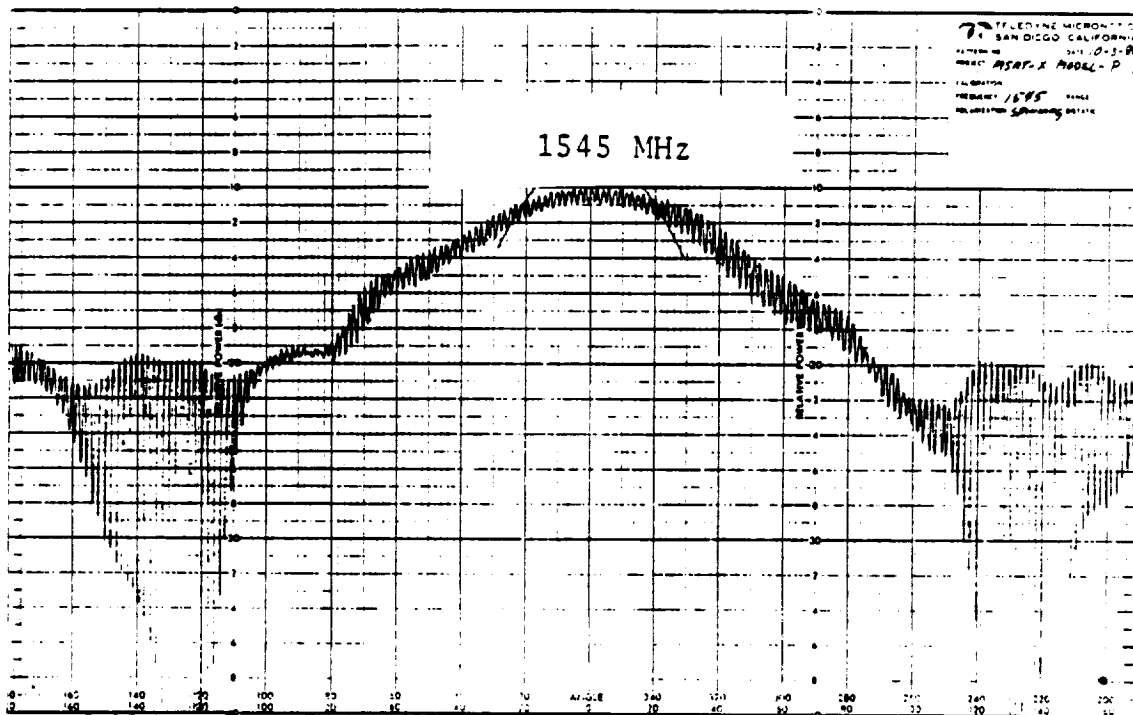
ORIGINAL PAGE IS  
OF POOR QUALITY



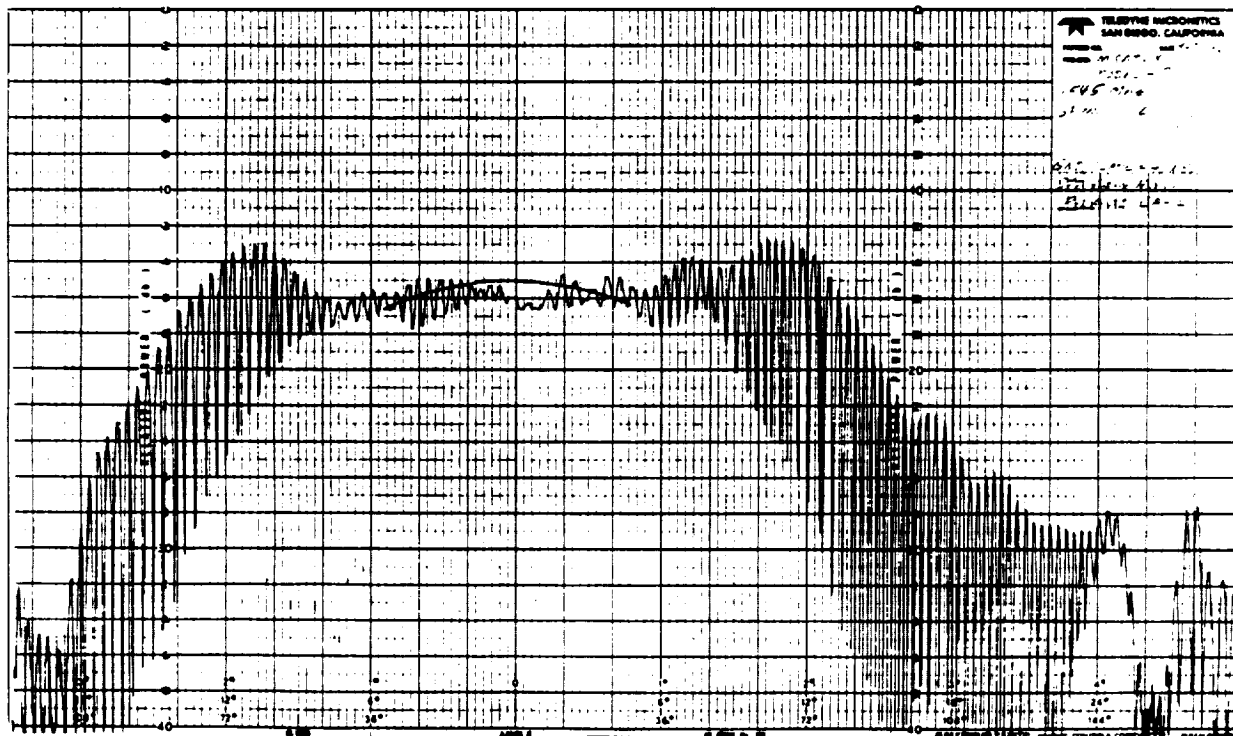
**LEGEND**

<b>A</b>	<b>WITH:</b>	<b>2-180° HYBRIDS</b>	<b>B</b>	<b>PORTS 1 &amp; 3 +</b>	<b>C</b>	<b>PORTS 2 &amp; 4 +</b>
<u>          </u>		<b>&amp; 1-90° HYBRID</b>	<u>          </u>	<b>180° HYBRID</b>	<u>          </u>	<b>180° HYBRID</b>

Figure 3-6. Measured Impedance Plot for Crossed-Slot Model-P



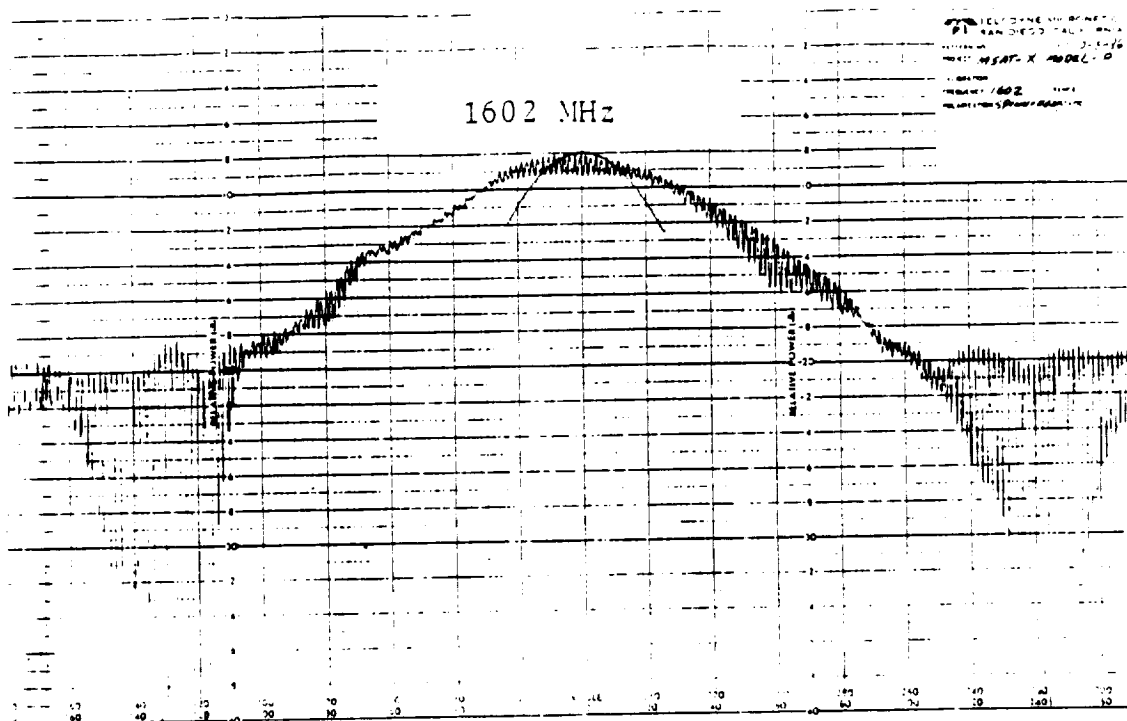
(A) W/O 40" X 50" GROUND PLANE



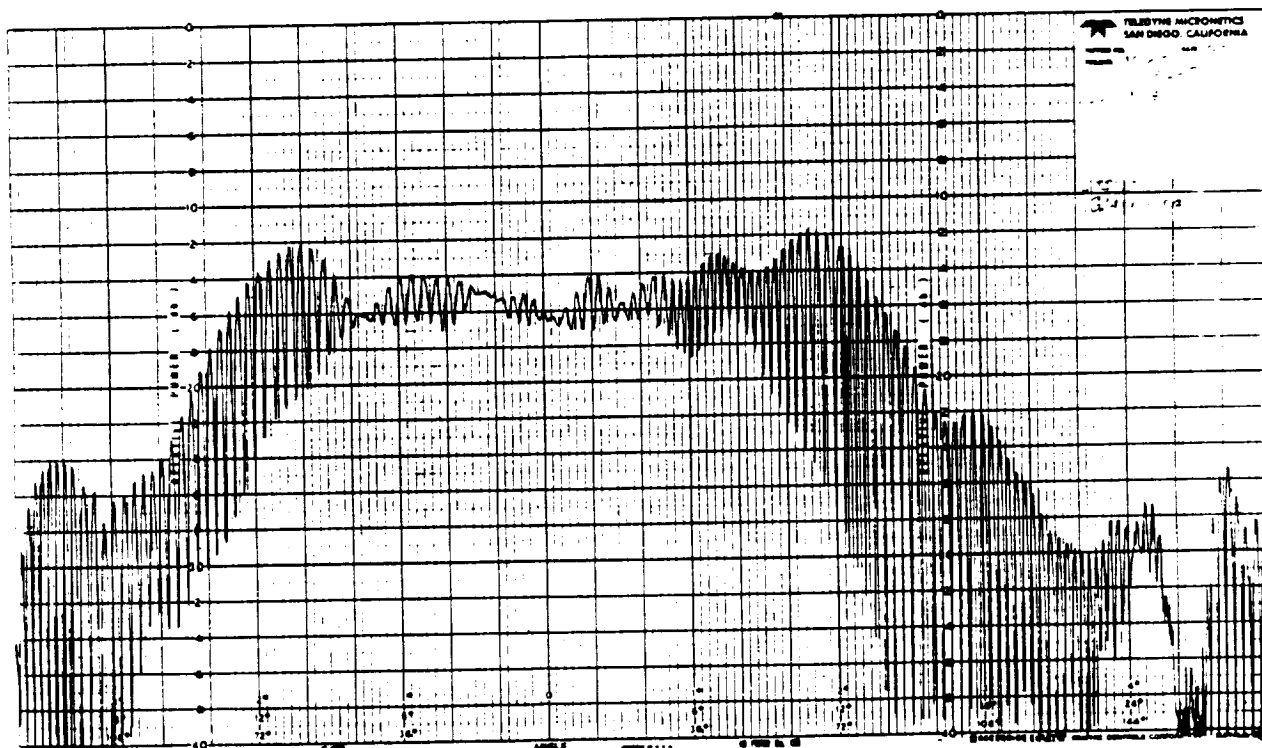
(B) W/40" X 50" GROUND PLANE

Figure 3-7. Spinning Linear Pattern at 1545 MHz

ORIGINAL PAGE IS  
OF POOR QUALITY

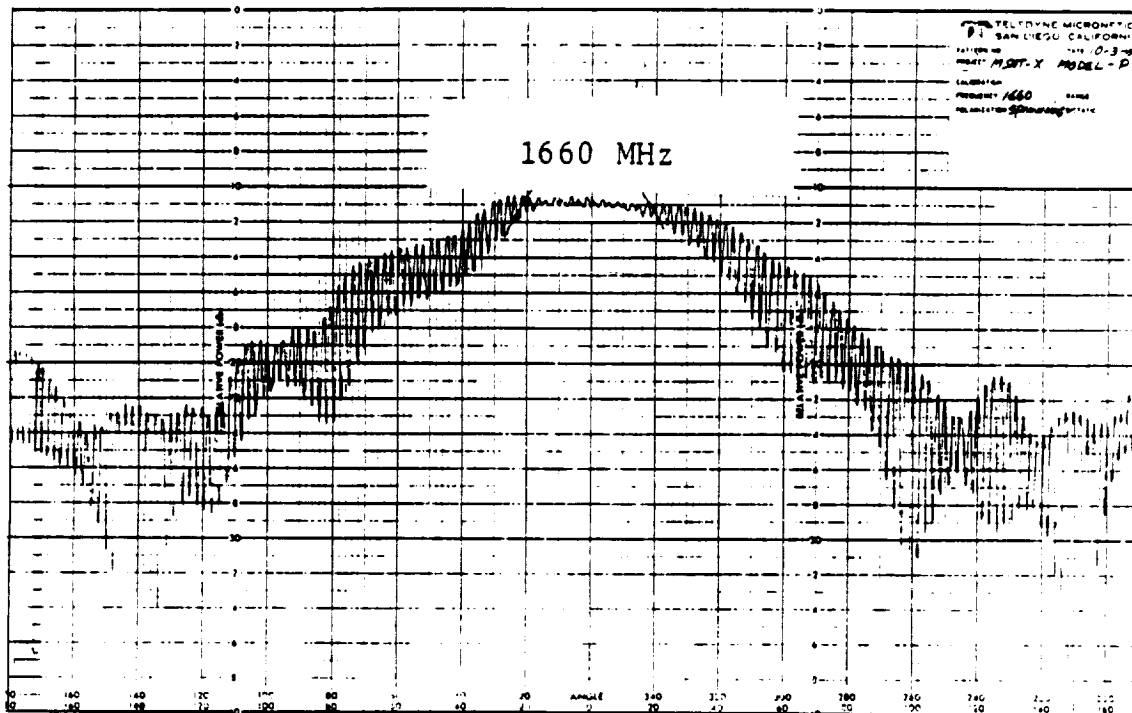


(A) W/O 40" X 50" GROUND PLANE

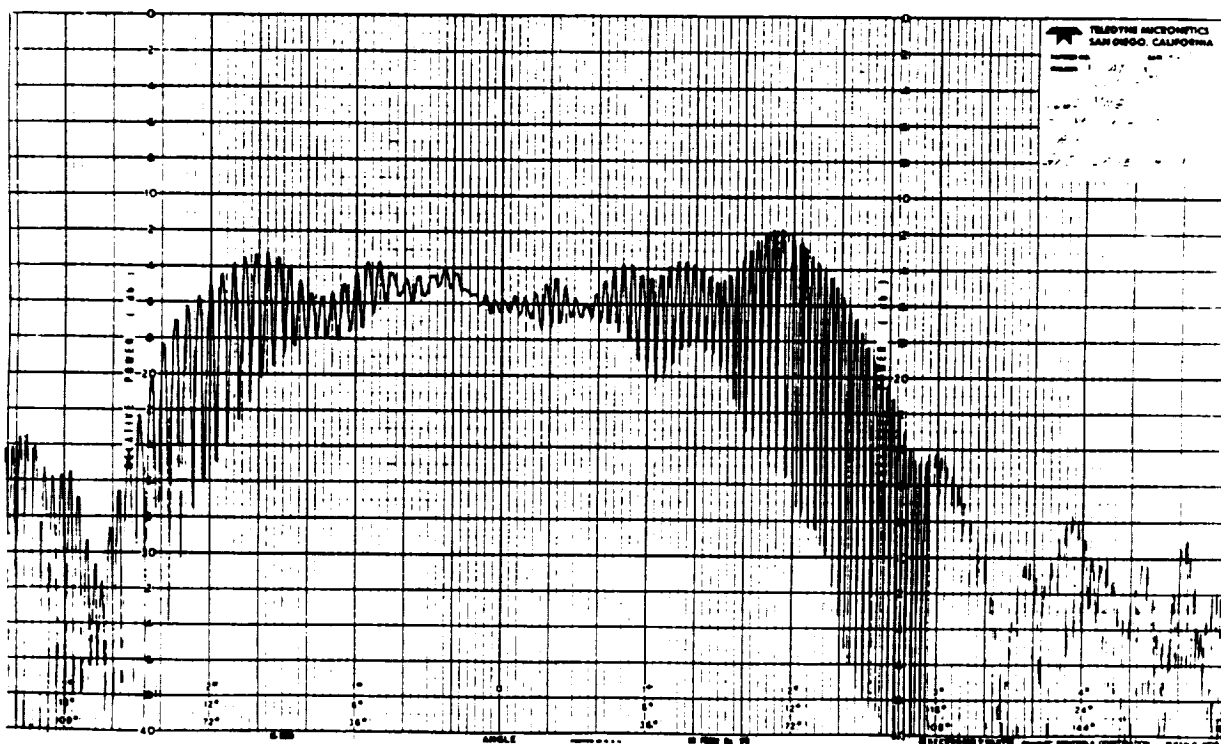


(B) W/40" X 50" GROUND PLANE

Figure 3-8. Spinning Linear Pattern at 1602 MHz



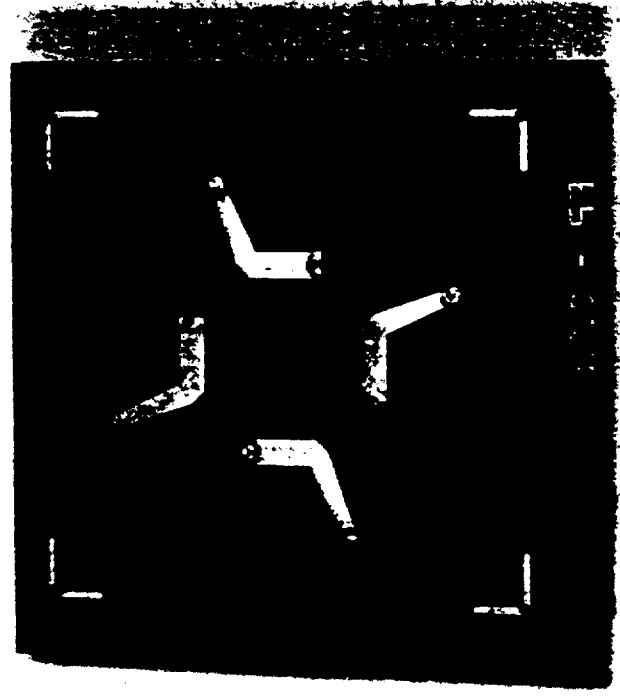
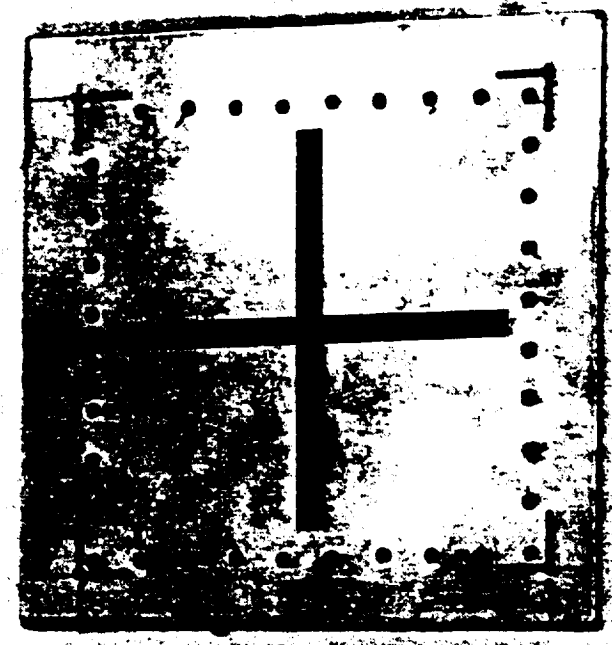
(A) W/O 40" X 50" GROUND PLANE



(B) W/40" X 50" GROUND PLANE

Figure 3-9. Spinning Linear Pattern at 1660 MHz

ORIGINAL PAGE IS  
OF POOR QUALITY

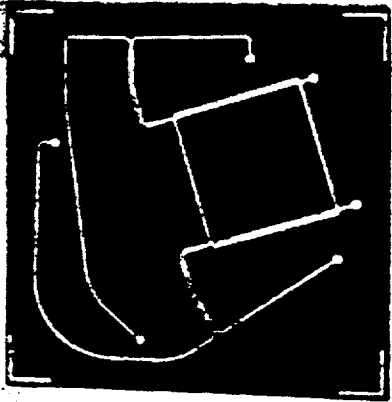
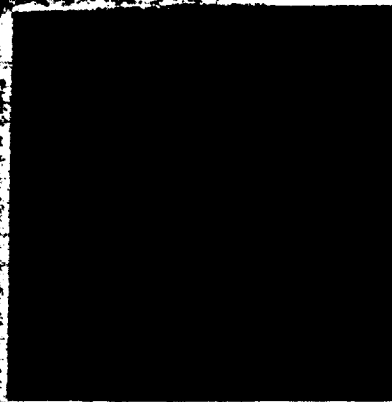
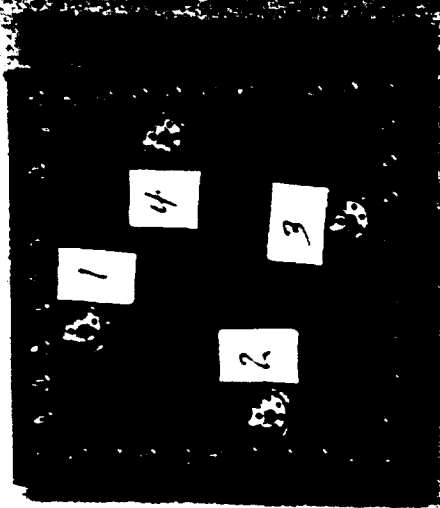


TELEDYNE RYAN ELECTRONICS

TELEDYNE RYAN ELECTRONICS

TELEDYNE RYAN ELECTRONICS

Figure 3-10. Breadboard Crossed-Slot Element



TELEDYNE RYAN ELECTRONICS

TELEDYNE RYAN ELECTRONICS

TELEDYNE RYAN ELECTRONICS

Figure 3-11. Hybrid Feed Network for Circular Polarization

ORIGINAL PAGE IS OF POOR QUALITY

Table 3-3. Measured Hybrid Network Performance

Test Data Summary - Frequency (MHz)			
Parameter	1545	1603	1660
INPUT VSWR	1.15	1.16	1.26
PORT-1 $S_{21}$ -DB	6.53	6.64	6.69
PORT-2 $S_{21}$ -DB	6.05	5.89	5.90
PORT-3 $S_{21}$ -DB	6.68	6.52	6.79
PORT-4 $S_{21}$ -DB	5.90	5.70	5.79
UNBAL 1-3-DB	0.16	0.12	0.10
UNBAL 2-4-DB	0.15	0.19	0.18
1-3 (180°)	186	184	179
2-4 (180°)	175	174	180
1-2 (90°)	91	93	94
3-4 (90°)	87	87	84
1-4 (90°)	89	92	93
2-3 (90°)	95	88	94

To implement the feed network for the crossed-slot element into a completely integrated structure, two types of feed circuits were designed. Type-1, as shown in Figure 3-12, consists of a 90 degree branch line hybrid with two 180 degree corporate feeds to drive the four feed points, and provide the 0-90-180-270 degree phase sequence. Type-2, shown in Figure 3-13, also has a 90 degree branch line hybrid. Instead of the 180 degree reactive power divider, however, two 180 degree Wilkinson type power dividers are utilized. The advantage of this design is that the Wilkinson Power Dividers provide isolation (on the order of 20 db) between the feed points at opposite ends of the same slot. This could be very beneficial for wide angle scanning. However, it is more difficult to implement Wilkinson power dividers in stripline form, since for proper operation, isolation resistors are required at locations A and B of Figure 3-11. As a result, there would be an impact on both material and fabrication cost. Also, because of the more complex circuitry, the overall network would have a higher insertion loss. In view of this, it was decided to use the Type-1 feed network for the final design.

The integrated unit of the crossed-slot consists of four boards - a top crossed-slot board, a stripline excitation feeder board, a hybrid/corporate feed network board, and a bottom ground plane board. The top layer of crossed slot elements is etched on a single sided,

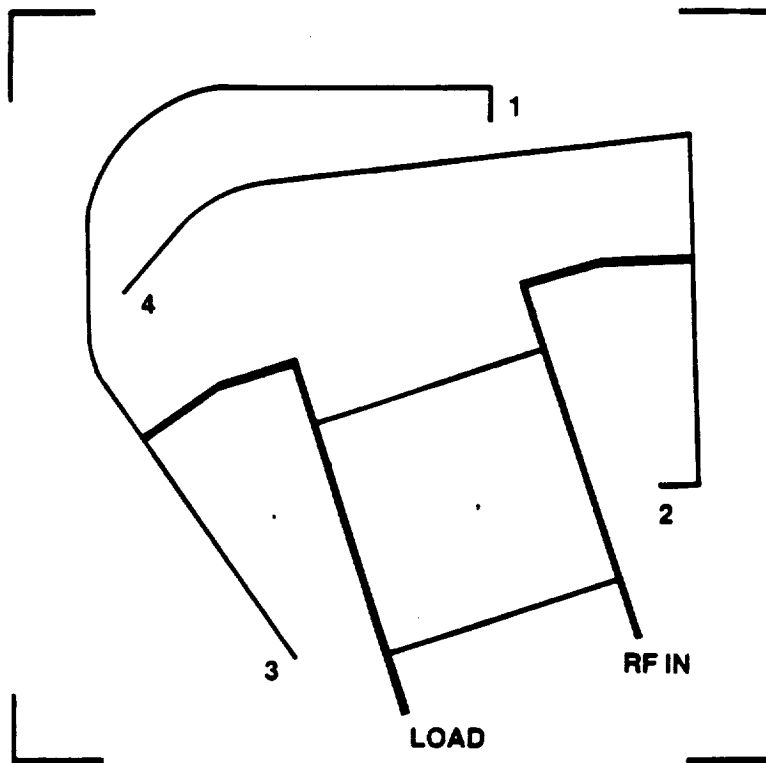


Figure 3-12. 90 Degree Branch Line Hybrid with Two 180 Degree Corporate Feed Circuit

copper clad teflon fiberglass board. The thicknesses of the boards are 0.09 inches and 0.125 inches for breadboard units #1 and #2. The thicker board was used for unit #2 to increase the antenna's bandwidth. The next layer is the crossed slot excitation feeders which are etched on another copper clad teflon fiberglass board having the same thickness as the slotted board. A set of plated through holes around the crossed slots is required to form the cavity wall for the crossed slot element. The bottom two layers of the antenna have thicknesses of 0.031 inch each and constitute the stripline hybrid/corporate feed network boards used to form the required right hand circular polarization pattern. These four boards were held together with the 0.125 inch stiffener aluminum plate by means of brass screws inserted through the plated cavity holes. RF connectors were attached to both the input and the isolated ports of the hybrid circuit, via the bottom ground plane board. The unit is now ready for testing.

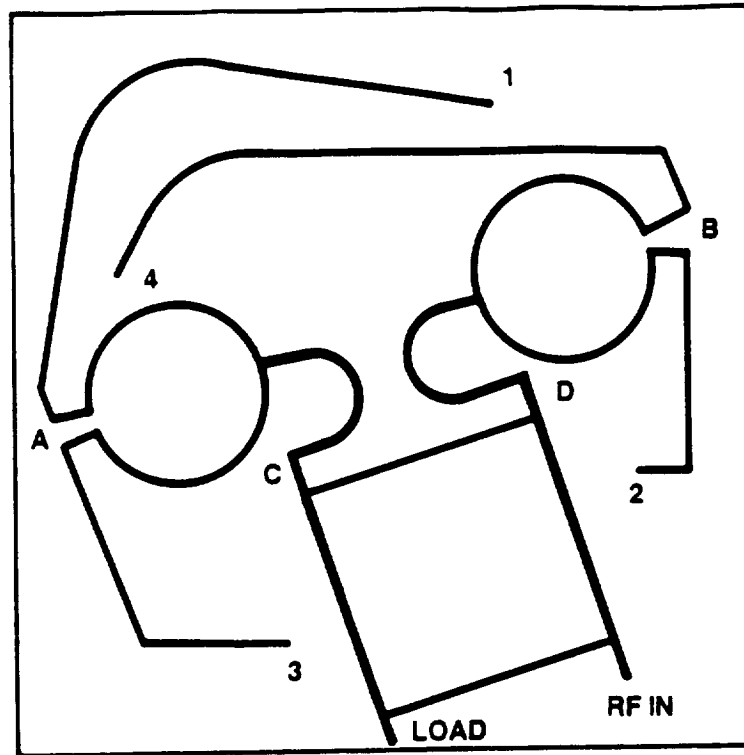


Figure 3-13. 90 Degree Branch Line Hybrid with Two 180 Degree Wilkinson Power Divider Feed Circuits

### 3.3.3 Measured Antenna Performance And Gain Analysis

The measured return losses for unit #1 and #2 elements are shown in Figures 3-14 and 3-15, respectively. The results show that a good input VSWR was achieved. However, one should be cautious at this point because these data still do not tell the whole story. The hybrid could mask the mismatch information at the four feeders through the load port of the branch line hybrid. As shown in Figures 3-16 and 3-17, poor isolation between the input port and the load port was measured. These data indicate that the impedance matching at the four feed points of the crossed-slot needs to be improved further. As can be seen from Figure 3-18, dissipation losses at the load port of the unit #2 crossed-slot are 1.05 dB and 1.25 dB at frequencies 1545 MHz and 1660 MHz, respectively. This loss must be reduced to improve the antenna gain. It is noted from Figures 3-16 and 3-17 that the thicker material used in the second unit has increased the antenna bandwidth. The measured RHCP patterns of the unit #2 crossed-slot along two principal cuts are shown in Figures 3-19 to 3-22. The measured beamwidth is 140 degrees. The measured element gain (average) of the unit #2 crossed-slot at 20 degrees elevation angle (above the horizon) are -0.1 dBic and -0.8 dBic for frequencies of 1545 MHz and 1660 MHz, respectively, as shown in Figures 3-23 and 3-24. Note that the element gain of unit #2 is 0.5 dB better than that of unit #1.

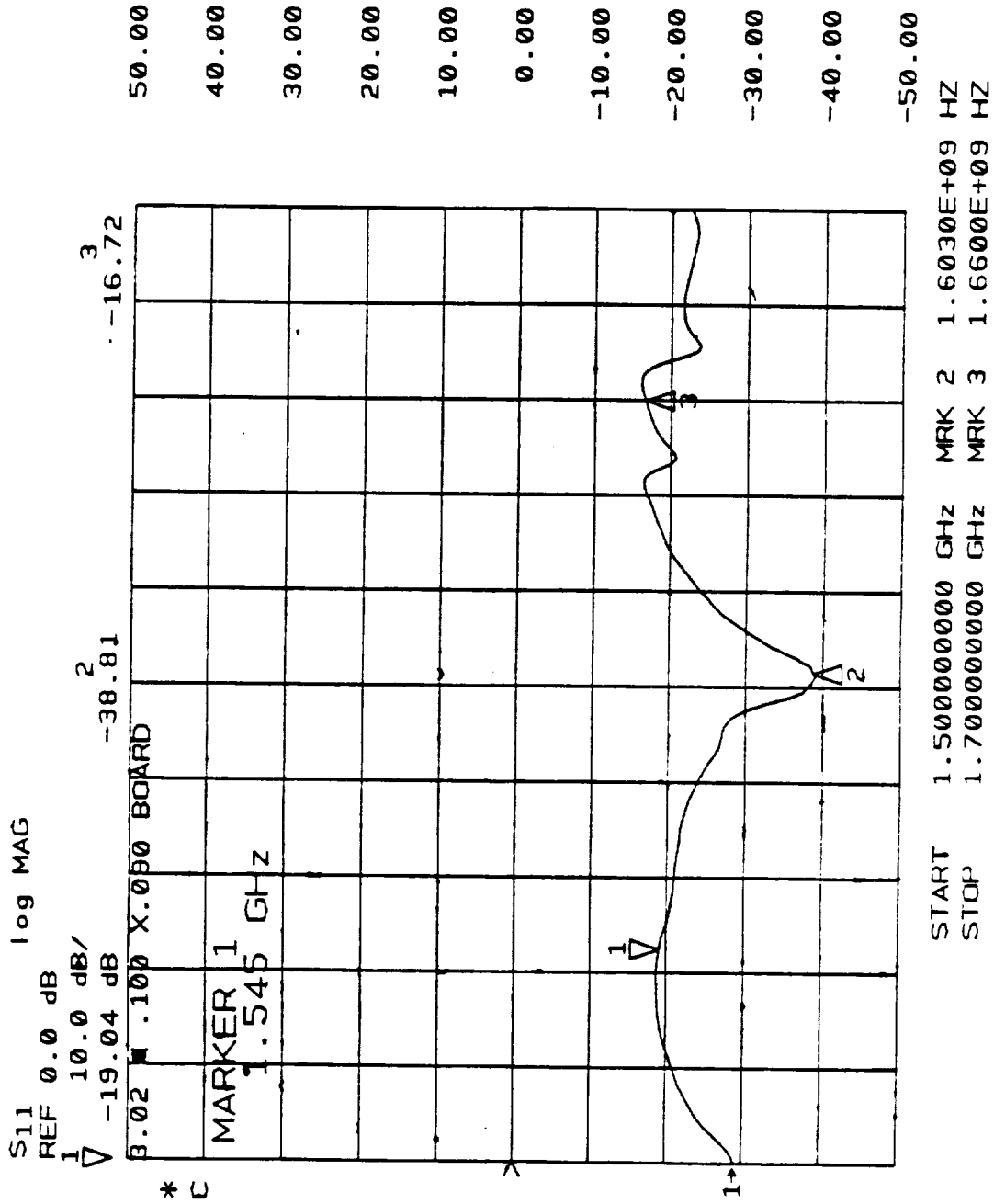


Figure 3-14. Measured Return Loss of Unit #1 Crossed-slot Element

6 NOV 1987  
16:35:26

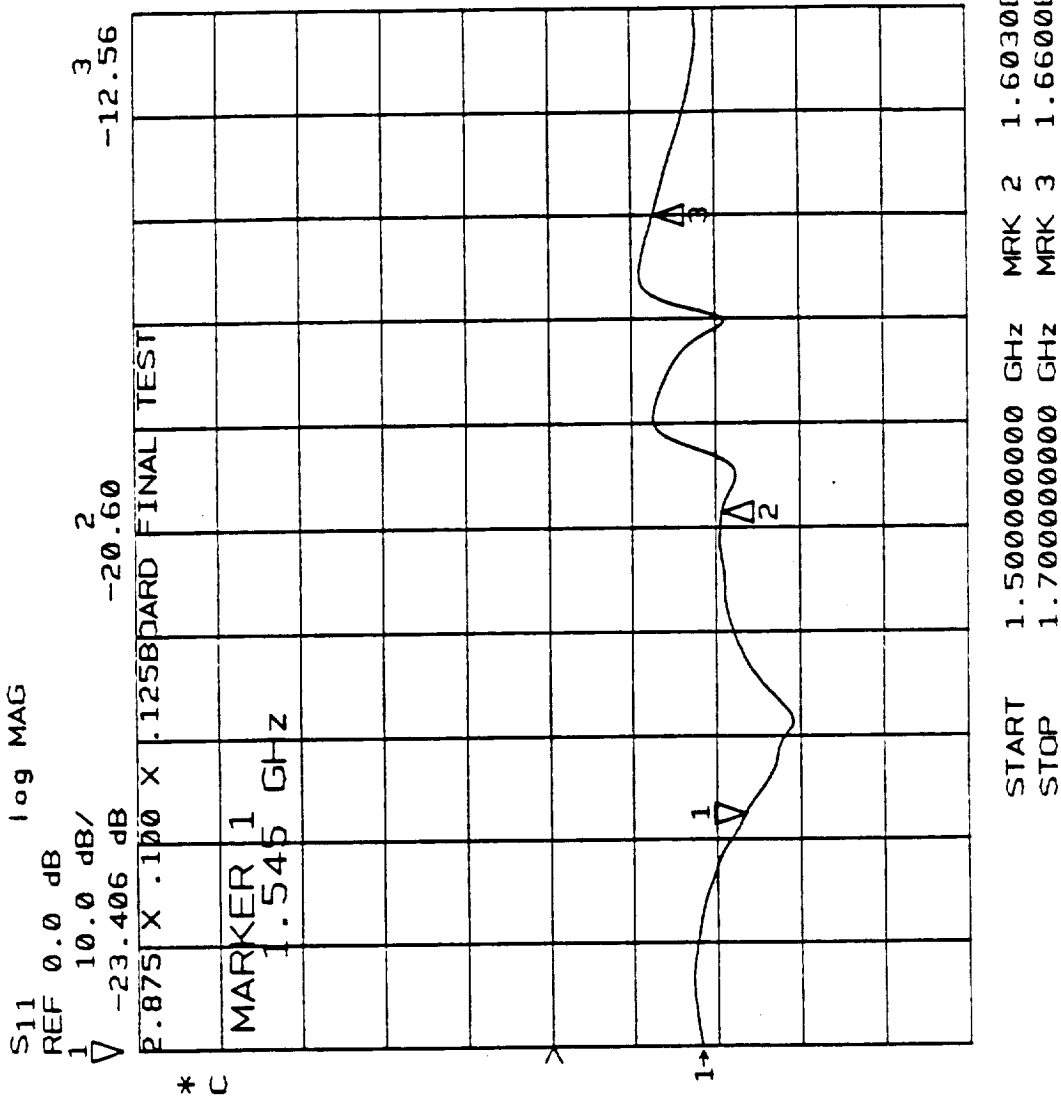


Figure 3-15. Measured Return Loss of the Unit #2 Crossed-slot Element

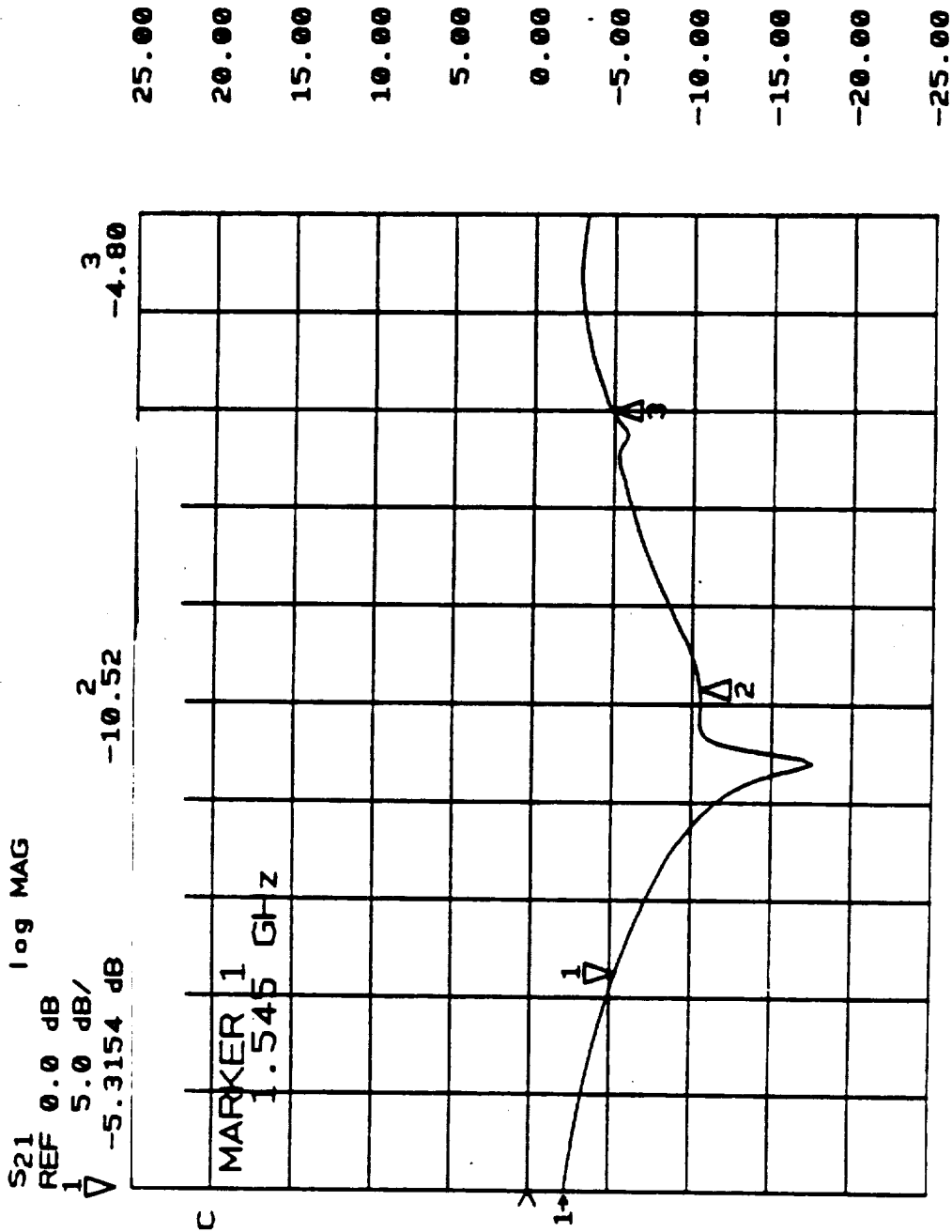


Figure 3-16. Measured Isolation between the Input and the Load Port of the Unit #1 Crossed-slot Element

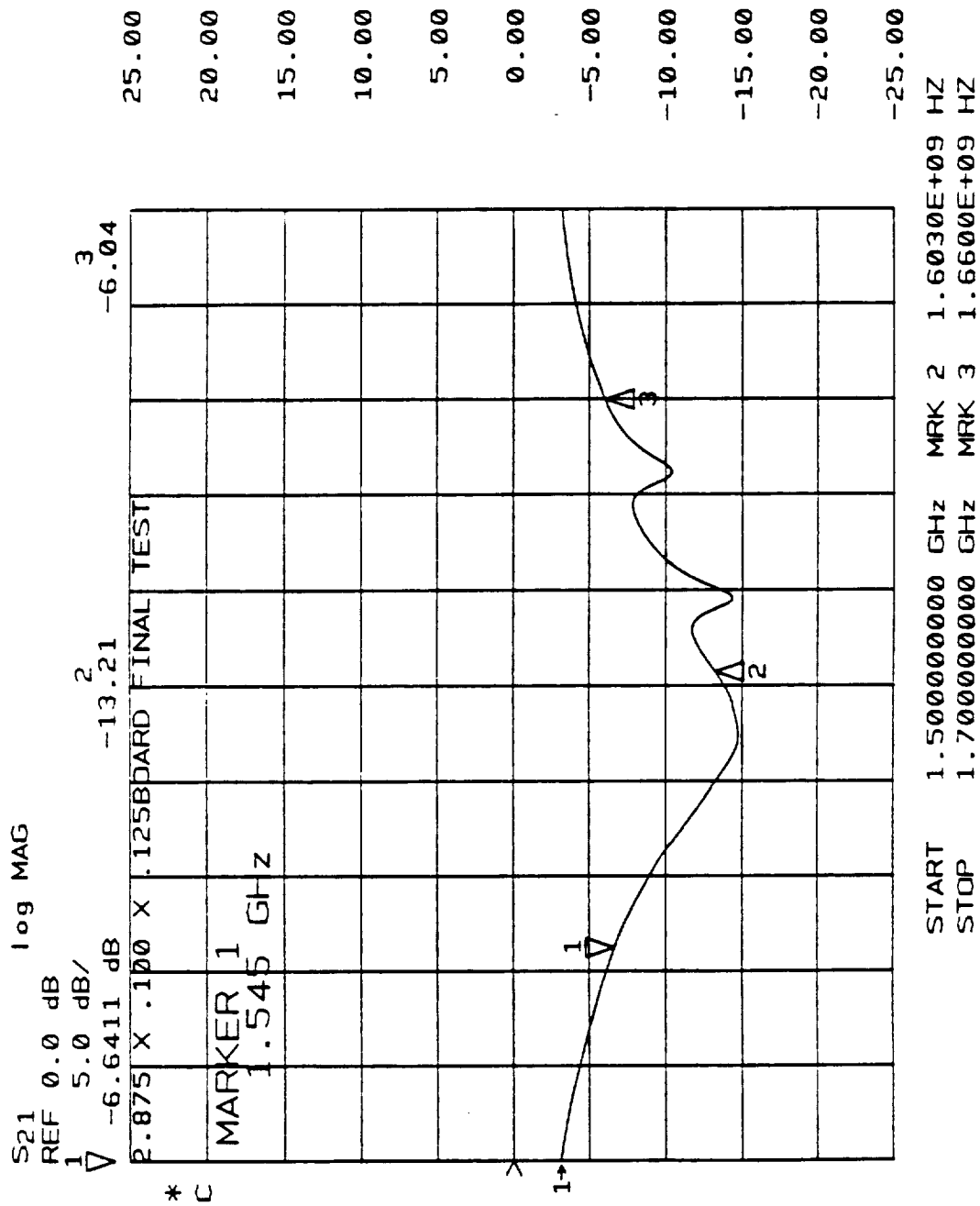


Figure 3-17. Measured Isolation Between the Input and the Load Port of the Unit #2 Crossed-slot Element

# ELEMENT GAIN REDUCTION VS LOAD PORT ISOLATION

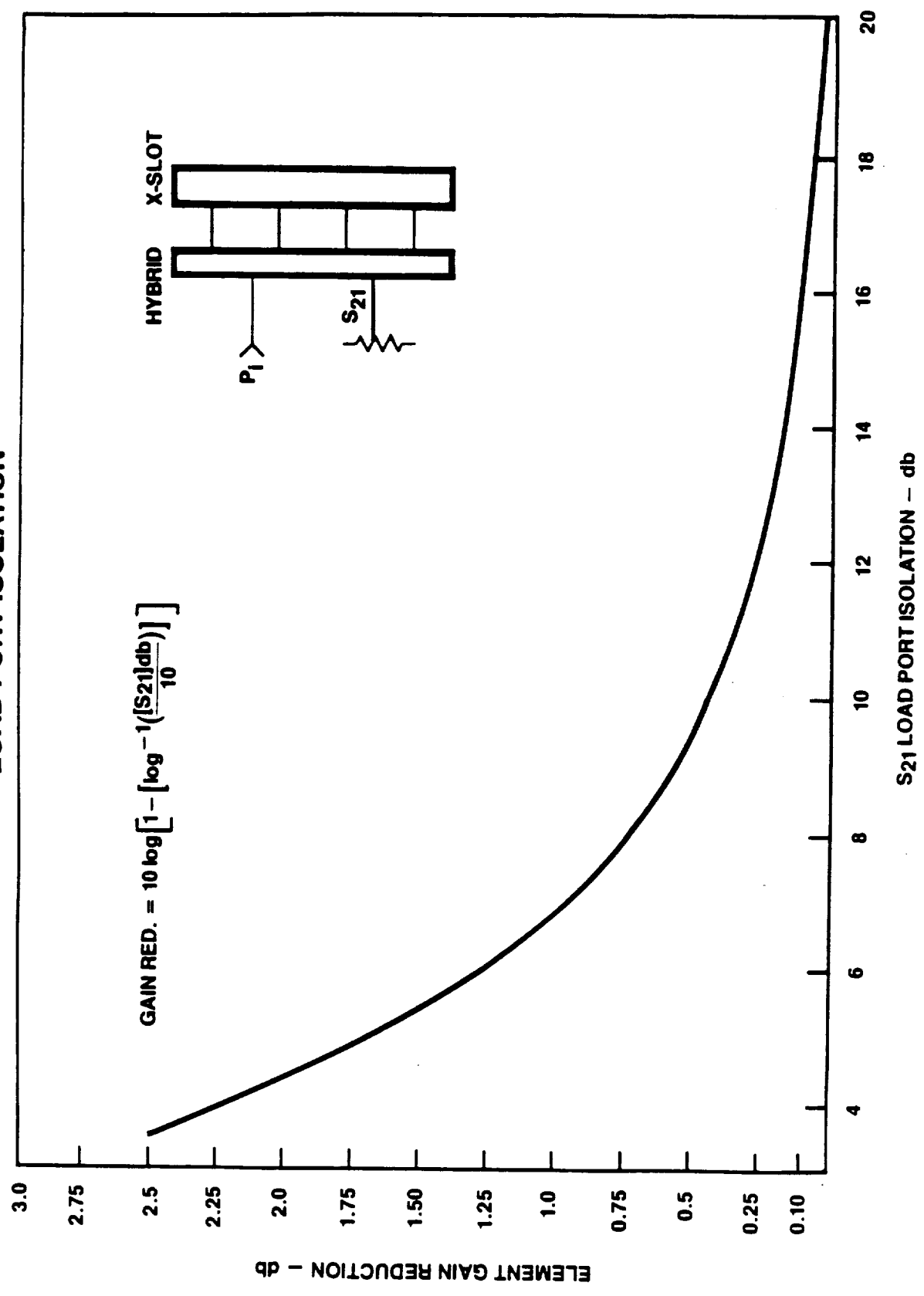


Figure 3-18. Element Gain Reduction versus Load Port Isolation

ORIGINAL PAGE 16  
OF POOR QUALITY

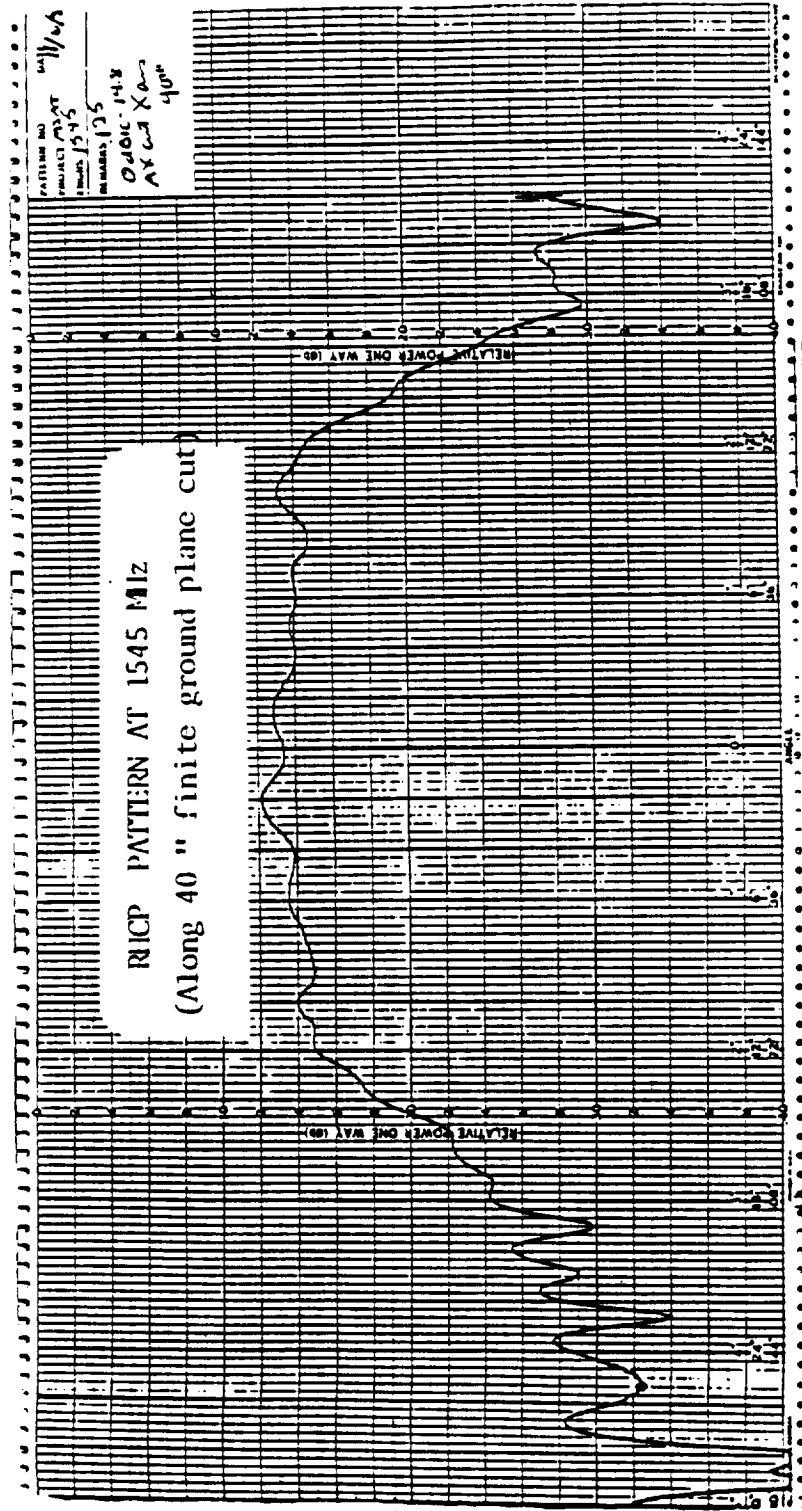


Figure 3-19. Measured RHCP Elevation Pattern of the Unit #2 Crossed-slot Along the 40" Ground Plane Cut at 1545 MHz.  
Note: Antenna was mounted on the center of a 40" x 50" finite ground plane.

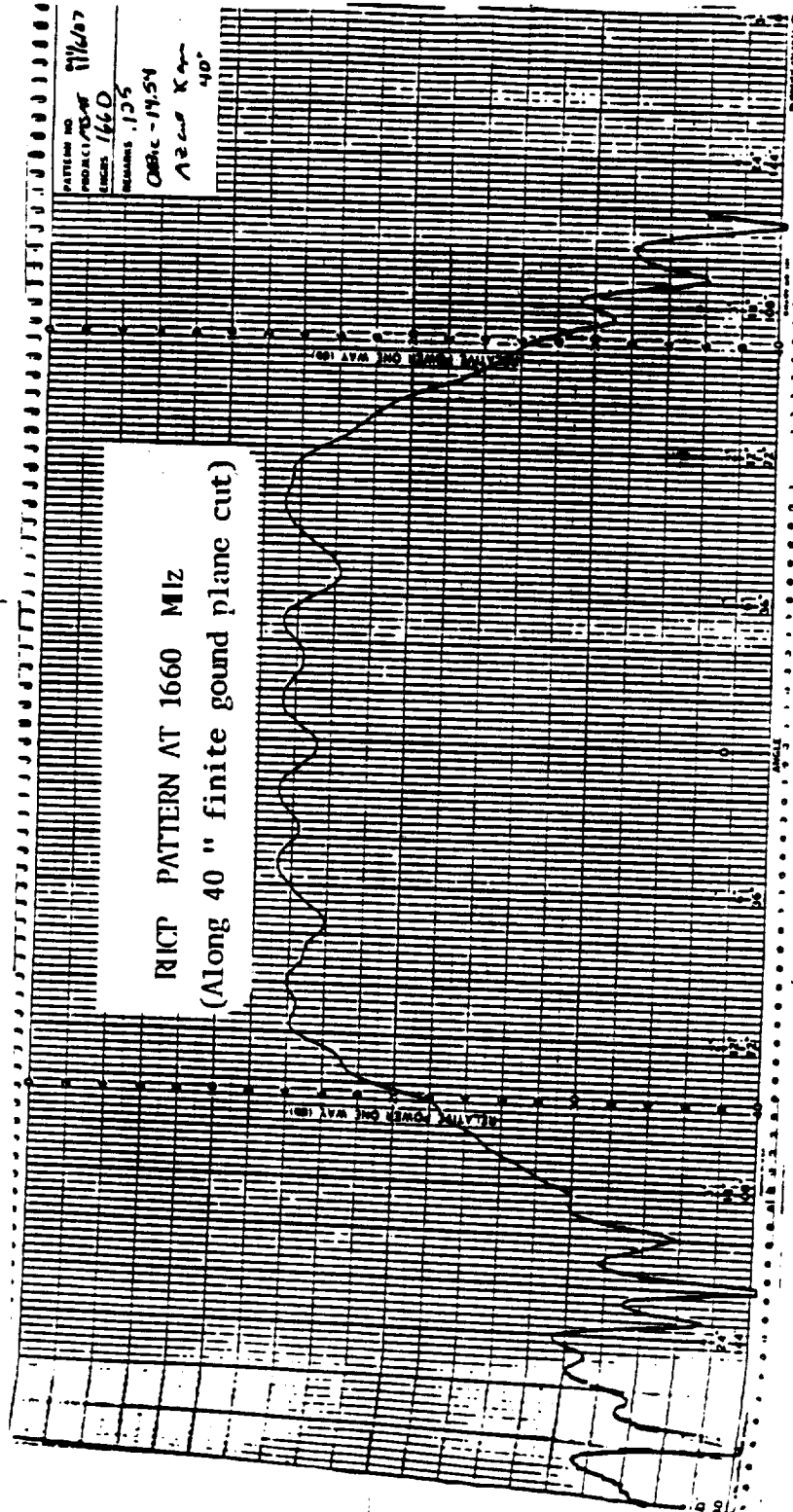


Figure 3-20. Measured RHCP Elevation Pattern of the Unit #2 Crossed-slot Along the 40° Ground Plane Cut at 1660 MHz.  
 Note: Antenna was mounted on the center of a 40" x 50" finite ground plane.

ORIGINAL PAGE IS  
OF POOR QUALITY

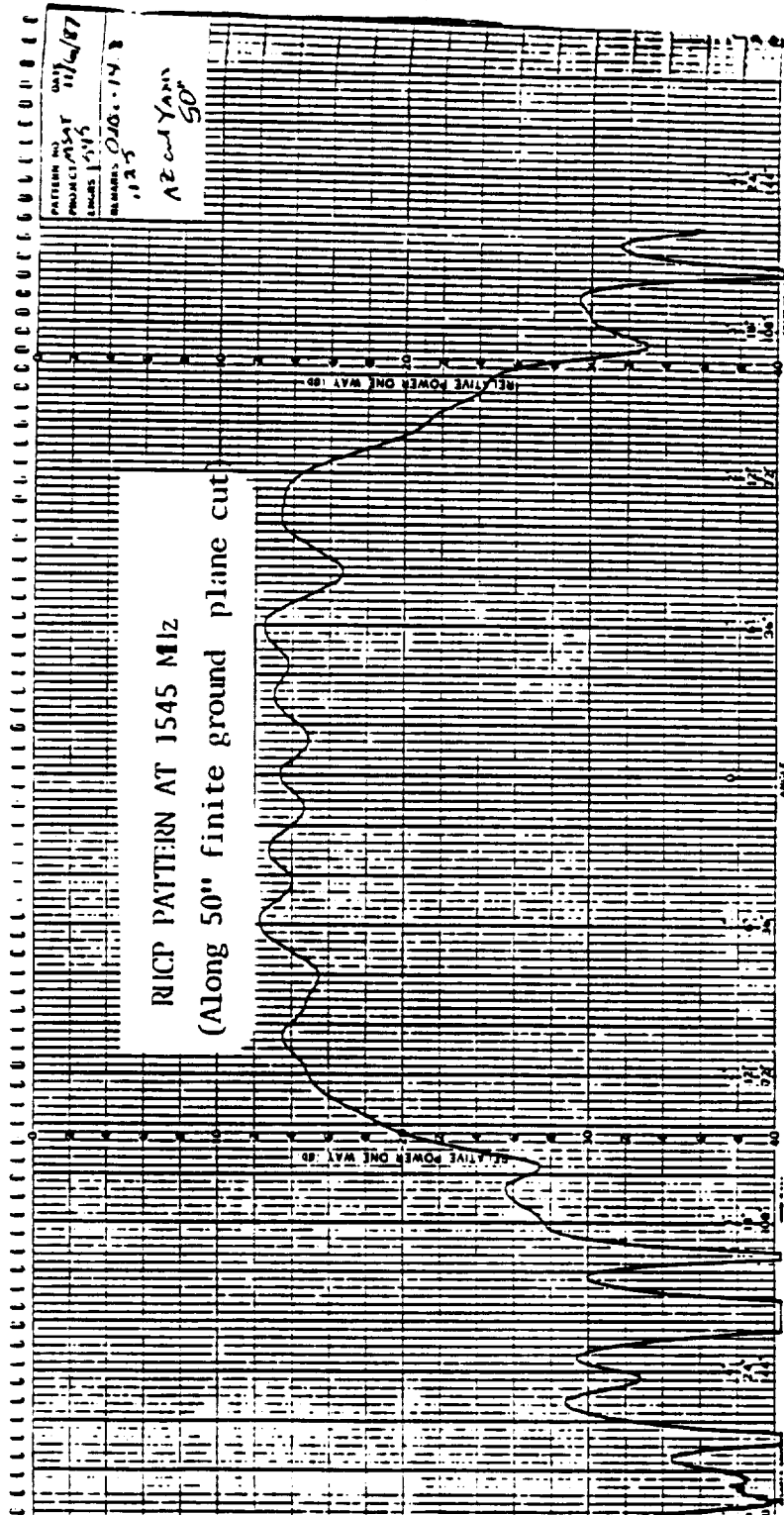


Figure 3-21. Measured RHCP Elevation Pattern of the Unit #2 Crossed-slot Along the 50" Ground Plane Cut at 1545 MHz.  
Note: Antenna was mounted on the center of a 40" x 50" finite ground plane.

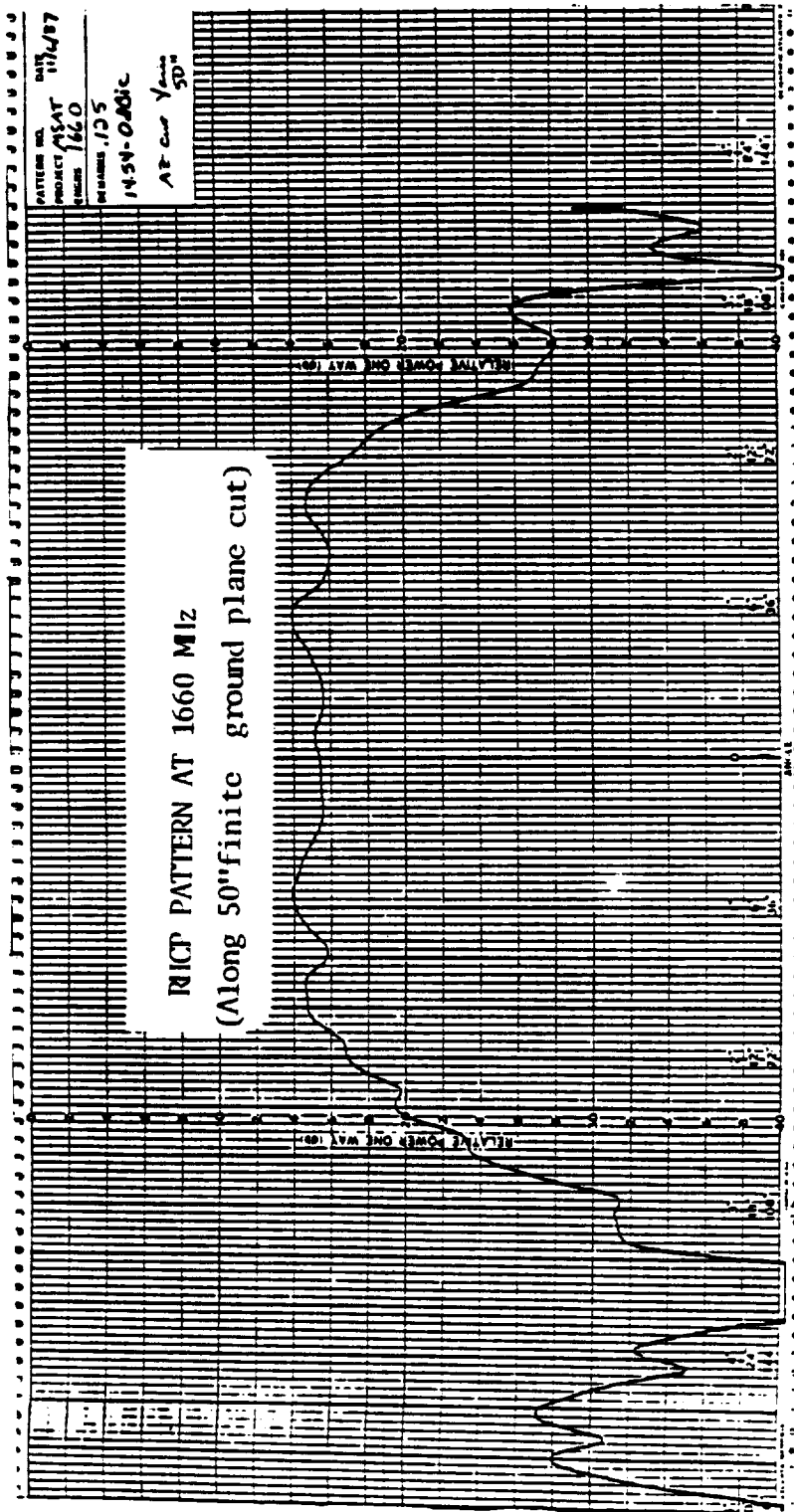
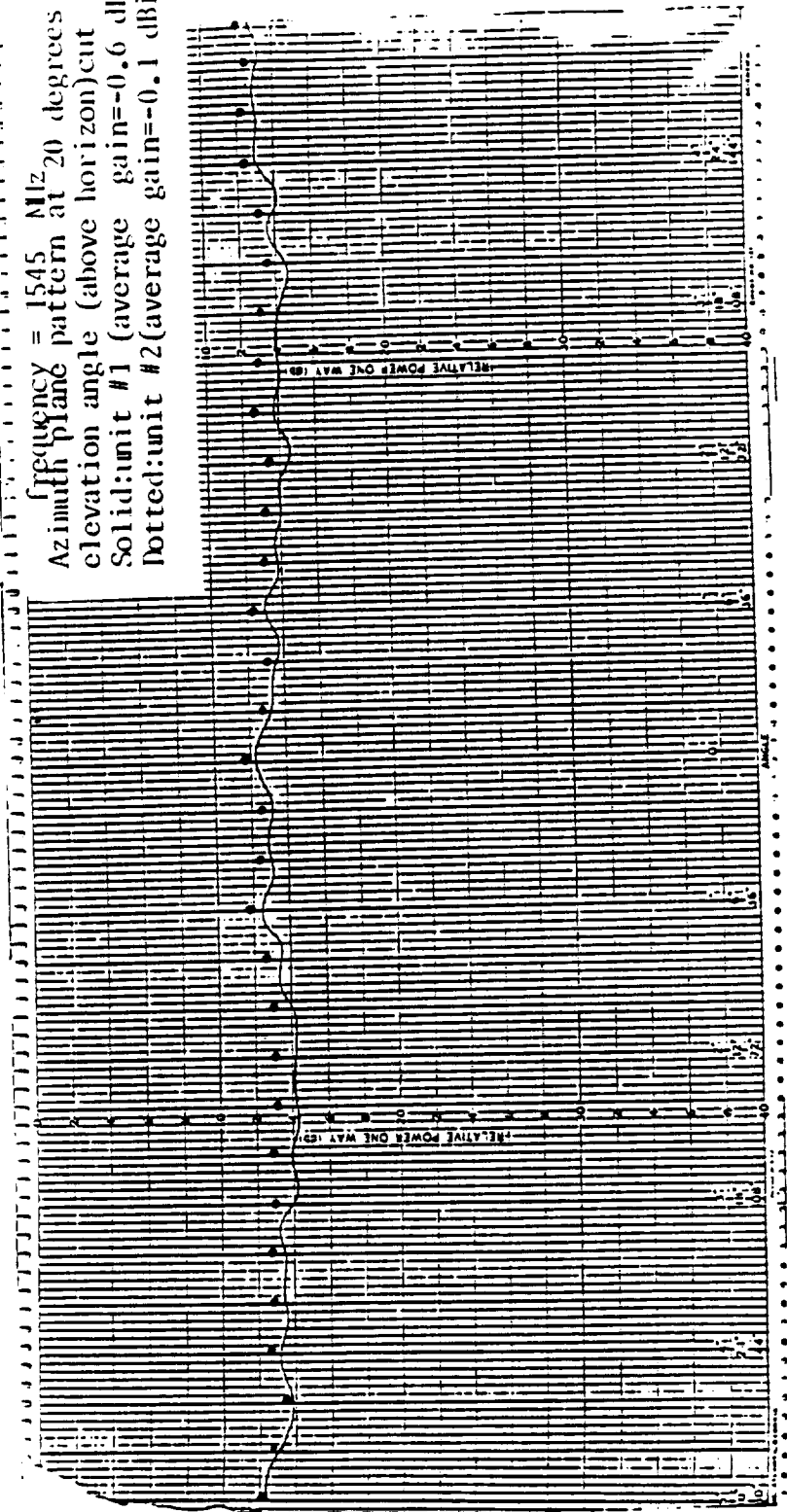


Figure 3-22. Measured RHCP Elevation Pattern of the Unit #2 Crossed-slot Along the 50" Ground Plane Cut at 1660 MHz.

Note: Antenna was mounted on the center of a 40" x 50" finite ground plane.

ORIGINAL PAGE IS  
OF POOR QUALITY

frequency = 1545 MHz  
Azimuth plane pattern at 20 degrees  
elevation angle (above horizon) cut  
Solid: unit #1 (average gain=-0.6 dBic)  
Dotted: unit #2 (average gain=-0.1 dBic)



ORIGINAL PAGES  
OF POOR QUALITY

Figure 3-23. Measured RHCP Azimuth Pattern at 20 Degrees Elevation Angle (Above Horizon), at frequency of 1545 MHz

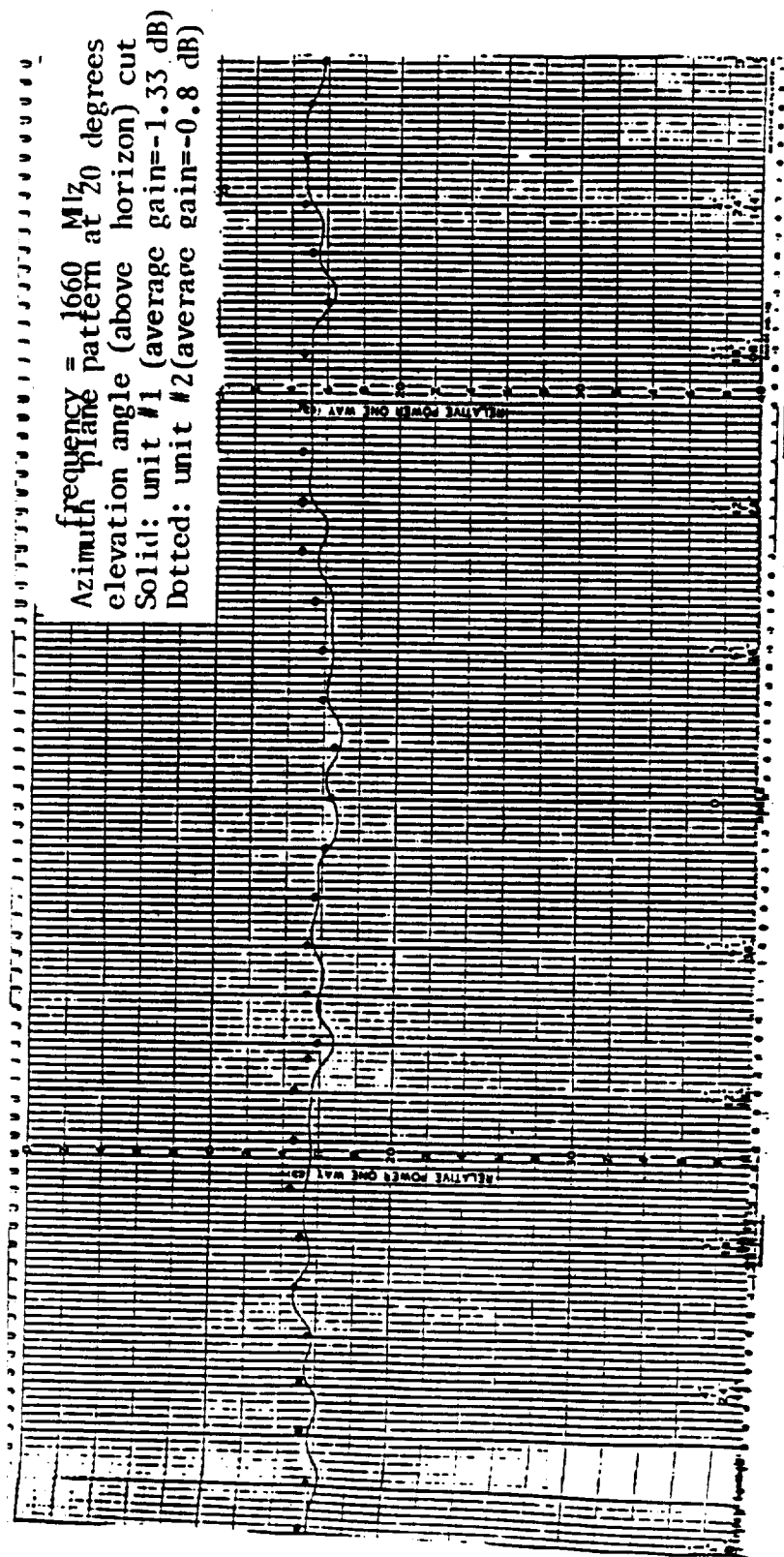


Figure 3-24. Measured RHCP Azimuth Pattern at 20 Degrees Elevation Angle (Above Horizon), at frequency of 1660 MHz

ORIGINAL PAGE IS  
 OF POOR QUALITY

In order to improve the element gain, the loss budget and gain analysis was analyzed and summarized in Table 3-4. The loss budget shows that (1) the dissipation loss at the isolation port of the hybrid, and (2) the radiation efficiency loss must be reduced. The dissipation loss at the isolation port of the hybrid is mainly due to mismatch at the four excitation feeders of the crossed slot, hence efforts to optimize the antenna matching is required for future work. Possible gain improvement on this loss is estimated to be 0.6 dB and 0.8 dB for frequencies of 1545 MHz and 1660 MHz, respectively.

Table 3-4. Element Gain Analysis

Directivity (dB)	Frequency (MHz)		Remarks
	1545	1660	
Loss Budget:			
Antenna Mismatch Loss (dB) at RF input port	-0.2	-0.2	
Hybrid loss	-0.25	-0.25	
Dissipation loss at hybrid load (dB)	-1.05	-1.25	Mismatch at the four feeders
Junction and radiation efficiency loss (dB)	-0.4	-1.0	Excitation feeder
Total Loss (dB)	-1.8	-2.7	
Gain at Peak	3.05	2.5	
Gain at 20 degrees elevation angle	-0.1	-0.8	

Proper excitation feeder design could be the key to improve the radiation efficiency of the crossed slot. The dog leg shape (bent stripline) of the excitation feeder in the current design is not desirable because it could generate additional higher order modes inside the cavity which in turn will degrade the radiation efficiency. Efforts to optimize the feed point of the stripline are also required to improve the radiation efficiency. Not that balanced cavity excitation requires four perfectly symmetrical probe feeds located at the four quadrants and along the diagonal of the crossed-slot. In addition, the bandwidth of the crossed-slot must be increased. A thicker cavity and the use of a flared shape slot to broaden the bandwidth are being pursued. Another area that will improve the gain performance of the array is to bond it together. The potentially uneven tightness of each

screw will generate higher order modes inside the crossed-slot and also degrade the stripline hybrid circuit performance. Possible gain improvement on the radiation efficiency is estimated to be around 0.4 dBic and 0.8 dBic for frequencies of 1545 MHz and 1660 MHz respectively.

### 3.3.4 Conclusions Derived from Breadboard Design Phase

As a result of the analysis of the test data obtained during the breadboard single element design phase, the following conclusions were made:

1. A stripline fed crossed-slot, using the four point feed method would be the radiating element used for the final design.
2. A 90 degree branch line hybrid with two 180 degree corporate feeds would be the network configuration used to feed the radiating element.
3. Optimization of the four excitation feeders in the cavity, would be pursued.
4. The bandwidth of the crossed-slot element must be improved.
5. The antenna should be bonded together.
6. Optimization of the hybrid feed network, with respect to amplitude and phase balance, would be undertaken.

### 3.4 BREADBOARD ARRAY ELEMENT DEVELOPMENT

Using the single element and feed network configuration established during the breadboard design phase, an experimental seven element array was fabricated (Figures 2-9 and 2-10) to investigate the mutual coupling effects on the individual antenna's performance under an array environment. The measured VSWR of the center element of the experimental array is shown in Figure 3-25. The data showed that the VSWR of the element was under 1.5:1. The analysis of the active scanning impedance (Section 2) showed that the mutual coupling effect was insignificant. The measured typical element patterns embedded in the array environment are shown in Figures 3-26. The measurement was taken on the center element, with the array mounted on a 40" x 50 " finite ground plane. The data showed that the element was well behaved. The data taken on the other elements in the array was very similar to that of the center element, signifying that the mutual coupling effect was small.

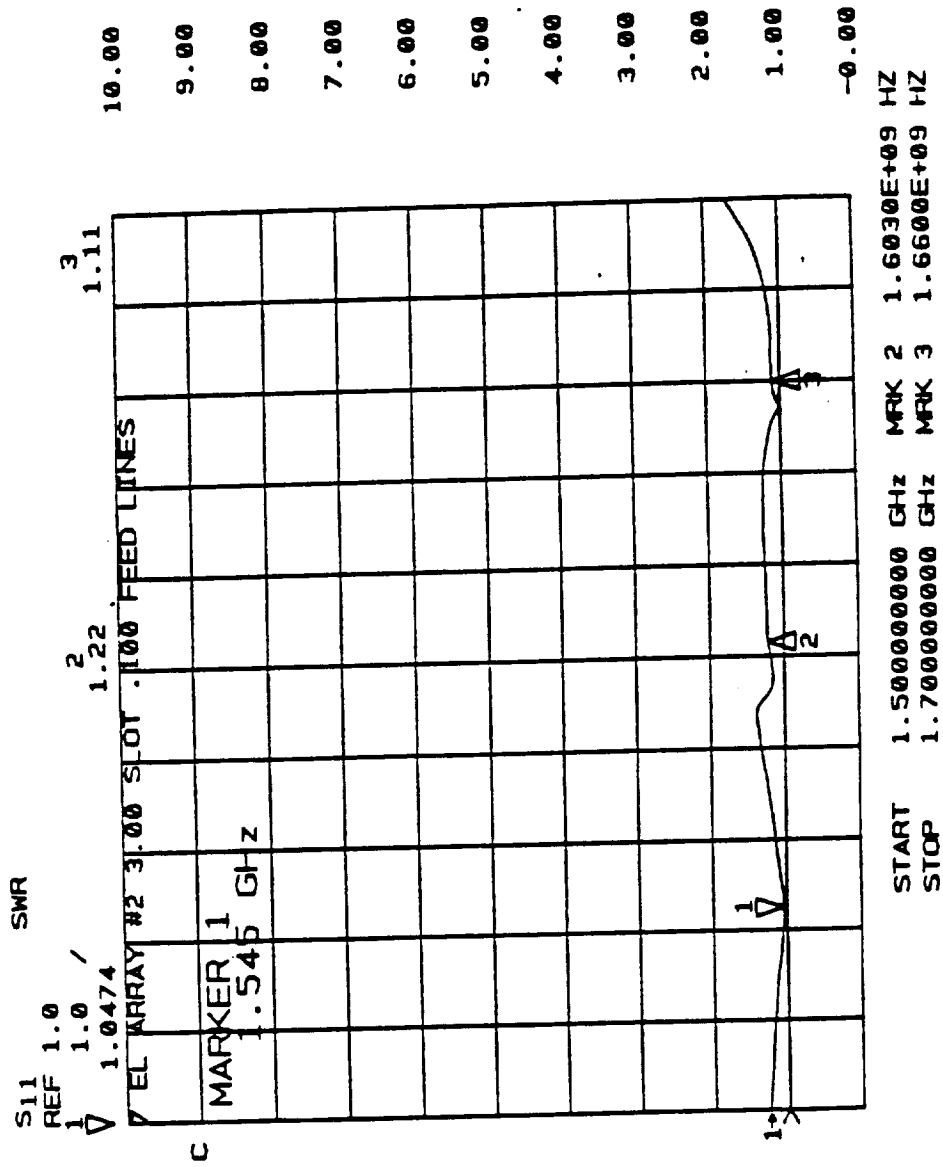


Figure 3-25. Measured VSWR of the Crossed-Slot

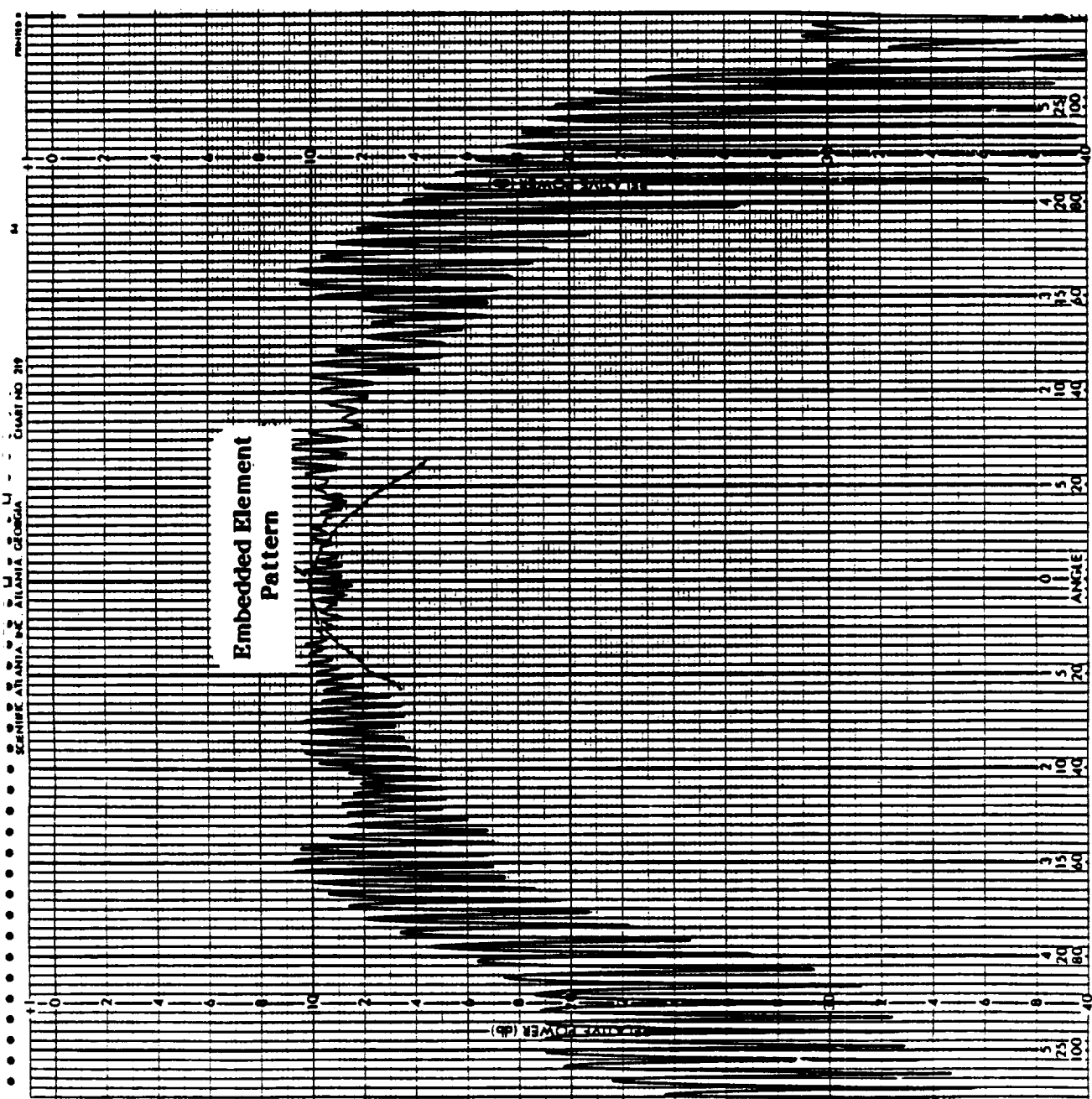


Figure 3-26. Embedded Element Pattern of the Center Element of the Seven Element Array at 1660 MHz

ORIGINAL PAGE IS  
OF POOR QUALITY

An experimental nineteen element array was also fabricated to facilitate the optimization process of the antenna design under an array environment. The array assembly was discussed in Section 2.3 and will not be repeated here. The optimization of the excitation feeder and the hybrid network design are discussed in the following subsections.

#### 3.4.1 Optimization of Feed Network Design

With the assembly described previously, it was possible to obtain test data on the various elements in an array environment. This data was then analyzed and used to optimize the design of the feed network. For example, one optimization that was performed was on the width of the feedlines. The effect of this parameter on element performance is depicted by the curves shown in Figures 3-27. As noted, the line width effects the impedance, which in turn translates to a mismatch between the feedline drive point and the hybrid network. This match degradation is actually a measure of the isolation between the input port and the isolated port of the hybrid network. As shown in Figure 3-18, when the load port isolation increases, the element gain decreases from some optimum value.

As an illustration, some early test data taken prior to optimization is shown in Figure 3-28. The upper curve is a measure of  $S_{21}$ , which represents the isolation between the input and load port of the hybrid network. The lower curve is a measure of the input port VSWR under the same test environment. The goal for optimization is for  $S_{21}$  to be not less than 10 dB over the antenna operating frequency, with a value of 12 to 15 db being very desirable. With regard to input VSWR, the value should be as low as possible, however a VSWR of not greater than 1.5 is set as an upper limit.

#### 3.4.2 Optimization of Hybrid Network

Optimization was also performed on the hybrid network with respect to amplitude and phase balance. Since the axial ratio of the circular polarized wave (from the radiating element) is dependent upon the balance in both amplitude and phase of the signals feeding the two crossed slots, it is important to keep the error associated with these two parameters as small as possible. Figure 3-29 depicts the relationship between axial ratio and amplitude phase unbalance. For example, to limit the axial ratio to not greater than 1 db, the amplitude unbalance cannot exceed 1 db. Likewise, the phase unbalance must be somewhere between 0 and 5 degrees. The following equations were used to evaluate each hybrid network's performance.

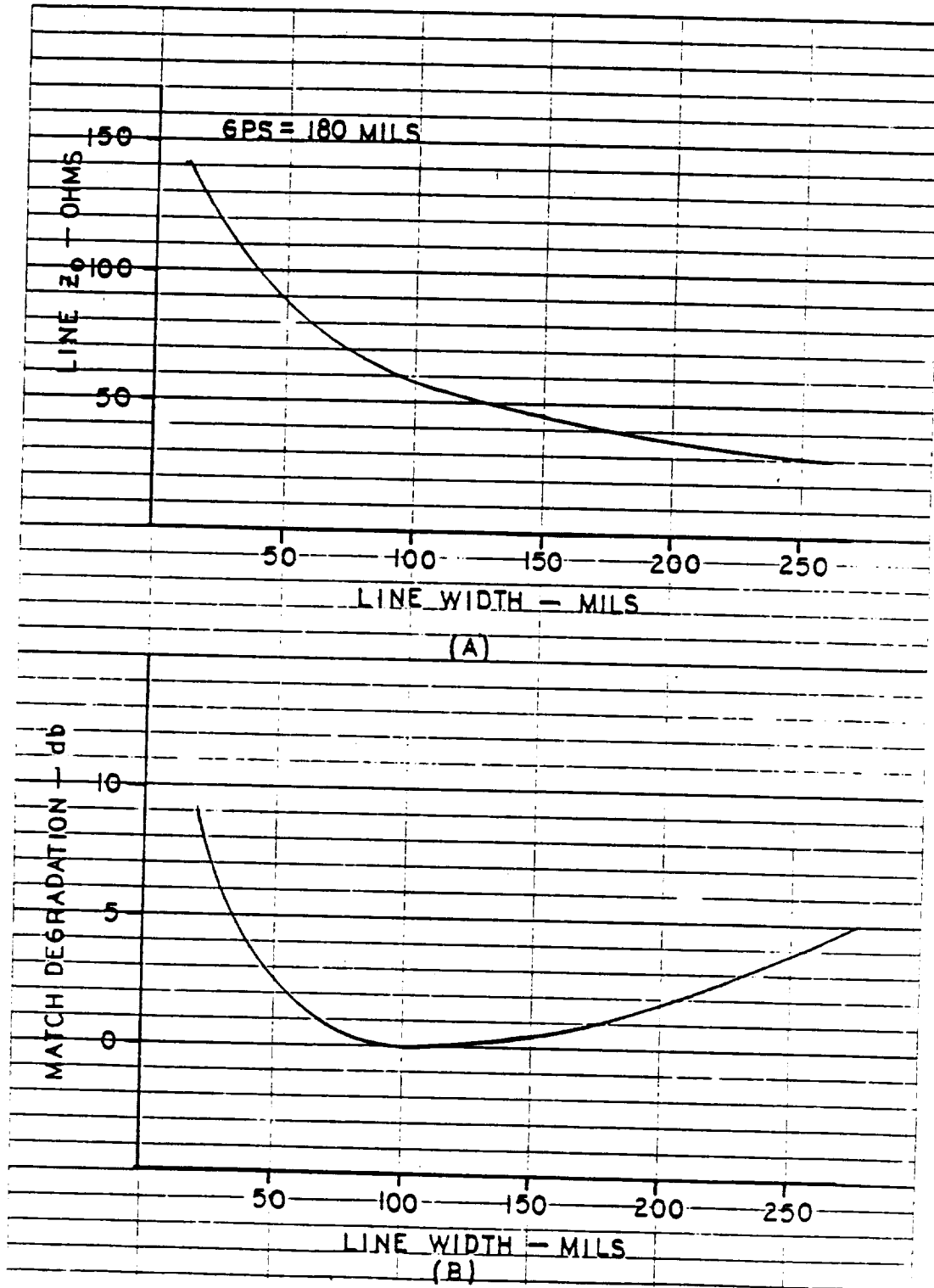


Figure 3-27. Feed Line Characteristics

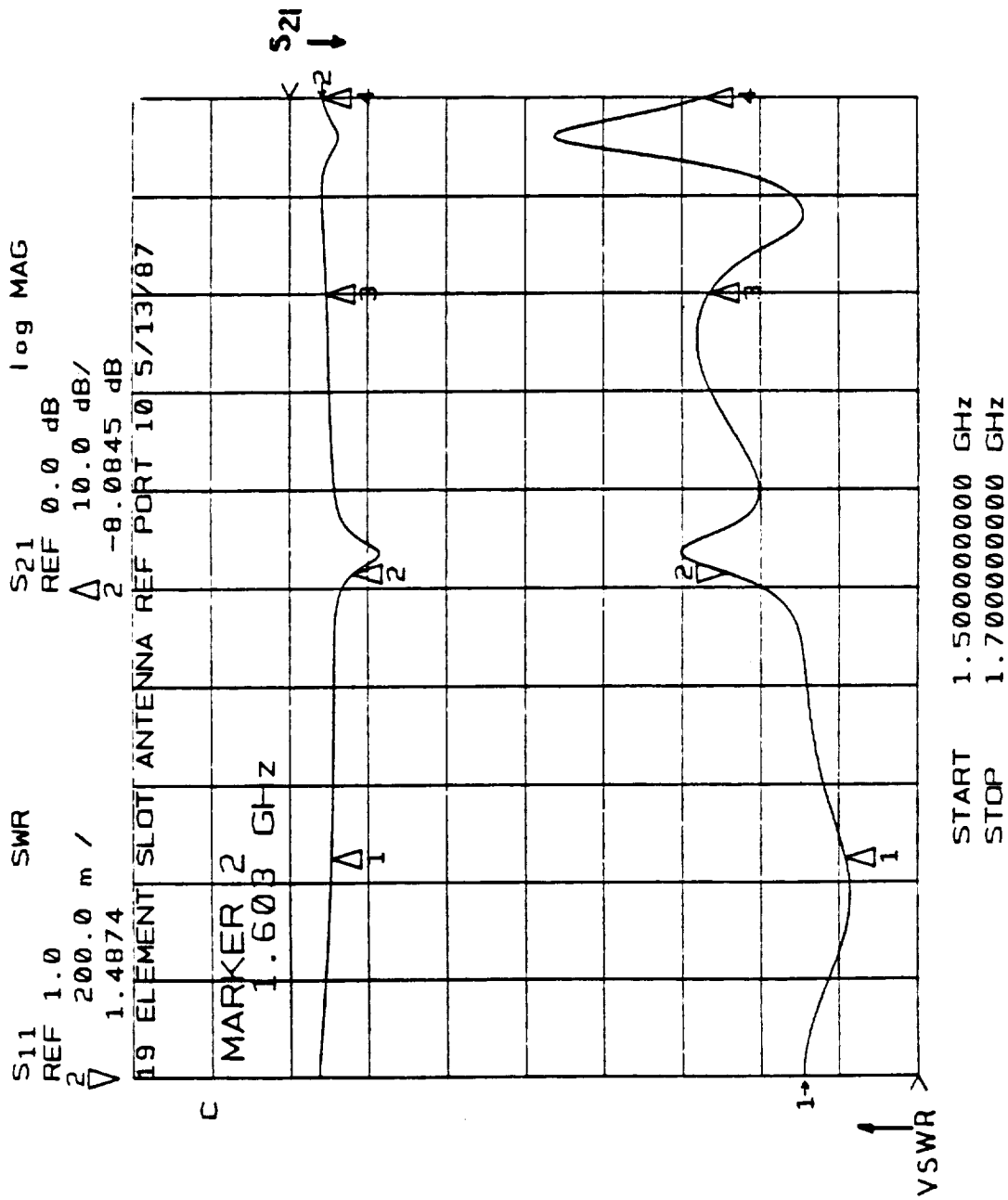


Figure 3-28. Measured VSWR and S<sub>21</sub> Characteristics on a Typical Element in an Array with the Feed Circuit Optimized

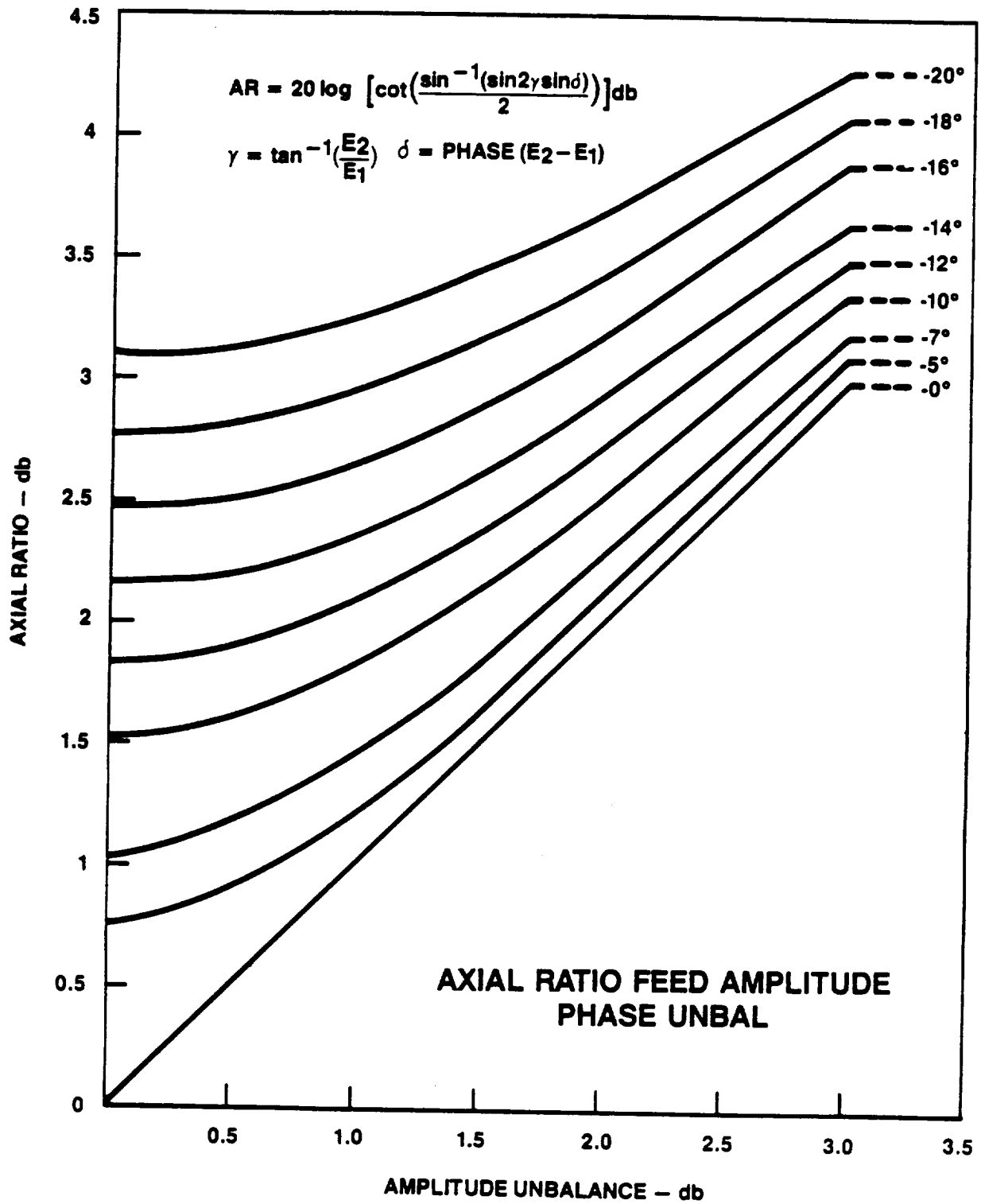


Figure 3-29. Axial Ratio versus Feed Amplitude/Phase Unbalance

Insertion Loss:

$$I_L = 10 \text{ Log } [1 + (1 - (P_V + P_H))] \text{ dB}$$

Slot Power Unbalance:

$$P_{SU} = 10 \text{ Log } (P_V/P_H) \text{ dB}$$

Quadrature Phase Error:

$$\phi_e = 90 - [((\Delta\phi_{1-2})^2 + (\Delta\phi_{2-3})^2 + (\Delta\phi_{3-4})^2 + (\Delta\phi_{4-1})^2)/4]^{1/2}$$

The performance of the hybrid network used in the final array assembly is summarized in Table 3-5. Note that the phase performance was optimized. The amplitude unbalance, however, can further be improved.

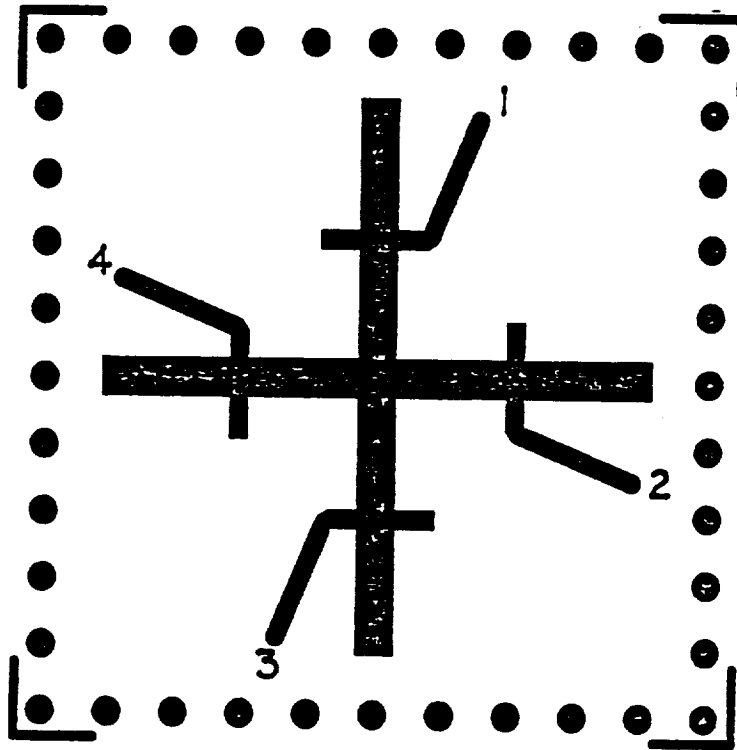
Table 3-5. Performance Summary of Typical Hybrid Network

Parameter	Frequency (MHz)		
	1545	1603	1660
IL - dB	0.25	0.21	0.24
P <sub>SU</sub> - db	0.64	0.78	0.90
φ <sub>e</sub> - deg.	0.55	0.04	1.35

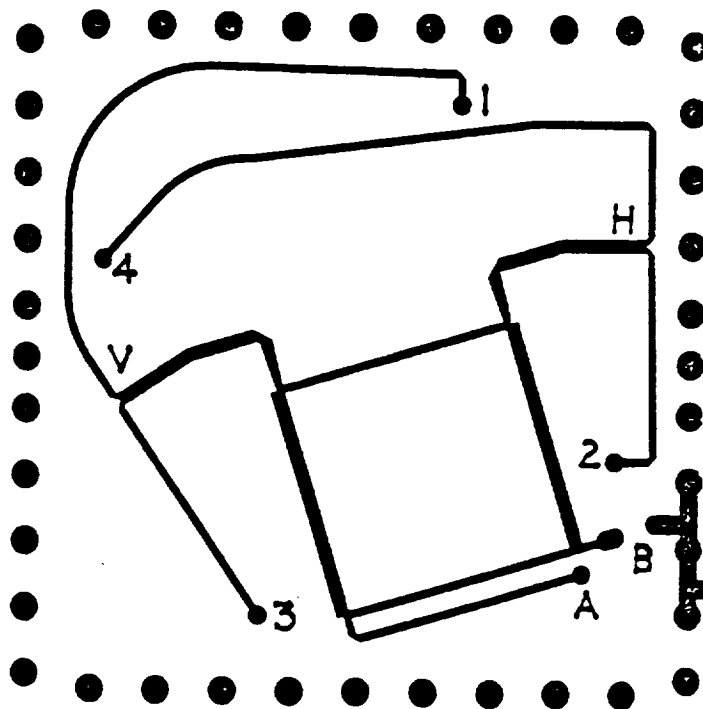
### 3.4.3 Modifications Required of Hybrid Network

The development model of a 19-element array built was left hand circularly polarized. The requirement is right hand circular polarization. Therefore, the modification of the hybrid network is required and shown in Figure 3-30.

As shown in Figure 3-30B, originally points A and B were brought out parallel and perpendicular to the branch line of the quadrature coupler. Port-A is connected to the beamformer board with a vertical pin, and Port-B is terminated with a surface mount chip resistor on the hybrid network board. Ground for the resistor is provided by several plated-through cavity holes. Clearance for the chip resistor is provided by a cut-out in the ground plane board of the hybrid.



(A)



(B)

Figure 3-30. Element Feed Configuration

CONCLUSIONS

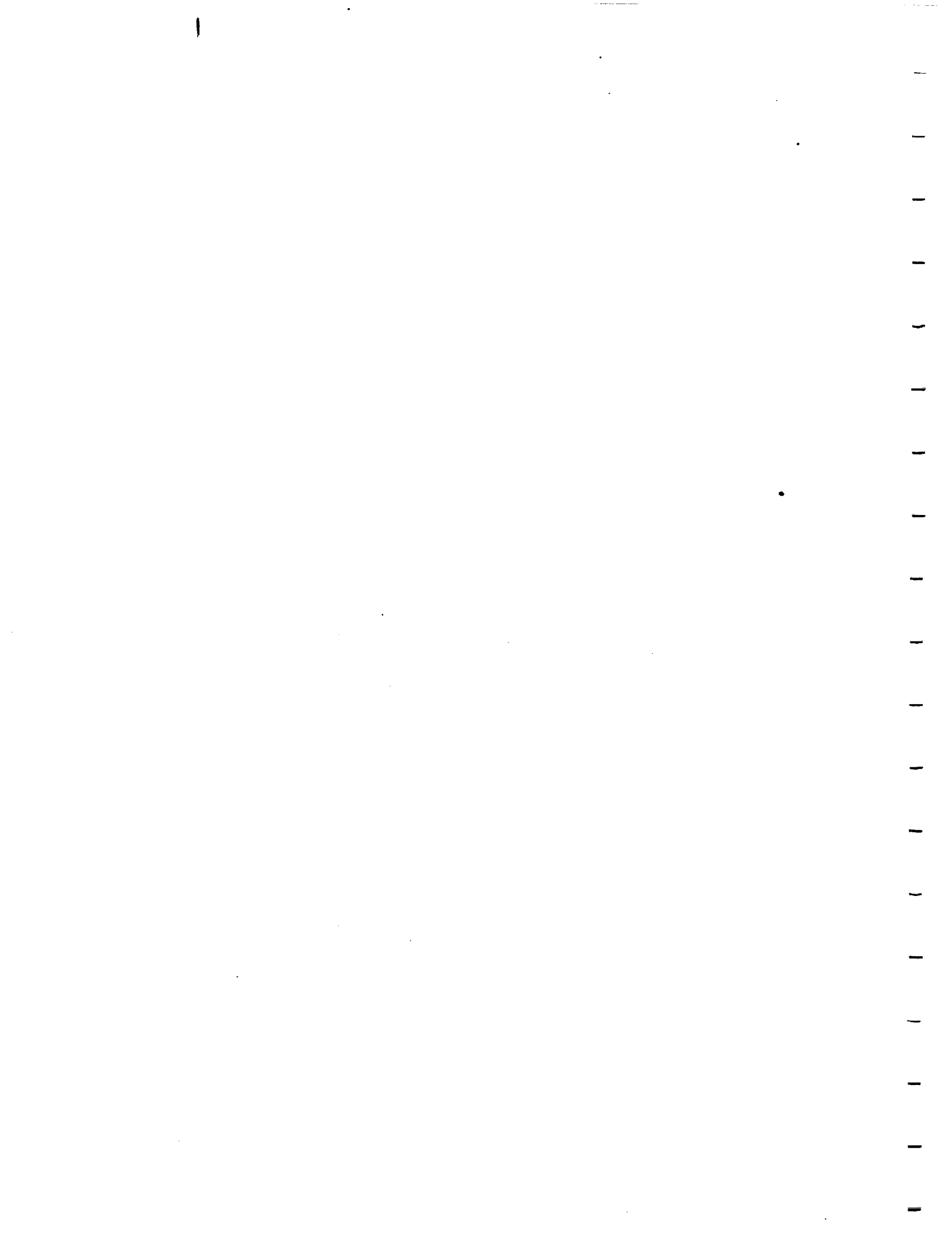
A printed stripline-fed cavity-backed crossed-slot has been successfully developed. Based on the development work, one can draw the following conclusions:

1. Two excitation mechanisms are involved in this antenna: the "coupling excitation" mode from the stripline across the slot and the "cavity excitation" mode of the probe feed.
2. Four symmetrical excitation feeders located at the four quadrants and with 0-90-180-270 degrees phase rotation are required in the feed design. The optimal positions of the four probe feed points are located along the diagonal of the crossed-slot.
3. Good impedance matching at the four feed points, balanced excitation between two orthogonal slots, and even excitation between the two feeds at each of the two orthogonal slots are required to have good radiation efficiency of the antenna.
4. Minimum metal should be used in the feed design.
5. Unnecessary bending of the stripline feed should be avoided.

RECOMMENDATIONS

In order to improve the antenna gain, the following tasks are recommended for the future development work.

1. Improve the antenna matching at the four excitation feeders of the current design. Improper location of the plated through ground holes of the crossed-slot (shown in Figure 2-20) must be corrected. Eliminate the dog leg shape of the feeder.
2. Theoretical and experimental investigation of the optimal excitation mechanism is needed. The four probe excitation method is recommended because it could reduce the unnecessary metal inside the cavity of the crossed-slot, which in turn can improve the antenna radiation efficiency.
3. Investigate the broadbanding technique to improve the antenna gain across the required frequency band. The slot with a flared shape is worth further study.
4. Bonding techniques must be used to improve the radiation efficiency and the operating stability.
5. Optimization of the hybrid feed network, with respect to amplitude and phase balance, should be continued.



## SECTION 4 BEAMFORMER NETWORK

After a brief synopsis of the work described in the interim report this section discusses subsequent beamformer advances and results. Also to be discussed are certain problems uncovered in testing the first two beamformer assemblies. The section ends with a listing of the tasks to be done in the next segment of work, provided Teledyne Ryan Electronics is chosen to perform the next phase. In essence the results of this phase prove the basic beamformer concepts are valid and promising to economical production costs and to improve performance further.

### 4.1 SUMMARY OF THE DEVELOPMENT OF THE PHASE SHIFTER AND DIVIDER

In the following paragraphs the design and development of the 3 bit phase shifter and nineteen way unequal divider are described. Optimization via Touchstone software was applied to obtain the design. The prototype assemblies used this design with only a small amount of phase correction on the phase shifter. The nineteen way divider is essentially as originally designed with the exception of a change of resistor types as the first ones had very poor microwave properties.

The 3 bit phase shifter uses the switched line principle. This was selected to give the least phase shift error over the entire band. Performance was compared with a hybrid coupled phase shifter which did not project to be as accurate over frequency. The switched line shifter projects an 11 degree error while the hybrid one projects a 19 degree error over the same frequency band. The results of the calculations were the determining factor in selecting the switched line shifter over the hybrid coupled unit.

The requirement is to provide two way low loss phase shifting with power handling of about 1 watt. This means a diode must be selected to have a breakdown voltage in excess of 100 volts. Since 18 phase shifters are required with 216 pin diodes, these diodes must be inexpensive. A surface mount diode, Metelics MPN7484 on a ceramic carrier, was selected. Vendor data showed this diode has low junction and case capacitances permitting a series configuration to be used. However, results using this diode has led us to question the exact value of the capacitances because of excessive loss in some modes. This will be

described later. Future phases will devote a reasonable effort to understand and correct the problem. Also reserved for the future is developing manufacturing assembly techniques suitable for this rather new diode package.

Early in the program a breadboard 3 bit phase shifter was tested. Everything looked reasonably well except that the switched phase shifts were approximately 10% lower than desired. All this was corrected in the prototype units. The prototype design had to make layout changes to avoid RF lines crossing other RF or control lines. Table 4-1 compares the delta phase, loss, and VSWR for the original phase shifter, the prototype phase shifter, and a self biased phase shifter developed as a potentially low cost circuit. It can be seen that the #1 shifter misses the desired phase by about 10% while the prototype or array shifter comes considerably closer to the desired values. However, an iteration on that shifter, to further adjust phase, still appears desirable for the next contract.

As previously mentioned, there is a small loss problem with the array shifter. This is probably due to the diode parasitics being higher than expected and possibly due to the proximity of the biasing circuits. Figure 4-1 shows a sketch of the #1 microstrip phase shifter. It can be seen that the bias circuits are brought from below the phase shifter to move them out of the vicinity of the RF fields. In the array, this is not possible because all circuits must be planar since the ground side is not accessible. A sketch of the first array design is shown in Figure 4-2. This circuit had a very bad loss problem because the RF energy was being sucked out by the bias circuits. To solve this problem additional decoupling was added as shown in Figure 4-3. That particular shifter, with the addition of a small stub to the 180° phase shift line performed as shown in Table 4-1. Loss still appears somewhat high when the 90° section is activated. This loss appears to be related to VSWR.

If we hypothesize that the junction and case capacitances equal .13 pf instead of .06 pf and .07 pf, respectively, as claimed by the vendor, a loss of 1.5 db for a 315° shift is calculated as shown in Figure 4-4. With smaller capacitances the loss calculates to be about 1 db.

In the overall array assembly it appears the losses are somewhat different as can be seen by a later discussion of the data. This is not surprising because there are many more circuits near the phase shifters in the entire array interacting with the RF path. All this points to investigations needed for the next phase. Complicating our understanding of why the losses

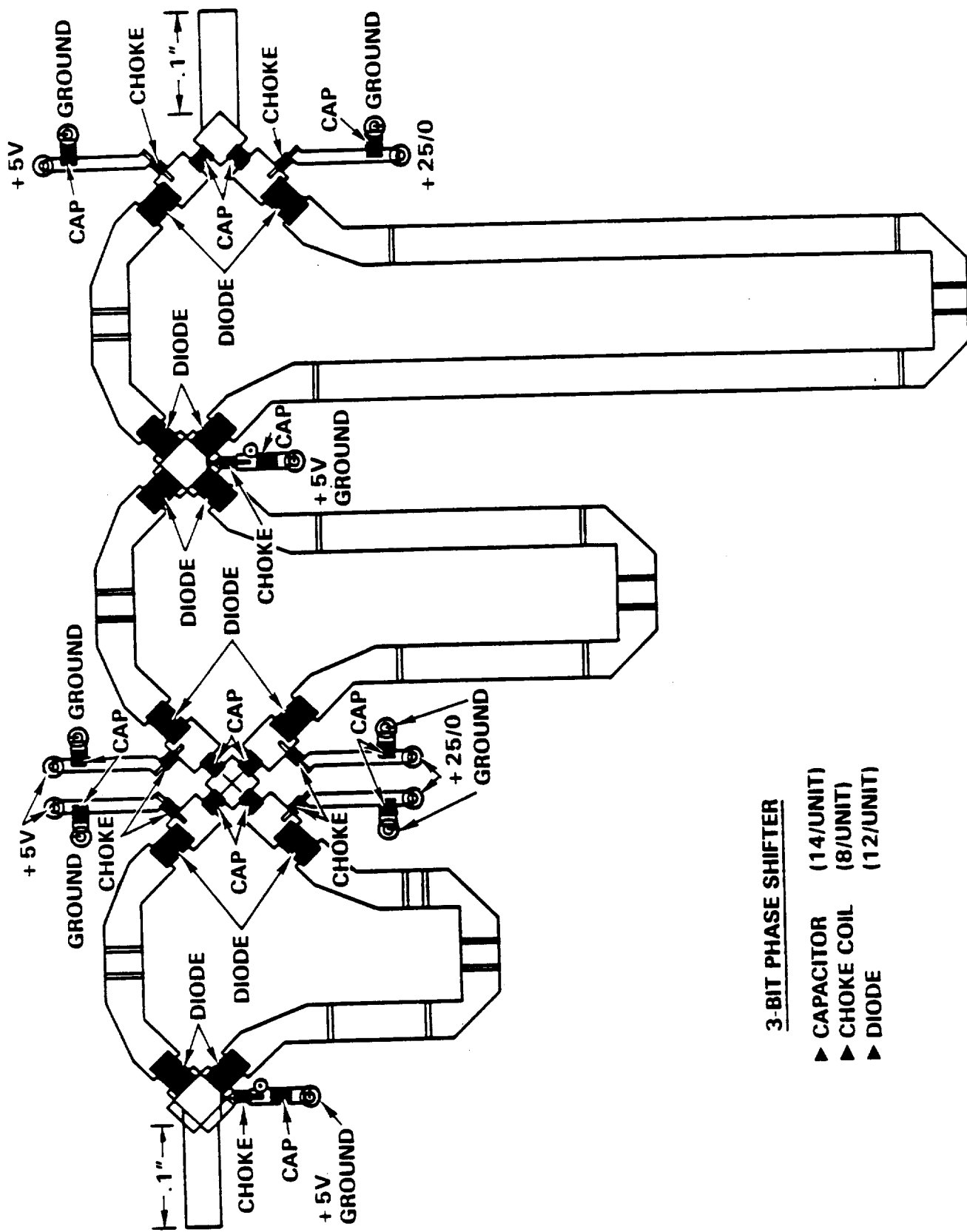


Figure 4-1. Sketch of Phase Shifter #1. Bias comes up from beneath the ground plane.

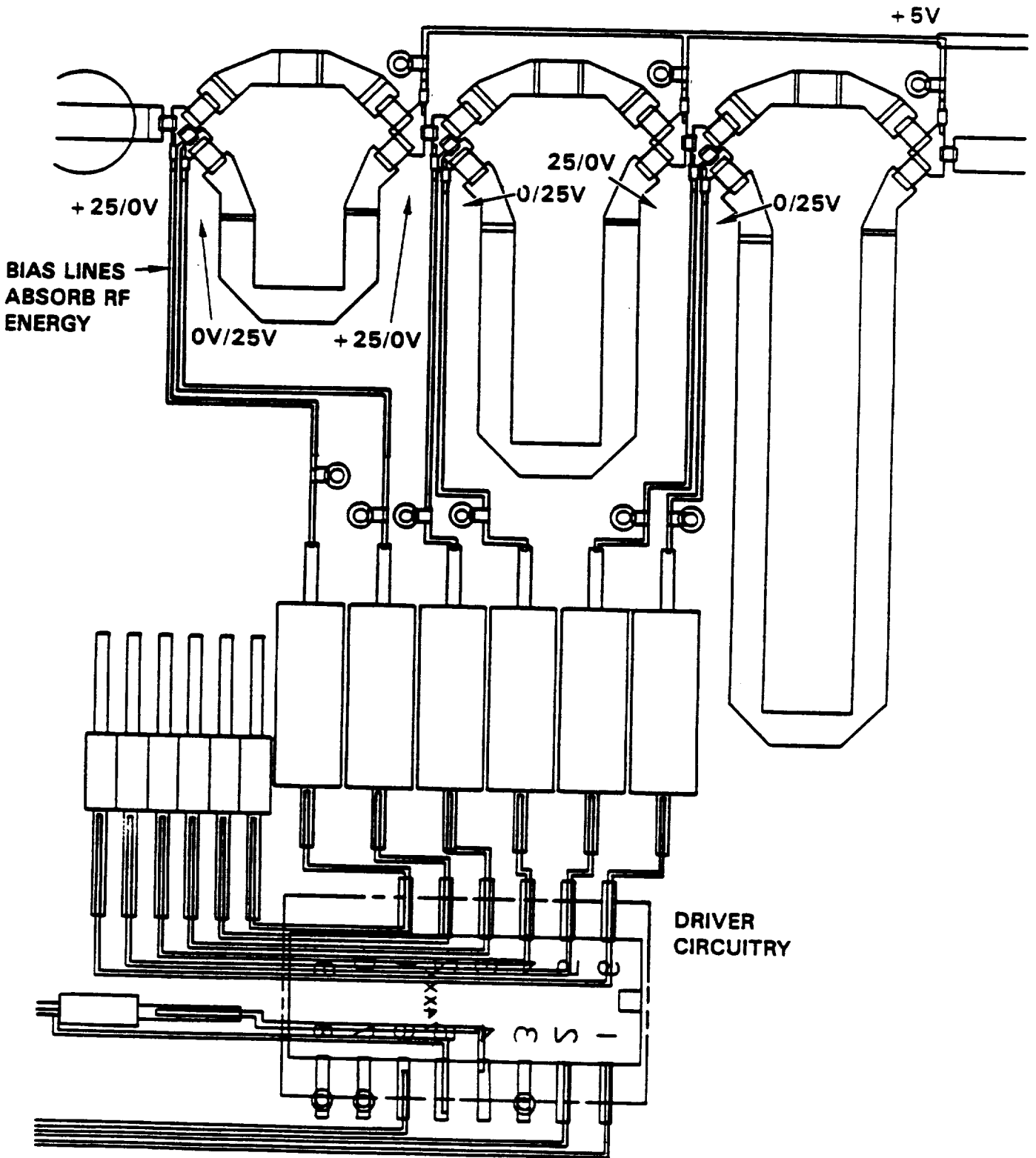


Figure 4-2. First Design of Array Phase Shifter

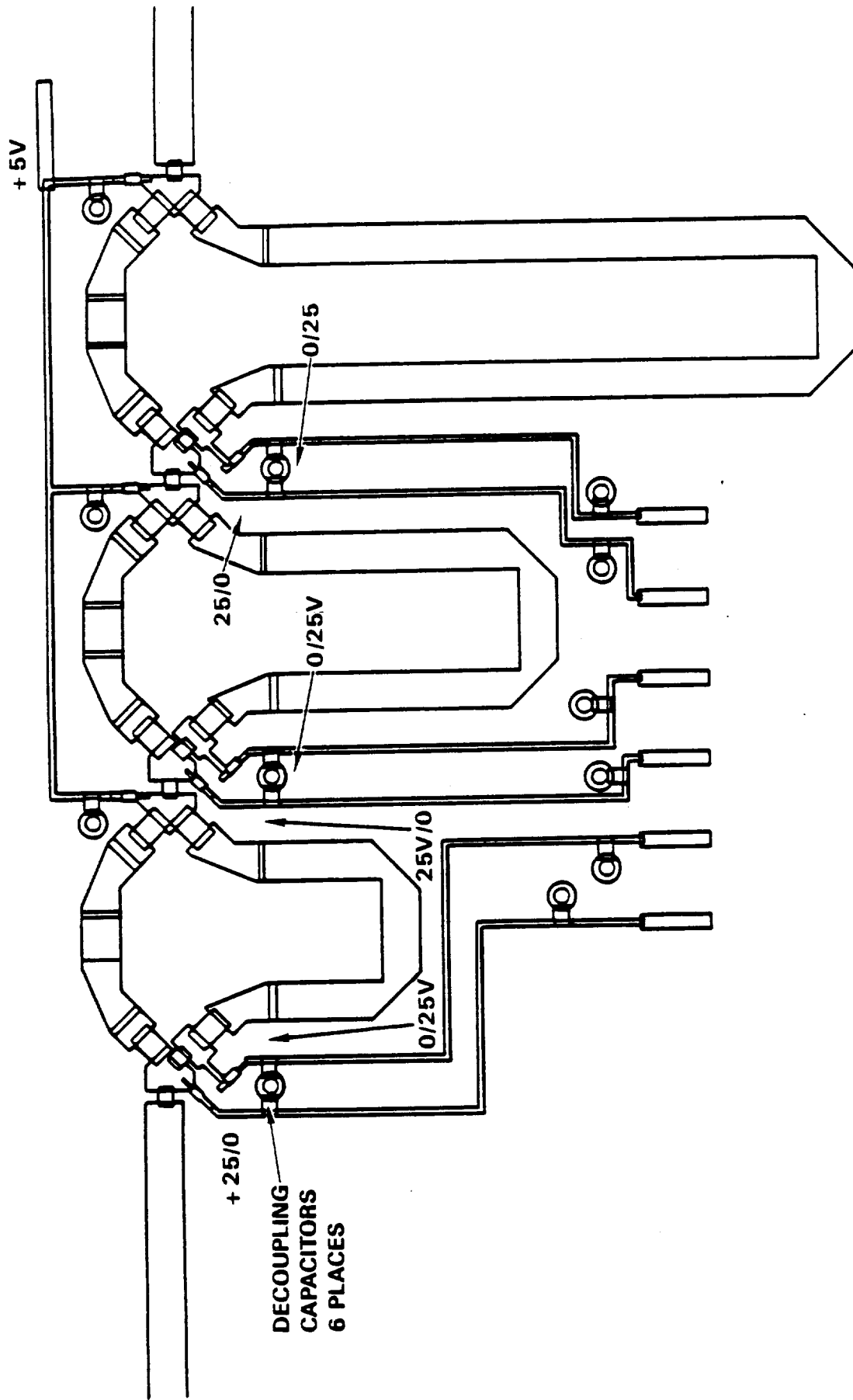


Figure 4-3. Revised Array Phase Shifter Design. Chip decoupling capacitors were added to stop the absorption of RF in the bias lines.

Table 4-1. Summary of Mid Frequency Phase Shifter Data for Three Designs

<u>Phase Shifter Setting</u>	<u>#1 Phase Shifter ΔPhase</u>	<u>Array Phase Shifter ΔPhase</u>	<u>Self Biased Phase Shifter ΔPhase</u>
0°	0°	0°	0°
-45°	-38.1°	-42.9°	-46°
-90°	-81.5°	-81.4°	-88°
-135°	-118°	-124.2°	-133°
-180°	-166.9°	-181.2°	-177°
-225°	-204.7°	-225.2°	-223°
-270°	-246°	-264.7°	-268°
-315°	-283.3°	-306.9°	-312°
	<u>Loss (dB/VSWR)</u>	<u>Loss (dB/VSWR)</u>	<u>Loss (dB/VSWR)</u>
0°	1.0/No VSWR Data	1.1/1.14	1.1/1.14
-45°	1.04/No VSWR Data	1.18/1.25	1.45/1.42
-90°	1.04/No VSWR Data	1.48/1.79	1.82/1.82
-135°	.95/No VSWR Data	1.29/1.27	1.44/1.38
-180°	1.07/No VSWR Data	1.2/1.3	1.21/1.21
-225°	1.15/No VSWR Data	1.24/1.16	1.26/1.24
-270°	1.12/No VSWR Data	1.4/1.49	1.74/1.89
-315°	1.03/No VSWR Data	1.3/1.19	1.47/1.37

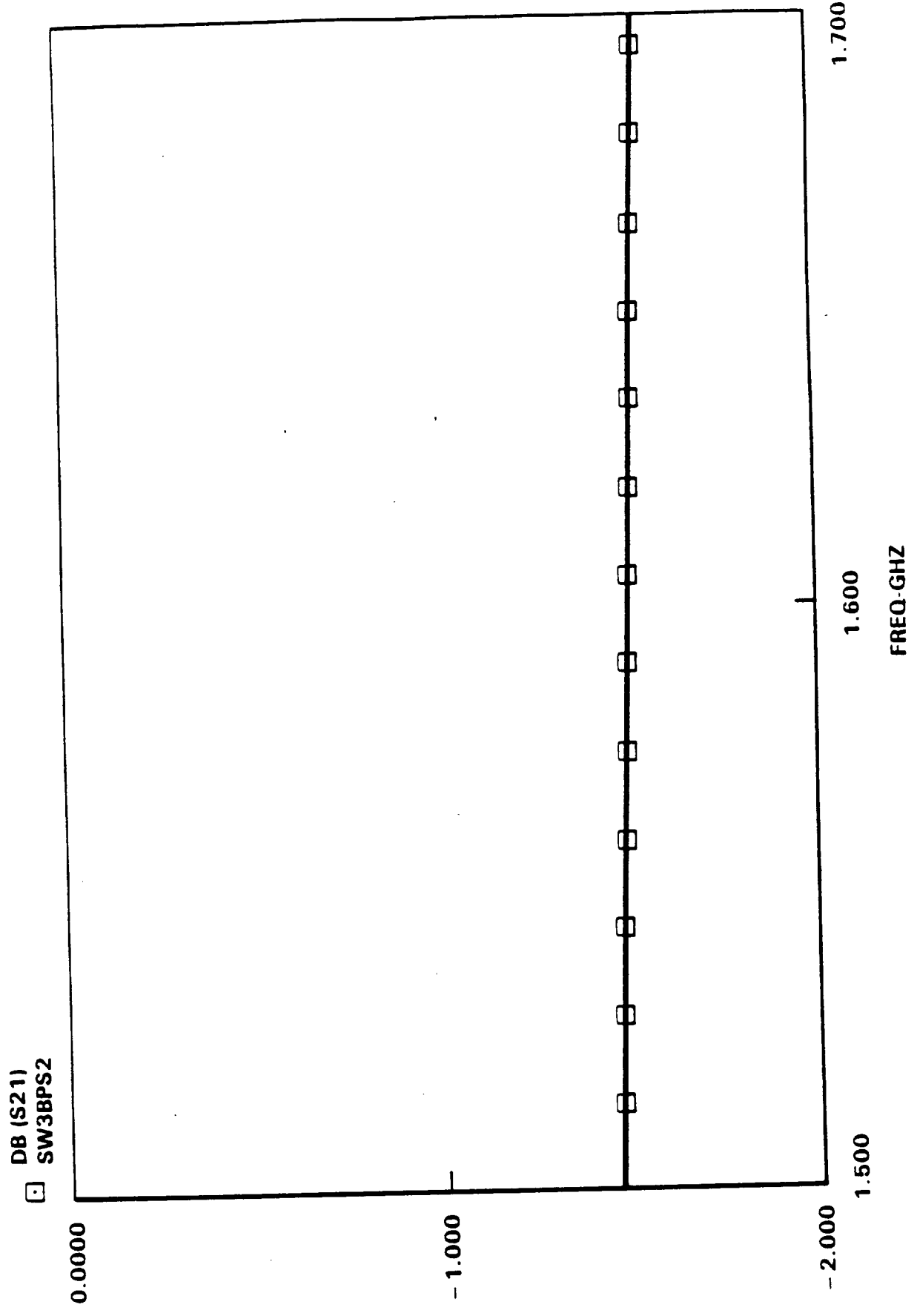


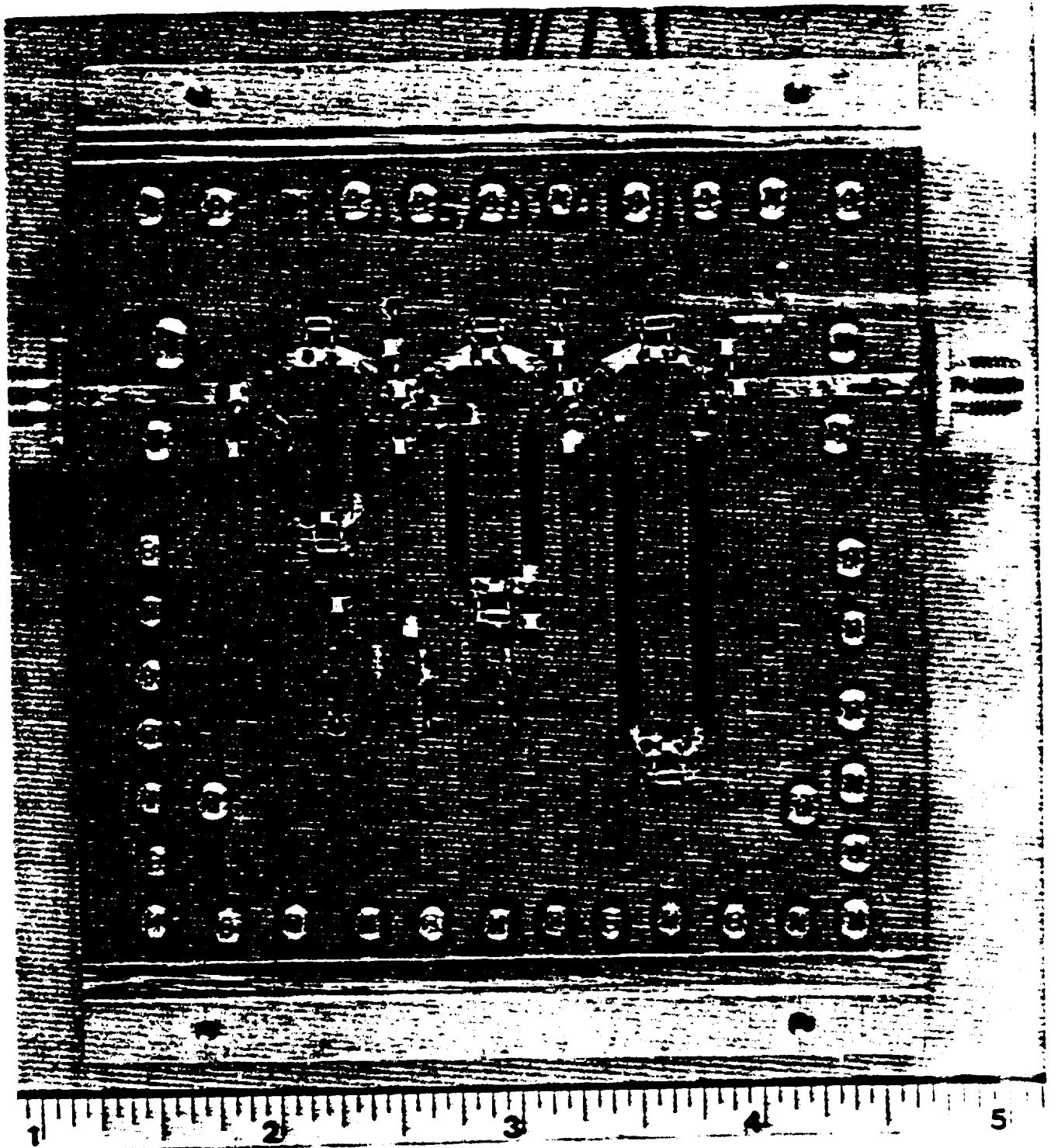
Figure 4-4. Theoretical phase shifter loss in the 315° condition assuming  $C_J$  and  $C_C = .13$  pF for the PIN diodes. The vendor catalogue lists  $C_J$  and  $C_C$  on .06 pF and .07 pF respectively.

are somewhat higher than anticipated, was the discovery of wire bonding problems on one lot of diodes and diode soldering problems for the entire assembly. We believe those problems are now solved, but their effect contaminates some of the earlier data.

The self biased phase shifter experiment was made to determine if pairs of diodes can be brought to a common junction (for future integration), and if only one switched voltage form could be used. The "on" diodes provide "off" bias in each switched line shifter. We found that in order to do this, the "on" arm voltage drop had to be increased by using bypassed resistors. The assembly for this experiment is shown photographically in Figure 4-5. The results shown in Table 4-1 are encouraging enough to continue this line of experimentation.

The nineteen way divider presented a challenge since tapering of power for the antennas was desired for the circular geometry. Starting from the outside going towards the center, three circular rings of relative power -6db, -5.2db, and -3db, respectively for each radiator compared to 0 db reference at the center are provided. To do this most effectively, it was decided to use a uniform one-to-seven way divider followed by six unequal one-to-three dividers. These dividers were based on the Wilkinson divider principle. The Touchstone program was used to determine the line impedances and balancing resistor values. Figure 4-6 shows a schematic diagram of the nineteen way divider with the line impedances and balancing resistors given. The left hand network is an equal 7 way divider, and the right hand side is six unequal 3 way dividers. Figure 4-7 shows the layout of a test divider without the resistors.

Microwave evaluations were performed on both a separate 7 way divider and the 19 way divider shown on Figure 4-7. Table 4-2 summarizes the results for the 7 way divider. The loss performance is quite uniform and good. There are some small differences in phase with the outside lines having less phase. This is no problem because a phase trim is done on the final assembly. Table 4-3 summarizes the 19 way divider performance with no resistors. No resistors were used because at the time of the evaluation, we had no satisfactory resistors, as will be shown in the next paragraph, and it was hoped resistors would not be needed. In later work this proved to be false; resistors are needed. As seen in Table 4-3 amplitude results of the test divider are quite good. These are summarized by using statistical analysis, the results of which are shown at the bottom of the table. Again the phase data has some scatter, but as previously mentioned we do a phase trim on the



## TELEDYNE RYAN ELECTRONICS

Figure 4-5. Photograph of the self-biased PIN Diode Phase Shifter. With added dropping resistors, results were close to those obtained by the switched bias scheme.

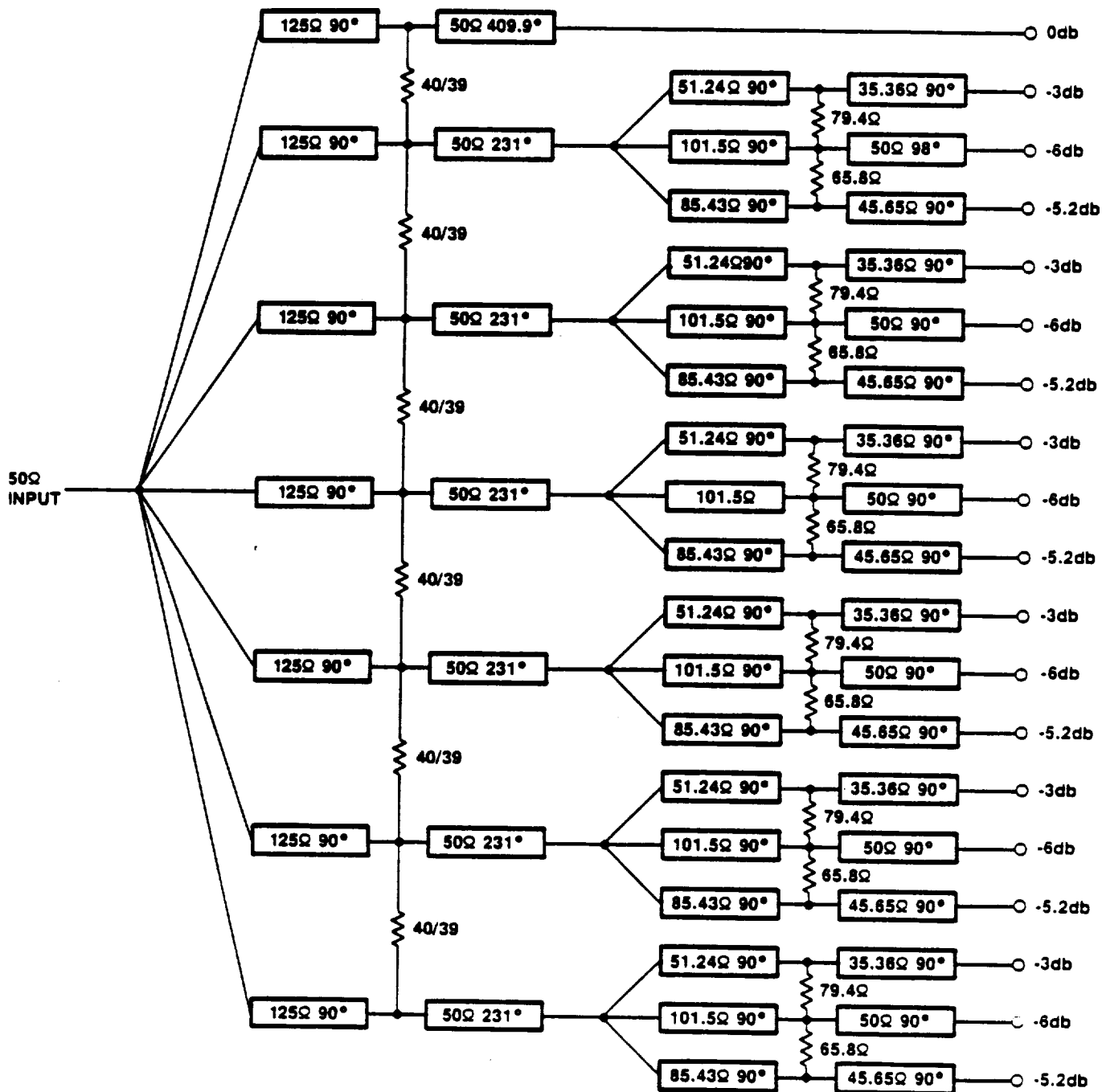


Figure 4-6. Schematic Diagram of MSAT-X 1:19 Unequal Power Divider

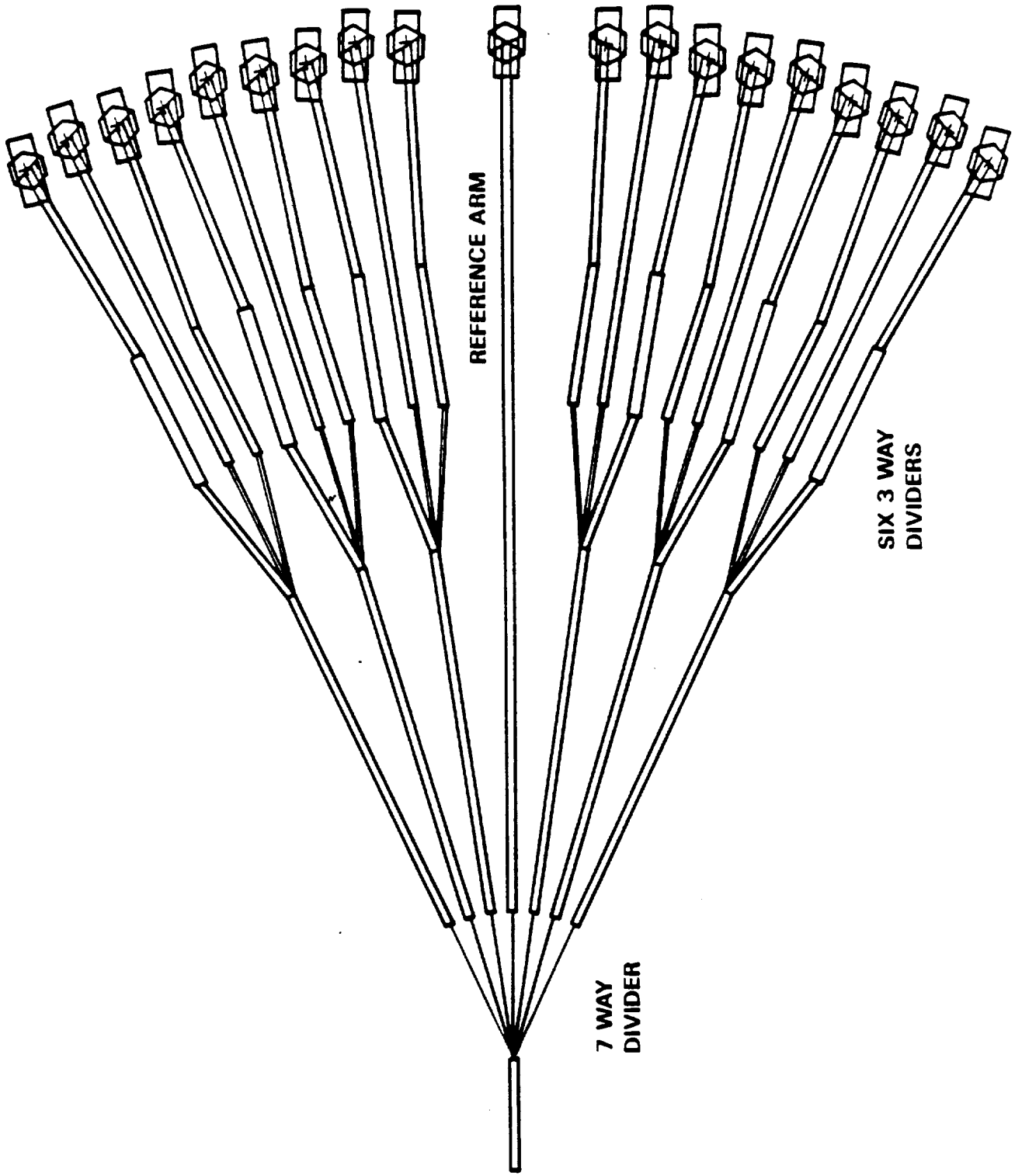


Figure 4-7. Layout of the Test 19-Way Divider

12.000

Table 4-2. 7-Way Divider Data (No Resistors)

Port#	S <sub>21</sub> dB			S <sub>21</sub> PHASE		
	<u>1545 MHZ</u>	<u>1600 MHZ</u>	<u>1660 MHZ</u>	<u>1545 MHZ</u>	<u>1600 MHZ</u>	<u>1660 MHZ</u>
1	-9.3	-9.2	-9.3	-48	-67	-88
2	-9.3	-9.2	-9.4	-50	-70	-90
3	-9.3	-9.2	-9.2	-52	-72	-91
4	-9.3	-9.2	-9.1	-52	-72	-91
5	-9.3	-9.2	-9.1	-53	-73	-91
6	-9.0	-9.0	-9.0	-52	-71	-90
7	-9.0	-8.9	-9.0	-48	-68	-89

Table 4-3. 19-Way Divider Data (No Resistors)

Port #	Des. Loss DB (IDEAL)	S <sub>12</sub> (dB)			S <sub>12</sub> PHASE (DEG.)		
		1540 MHZ	1600 MHZ	1660 MHZ	1540 MHZ	1600 MHZ	1660 MHZ
1	11.45	11.87	11.96	12.24	-26	-59	-92
2	14.45	15.12	15.07	15.07	-31	-65	-100
3	13.65	14.03	13.98	14.10	-24	-57	-93
4	11.45	12.69	12.50	12.54	-29	-62	-96
5	14.45	15.76	15.50	15.41	-35	-69	-104
6	13.65	14.77	14.59	14.55	-29	-62	-98
7	11.45	12.74	12.72	12.98	-35	-68	-102
8	14.45	15.71	15.62	15.73	-39	-73	-108
9	13.65	15.02	14.99	15.23	-33	-66	-99
10	8.45	8.86	8.45	8.35	-28	-58	-91
11	13.65	14.89	14.95	15.24	-32	-65	-99
12	14.45	15.81	15.78	15.91	-40	-73	-108
13	11.45	12.24	12.30	12.74	-34	-67	-101
14	13.65	14.79	14.65	14.82	-30	-64	-98
15	14.45	15.61	15.44	15.49	-36	-70	-105
16	11.45	12.65	12.65	12.95	-31	-64	-97
17	13.65	13.99	14.06	14.37	-27	-61	-95
18	14.45	15.10	15.05	15.32	-33	-66	-101
19	11.45	11.89	12.02	12.47	-27	-59	-93
<hr/>							
Total Loss (dB)			.66	.56	.73		
-3dB MEAN			12.35	12.36	12.66		
-3dB STD. DEV.			.40	.32	12.66		
-5.2dB MEAN			14.58	14.54	14.72		
-5.2dB STD.DEV			.45	.43	.46		
-6dB MEAN			15.52	15.41	15.49		
-6dB STD.DEV.			.32	.29	.30		

final assembly. Future versions of the final assembly will try to correct phase errors by printed line length adjustments. In summation, the divider appeared to meet all requirements, and the design was incorporated in the array design.

To close out the discussion of the divider development a sample of data taken on resistors will be given. Figure 4-8 shows two HP8510 analyzer plots on 50 ohm resistors. The left hand Smith chart display is for the IMS chip, and the right hand Smith chart is for the Component General chip. At 1.6 Ghz the IMS 50 ohm chip measures 27.8-j26 ohms while the Component General chip measures 58.5-j33.3 ohms. While neither result is as good as we would like, the IMS resistor is clearly unacceptable. At least the Component General chip has an acceptable resistance value. It also has some undesirable capacitance. It is planned to take this subject up in the next phase.

The entire beamformer concept, shown conceptually in Figure 4-9, has not changed significantly from what has originally been presented. The one change is the rearrangement of the bias circuits allowing an easier full array assembly without cross-over microwave paths. The next sections will further discuss the Beamformer layout and give results for Beamformer Assemblies 1 and 2.

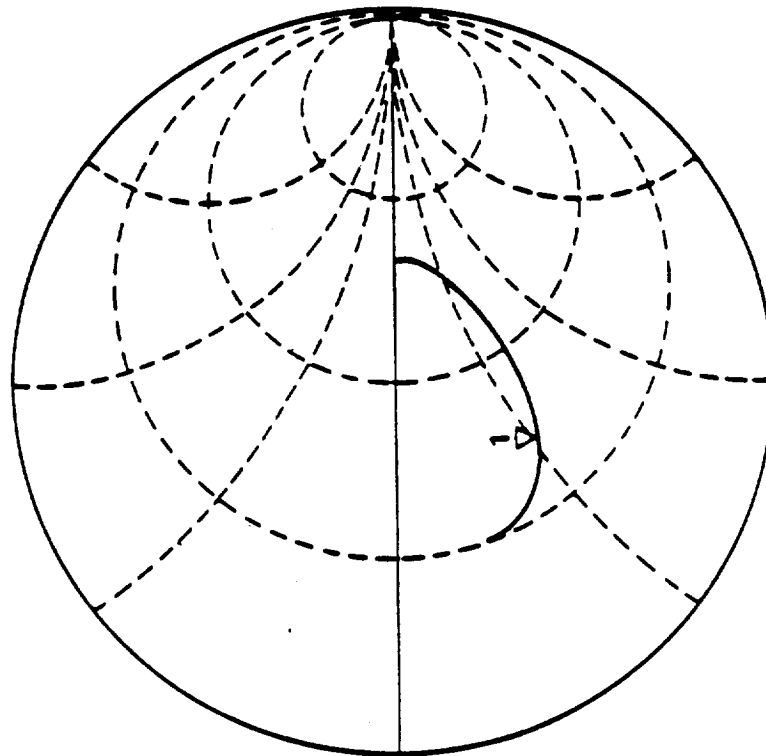
#### 4.2 DESCRIPTION OF THE BEAMFORMER ASSEMBLY

A photograph of the prototype beamformer assembly is shown in Figure 4-10 and a drawing of the assembly in Figure 4-11. The microstrip assembly is built on .031" thick Oak 601 Teflon fiberglass material. This material has a dielectric constant of 2.55.

The RF input from the transceiver is approximately in the center of the microstrip assembly. The signal immediately goes into the 7 way divider terminated by resistors R12, R15, R18, R22, R25 and R28. Following the divider are meandering delay sections to equalize the phase to each phase shifter, thus preventing large frequency dispersions. The layout of these delay sections represented one of the most difficult tasks in the design of the beamformer. Using a sophisticated CAD system the mechanical designer has managed to achieve an equal phase distribution without a single RF cross-over of either other RF lines or the bias lines. This enhances performance by keeping the signals isolated. Represented in Figure 4-11 is the first attempt at achieving the equal phase. For the first two prototypes some adjustment of phase has proven necessary. This has been accomplished by two ways.

**S<sub>11</sub>**      **Z**  
**REF**    **1.0 UNITS**  
**1**      **200.0 mUNITS/**  
**▽**      **27.772Ω - 25.992jΩ AT 1.6 GHz R + jX**  
**FLAT RESISTOR COVERED COVER.182 IN 12/2/85**

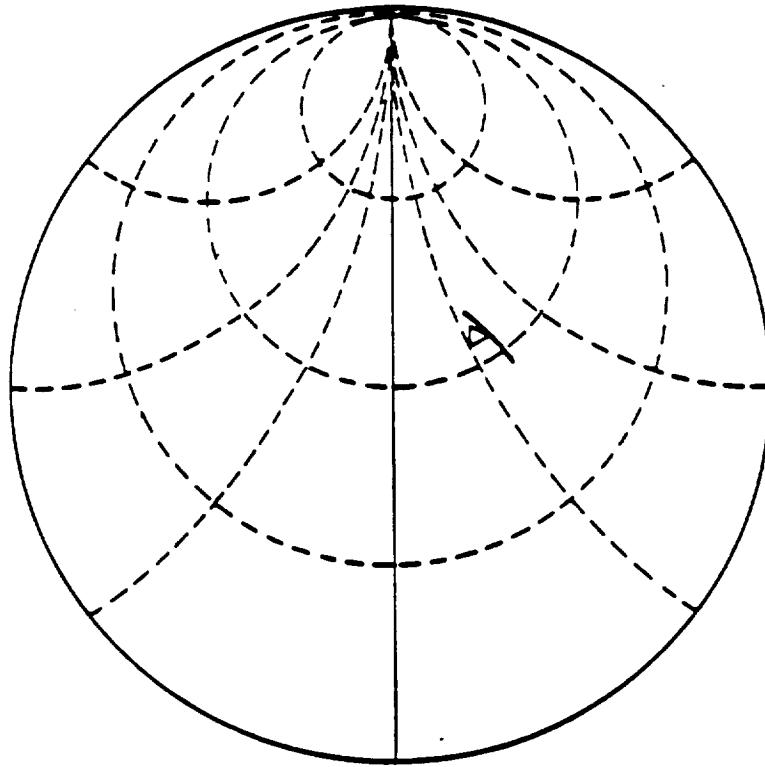
**ELECTRICAL DELAY**  
**300.0 ps**  
**89.938 mm**



**START**    **0.050000000 GHz**  
**STOP**     **2.550000000 GHz**  
**IMS 50Ω RESISTOR**

**S<sub>11</sub>**      **Z**  
**REF**    **1.0 UNITS**  
**▽**      **200.0 mUNITS/**  
**58.5Ω - 33.3jΩ AT 1.6 GHz R + jX**  
**#1 SMALL 50 OHM WITH LID 03 JAN**

**ELECTRICAL DELAY**  
**300.0 ps**  
**89.938 mm**



**START**    **0.300000000 GHz**  
**STOP**     **1.900000000 GHz**  
**COMPONENT GENERAL 50Ω RESISTOR**

Figure 4-8. Comparison of Microwave Performance of IMS and Component General 50 Ohm Chip Resistors.

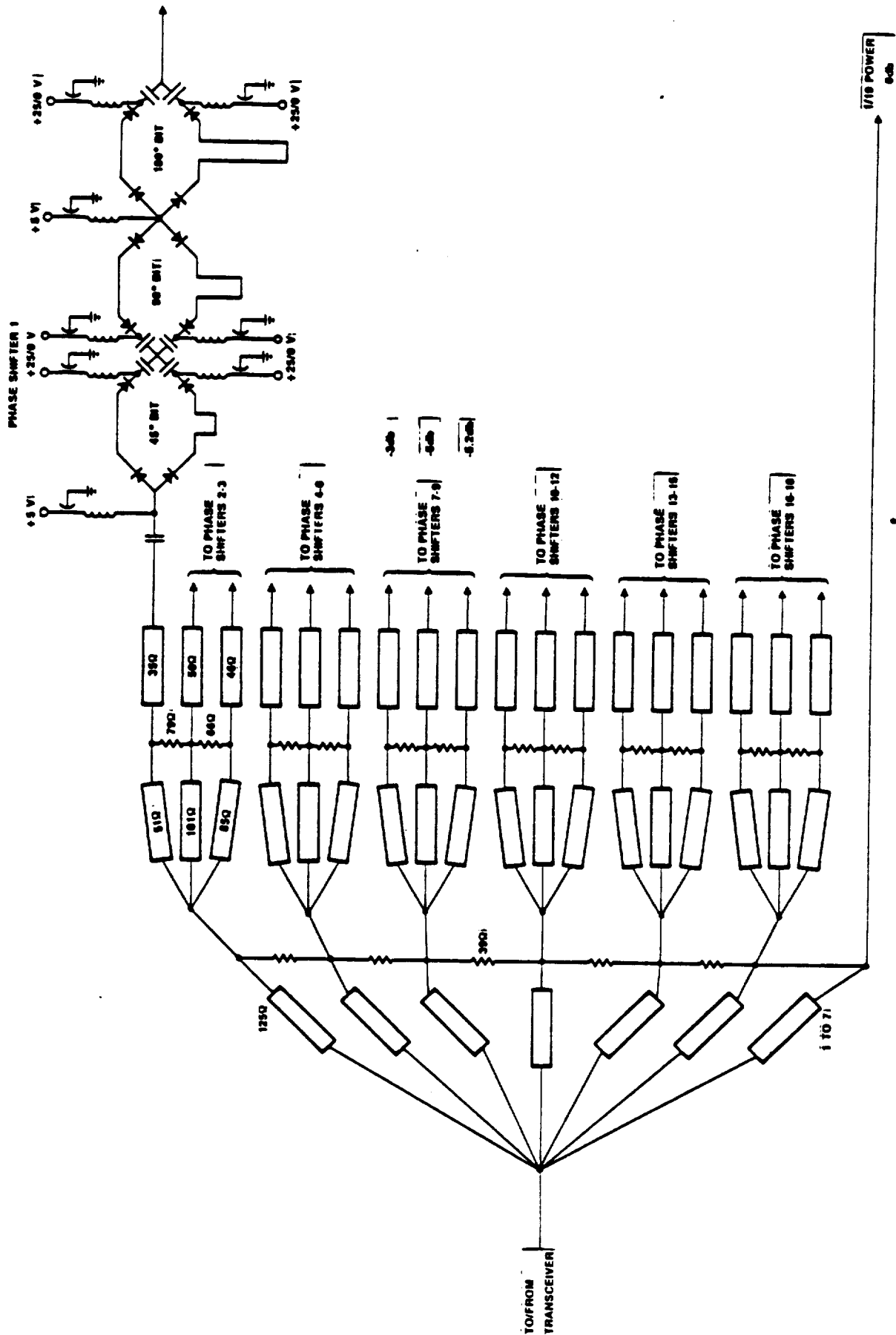


Figure 4-9. Schematic Representation of Power/Combiner and 3-Bit Phase Shifter

ORIGINAL PAGE  
BLACK AND WHITE PHOTOGRAPH

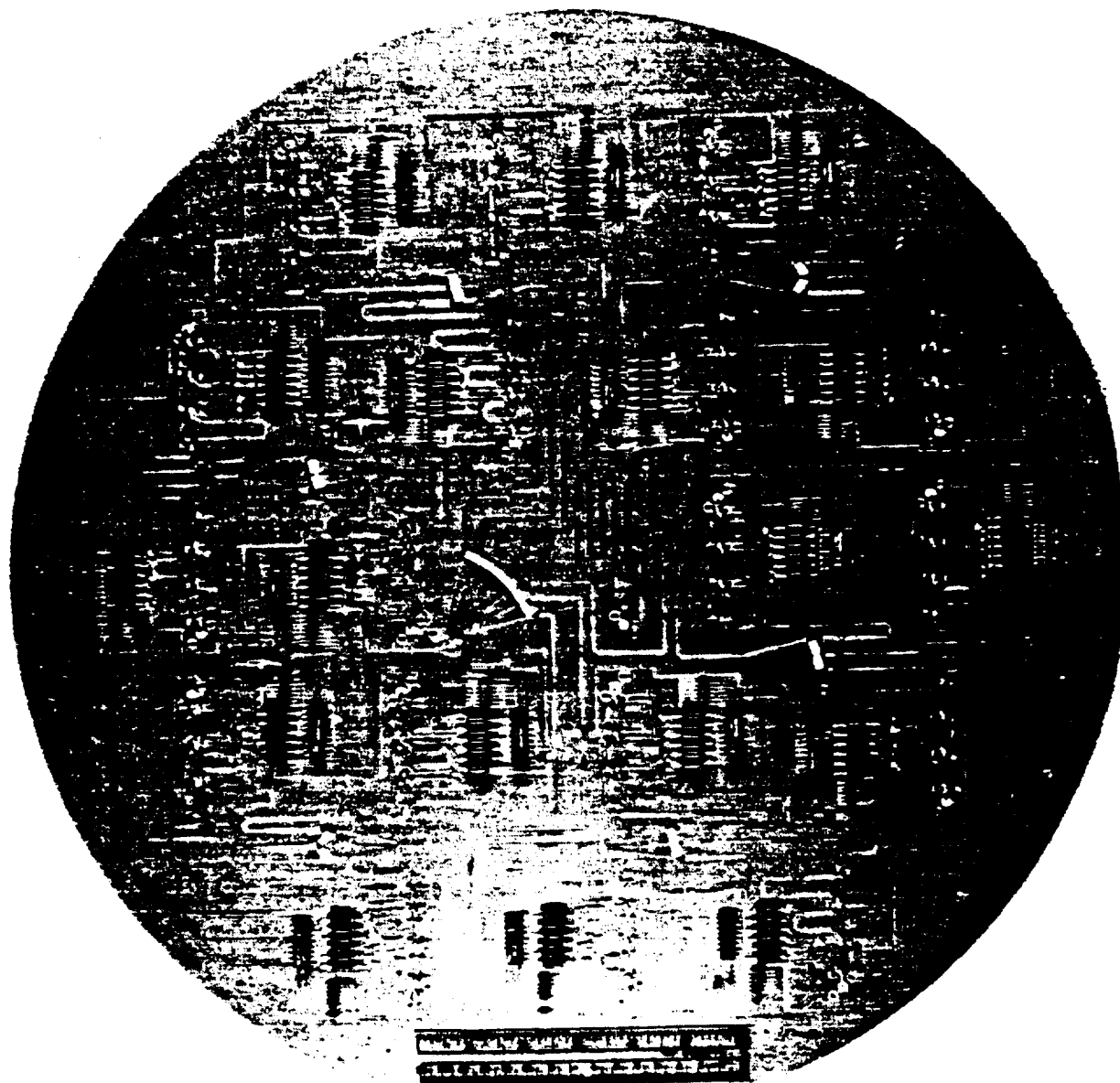


Figure 4-10. Photograph of Prototype #1

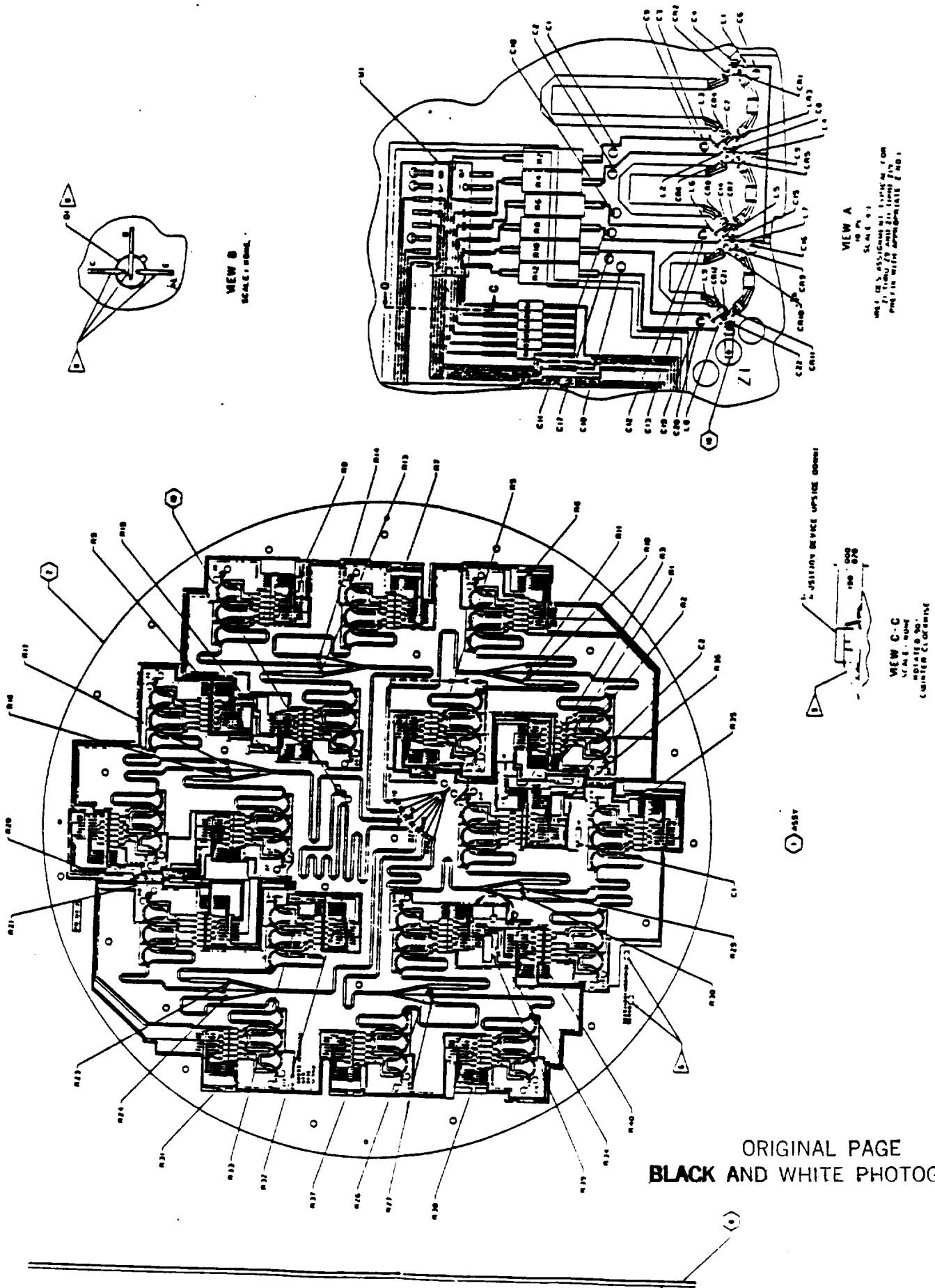


Figure 4-11. Layout of the Beamformer

One way was to cut and patch lines that were too long. The other, and preferred way, was to cover the lines appropriately with dielectric to add phase. By using these techniques we have managed to have all phases equal within  $\pm 10$  degrees with all phase shifters set at  $0^\circ$ .

Continue tracing the signal paths. Notice that at the end of each delay section, except the center one (reference), is an unequal 3-way divider. Initially there was concern about achieving a reasonable unequal divider, but measured performance of the entire 19-way divider have been quite satisfactory. Following the unequal dividers are more delay sections to even the phase going to each phase shifter. Each shifter feeds antenna elements comprising the three rings around the center as shown in Figure 2-1. The outer ring is supposed to have energy down 6 db below the center element. The middle ring has energy down 5.3 db below the center element. Again the layout achieved this distribution without any crossovers. Careful layout of the phase shifter bias circuits helped to achieve this geometry.

In the phase shifters, the circuit is orientated so all +5 volt lines face one way, and all lines going to drivers, face the driver elements which are mounted in close proximity to their respective phase shifters. This is shown in Figure 4-2 where the +5 volt line is on top and the lines to the driver are on the bottom. Also shown are the driver circuits. As was previously described in Section 4.2 extra decoupling capacitors had to be added. Therefore, the phase shifter design used in the array is based on that shown in Figure 4-3. Directly after the phase shifters the signals exit the beamformer board via right angle feedthroughs to the following hybrid board. To control moding, extra grounding screws had to be added around each feedthrough. The test results of the first two prototypes, built as described herein, are reasonably good for an initial attempt at this complicated board. These results are discussed in the next section.

#### 4.3 TEST RESULTS FOR THE FIRST TWO BEAMFORMERS

Both prototype beamformers have been evaluated using the HP 8510 network analyzer for phase, amplitude, and match. The results are discussed in this section. Considerably more time has been spent with beamformer #2 than #1 as will be evident by the volume of data presented. In general the performance is reasonable for an assembly in this state of development.

A summary of Beamformer #1's data is given in Table 4-4. Loss and phase angle are given for each port. The reference port number is 10. Ideal loss is also given on one of the top rows. Below the port data, is the match and loss data along with a statistical analysis of the loss data. All this data is for the beamformer phase shifters in the 0° position. The loss data represents the total power exiting the beamformer divided by the input power. However, these losses cannot be used for gain calculation because they do not account for the required power distribution needed at each antenna element. Our antenna system engineers, though, can take the specific powers going to each antenna element, couple it with antenna element gain, and calculate antenna gain.

The next series of tables summarizes data for beamformer #2. In this case we took data for many azimuth and elevation positions as well as having the phase shifters all in given phase shift positions. A computer program was developed to put this data in summary form. A complete data package is given in Table 4-7 in Appendix B. In the appendix, the given data includes beam position, desired loss, desired angle, measured loss and angles, total loss, statistical studies on power, VSWR (only taken for equal phase positions), mean delta phase shift from desired, and standard deviation on that delta angle. Somewhat more effort was spent trimming phase on beamformer #2 than #1 with the result that the gain is a little better. A summary of loss data for all these positions is given in Tables 4-5 and 4-6 for three frequencies. It can be seen in Table 4-5 that total loss varies up to .3 db for various positions of beam angle. This is probably caused by internal VSWR's phasing in and out within the beamformer. The situation is even more pronounced with the phase shifters set to the same angle. Graphical representation of this loss data versus beam position or uniform phase shift settings is shown in Figure 4-12.

Table 4-6 and Figure 4-13 gives a summary of the mean phase delta for the various positions. Ideally the 1545 Mhz data should be just as positive as the 1660 Mhz data is negative. The mean phase delta needs to be increased a little at the low frequency and decreased a little at the high frequency. Trimming the reference element by adding line length should help this. When all phase shifters are set to the same phase angle, the effect of growth of phase with frequency in the phase shifters can be seen. With the higher phase shift settings, the difference between low frequency and high frequency phase separates, as would be expected, since phase is proportional to frequency. The longer the path lengths, (needed by the higher phase shift positions), the more the low and high frequency phases separate.

Table 4-4. Beamformer #1 Performance Summary

Port #	1	2	3	4	5	6	7	8	9	10	11	12	13	14	15	16	17	18	19	
Ideal Loss	11.63	13.83	14.63	11.63	14.63	13.83	13.83	14.63	13.83	8.63	11.63	13.83	14.63	11.63	14.63	13.89	13.83	14.63	14.63	11.63

Freq. (MHz)	Loss (dB)	Phase (°)
1545	-46	-67
1600	-13	-106
1660	-13	-173

Freq. MHz	S11 MAG.	Total Loss	-3 dB Ref Ave	-3 dB STD. DEV.	-5.2 dB AVE.	-5.2 dB STD. DEV.	-6 dB REF. AVG.	-6 dB STD. DEV.
	VSMR	dB	dB	dB	dB	dB	dB	dB
1545	1.54	-2.03	-13.5	.30	-16.1	.35	-16.9	.6
1600	1.41	-2.04	-13.4	.47	-16.3	.25	-17	.47
1660	1.21	-1.90	-13.4	.37	-16.3	.42	-16.9	.45

Inner Ring Ports #1, 4, 7, 11, 14, 17  
 Middle Ring Ports #2, 6, 9, 12, 16, 19  
 Outer Ring Ports #3, 5, 8, 13, 15, 18  
 Reference Port #10

NOTE: All Phase Shifters at 0°

Table 4-5. Summary of Beamformer Losses for Various Beamformer Configurations  
Loss Data

Beamformer Status	1545 MHz				1600 MHz				1660 MHz			
	Tot Loss (dB)	Mean Inner Ring Loss (dB)	Mean Middle Ring Loss (dB)	Mean Outer Ring Loss (dB)	Tot Loss (dB)	Mean Inner Ring Loss (dB)	Mean Middle Ring Loss (dB)	Mean Outer Ring Loss (dB)	Tot Loss (dB)	Mean Inner Ring Loss (dB)	Mean Middle Ring Loss (dB)	Mean Outer Ring Loss (dB)
All Shifters -315°	2.03	13.7	16.2	16.8	2.03	14.1	16.5	17.2	2.14	14.0	16.3	17.1
All Shifters -270°	2.07	13.7	16.2	17.0	2.07	13.5	15.9	16.7	1.79	13.5	16.1	16.8
All Shifters -225°	2.45	14.3	16.4	17.3	2.45	13.8	16.0	16.9	2.17	14.1	16.5	17.3
All Shifters -180°	1.97	13.5	16.2	16.9	1.97	13.7	16.1	16.9	1.84	13.6	16	16.8
All Shifters -135°	1.97	13.5	16.2	17	1.97	13.9	16.4	17.2	2.04	13.8	16.3	17
All Shifters -90°	2.07	13.6	16.2	17	2.07	13.3	15.9	16.7	1.72	13.4	16	16.8
All Shifters -45°	2.34	13.9	16.4	17.4	2.34	13.5	15.9	16.9	2.05	13.8	16.4	17.3
All Shifters -0°	1.86	13.4	16	16.8	1.86	13.4	15.9	16.8	1.72	13.4	15.9	16.8
AZ = 315°, EL = 20°	2.11	13.9	16.1	16.9	2.11	13.7	16.1	17.1	1.95	13.6	16.2	17
AZ = 270°, EL = 20°	1.96	13.4	16.3	16.9	1.96	13.4	16	16.8	1.78	13.4	16	16.9
AZ = 225°, EL = 20°	2.10	13.8	16.1	16.9	2.10	13.7	16	16.9	1.92	13.6	16.2	17
AZ = 180°, EL = 20°	1.97	13.6	16.2	17	1.97	13.6	16.2	17.1	1.89	13.6	15.9	17.4
AZ = 135°, EL = 20°	2.13	13.8	16.1	17.1	2.13	13.5	16.1	17	1.97	13.7	16.3	17.3
AZ = 90°, EL = 20°	1.98	13.4	16.2	17	1.98	13.4	16	16.9	1.79	13.5	16.0	16.9
AZ = 45°, EL = 20°	2.12	13.7	16.3	17	2.12	13.6	16.1	17	1.95	13.7	16.2	17.2
AZ = 0°, EL = 20°	2.11	13.7	16.4	16.9	2.11	13.6	16.3	17	2.01	13.8	16.6	17.1
AZ = 0°, EL = 30°	2.08	13.9	16.2	16.8	2.08	13.6	16.2	16.7	1.95	13.8	16.5	16.9
AZ = 0°, EL = 40°	2.13	13.8	16.3	17	2.13	13.6	16.5	17	2.06	13.9	16.3	17.2
AZ = 0°, EL = 50°	2.04	13.6	16.3	17	2.04	13.4	16.1	17	1.88	13.5	16.2	17.1
AZ = 0°, EL = 60°	1.98	13.5	16.3	16.9	1.98	13.4	16	16.8	1.80	13.5	16	16.9

Table 4-6. Summary of Beamformer Mean Phase Errors for Various Beamformer Configurations

Beamformer Status	1545 MHz		1600 MHz		1660 MHz	
	Mean Phase Error for All Ports (Deg.)	Std. Dev. For Mean Phase Error (Deg.)	Mean Phase Error for All Ports (Deg.)	Std. Dev. For Mean Phase Error (Deg.)	Mean Phase Error for All Ports (Deg.)	Std. Dev. For Mean Phase Error (Deg.)
All Shifters -315°	+8.61	+5.02	-5.89	5.36	-16.89	6.36
All Shifters -270°	+11.50	5.7	-3.89	4.79	-15.39	5.69
All Shifters -225°	+11.44	5.5	-4.17	3.93	-14.89	4.79
All Shifters -180°	+6.00	4.53	-3.94	4.40	-12.78	4.80
All Shifters -135°	-.67	4.11	-9.28	4.92	-14.44	5.67
All Shifters -90°	+2.11	4.40	-8.50	4.54	-12.67	5.05
All Shifters -45°	+2.50	3.95	-8.61	3.83	-11.50	4.14
All Shifters 0°	-2.44	3.2	-8.39	3.7	-8.17	4.3
AZ=315°, EL=20°	+4.67	6.41	-5.50	4.43	-13.06	6.11
AZ=270°, EL=20°	+5.94	7.8	-5.44	5.43	-11.61	5.34
AZ=225°, EL=20°	+1.83	6.3	-5.94	5.96	-12.22	6.11
AZ=180°, EL=20°	-.50	7.83	-6.61	6.42	-11.22	4.89
AZ=135°, EL=20°	+6.06	7.91	-8.94	5.44	-14.94	6.28
AZ=90°, EL=20°	+3.33	5.44	-7.44	4.67	-11.06	5.76
AZ=45°, EL=20°	+6.39	7.25	-7.94	5.61	-16.39	5.57
AZ=0°, EL=20°	+7.61	7.68	-6.94	6.12	-16.33	7.93
AZ=0°, EL=30°	+7.94	6.71	-6.28	4.68	-16.06	7.60
AZ=0°, EL=40°	+6.61	5.75	-6.67	4.65	-15.17	7.49
AZ=0°, EL=50°	+6.67	5.31	-5.17	4.18	-14.11	6.57
AZ=0°, EL=60°	+5.33	6.66	-5.61	4.54	-12.39	6.17

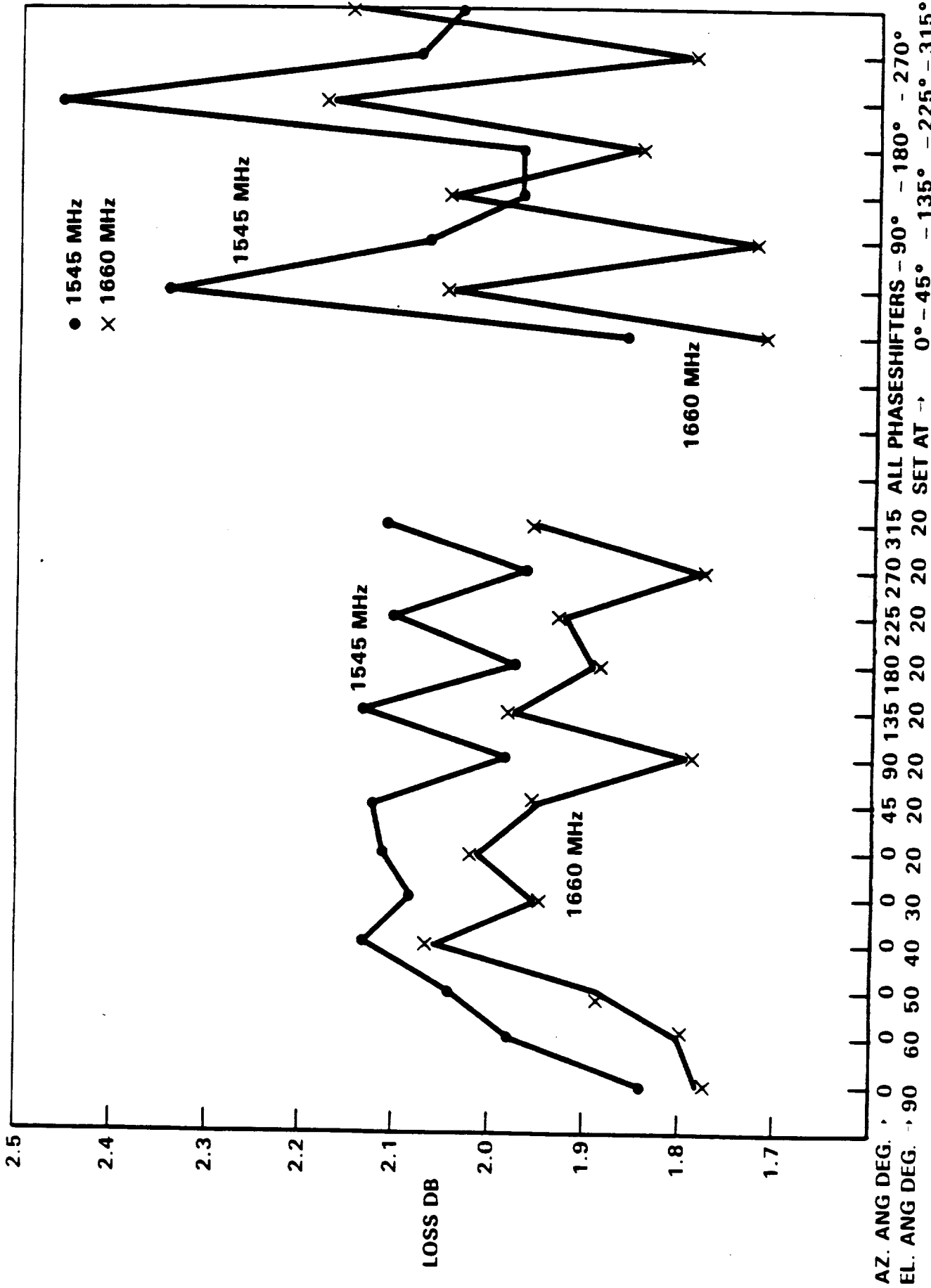
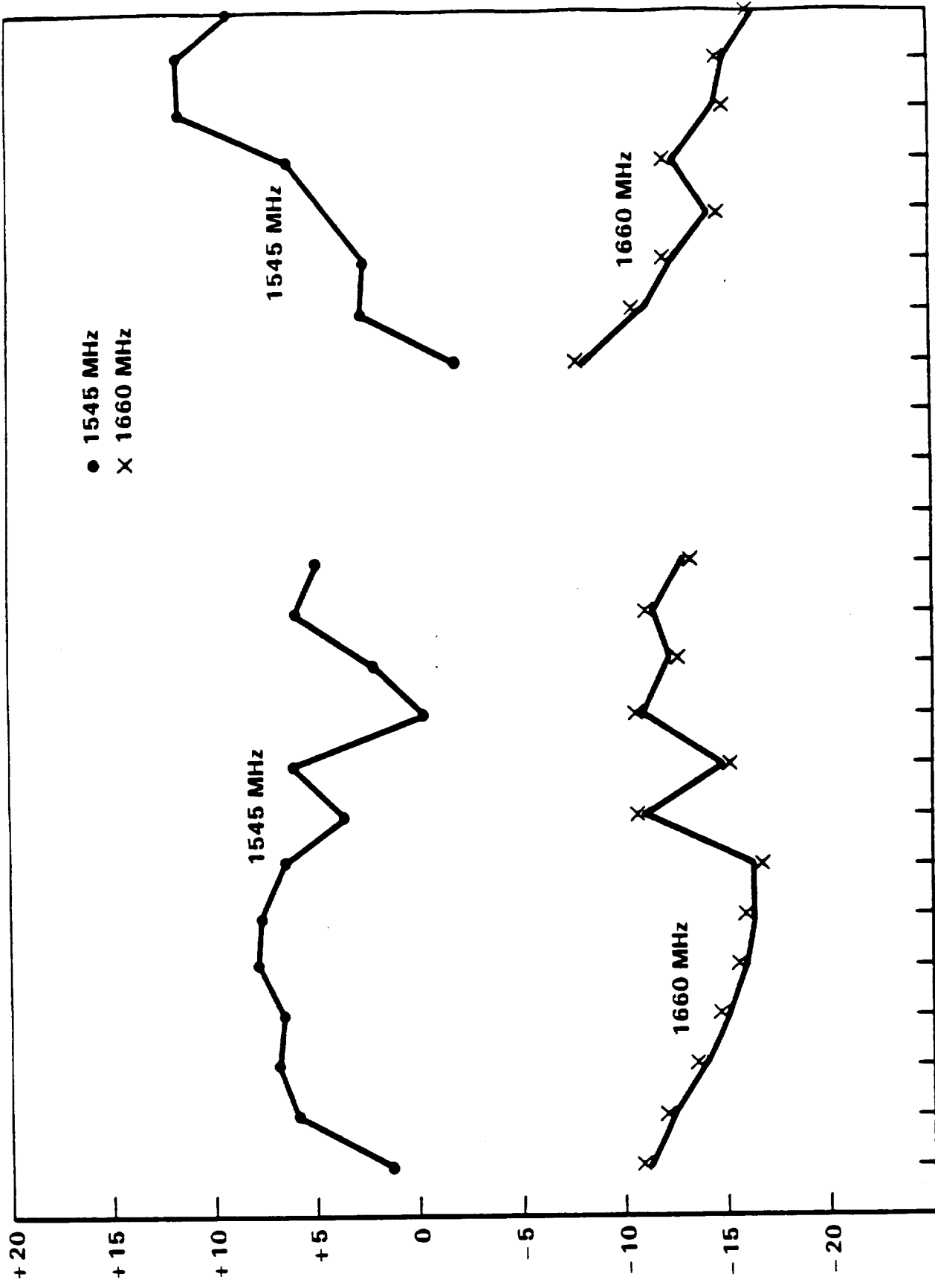


Figure 4-12. Beamformer Loss vs. Pointing Angle or Phase Shifter Setting



AZ. ANG DEG. → 0 0 0 0 0 0 0 0 45 90 135 180 225 270 315 ALL PHASESHIFTERS - 90° - 180° - 270°  
 EL. ANG DEG. → 90 60 50 40 30 20 20 20 20 20 20 20 SET AT 0° - 45° - 135° - 225° - 315°

Figure 4-13. Beamformer Phase Delta from Desired vs. Pointing Angle or Phase Shifter Setting

4.4

## FEATURES

The major feature or achievement is that the design works and works pretty much as calculated the first time it was tried in its entirety. While there are some deficiencies as will be discussed in the next section, these are relatively minor and will easily be corrected in the hoped for follow on work.

Basically, the feasibility of an extremely large single beamforming board has been proven along with the concept of unequal power dividers. Also proven is that potentially low cost, large scale surface mount techniques, will work for this phased array application.

4.5

## DEFICIENCIES AND WORK TO BE DONE IN THE NEXT PHASE

There are some apparent deficiencies in the beamformer which should be corrected in future iterations. These include the fact that the meandering delay sections do not exactly equalize the phases. Various lengths have to be changed in an appropriate manner. Secondly, the exact power splits on the equal 7-way divider and on the unequal 3-way divider needs to be individually confirmed. In addition a study should be conducted to pick the best possible microwave resistor considering both microwave performance and cost. The phase shifters have to be optimized so that mismatch and loss problems are eliminated. A diode study needs to be conducted to pick a reliable, high performance, and low cost part. Finally, a new mechanical design needs to be evolved to eliminate the numerous screws that currently provide adequate grounding and mode suppression. All this will be planned for the next phase.

## SECTION 5

### ANTENNA BEAM ANGLE STEERING CONTROL

The angle tracking servomechanism is designed to minimize angle tracking error over a wide number of contingencies. Basically, the fast response operations are controlled by the angle rate sensor while the radio link corrects the rate sensor errors. Because the rate sensor bias error changes relatively slowly, the radio link data is averaged over a 30 second period before correcting the rate sensor. This will filter out any attitude perturbations, shadowing or fading (multipath) effects in the radio link. Future tests will indicate whether this time constant needs to be modified.

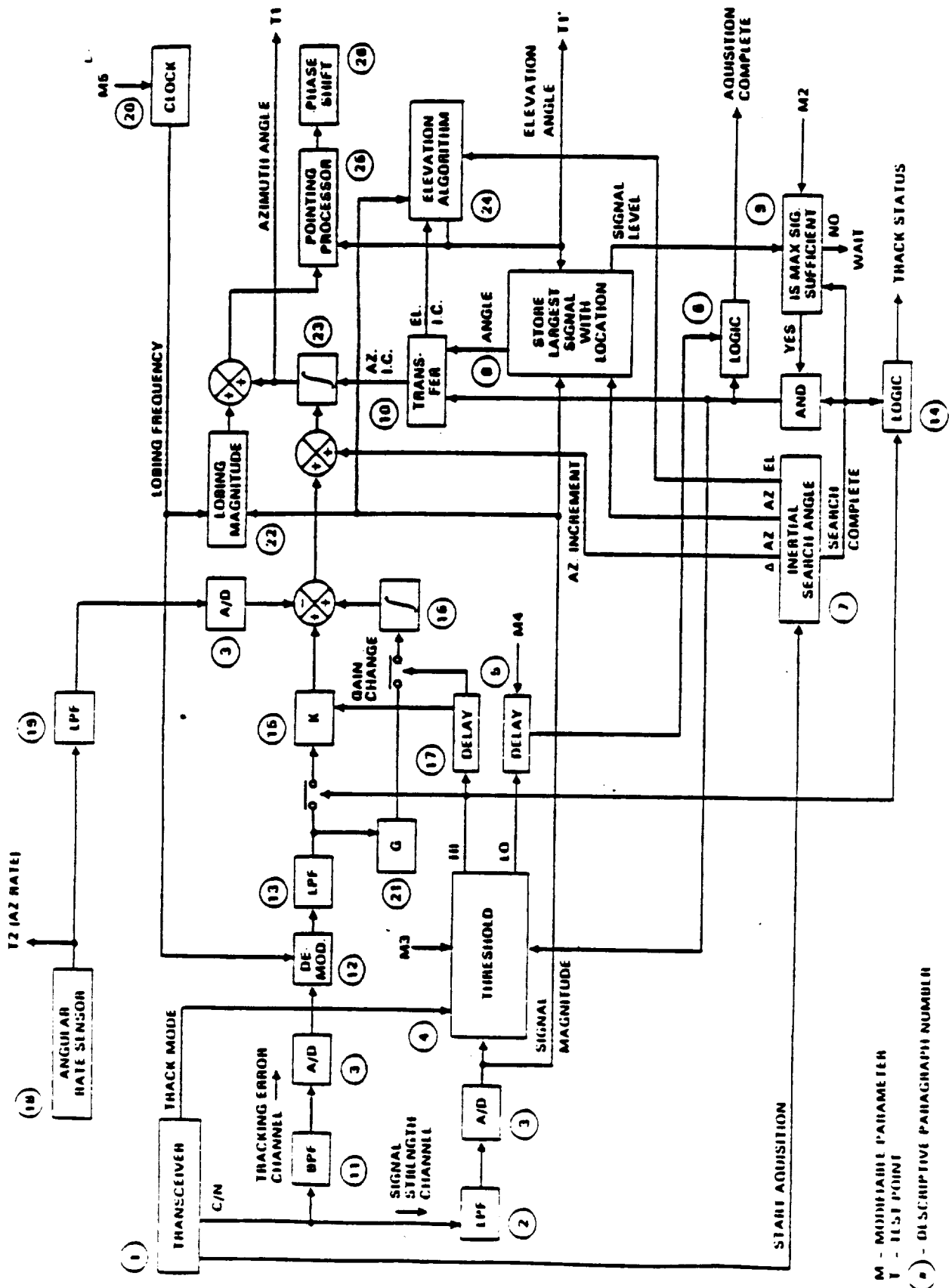
When the rate sensor is disconnected, the rate sensor correction is eliminated and the radio link loop gain is automatically increased. This allows somewhat less accurate but still adequate satellite tracking on pilot signal alone; however, it will no longer be able to follow vehicle turns during signal outages.

The sequential lobing dither of the radio link is held to plus and minus 1.5 degrees under normal signal strength conditions in order to have maximum intersatellite isolation. The dither magnitude is only increased if signal level drops. This is done automatically by sensing the strength of the pilot signal. The dither frequency is a modifiable parameter which can be adjusted between 10 and 200 Hz.

The elevation angle of the antenna beam is controlled by searching for maximum signal strength. Because of the wide antenna beamwidth and the generally slow variation of satellite elevation angle, this search is done at a rate of one incremental beam shift per second from 20° through 60° in increments of 5°. The total number of incremental elevation beams is nine. A tenth one (90°) is available in the manual mode. The low search rate also separates the elevation servo information from the azimuth servo to prevent cross-coupling.

#### 5.1 STEERING CONTROL SYSTEM DESCRIPTION

A block diagram of the Antenna Steering Control is shown in Figure 5-1. Each block has a number identifying the paragraph below which explains the block.



M - MODIFIABLE PARAMETER  
 T - TEST POINT  
 ( ) - DESCRIPTIVE PARAGRAPH NUMBER

Figure 5-1. MSAT-X Antenna Steering Control

## 1. Transceiver

The receiver portion of the transceiver amplifies the pilot signal coming from the MSAT-X antenna. It will have a bandwidth sufficient to accommodate the AM sidebands produced by sequential lobing. A sequential lobing at a constant rate to the right and left of boresight produces a square wave modulation which has a large number of sidebands. The first sideband pair at the lobing frequency has over 81% of the total sideband power. If we include the next sideband pair (which is at the third harmonic) we get 9% more power, and the fifth harmonic adds 3.2% additional. The signal processor following the receiver is a matched filter to the lobing signal such that any loss in sideband energy reflects directly as a loss in signal-to-noise ratio. For this reason, a lobing frequency just above the multipath interference band would allow reception of most of the sideband energy with modest bandwidth. At a minimum, at least the first sideband pair should be accepted giving a sequential lobing signal-to-noise ratio loss of 0.9 dB.

The receiver C/N output which is fed to the steering control servomechanism represents either the in phase coherent component (C) of the IF signal mixed to base band by the phase locked loop, or a noncoherent detection output (N). The C signal is present when the phase locked loop is locked during normal angle tracking, while the N signal is present during acquisition. In either case, the voltage is directly proportional to the IF envelope. The average envelope magnitude is a measure of signal strength and the amplitude modulation is a measure of the antenna pointing error. According to the interface signal specification, this output will be a nominal -1 volt corresponding to a -137 dBW receiver input level. At present, there are no plans to incorporate an automatic gain control on the received signal so that the C/N voltage will change directly with the transceiver input signal level.

The Track Mode command from the transceiver to the antenna commands the antenna into hybrid tracking mode when low and into open loop (inertial tracking only) mode when high. Normally, the signal is low, allowing the antenna to determine the appropriate mix of inertial and pilot signal steering based on the received signal power history. During acquisition the Track Mode command is high which will force the antenna into a purely inertial tracking mode. The C/N output is N (noncoherent) during acquisition. After the signal has been acquired and the receiver C/N output is C (coherent), the Track Mode command will go low (hybrid tracking mode).

A Start Acquisition command from the transceiver to the antenna is a pulse of at least 10 msec and no more than 100 msec at TTL levels. The signal is negative true. As the name implies, the signal commands the antenna to start its azimuth scanning sequence.

## 2. Carrier Amplitude Low Pass Filter

The C/N channel output is a measure of the IF signal instantaneous envelope. This envelope contains an average value which represents the carrier level and an alternating component which is proportional to the antenna steering error. The low pass filter removes the alternating component so that only the average carrier level remains. This output is used to determine whether or not the steering control loop has sufficient signal strength to permit closed loop tracking. The low pass filter time constant is 0.12 second, which matches the half power beamwidth time on signal during the search phase of operation.

## 3. Analog-to-Digital Conversion

Analog-to-digital conversion is used in three places to separate the analog and digital processing. Much of the processing can be done either in the analog or digital domain. The dividing line was determined by engineering judgment. The A/D converters are 10 bit and operate on DC signals from 0 to 5 volts.

## 4. Threshold Circuit

The threshold circuit determines whether or not the signal level is sufficient for closed loop tracking. This is a Modifiable Operational Parameter (M3) for testing purposes. The threshold circuit is not activated until the Track Mode Command is low. If the C/N signal level is above threshold level, the steering control loop is immediately closed, otherwise it is opened. The tracking status is sent to the outside world.

## 5. Signal Search Delay (Open Loop Time-Out)

If the signal fades, the steering control gets no information from the receiver. Angle tracking is then accomplished solely from the angular rate sensor. Depending upon the quality of the angular rate sensor, the antenna can remain pointed at the satellite within a beamwidth for a considerable time while waiting for the signal to return. Eventually, however, the pointing accuracy degrades to such an extent that the probability of pointing at a satellite is sufficiently small to inform the transceiver by setting the 'Acquisition

Complete' interface control signal low. This search delay is a Modifiable Operational Parameter (M4) for use during testing.

#### 6. Logic for Acquisition Complete (AC) Signal

The 'Acquisition Complete' line is low when:

1. The antenna is in the search mode, or
2. The antenna has completed the search mode (or not started the search mode) but has found no signal exceeding the threshold level determined by Modifiable Parameter 2, or
3. The received signal has dropped below threshold determined by Modifiable Parameter 3 for a time period exceeding that determined by Modifiable Parameter 4.

The 'Acquisition Complete' line is high when:

1. The antenna has completed the search mode, and
2. The searched for signal is above the threshold determined by Modifiable Parameter 2, and
3. The present signal has not been below the threshold determined by Modifiable Parameter 3 for a period exceeding that determined by Modifiable Parameter 4.

#### 7. Inertial Search Angle Sequence

The antenna is scanned in azimuth and elevation whenever it receives a Start Acquisition command. The scan in azimuth is done in inertial space because the vehicle carrying the antenna may be in motion and turning during the search phase of operation. The inertial coordinate search is only possible if the azimuth angular rate sensor is in operation, otherwise, the search is done in vehicle coordinates. The elevation angle search is always done in vehicle coordinates because: (1) there is no vertical rate sensor and, (2) the vertical beamwidth is wide enough to span most expected vertical excursions of the vehicle.

The azimuth angles are scanned at a rate of 250 degrees/second at a 30 degree elevation, and 338 degrees/second at a 50 degree elevation. This permits the search for one pilot signal to be accomplished in 2.5 seconds with half power time on target of 0.12 sec. When the search is complete, the 'Track Status' output is set high and the maximum signal level

measured during the search is tested for tracking adequacy. If the maximum signal level exceeds that determined by Modifiable Parameter 2, the 'Acquisition Complete' output is also set high.

#### 8. Maximum Signal Level Storage

During the signal search mode described for Block 7, the signal magnitude for each angle is measured. If the signal level is stronger than that previously measured during the search, its magnitude along with the corresponding antenna azimuth and elevation angles is stored. Only one storage location is necessary because the stronger signal always replaces the weaker.

#### 9. Signal Strength Test

After all antenna positions have been sampled for signal availability during the antenna scan, the search is stopped and the maximum signal level stored in Block 8 is tested for sufficiency as determined by Modifiable Operational Parameter 2. If the maximum measured signal strength is sufficient, the 'Acquisition Complete' output is set high. The antenna steering control is simultaneously set at the azimuth and elevation angles through Block 10. The antenna steering loop is now ready to start closed loop tracking when the Track Mode signal from the transceiver is set low.

Modifiable Operational Parameter 2 (Acquisition Minimum Signal Level) is called out separately from Parameter 3 (Open Loop/Closed Loop Threshold Signal Level) in the addendum to Exhibit 1, Antenna System Requirements. In all likelihood, these parameters should be the same; any acquisition minimum signal level should also be an acceptable closed loop signal level.

#### 10. Angle Transfer

The azimuth and elevation angles stored in Block 8 give the antenna position where the maximum signal strength was measured during antenna scan. The low pass filter in Block 2 effectively integrates the signal return for the time the satellite is within the antenna beamwidth. Consequently, the full signal strength is not indicated until the antenna beam has passed the peak gain position. The low pass filter output reaches a maximum approximately 60 milliseconds after the antenna passes the satellite line of sight due to capacitive storage. At the 30 degree elevation search angle, the scan rate is 250 degrees per second (see Block 7) which causes the peak output to register 15 degrees after the

beam passes line of sight. At 50 degrees elevation, the search rate is 338 degrees per second, which causes the peak output to register 20 degrees after the beam passes the line of sight. These offsets are subtracted in Block 10 from the stored azimuth before being added to the azimuth angle integrator (Block 23). The elevation angle (either 30° or 50°) is transferred without modification.

#### 11. Error Signal Band Pass Filter

The error signal band pass filter separates the amplitude modulation component from the DC carrier in the C/N channel. This reduces the dynamic range requirement for the following analog-to-digital converter. Because the AM component is driven toward 0 volts by the angle tracking loop, the band pass filter will also amplify the signal by a factor of 50 so as to fully utilize the analog-to-digital converter capability.

#### 12. Demodulator

The closed loop steering information is carried in the amplitude of the square wave modulation arriving at the demodulator. By multiplying its signal with a fixed amplitude replica of the dither signal, the square wave modulation is converted to a dc voltage proportional to the antenna beam pointing error.

#### 13. Antenna Error Angle Low Pass Filter

The low pass filter eliminates the excess noise and multipath interference passed by the receiver because of its wide bandwidth to accommodate the dither sidebands discussed in Block 1. The low pass bandwidth need only be wide enough to permit the dynamic passage of pointing errors accumulated by the angular rate sensor control. This is in the order of fractions of a Hertz. However, since the bandwidth of the closed loop will be controlled by other parameters, it will not be necessary to reduce the bandwidth to less than a few Hertz. The reduced bandwidth allows the digital processor to operate at a lower sampling rate without suffering the effects of aliasing.

#### 14. Track Status Logic

Track status is a signal from the antenna to the transceiver. During acquisition, this signal is set low while the antenna is scanning and is set high at the completion of the scanning sequence. In track mode, this signal indicates the type of antenna tracking. A low TTL level indicates hybrid tracking and a high TTL level indicates open loop tracking.

### 15. Closed Loop Gain Control

The closed loop gain of the antenna steering control is determined by the sum of all the component gains in the closed loop path. The value of K shown in the block is merely a convenient place to modify the loop gain for the two conditions of rate aided tracking and non-rate aided tracking. The theory and computations for the value of K are given in Appendix C. The value of K is 2 degrees per second per volt peak-to-peak error during normal operation. However, for one second after initial signal acquisition, the gain is increased by a factor of 20 to assure rapid antenna positioning to the satellite.

### 16. Integral Control

Without integral control, the pilot signal can only correct a constant angular rate sensor error by having a corresponding offset error in the pointing angle. Increasing the loop gain K reduces the offset error, but increases jitter from the noise accompanying the error signal. In addition, if the signal fades, the antenna beam will move away from the satellite at a rate proportional to the uncorrected angular rate sensor error.

The purpose of the integral control is to reduce the constant or slowly varying angular offset error of the angular rate sensor to zero when the pilot signal is present. The output of the integrator is then equal but opposite to the angular sensor error. If the signal fades, the integrator holds its output at its last value, removing the angular rate sensor error during open loop tracking.

### 17. Integral Control Delay

When the pilot signal exceeds the threshold as determined by Block 4, the direct control loop through Block 15 is closed immediately, but the loop through the Integral Control Block 16 is delayed. This is because prior to detecting the signal, the antenna will probably have an offset, either due to antenna angle wander when under open loop control, or due to the initial error in measuring the azimuth beam angle during search. It is necessary for the direct control to remove these initial errors before the integral control is closed to remove steady state errors. The delay is presently set for one second. The delay is used only when inserting integral control; there is no delay when the integrator input is opened. The integrator input is always open if there is no Angular Rate Sensor.

### 18. Angular Rate Sensor

The angular rate sensor produces a DC voltage proportional to the antenna azimuth rotation rate in vehicle coordinates. This signal is the major input to the antenna control in that it enables removal of most of a beam pointing error caused by vehicle turns. The primary task of the closed loop pilot signal channel is to correct for the errors in the angular rate sensor.

### 19. Angular Rate Low Pass Filter

The purpose of the low pass filter is to ensure that there are no extraneous high frequency noise voltages to cause aliasing effects on the output of the analog-to-digital converter.

### 20. Clock Frequency Generator

The clock determines the antenna lobing dither rate. The theory of closed loop operation is independent of lobe frequency as long as the frequency is above the response function of the servomechanism. It follows then that the dither frequency could be continuously variable or random. In general, the dither waveform would be ideally selected for maximum immunity to signal fades. The optimization of dither waveform will have to await the results of field tests under actual operating conditions. For the present, the dither rate is controlled by the Modifiable Operational Parameter 5 which is adjustable from 10 Hz to 200 Hz.

### 21. Integral Control Gain

The integral control gain  $G$  determines the averaging time over which the angular rate sensor drift error is determined. It is only effective after the pilot signal search phase has been completed and all the transients have died out. The theory and computation for the value of  $G$  are given in Appendix C. The value of  $G$  is  $(1/15)$  deg/sec/sec per volt peak to peak.

### 22. Dither Magnitude Control

The dither magnitude is controlled automatically by the signal amplitude. The dither magnitude has a direct influence on the closed loop servomechanism gain, error channel signal to noise ratio and second satellite signal rejection. In general, it is desired that the dither be kept to a minimum to reject the second satellite signal; however, it is necessary that the dither be sufficient to prevent angle track loss. Obviously then, the dither can only

be a minimum at high signal-to-noise ratio and must be increased as the signal level decreases. This also keeps the angle tracking loop gain constant which is a desirable feature.

### 23. Azimuth Angle Integrator

The azimuth angle integrator takes the sum of all input digits and when the output reaches 3 degrees, increments the azimuth angle by this amount. The initial starting angle is the largest signal amplitude location determined during the antenna scan mode. The azimuth angle is also an output at test point 1.

### 24. Elevation Algorithm

It was originally envisioned that elevation track would be accomplished by testing the signal level periodically at 30 and 50 degrees and staying predominantly at the angle of greatest signal strength. Further analysis indicated that the signal level could drop as much as 5 dB when moving from a favorable to an unfavorable elevation angle. For this reason, it was decided to move the elevation angle in smaller steps. The step size is small enough such that the maximum antenna gain loss is less than 1 dB.

The elevation tracking loop utilizes the signal strength channel rather than the tracking error channel. This separates the elevation tracking loop from the azimuth tracking loop. The elevation angles are incremented in steps toward the strongest signal return. The period between steps is on the order of one second.

Elevation control is initiated immediately after acquisition is complete and the transceiver interface track mode signal indicates "Normal Tracking". The search algorithm operates as follows:

1. Move the beam one resolution angle up if the acquisition was accomplished on the lower search beam, one down if the acquisition was accomplished on the upper beam.
2. Determine the pilot signal strength averaged over one second in the new beam position.
3. If the signal strength is larger than that measured in the previous position, move an additional resolution angle step in the same direction; otherwise, move back one resolution step. If the limits of elevation have been reached such that there is no further resolution angle step in the same direction, move to the previous angle step.

4. Go to instruction 2.

## 25. Pointing Processor

The pointing processor converts the azimuth and elevation angles into the 18 equivalent phase shifts which feed the radiating elements.

## 26. Phase Shifters

The phase shifters are located in the RF lines leading to the antenna elements.

## 5.2 POINTING ELECTRONICS

The pointing electronics hardware provides the requisite analog and digital circuitry needed to implement the pointing subsystem algorithm. It also provides an interface with the transceiver, rate sensor, antenna, user, and test equipment. To provide these features, the electronics is divided and placed at two different locales, namely the electronics box and the antenna. All the circuits associated with power conditioning, input signal processing, and test interfacing is housed in the electronics box. The shift registers, which drive the phase shifters, are part of the beamformer assembly - a board constituting the fifth layer of the antenna. A frontal view of the electronics box is shown in Figure 5-2 with the main circuit boards comprising the box depicted in Figure 5-3. The reader is referred to Figure 4-10 of Section 4 of this report for a view of that portion of the electronics located on the beamformer board.

### 5.2.1 Hardware Description

It is altogether fitting to begin a discussion of the electronics hardware by referring to a block diagram/cable interconnect of the overall system as shown in Figure 5-4. Four major blocks are shown, namely an electronics assembly (box), the beamformer, an antenna subassembly, and a receiver test set. The latter item is for system test purposes only and would be replaced with a transceiver in an actual commercial installation. The two former items are the subject of discussion in this Section with the majority of the pointing/control electronics located in the electronics box. The advantages of having a separate electronic box are as follows:

- It gives a chance to move the electronics away from harsh "open air" conditions.
- The concentration of many low reliability, low cost components in one assembly makes it possible to become a "throw away" item.

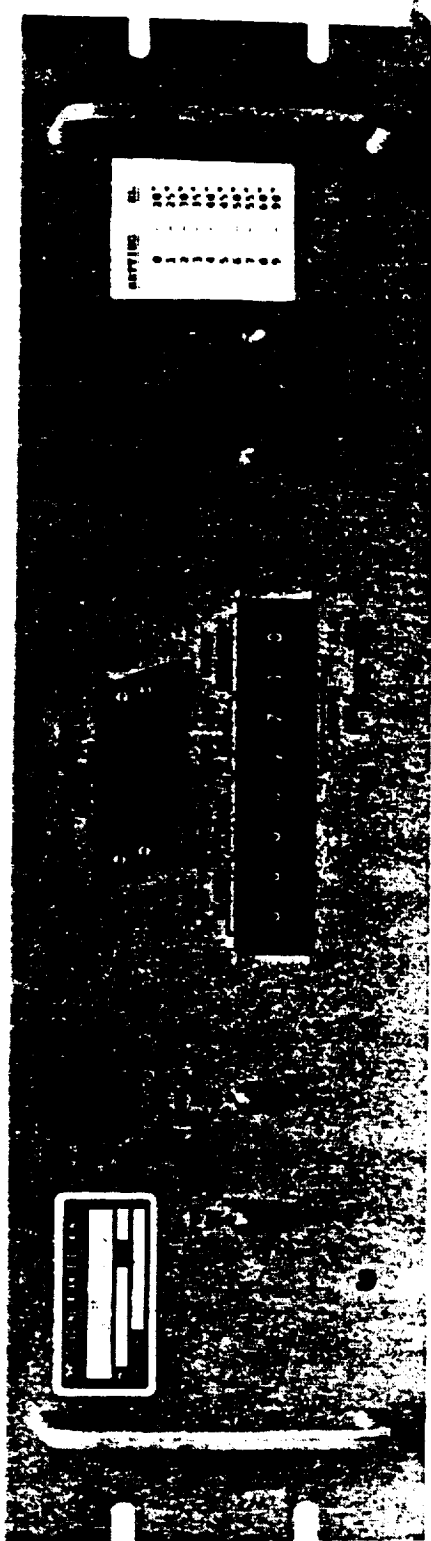


Figure 5-2. A Front Panel View of the Electronics Box

ORIGINAL PAGE  
BLACK AND WHITE PHOTOGRAPH

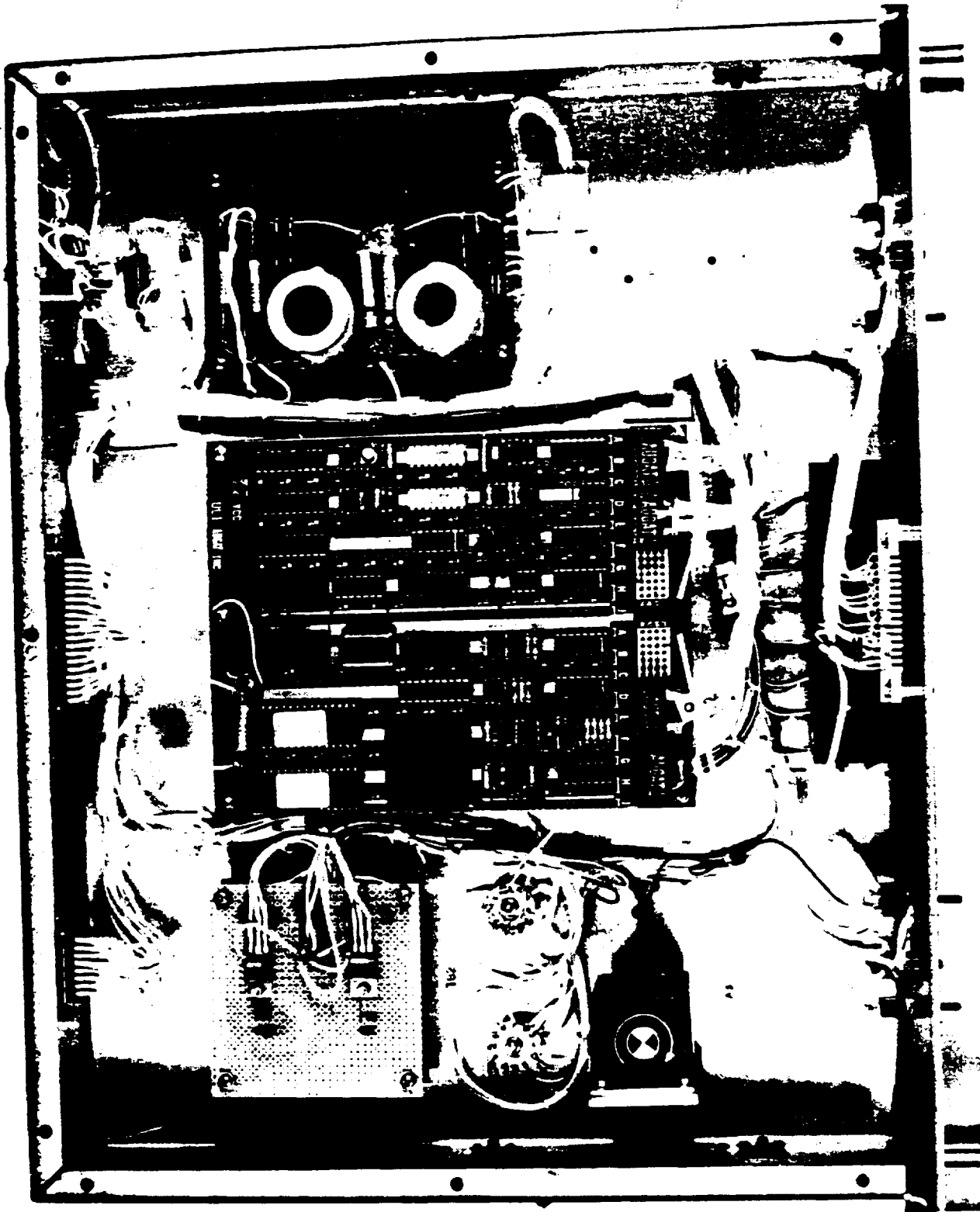


Figure 5-3. View of the Electronics Box with the Top Cover Removed

The signal processing "mother" board is located in the center. To the right is the power transformer board. In the upper left is the voltage regulator board. The angular rate sensor is located at the lower left of the mother board.



- It does not affect the size of the antenna, and
- It is easy to maintain.

### 5.2.2 Transceiver Interface

A block diagram of the transceiver interface is shown in Figure 5-5. It also serves as a signal flow description. The hardware supports two different modes of operation. With the first mode, only the radio links signal serves as an input to the antenna's steering servo-loop. In the second mode, the radio link signal is inputted along with the vehicle's turn rate as measured by the angular rate sensor. Either of these modes is selected via the "ANGULAR RATE SENSOR" switch on the front panel (see Figure 5-2). The operation of this interface circuitry is as follows:

- The transceiver output signal is band-limited and is shifted in level thereby adapting it to the microcontroller's A/D converter.
- The aforementioned input signals are conditioned in bandwidth and level by active filters prior to being inputted at the A/D converter, the latter being part of an intel 8097 microcontroller loop. One filter (bandpass) has a gain of 26 and a 3dB passband from 10Hz to 400Hz. The other filter is a low pass design with a gain of 5 and a low frequency corner of 1.3Hz.
- Two discrete inputs and two discrete outputs form a handshake mode of operation by which the transceiver directs the operation of the pointing system. The "START ACQUISITION" pulse is buffered and accepted by the High Speed Input of the microcontroller which then measures the direction of this pulse, making sure it lasts 10 milliseconds, minimum. The "TRACKING MODE" input is buffered and read by the microcontroller's PORT 1.
- Discrete output signals, "TRACKING STATUS" and "ACQUISITION COMPLETE", are entered in parallel at DATA BUS and stored in U16 (see Appendix D, Dwg. No. 1056C0002) transparent latch.

### 5.2.3 User Interface

Two modes of operation are available - "MANUAL" and "AUTO". In the "AUTO" mode, the pointing system exercises search or tracking algorithms which can be altered by four modifiable parameters. These parameters are controlled by a set of thumbwheel switches. In the "MANUAL" mode, the right half of the thumbwheel switch set is used to control or steer the antenna's beam to a desired position in azimuth and elevation.

The modifiable sets of parameters are entered into the system by depressing the "LOAD" pushbutton. This event also initiates the sequence which allows these parameters to be

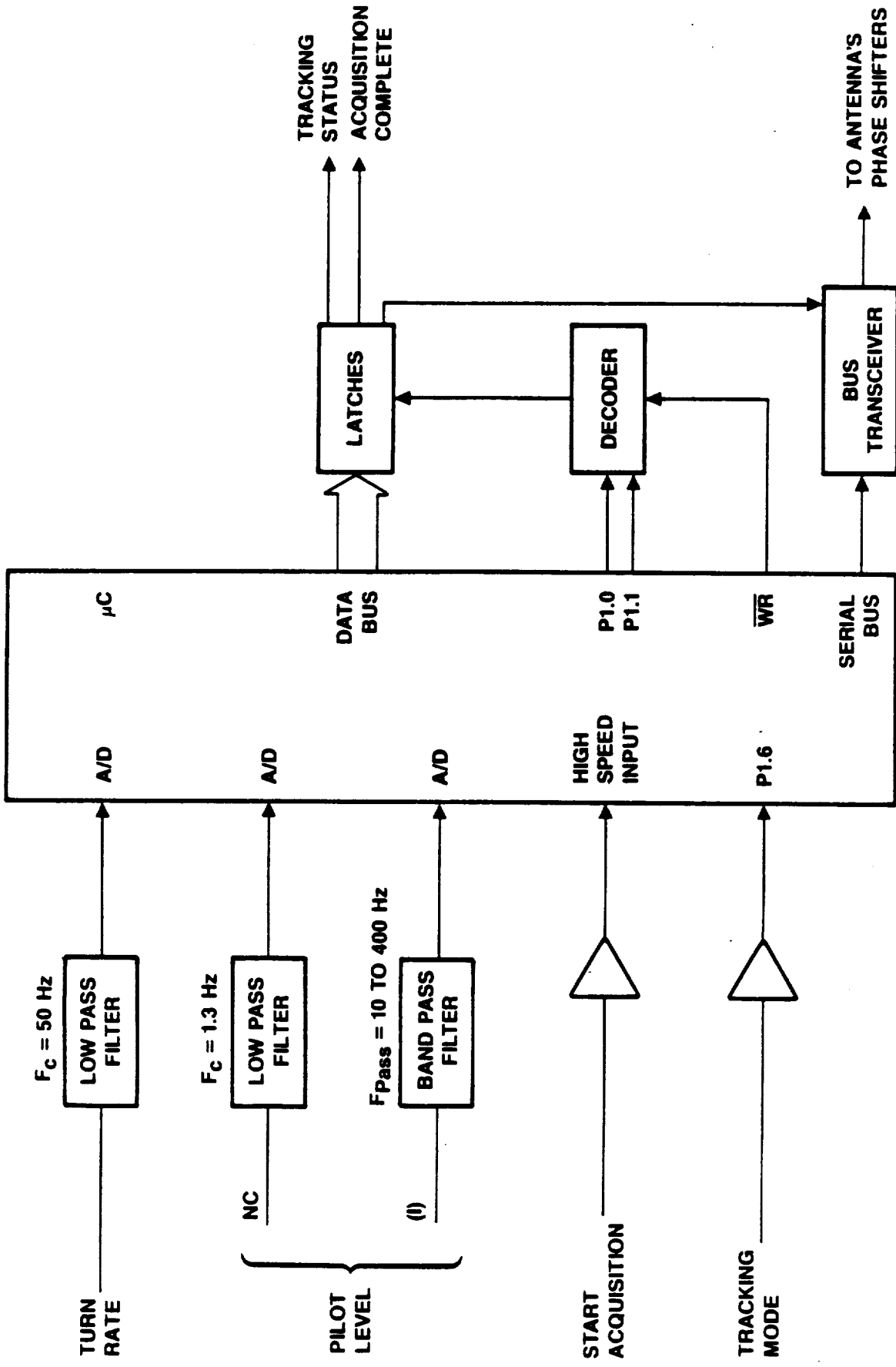


Figure 5-5. Block Diagram of Transceiver Interface

recorded by the user's test equipment. Figures 5-6 and 5-7 describes this interface which is supported by the "HS INPUT" and "HS OUTPUT" handshake pair of discrete signals.

#### 5.2.3.1 Dither, Search, and Track

Regarding the modifiable parameters mentioned above, each one is preset by two digits. For the search and track signal threshold, they represent a percentage of one volt (e.g. "99" => .99 volt). The open loop delay is in seconds (e.g. "20" => 20 seconds). The dither frequency is in multiples of 10 Hertz (e.g. "20" => 200 Hz, "04" => 40 Hz), and is limited by the software to range from 10 Hz to 200 Hz.

#### 5.2.3.2 Elevation and Azimuth

Four thumbwheel switches located at the right, center (see Figure 5-2) of the front panel are used for steering the antenna to a desired location when the system is in the "MANUAL" mode. "AZIMUTH" is represented by three switches whereas "ELEVATION" is set by one digit and is not direct reading, but is coded as shown in Table 5-1. The mean antenna position is displayed using the set of LEDS above the thumbwheel switches (see Figure 5-2). A circuit synopsis of the events that occur at a particular thumbwheel setting are as follows:

- At "POWER ON", the thumbwheel switch S1 reset setting is latched into Parallel In/Serial Out Shift Registers (U1, U2, U3, and U4), read through the microcontroller's Serial Bus, and stored in memory for future use.
- In the "MANUAL" mode, S1 is read by depressing the "LOAD" pushbutton. The antenna is steered to a desired position according to the setting of S1.
- "ARS" switch (SW2) distinguishes between the operation with and without the angular rate sensor.
- The "MALFUNCTION" LED (DS5) indicates the discovery of errors in the "wrap-around" self test (the first bit in the 144 bit word is remembered and checked, thence updating the position of the antenna), or during the A/D self test, when a set voltage is read at ACHO.

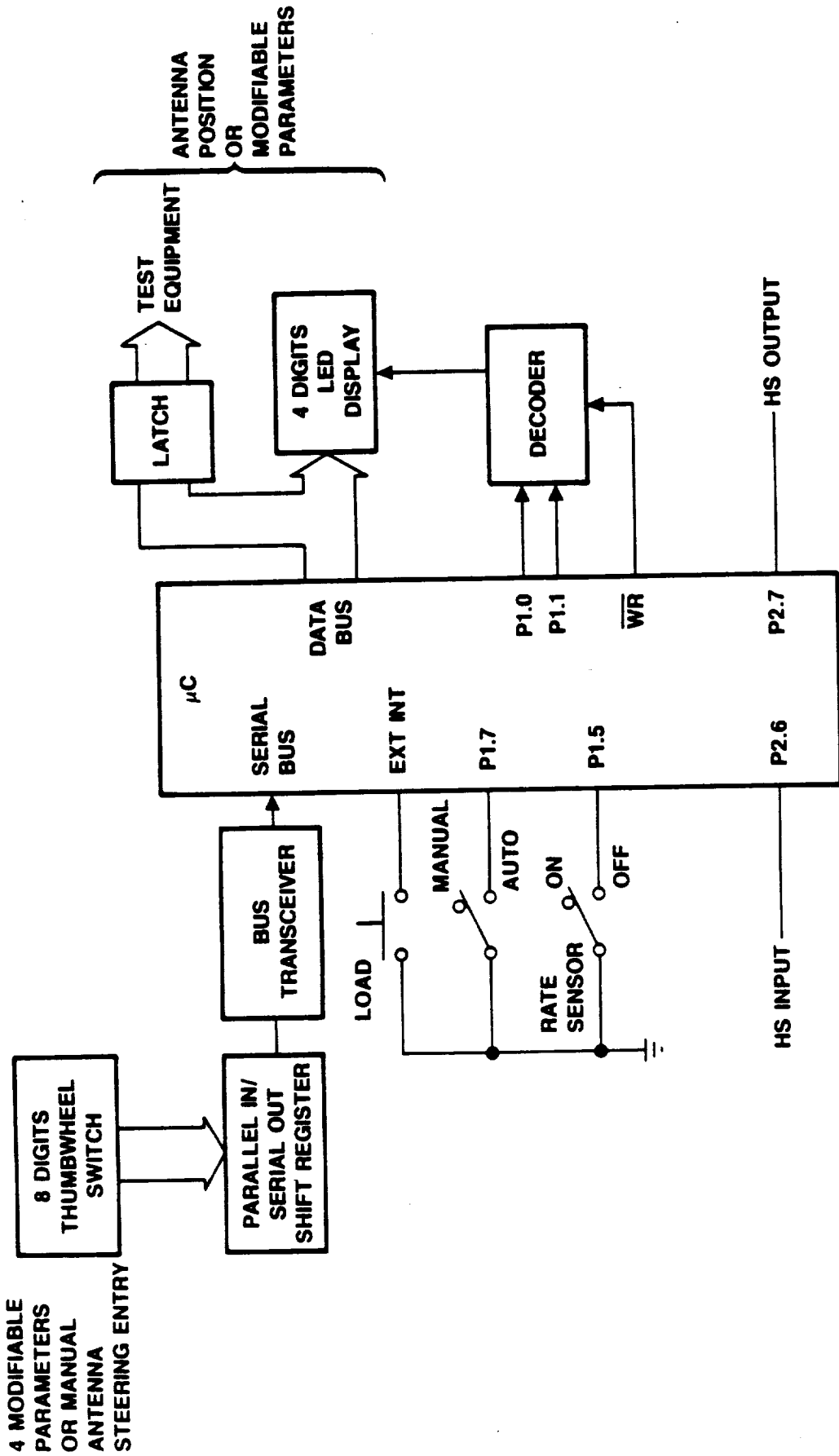
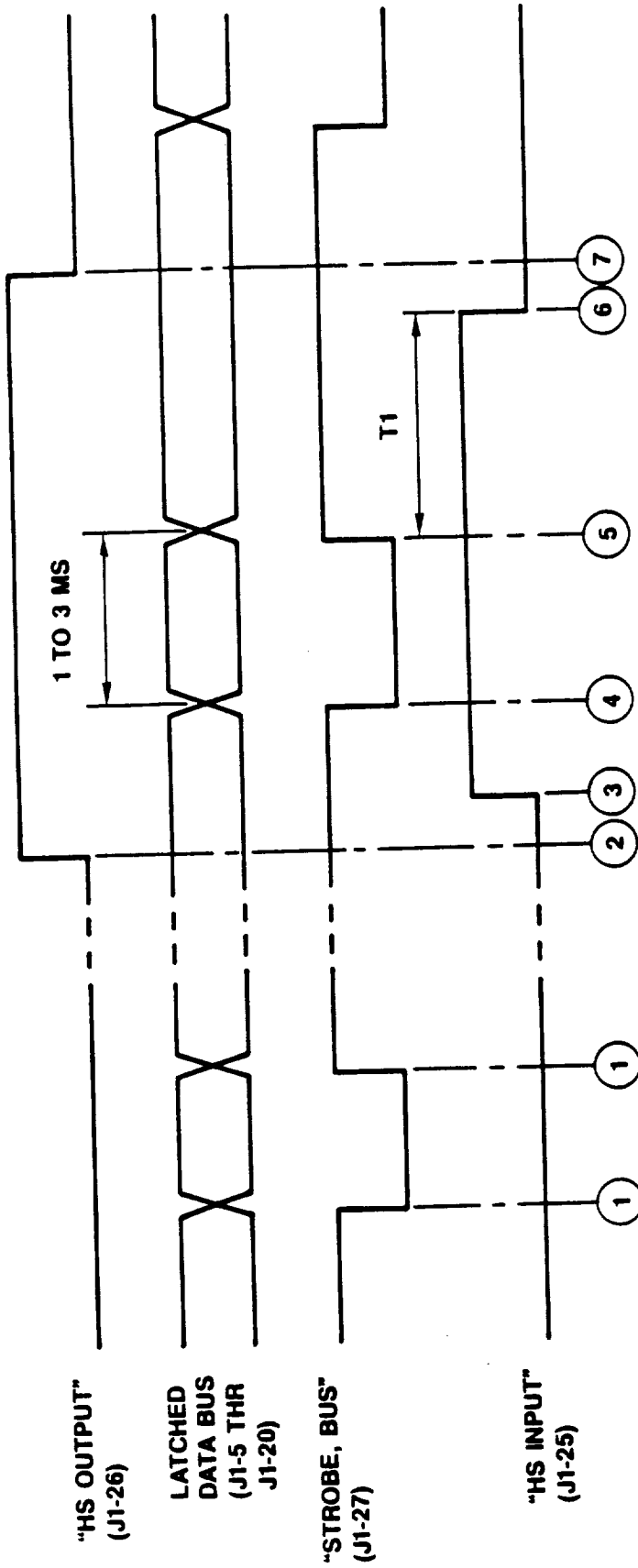


Figure 5-6. Block Diagram of MSAT-X User Interface



1. ANTENNA MEAN POSITION IS UPDATED DURING NORMAL AUTO MODE OPERATION
2. NEW SET OF MODIFIABLE PARAMETERS HAD BEEN ENTERED
3. TEST EQUIPMENT IS READY TO RECORD THE NEW SET OF MODIFIABLE PARAMETERS
4. "M4" AND "M5" BCD CODE IS ON DATA BUS
5. "M2" AND "M3" BCD CODE IS ON DATA BUS
6. NEW SET OF MODIFIABLE PARAMETERS HAD BEEN SUCCESSFULLY RECORDED IF  $T1 > 10$  MS, IT IS ASSUMED THAT FAILURE IN COMMUNICATION HAS OCCURRED, AND SEQUENCE 4 & 5 WILL BE REPEATED.
7. NORMAL AUTO MODE OF OPERATION HAS BEEN REENTERED.

1. ANTENNA MEAN POSITION IS UPDATED DURING NORMAL AUTO MODE OPERATION
2. NEW SET OF MODIFIABLE PARAMETERS HAD BEEN ENTERED
3. TEST EQUIPMENT IS READY TO RECORD THE NEW SET OF MODIFIABLE PARAMETERS
4. "M4" AND "M5" BCD CODE IS ON DATA BUS
5. "M2" AND "M3" BCD CODE IS ON DATA BUS
6. NEW SET OF MODIFIABLE PARAMETERS HAD BEEN SUCCESSFULLY RECORDED IF  $T1 > 10$  MS, IT IS ASSUMED THAT FAILURE IN COMMUNICATION HAS OCCURRED, AND SEQUENCE 4 & 5 WILL BE REPEATED.
7. NORMAL AUTO MODE OF OPERATION HAS BEEN REENTERED.

Figure 5-7. Test Equipment Parallel Bus Definition

Table 5-1. LED Reading versus Elevation Angle

LED Digital Reading	Elevation Angle (Degrees above Horizon)
0	20
1	25
2	30
3	35
4	40
5	45
6	50
7	55
8	60
9	90

#### 5.2.4 Antenna Interface

Control of the phase shifters in the antenna's beamforming network is by commands from the electronics box transmitted to the antenna via a 15 conductor cable. This operation is as follows:

- One 144 bit serial word is sent to the Antenna Phase Shift Latches every time the portion of the antenna is updated. The microcontroller's serial bus is used for this function and requires minimum software control. The shift clock for this operation will be set at 500 KHz.
- Bus Driver U17 is used to drive the control cable. This IC is also used as a bi-directional buffer to allow the microcontroller's serial bus to be shared between sending the data into the antenna and reading the thumbwheel switch as described above.

#### 5.2.5 Power Supply

The power supply has been altered, during the system development, to accommodate changing requirements. At this time, it doesn't represent the best possible approach. The performance is acceptable, however, for the breadboard level of the development phase. Another scheme, recently developed and tested by TRE, will be recommended for follow-on phases.

As configured, the power supply consists of two-states: 1) a bucking regulator which supplies a high current, 5 volt output for biasing the beamformer diodes; and 2) a DC-DC converter used as a source to derive all the other voltages used by the MSAT-X antenna system. Table 5-2 lists these voltages in the form of output versus input voltage. This same table also shows the efficiency of the power supply.

Table 5-2 Output versus Input Voltage  
(Efficiency at  $V_{IN} = 12V$  is 68%)

Input Voltage	Output Voltages					
	5V bias (3A)	5V (.9A)	5V SP (.08A)	+15V (.06A)	-15V (.02A)	+28V (.03A)
12V	5.27	4.98	4.80	14.44	-14.65	26.83
8V	5.17	4.75	4.82	14.72	-14.84	27.89
18V	5.35	4.91	4.51	14.62	-14.67	27.10

Reference is made to Appendix D for a comprehensive set of drawings of the electronics box hardware. These drawings, in addition to being of general interest to the readers of this Report, are included to serve as a guide during the installation and maintenance of this system. In the case of inconsistencies between the electrical and mechanical sets of drawings, the electrical schematics should be regarded as more accurate. Table 5-3 lists the drawings, along with a synoptic description of the subject matter, included in the aforementioned Appendix.

### 5.3 POINTING SOFTWARE

The software for MSAT-X has been designed, coded, and tested. The code is written in 8096 assembly language and was developed on an IBM compatible personal computer. The code and the system was debugged and integrated using an Intel VLSICE-96P (in circuit emulator). The program is stored in 16 kilobytes of ROM, most of which is used to contain the phased array position tables. The code is modular and well commented including procedure headers and flowcharts of all of the main subroutines. Each of the main routines is summarized below and a processor I/O diagram is shown in Figure 5-8 to enhance the descriptions.

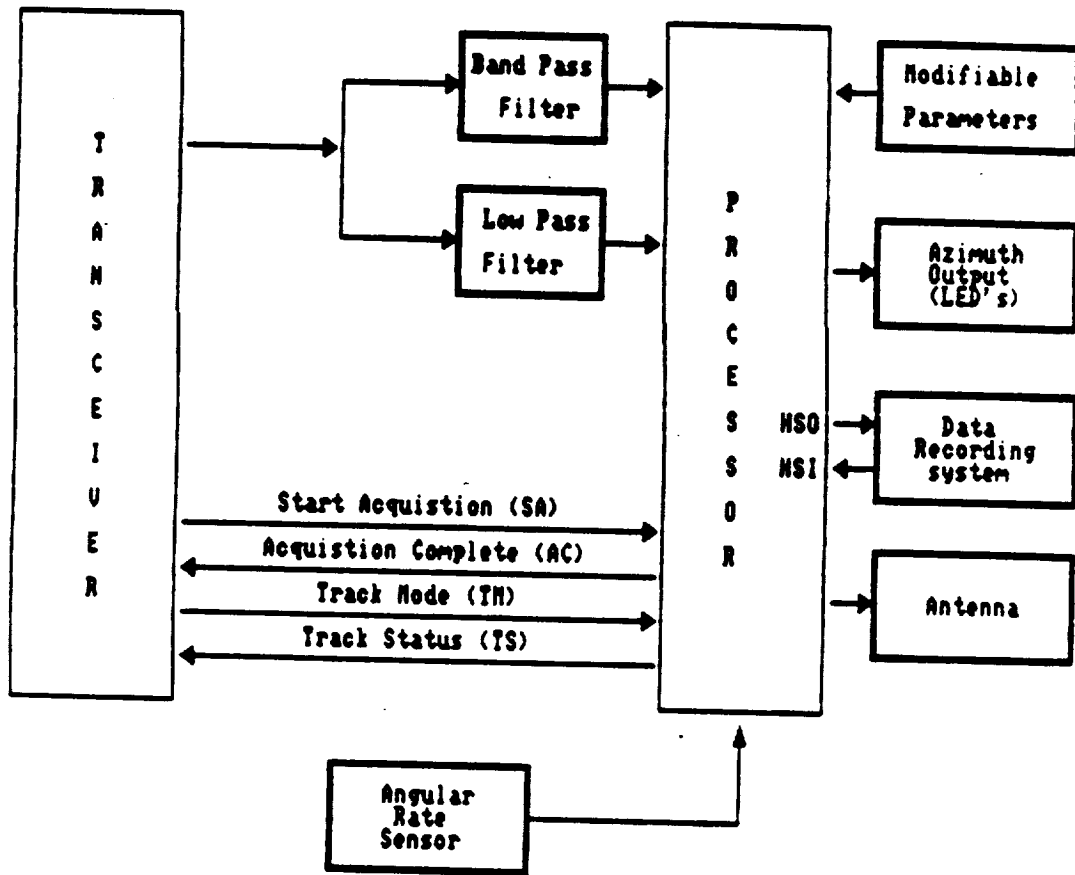


Figure 5-8. MSAT-X Processor Block Diagram

Table 5-3. List of Electronics Box Drawings and Context Matter

Item	Drawing No.	Description
1.	1056A0001	Electronics Box Assembly
2.	1056A0002	Electronics Box Schematic Diagram
3.	1056B0005	Cable interface of Electronics Box with antenna and test receiver. Refer to Drawing 1056B0025 for details of W4 cable. Refer to Drawing 1056A0132 for details of W3 cable.
4.	1056C0141, 1056C0151, 1056C0161	Components location on wirewrap and two terminal boards... which are part of the electronics box.

### 5.3.1 MSAT-X Software Procedure Descriptions

#### MSATX-EXEC:

This is a real time loop which monitors the Start Acquisition (SA) input (shown in Figure 5-8) and the external interrupt input. Once a SA pulse is detected, the procedure POSITION-SCAN is called to search for the antenna's position. On returning from the POSITION-SCAN procedure, if the Acquisition Completed (AC) condition is met, then a second loop is entered for tracking. The tracking loop is discussed below. A detailed flowchart is given in Figure 5-9, sheets 1 and 2.

#### POSITION\_SCAN:

This procedure scans 120 positions of azimuth and two elevations (30 and 50 degrees). At each position an average signal strength reading is taken. The maximum signal strength reading will be stored and if above a given threshold, the antenna position is set. A subroutine "SET-POSITION" is called to shift out the correct position pattern for the scanned azimuth and elevation. Due to filtering in the hardware, the actual antenna azimuth will lag the azimuth found by the scan. For this reason an offset of either 15 or 20 degrees (depending on the elevation) will be subtracted from the scanned azimuth. The

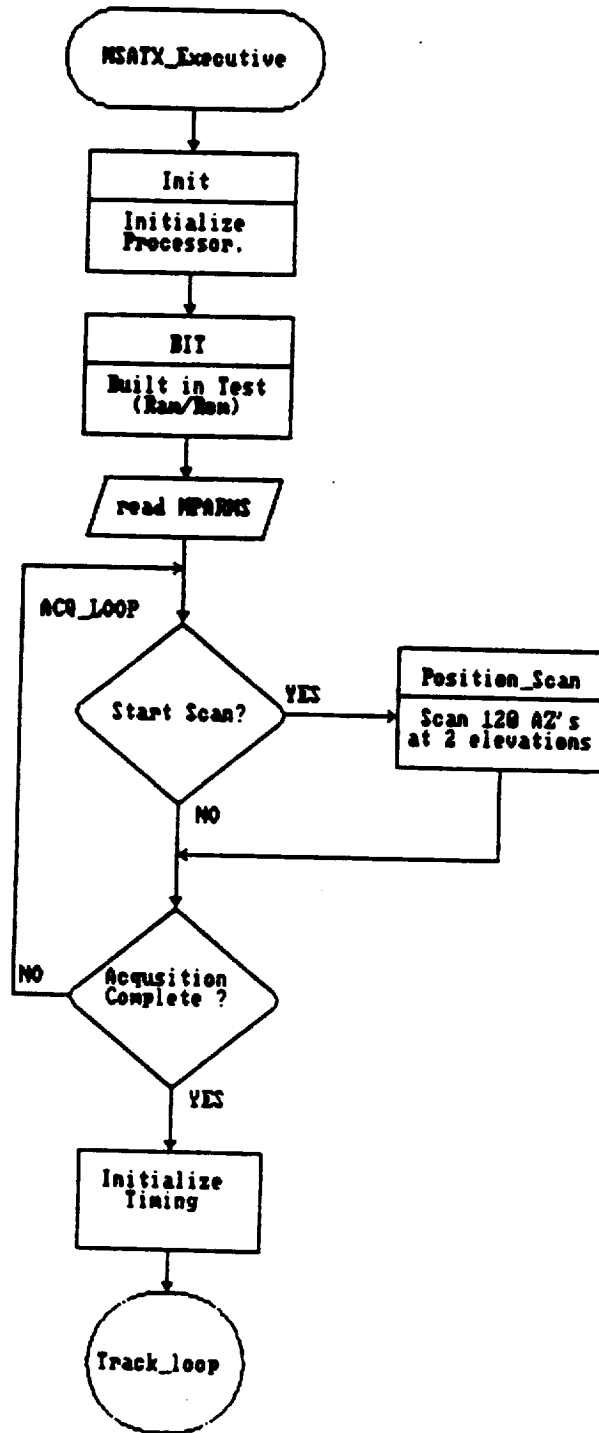


Figure 5-9. MSAT-X Executive Flowchart (Sheet 1 of 2)

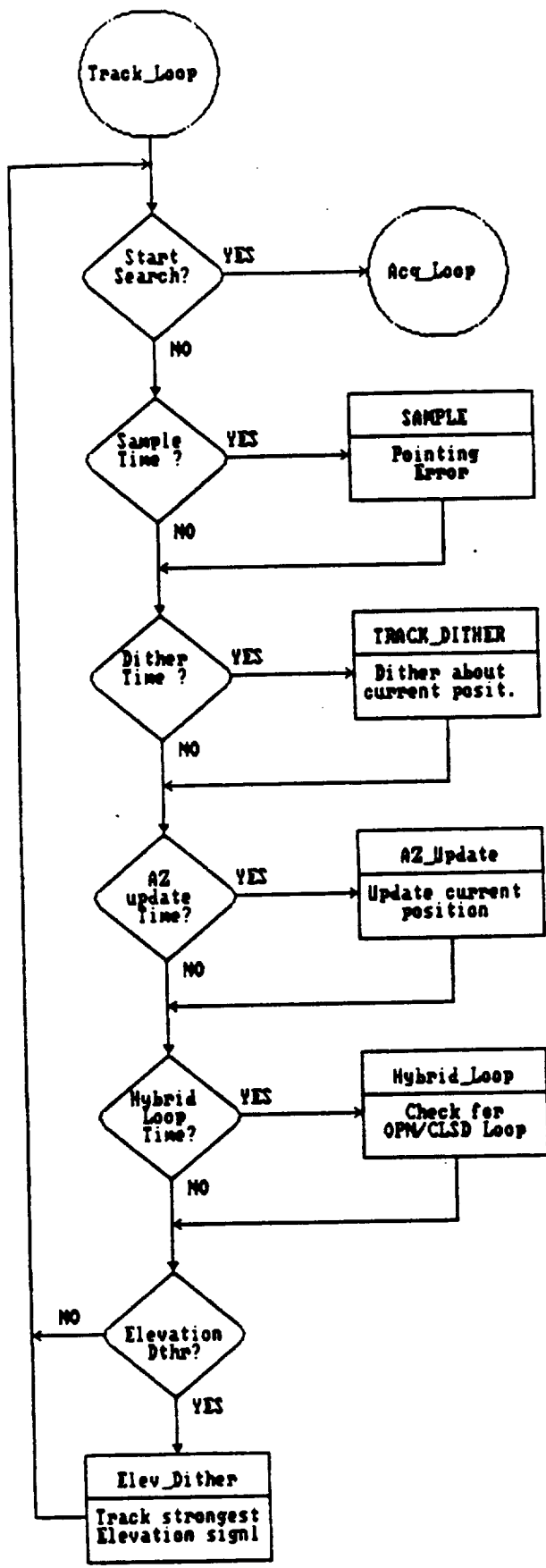


Figure 5-9. MSAT-X Executive Flowchart (Sheet 2 of 2)

two interface lines (AC, TS) will be set or cleared depending on acquisition. These interface lines are shown in Figure 5-8. The POSITION-SCAN procedure takes 2.5 seconds to execute. A detailed flowchart of POSITION-SCAN is given in Figure 5-10.

#### TRACK:

TRACK is another real time loop of the executive (control loop) which constantly monitors the processor timer for preset time intervals. If a time interval has elapsed, the proper procedure is called, otherwise the loop continually cycles. The interrupting procedures are TRACK-DITHER, AZ-Update, Sample, Hybrid-Loop, and Elev-Dither. A detailed flowchart of TRACK is given in Figure 5-9, Sheet 2 of 2. This cycle will track the signal (found during the position scan) over 120 positions in azimuth and in 9 elevations. This cycle takes 1.8 milliseconds at worst case before repeating. The azimuths start at 0 degrees and increase to 357 degrees in increments of 3 degrees. The elevations begin at 20 degrees and range to 60 degrees in increments of 5 degrees. Descriptions and flowcharts of each of the interrupting procedures are given below.

#### TRACK-DITHER:

Low pass filtering (quantization) and dithering is accomplished in this procedure. The procedure takes one last sample, loads the current antenna position, then shifts out the next position. This sequence ensures that the samples will be taken when they are most valid. The frequency of this procedure is determined by modifiable parameter five. Each time it is called, a new position is calculated and set by adding the dither magnitude to the current average position. All of the samples of the pointing error that were collected at the current antenna position are summed and the dither count is incremented. It is this averaged sum that is used to compute the increment of azimuth due to pointing error. The TRACK-DITHER routine take 1.3 milliseconds to execute at worst case. A detailed flowchart is given in Figure 5-11.

#### AZ\_UPDATE:

This procedure is called every 50 milliseconds and updates the current azimuth position because of changes from the rate sensor and the pointing error signal. The antenna position azimuth is stored by the processor as a 16 bit BAM (Binary Angular Measurement). The calculation of the BAM increment is done in this procedure and includes system gain (K) and the ARS DC offset, if any. The increment is also limited

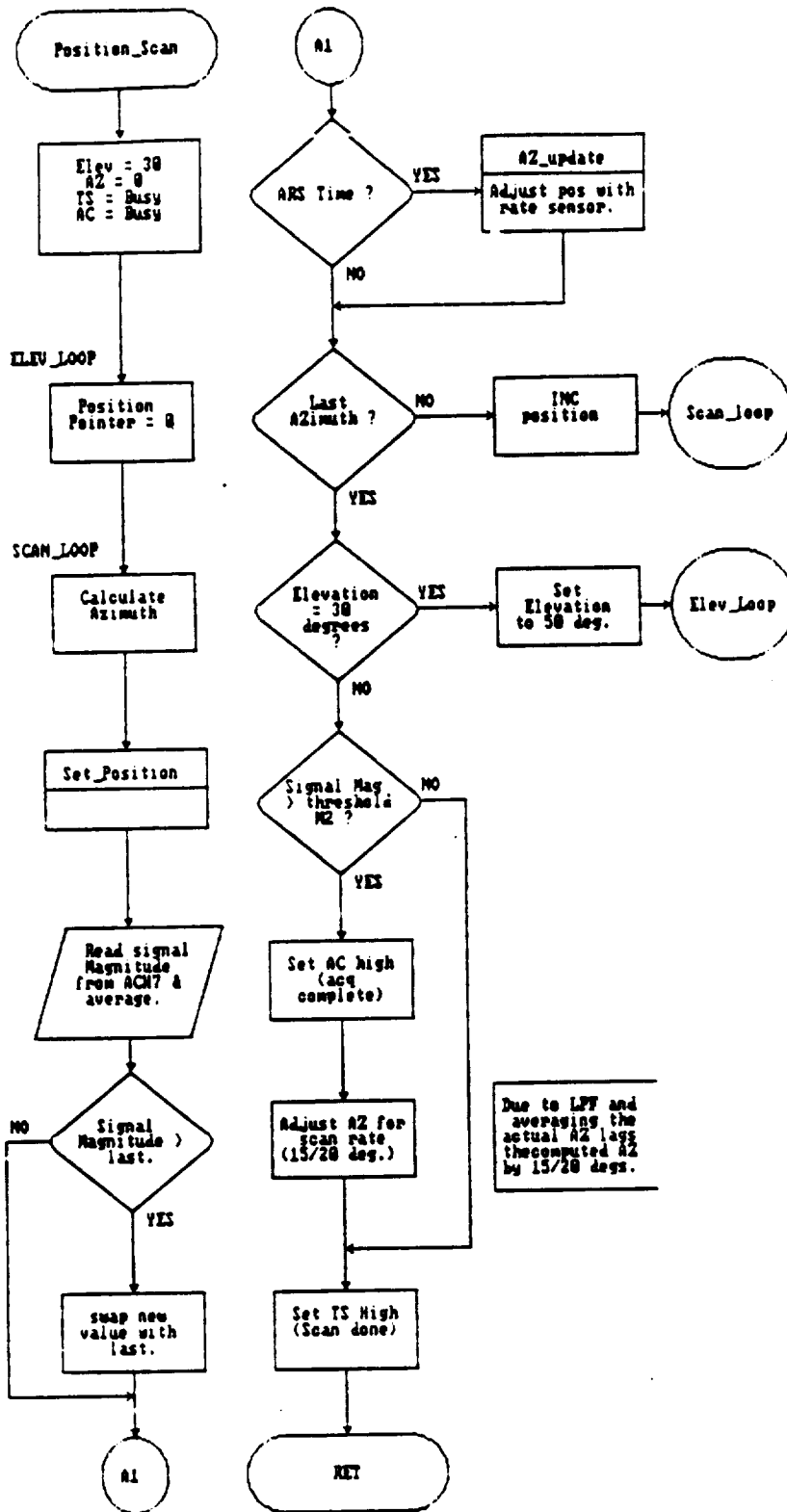


Figure 5-10. MSAT-X Position Scan Flowchart

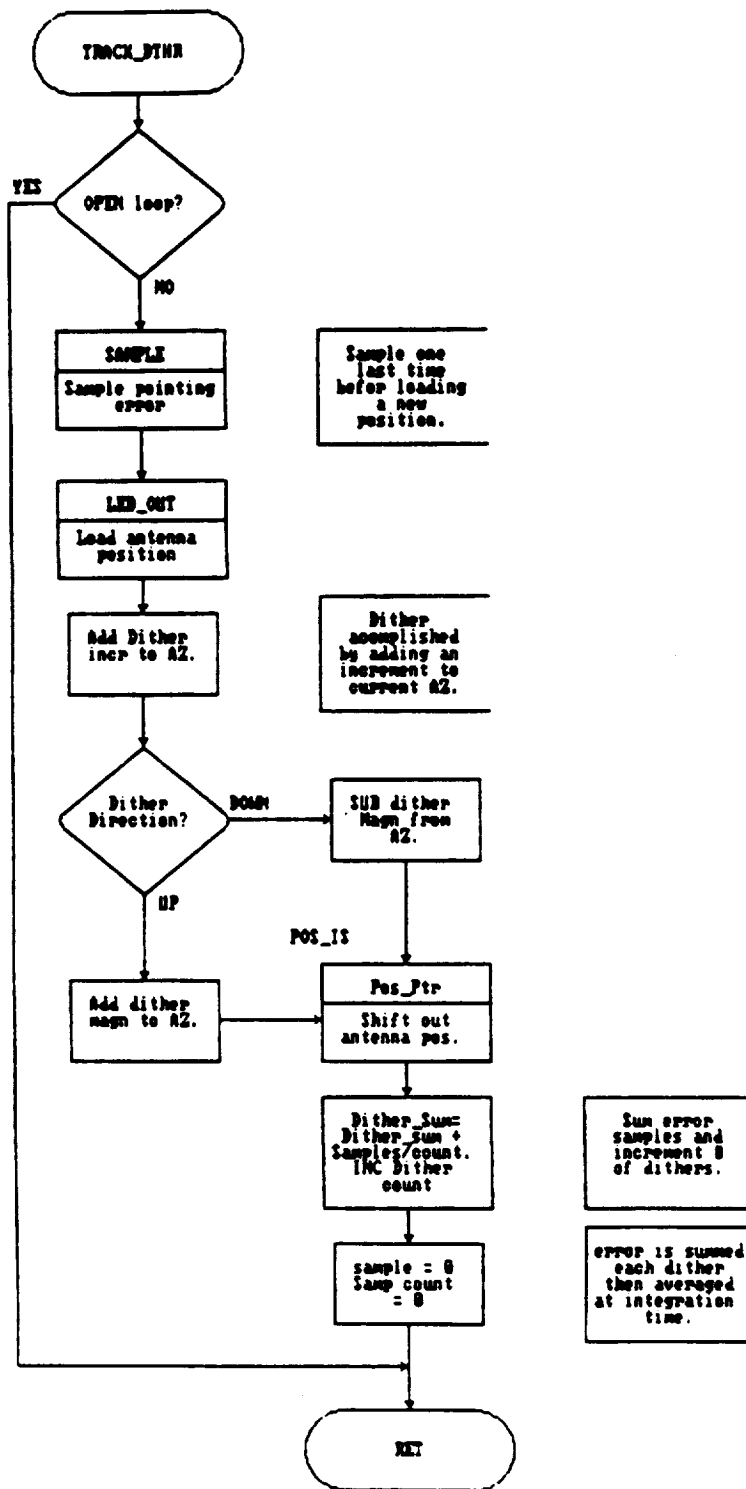


Figure 5-11. MSAT-X Track Dither Flowchart

within 4 degrees to avoid losing track due to glitches. The 4 degrees will still allow a turn rate of 75 degrees/second since this increment is done every 1/20 of a second. The signal magnitude is also sampled at this time and then averaged later. The AZ-UPDATE procedure takes 285 microseconds to execute at worst case. A detailed flowchart is given in Figure 5-12, Sheets 1 and 2.

#### HYBRID\_LOOP:

This procedure is called every 100 milliseconds and tests the TM (Track Mode) input for OPEN or CLOSED loop tracking. If the transceiver selects open loop tracking, a delay is implemented before the track mode exits. If closed loop tracking is selected, the filter and dither routine will begin executing. The software flag IC (Integral Control) is tested in this routine; IC is also tested during the first second of the "TRACK" mode if a wait condition is entered. After 1 second, IC is set to go and the ARS DC biasing begins. The HYBRID-LOOP procedure takes 30 microseconds to execute. A detailed flowchart is given in Figure 5-13, Sheets 1 and 2.

#### ELEV\_DITHER:

Elevations from 20 degrees above the horizon to 60 degrees are scanned for the greatest signal strength. This procedure will cause the antenna to dither about this elevation and the two adjacent elevations. The signal magnitude used is an averaged value which was sampled in the AZ-UPDATE routine. This procedure takes 55 microseconds to execute. A detailed flowchart is given in Figure 5-14.

#### EXT-INTR:

This procedure is called when the "LOAD" push button is pressed. If the system is in the automatic mode then the current modifiable parameters are sent out over the parallel port. If it is in the manual mode, the current azimuth on the thumbwheel switches is sent to the antenna. A detailed flowchart is given in Figure 5-15.

#### SAMPLE:

This routine reads the pointing error signal via an analog-to-digital converter. The sample is summed and then averaged at a later time. The sample routine is called at a rate of 2000 Hz and takes 65 microseconds. A detailed flowchart is given in Figure 5-16.

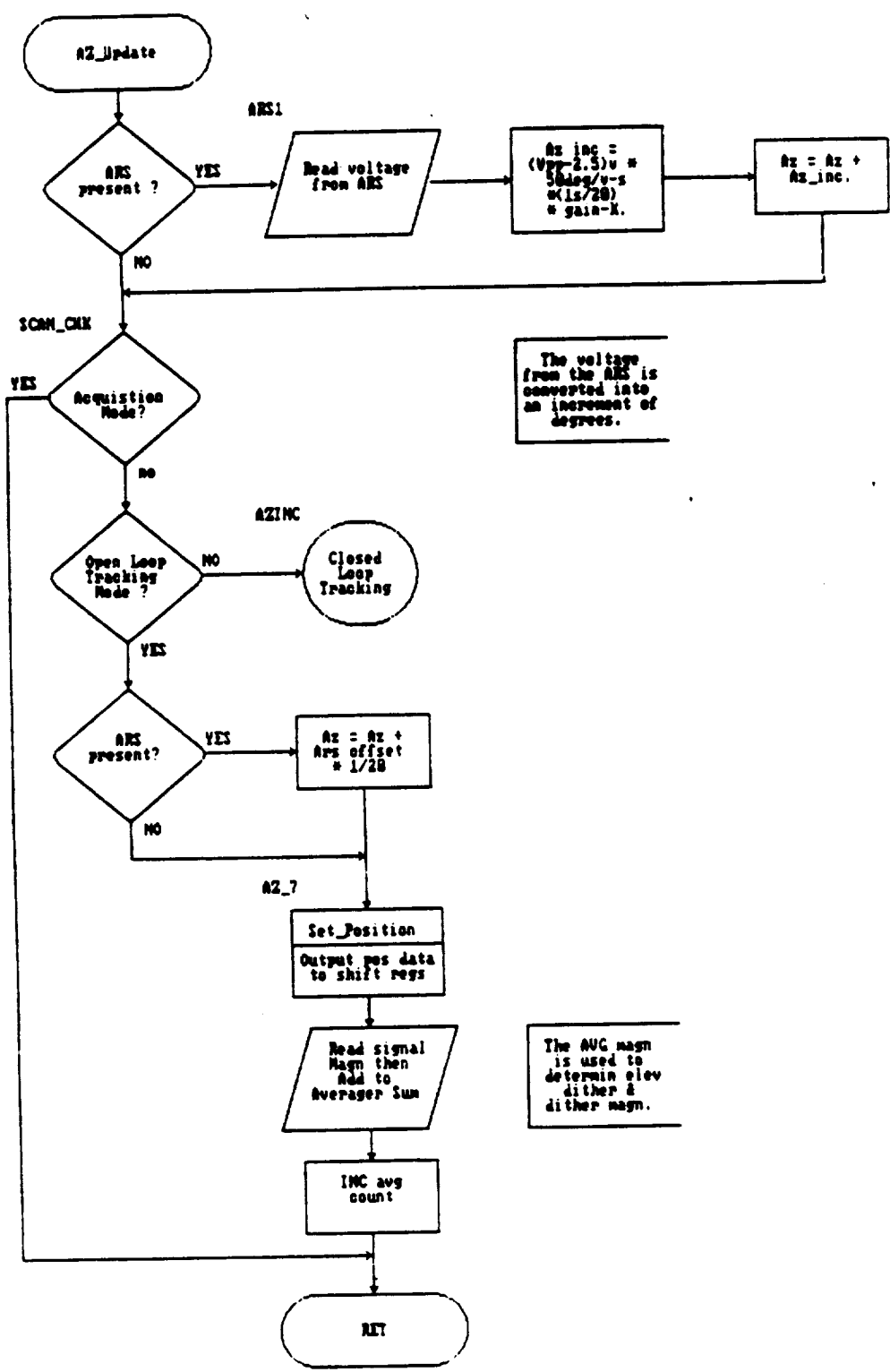


Figure 5-12. MSAT-X Azimuth Update Flowchart (Sheet 1 of 2)

ORIGINAL PAGE IS  
OF POOR QUALITY

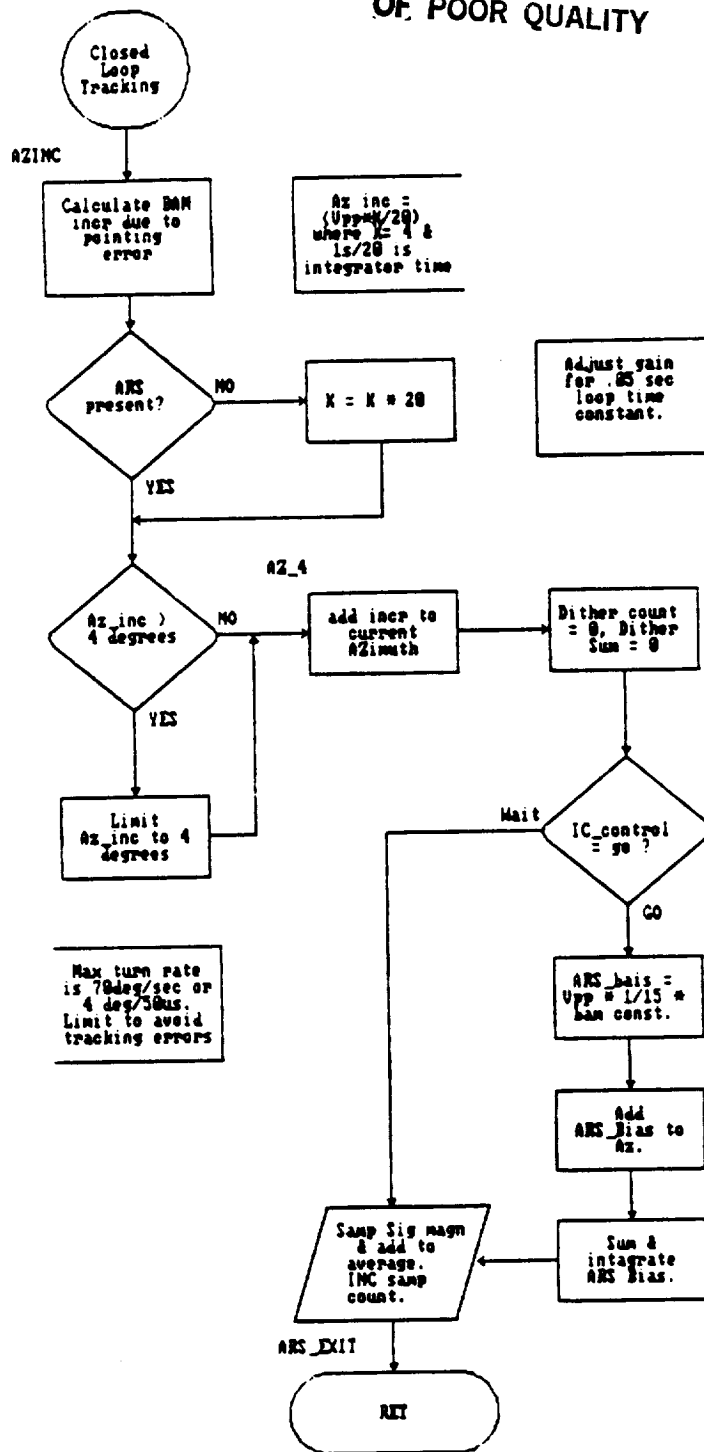


Figure 5-12. MSAT-X Azimuth Flowchart (Sheet 2 of 2)

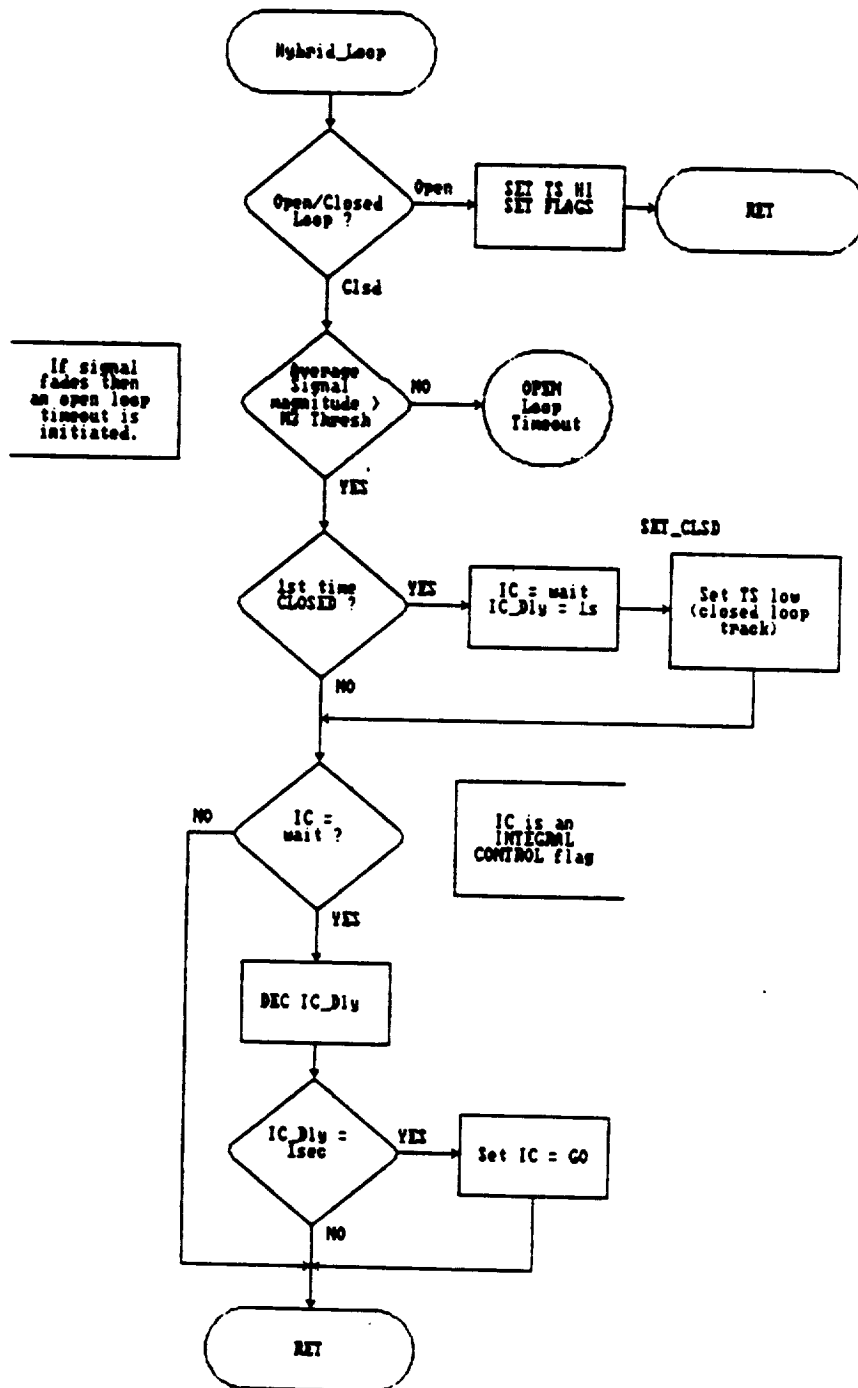
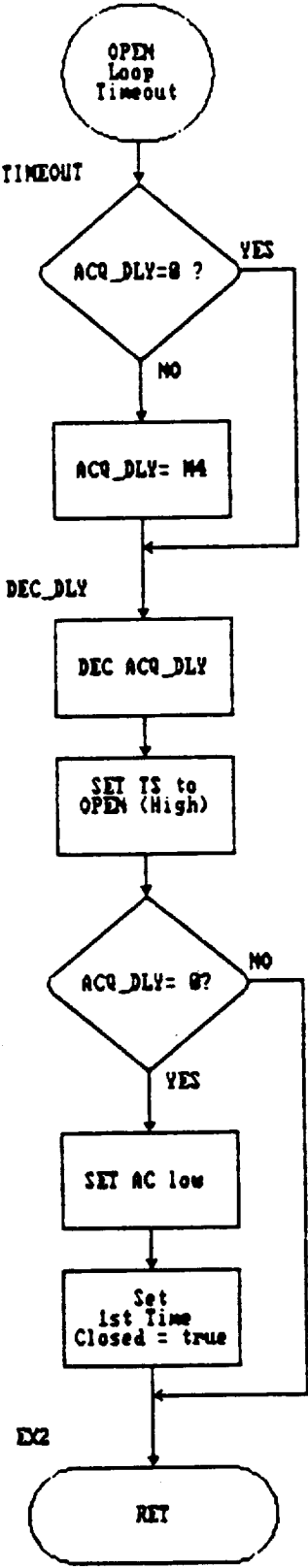


Figure 5-13. Hybrid Loop Procedure Flowchart (Sheet 1 of 2)

ORIGINAL PAGE IS  
OF POOR QUALITY



If the signal fades for a time M5 then force OPEN LOOP mode.

Figure 5-13. Hybrid Loop Procedure Flowchart (Sheet 2 of 2)

ORIGINAL PAGE IS  
OF POOR QUALITY

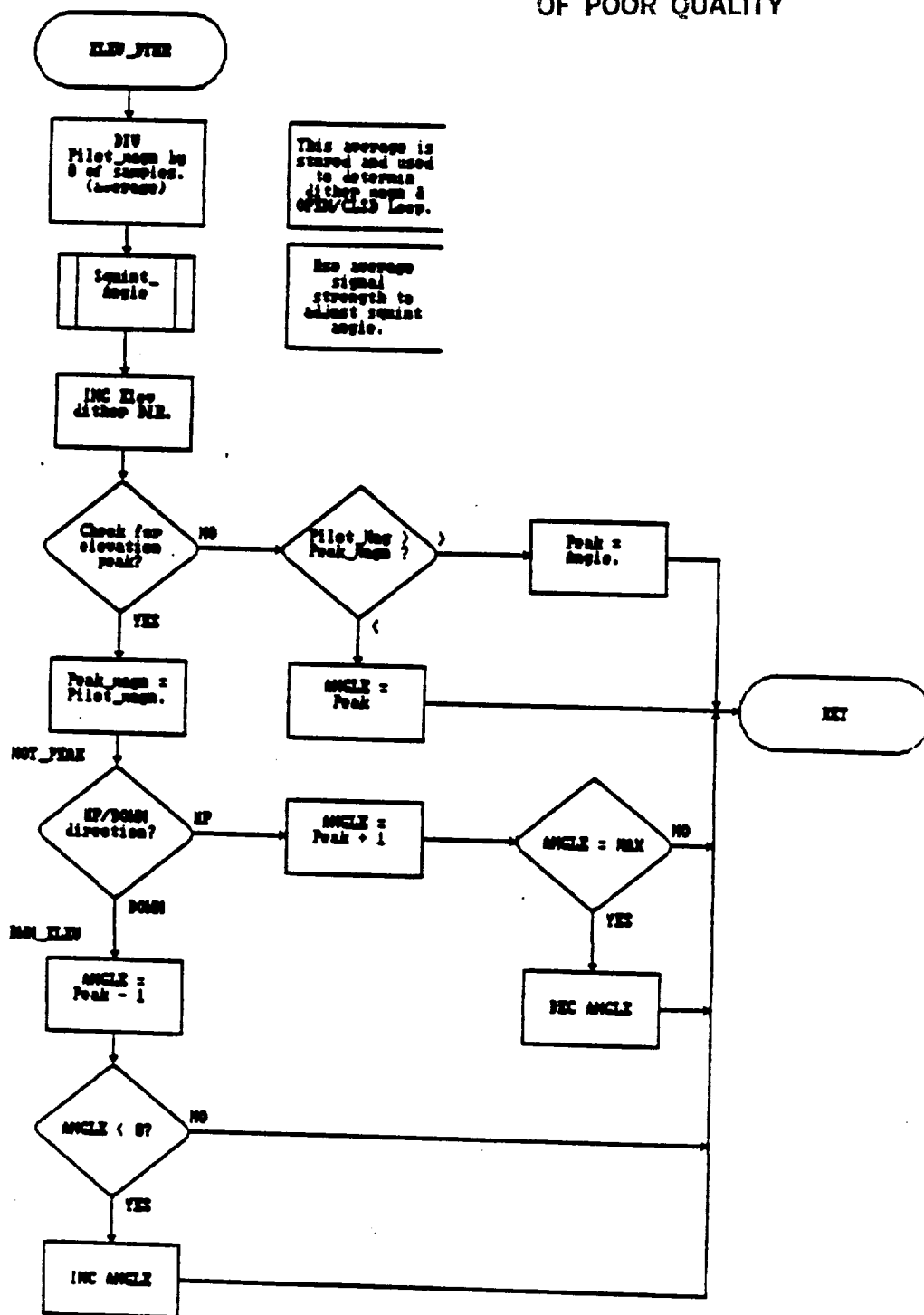


Figure 5-14. MSAT-X Elevation Dither Procedure Flowchart

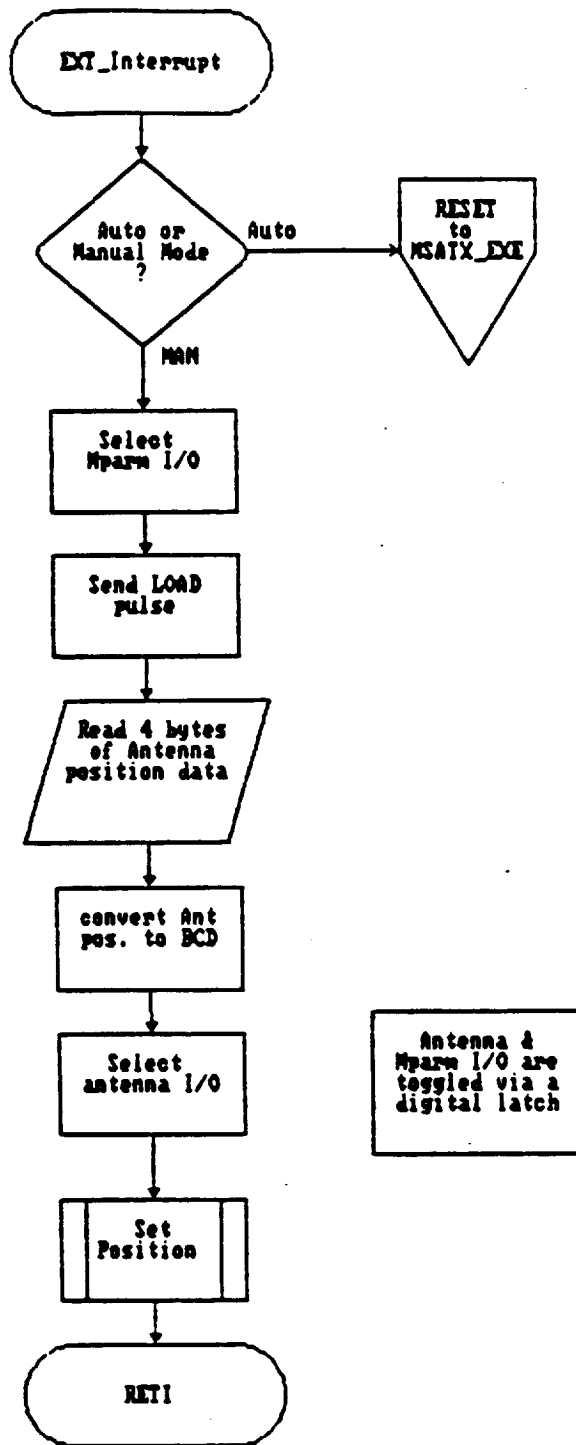


Figure 5-15. External Interrupt Flowchart

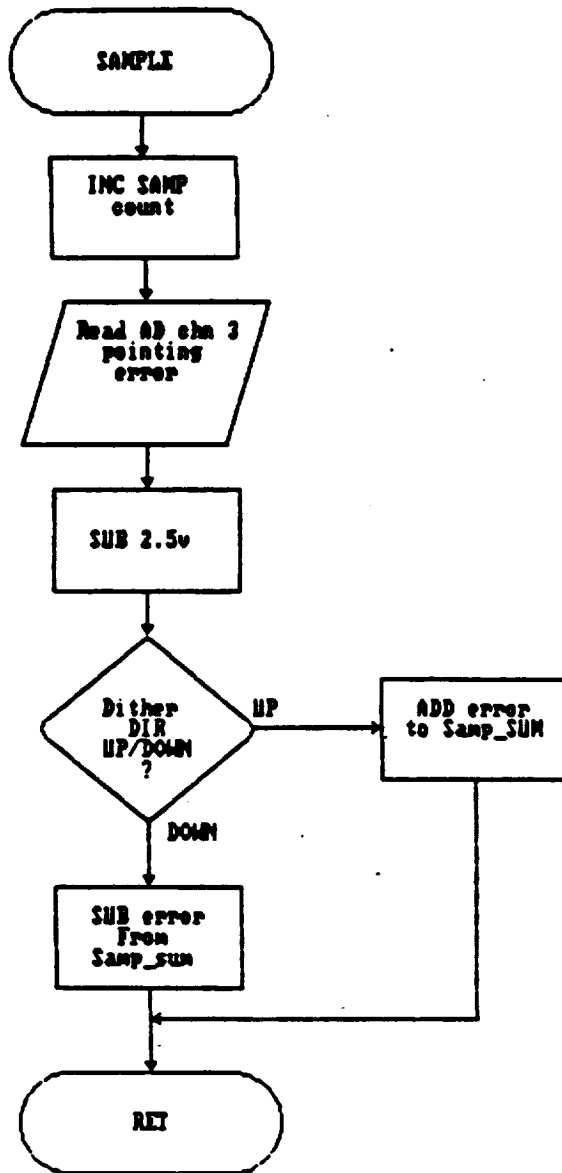


Figure 5-16. Pointing Error Sample Flowchart

## SECTION 6 MSAT-X MECHANICAL DESIGN

### 6.1 GENERAL DESCRIPTION

Mechanically, the MSAT-X breadboard development antenna is a very thin multi-layer wafer just 0.75 inch thick by 22 inches in diameter... exclusive of the R.F. and power connector which exit from the bottom of the unit. Its overall weight is approximately 15 pounds. The antenna, shown in Figure 6-1, is an assembly of etched circuit boards joined together with screws to allow disassembly for tuning adjustments. The majority of these screws also serve the additional purpose of forming the walls of the 19 cavities.

The antenna also contains a supporting aluminum plate for the beamformer. This plate provides the threaded holes for the screws, stiffness to support the beamformer, printed circuit board, and provisions for the attachment of coaxial connectors used for testing prior to the final assembly. Stripline and microstripline boards comprising the antenna are: crossed-slots, feeders, hybrid couplers, and phase shifters. A bottom cover completes the assembly. These boards and how they make up the composite antenna are depicted in Figure 6-2. Figure 6-3 shows how a typical system might mount in a vehicle.

### 6.2 MECHANICAL DESIGN

It is worthwhile to include a brief description of the various boards that comprise the antenna. The exact circuit detail of these boards is described elsewhere in this report. All the circuit boards described herein are DI-CLAD woven PTFE (teflon) microwave composite laminates of the 522 series by Keene Corporation of Bear, Delaware. This material is quite stable, has a low loss tangent, a dielectric constant of approximately 2.5, a thermal expansion coefficient of 10-12 ppm/°C (in the x-y direction), and is supplied with one ounce copper on both sides. Its major disadvantage is cost which is discussed later in this report.

A brief description of the printed circuit boards that comprise the antenna is given in the following paragraphs. One is encouraged to refer to Sections 2, 3, and 4 of this report for photographs and/or drawings of each of the p-c boards or assemblies described below.

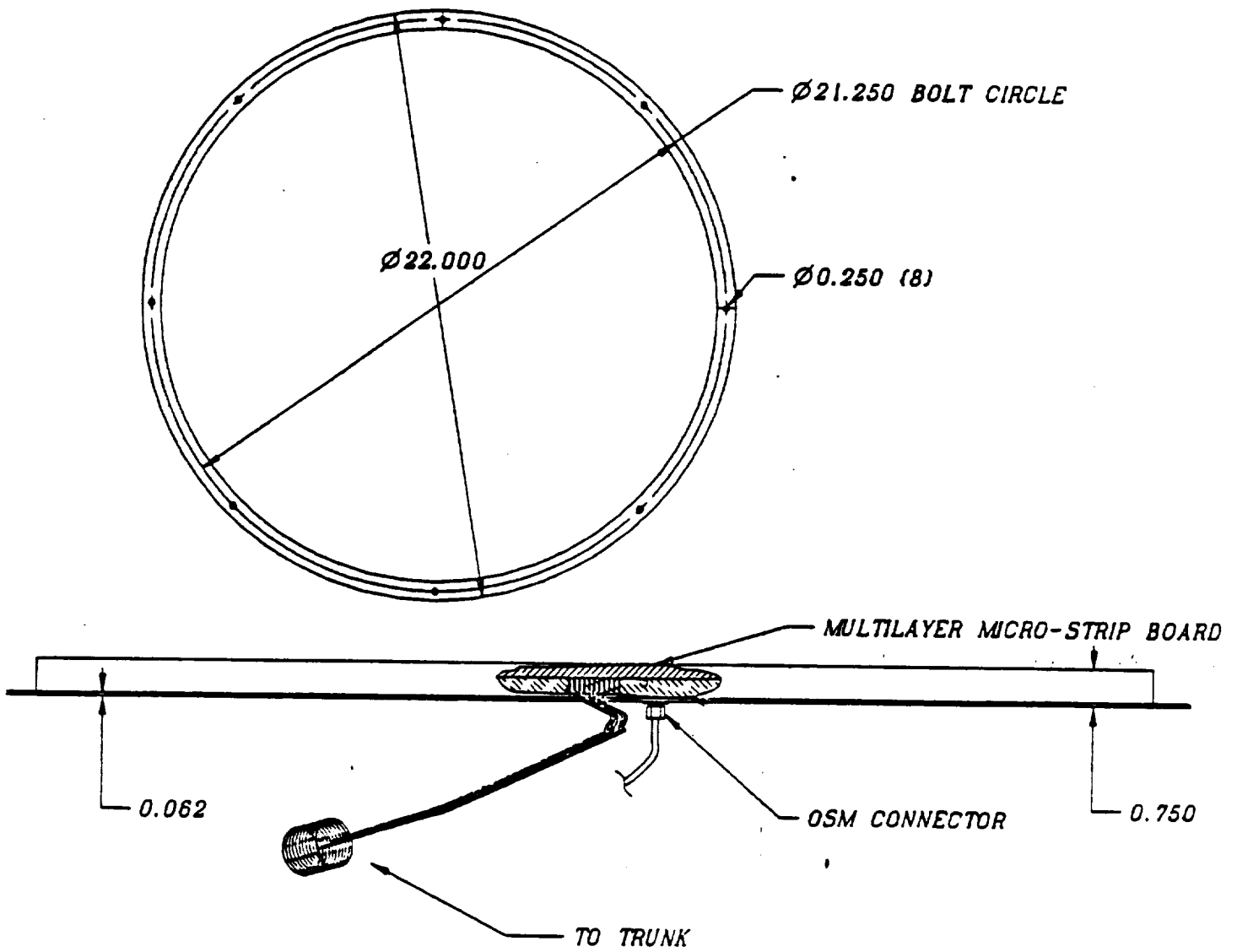


Figure 6-1. Planar Views of MSAT-X Vehicle Antenna

ORIGINAL PAGE IS  
OF POOR QUALITY

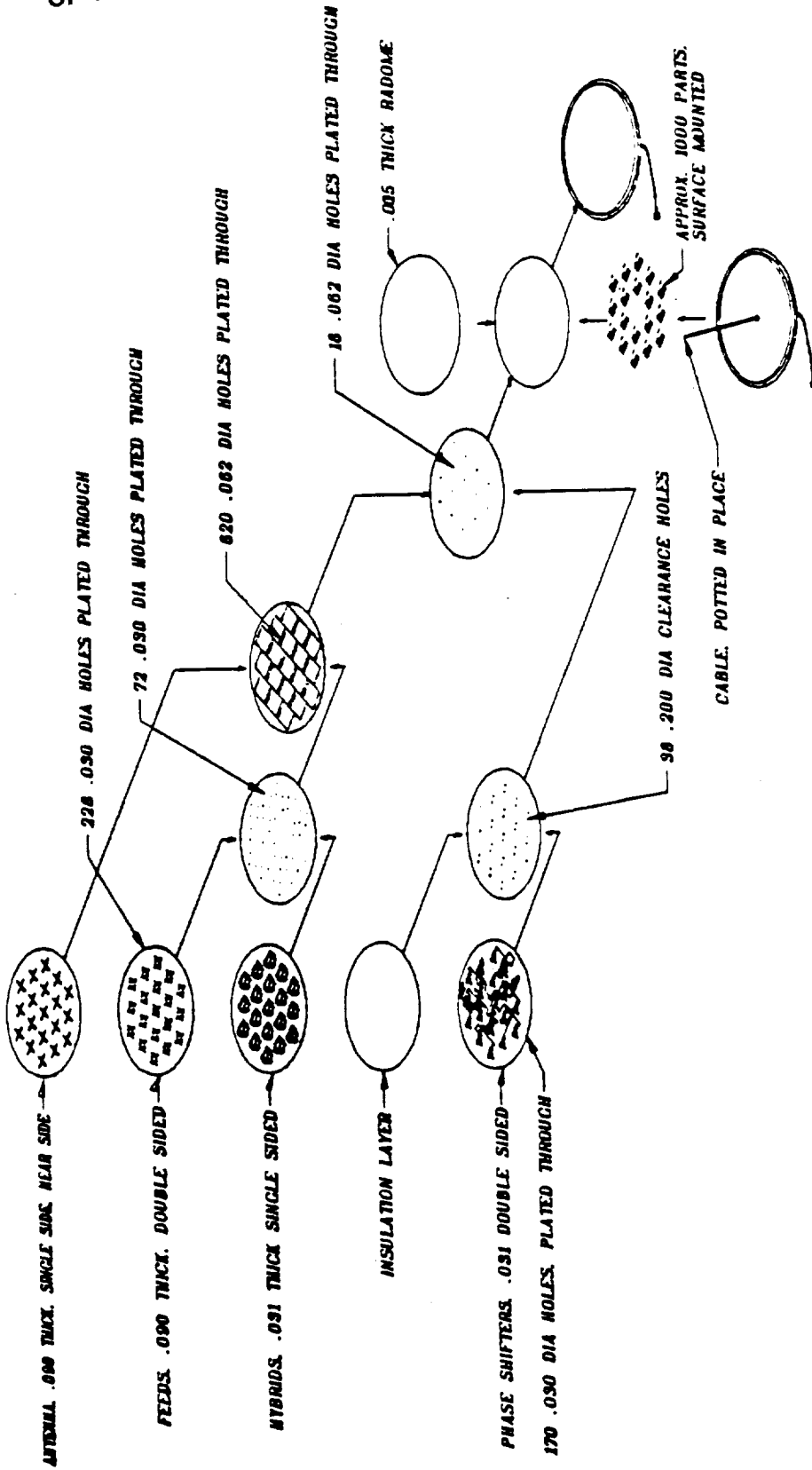


Figure 6-2. Exploded View of MSAT-X Vehicle Antenna

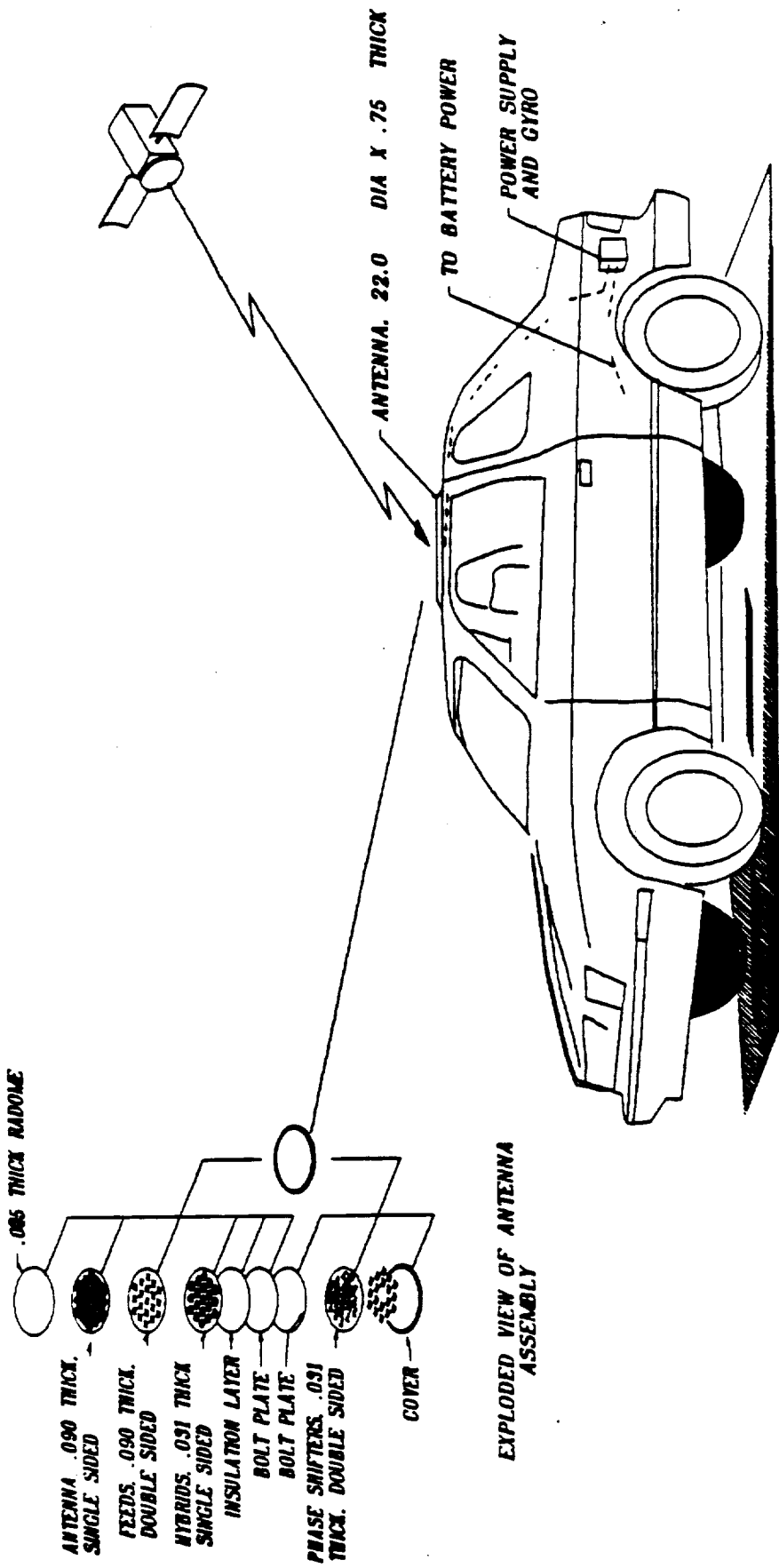


Figure 6-3. MSAT-X Vehicle Antenna System

### 6.2.1 Beamformer

The beamformer consists of an etched .031" thick teflon p-c board bonded to a sheet of .125" thick aluminum for stiffness. Originally, the stiffener plate was planned to be .125 plated teflon but the integrity of threaded holes in this material was unsatisfactory, hence this approach was rejected.

The parts count for this board numbers 1033 coils, diodes, capacitors, integrated circuits, and transistors. All components are surface mounted using SN 63 solder except in the case of the diodes which are affixed with Indalloy #2 solder. Basically, the circuit board is comprised of 18, 3-bit phase shifters, 6 3-way, and 1 7-way power divider. Each phase shifter consists of three loops interconnected with PIN diodes and chip capacitors. DC connections are made using choke coils and capacitors to the surface mounted 14 pin DIPS. These parts are mounted by spreading and cutting the leads to solder flat on the microstripline board.

### 6.2.2 Cover

The next layer up from the bottom of the antenna stack is a .031" teflon cover. It has slots cut in it to recess the 50 ohm chip resistors serving on terminations for the hybrids. Holes in the board accommodate the pins linking the output of the beamformer phase shifters to the hybrids. The sole function of this board is to serve as a ground plane cover for the stripline hybrids.

### 6.2.3 Hybrid Layer

The hybrid p-c board is of .031" teflon material and serves as the polarization designator (RHCP in this case) for the antenna along with its other major function of feeding the feed circuits. Nineteen hybrids and load resistors make up this board.

### 6.2.4 Feeders

This board is of .090" and .125" teflon material for the first and second breadboard units respectively. The feeders are tied to the hybrid layer via plated through holes and pins. They are grounded to the antenna's ground plane by plated through holes.

## 6.2.5 Radiator Layer

The antenna consists of slots etched in the innermost metal layer and isolated from each other by means of plated through holes spaced approximately .4" apart. This layer forms the top half of the cavities and in .090" and .125" thick teflon respectively in units #1 and #2.

## 6.2.6 Radome

Originally, it was intended to have a radome comprised of .005" PTFE bonded to the top of the radiator layer, hence covering the slots and providing protection against the environment. However, this did not materialize with these models since they were bolted together. Instead, a radome was painted on using a white, translucent radome paint .002 thick. It seals the top of the antenna nicely and has losses of less than .2 dB at 1600 MHz.

## 6.2.7 Back Cover

The back cover serves as an EMI and environmental shield. The unit is bolted to the beamformer baseplate leaving an air gap of .200" between it and the circuit board. This provides adequate clearance for the components and is factored into the design of the microstripline circuitry of the board. The present cover is anodized aluminum. However, future covers could be made of thin film deposited metal, high impact plastic to conserve weight and cost, yet perform its electrical and environmental protection functions adequately.

## 6.2.8 Connectors

### 6.2.8.1 R.F.

The design of the RF connector/launcher proved inadequate on the first deliverable unit and subsequently needed strengthening to prevent mechanical breakage of the solder bond between the center conductor of the connector and the beamformer board. For the purpose of the development module, the aforementioned connector is really a short piece of RG-141/U semi-rigid coax soldered to a collar and having an OSM connector on one end. An additional supporting collar had to be machined to secure this assembly and prevent damage to it. The unit is now very sturdy.

### 6.2.8.2 Power And Signal

A 15 pin TRW "D" type subminiature connector brings the power and signal circuits to the antenna from the electronics box. The connector is securely mounted to a bracket affixed to the back cover with screws and nut plates. A bead of silicone RTV serves as a seal where the wires pass through the cover. The entire assembly is quite sturdy.

### 6.3 FABRICATION

Fabrication of the antenna/beamformer array was done as follows. This will also give same insight into the repair of the unit if the need arises. Refer to Figure 6-4.

1. Detail boards will be etched and holes drilled and plated through.
2. The beamformer board and the stiffness plate will be bonded together using silver-loaded epoxy.
3. The hybrid, feeders, antenna, and cover board will be etched and 620 .094" diameter holes drilled and plated through. Additional holes (per unit) will be drilled and processed (again per print) as required per board.
4. The hybrid and feeder board will be pinned and soldered together per engineering direction.
5. Nineteen, 50 ohm chip resistors will be attached to the hybrid board per print. Slots will be cut in the cover sheet to recess the resistors. Pins will be soldered to the input pads of the nineteen hybrids.
6. The crossed-slot, feeder, and hybrid boards are combined with threaded fasteners for testing. The phase shifter board needs the cover along with an aluminum plate for testing.
7. After testing, the aluminum assembly plate for the antenna will be removed and all four boards will be keyed together along with the beamformer. They will be bolted together using 620 brass 2 x 56 binder head machine screws of the appropriate length. Each screw is tightened to 1.7 in-oz of torque.
8. Teflon spacers are inserted over each pin and in the holes leading from the phase shifter outputs to the hybrid board. A strap is attached from the output of each phase shifter to the appropriate pin to each hybrid.
9. Attach the shield or environmental cover. At the conclusion of testing, seal and paint.

Many of the features that are needed for a development unit are not needed in a production unit. Other ways of providing the same functional performance without the

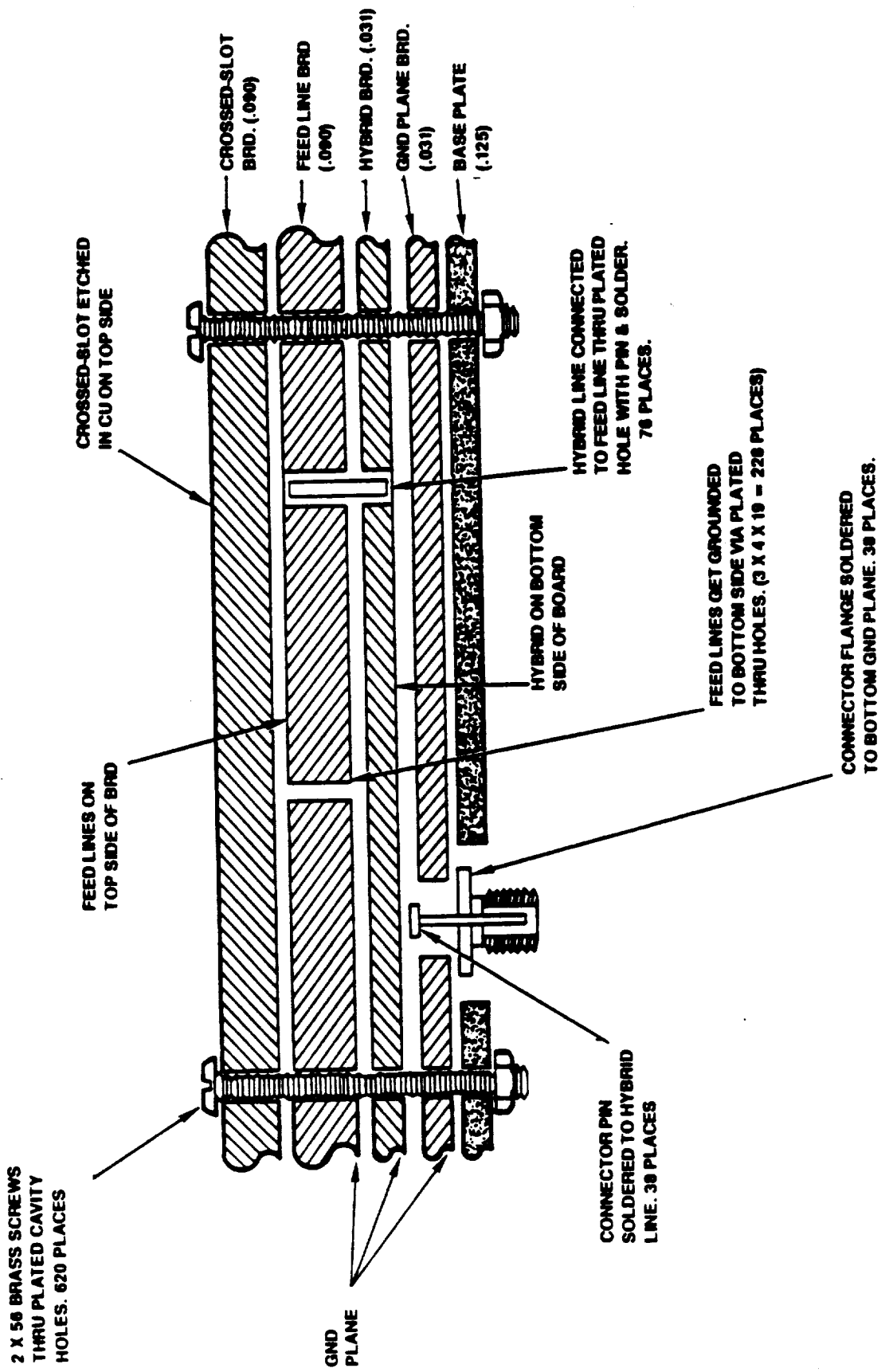


Figure 6-4. 19-Element Fabrication Experimental Model

numerous screws that now hold the antenna together or the aluminum plates must be designed.

## 6.4 MECHANICAL TECHNIQUES ASSOCIATED WITH MSAT-X

### 6.4.1 Bonding

The time required to optimize the antenna element design did not leave time to develop tools and processes to bond the assembly or test the individual boards before bonding. Since this antenna represents stripline and microstripline boards much larger than the average microwave circuitry, the problems of differentiated expansion, and restraining parts during high temperature bonding procedures are magnified. Add to this, the requirement to make connections between boards without penetrating the antenna element cavities and the problems become very apparent.

The two breadboard antennas delivered under contract were bolted together because TRE could not successfully bond the four layers together in the exercise of this phase of the program. More testing and study needs to be carried out in this area to determine the correct temperatures, pressure, and adhesives required for the job. Bond tests were conducted on specimen boards of the size used in these antennas; however, the results were not satisfactory. Cooling differentials within the layers caused a buckling of the copper and a shearing of some of the plated-through barrels, most noticeably at the interface between layers where the lip would tear away from the body or central shaft. Also noticed was bowing of the bonded specimen after it was removed from the autoclave.

### 6.4.2 Connectors

Another mechanically weak spot in the antenna is how the R.F. connector launches onto the beamformer board. Presently, a piece of RG-141/U semi-rigid coax is affixed to a mechanical collar (for mechanical support), its center conductor bent at right angles, and the whole assembly soldered to the input of the microstripline 7-way power divider. This serves as the input port of the beamformer circuit. Where the connector is soldered to the board also constitutes a small area which is vulnerable to cracking and breakage.

When it was discovered this was a problem, steps were taken to alleviate it by "beefing-up" the mechanical support anchoring the coaxial input line in place. This was done by machining a special pyramidal shaped collar that clamps around the connector where it

egresses from the cover. A three-point bolt arrangement at the base of the collar (attaching it to the cover) further stabilizes this connector.

A glance at Figure 6-1 shows that the R. F. and power connectors exit the antenna from the bottom. It is desired of future models to have these connectors exit the antenna at the edge. This would make a true low profile antenna approximately .75" thick overall. The present models are indeed of this thickness, but this is exclusive of the connectors.

#### 6.4.3 Plating

The boards on these antennas are tin plated, in the interest of economy. Unfortunately, tin plating tends to oxidize badly. Additionally, the complex circuitry of the beamformer board meant that its plating had to be of the "electro-less" type. This had the tendency to make the plating on that particular board non-uniform and very thin. Future models must have a different type of plating; something more stable (like gold, perhaps), yet easily soldered.

#### 6.4.4 Soldering Techniques

Initially, all the components of the beamformer board were soldered in place using SN63 solder with a temperature controlled soldering iron at 600° F. Later, some diode failures were noted. Reliability analysis plus discussions with the supplier of the diodes unearthed the fact that the die/frit interface of these PIN diodes would rapidly deteriorate at temperatures above 300°C since the gold would migrate into the solder leaving this interface brittle. For these antennas, the problem was solved by using Indalloy #2 (melting point, 150°C) solder and a low temperature, variac-controlled soldering iron. Future units should employ vapor-phase soldering techniques or something similar to avoid these problems.

#### 6.4.5 Intra-Antenna Interconnects

Launching from the beamformer to the hybrid board is now done with pins and straps. The heads of the pins are soldered to the stripline circuitry of the hybrid board, a delicate process that can lead to lifted pads if one is not careful. Also, great care must be exercised to center the pins. Following this action, the stripline cover is bolted in place, teflon inserts placed over the pins in the holes, and the straps formed and soldered to the top of the pins. Obviously, this can present quite an alignment problem with risk of damage to the circuit

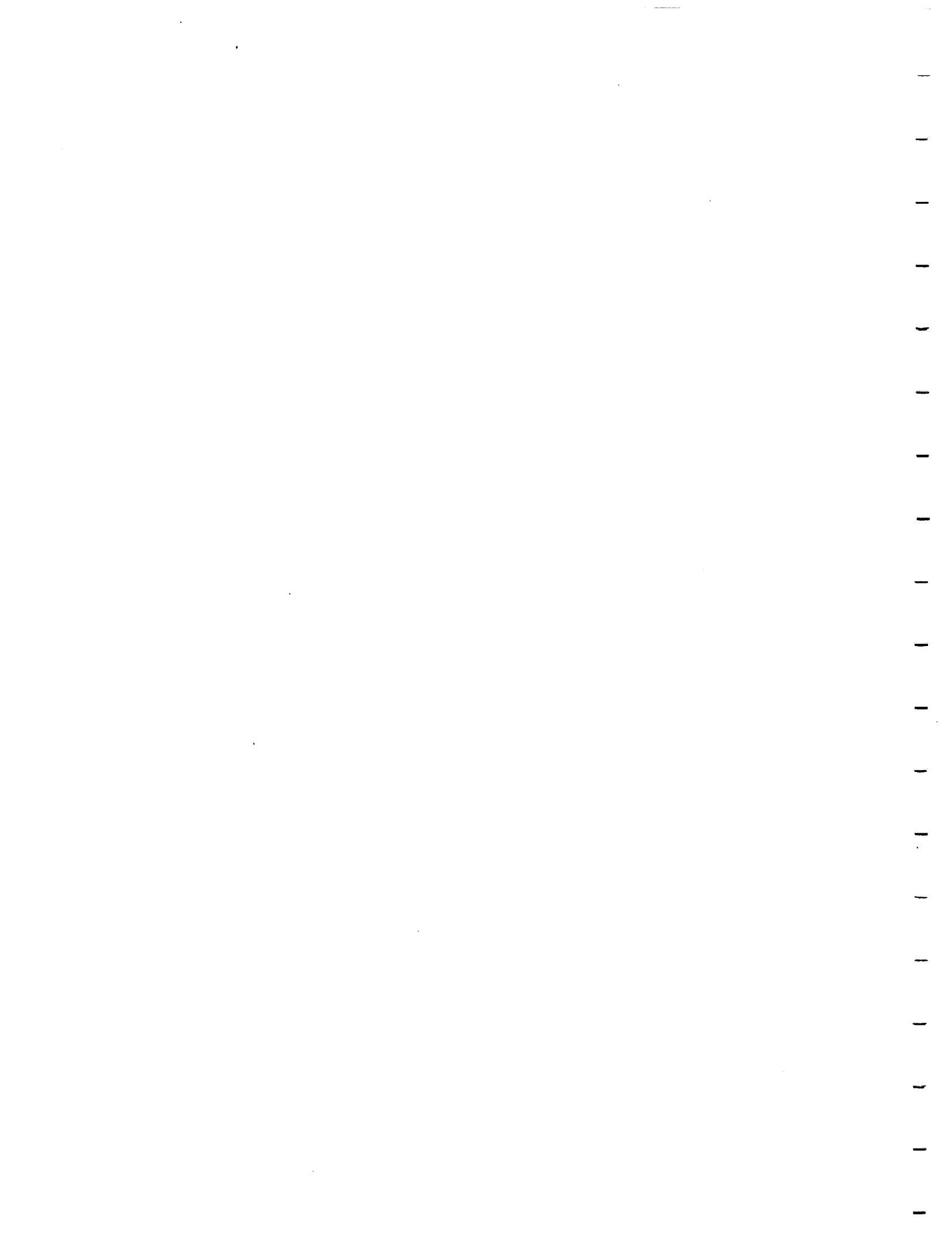
boards if care is not exercised. More work is required in this area to simplify this process and improve its reliability.

#### 6.4.6 Sealing

As presently configured, the bottom cover of the antenna (over the beamformer) is held in place with over 60 steel studs that screw into the aluminum support plate of the beamformer. Spacers are screwed over the studs to maintain proper clearance (.20") between the inner surface of the cover and the beamformer board. The studs are held tightly in place by "torque-seal". The cover is installed and tightened down at 1.7 in-oz. of torque per stud. There is nothing wrong with this procedure, however, sometimes when the cover is removed, an occasional stud may come off with the cover. A better arrangement will be devised on future models to affix the cover.

#### 6.5 CONCLUSION

The MSAT-X antenna represents a major advancement in the size and complexity of combining digital and high frequency circuitry into a thin integrated package. The bolts and aluminum threaded plate add to the complexity, but are adequate and do allow development testing. Improvements can be made. The relatively expensive cover and spacers can be injection molded in one piece, for instance, and metallized. The phase shifter board can be held to a stiffener tool with vacuum during parts installation and testing. Methods of mass producing very reliable solder connections must be considered, such as vapor deposition. Surface mount robotics would improve the cost of fabrication. Low temperature and pressure bonding materials must be developed. These are tasks that will be addressed in later versions of this product.



**SECTION 7**  
**MSAT-X PRODUCTION ANTENNA COST ANALYSIS**

This section summarizes the material/labor cost breakdown for yearly production quantities of 1000, 5000, and 10,000 MSAT-X phased array vehicle antennas over a five year period beginning in 1990. Additionally, a one-time production quantity of 11 units is also priced. Manufacturer's selling price, wholesale price and retail price. The data presented herein presents TRE's realistic progression to reach the customer's manufacturers' cost goal of \$1500 or less per unit in yearly lots of 10,000. TRE is taking the approach that this goal can be met with such labor cost reducing methods as automation (robotics) and perhaps off-shore manufacturing facilities.

Table 7-1 shows a summary of the cost analysis. Note that the estimated manufacturer's unit cost is \$1363 for 10,000 units per year for 5 years, using a dedicated offsite operation. The confidence level (under our assumptions) of this estimated cost of \$1363 is within 5%. Therefore, the ultimate cost goal of \$1500 or less has been met. For a local plant (inside the U.S.A.), however, the unit cost is \$1848 which is higher than the targeted value of \$1500.

Table 7-1. Cost Analysis Summary

Quantity per year	Manufacturer's Cost (\$)	Manufacturer's Selling Price (\$)	Wholesale Price (\$)	Retail Price (\$)
10,000 (A)*	1363	1800	2215	2770
10,000 (B)**	1848	2595	3195	3995
5000	2060	2890	3560	4450
1000	2589	3635	4480	5595
11	4461	6260	7710	9640

\* Antennas manufactured at a TRE dedicated offsite operation (commercial profit center outside the U.S.A.).

\*\* Antenna manufactured at a facility within the confines of the U.S.A.

The high cost driver items have been identified and are summarized in Table 7-2. It is noted that the most costly item is the dielectric circuit board material, which uses the teflon fiberglass to minimize RF circuit losses. By using lower cost circuit board material, reducing the overhead cost, and improving the manufacturing technique, the targeted unit cost of \$1500 will be met for the local plant (inside the U.S.A.).

Table 7-2. High Cost Driver Items for 10,000 Units per Year

Items	Cost	Percent of Total Parts Cost
Dielectric Circuit Boards	\$293	25.7%
Phase Shifters	\$259	22.7%
Electronics	\$250	21.9%
Angular Rate Sensor	\$180	15.8%

## 7.1 COST ANALYSIS

The method used for the cost analysis is to break the unit cost into six distinct groups as suggested by Jet Propulsion Laboratory (JPL). These groups are:

- Material and Parts
- Assembly/Labor
- Manufacturer's Cost
- Manufacturer's Selling Price
- Wholesale Price
- Retail (User's) Price

Each of the six groups will be discussed in the following subsections.

### 7.1.1 Material and Parts

A parts list has been generated for each antenna system. Based on the parts list; total material cost has been determined for different quantities of production units per year. Results are summarized below:

<u>Number of Units</u>	<u>Material Cost</u>
11	\$1806
1000	\$1290
5000	\$1084
10,000 (A)	\$1018
10,000 (B)	\$1018

Based on the above results, the material cost is still somewhat high. Therefore, different types of material should be explored to reduce the cost. In addition, the design concept should be re-evaluated to reduce the required material. Note that the total material cost includes the rate sensor. The total material cost for the phased array antenna is only \$838 for the case of 10,000 units per year. Therefore, the cost of the rate sensor is a significant factor.

#### 7.1.2 Assembly/Labor

The assembly/labor required to build the antenna system was analyzed.

<u>Number of Units</u>	<u>Assembly/Labor</u>
11	\$991
1000	\$469
5000	\$348
10,000 (A)	\$122
10,000 (B)	\$292

Based on the above cost, it was concluded that the assembly/labor is not a cost driving item.

#### 7.1.3 Manufacturer's Cost (MC)

The manufacturer's cost is defined as follows:

$$MC = \text{Material and Parts} + \text{Assembly/Labor} + \text{Overhead}$$

For the MSAT-X production antennas, this illustrated as follows.

<u>Number of Units</u>	<u>Material Cost</u>
11	\$4461
1000	\$2589
5000	\$2060
10,000 (A)	\$1363
10,000 (B)	\$1848

Note that the estimated manufacturer's unit cost is \$1363 for TRE's offsite operation for 10,000 units per year for five years. The estimated value of \$1363 is lower than the targeted unit cost value of \$1500. For the local plant (inside the U.S.A.), however, the estimated unit cost is \$1848 which is higher than the targeted unit price. The major cost difference between the offsite and local plan facilities is the assembly/labor and the overhead cost.

#### 7.1.4 Manufacturer's Selling Price (MSP)

The manufacturer's selling price is defined as:

$$\text{MSP} = \text{MC} + \text{Gross Profit}$$

The estimated MSP is summarized below:

<u>Number of Units</u>	<u>Material Cost</u>
11	\$6260
1000	\$3635
5000	\$2890
10,000 (A)	\$2595
10,000 (B)	\$1800

#### 7.1.5 Wholesale Price and Retail Price

Based on a limited survey of current cellular communications hardware, the cost of distribution and retailing represent as markup of the manufacturer's selling price of roughly 54% as follows:

Manufacturer's Selling Price	-	\$MSP
Distribution Selling Price (DSP)	-	111% x MSP

Wholesaler Selling Price (WSP)	-	111% x DSP
Retailer's Selling Price (RSP)	-	125% x WSP

This chain results in the Retailer's Selling Price equaling 154% x the Manufacturer's Selling Price. It may be possible to reduce one of the distribution levels and thereby reduce the price the customer ultimately has to pay.

The results are given below:

<u>Number of Units</u>	<u>Wholesale Price</u>	<u>Retail Price</u>
11	\$7710	\$9640
1000	\$4480	\$5595
5000	\$3560	\$4450
10,000 (A)	\$3195	\$3995
10,000 (B)	\$2215	\$2770

## 7.2 RESULTS

In order to provide an overall picture about the cost of a complete antenna system, all component costs are summarized together in Tables 7-3, 7-4, 7-5, 7-6, and 7-7 for production units of 11, 1000, 5000, and 10,000 per year, over a 5-year period. The high cost items are the teflon/fiberglass circuit board material, phase shifters, electronics circuits and angular rate sensor. In addition, the overhead cost is also very significant. Using the offsite operation, TRE's estimated manufacturer's unit cost is \$1363 which meets the ultimate goal of \$1500. The error in cost estimate is about 5%.

It should be noted that the manufacturer's unit cost comes down drastically from the first 11 units (\$4461) to the 10,000 units per year which is \$1363.

## 7.3 CONCLUSIONS AND RECOMMENDATIONS

In view of the cost analysis results, TRE concludes that the \$1500 manufacturer's unit cost goal can be met with the offsite operation. The estimated unit cost is \$1363. For the local plant (inside the U.S.A.), the unit cost goal could be met by using lower cost circuit board material, reducing overhead cost and improving the manufacturing technology. at the present time, the estimated unit cost is \$1848. TRE is committed to the MSAT-X program and will continue to investigate the methods of achieving lower cost for future MSAT-X

Table 7-3. TRE Fab. and Assy. Complete, 11 Units

Phased Array Antenna Parts and Labor Costs  
(per unit manufacturing costs)

A. Material and Parts	1986 \$'s Absolute Cost	% of Total Cost
o Radome	23	.3
o Dielectric circuit boards	(397)	(14.2)
- radiator layer	261	9.3
- hybrid layer	91	3.3
- phase shifter layer	45	1.6
o Phase shifters	(702)	(25.1)
- Pin diodes	529	18.9
- resistors	10	.4
- capacitors and chokes	163	5.8
- etc.		
o Open-loop pointing sensor	300	10.7
o Electronics	(360)	(12.9)
- Microprocessor	90	3.2
- Peripheries	270	9.7
o Mechanical structures	5	.2
o Cable, connectors, etc.	19	.7
Subtotal	\$1,806	64.6%
B. Assembly/Labor		
o Radome	99	3.5
o Radiators	471	16.8
o Hybrids	187	6.7
o Phase shifter layer	94	3.4
o Phase shifters	36	1.3
o Electronics	49	1.8
o Mechanical Structures	29	1.0
o Antenna integration	26	.9
Subtotal	\$ 991	35.4%
C. Overhead Cost	\$1,664	
Grand Total (Manufacturer's Cost)	\$4,461	
Gross Profit	\$1,799	
Manufacturer's Sales Price	\$6,260	
Wholesale Price	\$7,710	
Retail Price	\$9,640	

Table 7-4. TRE Fab. and Assy. Complete, 1000 Units/Yr - over a 5-year period

Phased Array Antenna Parts and Labor Costs  
(per unit manufacturing costs)

A.	Material and Parts	1986 \$'s Absolute Cost	% of Total Cost
	o Radome	19	1.1
	o Dielectric circuit boards	(331)	(13.7)
	- radiator layer	217	12.3
	- hybrid layer	76	4.3
	- phase shifter layer	38	2.1
	o Phase shifters	(461)	(26.2)
	- Pin diodes	344	19.5
	- resistors	10	.6
	- capacitors and chokes	107	6.1
	- etc.		
	o Open-loop pointing sensor	200	11.4
	o Electronics	(260)	(14.3)
	- Microprocessor	56	3.2
	- Peripherals	204	11.6
	o Mechanical structures	4	.2
	o Cable, connectors, etc.	15	.9
	Subtotal	\$1,290	73.3%
B.	Assembly/Labor		
	o Radome	46	2.6
	o Radiators	207	11.3
	o Hybrids	93	4.7
	o Phase shifter layer	41	2.3
	o Phase shifters	36	2.1
	o Electronics	29	1.7
	o Mechanical Structures	14	.8
	o Antenna integration	13	.7
	Subtotal	\$ 462	26.7%
C.	Overhead Cost	\$ 330	
	Grand Total (Manufacturer's Cost)	\$2,589	
	Gross Profit	\$1,046	
	Manufacturer's Sales Price	\$3,635	
	Wholesale Price	\$4,480	
	Retail Price	\$5,595	

Table 7-5. TRE Fab. and Assy. Complete, 5000 Units/Yr - over a 5-year period

Phased Array Antenna Parts and Labor Costs  
(per unit manufacturing costs)

A.	Material and Parts	1986 \$'s Absolute Cost	% of Total Cost
	o Radome	17	1.2
	o Dielectric circuit boards	(303)	(21.1)
	- radiator layer	199	13.9
	- hybrid layer	69	4.8
	- phase shifter layer	35	2.4
	o Phase shifters	(302)	(21.1)
	- Pin diodes	193	13.5
	- resistors	10	.7
	- capacitors and chokes	99	6.9
	- etc.		
	o Open-loop pointing sensor	190	13.3
	o Electronics	(253)	(17.7)
	- Microprocessor	56	3.9
	- Peripherals	197	13.8
	o Mechanical structures	4	.3
	o Cable, connectors, etc.	15	1.0
	Subtotal	\$1,084	75.7%
B.	Assembly/Labor		
	o Radome	33	2.3
	o Radiators	145	10.1
	o Hybrids	60	4.2
	o Phase shifter layer	30	2.1
	o Phase shifters	36	2.5
	o Electronics	25	1.8
	o Mechanical Structures	10	.7
	o Antenna integration	9	.6
	Subtotal	\$ 348	24.3%
C.	Overhead Cost	\$ 628	
	Grand Total (Manufacturer's Cost)	\$ 2060	
	Gross Profit	\$ 930	
	Manufacturer's Sales Price	\$2,990	
	Wholesale Price	\$3,560	
	Retail Price	\$4,450	

Table 7-6. TRE Fab. and Assy. Complete, 10,000 Units/Yr - over a 5-year period

Phased Array Antenna Parts and Labor Costs  
(per unit manufacturing costs)

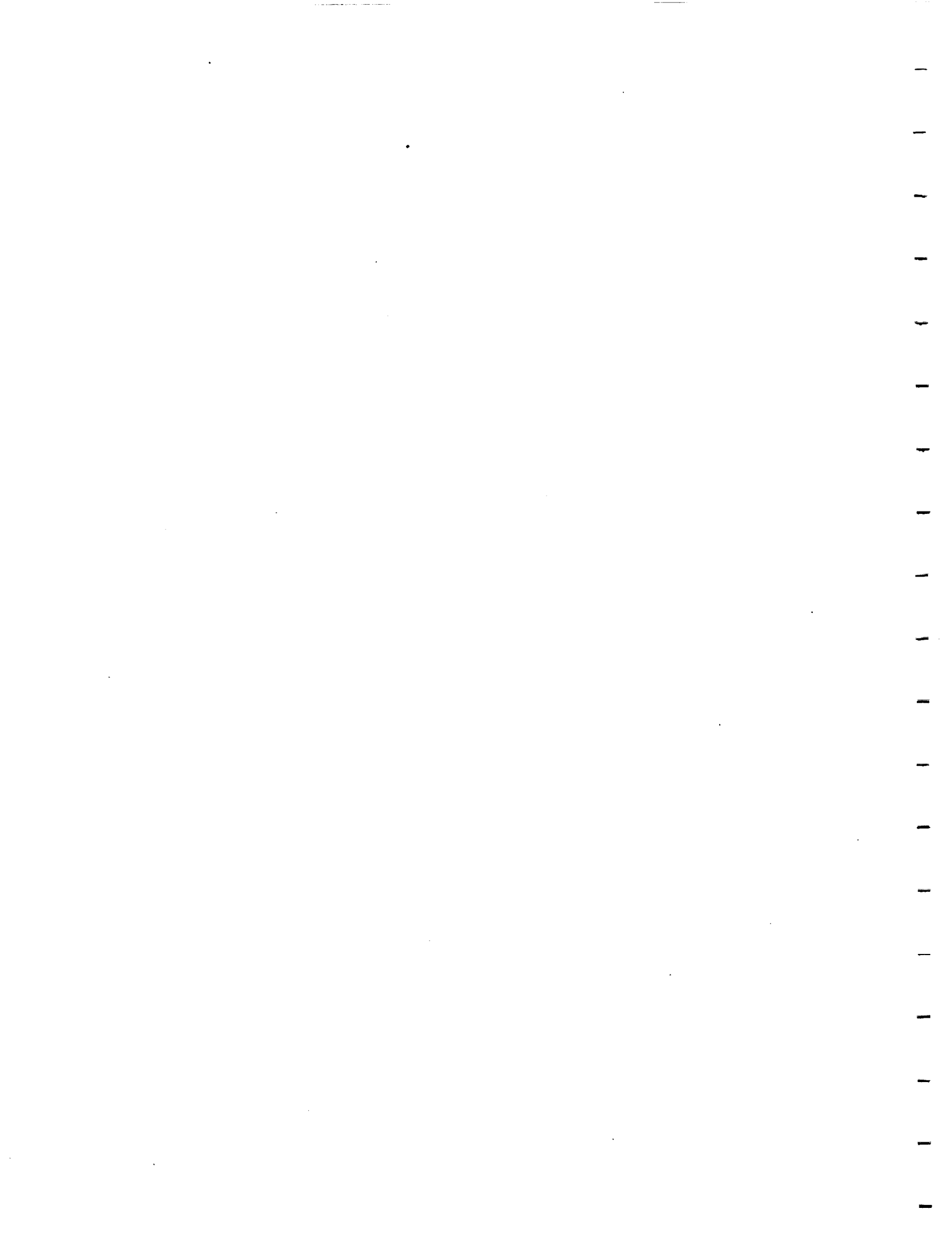
A.	Material and Parts	1986 \$'s Absolute Cost	% of Total Cost
	o Radome	17	1.3
	o Dielectric circuit boards	(293)	(22.4)
	- radiator layer	194	14.8
	- hybrid layer	66	5.1
	- phase shifter layer	33	2.5
	o Phase shifters	(259)	(12.8)
	- Pin diodes	151	11.5
	- resistors	10	.8
	- capacitors and chokes	98	7.5
	- etc.		
	o Open-loop pointing sensor	180	13.7
	o Electronics	(250)	(19.1)
	- Microprocessor	56	4.3
	- Peripherals	194	14.8
	o Mechanical structures	4	.3
	o Cable, connectors, etc.	15	1.1
	Subtotal	\$1,019	77.7%
B.	Assembly/Labor		
	o Radome	28	2.1
	o Radiators	116	8.9
	o Hybrids	48	3.7
	o Phase shifter layer	24	1.8
	o Phase shifters	36	2.7
	o Electronics	22	1.7
	o Mechanical Structures	9	.7
	o Antenna integration	9	.7
	Subtotal	\$ 292	22.3%
C.	Overhead Cost	\$ 338	
	Grand Total (Manufacturer's Cost)	\$1,648	
	Gross Profit	\$ 747	
	Manufacturer's Sales Price	\$2,395	
	Wholesale Price	\$3,195	
	Retail Price	\$3,995	

Table 7-7. TRE Decated Offsite Operation, 10,000 Units/Yr - over a 5-year period

Phased Array Antenna Parts and Labor Costs  
(per unit manufacturing costs).

A.	Material and Parts	1986 \$'s Absolute Cost	% of Total Cost
	o Radome	17	1.5
	o Dielectric circuit boards	(293)	(25.7)
	- radiator layer	194	17.0
	- hybrid layer	66	5.8
	- phase shifter layer	33	2.9
	o Phase shifters	(259)	(22.7)
	- Pin diodes	151	13.2
	- resistors	10	.9
	- capacitors and chokes	98	8.6
	- etc.		
	o Open-loop pointing sensor	180	15.8
	o Electronics	(250)	(21.9)
	- Microprocessor	56	4.9
	- Peripherals	194	17.0
	o Mechanical structures	4	.4
	o Cable, connectors, etc.	15	1.3
	<b>Subtotal</b>	<b>\$1,018</b>	<b>89.3%</b>
B.	<b>Assembly/Labor</b>		
	o Radome	12	1.0
	o Radiators	48	4.2
	o Hybrids	20	1.7
	o Phase shifter layer	10	.9
	o Phase shifters	15	1.3
	o Electronics	9	.8
	o Mechanical Structures	4	.4
	o Antenna integration	4	.4
	<b>Subtotal</b>	<b>\$ 122</b>	<b>10.7%</b>
C.	<b>Overhead Cost</b>	<b>\$ 223</b>	
	<b>Grand Total (Manufacturer's Cost)</b>	<b>\$1363</b>	
	<b>Gross Profit</b>	<b>\$ 437</b>	
	<b>Manufacturer's Sales Price</b>	<b>\$1800</b>	
	<b>Wholesale Price</b>	<b>\$2215</b>	
	<b>Retail Price</b>	<b>\$2770</b>	

program and will continue to investigate the methods of achieving lower cost for future MSAT-X electronically steered antenna system. Therefore, TRE would like to recommend a joint program, TRE and JPL, to explore the possible techniques to reduce the material cost for the antenna system.



**SECTION 8**  
**TEST PLAN/PROCEDURE**

8.1           TEST PLAN

8.1.1         Introduction

This section summarizes Teledyne Ryan Electronics' (TRE's) breadboard test plan to evaluate the MSAT-X satellite antenna during its development and prior to delivery to JPL. This document was generated to satisfy Item 6 under Contract 957468.

8.1.2         Scope

The major scope of this test plan is to describe the proposed approach in verifying the performance of the breadboard antenna system. It is here in its entirety as presented in Part I of TRE Report No. TRE/SD105662-1B, entitled "Breadboard Test Plan/Procedure for MSAT-X Satellite Communications Antennas."

8.1.3         Differences Between Breadboard and Production Tests

This document covers the first phase of a continuing development leading to a commercially affordable antenna that provides reliable mobile communications without dependence on local fixed stations. Consequently, these tests will have different objectives than the final production test. These breadboard tests are needed to prove a sound design and to define areas of improvement that might be beneficial in the next phase. A comparison matrix between the two test philosophies is shown below:

**Breadboard Tests**

**Goals**

- Verify the design with intensive tests.

**Characteristics**

- Labor intensive, manual tests are typical.

- Use existing equipment for best cost affectivity.
- Manufacturing errors or defective parts have to be corrected but the main effect is a small delay in delivery.

### Production Tests

#### Goals

- Low recurring cost contribution.
  - Requires low labor input and use of non-skilled labor.
  - Requires low cycle time for each test.
- Must be integrated into the production test flow.
  - Must provide a high probability of capturing defective components and manufacturing errors without filling the pipeline with defects.
  - The test intensity must be greatest at the lowest levels of assembly.
  - Must provide automatic fault isolation with a paperless record system.
  - Must provide quick feedback into the manufacturing process.

#### Characteristics

- Requires a high capital investment of dedicated test facilities and equipment.
- Highly automated tests are mandatory.
- Higher test equipment reliability is required than for breadboard tests but the test equipment is also far more complex, putting a premium on intrinsic reliability and rapidity of repair.
- Each test must be designed for maximum cost affectivity.

#### 8.1.4 Location of Tests and Witnessing

##### 8.1.4.1 Location

Testing will be performed at two locations:

Lower level tests will be performed at TRE's engineering laboratories by TRE engineers who designed the equipment. All tests will be witnessed by a TRE Quality Assurance engineering.

The final system integration and acceptance tests will be performed at TRE's outdoor pattern range which is located at 5658 Kearney Mesa Road, about 3 miles from the TRE plant.

##### 8.1.4.2 Witnessing

JPL will be advised in advance of the System Acceptance Tests and Spike tests to allow them the opportunity of witnessing these tests. This will also provide the opportunity for informal comparison of data with the design and requirements and determining the acceptability of the equipment prior to formal submission of the test report.

#### 8.1.5 Description of the Test Range

TRE will perform antenna module pattern tests as well as final system acceptance tests on an outdoor far field pattern range. The range length is 88 feet and the height above grade is approximately 20 feet. The facility contains a small Scientific Atlanta Azimuth over Elevation over azimuth antenna positioner with pattern recorder. The following range modifications were performed by TRE to optimize the MSAT-X test results:

- The microwave absorber lining on the primary tower anechoic walls was replaced with longer pyramids. This was necessary to measure the sidelobes of this lower frequency broader band antenna, when compared to the normal use.
- A dual polarization L band antenna was mounted in the secondary tower, along with a tunable source as shown in Figure 8-1. This antenna will provide four transmission modes (Right Hand Circular, Left Hand Circular, Vertical Linear and Horizontal Linear) to measure cross polarization isolation and ellipticity. This antenna will have somewhat more directivity than the test item in order to minimize ground reflection effects.
- A second LHC polarized antenna and source is placed on an adjacent structure to approximate the average view angle to the second satellite.

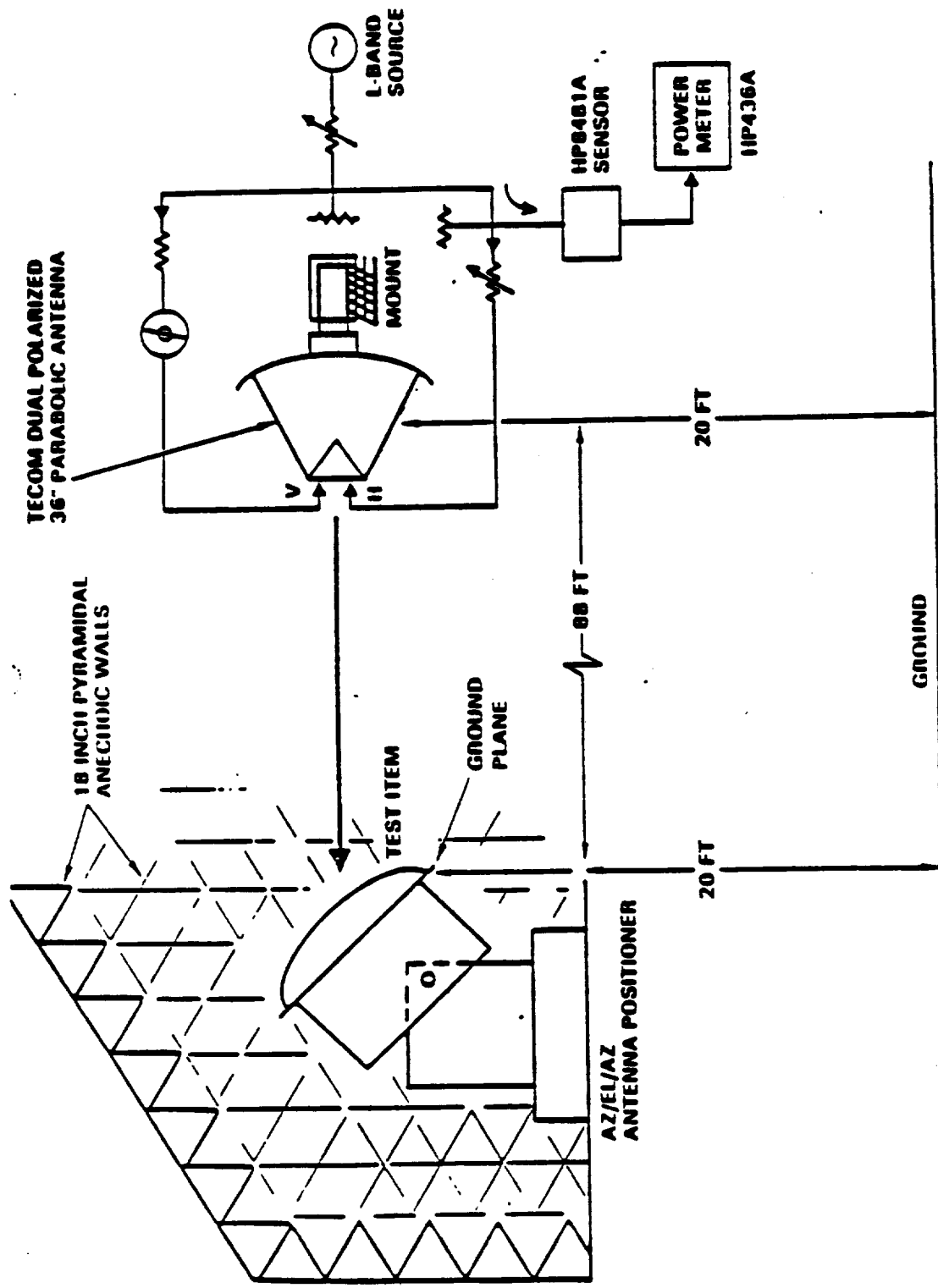


Figure 8-1. Antenna Test Range

## 8.1.6 Test Plan Details

### 8.1.6.1 Test Flow

TRE will perform the following tests in the general order indicated below. Some of the tests, which do not involve dependent constraints, may be performed in parallel.

- **Beam Steering Electronics Subassembly Tests**
  - **Power Supply Functional Tests**
  - **Software/Hardware Integration Tests and Software Margin Tests**
  - **Search Mode Functional Tests**
  - **Track Mode Transfer Function Tests**
  - **Primary Power Margin Tests**
- **Antenna Assembly Tests**
  - **Tests of Individual Phase Shifters**
  - **Steering Coverage Tests**
  - **360 Degree Azimuth Pattern Tests at Selected Steering Angles**
  - **Polarization Isolation and Ellipticity Tests**
- **TRE Receiver Tests**
  - **Isolation Tests**
  - **Acquisition Sensitivity**
- **Functional System Integration Tests**
  - **Acquisition Tests**
  - **Dynamic Tracking Tests**
  - **Dynamic Fading Simulation Tests**

(The foregoing Functional system Tests will include an interfering cross polarized signal from a simulated second satellite.)

## 8.1.6.2 Beam Steering Electronics Assembly Test

### 8.1.6.2.1 Power Supply Functional Tests

The breadboard Beam Steering Assembly does not contain a separate power supply subassembly. The power supply is TRE's design and is both functionally and mechanically interrelated with the beam steering electronics. The power supply is not a commercial on shelf item. This design approach was chosen for lowest producible cost. The power supply uses the beam steering computer to regulate the power forms for the non logic loads. The logic loads use a linear pass regulator. Consequently, the 5 V logic form will be initially tested. Following this, the computer will be powered from the 5 V logic form on the power supply under test and the other output forms will be dummy loaded. Finally, the other forms will be connected to their loads. (These are used in the antenna and in the rate gyro which is also contained in the Beam Steering Assembly.) The following tests will be performed on each form:

- With the input form at 8 V then at 18 V, the following parameters will be measured:
  - Average input current
  - Input current waveform
  - Output voltages
  - Output ripple
  - Load regulation, 50 to 120% of design load, varied one at a time
- Each form will be sequentially short circuited and the primary power will be applied. Input current will be recorded up to equilibrium. That short will be removed prior to shorting the next output form.

Typical test data sheets are included in Appendix A of TRE Document No. TRE/SD105662-1B.

### 8.1.6.2.2 Hardware/Software Integration and Software Margin Tests

The breadboard is being constructed with some built in features (switches and monitor LEDs) to facilitate the basic operational checkout. Appendix B of the aforementioned report provides a basic guideline for the hardware/software integration test.

#### 8.1.6.2.3 Search Mode Functional Tests

A logic analyzer will be connected to the serial data output of the the Electronics Assembly. Start search will be commanded. The analyzer memory data contents will be compared with the known stored search pattern. These data represents three bit phase commands to the phase shifters that are wired to the single long shift register in the Antenna Assembly.

Next, the sweep will again be started and during the sweep, the analog input will be momentarily raised above the track threshold. The existence of only a partial pattern capture will be verified.

#### 8.1.6.2.4 Track Mode Transfer Function Tests

Referring to the Antenna Steering Control Block Diagram (Figure 8-2), an input ripple signal will be summed in with a coherent ("C") state bias at the C/N analog input from the receiver. The azimuth integrator output test point, T1, will be observed on an oscilloscope. The input ripple frequency will be varied about the dither rate. The resulting beat frequency provides a simple but thorough end-to-end analog transfer function test. The open loop frequency response may be measured by varying this beat frequency and noting the relative T1 amplitude.

Turning the module while observing T1 when temporarily in the non-coherent ("N") input state, will test the rate sensor and its algorithm. Putting the input back at the "C" level should reduce the T1 value back to zero after the delay period.

#### 8.1.6.2.5 Power Form Margin and Noise Tests

The specification requires the use of filters and compliance with unspecified spike levels. There is no other requirement for electromagnetic compatibility. Compliance is a cost driver in a cost sensitive product. The design will comply with the specified voltage range but not the environment described in Sections 4.9 through 4.11 of SAE Handbook J1211. More hardening would be required for protection against external electromagnetics effects. Finally, no requirement for compatibility with SAE J551, or FCC Part 15J emissions requirements are described. Even these specifications will not necessarily assure compatibility with broadcast AM or CB receivers on the same vehicle.



In view of the above, TRE suggests the following tests:

- Measure the item and frequency domain input current waveforms with MIL-STD-462 10 f coaxial filter line impedance stabilization. The test report will discuss the potential interference which is likely from this.
- Perform the spike tests. TRE will apply increasing levels of input stimulus while observing the secondary forms for pulse transfer. the level will not be increased beyond the maximum safe value for the input protective avalanche diode or the point where pulse transfer to the load is observed to approach the maximum safe component rail voltage.

TRE recommends that these issues all be a part of the next two phases. The second phase should provide cost studies in hardening to different scenarios described in the above references. These would lead to an optimum degree of emissions and susceptibility control. The third phase would then test a pilot production model to these performance requirements.

#### 8.1.6.3 Antenna Assembly Tests

The antenna assembly will be subjected to bench and antenna range performance tests. The antenna assembly receives steering commands by means of a serial data link from the Electronics Assembly. It also receives secondary power forms for the shift register and phase shifts from the Electronics Assembly. While the production version contains a single coaxial rf connector for the transmit and receive signals, the breadboard has connector separable interfaces between each phase shifter and each antenna element. The Antenna Assembly will be powered from bench supplies. A word generator will provide steering commands. The required data content will be predetermined by means of an external computer which will generate standard beam pointing angle exercises to be used for pattern tests.

##### 8.1.6.3.1 Bench Tests

Prior to testing the actual beam pointing angles or patterns, it is necessary to independently assure that each phase shifter creates the expected microwave phase shift in each of the

eight states. Without doing this first, it would not be possible to evaluate or troubleshoot range performance anomalies. As stated above, the breadboard antenna has a connector separable interface between the phase shifter and antenna hybrid planes.

First each antenna element will be tested for VSWR ( $S_{11}$ ) and Isolation to the hybrid termination ( $S_{21}$ ).

Next, each of the 18 phase shifters will be tested in all 8 states using a HP 8510 network analyzer. The results will be printed by the controlling computer. A word generator will program the phase shifts with a precomputed pattern for each desired state.

Other tests will be current consumption from each power form and injected ripple susceptibility on each power form.

Later, integrated antennas will receive the equivalent of the above tests using a near field antenna range. This technique can detect individual phase shifter/element problems (but not separate the phase shifter from the element. In an integrated antenna, only the phase shifter diodes can be replaced.) At PDR, single element coupling probe tests were proposed. In retrospect, this does not appear to be workable because the probe will disturb the antenna and reflect power back into it in an uncontrolled manner.

#### 8.1.6.3.2 Range Tests

The Antenna Assembly will be mounted on the antenna positioner described in paragraph 8.1.5 herein. The lower elevation motion will only be used for initial indexing of the electronic steering angle and upper azimuth motion zero position. The elevation axis will be tipped downward to allow the beam (which is steered to a finite elevation angle) to point parallel to the earth at the secondary tower which contains the source antenna. Once this is done, the azimuth pattern can now be obtained by rotating the upper azimuth motion by 360 degrees. The high performance microwave absorber (18 inch pyramids) will minimize scattered power from the main beam and provide accurate minor lobe structures.

Owing to the very large number of possible beam pointing angles, it is necessary to plan the test so as to provide the most useful information to characterize expected performance in operational deployment with the maximum amount of data to review. This can be done by exploiting the symmetry of the antenna. The azimuth beam steering has 60 degree cyclic redundancy. Within this it has 30 degree mirror symmetry. One electronic beam steering

exercise set from zero to 30 degrees of azimuth would effectively characterize the antenna behavior over the entire azimuth circle. However, the addition of the ground plane alters the inherent 30 degree symmetry to 90 degrees. In view of these considerations, TRE will perform the following tests at  $f_{\min}$  and  $f_{\max}$ :

Steer the antenna to each of 30 beam pointing angles from 0 to 90 degrees azimuth. Record a 360 degree azimuth pattern at each commanded beam position.

Steer the antenna to each of 10 azimuth positions from 0 to 90 degrees. Rotate the lower azimuth positioner axis to point the beam at the source. Record an elevation pattern from zero to 90 degrees.

The secondary tower will be equipped with a Tecom Industries Model 202019 36 inch dual polarized parabolic antenna, or equivalent. This provides approximately 12 dB gain to minimize ground reflection errors. The two ports of the antenna will be fed with a variable phase shifter and attenuator in one branch so as to provide the ability to compensate for differential VSWR effects at the test frequency. These items will be empirically adjusted to equalize the response of a spinning linear receiver element. The two branches will be fed from a common source via a power divider.

This antenna provides the ability to make both ellipticity measurements and cross polarization isolation measurements with one source antenna.

#### 8.1.6.3.3 Receiver Tests

TRE has purchased an ICOM IC-R7000 Receiver. However, it is not a complete ground terminal receiver. Consequently, TRE, has designed and provided extra components as shown in Figure 8-3. This assembly will then be tested. Tests will consist of acquisition sensitivity and the isolation of the CFE diplexer plus preselector.

#### 8.1.6.4 System Integration and Acceptance Tests

The Electronics and Antenna Modules will be connected together and tested on the same range used for pattern tests. Meaningful tests require the use of the system receiver (which TRE already has) and one CFE diplexer. The latter is required in order to simultaneously transmit and receive. This is necessary to assure that the specified power does not cause unexpected pin diode behavior. Possible effects might be parametric pumping of the I (intrinsic) layer width from the high level transmitter carrier. This could effect the steering performance and generate intermodulation terms, as well as radiate transmitter harmonics.

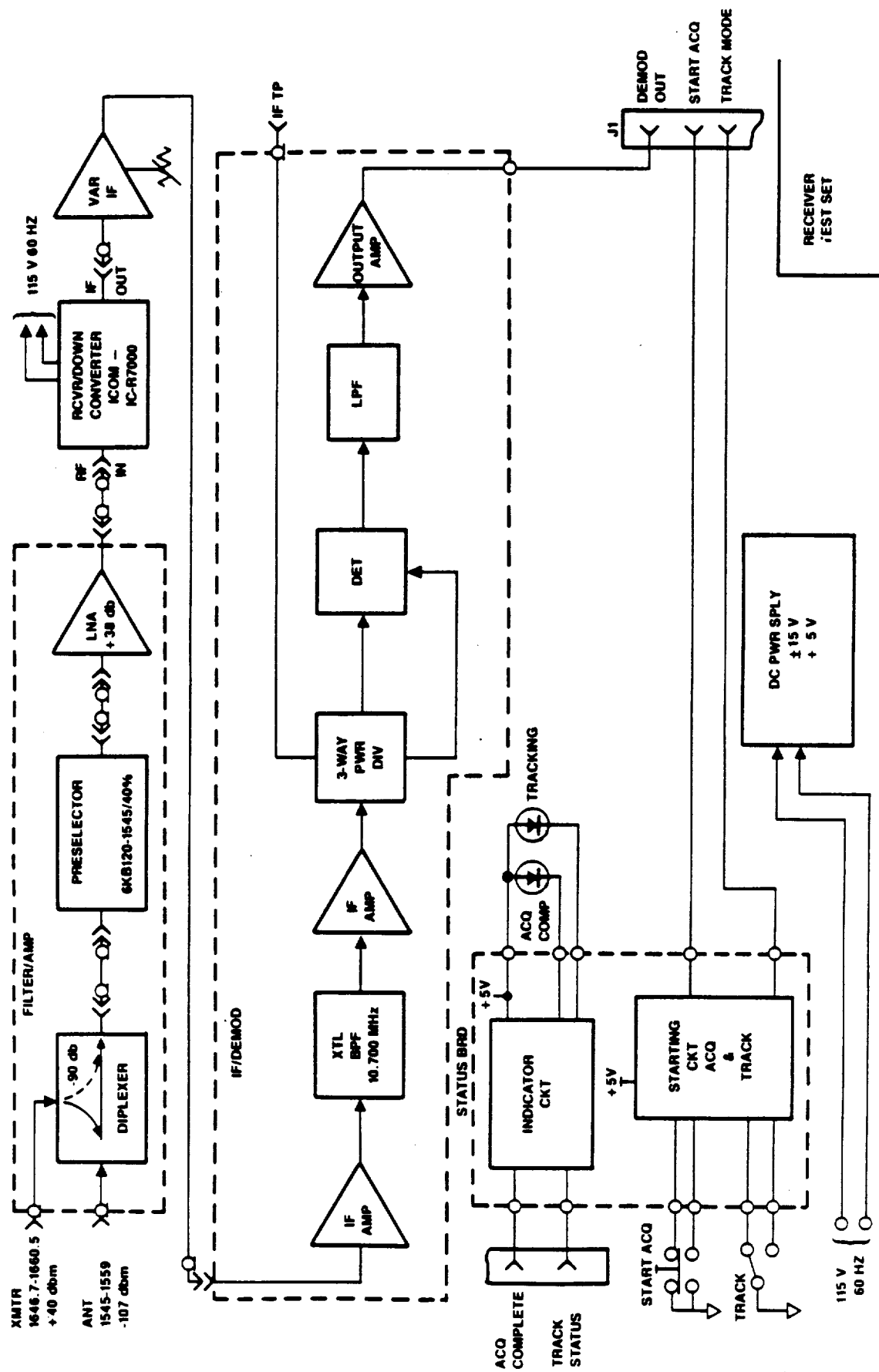


Figure 8-3. ICOM Reference Antenna Receiver

A far field antenna range provides the most accurate method of measuring the sensitivity of a receiving system that includes an antenna aperture. A power meter and variable attenuator at the source end will provide a means of accurately knowing the power to the transmitting antenna. The latter's gain will be initially measured at the two frequencies of interest. Mismatch losses are automatically included in the gain value. By using the communications equation, this will provide a known power density at the receiving aperture.

A second source at the same frequency will be put on an adjacent secondary tower. The position will approximate one point in the separation envelope between the two satellites. A second source will be used here to avoid the multipath spatial beat patterns that a coherent source would cause. This source will use a simple cross polarized (LHCP) antenna and the power will be adjusted for approximately equal power densities at the test aperture.

The test procedure (Part II of TRE Report No. TRE/SD105662-1B) is designed to establish the following results.

The following tests will be performed with both satellites transmitting:

- Measure the signal/noise ratio for acquisition threshold at various elevation angles, with and without the second satellite transmitting. This test will verify that the antenna has adequate gain and the the closed loop design makes the system relatively insensitive to variable signal-to-noise ratio.
- Measure the ability to maintain pointing angle and recover during fades.
- Demonstrate that the rate sensor can maintain inertial track for at least ten seconds after signal loss.
- Demonstrate the resumption of search after a modifiable period of signal loss.
- Demonstrate that the beam steering system does not cause more than 1 dB peak-to-peak amplitude fluctuation and 10 degrees peak-to-peak phase fluctuation on the received signal.
- Demonstrate that the tracking system operates satisfactorily for all specified antenna azimuth rates.
- The existing antenna positioner is only capable of 10 degrees/second azimuth rotation. The required speed of the rate table is 75 degrees/second. TRE is planning to increase the rotating speed from 10 degrees/sec to about 45 degrees/sec by using a separate motor.

## 8.2 ENGINEERING TEST PROCEDURE

### 8.2.1 Introduction

The Engineering Test Procedure (ETP) is a somewhat lengthy, self-contained document applied to JPL under Report No. TRE/SD105662-1B, entitled "Breadboard Test Plan/Procedure for MSAT-X Satellite Communications Antenna," dated September 2, 1987. The procedure consists of an introductory section, functional tests, preliminary set-up, and system tests. All the necessary data sheets, diagrams, phase shifter tables, and instructions to perform a complete acceptance test on the MSAT-X phased array antenna system. Preliminary conditions and test equipment are as follows.

### 8.2.2 Applicable Documents

The M1056 antenna system consists of a 19 element array, the electronic control box, and the receiver test set. applicable documents include:

Assembly Drawing	-	1056A0033
Schematic Drawing	-	1056A0001
Test Data Sheet	-	1056AS01
System Interconnect	-	1056B0005

### 8.2.3 Test Requirements

the test conditions and test equipment needed to perform the ETP are as follows.

#### 8.2.3.1 Test Conditions

Temperature	:	+25°C ±15°C
Altitude	:	normal ground
Vibration	:	none
Humidity	:	up to 95% RH

### 8.2.3.2 Test Equipment

Network Analyzer	:	HP8510 or equivalent
Test Cable	:	8 feet (2 required) Adams-Russell #9199-0096
Signal Generator	:	HP8663C
Spinning Mount	:	TRE
Receiver	:	Scientific Atlanta, Model 1711
Position Controller	:	Scientific Atlanta
Pattern Controller	:	Scientific Atlanta
Standard Gain Horn	:	Polarad CA-L (2 required)
Three Axis Positioner	:	Scientific Atlanta
Signal Generator	:	HP8642B (3 required)
Spectrum Analyzer	:	HP8562A
TWT Power Amplifier	:	Hughes 1177H09
Dual Polarized Antenna	:	Tecom 202019
LHCP Antenna	:	Tecom 401020L
RHCP Antenna	:	Tecom 401020R

### 8.2.4 List of ETP Tests

Reference is made to ETP #1056AS01 for further information regarding the tests. However, it is worth noting that the procedure delimitates and explains the following tests.

- Preliminary Set-up
- Antenna Patterns
- Antennas Cross-Polarization
- Intersatellite Isolation
- Acquisition
- Track
- Signal Loss
- Manual Steering Response
- Carrier-to-Noise (C/No)
- Dynamic Tracking and Fading
- High Power Test

Appropriate illustrations, drawings, and details are covered to fully evaluate the MSAT-X antenna system.

### 8.3 SYNOPSIS OF ACCEPTANCE TESTS

This section is a review of the acceptance tests performed on a typical MSAT-X developmental antenna system. All the tests are described fully in Report TRE/SD105662-1B entitled "Breadboard Test Plan/Procedure for MSAT-X Satellite Communications Antenna", September 2, 1987, pages II-1 through II-22. Consult Appendices D and E for a condensation of the test results on units #1 and #2 respectively.

#### 8.3.1 VSWR Tests

Prior to any range tests, the antenna in test must have the input VSWR ( $S_{11}$ ) checked over the frequency range of 1545 MHz to 1660 MHz. This is done using an HP-8510 Network Analyzer and the arrangement shown in Figure 8-4. The 18 3-bit phase shifters are exercised using a manual beam steering controller. Maximum acceptable VSWR is 1.5:1. In some cases, it was noted that the VSWR could run as high as 2.0:1 at either the high or low frequencies for some settings of the phase shifters.

#### 8.3.2 Antenna Patterns

##### 8.3.2.1 General Description of Test Set-up

The far field range at TRE used for the RF performance tests has a length of 88 feet with a height above grade of approximately 20 feet. The facility contains a Scientific Atlanta Series 5100/5300 azimuth over elevation over azimuth antenna positioner with pattern recorder. A diagram showing the essential elements of the range, as it was configured for these acceptance tests, is given in Figure 8-5. A brief description of the test set-up follows.

A dual polarized, L band parabolic antenna (TECOM Model 202019) was mounted in the secondary tower. This antenna is 36 inches in diameter and provides a gain of approximately 21 dB at 1600 MHz. Its relatively narrow beamwidth of 14° is a useful factor in minimizing ground reflections for these tests. The two ports of the antenna are fed with the quadrature arms of a 90° hybrid. Axial ratio is maintained to within 0.25 dB in the circular polarization (CP) mode by incorporating a variable phase shifter in

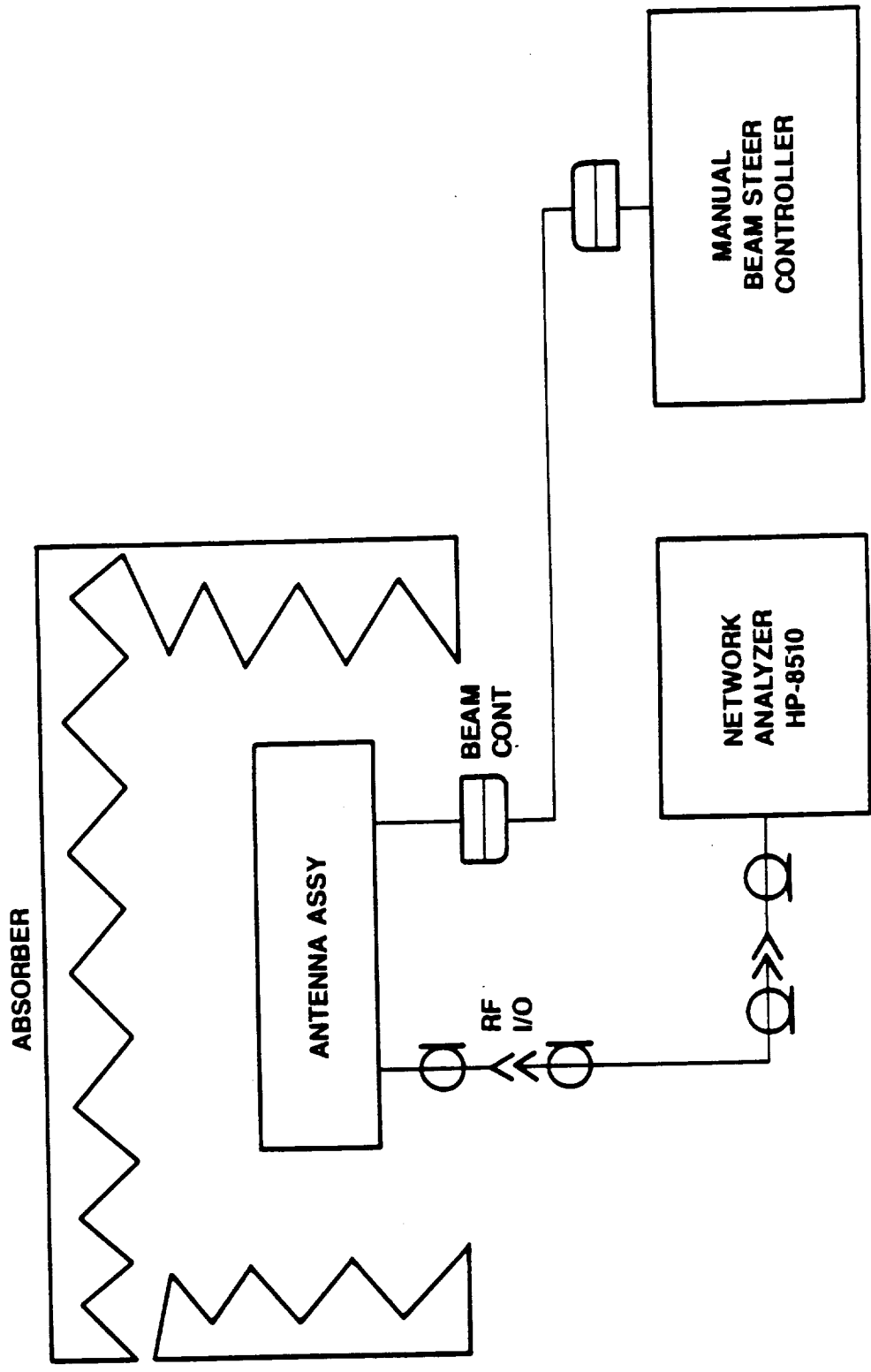


Figure 8-4. Block Diagram Depicting how MSA T-X Equipment is Interconnected for Functional Tests

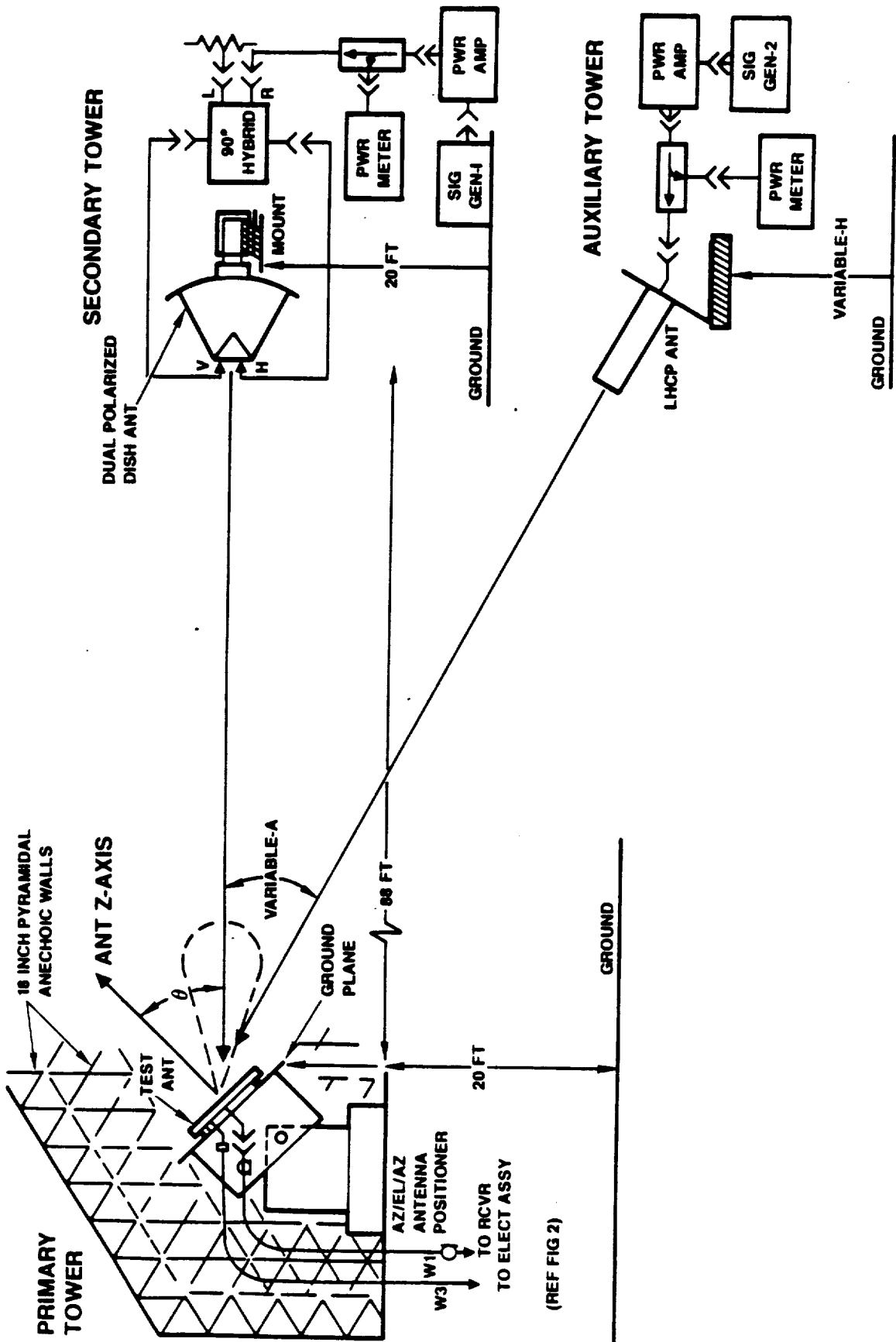


Figure 8-5. Pictorial/Block Diagram Depicting Equipment Hook-up for MSAT-X Systems Tests on Outdoor Antenna Range

one of the feed arms. As configured, the antenna provides four transmission modes (RCH, LHC, vertical linear, and horizontal linear) to measure cross-polarization isolation, and ellipticity. AN HP 8642 signal generator provides a source signal to the antenna.

A second antenna (TECOM Model 401020L, Helix, LHCP) was placed as an adjacent tower to approximate an average view angle to the second satellite. This antenna was likewise driven by an HP 8642 signal generator. The primary purpose of this set-up was to measure intersatellite isolation. The gain of the helix is approximately 13 dBic at 1600 MHz with a beamwidth of approximately 36°.

Axial ratio measurements were conducted using a spinning linear standard gain horn antenna (POLARAD Model CA-L) on a TRE mount in the secondary tower.

### 8.3.2.2 Broadside Antenna Patterns

Broadside antenna patterns were taken in both the horizontal (x-cut) and vertical (y-cut) planes. The MSAT-X antenna was mounted to a 40" x 50" ground plane which in turn was mounted on the positioner using the orientation of Figure 8-6. The equipment was hooked-up as shown in Figure 8-7, and the system calibrated by using a TECOM model 401020R helix antenna affixed to the ground plane of the antenna under test (AUT). Calibration is done with the positioner table at 90° elevation and 0° azimuth.

Once calibration is logged, the switches in the electronics box are set to steer the beam to 0° azimuth at 90° elevation. In this test, the y-axis of the antenna is vertical and the x-axis is horizontal. A 360° rotation of the positioner about the y-axis (x-cut) will establish a broadside pattern. Rotating the antenna 90° and repeating the above will generate a y-cut broadside pattern. Broadside gain and sidelobe levels are readily available from these patterns. This procedure was run at both 1545 MHz and 1660 MHz.

### 8.3.2.3 Azimuth And Elevation

Azimuth cuts were taken at 0° and over elevation angles of 20°, 30°, 40°, 50°, and 60°. A typical test set-up was done as follows using a beam setting of 0° azimuth and a beam elevation of 50°.

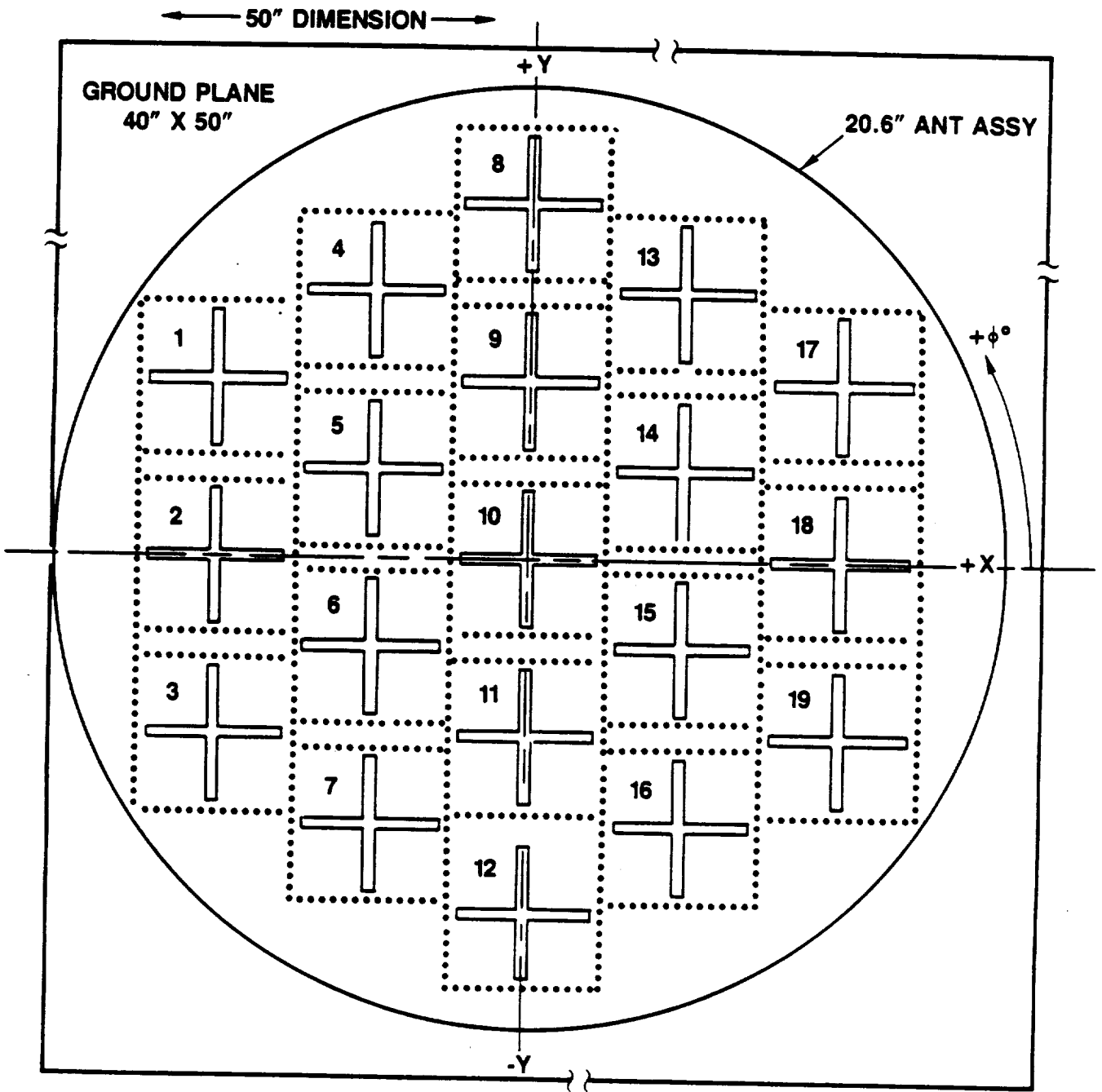


Figure 8-6. 19-Element Array, Top View

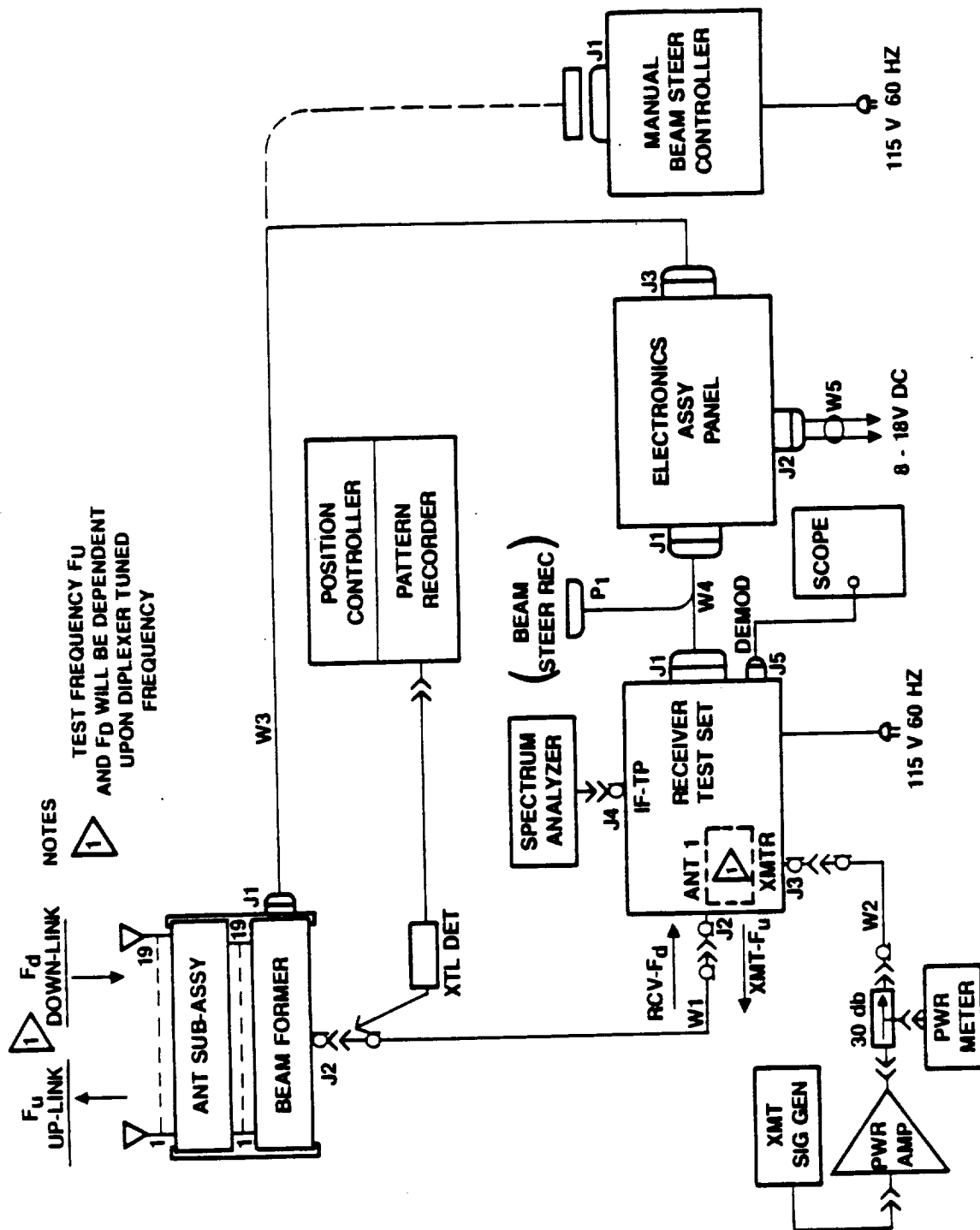


Figure 8-7. Block Diagram Depicting Equipment Hook-up for Antenna Pattern Tests

The switches on the electronics controller were set to steer the beam to 0° azimuth and 50° elevation. The antenna positioner was rotated to point the z-axis to 40° from zenith (50° from horizontal) and repositioned slightly to peak the signal. Next, the positioner was rotated about the z-axis to generate a pattern cut in azimuth at 50° elevation. Once the sets were generated, it was possible to determine gain, sidelobe and backlobe levels, and low angle drop-off rate. Representative patterns are shown in Appendix A.

An area of primary interest was the gain at an elevation angle of 20° with the beam at azimuth angles of 0° through 360° in 45° increments. A typical test set-up was done as follows using a beam setting of 45° azimuth and 20° elevation as an example.

The switches on the electronics controller were set to steer the beam to 45° azimuth and 20° elevation. The settings were entered and the positioner rotated to place the antenna in a vertical plane, then rotated about the vertical axis and z-axis of the antenna to position the beam horizontally and pointing to the dish antenna in the secondary tower. The positioner was then rotated about the vertical axis of the antenna to generate the required pattern. Representative patterns are shown in Appendix A.

### 8.3.3 Cross-Polarization

Cross-polarization levels were determined by changing the dish antenna in the secondary tower to the LHCP mode, running specific pattern plots as outlined in Paragraph 8.3.2, and comparing the results with those obtained in the RHCP tests. Typical patterns exhibiting LHCP plots superimposed over RHCP plots at selected azimuths and elevations are displayed in appendix D.

### 8.3.4 Intersatellite Isolation

This phase of the acceptance tests was designed to measure the antenna system's ability to discriminate between wanted and unwanted reception. The requirements are for the antenna to provide adequate gain to the desired satellite and also maintain a carrier-to-interference ratio of at least 20 dB to the undesired satellite anywhere within the continental United States (CONUS). Beam pointing error is included in this figure, but not propagation shadowing or ground multipath.

An idea of the range configuration can be gained by glancing at Figure 8-5. A twelve-foot movable boom was rigged to the roof of the auxiliary tower on the range. An LHCP helical

antenna was attached to the end of the boom to serve as the undesired signal source. While this affair could not approximate all the possible geometries in the CONUS between two satellite sources and the antenna test specimen, it did give some idea of what to expect.

A test frequency of 1545 MHz at + 16 dBm was fed to the dish antenna in the RHCP mode. A 1 MHz offset of this frequency was fed to the LHCP antenna at a level commensurate to give equal power density with respect to the dish antenna. Effective intersatellite isolation (I.S.) was measured by observing the received signals on a spectrum analyzer at the test receiver output (see Figure 8-8). Table 2-8 of Section 2 of this report lists the measured I.S. as 26 dB, a comfortable margin.

### 8.3.5 System Acquisition/Track/Steering

#### 8.3.5.1 Set-Up

The acquisition, tracking, and steering portions of the acceptance tests were conducted using the test set-up shown in Figure 8-5 and E-1 of this report. One of the requirements of these tests was to observe the effects of amplitude and phase induced by the tracking system on the received CW source carrier. As this wasn't possible with the TRE receiver (it had no "Q" or phase output), the JPL PIFEX transceiver was substituted. This is a precision calibrated receiver with a known correspondence between the received  $C/N_0$  and the DC output of the "I" signal.

It was noticed during the start of these tests that proper operation of the pointing subsystem could only be achieved by inserting a DC amplifier between the "I" output of the transceiver and the pointing subsystem's detected signal input. This amplifier was adjusted to a voltage gain of 10, which at a received  $C/N_0$  of 55 dB, provided a DC level of 1.1 volts to the detected signal. Likewise, it gave an output DC level of .11 volts to the detected signal at a  $C/N_0$  of 35 dB.

Data was taken on antenna system #1 only and is tabulated in Appendix E. No data was taken on system #2 as time did not permit this to be done.

**INTERSATELLITE ISOLATION  
SPECTRUM ANALYZER DISPLAY**

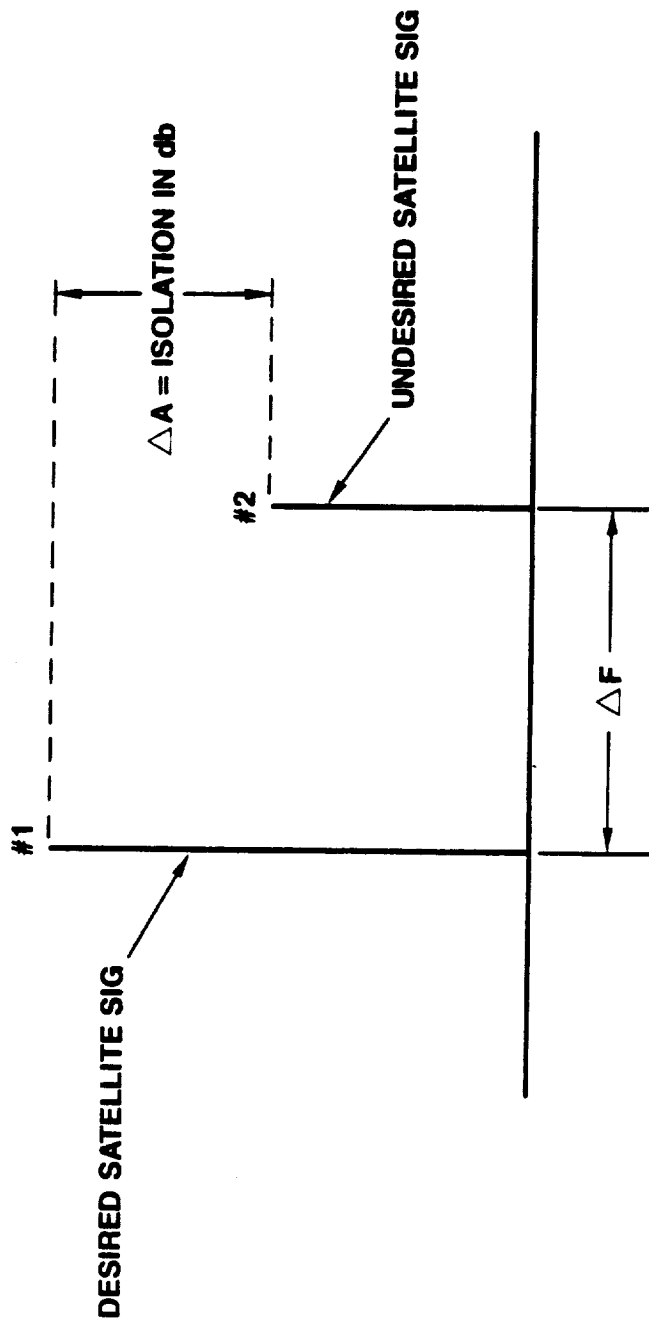


Figure 8-8. Intersatellite Isolation Spectrum Analyzer Display

### 8.3.5.2 Acquisition And Track

Acquisition measures the ability of the antenna beam to seek and acquire to the signal source from turn-on and random azimuth and elevation angles of the antenna. In these tests, the elevation angle of the antenna was 30°. Acquisition time was measured at C/N<sub>0</sub> levels from 55 dB to threshold. At 55 dB, 45 dB, and 38 dB (threshold) acquisition was timed at physical positions of the antenna of 0°, 45°, 90°, 135°, 180°, 270°, and 360°. In every case, the acquisition time was roughly 2 1/2 seconds. In a 4-beam system this would total 10 seconds, the specification limit.

During the acquisition and track tests, gain and phase transients were examined. The C/N<sub>0</sub> level for this observation was 70 dB to ensure that the received signal was elevated well above the system noise temperature. It was noted that peak-to-peak gain variations were 1.5 dB max., with a maximum phase variation of 15 degrees peak-to-peak. The spec limit of 1 dB and 10° for these items was not exceeded more than 95% of the time, according to best estimates.

### 8.3.5.3 Signal Loss Test

During this test, the system was placed in the track mode with the rate sensor turned on and closed loop tracking initiated with the antenna rotating at 10°/second. The source signal in the secondary tower was turned off for 10 seconds, then on again. No loss of tracking was noted.

### 8.3.5.4 Manual Steering Response

This test merely confirmed that the antenna beam was peaked in accordance with the settings entered and displayed on the front panel of the electronics box.

A specific elevation and azimuth for the antenna was loaded into the system which then steered the beam to that location. The antenna is physically steered to note a peak response. In all cases, the antenna system under test had the beam peaked in accordance with the data entered in the system.

#### 8.3.5.5 Dynamics Tracking And Fading

The dynamic tracking phase of this test involved verification that the system would track the same signal in the auto-track mode. This meant rotating the antenna away from the source and observing if the system tracked... which it did.

The fading test used an amplitude modulated test signal with a modulation index of .44 to simulate a 5 dB fade at a 40 Hz rate. No impairment of acquisition or tracking was noted, even when the antenna was spun at 10°/second.

#### 8.3.5.6 High Power Test

The purpose of this test was to note if any cross-modulation or deleterious spurious products were formed in the receiving system in the presence of a 20 watt signal fed into the transmitter port of the transceiver at 1655 MHz when the receiver is tuned to 1554 MHz. Considering losses, it was estimated that 10 watts of power was transmitted from the array. No impairment of operation was noted.

**SECTION 9**  
**CONCLUSIONS AND RECOMMENDATIONS**

9.1            CONCLUSIONS

An L-band electronically steered phased array antenna system has been successfully developed for the mobile satellite experimentation under NASA contract through Jet Propulsion Laboratory (JPL). The major features of the developed phased array are:

1. Low profile - Total array/antenna thickness is around 0.75 inch, which is less than one inch as the contract specified, without the inclusion of connectors.
2. Small size - Total of 22 inches in diameter, including mounting areas, which is well within the specified value of the 24 inches.
3. Low sidelobes - At broadside of array, the measured sidelobes are below 18 dB.
4. Good axial ratio - better than 5 dB was achieved within 95% of the required space coverage across the frequency band.
5. Good Intersatellite Isolation (26 dB) was achieved.
6. Satisfactory multipath rejection capability was realized.
7. Good Pointing Performance - The measured data showed fast acquisition time (10 seconds) during search mode and good tracking performance over wide signal to noise ratio ranges, even under fading and high power conditions.

The key factors in achieving the above performance are the result of the success of developing the cavity-backed, stripline feed, printed-circuit crossed-slot array element and the sound approach used in the design analysis of the array and pointing system. The former provides good element gain coverage at the low elevation angle of 20 degrees above the horizon. The latter forms the basis of selecting the right design of the array lattice, element spacing, 3-bit diode phase shifter circuits, beamforming network, and the beam pointing algorithm.

The only important performance that did not meet the design specification is the array gain at the low elevation angle of 20 degrees. However, the gain can be improved in the near future as discussed in Section 2.4.2. For comparison, the measured array gain (averaged over a 360 degree azimuth scan in 45 degree steps) and the broadside array gain are given in Table 9-1, together with the design specification.

Table 9-1. Array Gain Performance

Frequency (MHz)	Elevation Angle (Degrees)	Design Specification (DBIC)	Measured Gain (DBIC)
1545	90	10.0	12.6 (#1) 12.5 (#2)
	20	10.0	9.2 (#1) 9.3 (#2)
	90	10.0	13.7 (#1) 13.7 (#2)
	20	10.0	7.7 (#1) 8.3 (#2)

The main reasons for not meeting the gain specification are due to:

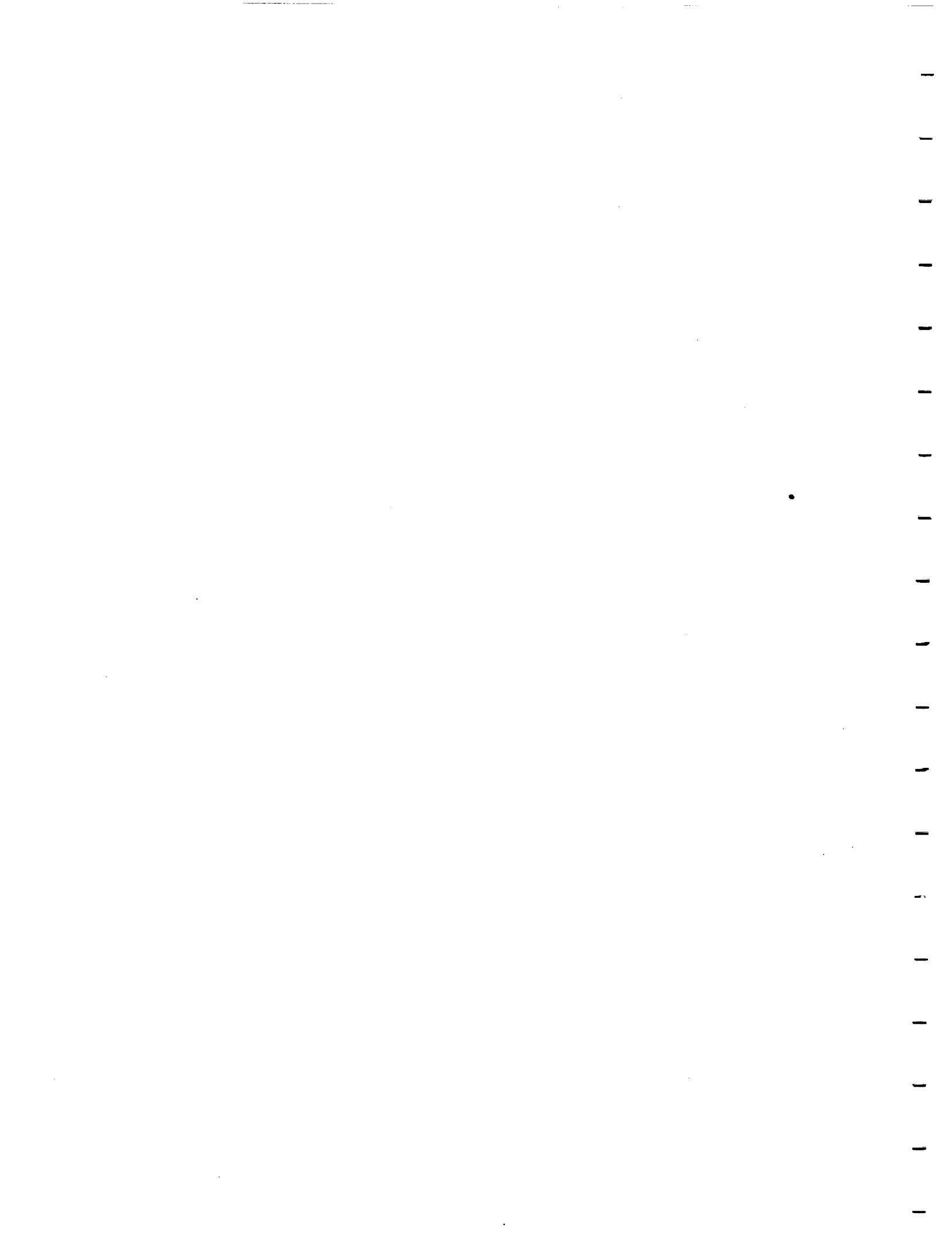
- The poor isolation between the right hand circular polarization (RHCP) and left hand circular polarization (LHCP) ports of each crossed-slot array element. The measured isolation is 6.64 dB and 6.04 dB for frequencies of 1545 and 1660 MHz respectively.
- The lack of calibration to optimize array beam scan positions. That is, at some azimuth angles, the beam did not scan far enough to the low elevation angles. As a result, the gain loss is very significant.
- The excessive loss in the beamforming network. The aperture amplitude and phase distributions realized exceed the design goal. As a result, the scan loss due to aperture distribution errors is very significant.

## 9.2 RECOMMENDATIONS

To further improve the array gain coverage at low elevation angles and to reduce manufacturing costs, the following areas are recommended for future studies:

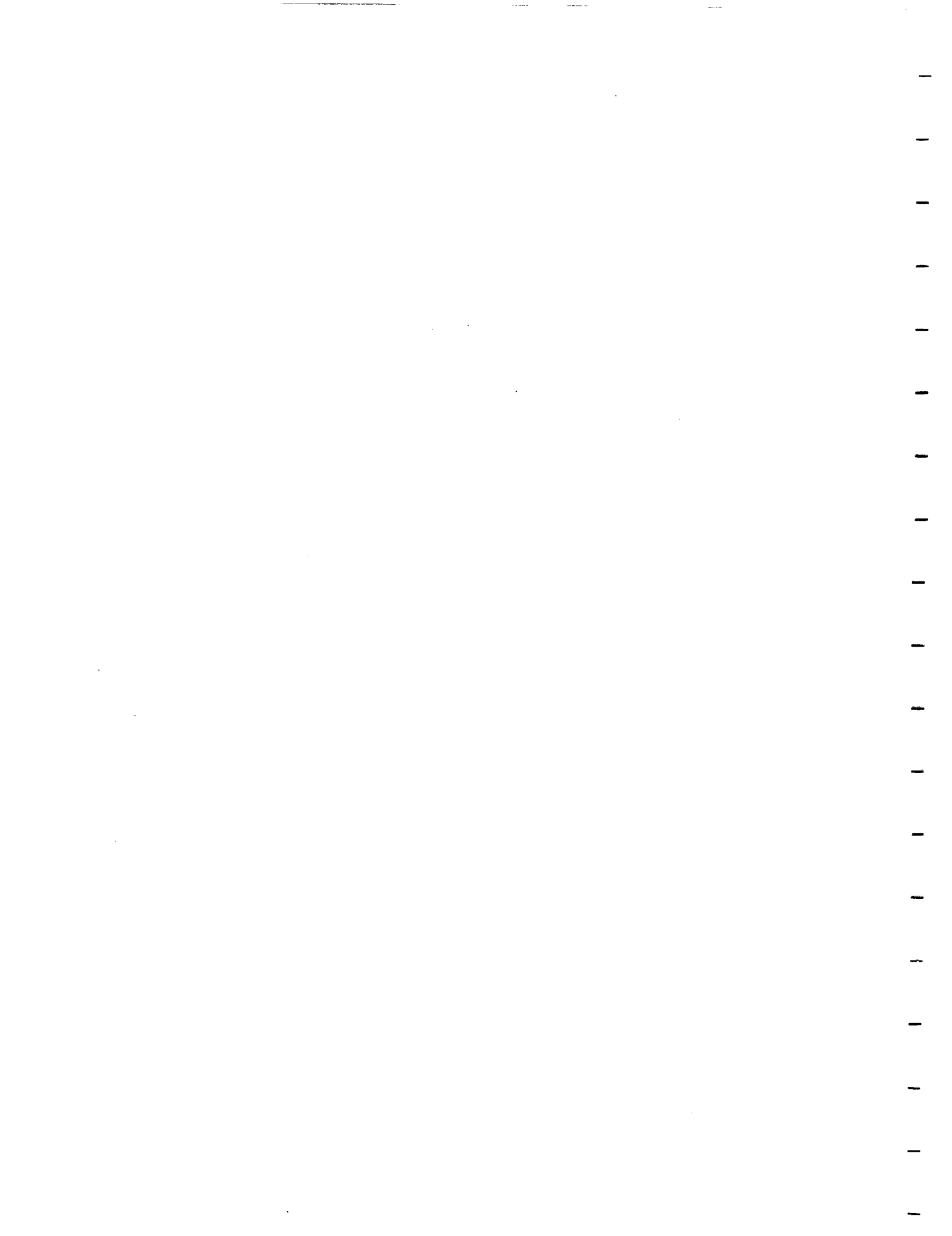
1. The excitation of a cavity-backed, printed-circuit crossed slot element needs to be reinvestigated to improve the isolation between the two polarization ports (RHCP and LHCP). The suggested approach is to optimize the excitation feed design; it is expected that an isolation factor of 10 dB should be realizable. The anticipated result is an improvement in the element gain and low elevation angle coverage of 0.6 dB and 1.2 dB at 1545 MHz and 1660 MHz respectively.
2. The amplitude and phase distributions of the beamforming network needs to be improved, so the beam can be steered to the correct elevation angle. As a result, low elevation angle gain can be improved by about 0.6 dB.

3. The bonding of the array has to be studied. Presently, the whole array was assembled together by screws. During the program we did some preliminary experiments which showed promising results. Additional effort is required to establish a bonding procedure and to evaluate bonding effects on array performance.
4. The modular approach for future production should be investigated. The modular approach may be defined as that each element forms a module which includes a crossed-slot, excitation circuit, and a 90 degree hybrid. The advantage of this approach is that the multiple-layer bonding applies to a much smaller area as compared to a whole array. This bonding process will be simpler and more cost effective. It can be envisioned that each element will be assembled by screws to a common ground plane to form the array aperture. Each array port of the beam forming network will be connected to each array element via a plug-in type connector. In addition, integrating a 3-bit diode phase shifter onto each element module should also be investigated to lower the manufacturing cost.



**APPENDIX A**

**TEST PATTERNS:  
MSAT-X ANTENNA SYSTEMS #1 AND #2**



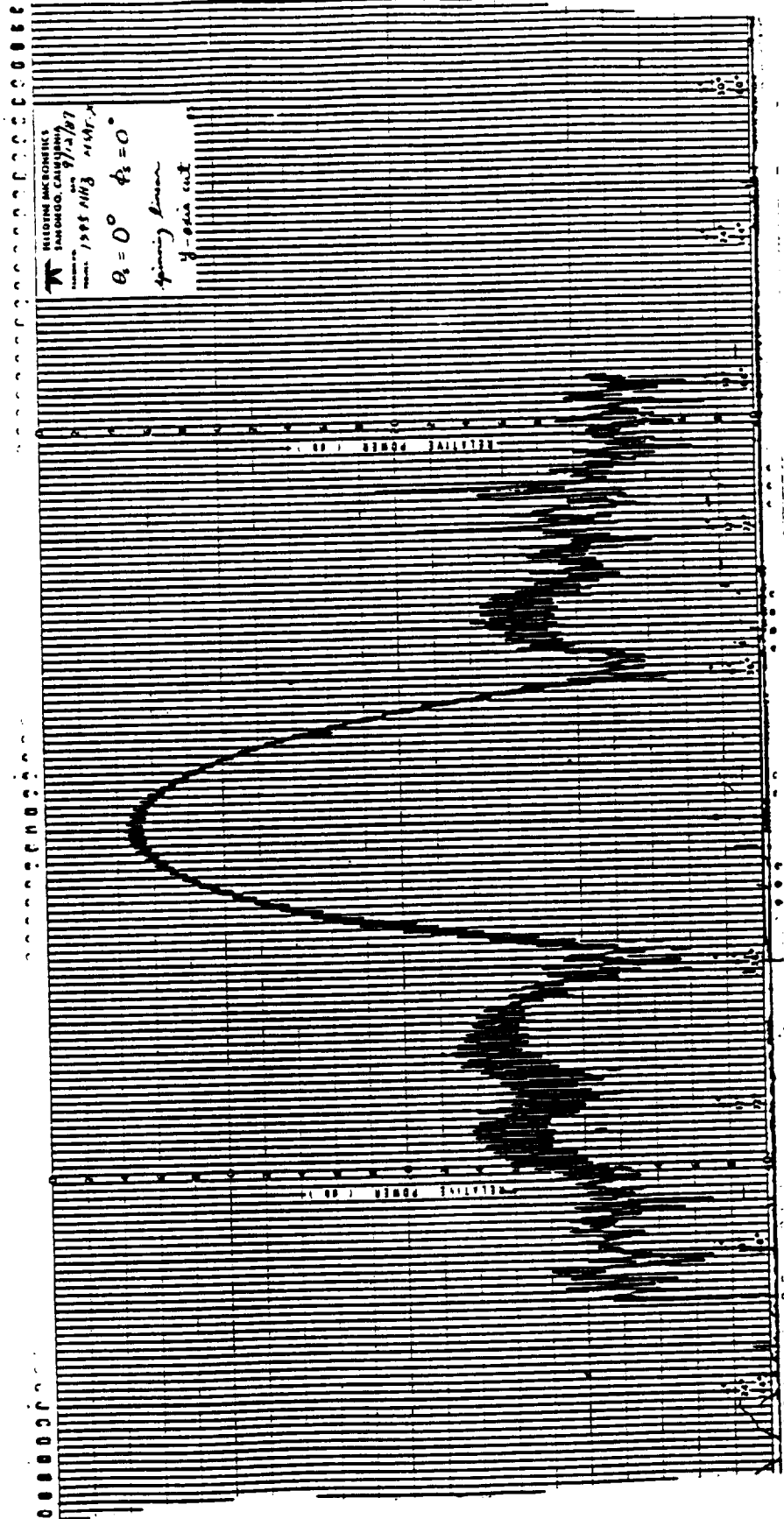


Figure A-1. Measured Spinning Linear Pattern at 1545 MHz (y-Axis Cut,  $\theta_s = 0^\circ$ ,  $\phi_s = 0^\circ$ )

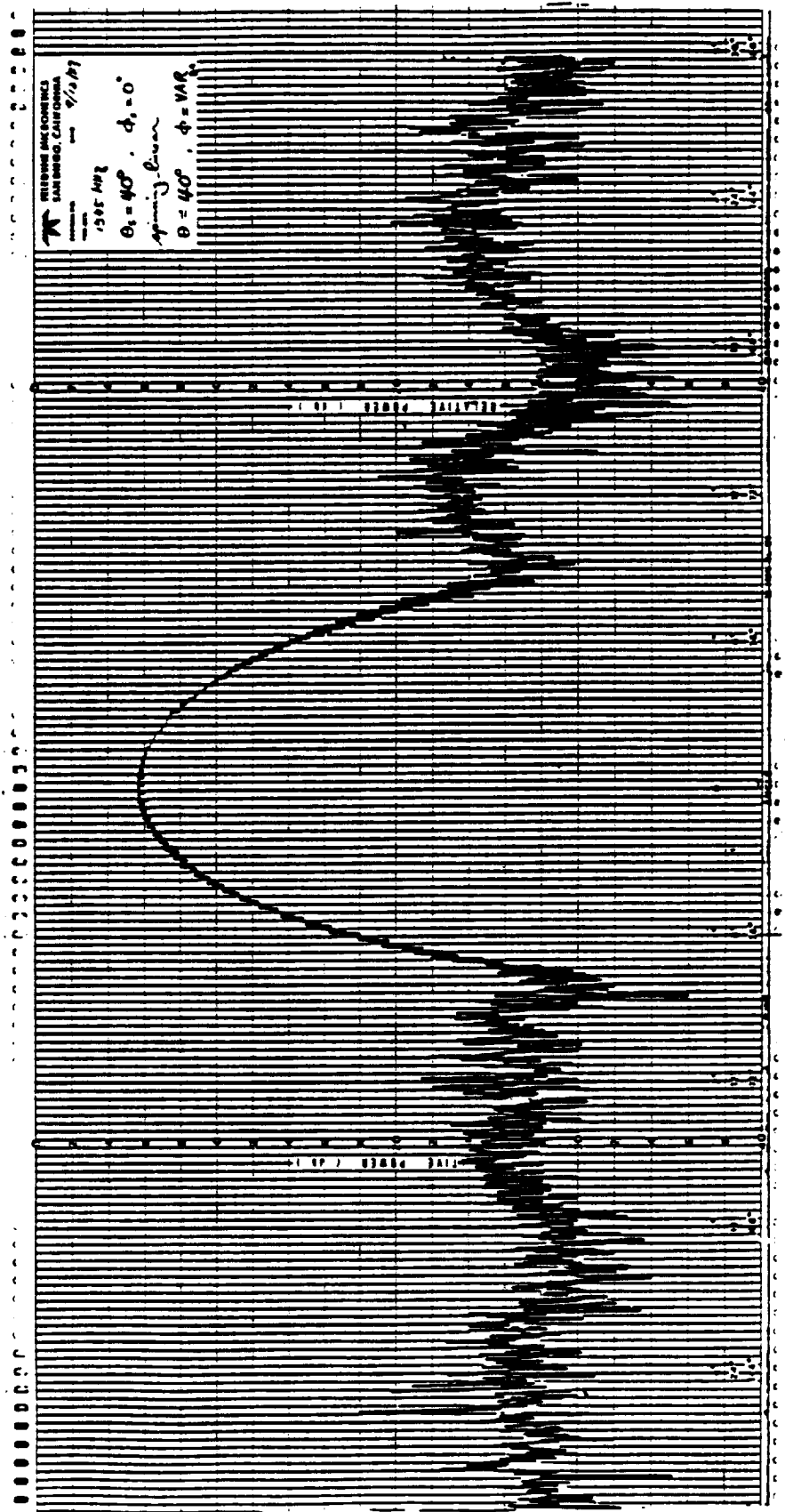


Figure A-2. Measured Spinning Linear Pattern at 1545 MHz ( $\theta_s = 40^\circ, \phi_s = 0^\circ, \theta = 40^\circ, \phi = \text{VAR}$ )

ORIGINAL PAGE IS  
OF POOR QUALITY

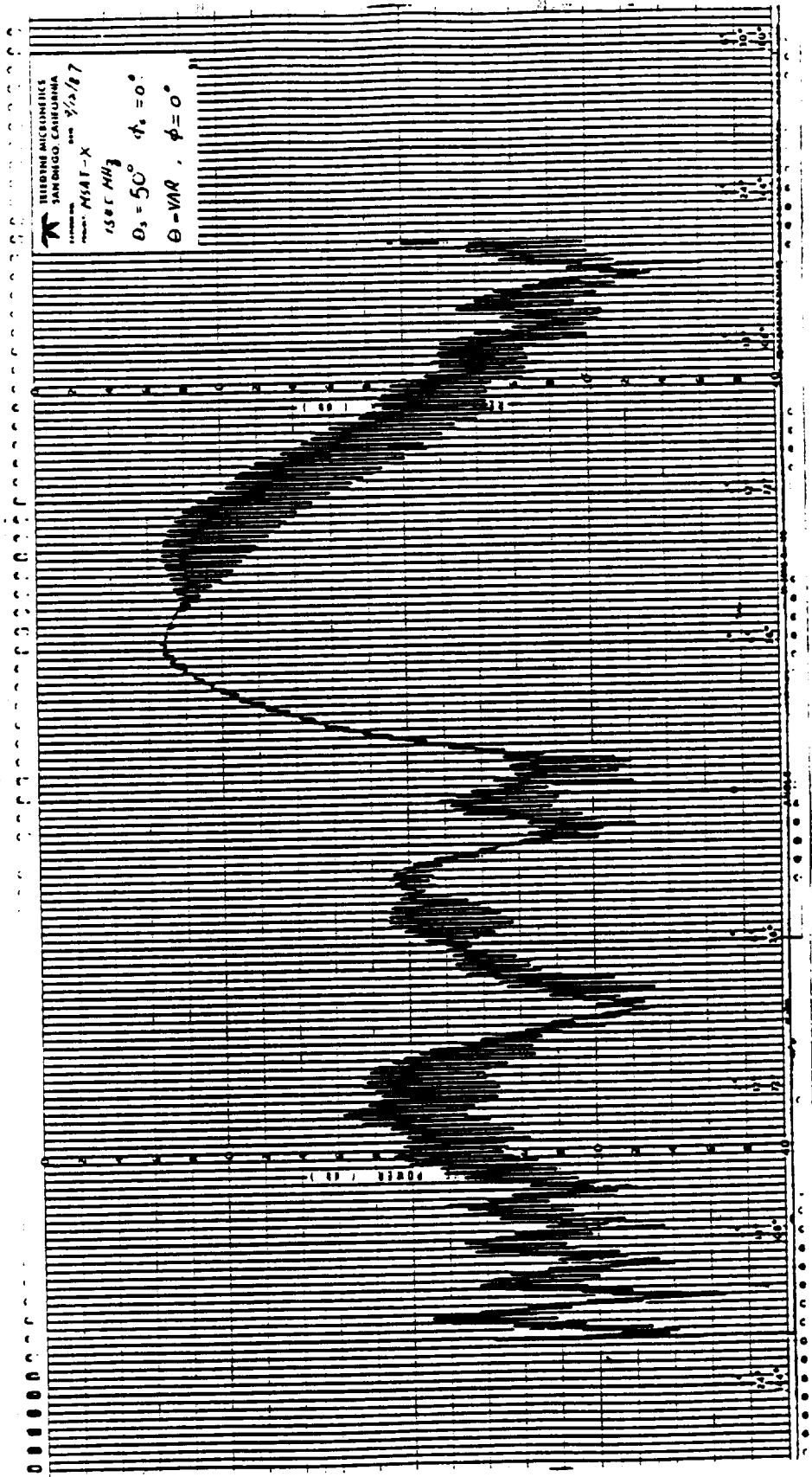


Figure A-3. Measured Array Pattern at 1545 MHz ( $\theta_s = 50^\circ$ ,  $\phi_s = 0^\circ$ ,  $\theta = \text{VAR}$ ,  $\phi = 0^\circ$ )

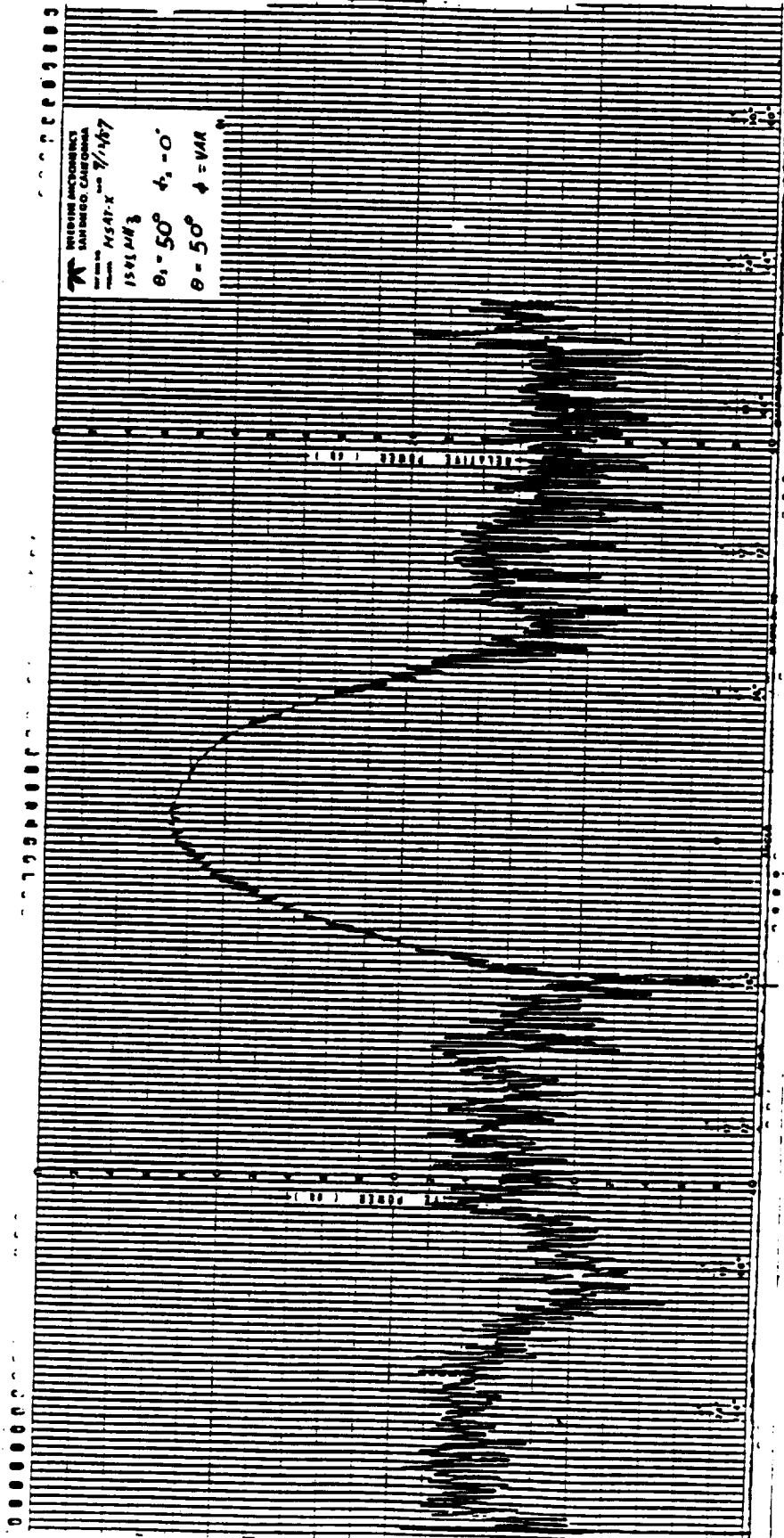


Figure A-4. Measured Array Pattern at 1545 MHz ( $\theta_s = 50^\circ$ ,  $\phi_s = 0^\circ$ ;  $\theta = 50^\circ$ ;  $\phi = \text{VAR}$ )

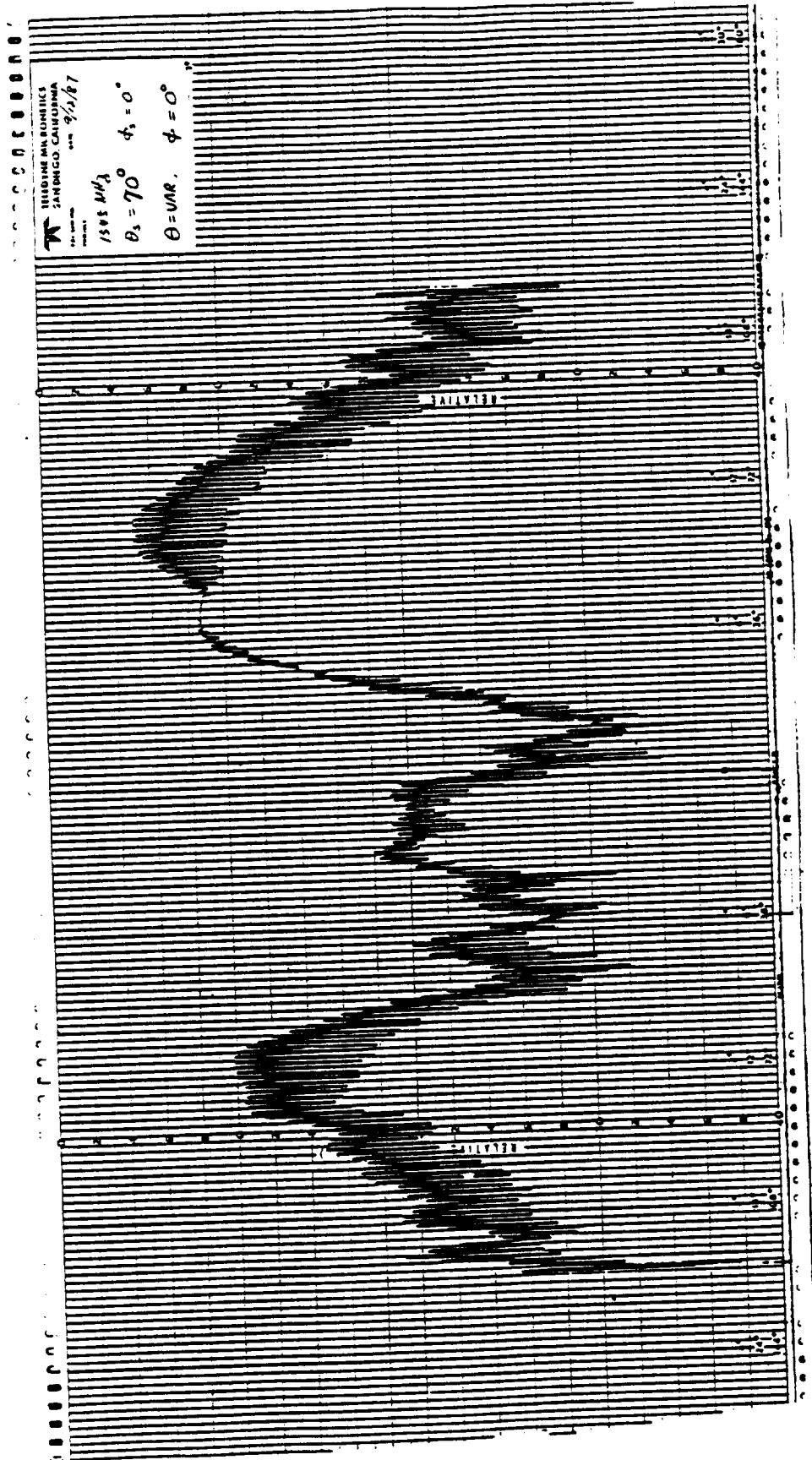


Figure A-5. Measured Array Pattern at 1545 MHz ( $\theta_s = 70^\circ$ ,  $\phi_s = 0^\circ$ ,  $\theta = \text{VAR.}$ ,  $\phi = 0^\circ$ )

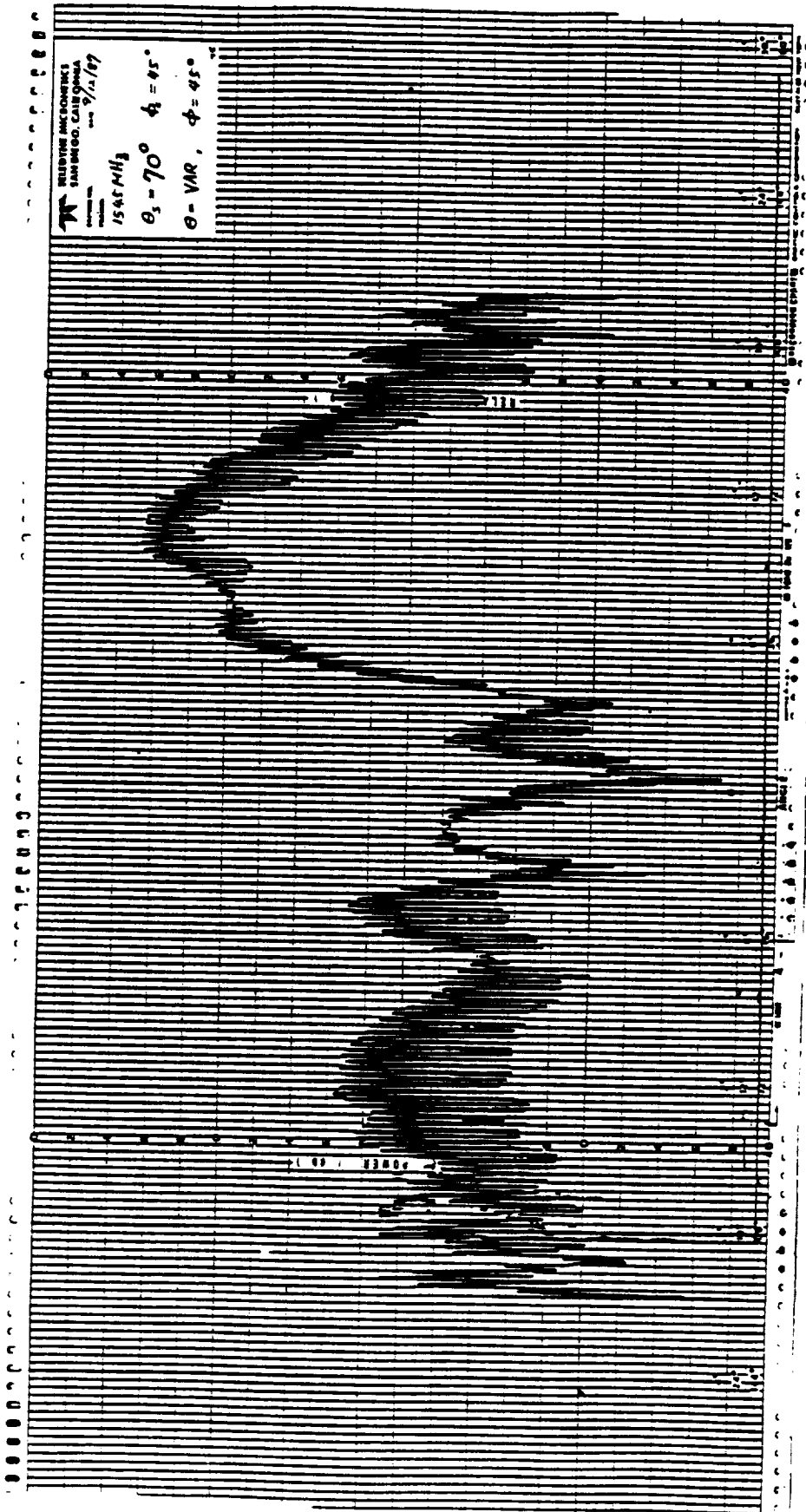


Figure A-6. Measured Array Pattern at 1545 MHz ( $\theta_s = 70^\circ$ ,  $\phi_s = 45^\circ$ ,  $\theta = \text{VAR}$ ,  $\phi = 45^\circ$ )



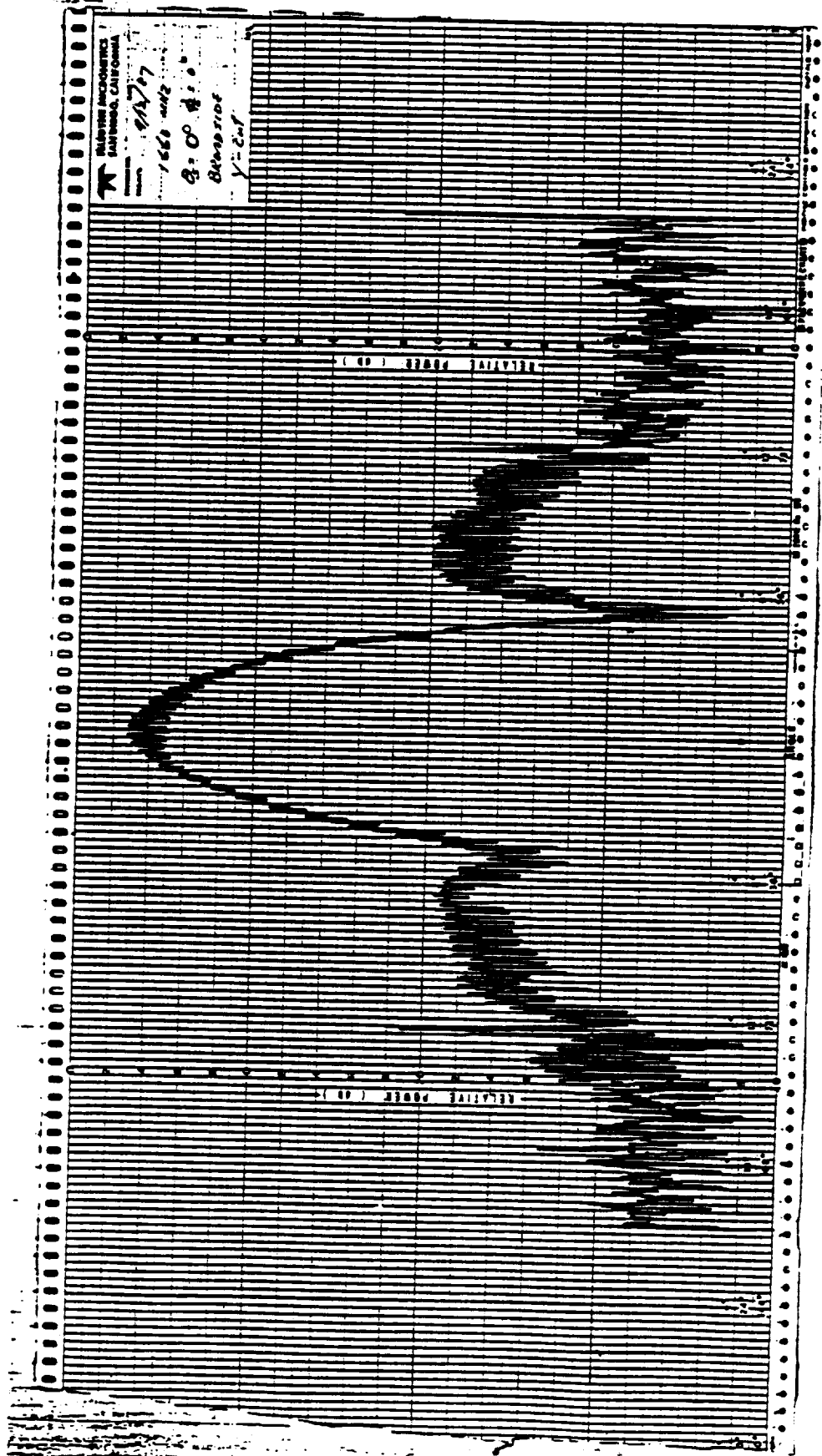


Figure A-8. Measured Broadside Array Pattern at 1660 MHz ( y-Axis Cut,  $\theta_s = 0^\circ$ ,  $\phi_s = 0^\circ$  )

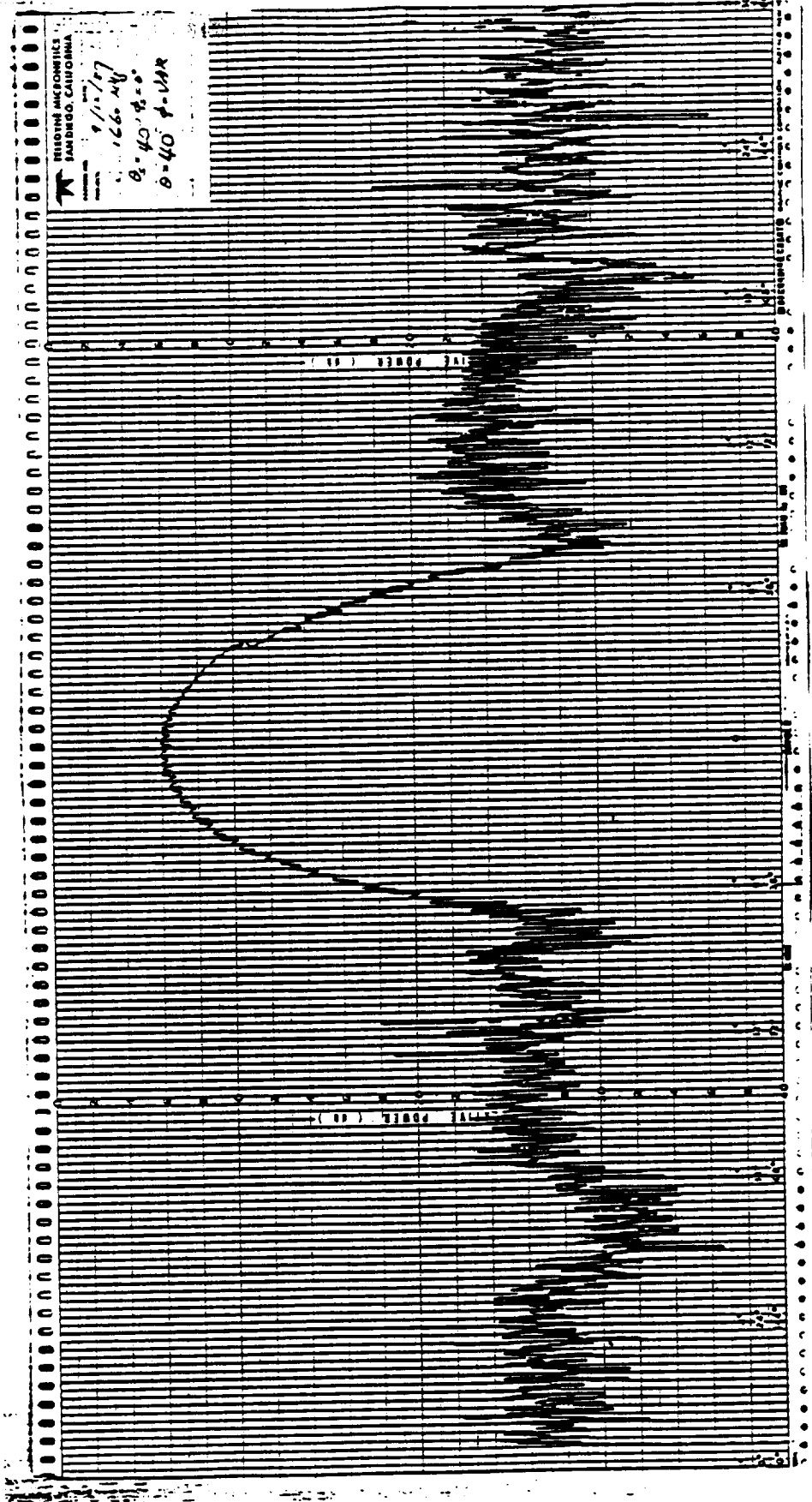


Figure A-9. Measured Array Pattern at 1660 MHz ( $\theta_s = 40^\circ, \phi_s = 0^\circ, \theta = 40^\circ, \phi = \text{VAR}$ )

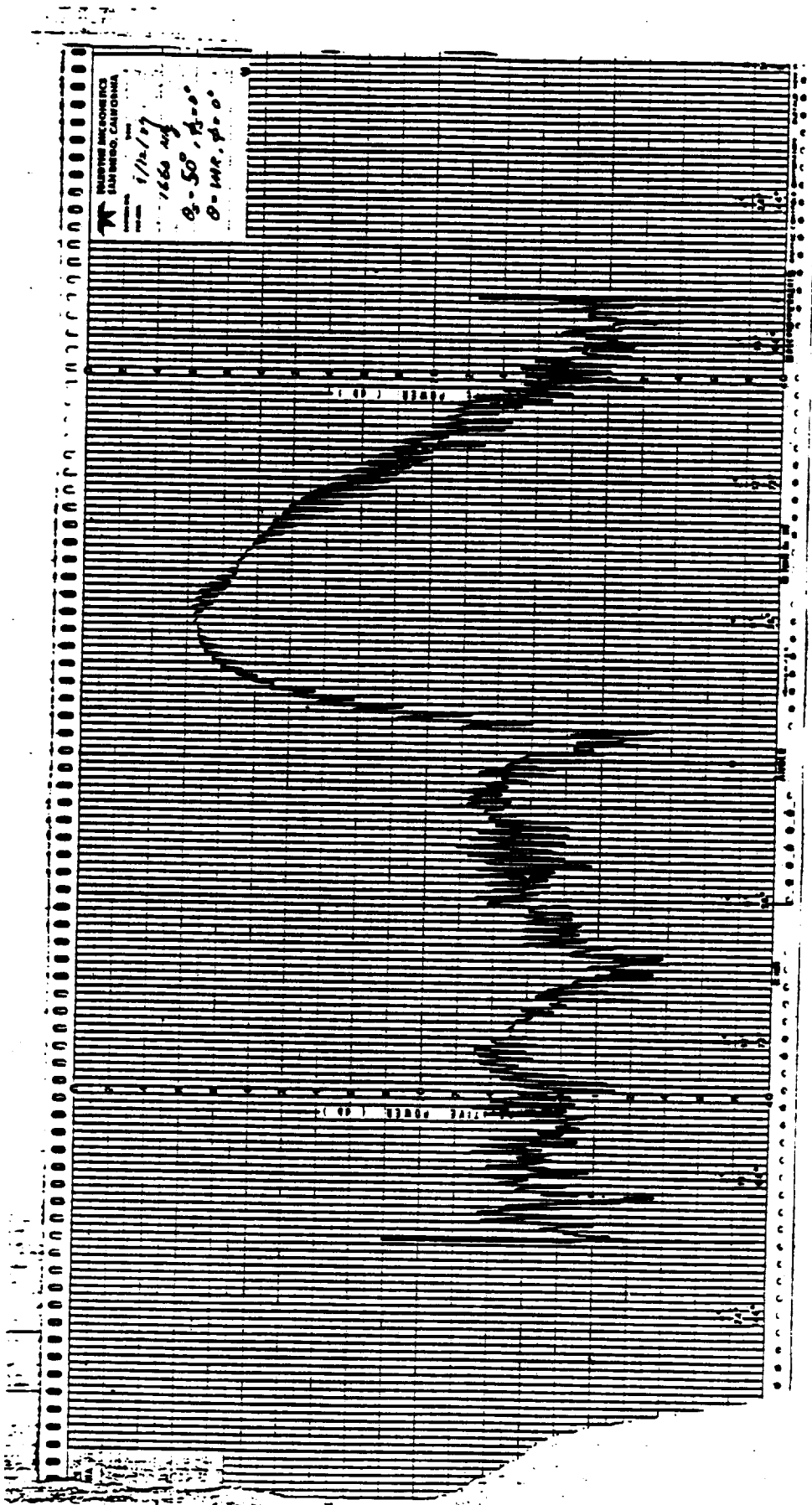


Figure A-10. Measured Array Pattern at 1660 MHz ( $\theta_s = 50^\circ$ ,  $\phi_s = 0^\circ$ ,  $\theta = \text{VAR}$ ,  $\phi = 0^\circ$ )

ORIGINAL PAGE IS  
OF POOR QUALITY

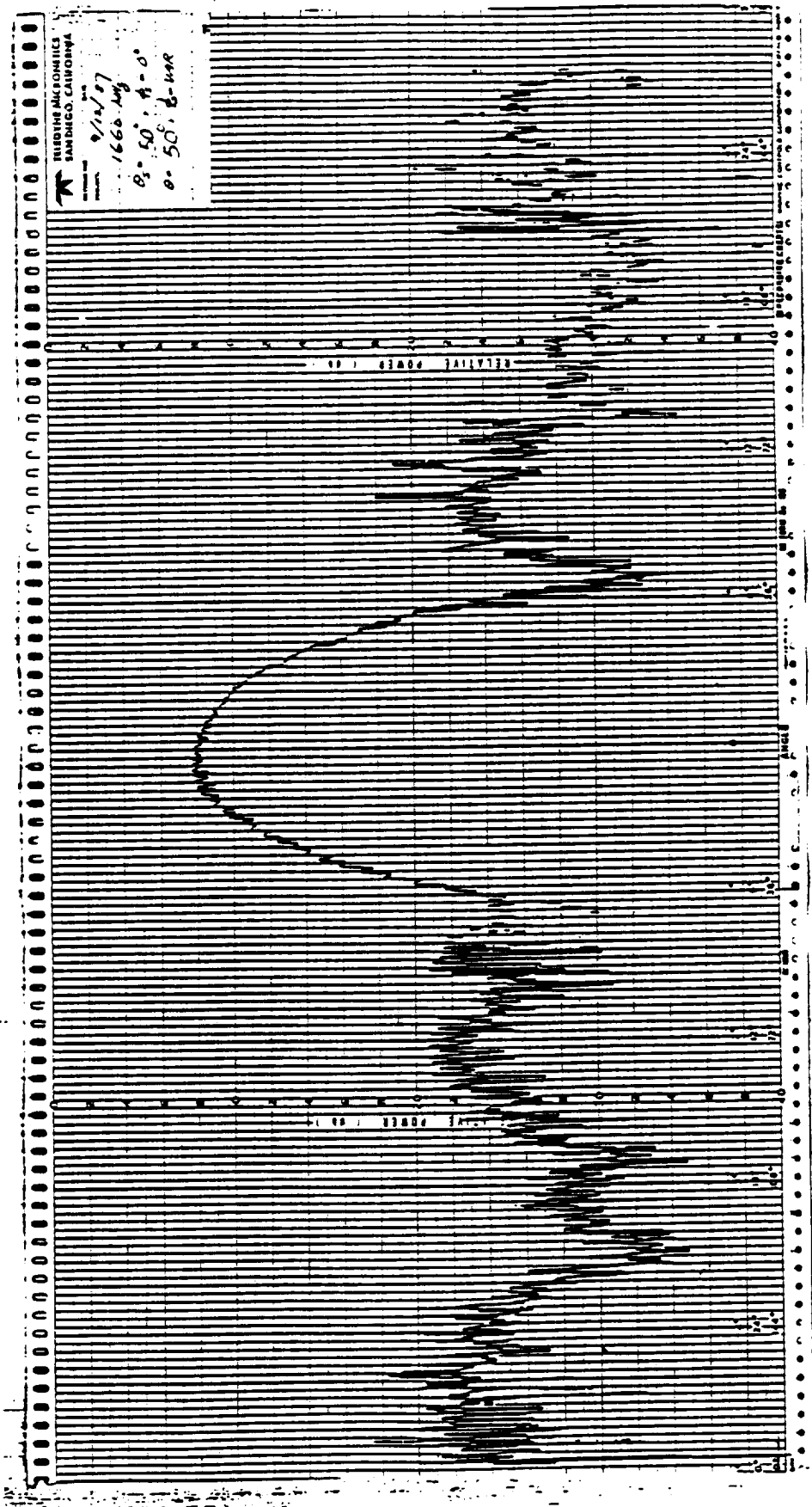
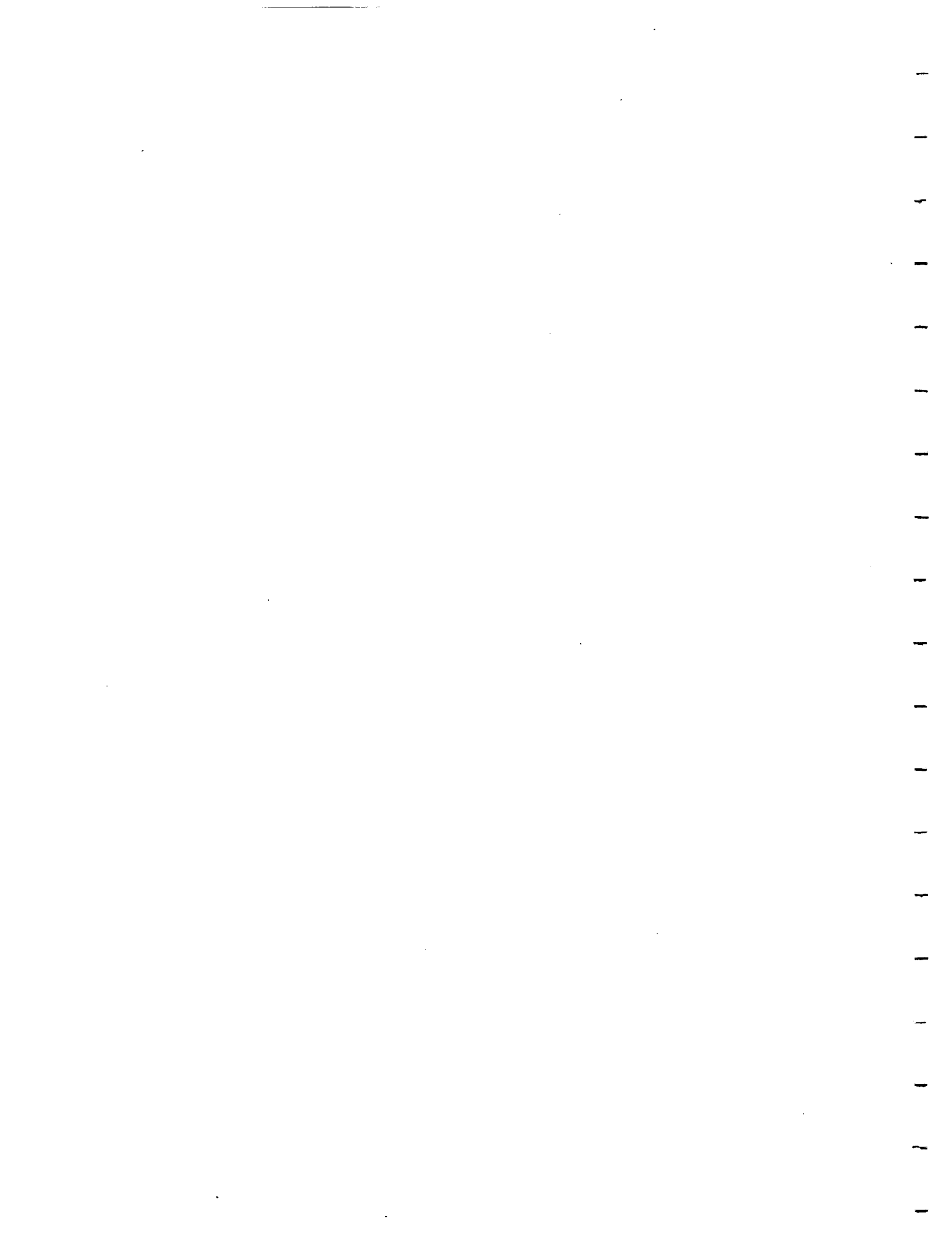


Figure A-11. Measured Array Pattern at 1660 MHz ( $\theta_s = 50^\circ$ ,  $\phi_s = 0^\circ$ ,  $\theta = 50^\circ$ ,  $\phi = \text{VAR}$ )



**APPENDIX B**

**TABLES OF BEAMFORMER CALCULATIONS**



## Table B-1. Beamformer Calculations

BEAMFORMER CALCULATIONS

10/16/87

MSAT, BFM2, TRIM3, COVERED, ALL PHASESHIFTERS SET AT 0°

NUMBER OF OUTPUT PORTS = 19  
 LOW FREQUENCY IN MHZ = 1545  
 MID FREQUENCY IN MHZ = 1600  
 HIGH FREQUENCY IN MHZ = 1660

BEAMFORMER ANALYSIS

PORT DES. DES. F1=1545 MHZ F2=1600 MHZ F3=1660 MHZ  
 NO. -DB ANG. MS12 AS12 MS12 AS12 MS12 AS12  
 Z -DB DEG. -DB DEG. -DB DEG.

1	11.6	+0	13.6	-98	13.3	-158	13.3	-226
2	13.8	+0	16.0	-94	15.8	-154	15.8	-223
3	14.6	+0	17.0	-92	16.9	-152	16.9	-219
4	11.6	+0	13.5	-96	13.2	-156	13.3	-226
5	14.6	+0	17.6	-96	17.3	-157	17.5	-226
6	13.8	+0	16.1	-93	15.8	-153	15.9	-222
7	11.6	+0	13.4	-93	13.5	-152	13.2	-217
8	14.6	+0	16.6	-90	16.6	-151	16.5	-216
9	13.8	+0	16.0	-89	16.0	-150	15.8	-216
10	8.6	+0	10.1	-91	9.7	-145	9.4	-212
11	11.6	+0	13.1	-98	13.3	-159	13.3	-225
12	13.8	+0	16.2	-87	16.2	-148	16.1	-214
13	14.6	+0	16.6	-91	16.6	-151	16.5	-218
14	11.6	+0	13.2	-95	13.5	-154	13.6	-218
15	14.6	+0	16.4	-98	16.7	-158	16.9	-223
16	13.8	+0	15.8	-95	16.1	-154	16.2	-220
17	11.6	+0	13.5	-92	13.5	-151	13.5	-217
18	14.6	+0	16.5	-95	16.5	-154	16.2	-221
19	13.8	+0	15.7	-90	15.7	-149	15.6	-216

LOSS DB =	-1.86	-1.86	-1.72
-3DBLOSS MEAN =	13.4	13.4	13.4
-3DB STD. DEV. =	0.18	0.12	0.14
-5.2DBLOSS MEAN =	16.0	15.9	15.9
-5.2DB STD. DEV. =	0.17	0.18	0.20
-6DBLOSS MEAN =	16.8	16.8	16.8
-6DB STD. DEV. =	0.41	0.27	0.42
INPUT VSWR =	1.55	1.42	1.17

BEAMFORMER ANGLE ANALYSIS

PORT DES. DES. F1=1545 MHZ F2=1600 MHZ F3=1660 MHZ  
 NO. ANG. MANG. DELTA MANG. DELTA MANG. DELTA  
 Z DEG. F1DA DF1DA F2DA DF2DA F3DA DF3DA

1	+0	-7	-7	-13	-13	-14	-14
2	+0	-3	-3	-9	-9	-11	-11
3	+0	-1	-1	-7	-7	-7	-7
4	+0	-5	-5	-11	-11	-14	-14
5	+0	-5	-5	-12	-12	-14	-14
6	+0	-2	-2	-8	-8	-10	-10
7	+0	-2	-2	-7	-7	-5	-5
8	+0	+1	+1	-6	-6	-4	-4
9	+0	+2	+2	-5	-5	-4	-4
10	+0	+0	+0	+0	+0	+0	+0
11	+0	-7	-7	-14	-14	-13	-13
12	+0	+4	+4	-3	-3	-2	-2
13	+0	+0	+0	-6	-6	-6	-6
14	+0	-4	-4	-9	-9	-6	-6
15	+0	-7	-7	-13	-13	-11	-11
16	+0	-4	-4	-9	-9	-8	-8
17	+0	-1	-1	-6	-6	-5	-5
18	+0	-4	-4	-9	-9	-9	-9
19	+0	+1	+1	-4	-4	-4	-4
MEAN DELTA ANG. =	-2.44			-8.39		-8.17	
STD. DEV. FOR DEL. =	+3.20			+3.70		+4.30	

Table B-1. Beamformer Calculations (Continued)

BEAMFORMER CALCULATIONS									
10/16/87									
MSAT, BFM2, TRIM3, COVERED, ALL PHASESHIFTERS SET AT -45°									
NUMBER OF OUTPUT PORTS = 19									
LOW FREQUENCY IN MHZ = 1545									
MID FREQUENCY IN MHZ = 1600									
HIGH FREQUENCY IN MHZ = 1660									
BEAMFORMER ANALYSIS									
PORT NO.	DES.	DES.	F1=1545 MHZ		F2=1600 MHZ		F3=1660 MHZ		Z
	-DB	ANG.	MS12	AS12	MS12	AS12	MS12	AS12	
			-DB	DEG.	-DB	DEG.	-DB	DEG.	
1	11.6	-45	14.1	-140	13.6	-201	13.6	-270	
2	13.8	-45	16.6	-138	16.2	-199	16.4	-269	
3	14.6	-45	17.5	-136	17.2	-196	17.2	-265	
4	11.6	-45	13.9	-138	13.3	-200	13.6	-271	
5	14.6	-45	18.2	-140	17.7	-202	18.1	-272	
6	13.8	-45	16.6	-134	15.9	-197	16.2	-267	
7	11.6	-45	13.9	-135	13.2	-199	13.9	-267	
8	14.6	-45	17.2	-132	16.5	-197	17.3	-265	
9	13.8	-45	16.4	-129	15.7	-194	16.4	-265	
10	8.6	+0	10.3	-93	10.0	-144	9.1	-210	
11	11.6	-45	13.9	-140	13.2	-203	14.0	-272	
12	13.8	-45	16.4	-127	15.7	-192	16.6	-262	
13	14.6	-45	17.1	-130	16.3	-194	17.0	-264	
14	11.6	-45	13.7	-137	13.6	-198	13.9	-264	
15	14.6	-45	17.0	-140	16.9	-202	17.4	-268	
16	13.8	-45	16.3	-137	16.2	-199	16.8	-266	
17	11.6	-45	14.1	-137	13.8	-195	13.8	-263	
18	14.6	-45	17.1	-137	16.7	-197	16.7	-265	
19	13.8	-45	16.2	-132	15.9	-192	15.9	-262	
-----									
LOSS DB =			-2.34		-2.34		-2.05		
-3DBLOSS MEAN =			13.9		13.5		13.8		
-3DB STD. DEV. =			0.14		0.23		0.15		
-5.2DBLOSS MEAN =			16.4		15.9		16.4		
-5.2DB STD. DEV. =			0.15		0.21		0.29		
-6DBLOSS MEAN =			17.4		16.9		17.3		
-6DB STD. DEV. =			0.41		0.46		0.43		
INPUT VSWR =			1.99		1.26		1.54		
-----									
BEAMFORMER ANGLE ANALYSIS									
PORT NO.	DES.	F1=1545 MHZ	F2=1600 MHZ	F3=1660 MHZ	Z	MANG. DELTA		MANG. DELTA	
	ANG.	MANG.	DELTA	MANG.	DELTA	MANG.	DELTA	MANG.	DELTA
	DEG.	F1DA	DF1DA	F2DA	DF2DA	F3DA	DF3DA	F3DA	DF3DA
-----									
1	-45	-47	-2	-5	-12	-60	-15		
2	-45	-45	+0	-55	-10	-59	-14		
3	-45	-43	+2	-52	-7	-55	-10		
4	-45	-45	+0	-56	-11	-61	-16		
5	-45	-47	-2	-58	-13	-62	-17		
6	-45	-41	+4	-53	-8	-57	-12		
7	-45	-42	+3	-55	-10	-57	-12		
8	-45	-39	+6	-53	-8	-55	-10		
9	-45	-36	+9	-50	-5	-55	-10		
10	+0	+0	+0	+0	+0	+0	+0		
11	-45	-47	-2	-59	-14	-62	-17		
12	-45	-34	+11	-48	-3	-52	-7		
13	-45	-37	+8	-50	-5	-54	-9		
14	-45	-44	+1	-54	-9	-54	-9		
15	-45	-47	-2	-58	-13	-58	-13		
16	-45	-44	+1	-55	-10	-56	-11		
17	-45	-44	+1	-51	-6	-53	-8		
18	-45	-44	+1	-53	-8	-55	-10		
19	-45	-39	+6	-48	-3	-52	-7		
-----									
MEAN DELTA ANG. =			+2.50		-8.61		-11.50		
STD. DEV. FOR DEL. =			+3.95		+3.83		+4.14		

Table B-1. Beamformer Calculations (Continued)

BEAMFORMER CALCULATIONS 10/16/87  
MSAT, BFM2, TRIM3, COVERED, ALL PHASESHIFTERS SET TO -90°

NUMBER OF OUTPUT PORTS = 19  
 LOW FREQUENCY IN MHZ = 1545  
 MID FREQUENCY IN MHZ = 1600  
 HIGH FREQUENCY IN MHZ = 1660

BEAMFORMER ANALYSIS  
 F1=1545 MHZ F2=1600 MHZ F3=1660 MHZ  
 PORT DES. DES. MS12 AS12 MS12 AS12 MS12 AS12  
 NO. -DB ANG. -DB DEG. -DB DEG. -DB DEG.  
 Z

PORT NO.	DES. -DB	DES. ANG.	F1=1545 MS12 -DB	F1=1545 AS12 DEG.	F2=1600 MS12 -DB	F2=1600 AS12 DEG.	F3=1660 MS12 -DB	F3=1660 AS12 DEG.
1	11.6	-90	13.7	-187	13.4	-248	13.2	-318
2	13.8	-90	16.4	-183	16.2	-245	16.0	-316
3	14.6	-90	17.4	-179	17.0	-240	16.9	-312
4	11.6	-90	13.8	-185	13.3	-248	13.3	-321
5	14.6	-90	17.4	-184	17.0	-248	17.2	-319
6	13.8	-90	16.1	-180	15.8	-243	15.8	-315
7	11.6	-90	13.4	-177	13.1	-242	13.2	-310
8	14.6	-90	16.9	-177	16.7	-241	16.7	-309
9	13.8	-90	16.3	-177	16.0	-242	16.0	-311
10	8.6	+0	10.2	-92	9.8	-145	9.2	-211
11	11.6	-90	13.6	-182	13.1	-248	13.5	-318
12	13.8	-90	16.1	-172	15.7	-238	16.1	-309
13	14.6	-90	17.1	-176	16.5	-241	16.6	-311
14	11.6	-90	13.3	-182	13.3	-246	13.5	-314
15	14.6	-90	16.6	-185	16.6	-249	17.0	-318
16	13.8	-90	16.0	-182	16.1	-246	16.4	-314
17	11.6	-90	13.8	-180	13.4	-242	13.4	-312
18	14.6	-90	16.9	-180	16.6	-243	16.6	-314
19	13.8	-90	16.1	-170	15.6	-233	15.7	-305

LOSS DB =	-2.07	-2.07	-1.72
-3DBLOSS MEAN =	13.6	13.3	13.4
-3DB STD. DEV. =	0.19	0.12	0.13
-5.2DBLOSS MEAN =	16.2	15.9	16.0
-5.2DB STD. DEV. =	0.14	0.22	0.22
-6DBLOSS MEAN =	17.0	16.7	16.8
-6DB STD. DEV. =	0.29	0.20	0.22
INPUT VSWR =	1.87	1.30	1.24

BEAMFORMER ANGLE ANALYSIS  
 F1=1545 MHZ F2=1600 MHZ F3=1660 MHZ  
 PORT DES. MANG. DELTA MANG. DELTA MANG. DELTA  
 NO. ANG. DEG. F1DA DF1DA F2DA DF2DA F3DA DF3DA  
 Z

PORT NO.	DES. ANG. DEG.	F1=1545 MANG. DELTA	F1=1545 DF1DA	F2=1600 MANG. DELTA	F2=1600 DF2DA	F3=1660 MANG. DELTA	F3=1660 DF3DA
1	-90	-95	-5	-103	-13	-107	-17
2	-90	-91	-1	-100	-10	-105	-15
3	-90	-87	+3	-95	-5	-101	-11
4	-90	-93	-3	-103	-13	-110	-20
5	-90	-92	-2	-103	-13	-108	-18
6	-90	-88	+2	-98	-8	-104	-14
7	-90	-85	+5	-97	-7	-99	-9
8	-90	-85	+5	-96	-6	-98	-8
9	-90	-85	+5	-97	-7	-100	-10
10	+0	+0	+0	+0	+0	+0	+0
11	-90	-90	+0	-103	-13	-107	-17
12	-90	-80	+10	-93	-3	-98	-8
13	-90	-84	+6	-96	-6	-100	-10
14	-90	-90	+0	-101	-11	-103	-13
15	-90	-93	-3	-104	-14	-107	-17
16	-90	-90	+0	-101	-11	-103	-13
17	-90	-88	+2	-97	-7	-101	-11
18	-90	-88	+2	-98	-8	-103	-13
19	-90	-78	+12	-88	+2	-94	-4
MEAN DELTA ANG. =	+2.11			-8.50		-12.67	
STD. DEV. FOR DEL. =	+4.40			+4.54		+5.05	

Table B-1. Beamformer Calculations (Continued)

BEAMFORMER CALCULATIONS

10/16/87

MSAT, BFM2, TRIM3, COVERED, ALL PHASESHIFTERS SET AT -135°

NUMBER OF OUTPUT PORTS = 19  
 LOW FREQUENCY IN MHZ = 1545  
 MID FREQUENCY IN MHZ = 1600  
 HIGH FREQUENCY IN MHZ = 1660

BEAMFORMER ANALYSIS

PORT NO. Z	DES. -DB	DES. ANG.	F1=1545 MHZ		F2=1600 MHZ		F3=1660 MHZ	
			MS12 -DB	AS12 DEG.	MS12 -DB	AS12 DEG.	MS12 -DB	AS12 DEG.
1	11.6	-135	13.8	-232	14.0	-295	14.1	-366
2	13.8	-135	16.5	-227	16.5	-292	16.4	-364
3	14.6	-135	17.4	-223	17.3	-288	17.4	-362
4	11.6	-135	13.8	-230	13.8	-295	13.8	-369
5	14.6	-135	17.4	-228	17.2	-297	17.2	-368
6	13.8	-135	16.2	-225	16.2	-289	16.1	-363
7	11.6	-135	13.4	-225	14.0	-289	13.5	-364
8	14.6	-135	16.8	-225	17.4	-289	16.8	-363
9	13.8	-135	16.3	-223	16.9	-287	16.3	-364
10	8.6	+0	10.0	-90	9.5	-146	9.5	-213
11	11.6	-135	13.1	-230	13.7	-295	13.4	-365
12	13.8	-135	15.7	-217	16.1	-282	15.8	-352
13	14.6	-135	16.9	-223	17.2	-287	16.7	-357
14	11.6	-135	13.4	-228	13.9	-292	13.9	-360
15	14.6	-135	16.6	-230	17.0	-295	17.1	-366
16	13.8	-135	16.0	-227	16.5	-291	16.7	-362
17	11.6	-135	13.5	-227	13.7	-292	14.0	-364
18	14.6	-135	16.8	-226	17.0	-290	17.1	-363
19	13.8	-135	16.2	-216	16.3	-280	16.2	-352

LOSS DB =	-1.97	-1.97	-2.04
-3DBLOSS MEAN =	13.5	13.9	13.8
-3DB STD. DEV. =	0.24	0.13	0.25
-5.2DBLOSS MEAN =	16.2	16.4	16.3
-5.2DB STD. DEV. =	0.25	0.26	0.28
-6DBLOSS MEAN =	17.0	17.2	17.0
-6DB STD. DEV. =	0.31	0.15	0.24
INPUT VSWR =	1.49	1.64	1.26

BEAMFORMER ANGLE ANALYSIS

PORT NO. Z	DES. ANG. DEG.	F1=1545 MHZ		F2=1600 MHZ		F3=1660 MHZ	
		MANG. DELTA F1DA	DF1DA	MANG. DELTA F2DA	DF2DA	MANG. DELTA F3DA	DF3DA
1	-135	-142	-7	-149	-14	-153	-18
2	-135	-137	-2	-146	-11	-151	-16
3	-135	-133	+2	-142	-7	-149	-14
4	-135	-140	-5	-149	-14	-156	-21
5	-135	-138	-3	-151	-16	-155	-20
6	-135	-135	+0	-143	-8	-150	-15
7	-135	-135	+0	-143	-8	-151	-16
8	-135	-135	+0	-143	-8	-150	-15
9	-135	-133	+2	-141	-6	-151	-16
10	+0	+0	+0	+0	+0	+0	+0
11	-135	-140	-5	-149	-14	-152	-17
12	-135	-127	+8	-136	-1	-139	-4
13	-135	-133	+2	-141	-6	-144	-9
14	-135	-138	-3	-146	-11	-147	-12
15	-135	-140	-5	-149	-14	-153	-18
16	-135	-137	-2	-145	-10	-149	-14
17	-135	-137	-2	-146	-11	-151	-16
18	-135	-136	-1	-144	-9	-150	-15
19	-135	-126	+9	-134	+1	-139	-4
MEAN DELTA ANG. =	-0.67			-9.28		-14.44	
STL. DEV. FOR DEL. =	+4.11			+4.92		+5.67	

## Table B-1. Beamformer Calculations (Continued)

BEAMFORMER CALCULATIONS

10/16/87

MSAT, SPM2, TRIM3, COVERED, ALL PHASESHIFTERS SET AT -180°

NUMBER OF OUTPUT PORTS = 19  
 LOW FREQUENCY IN MHZ = 1545  
 MID FREQUENCY IN MHZ = 1600  
 HIGH FREQUENCY IN MHZ = 1660

BEAMFORMER ANALYSIS

PORT DES. DES. F1=1545 MHZ F2=1600 MHZ F3=1660 MHZ  
 NO. -DB ANG. MS12 AS12 MS12 AS12 MS12 AS12  
 Z -DB DEG. -DB DEG. -DB DEG.

PORT NO.	DES. -DB	DES. ANG.	F1 MS12 -DB	F1 AS12 DEG.	F2 MS12 -DB	F2 AS12 DEG.	F3 MS12 -DB	F3 AS12 DEG.
1	11.6	-180	13.8	-269	13.6	-334	13.5	-409
2	13.8	-180	16.4	-264	16.1	-330	16.0	-406
3	14.6	-180	17.1	-262	17.0	-327	17.0	-401
4	11.6	-180	13.4	-266	13.3	-333	13.4	-408
5	14.6	-180	17.5	-266	17.2	-333	17.2	-409
6	13.8	-180	16.3	-264	16.2	-330	16.2	-404
7	11.6	-180	13.3	-263	13.6	-328	13.4	-401
8	14.6	-180	16.7	-262	16.9	-328	16.6	-400
9	13.8	-180	16.2	-259	16.2	-325	15.9	-399
10	8.6	+0	10.0	-90	9.6	-146	9.4	-211
11	11.6	-180	13.5	-273	13.9	-330	13.8	-410
12	13.8	-180	16.2	-253	15.9	-320	15.7	-397
13	14.6	-180	16.8	-263	16.5	-329	16.4	-404
14	11.6	-180	13.7	-266	14.1	-331	13.9	-401
15	14.6	-180	16.6	-270	16.9	-337	17.0	-408
16	13.8	-180	15.8	-266	16.3	-332	16.5	-404
17	11.6	-180	13.4	-262	13.4	-328	13.5	-402
18	14.6	-180	16.8	-264	16.7	-329	16.7	-404
19	13.8	-180	16.1	-260	15.8	-326	15.7	-401

LOSS DB =	-1.97	-1.97	-1.84
-3DBLOSS MEAN =	13.5	13.7	13.6
-3DB STD. DEV. =	0.18	0.28	0.20
-5.2DBLOSS MEAN =	16.2	16.1	16.0
-5.2DB STD. DEV. =	0.19	0.18	0.28
-6DBLOSS MEAN =	16.9	16.9	16.8
-6DB STD. DEV. =	0.30	0.22	0.27
INPUT VSWR =	1.53	1.48	1.22

BEAMFORMER ANGLE ANALYSIS

PORT DES. F1=1545 MHZ F2=1600 MHZ F3=1660 MHZ  
 NO. ANG. MANG. DELTA MANG. DELTA MANG. DELTA  
 Z DEG. F1DA DF1DA F2DA DF2DA F3DA DF3DA

PORT NO.	DES. ANG.	F1 MANG. DELTA	F1 DF1DA	F2 MANG. DELTA	F2 DF2DA	F3 MANG. DELTA	F3 DF3DA
1	-180	-179	+1	-188	-8	-198	-18
2	-180	-174	+6	-184	-4	-195	-15
3	-180	-172	+8	-181	-1	-190	-10
4	-180	-176	+4	-187	-7	-197	-17
5	-180	-176	+4	-187	-7	-198	-18
6	-180	-174	+6	-184	-4	-193	-13
7	-180	-173	+7	-182	-2	-190	-10
8	-180	-172	+8	-182	-2	-189	-9
9	-180	-169	+11	-179	+1	-188	-8
10	+0	+0	+0	+0	+0	+0	+0
11	-180	-183	-3	-193	-13	-199	-19
12	-180	-163	+17	-174	+6	-186	-6
13	-180	-173	+7	-183	-3	-193	-13
14	-180	-176	+4	-185	-5	-190	-10
15	-180	-180	+0	-191	-11	-197	-17
16	-180	-176	+4	-186	-6	-193	-13
17	-180	-172	+8	-182	-2	-191	-11
18	-180	-174	+6	-183	-3	-193	-13
19	-180	-170	+10	-180	+0	-190	-10
MEAN DELTA ANG. =	+6.00			-3.94		-12.78	
STD. DEV. FOR DEL. =	+4.53			+4.40		+4.80	

Table B-1. Beamformer Calculations (Continued)

BEAMFORMER CALCULATIONS

10/16/87

MSAT, BFM2, TRIM3, COVERED, ALL PHASESHIFTERS SET AT -225°

NUMBER OF OUTPUT PORTS = 19  
 LOW FREQUENCY IN MHZ = 1545  
 MID FREQUENCY IN MHZ = 1600  
 HIGH FREQUENCY IN MHZ = 1660

BEAMFORMER ANALYSIS

PORT DES. DES. F1=1545 MHZ F2=1600 MHZ F3=1660 MHZ  
 NO. -DB ANG. MS12 AS12 MS12 AS12 MS12 AS12  
 Z -DB DEG. -DB DEG. -DB DEG.

1	11.6	-225	14.4	-311	13.9	-377	13.7	-453
2	13.8	-225	16.7	-309	16.4	-375	16.6	-451
3	14.6	-225	17.4	-305	17.3	-370	17.2	-445
4	11.6	-225	13.8	-309	13.4	-376	13.6	-452
5	14.6	-225	17.8	-309	17.5	-377	17.6	-452
6	13.8	-225	16.6	-305	16.3	-373	16.5	-449
7	11.6	-225	14.0	-305	13.5	-373	14.1	-449
8	14.6	-225	17.3	-304	16.6	-373	17.3	-449
9	13.8	-225	16.6	-299	15.8	-368	16.3	-446
10	8.6	+0	10.2	-92	10.0	-144	9.1	-209
11	11.6	-225	14.4	-313	13.5	-379	14.3	-456
12	13.8	-225	16.1	-293	15.1	-365	16.4	-444
13	14.6	-225	17.2	-301	16.2	-372	17.0	-450
14	11.6	-225	15.1	-306	14.9	-372	15.0	-444
15	14.6	-225	16.9	-312	17.0	-380	17.4	-451
16	13.8	-225	16.0	-308	16.4	-375	17.2	-450
17	11.6	-225	14.1	-305	13.6	-372	13.9	-447
18	14.6	-225	17.3	-305	16.8	-372	17.0	-447
19	13.8	-225	16.4	-301	15.7	-368	15.9	-445

LOSS DB =	-2.45	-2.45	-2.17
-3DBLOSS MEAN =	14.3	13.8	14.1
-3DB STD. DEV. =	0.42	0.52	0.47
-5.2DBLOSS MEAN =	16.4	16.0	16.5
-5.2DB STD. DEV. =	0.26	0.47	0.39
-6DBLOSS MEAN =	17.3	16.9	17.3
-6DB STD. DEV. =	0.27	0.43	0.21
INPUT VSWR =	2.02	1.34	1.57

BEAMFORMER ANGLE ANALYSIS

PORT DES. F1=1545 MHZ F2=1600 MHZ F3=1660 MHZ  
 NO. ANG. MANG. DELTA MANG. DELTA MANG. DELTA  
 Z DEG. F1DA DF1DA F2DA DF2DA F3DA DF3DA

1	-225	-219	+6	-233	-8	-244	-19
2	-225	-217	+8	-231	-6	-242	-17
3	-225	-213	+12	-226	-1	-236	-11
4	-225	-217	+8	-232	-7	-243	-18
5	-225	-217	+8	-233	-8	-243	-18
6	-225	-213	+12	-229	-4	-240	-15
7	-225	-213	+12	-229	-4	-240	-15
8	-225	-212	+13	-229	-4	-240	-15
9	-225	-207	+18	-224	+1	-237	-12
10	+0	+0	+0	+0	+0	+0	+0
11	-225	-221	+4	-235	-10	-247	-22
12	-225	-201	+24	-221	+4	-235	-10
13	-225	-209	+16	-228	-3	-241	-16
14	-225	-214	+11	-228	-3	-235	-10
15	-225	-220	+5	-236	-11	-242	-17
16	-225	-216	+9	-231	-6	-241	-16
17	-225	-213	+12	-228	-3	-238	-13
18	-225	-213	+12	-228	-3	-238	-13
19	-225	-209	+16	-224	+1	-236	-11

MEAN DELTA ANG. = +11.44      -4.17      -14.89  
 STD. DEV. FOR DEL. = +5.50      +3.93      +4.79

Table B-1. Beamformer Calculations (Continued)

BEAMFORMER CALCULATIONS 10/16/87  
 NSAW, BFMS, TRIMS COVERED, ALL PHASESHIFTERS SET TO -270

NUMBER OF OUTPUT PORTS = 19  
 LOW FREQUENCY IN MHZ = 1545  
 MID FREQUENCY IN MHZ = 1600  
 HIGH FREQUENCY IN MHZ = 1660

BEAMFORMER ANALYSIS

PORT NO.	DES.		F1=1545 MHZ		F2=1600 MHZ		F3=1660 MHZ	
	-DB	ANG.	MS12	AS12	MS12	AS12	MS12	AS12
			-DB	DEG.	-DB	DEG.	-DB	DEG.
1	11.8	-270	13.9	-357	13.6	-425	13.3	-503
2	13.8	-270	16.8	-353	16.2	-422	16.2	-500
3	14.8	-270	17.4	-349	17.0	-417	16.8	-500
4	11.8	-270	13.7	-355	13.4	-425	13.4	-504
5	14.8	-270	16.9	-354	16.7	-423	16.8	-501
6	13.8	-270	16.0	-350	15.9	-420	16.1	-498
7	11.8	-270	13.8	-348	13.3	-417	13.3	-494
8	14.8	-270	16.9	-348	16.7	-418	16.8	-494
9	13.8	-270	16.3	-347	15.9	-417	16.0	-495
10	8.8	+0	10.1	-92	9.7	-146	9.3	-212
11	11.8	-270	13.8	-356	13.6	-426	13.9	-502
12	13.8	-270	16.0	-358	15.5	-410	15.9	-489
13	14.8	-270	17.0	-347	16.2	-419	16.4	-498
14	11.8	-270	13.4	-352	13.5	-421	13.6	-496
15	14.8	-270	16.7	-357	16.7	-426	17.1	-501
16	13.8	-270	16.0	-353	16.3	-423	16.6	-497
17	11.8	-270	13.8	-352	13.6	-420	13.5	-497
18	14.8	-270	17.0	-352	16.7	-420	16.7	-497
19	13.8	-270	16.1	-341	15.6	-409	15.5	-487

AVERAGE LOSS DB =	-2.07	-2.07	-1.79
3-DBS LOSS MEAN =	13.7	13.5	13.5
3-DBS STD. DEV. =	0.18	0.12	0.21
5-DBS LOSS MEAN =	16.2	15.9	16.1
5-DBS STD. DEV. =	0.19	0.29	0.33
7-DBS LOSS MEAN =	17.0	16.7	16.8
7-DBS STD. DEV. =	0.21	0.34	0.21
10-DBS LOSS MEAN =	1.84	1.35	1.27

BEAMFORMER ANGLE ANALYSIS

PORT NO.	DES.		F1=1545 MHZ		F2=1600 MHZ		F3=1660 MHZ	
	ANG.	MANG.	DELTA	MANG.	DELTA	MANG.	DELTA	
	DEG.	DF1DA	DF1DA	DF2DA	DF2DA	DF3DA	DF3DA	
1	-270	-265	+5	-279	-9	-291	-21	
2	-270	-261	+9	-276	-6	-288	-18	
3	-270	-257	+13	-271	-1	-288	-16	
4	-270	-263	+7	-279	-9	-292	-22	
5	-270	-262	+8	-277	-7	-289	-19	
6	-270	-258	+12	-274	-4	-286	-16	
7	-270	-256	+14	-271	-1	-282	-12	
8	-270	-256	+14	-272	-2	-282	-12	
9	-270	-255	+15	-271	-1	-283	-13	
10	+0	+0	+0	+0	+0	+0	+0	
11	-270	-254	+6	-280	-10	-290	-20	
12	-270	-248	+24	-264	+6	-277	-7	
13	-270	-255	+15	-273	-3	-286	-16	
14	-270	-260	+10	-275	-5	-284	-14	
15	-270	-263	+5	-280	-10	-289	-19	
16	-270	-261	+9	-277	-7	-285	-15	
17	-270	-260	+10	-274	-4	-285	-15	
18	-270	-260	+10	-274	-4	-285	-15	
19	-270	-249	+21	-263	+7	-275	-5	

BEAM DELTA ANG. =	+11.50	-3.89	-15.39
BEAM DELTA ANG. =	+5.70	+4.73	+5.63

Table B-1. Beamformer Calculations (Continued)

CIN -> BEAMFORMER CALCULATIONS

10/16/87

MSAT, BFM2, TRIMS, COVERED, ALLSHIFTERS SET TO -315°

NUMBER OF OUTPUT PORTS = 19  
 LOW FREQUENCY IN MHZ = 1545  
 MID FREQUENCY IN MHZ = 1600  
 HIGH FREQUENCY IN MHZ = 1660

BEAMFORMER ANALYSIS

PORT NO.	DES. ANG. Z	F1=1545 MHZ		F2=1600 MHZ		F3=1660 MHZ	
		MS12 -DB	AS12 DEG.	MS12 -DB	AS12 DEG.	MS12 -DB	AS12 DEG.
1	11.6 -315	14.2	-401	14.2	-473	14.2	-550
2	13.8 -315	16.7	-396	16.7	-467	16.8	-548
3	14.6 -315	17.0	-394	17.4	-466	17.7	-542
4	11.6 -315	13.8	-400	13.9	-472	13.9	-553
5	14.6 -315	16.9	-397	17.0	-469	17.1	-550
6	13.8 -315	16.2	-395	16.5	-467	16.5	-546
7	11.6 -315	13.5	-396	14.1	-466	13.6	-541
8	14.6 -315	16.8	-396	17.4	-466	16.9	-542
9	13.8 -315	16.2	-392	16.7	-462	16.2	-541
10	2.6 +0	9.9	-90	9.5	-146	9.5	-213
11	11.6 -315	13.5	-403	14.1	-475	14.2	-551
12	13.8 -315	16.0	-383	15.9	-454	15.3	-535
13	14.6 -315	16.9	-397	17.3	-466	16.6	-542
14	11.6 -315	13.6	-399	14.3	-468	14.0	-544
15	14.6 -315	16.6	-402	17.1	-472	17.2	-549
16	13.8 -315	16.1	-400	16.8	-469	16.7	-546
17	11.6 -315	13.6	-398	13.8	-469	14.1	-547
18	14.6 -315	16.8	-396	17.0	-467	17.2	-546
19	13.8 -315	16.2	-390	16.2	-456	16.0	-535

LOSS DB =	-2.03	-2.03	-2.14
-3DB LOSS MEAN =	13.7	14.1	14.0
-3DB STD. DEV. =	0.24	0.17	0.21
-5.2DB LOSS MEAN =	16.2	16.5	16.3
-5.2DB STD. DEV. =	0.22	0.32	0.51
-6DB LOSS MEAN =	16.8	17.2	17.1
-6DB STD. DEV. =	0.12	0.17	0.33
INPUT VSWR =	1.41	1.67	1.28

BEAMFORMER ANGLE ANALYSIS

PORT NO.	DES. ANG. Z	F1=1545 MHZ		F2=1600 MHZ		F3=1660 MHZ	
		MANG. F1DA	DELTA DF1DA	MANG. F2DA	DELTA DF2DA	MANG. F3DA	DELTA DF3DA
1	-315	-311	+4	-327	-12	-337	-22
2	-315	-306	+9	-321	-6	-335	-20
3	-315	-304	+11	-320	-5	-329	-14
4	-315	-310	+5	-326	-11	-340	-25
5	-315	-307	+6	-323	-8	-337	-22
6	-315	-305	+10	-321	-6	-333	-18
7	-315	-306	+9	-320	-5	-328	-13
8	-315	-306	+9	-320	-5	-329	-14
9	-315	-302	+13	-316	-1	-328	-13
10	+0	+0	+0	+0	+0	+0	+0
11	-315	-313	+2	-329	-14	-336	-23
12	-315	-293	+22	-308	+7	-322	-7
13	-315	-307	+8	-320	-5	-329	-14
14	-315	-309	+6	-322	-7	-331	-16
15	-315	-312	+3	-326	-11	-336	-21
16	-315	-310	+5	-323	-8	-333	-18
17	-315	-306	+7	-323	-8	-334	-19
18	-315	-306	+9	-321	-6	-333	-18
19	-315	-300	+15	-310	+5	-322	-7

MEAN DELTA ANG. = +8.61  
 STD. DEV. FOR DEL. = +5.02

Table B-1. Beamformer Calculations (Continued)

BEAMFORMER CALCULATIONS

NO. OF SENS. TRNGS. COVERED, ACROSS ELEMENTS

NUMBER OF OUTPUT PORTS = 12  
 LOW FREQUENCY IN MHZ = 1345  
 MID FREQUENCY IN MHZ = 1500  
 HIGH FREQUENCY IN MHZ = 1680

BEAMFORMER ANALYSIS

PORT	DEG.	DBS.	F1=1345 MHZ		F2=1500 MHZ		F3=1680 MHZ	
			MS12	AS12	MS12	AS12	MS12	AS12
			-DB	DBS.	-DB	DBS.	-DB	DBS.
1	11.2	-312	13.9	-336	13.5	-478	13.1	-553
2	12.9	-318	13.5	-331	13.0	-471	12.8	-550
3	14.6	-315	13.3	-330	12.8	-470	12.6	-544
4	16.3	-312	13.0	-327	12.6	-475	12.5	-553
5	18.0	-315	12.7	-334	12.5	-473	12.3	-551
6	19.8	-318	12.4	-338	12.3	-469	12.1	-546
7	21.6	-320	12.2	-350	12.1	-331	12.1	-403
8	23.4	-325	12.0	-358	11.9	-329	11.9	-400
9	25.2	-330	11.8	-319	11.8	-288	11.7	-358
10	27.0	-340	11.6	-92	11.6	-145	9.1	-210
11	28.8	-345	11.5	-314	11.5	-375	11.3	-455
12	30.6	-351	11.4	-308	11.4	-368	11.2	-444
13	32.4	-355	11.3	-308	11.3	-373	11.1	-449
14	34.2	-358	11.2	-311	11.2	-371	11.0	-450
15	36.0	-360	11.1	-317	11.1	-387	10.9	-453
16	37.8	-365	11.0	-312	11.0	-378	10.8	-450
17	39.6	-370	10.9	-35	10.9	-145	10.7	-216
18	41.4	-375	10.8	-103	10.8	-152	10.6	-220
19	43.2	-380	10.7	-139	10.7	-190	10.5	-220
MEAN =			-2.11		-2.11		-2.01	
STANDARD DEVIATION =			13.7		13.6		13.9	
CORRELATION COEFF. =			0.23		0.28		0.30	
CORRELATION COEFF. (DB) =			16.4		16.3		16.6	
CORRELATION COEFF. (DB) =			4.20		4.28		4.30	
CORRELATION COEFF. (DB) =			16.9		17.0		17.1	
CORRELATION COEFF. (DB) =			0.37		0.34		0.34	
CORRELATION COEFF. (DB) =			1.80		1.89		1.89	

BEAMFORMER ANGLE ANALYSIS

PORT	DEG.	DBS.	F1=1345 MHZ		F2=1500 MHZ		F3=1680 MHZ	
			MANG.	DELTA	MANG.	DELTA	MANG.	DELTA
			F1DA	DF1DA	F2DA	DF2DA	F3DA	DF3DA
1	11.2	-304	+11	-331	-12	-343	-17	
2	12.9	-315	+16	-327	-12	-340	-22	
3	14.6	-318	+17	-325	-10	-334	-19	
4	16.3	-315	+10	-330	-15	-343	-28	
5	18.0	-312	+13	-327	-12	-341	-26	
6	19.8	-318	+15	-324	-9	-336	-21	
7	21.6	-320	+12	-326	-6	-333	-13	
8	23.4	-325	+13	-324	-4	-330	-10	
9	25.2	-330	+9	-343	-8	-340	-13	
10	27.0	-340	+0	+0	+0	+0	+0	
11	28.8	-345	+3	-323	-6	-343	-20	
12	30.6	-351	+15	-321	+4	-334	-9	
13	32.4	-355	+7	-317	-2	-329	-11	
14	34.2	-358	+7	-316	-1	-326	-11	
15	36.0	-360	+5	-343	-17	-343	-18	
16	37.8	-365	+5	-337	-2	-340	-15	
17	39.6	-370	-3	+0	+0	-6	-6	
18	41.4	-375	-11	-11	-7	-10	-10	
19	43.2	-380	-2	-42	+1	-10	-5	
MEAN =			+7.81		-2.34		-10.23	
STANDARD DEVIATION =			13.00		13.10		13.10	

Table B-1. Beamformer Calculations (Continued)

BEAMFORMER CALCULATIONS

10/16/87

MSAT, 8FM2, TRIM3, COVERED, AZ=45°, EL=20°

NUMBER OF OUTPUT PORTS = 19  
 LOW FREQUENCY IN MHZ = 1545  
 MID FREQUENCY IN MHZ = 1600  
 HIGH FREQUENCY IN MHZ = 1660

BEAMFORMER ANALYSIS  
 PORT DES. DES. F1=1545 MHZ F2=1600 MHZ F3=1660 MHZ  
 NO. -DB ANG. MS12 AS12 MS12 AS12 MS12 AS12  
 Z -DB DEG. -DB DEG. -DB DEG.

1	11.6	+0	13.7	-101	13.7	-158	13.0	-225
2	13.8	-90	16.7	-183	16.4	-242	15.3	-315
3	14.6	-315	17.3	-398	17.6	-465	17.2	-544
4	11.6	-225	13.9	-309	13.1	-376	13.6	-454
5	14.6	-90	17.5	-183	16.7	-248	17.5	-323
6	13.8	-225	17.0	-306	16.0	-371	16.3	-452
7	11.6	-45	13.6	-139	13.8	-199	13.6	-265
8	14.6	-315	16.9	-397	17.4	-468	17.5	-544
9	13.8	-270	16.5	-343	15.8	-413	15.1	-493
10	8.6	+0	10.1	-92	9.9	-145	9.2	-210
11	11.6	-180	13.8	-267	13.1	-336	13.6	-411
12	13.8	-90	15.9	-173	15.6	-240	16.5	-311
13	14.6	-225	17.0	-306	16.8	-376	17.3	-449
14	11.6	-315	13.5	-400	14.3	-479	14.2	-544
15	14.6	-90	16.5	-183	16.7	-248	16.6	-316
16	13.8	-315	15.8	-401	16.9	-473	17.4	-545
17	11.6	-135	13.8	-224	13.3	-292	14.2	-366
18	14.6	-225	16.9	-305	16.6	-374	17.0	-450
19	13.8	-270	15.8	-343	15.9	-415	16.7	-488

LOSS DB =		-2.12		-2.12		-1.95
-3DBLOSS MEAN =		13.7		13.6		13.7
-3DB STD. DEV. =		0.13		0.43		0.41
-5.2DBLOSS MEAN =		16.3		16.1		16.2
-5.2DB STD. DEV. =		0.47		0.43		0.80
-6DBLOSS MEAN =		17.0		17.0		17.2
-6DB STD. DEV. =		0.32		0.39		0.31
INPUT VSWR =		0.00		0.00		0.00

BEAMFORMER ANGLE ANALYSIS  
 PORT DES. F1=1545 MHZ F2=1600 MHZ F3=1660 MHZ  
 NO. ANG. MANG. DELTA MANG. DELTA MANG. DELTA  
 Z DEG. F1DA DF1DA F2DA DF2DA F3DA DF3DA

1	+0	-9	-9	-13	-13	-15	-15
2	-90	-91	-1	-97	-7	-105	-15
3	-315	-306	+9	-320	-5	-334	-19
4	-225	-217	+8	-231	-6	-244	-19
5	-90	-91	-1	-103	-13	-113	-23
6	-225	-214	+11	-226	-1	-242	-17
7	-45	-47	-2	-54	-9	-55	-10
8	-315	-305	+10	-323	-8	-334	-19
9	-270	-251	+19	-268	+2	-283	-13
10	+0	+0	+0	+0	+0	+0	+0
11	-180	-175	+5	-191	-11	-201	-21
12	-90	-81	+9	-95	-5	-101	-11
13	-225	-214	+11	-231	-6	-239	-14
14	-315	-308	+7	-334	-19	-334	-19
15	-90	-91	-1	-103	-13	-106	-16
16	-315	-309	+6	-328	-13	-335	-20
17	-135	-132	+3	-147	-12	-156	-21
18	-225	-213	+12	-229	-4	-240	-15
19	-270	-251	+19	-270	+0	-278	-8

MEAN DELTA ANG. = +6.39 -7.94 -16.39  
 STD. DEV. FOR DEL. = +7.25 +5.61 +5.57

Table B-1. Beamformer Calculations (Continued)

BEAMFORMER CALCULATIONS

10/16/87

MSAT, 8FM2, TRIM3, COVERED, AZ=90°, EL=20°

NUMBER OF OUTPUT PORTS = 19  
 LOW FREQUENCY IN MHZ = 1545  
 MID FREQUENCY IN MHZ = 1600  
 HIGH FREQUENCY IN MHZ = 1660

BEAMFORMER ANALYSIS

PORT DES. DES. F1=1545 MHZ F2=1600 MHZ F3=1660 MHZ  
 NO. -DB ANG. MS12 AS12 MS12 AS12 MS12 AS12  
 Z -DB DEG. -DB DEG. -DB DEG.

1	11.6	-270	13.7	-357	13.7	-425	13.4	-503
2	13.8	-90	16.5	-182	16.1	-244	15.8	-317
3	14.6	-180	17.5	-265	17.1	-326	16.8	-401
4	11.6	-90	13.4	-186	13.4	-250	13.4	-320
5	14.6	-180	17.6	-267	17.3	-333	17.1	-408
6	13.8	+0	16.4	-90	15.8	-151	15.8	-221
7	11.6	+0	13.6	-93	13.4	-152	13.1	-217
8	14.6	-180	16.7	-265	17.0	-331	16.9	-400
9	13.8	-90	16.0	-178	16.1	-242	16.0	-312
10	8.6	+0	10.1	-92	9.7	-145	9.3	-212
11	11.6	-270	13.4	-354	13.2	-426	13.8	-502
12	13.8	-90	16.2	-171	15.7	-237	16.0	-308
13	14.6	+0	17.2	-91	16.6	-151	16.6	-217
14	11.6	-90	12.9	-185	13.4	-248	13.6	-314
15	14.6	+0	16.4	-98	16.6	-159	17.0	-224
16	13.8	-180	16.3	-263	16.2	-331	16.4	-404
17	11.6	-180	13.6	-262	13.3	-328	13.6	-402
18	14.6	+0	16.6	-97	16.6	-156	16.8	-221
19	13.8	-90	15.9	-172	15.9	-234	15.8	-304

LOSS DB =	-1.98	-1.98	-1.79
-3DBLOSS MEAN =	13.4	13.4	13.5
-3DB STD. DEV. =	0.26	0.15	0.22
-5.2DBLOSS MEAN =	16.2	16.0	16.0
-5.2DB STD. DEV. =	0.21	0.18	0.21
-6DBLOSS MEAN =	17.0	16.9	16.9
-6DB STD. DEV. =	0.46	0.28	0.16
INPUT VSWR =	0.00	0.00	0.00

BEAMFORMER ANGLE ANALYSIS

PORT DES. F1=1545 MHZ F2=1600 MHZ F3=1660 MHZ  
 NO. ANG. MANG. DELTA MANG. DELTA MANG. DELTA  
 Z DEG. F1DA DF1DA F2DA DF2DA F3DA DF3DA

1	-270	-265	+5	-280	-10	-291	-21
2	-90	-90	+0	-99	-9	-105	-15
3	-180	-173	+7	-181	-1	-189	-9
4	-90	-94	-4	-105	-15	-108	-18
5	-180	-175	+5	-188	-8	-196	-16
6	+0	+2	+2	-6	-6	-9	-9
7	+0	-1	-1	-7	-7	-5	-5
8	-180	-173	+7	-186	-6	-188	-8
9	-90	-86	+4	-97	-7	-100	-10
10	+0	+0	+0	+0	+0	+0	+0
11	-270	-262	+8	-281	-11	-290	-20
12	-90	-79	+11	-92	-2	-96	-6
13	+0	+1	+1	-6	-6	-5	-5
14	-90	-93	-3	-103	-13	-102	-12
15	+0	-6	-6	-14	-14	-12	-12
16	-180	-171	+9	-186	-6	-192	-12
17	-180	-170	+10	-183	-3	-190	-10
18	+0	-5	-5	-11	-11	-9	-9
19	-90	-80	+10	-89	+1	-92	-2

MEAN DELTA ANG. = +3.33 -7.44 -11.06  
 STD. DEV. FOR DEL. = +5.44 +4.67 +5.76

Table B-1. Beamformer Calculations (Continued)

BEAMFORMER CALCULATIONS

10/16/87

MSAT, BFM2, TRIM3, COVERED, AZ=135°, EL=20°

NUMBER OF OUTPUT PORTS = 19  
 LOW FREQUENCY IN MHZ = 1545  
 MID FREQUENCY IN MHZ = 1600  
 HIGH FREQUENCY IN MHZ = 1660

BEAMFORMER ANALYSIS

PORT DES. DES. F1=1545 MHZ F2=1600 MHZ F3=1660 MHZ  
 NO. -DB ANG. MS12 AS12 MS12 AS12 MS12 AS12  
 Z -DB DEG. -DB DEG. -DB DEG.

1	11.6	-135	14.3	-229	13.7	-293	13.8	-366
2	13.8	-270	16.4	-351	16.0	-422	16.5	-501
3	14.6	-270	16.8	-348	16.7	-421	17.6	-498
4	11.6	+0	13.5	-97	13.3	-157	13.6	-226
5	14.6	-45	18.2	-138	17.6	-199	17.4	-270
6	13.8	-135	16.3	-226	16.3	-290	16.5	-363
7	11.6	-45	13.6	-136	13.4	-199	13.9	-267
8	14.6	-315	17.0	-396	17.1	-469	17.8	-545
9	13.8	-90	16.4	-172	15.6	-238	15.4	-311
10	8.6	+0	10.2	-93	10.1	-144	9.0	-210
11	11.6	-45	13.7	-141	13.4	-204	14.0	-271
12	13.8	-270	16.2	-342	15.7	-414	16.3	-492
13	14.6	-270	17.1	-346	16.3	-419	16.5	-497
14	11.6	-180	13.6	-264	13.7	-329	13.3	-400
15	14.6	-135	16.5	-234	17.3	-300	17.9	-367
16	13.8	-45	15.7	-140	16.5	-201	16.6	-263
17	11.6	-135	13.9	-225	13.6	-289	13.7	-363
18	14.6	-225	17.1	-307	16.9	-372	16.5	-448
19	13.8	-90	15.8	-173	16.3	-237	16.5	-301

LOSS DB =	-2.13	-2.13	-1.97
-3DBLOSS MEAN =	13.8	13.5	13.7
-3DB STD. DEV. =	0.27	0.16	0.23
-5.2DBLOSS MEAN =	16.1	16.1	16.3
-5.2DB STD. DEV. =	0.28	0.33	0.41
-6DBLOSS MEAN =	17.1	17.0	17.3
-6DB STD. DEV. =	0.53	0.42	0.58
INPUT VSWR =	0.00	0.00	0.00

BEAMFORMER ANGLE ANALYSIS

PORT DES. F1=1545 MHZ F2=1600 MHZ F3=1660 MHZ  
 NO. ANG. MANG. DELTA MANG. DELTA MANG. DELTA  
 Z DEG. F1DA DF1DA F2DA DF2DA F3DA DF3DA

1	-135	-136	-1	-149	-14	-156	-21
2	-270	-258	+12	-278	-8	-291	-21
3	-270	-255	+15	-277	-7	-288	-18
4	+0	-4	-4	-13	-13	-16	-16
5	-45	-45	+0	-55	-10	-60	-15
6	-135	-133	+2	-146	-11	-153	-18
7	-45	-43	+2	-55	-10	-57	-12
8	-315	-303	+12	-325	-10	-335	-20
9	-90	-79	+11	-94	-4	-101	-11
10	+0	+0	+0	+0	+0	+0	+0
11	-45	-48	-3	-60	-15	-61	-16
12	-270	-249	+21	-270	+0	-282	-12
13	-270	-253	+17	-275	-5	-287	-17
14	-180	-171	+9	-185	-5	-190	-10
15	-135	-141	-6	-156	-21	-157	-22
16	-45	-47	-2	-57	-12	-53	-8
17	-135	-132	+3	-145	-10	-153	-18
18	-225	-214	+11	-228	-3	-236	-13
19	-90	-80	+10	-93	-3	-91	-1
MEAN DELTA ANG. =	+6.06			-8.94			-14.94
STD. DEV. FOR DEL. =	+7.91			+5.44			+6.28

Table B-1. Beamformer Calculations (Continued)

BEAMFORMER CALCULATIONS										10/16/87	
MSAT, BFM2, TRIM3, COVERED, AZ=180°, EL=20°											
NUMBER OF OUTPUT PORTS										= 19	
LOW FREQUENCY IN MHZ										= 1545	
MID FREQUENCY IN MHZ										= 1600	
HIGH FREQUENCY IN MHZ										= 1660	
BEAMFORMER ANALYSIS											
PORT NO.	DES.	DES.	F1=1545 MHZ		F2=1600 MHZ		F3=1660 MHZ				
Z	-DB	ANG.	MS12	AS12	MS12	AS12	MS12	AS12	-DB	DEG.	
Z	-DB	DEG.	-DB	DEG.	-DB	DEG.	-DB	DEG.	-DB	DEG.	
1	11.6	-45	14.3	-147	14.3	-197	12.6	-269			
2	13.8	-45	17.0	-145	16.9	-196	15.4	-268			
3	14.6	-45	17.8	-142	17.8	-192	17.8	-263			
4	11.6	-45	14.1	-142	13.7	-199	12.9	-270			
5	14.6	-45	18.4	-144	18.1	-200	17.5	-271			
6	13.8	-45	16.8	-138	16.3	-195	15.6	-267			
7	11.6	-180	14.0	-265	13.9	-325	12.6	-400			
8	14.6	-180	16.8	-267	17.2	-330	16.6	-402			
9	13.8	-225	16.4	-305	16.6	-369	15.8	-445			
10	8.6	+0	10.0	-90	9.4	-147	9.6	-213			
11	11.6	-135	12.9	-228	13.2	-299	14.1	-368			
12	13.8	-135	15.5	-215	15.7	-285	16.4	-355			
13	14.6	-135	16.6	-222	16.8	-290	17.3	-360			
14	11.6	-135	13.0	-227	13.6	-296	14.6	-362			
15	14.6	-135	16.2	-229	16.7	-300	17.9	-368			
16	13.8	-135	15.6	-226	16.1	-296	17.5	-364			
17	11.6	+0	12.9	-91	13.0	-157	14.7	-221			
18	14.6	+0	16.1	-91	15.8	-158	17.3	-225			
19	13.8	-315	15.8	-385	15.7	-461	14.4	-538			
LOSS DB =			-1.97		-1.97		-1.89				
-3DBLOSS MEAN =			13.6		13.6		13.6				
-3DB STD. DEV. =			0.65		0.43		0.31				
-5.2DBLOSS MEAN =			16.2		16.2		15.9				
-5.2DB STD. DEV. =			0.58		0.44		0.35				
-6DBLOSS MEAN =			17.0		17.1		17.4				
-6DB STD. DEV. =			0.84		0.76		0.42				
INPUT VSWR =			0.00		0.00		0.00				
BEAMFORMER ANGLE ANALYSIS											
PORT NO.	DES.	F1=1545 MHZ	F2=1600 MHZ	F3=1660 MHZ							
Z	ANG.	MANG.	DELTA	MANG.	DELTA	MANG.	DELTA	MANG.	DELTA	MANG.	DELTA
Z	DEG.	F1DA	DF1DA	F2DA	DF2DA	F3DA	DF3DA	F3DA	DF3DA	F3DA	DF3DA
1	-45	-57	-12	-50	-5	-56	-11				
2	-45	-55	-10	-49	-4	-55	-10				
3	-45	-52	-7	-45	+0	-50	-5				
4	-45	-52	-7	-52	-7	-57	-12				
5	-45	-54	-9	-53	-8	-58	-13				
6	-45	-48	-3	-48	-3	-54	-9				
7	-180	-175	+5	-178	+2	-187	-7				
8	-180	-177	+3	-183	-3	-189	-9				
9	-225	-215	+10	-222	+3	-232	-7				
10	+0	+0	+0	+0	+0	+0	+0				
11	-135	-138	-3	-152	-17	-155	-20				
12	-135	-125	+10	-138	-3	-142	-7				
13	-135	-132	+3	-143	-8	-147	-12				
14	-135	-137	-2	-149	-14	-149	-14				
15	-135	-139	-4	-153	-18	-155	-20				
16	-135	-136	-1	-149	-14	-151	-16				
17	+0	-1	-1	-10	-10	-8	-8				
18	+0	-1	-1	-11	-11	-12	-12				
19	-315	-295	+20	-314	+1	-325	-10				
MEAN DELTA ANG. =		-0.50		-6.61		-11.22					
STD. DEV. FOR DEL. =		+7.83		+6.42		+4.89					

Table B-1. Beamformer Calculations (Continued)

BEAMFORMER CALCULATIONS

10/16/87

MSAT, BFM2, TRIM3, COVERED, AZ=225°, EL=20°

NUMBER OF OUTPUT PORTS = 19  
 LOW FREQUENCY IN MHZ = 1545  
 MID FREQUENCY IN MHZ = 1600  
 HIGH FREQUENCY IN MHZ = 1660

BEAMFORMER ANALYSIS

PORT DES. DES. F1=1545 MHZ F2=1600 MHZ F3=1660 MHZ  
 NO. -DB ANG. MS12 AS12 MS12 AS12 MS12 AS12  
 Z -DB DEG. -DB DEG. -DB DEG.

1	11.6	+0	13.7	-96	13.1	-158	13.5	-226
2	13.8	-270	16.5	-352	15.9	-425	16.9	-502
3	14.6	-45	16.5	-134	16.5	-202	17.9	-270
4	11.6	-135	13.8	-230	13.8	-296	14.0	-368
5	14.6	-270	17.1	-352	16.6	-421	16.3	-500
6	13.8	-135	16.0	-227	16.3	-292	16.7	-363
7	11.6	-315	14.0	-391	13.6	-465	13.8	-544
8	14.6	-45	16.9	-133	16.8	-197	17.0	-263
9	13.8	-90	15.5	-180	16.0	-249	17.1	-314
10	8.6	+0	10.1	-90	9.5	-147	9.5	-213
11	11.6	-180	13.5	-272	13.7	-337	13.4	-409
12	13.8	-270	16.3	-345	16.2	-412	15.4	-489
13	14.6	-135	17.1	-226	17.4	-287	16.7	-357
14	11.6	-45	13.7	-137	13.5	-197	13.6	-266
15	14.6	-270	16.8	-360	16.7	-428	17.0	-505
16	13.8	-45	16.2	-137	16.1	-197	16.4	-266
17	11.6	-225	14.1	-312	14.3	-372	13.5	-446
18	14.6	-135	17.3	-232	17.7	-290	17.1	-361
19	13.8	-90	16.3	-171	15.7	-228	14.4	-305

LOSS DB =		-2.10		-2.10		-1.92
-3DBLOSS MEAN =		13.8		13.7		13.6
-3DB STD. DEV. =		0.20		0.36		0.21
-5.2DBLOSS MEAN =		16.1		16.0		16.2
-5.2DB STD. DEV. =		0.32		0.20		0.95
-6DBLOSS MEAN =		16.9		16.9		17.0
-6DB STD. DEV. =		0.26		0.44		0.48
INPUT VSWR =		0.00		0.00		0.00

BEAMFORMER ANGLE ANALYSIS

PORT DES. F1=1545 MHZ F2=1600 MHZ F3=1660 MHZ  
 NO. ANG. MANG. DELTA MANG. DELTA MANG. DELTA  
 Z DEG. F1DA DF1DA F2DA DF2DA F3DA DF3DA

1	+0	-6	-6	-11	-11	-13	-13
2	-270	-262	+8	-278	-8	-289	-19
3	-45	-44	+1	-55	-10	-57	-12
4	-135	-140	-5	-149	-14	-155	-20
5	-270	-262	+8	-274	-4	-287	-17
6	-135	-137	-2	-145	-10	-150	-15
7	-315	-301	+14	-318	-3	-331	-16
8	-45	-43	+2	-50	-5	-50	-5
9	-90	-90	+0	-102	-12	-101	-11
10	+0	+0	+0	+0	+0	+0	+0
11	-180	-182	-2	-190	-10	-196	-16
12	-270	-255	+15	-265	+5	-276	-6
13	-135	-136	-1	-140	-5	-144	-9
14	-45	-47	-2	-50	-5	-53	-8
15	-270	-270	+0	-281	-11	-292	-22
16	-45	-47	-2	-50	-5	-53	-8
17	-225	-222	+3	-225	+0	-233	-8
18	-135	-142	-7	-143	-8	-148	-13
19	-90	-81	+9	-81	+9	-92	-2
MEAN DELTA ANG. =		+1.83		-5.94		-12.22	
STD. DEV. FOR DEL. =		+6.30		+5.96		+6.11	

Table B-1. Beamformer Calculations (Continued)

BEAMFORMER CALCULATIONS

10/16/87

MSAT, BFM2, TRIM3, COVERED, AZ=270°, EL=20°

NUMBER OF OUTPUT PORTS = 19  
 LOW FREQUENCY IN MHZ = 1545  
 MID FREQUENCY IN MHZ = 1600  
 HIGH FREQUENCY IN MHZ = 1660

BEAMFORMER ANALYSIS

F1=1545 MHZ F2=1600 MHZ F3=1660 MHZ  
 PORT DES. DES. MS12 AS12 MS12 AS12 MS12 AS12  
 NO. -DB ANG. -DB DEG. -DB DEG. -DB DEG.  
 Z

1	11.6	-90	13.3	-183	13.4	-250	13.2	-318
2	13.8	-270	16.6	-352	16.3	-420	16.1	-499
3	14.6	-180	17.5	-262	17.0	-324	16.9	-402
4	11.6	-270	13.5	-356	13.4	-425	13.5	-504
5	14.6	-180	17.6	-269	17.4	-334	17.3	-408
6	13.8	+0	16.4	-93	16.0	-152	15.9	-221
7	11.6	+0	13.5	-93	13.4	-152	13.0	-217
8	14.6	-180	16.6	-263	16.9	-330	16.9	-400
9	13.8	-270	16.1	-346	15.9	-417	16.0	-495
10	8.6	+0	10.2	-92	9.7	-146	9.3	-212
11	11.6	-90	13.2	-184	13.2	-250	13.6	-318
12	13.8	-270	16.2	-341	15.8	-414	16.0	-491
13	14.6	+0	16.9	-89	16.5	-151	16.7	-217
14	11.6	-270	13.1	-354	13.5	-424	13.8	-497
15	14.6	+0	16.5	-99	16.6	-159	17.1	-224
16	13.8	-180	16.5	-266	16.3	-330	16.3	-404
17	11.6	-180	13.6	-262	13.4	-328	13.5	-402
18	14.6	+0	16.4	-95	16.5	-155	16.7	-221
19	13.8	-270	15.9	-342	15.8	-411	15.6	-487

LOSS DB =	-1.96	-1.96	-1.78
-3DBLOSS MEAN =	13.4	13.4	13.4
-3DB STD. DEV. =	0.18	0.09	0.26
-5.2DBLOSS MEAN =	16.3	16.0	16.0
-5.2DB STD. DEV. =	0.24	0.21	0.21
-6DBLOSS MEAN =	16.9	16.8	16.9
-6DB STD. DEV. =	0.47	0.32	0.21
INPUT VSWR =	0.00	0.00	0.00

BEAMFORMER ANGLE ANALYSIS

F1=1545 MHZ F2=1600 MHZ F3=1660 MHZ  
 PORT DES. MANG. DELTA MANG. DELTA MANG. DELTA  
 NO. ANG. F1DA DF1DA F2DA DF2DA F3DA DF3DA  
 Z DEG.

1	-90	-91	-1	-104	-14	-106	-16
2	-270	-260	+10	-274	-4	-287	-17
3	-180	-170	+10	-178	+2	-190	-10
4	-270	-264	+6	-279	-9	-292	-22
5	-180	-177	+3	-188	-8	-196	-16
6	+0	-1	-1	-6	-6	-9	-9
7	+0	-1	-1	-6	-6	-5	-5
8	-180	-171	+9	-184	-4	-188	-8
9	-270	-254	+16	-271	-1	-283	-13
10	+0	+0	+0	+0	+0	+0	+0
11	-90	-92	-2	-104	-14	-106	-16
12	-270	-249	+21	-268	+2	-279	-9
13	+0	+3	+3	-5	-5	-5	-5
14	-270	-262	+8	-278	-8	-285	-15
15	+0	-7	-7	-13	-13	-12	-12
16	-180	-174	+6	-184	-4	-192	-12
17	-180	-170	+10	-182	-2	-190	-10
18	+0	-3	-3	-9	-9	-9	-9
19	-270	-250	+20	-265	+5	-275	-5
MEAN DELTA ANG. =	+5.94			-5.44			-11.61
STD. DEV. FOR DEL. =	+7.80			+5.43			+5.34

Table B-1. Beamformer Calculations (Continued)

BEAMFORMER CALCULATIONS 10/16/87

MSAT, BFM2, TRIM3, COVERED, AZ=315°, EL=20°

NUMBER OF OUTPUT PORTS = 19  
 LOW FREQUENCY IN MHZ = 1545  
 MID FREQUENCY IN MHZ = 1600  
 HIGH FREQUENCY IN MHZ = 1660

BEAMFORMER ANALYSIS  
 PORT DES. DES. F1=1545 MHZ F2=1600 MHZ F3=1660 MHZ  
 NO. -DB ANG. MS12 AS12 MS12 AS12 MS12 AS12  
 Z -DB DEG. -DB DEG. -DB DEG.

PORT NO.	DES. -DB	DES. ANG.	F1=1545 MHZ MS12 -DB	F1=1545 MHZ AS12 DEG.	F2=1600 MHZ MS12 -DB	F2=1600 MHZ AS12 DEG.	F3=1660 MHZ MS12 -DB	F3=1660 MHZ AS12 DEG.
1	11.6	-225	14.3	-311	13.8	-378	13.9	-456
2	13.8	-90	16.5	-182	16.0	-244	15.8	-318
3	14.6	-90	17.3	-180	17.1	-240	16.6	-311
4	11.6	+0	13.9	-97	13.5	-153	12.8	-223
5	14.6	-315	16.9	-401	17.2	-471	17.5	-551
6	13.8	-225	16.3	-307	16.3	-373	16.3	-451
7	11.6	-315	14.2	-394	13.8	-463	13.5	-542
8	14.6	-45	17.0	-133	16.9	-195	16.7	-262
9	13.8	-270	15.7	-350	16.2	-423	16.8	-495
10	8.6	+0	10.1	-90	9.5	-146	9.6	-212
11	11.6	-315	13.8	-397	13.5	-470	13.7	-549
12	13.8	-90	15.8	-173	15.8	-239	16.0	-308
13	14.6	-90	16.6	-180	16.8	-244	17.0	-310
14	11.6	-180	13.2	-267	13.7	-332	13.7	-402
15	14.6	-225	17.0	-311	17.1	-377	16.6	-450
16	13.8	-315	16.0	-401	16.8	-471	17.1	-546
17	11.6	-225	13.8	-308	13.9	-375	14.1	-447
18	14.6	-135	16.8	-227	17.2	-292	17.7	-361
19	13.8	-270	16.0	-337	15.2	-408	15.1	-489

LOSS DB =	-2.11	-2.11	-1.95
-3DBLOSS MEAN =	13.9	13.7	13.6
-3DB STD. DEV. =	0.35	0.15	0.41
-5.2DBLOSS MEAN =	16.1	16.1	16.2
-5.2DB STD. DEV. =	0.28	0.49	0.66
-6DBLOSS MEAN =	16.9	17.1	17.0
-6DB STD. DEV. =	0.21	0.15	0.44
INPUT VSWR =	0.00	0.00	0.00

BEAMFORMER ANGLE ANALYSIS  
 PORT DES. F1=1545 MHZ F2=1600 MHZ F3=1660 MHZ  
 NO. ANG. MANG. DELTA MANG. DELTA MANG. DELTA  
 Z DEG. F1DA DF1DA F2DA DF2DA F3DA DF3DA

PORT NO.	DES. ANG.	F1=1545 MHZ MANG.	F1=1545 MHZ DELTA	F2=1600 MHZ MANG.	F2=1600 MHZ DELTA	F3=1660 MHZ MANG.	F3=1660 MHZ DELTA
Z	DEG.	F1DA	DF1DA	F2DA	DF2DA	F3DA	DF3DA
1	-225	-221	+4	-232	-7	-244	-19
2	-90	-92	-2	-98	-8	-106	-16
3	-90	-90	+0	-94	-4	-99	-9
4	+0	-7	-7	-7	-7	-11	-11
5	-315	-311	+4	-325	-10	-339	-24
6	-225	-217	+8	-227	-2	-239	-14
7	-315	-304	+11	-317	-2	-330	-15
8	-45	-43	+2	-49	-4	-50	-5
9	-270	-260	+10	-277	-7	-283	-13
10	+0	+0	+0	+0	+0	+0	+0
11	-315	-307	+8	-324	-9	-337	-22
12	-90	-83	+7	-93	-3	-96	-6
13	-90	-90	+0	-98	-8	-98	-8
14	-180	-177	+3	-186	-6	-190	-10
15	-225	-221	+4	-231	-6	-238	-13
16	-315	-311	+4	-325	-10	-334	-19
17	-225	-218	+7	-229	-4	-235	-10
18	-135	-137	-2	-146	-11	-149	-14
19	-270	-247	+23	-262	+8	-277	-7
MEAN DELTA ANG. =	+4.67			-5.56		-13.06	
STD. DEV. FOR DEL. =	+6.41			+4.43		+6.11	

Table B-1. Beamformer Calculations (Continued)

BEAMFORMER CALCULATIONS										10/16/87		
MSAT, BFM2, TRIM3, COVERED, AZ=0°, EL=30°												
NUMBER OF OUTPUT PORTS										= 19		
LOW FREQUENCY IN MHZ										= 1545		
MID FREQUENCY IN MHZ										= 1600		
HIGH FREQUENCY IN MHZ										= 1660		
BEAMFORMER ANALYSIS												
PORT DES. DES. F1=1545 MHZ F2=1600 MHZ F3=1660 MHZ												
NO.	-DB	ANG.	MS12	AS12	MS12	AS12	MS12	AS12	MS12	AS12		
Z			-DB	DEG.	-DB	DEG.	-DB	DEG.	-DB	DEG.		
1	11.6	-315	14.3	-398	13.9	-473	14.5	-551				
2	13.8	-315	16.2	-394	16.3	-472	17.7	-549				
3	14.6	-270	16.4	-346	16.6	-422	17.8	-496				
4	11.6	-315	14.1	-396	13.4	-471	14.2	-553				
5	14.6	-270	16.6	-350	16.2	-425	17.3	-502				
6	13.8	-270	15.3	-348	15.6	-425	17.2	-499				
7	11.6	-180	13.2	-261	13.4	-330	13.8	-402				
8	14.6	-180	16.8	-261	16.7	-328	16.7	-399				
9	13.8	-135	16.4	-220	16.4	-287	16.5	-357				
10	8.6	+0	10.0	-92	9.9	-145	9.1	-210				
11	11.6	-225	13.9	-313	13.7	-379	13.8	-455				
12	13.8	-225	16.4	-300	16.1	-366	16.1	-443				
13	14.6	-270	17.3	-351	16.7	-419	16.5	-499				
14	11.6	-225	13.8	-310	13.9	-374	13.7	-449				
15	14.6	-270	16.9	-360	17.0	-425	16.7	-502				
16	13.8	-270	16.6	-354	16.5	-417	15.8	-495				
17	11.6	+0	13.8	-93	13.6	-146	12.6	-217				
18	14.6	+0	16.8	-101	17.2	-153	16.3	-220				
19	13.8	-45	16.1	-137	16.4	-191	15.5	-261				
-----												
LOSS DB =										-2.08	-2.08	-1.95
-3DBLOSS MEAN =										13.9	13.6	13.8
-3DB STD. DEV. =										0.34	0.21	0.59
-5.2DBLOSS MEAN =										16.2	16.2	16.5
-5.2DB STD. DEV. =										0.42	0.30	0.77
-6DBLOSS MEAN =										16.8	16.7	16.9
-6DB STD. DEV. =										0.28	0.31	0.51
INPUT VSWR =										0.00	0.00	0.00
-----												
BEAMFORMER ANGLE ANALYSIS												
PORT	DES.	F1=1545 MHZ	F2=1600 MHZ	F3=1660 MHZ								
NO.	ANG.	MANG.	DELTA	MANG.	DELTA	MANG.	DELTA					
Z	DEG.	F1DA	DF1DA	F2DA	DF2DA	F3DA	DF3DA					
1	-315	-306	+9	-328	-13	-341	-26					
2	-315	-302	+13	-327	-12	-339	-24					
3	-270	-254	+16	-277	-7	-286	-16					
4	-315	-304	+11	-326	-11	-343	-28					
5	-270	-258	+12	-280	-10	-292	-22					
6	-270	-256	+14	-280	-10	-289	-19					
7	-180	-169	+11	-185	-5	-192	-12					
8	-180	-169	+11	-183	-3	-189	-9					
9	-135	-128	+7	-142	-7	-147	-12					
10	+0	+0	+0	+0	+0	+0	+0					
11	-225	-221	+4	-234	-9	-245	-20					
12	-225	-208	+17	-221	+4	-233	-8					
13	-270	-259	+11	-274	-4	-289	-19					
14	-225	-218	+7	-229	-4	-239	-14					
15	-270	-268	+2	-280	-10	-292	-22					
16	-270	-262	+8	-272	-2	-285	-15					
17	+0	-1	-1	-1	-1	-7	-7					
18	+0	-9	-9	-8	-8	-10	-10					
19	-45	-45	+0	-46	-1	-51	-6					
-----												
MEAN DELTA ANG. =										+7.94	-6.28	-16.06
STD. DEV. FOR DEL. =										+6.71	+4.68	+7.60

Table B-1. Beamformer Calculations (Continued)

BEAMFORMER CALCULATIONS										10/16/87	
MSAT, BFM2, TRIM3, COVERED, <u>AZ=0°, EL=40°</u>											
NUMBER OF OUTPUT PORTS										= 19	
LOW FREQUENCY IN MHZ										= 1545	
MID FREQUENCY IN MHZ										= 1600	
HIGH FREQUENCY IN MHZ										= 1660	
BEAMFORMER ANALYSIS											
PORT DES. DES. F1=1545 MHZ F2=1600 MHZ F3=1660 MHZ											
NO.	-DB	ANG.	MS12	AS12	MS12	AS12	MS12	AS12	MS12	AS12	
Z			-DB	DEG.	-DB	DEG.	-DB	DEG.	-DB	DEG.	
1	11.6	-315	14.5	-400	14.1	-471	14.0	-549			
2	13.8	-315	16.3	-397	17.5	-472	16.0	-550			
3	14.6	-225	16.5	-304	16.9	-376	17.9	-447			
4	11.6	-315	14.3	-397	13.5	-470	14.0	-552			
5	14.6	-225	17.3	-307	17.0	-379	17.9	-455			
6	13.8	-225	15.5	-306	16.0	-381	17.9	-453			
7	11.6	-180	13.2	-262	13.5	-330	13.6	-401			
8	14.6	-180	16.8	-262	16.9	-328	16.5	-399			
9	13.8	-135	16.4	-221	16.6	-286	16.3	-356			
10	8.6	+0	10.1	-91	9.8	-145	9.2	-211			
11	11.6	-225	13.6	-313	13.6	-381	14.2	-456			
12	13.8	-225	16.6	-298	15.9	-365	15.9	-443			
13	14.6	-315	17.5	-395	16.8	-466	17.1	-548			
14	11.6	-225	13.3	-311	13.9	-377	14.0	-449			
15	14.6	-315	17.0	-404	17.4	-471	17.1	-549			
16	13.8	-315	17.3	-397	16.8	-461	15.6	-543			
17	11.6	+0	13.7	-91	13.1	-148	13.8	-218			
18	14.6	+0	16.7	-99	16.9	-155	16.7	-221			
19	13.8	-45	16.0	-135	16.1	-193	15.8	-262			
-----											
LOSS DB =			-2.13		-2.13		-2.06				
-3DBLOSS MEAN =			13.8		13.6		13.9				
-3DB STD. DEV. =			0.48		0.32		0.19				
-5.2DBLOSS MEAN =			16.3		16.5		16.3				
-5.2DB STD. DEV. =			0.55		0.56		0.77				
-6DBLOSS MEAN =			17.0		17.0		17.2				
-6DB STD. DEV. =			0.34		0.20		0.54				
INPUT VSWR =			0.00		0.00		0.00				
-----											
BEAMFORMER ANGLE ANALYSIS											
PORT DES. F1=1545 MHZ F2=1600 MHZ F3=1660 MHZ											
NO.	ANG.	F1DA	DF1DA	F2DA	DF2DA	F3DA	DF3DA				
Z	DEG.										
1	-315	-309	+6	-326	-11	-338	-23				
2	-315	-306	+9	-327	-12	-339	-24				
3	-225	-213	+12	-231	-6	-236	-11				
4	-315	-306	+9	-325	-10	-341	-26				
5	-225	-216	+9	-234	-9	-244	-19				
6	-225	-215	+10	-236	-11	-242	-17				
7	-180	-171	+9	-185	-5	-190	-10				
8	-180	-171	+9	-183	-3	-188	-8				
9	-135	-130	+5	-141	-6	-145	-10				
10	+0	+0	+0	+0	+0	+0	+0				
11	-225	-222	+3	-236	-11	-245	-20				
12	-225	-207	+18	-220	+5	-232	-7				
13	-315	-304	+11	-321	-6	-337	-22				
14	-225	-220	+5	-232	-7	-238	-13				
15	-315	-313	+2	-326	-11	-338	-23				
16	-315	-306	+9	-316	-1	-332	-17				
17	+0	+0	+0	-3	-3	-7	-7				
18	+0	-8	-8	-10	-10	-10	-10				
19	-45	-44	+1	-48	-3	-51	-6				
MEAN DELTA ANG. =		+6.61		-6.67		-15.17					
STD. DEV. FOR DEL. =		+5.75		+4.65		+7.49					

Table B-1. Beamformer Calculations (Continued)

BEAMFORMER CALCULATIONS										10/16/87		
MSAT, BFM2, TRIM3, COVERED, AZ=0°, EL=50°												
NUMBER OF OUTPUT PORTS										= 19		
LOW FREQUENCY IN MHZ										= 1545		
MID FREQUENCY IN MHZ										= 1600		
HIGH FREQUENCY IN MHZ										= 1660		
BEAMFORMER ANALYSIS												
PORT NO.	DES.	DES.	F1=1545 MHZ	F2=1600 MHZ	F3=1660 MHZ							
Z	-DB	ANG.	MS12	AS12	MS12	AS12	MS12	AS12	MS12	AS12	-DB	DEG.
1	11.6	-270	14.0	-358	13.9	-423	12.8	-502				
2	13.8	-270	16.4	-356	16.5	-421	16.0	-500				
3	14.6	-225	17.1	-306	17.1	-372	16.8	-449				
4	11.6	-270	13.8	-356	13.4	-423	13.1	-504				
5	14.6	-225	17.6	-311	17.4	-378	17.3	-454				
6	13.8	-225	16.3	-309	16.3	-376	16.7	-452				
7	11.6	-180	13.7	-262	13.6	-326	13.0	-400				
8	14.6	-180	16.8	-266	17.2	-329	16.6	-400				
9	13.8	-90	16.0	-180	16.3	-241	15.7	-310				
10	8.6	+0	10.1	-91	9.6	-146	9.4	-212				
11	11.6	-270	13.3	-353	13.1	-427	14.0	-502				
12	13.8	-270	16.3	-341	15.6	-413	16.1	-492				
13	14.6	-315	17.5	-395	16.9	-467	17.3	-546				
14	11.6	-270	13.0	-353	13.4	-424	14.1	-498				
15	14.6	-315	16.8	-401	17.1	-473	17.6	-549				
16	13.8	-315	16.8	-396	16.5	-465	16.5	-545				
17	11.6	+0	13.5	-89	13.1	-151	13.8	-219				
18	14.6	+0	16.4	-96	16.3	-157	17.0	-223				
19	13.8	-90	15.7	-170	15.5	-235	16.1	-305				
-----												
LOSS DB =			-2.04		-2.04		-1.88					
-3DBLOSS MEAN =			13.6		13.4		13.5					
-3DB STD. DEV. =			0.33		0.28		0.52					
-5.2DBLOSS MEAN =			16.3		16.1		16.2					
-5.2DB STD. DEV. =			0.34		0.41		0.33					
-6DBLOSS MEAN =			17.0		17.0		17.1					
-6DB STD. DEV. =			0.42		0.35		0.34					
INPUT VSWR =			0.00		0.00		0.00					
-----												
BEAMFORMER ANGLE ANALYSIS												
PORT NO.	DES.	F1=1545 MHZ	F2=1600 MHZ	F3=1660 MHZ								
Z	ANG.	MANG.	DELTA	MANG.	DELTA	MANG.	DELTA					
Z	DEG.	F1DA	DF1DA	F2DA	DF2DA	F3DA	DF3DA					
1	-270	-267	+3	-277	-7	-290	-20					
2	-270	-265	+5	-275	-5	-288	-18					
3	-225	-215	+10	-226	-1	-237	-12					
4	-270	-265	+5	-277	-7	-292	-22					
5	-225	-220	+5	-232	-7	-242	-17					
6	-225	-218	+7	-230	-5	-240	-15					
7	-180	-171	+9	-180	+0	-188	-8					
8	-180	-175	+5	-183	-3	-188	-8					
9	-90	-89	+1	-95	-5	-98	-8					
10	+0	+0	+0	+0	+0	+0	+0					
11	-270	-262	+8	-281	-11	-290	-20					
12	-270	-250	+20	-267	+3	-280	-10					
13	-315	-304	+11	-321	-6	-334	-19					
14	-270	-262	+8	-278	-8	-286	-16					
15	-315	-310	+5	-327	-12	-337	-22					
16	-315	-305	+10	-319	-4	-333	-18					
17	+0	+2	+2	-5	-5	-7	-7					
18	+0	-5	-5	-11	-11	-11	-11					
19	-90	-79	+11	-89	+1	-93	-3					
MEAN DELTA ANG. =		+6.67		-5.17		-14.11						
STD. DEV. FOR DEL. =		+5.31		+4.18		+6.57						

Table B-1. Beamformer Calculations (Continued)

BEAMFORMER CALCULATIONS

10/16/87

MSAT, BFM2, TRIM3, COVERED, AZ=0°, EL=60°

NUMBER OF OUTPUT PORTS = 19  
 LOW FREQUENCY IN MHZ = 1545  
 MID FREQUENCY IN MHZ = 1600  
 HIGH FREQUENCY IN MHZ = 1660

BEAMFORMER ANALYSIS

PORT DES. DES. F1=1545 MHZ F2=1600 MHZ F3=1660 MHZ  
 NO. -DB ANG. MS12 AS12 MS12 AS12 MS12 AS12  
 Z -DB DEG. -DB DEG. -DB DEG.

1	11.6	-270	13.6	-356	13.5	-427	13.4	-504
2	13.8	-270	16.6	-352	16.2	-421	16.0	-500
3	14.6	-180	17.1	-261	16.7	-328	16.9	-403
4	11.6	-270	13.3	-356	13.4	-426	13.5	-504
5	14.6	-180	17.4	-268	17.2	-334	17.1	-410
6	13.8	-180	16.6	-264	16.1	-329	16.0	-405
7	11.6	-180	13.6	-261	13.4	-328	13.2	-401
8	14.6	-180	16.7	-265	16.9	-330	16.8	-401
9	13.8	-90	16.0	-178	16.1	-242	15.9	-311
10	8.6	+0	10.1	-92	9.7	-146	9.3	-212
11	11.6	-270	13.4	-355	13.2	-426	13.7	-502
12	13.8	-270	16.4	-342	15.9	-412	16.1	-491
13	14.6	+0	17.1	-92	16.6	-151	16.6	-218
14	11.6	-270	13.2	-354	13.5	-423	13.8	-498
15	14.6	+0	16.6	-100	16.8	-159	17.1	-224
16	13.8	+0	16.2	-95	16.1	-153	16.1	-220
17	11.6	+0	13.6	-91	13.3	-150	13.4	-219
18	14.6	+0	16.6	-98	16.5	-156	16.7	-222
19	13.8	-90	15.8	-172	15.7	-234	15.7	-306

LOSS DR =	-1.98	-1.98	-1.80
-3DBLOSS MEAN =	13.5	13.4	13.5
-3DB STD. DEV. =	0.16	0.11	0.20
-5.2DBLOSS MEAN =	16.3	16.0	16.0
-5.2DB STD. DEV. =	0.30	0.17	0.14
-6DBLOSS MEAN =	16.9	16.8	16.9
-6DB STD. DEV. =	0.30	0.23	0.19
INPUT VSWR =	0.00	0.00	0.00

BEAMFORMER ANGLE ANALYSIS

PORT DES. F1=1545 MHZ F2=1600 MHZ F3=1660 MHZ  
 NO. ANG. MANG. DELTA MANG. DELTA MANG. DELTA  
 Z DEG. F1DA DF1DA F2DA DF2DA F3DA DF3DA

1	-270	-264	+6	-281	-11	-292	-22
2	-270	-260	+10	-275	-5	-288	-18
3	-180	-169	+11	-182	-2	-191	-11
4	-270	-264	+6	-280	-10	-292	-22
5	-180	-176	+4	-188	-8	-198	-18
6	-180	-172	+8	-183	-3	-193	-13
7	-180	-169	+11	-182	-2	-189	-9
8	-180	-173	+7	-184	-4	-189	-9
9	-90	-86	+4	-96	-6	-99	-3
10	+0	+0	+0	+0	+0	+0	+0
11	-270	-263	+7	-280	-10	-290	-20
12	-270	-250	+20	-266	+4	-279	-9
13	+0	+0	+0	-5	-5	-6	-6
14	-270	-262	+8	-277	-7	-286	-16
15	+0	-8	-8	-13	-13	-12	-12
16	+0	-3	-3	-7	-7	-8	-8
17	+0	+1	+1	-4	-4	-7	-7
18	+0	-6	-6	-10	-10	-10	-10
19	-90	-80	+10	-88	+2	-94	-4

MEAN DELTA ANG. = +5.33 -5.61 -12.39  
 STD. DEV. FOR DEL. = +6.66 +4.54 +8.17

Table B-1. Beamformer Calculations (Continued)

BEAMFORMER CALCULATIONS 10/16/87

HEAT, SPM, TRIM, COVERED, AC=00, EL=900

NUMBER OF OUTPUT PORTS = 19  
 LOW FREQUENCY IN MHZ = 1545  
 MID FREQUENCY IN MHZ = 1600  
 HIGH FREQUENCY IN MHZ = 1660

BEAMFORMER ANALYSIS

PORT NO.	DES. ANG.	F1=1545 MHZ MS1B -DB	AS1B DEG.	F2=1600 MHZ MS1B -DB	AS1B DEG.	F3=1660 MHZ MS1B -DB	AS1B DEG.	
1	11.6	-180	13.3	-271	13.6	-337	13.8	-411
2	13.8	-180	13.2	-268	13.1	-333	13.0	-407
3	14.8	+0	13.3	-34	17.2	-154	17.1	-213
4	11.6	-180	13.3	-267	13.2	-334	13.3	-410
5	14.6	+0	17.4	-100	17.4	-160	17.7	-227
6	13.8	+0	15.5	-95	16.0	-156	16.2	-222
7	11.6	-180	13.3	-263	13.6	-329	13.4	-402
8	14.6	-180	16.7	-264	16.9	-330	16.7	-401
9	13.8	+0	15.9	-91	16.0	-151	15.8	-215
10	8.2	+0	10.0	-32	9.7	-146	9.2	-212
11	11.6	+0	13.1	-39	13.3	-153	13.3	-225
12	13.8	+0	16.4	-88	16.4	-149	16.3	-216
13	14.6	-180	16.8	-265	16.7	-332	16.7	-406
14	11.6	+0	13.2	-37	13.5	-154	13.4	-219
15	14.6	-180	16.7	-272	16.9	-337	16.9	-409
16	13.8	-180	16.1	-266	16.2	-331	16.4	-406
17	11.6	+0	13.3	-34	13.3	-152	13.5	-219
18	14.6	+0	16.4	-86	16.3	-155	16.5	-223
19	13.8	-180	16.1	-268	15.7	-327	15.7	-402

LOSS DB = -1.84 -1.84 -1.73  
 -3DB LOSS MEAN = 13.3 13.5 13.4  
 -3DB STD. DEV. = 0.12 0.15 0.11  
 -5.0DB LOSS MEAN = 16.1 16.1 16.1  
 -5.0DB STD. DEV. = 0.20 0.21 0.26  
 -6DB LOSS MEAN = 16.8 16.9 16.9  
 -6DB STD. DEV. = 0.30 0.35 0.39  
 NPORT VSWS = 1.00 1.00 1.00

BEAMFORMER ANGLE ANALYSIS

PORT NO.	ANG. DEG.	F1=1545 MHZ MANG. F1DA	DELTA DF1DA	F2=1600 MHZ MANG. F2DA	DELTA DF2DA	F3=1660 MHZ MANG. F3DA	DELTA DF3DA
1	-180	-179	+1	-191	-11	-199	-19
2	-180	-174	+6	-187	-7	-195	-15
3	+0	-2	-2	-8	-8	-6	-6
4	-180	-175	+5	-188	-8	-198	-18
5	+0	-8	-8	-14	-14	-15	-15
6	+0	-3	-3	-10	-10	-10	-10
7	-180	-171	+9	-183	-3	-190	-10
8	-180	-172	+8	-184	-4	-189	-9
9	+0	+1	+1	-5	-5	-4	-4
10	+0	+0	+0	+0	+0	+0	+0
11	+0	-7	-7	-13	-13	-13	-13
12	+0	+4	+4	-3	-3	-4	-4
13	180	-173	-7	180	-5	-194	-14
14	+0	-5	-5	-6	-6	-7	-7
15	-180	-180	+0	-191	-11	-197	-17
16	-180	-174	+6	-185	-5	-194	-14
17	+0	-2	-2	-5	-6	-7	-7
18	+0	-4	-4	-9	-9	-11	-11
19	-180	-170	+10	-181	-1	-190	-10

MEAN DELTA ANG. = +1.44 -7.23 -11.28  
 STD. DEV. FOR DEL. = +3.50 +3.33 +5.22



**APPENDIX C**

**THEORY OF THE ANTENNA AZIMUTH  
BEAM ANGLE STEERING CONTROL**



APPENDIX C  
THEORY OF THE ANTENNA AZIMUTH  
BEAM ANGLE STEERING CONTROL

The antenna azimuth beam angle servomechanism has two inputs which are used to keep the antenna beam pointed at the satellite. The first is the angular rate sensor which produces an output proportional to the vehicle azimuth turn rate. The second is the pilot signal radio link feeding through the antenna beam pattern. By dithering the antenna beam about the nominal beam center, a phase sensitive amplitude modulation is formed on the pilot signal which is directly proportional to the bearing error.

The angular rate sensor has a rapid response characteristic (100 Hz Bandwidth) such that any vehicle turn rate that would move the antenna away from the satellite can be almost instantaneously corrected. There is no inertia in the electronic steering so there is no lag associated with this link. (Even if the antenna had inertia, this would not be a hindrance but a benefit because the inertia would aid in maintaining a constant pointing angle.) Consequently, the angular rate sensor has a short term direct control of the antenna steering.

The angular rate sensor has three shortcomings: 1) the output may have a drift component (an angular rate offset), 2) the scale factor may not be exact (measured rate different from input rate), and 3) it does not know the initial position of the satellite. Fortunately, these deficiencies can be corrected by the radio link.

A mathematical block diagram of the antenna azimuth beam steering servomechanism is shown in Figure C-1. The figure is separated into two main areas, the real world and the servomechanism. The real world provides the inputs to the servomechanism. The major perturbation to the servomechanism is the vehicle turn rate  $\dot{\psi}_i$  in the real world. This is the input along the top of the diagram and is measured by the angular rate sensor. The integral of the turn rate is the vehicle azimuth  $\psi_i$  which is also shown. The difference between the vehicle azimuth and the satellite azimuth  $\psi_s$  is the satellite bearing  $\psi_d$ . The antenna bearing  $\psi_o$  is compared to the satellite bearing via the pilot signal radio link to give the bearing error  $(\psi_d - \psi_o)$ . This error is sensed by the antenna system by producing a modulation index on the received pilot signal proportional to the product of the dither magnitude  $M$  and bearing error. The dither magnitude is under software control



and is made inversely proportional to pilot signal magnitude A. This insures that the error signal voltage is always proportional to bearing error even though the received pilot signal level may fluctuate. In other words, the product MA in the block diagram is held constant by the microprocessor.

The radio link error is accompanied by system Noise N. The combined error signal and noise are amplified by a factor of 50 and converted to equivalent digital numbers by an analog to digital converter (not shown in the mathematical diagram since it has an equivalent gain of 1). The signal and noise are then multiplied by a proportional gain K and (in parallel) by an integral gain G/s. These radio link outputs are added together with the angular rate sensor output ( $\dot{\psi}_i + E$ ) to feed the azimuth integrator 1/s:

If the angular rate sensor were perfect, the error E would be zero and the radio link corrections would also be zero. In this case, the angular rate sensor  $\dot{\psi}_i$  would be equal but opposite in sign to the servomechanism antenna bearing rate  $\dot{\psi}_o$ , and the antenna bearing would always be equal to satellite bearing. If the angular rate sensor error E is not zero, the antenna bearing would not follow the satellite bearing exactly, and a radio link error  $\psi_d - \psi_o$  would appear. In the short term, when the servomechanism loop product  $50 \text{ MAK} (\dot{\psi}_d - \dot{\psi}_o)$  is equal to the angular rate sensor error E, the antenna bearing error will have a value equal to  $E/50\text{MAK}$ . Meanwhile, however, the parallel integral gain G/S will measure this error and remove it during the period K/G. The value for  $1/50\text{MAK}$  is set to 1 sec. and the value for K/G is 30 sec.

From inspection of Figure C-1, the closed loop Laplace transform equation for antenna bearing output  $\psi_o$  as a function of satellite bearing  $\dot{\psi}_d$ , angular rate sensor error E and radio link noise N is given by (remembering that  $\dot{\psi}_d = \dot{\psi}_i$ ):

$$\psi_o = \psi_d + (Es + 50 N (sK + G))/(s^2 + 50 \text{ MAK}s + 50 \text{ MAG})$$

where s is the Laplace transform complex variable. Note from this equation that the output  $\psi_o$  equals the input  $\dot{\psi}_i$  with no delay (except for the angular rate sensor delay which is so small (100 Hz response capability) compared to the vehicle dynamics that it was ignored in the analysis). Any steady state angular rate sensor error E is completely removed as evidenced by the multiplication by the derivative operator s. The receiver noise is passed through an effective single order low pass filter with a half power corner at 1 radian/sec ( $\sim 0.16\text{Hz}$ ) or a noise bandwidth of 0.25Hz. The reason the noise can be so

heavily filtered without affecting the system response is that most of the rapid regulating action is given to the angular rate sensor. The radio link serves only to correct the very slowly varying error in the rate sensor.

The foregoing equation and parameters are those for a normally operating servomechanism after signal acquisition. In order to establish proper initial conditions during a period of 1 second after acquisition, G is set to zero and K is increased by a factor of 20. This increases the radio link loop gain to properly position the antenna since the rate sensor has no angle sense, only rate sense. If the rate sensor is removed from the servomechanism, the increase in radio link gain is continuously maintained. The satellite can still be tracked but the operation will be more noisy because of the increased bandwidth. There will also be a lag in response as shown by the new closed loop equation (with  $G=0$  and  $\dot{\psi}_i + E = 0$ )

$$\psi_o = (50 \text{ MAK } \dot{\psi}_d + 50 \text{ KN}) / (s + 50 \text{ MAK})$$

**APPENDIX D**

**SCHEMATICS AND DIAGRAMS  
OF MSAT-X SYSTEM**

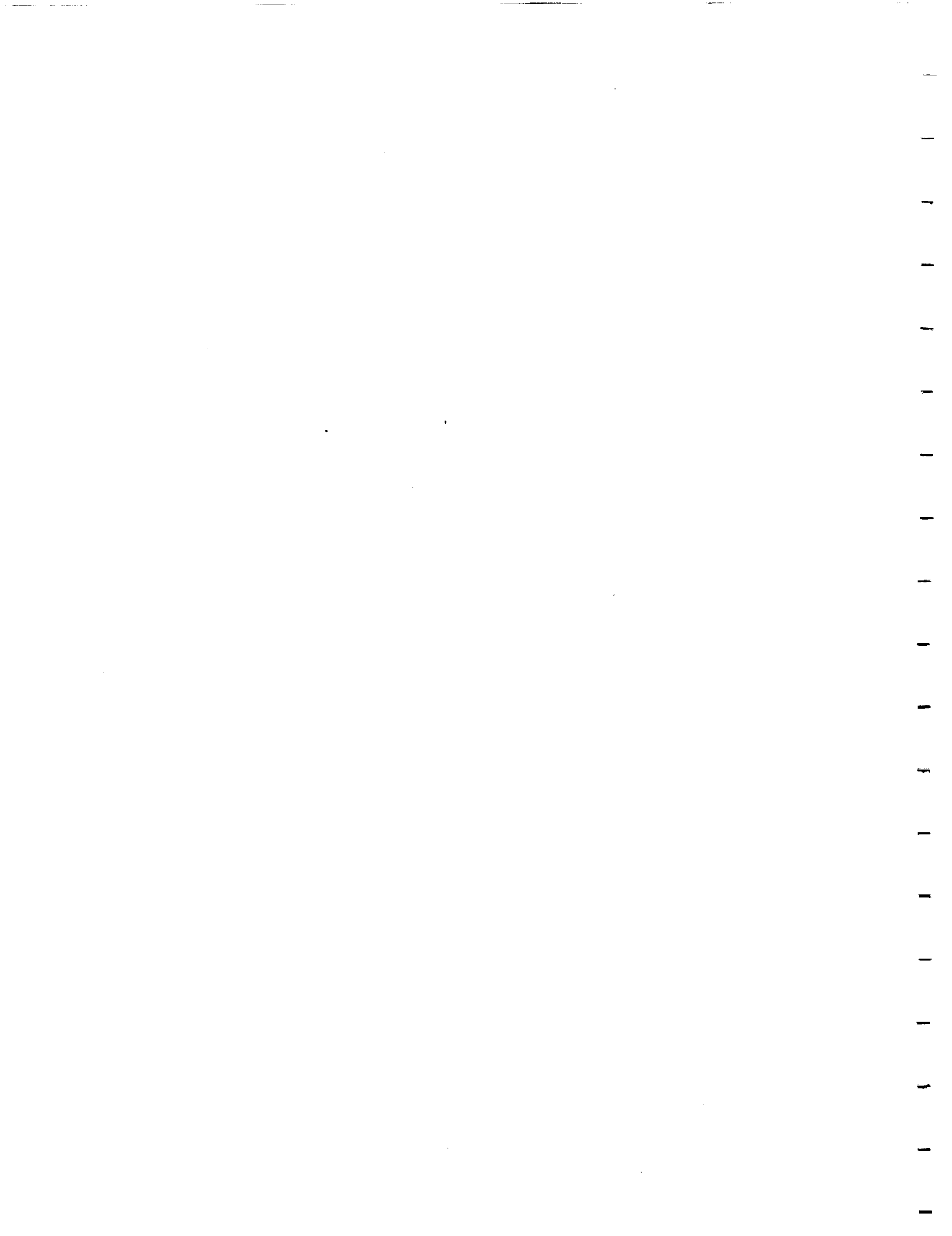
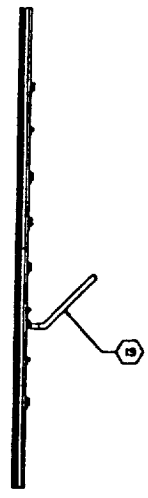
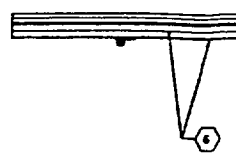


TABLE I - WIRING CHART

WIRE NO.	COLOR	ANTENNA TERM. NO.	J1 PIN NO.	SIGNAL
1	BLE	1	1	-28VDC
2	BRN	2	2	TEST
3	RED	3	3	-5V BIAS
4	ORB	3	4	-5V BIAS
5	YEL	4	5	-5V BIAS
6	BRN	4	6	-5V BIAS
7	BLU	5	7	SER IN
8	VIO	7	8	-5VDC
9	GRY	7	9	-5VDC
10	WHT	8	10	STROBE
11	WHT, BLE	9	11	-28VDC
12	WHT, BRN	10	12	-5V RYM
13	WHT, RED	11	13	GND
14	WHT, ORB	6	14	CLOCK
15	WHT, YEL	12	15	GND
SHLD		12		

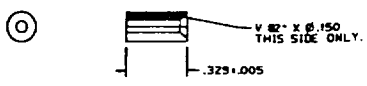
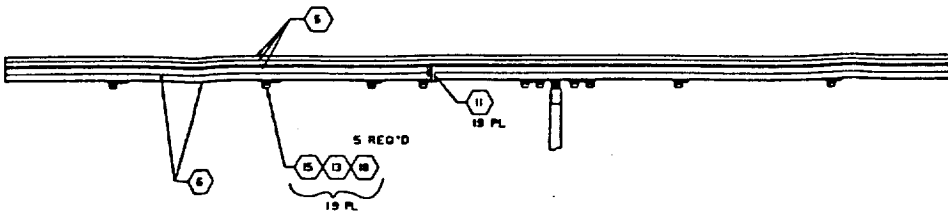


FOLDOUT FRAME

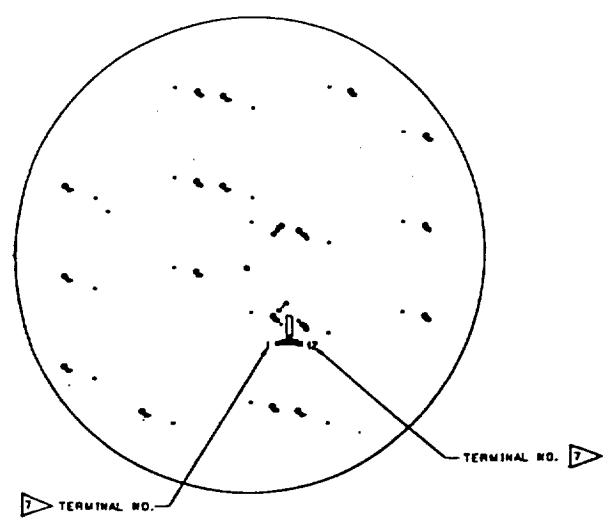
ORIGINAL PAGE IS  
OF POOR QUALITY



REVISIONS		REV	DATE	BY
A	SEE E.O./O.C.M. E19862 S.WEYQINT 87-G-5			



ORIGINAL PAGE IS  
OF POOR QUALITY



FOLDOUT FRAME

ASSY

C-24

STANDARD PROJ. NO.	WORK NO.	REV.
E 58853	1056A0001	A
SCALE 1/2	SHEET 2 OF 2	

Figure D-1. TRE Drawing No. 1056A0001. Antenna Assembly MSAT (Sheet 2 of 2)

D-3







NOTES: UNLESS OTHERWISE SPECIFIED

- 1. INTERPRET DRAWING PER DOD-STD-100.
- 2. SCHEMATIC SHOWN FOR ELEMENT NO. 1 IS TYPICAL FOR ALL ELEMENT NO'S.
- 3. FOR ANTENNA RHCP (RIGHT HAND CIRCULAR POLARIZATION), THE RF I/O MUST BE CONNECTED TO THE 1-PORT OF THE ELEMENT. THE 1-PORT IS DESIGNATED AS THE INPUT OF THE HYBRID WHICH DIRECTLY FEEDS THE CORPORATE LINE THAT EXCITES THE X-AXIS SLOT.

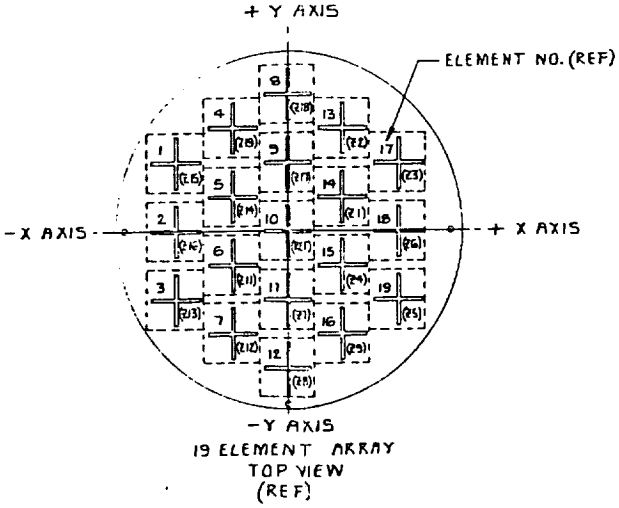
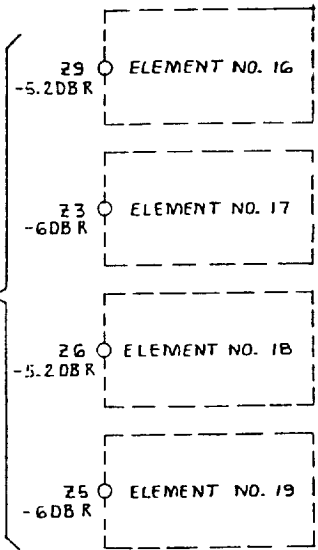
REVISIONS			
REV	DESCRIPTION	DATE	APPROVED

Applicable Engr. Orders	
NO	dup

- 0. 9
- 0. 10
- 10. 11
- 10. 12
- 0. 13
- 0. 14
- 0. 15

BEAM FORMER

RF I/O

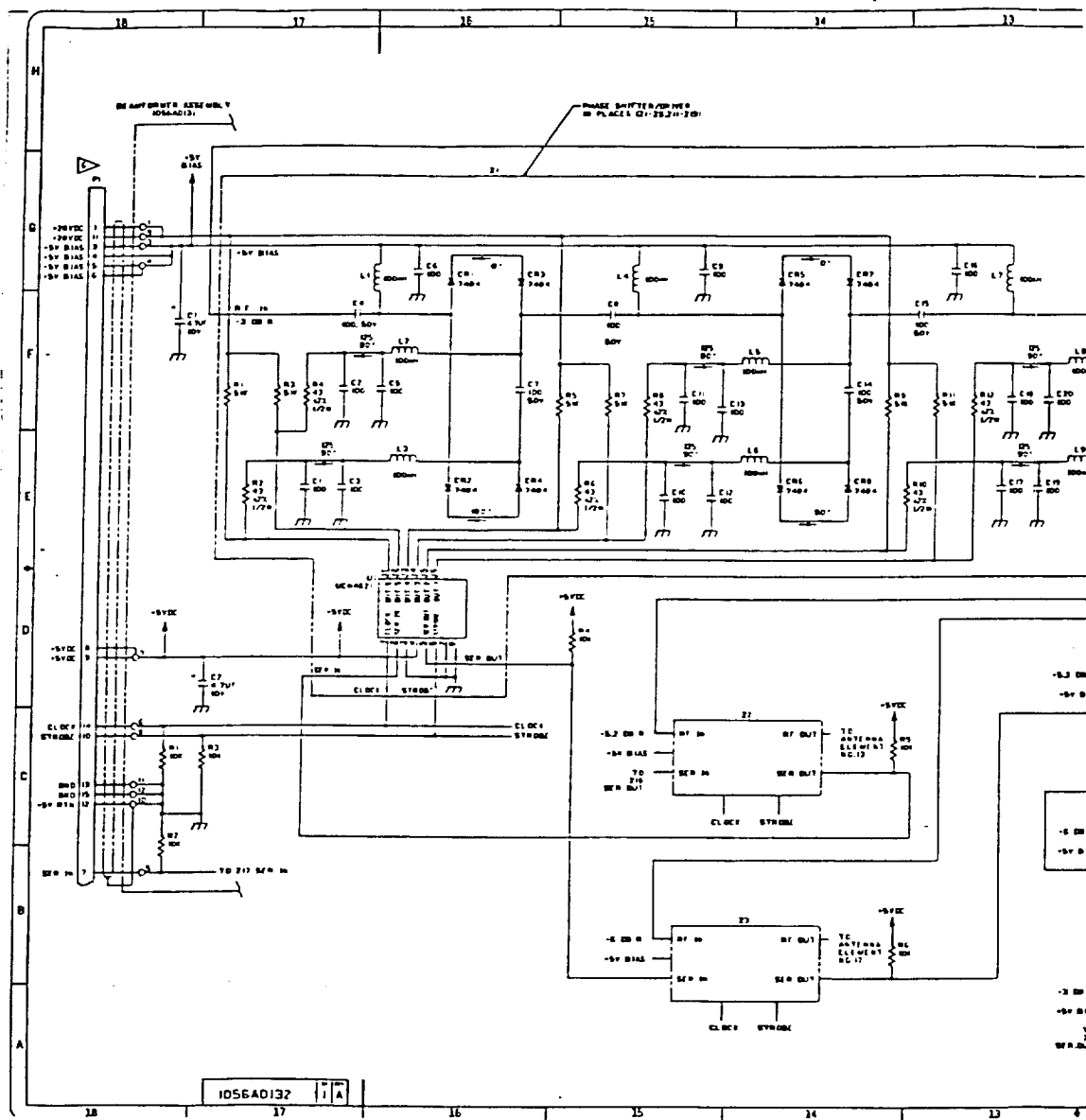


19 ELEMENT ARRAY TOP VIEW (REF)

RELEASE & DATE: <i>Edwards 12-5-27</i>	QTY REQD PER ASSY	FSCM NO.	PART NUMBER	DESCRIPTION	STOCK SIZE	MATERIAL/SPECIFICATION	SEE NOTE	FIND NO.
UNLESS OTHERWISE SPECIFIED: DIMENSIONS ARE IN INCHES AND INCLUDE CHEM APPLIED OR PLATED FINISHES		CONTRACT NUMBER 957468		TELEDYNE RYAN ELECTRONICS 2800 BALBOA AVENUE SAN DIEGO CALIFORNIA 92122				
TOLERANCES		SIGNATURES		DATE				
LINEAR X = .1 XX = .03 XXX = .010	ANGULAR DICK OF SHEET METAL FLANGES = 0° 30'	ORIS CHECK DATE	<i>J. P. ...</i>	<i>12-5-27</i>	ANTENNA - SCHEMATIC DIAGRAM			
DASH NO USED AT NEXT ASSY	NEXT ASSEMBLY	USED ON	PARTS TO BE FREE OF BURRS AND SHARP EDGES	DESIGN ACTIVITY	SIZE	FSCM NO.	DWG NO.	REV
					D	58853	1056A0002	-
APPLICATION		SIMILAR TO:		PROJECT	SCALE	WORK	SHEET 1 OF 1	

Figure D-2. TRE Drawing No. 1056A0002. Antenna Schematic Diagram D-4 2 FOLDOUT FRAME

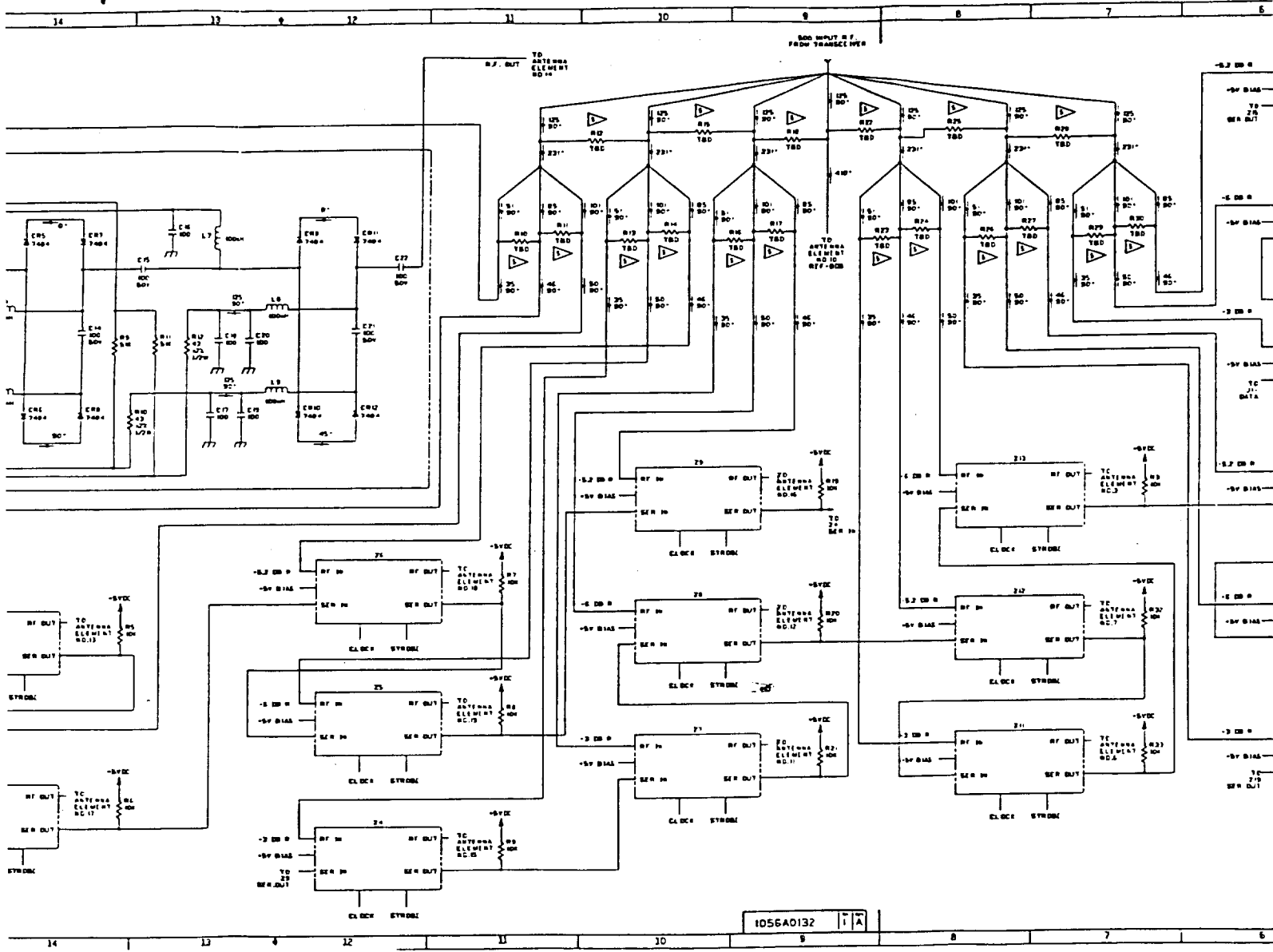




ORIGINAL PAGE IS  
OF POOR QUALITY

FOLDOUT FRAME

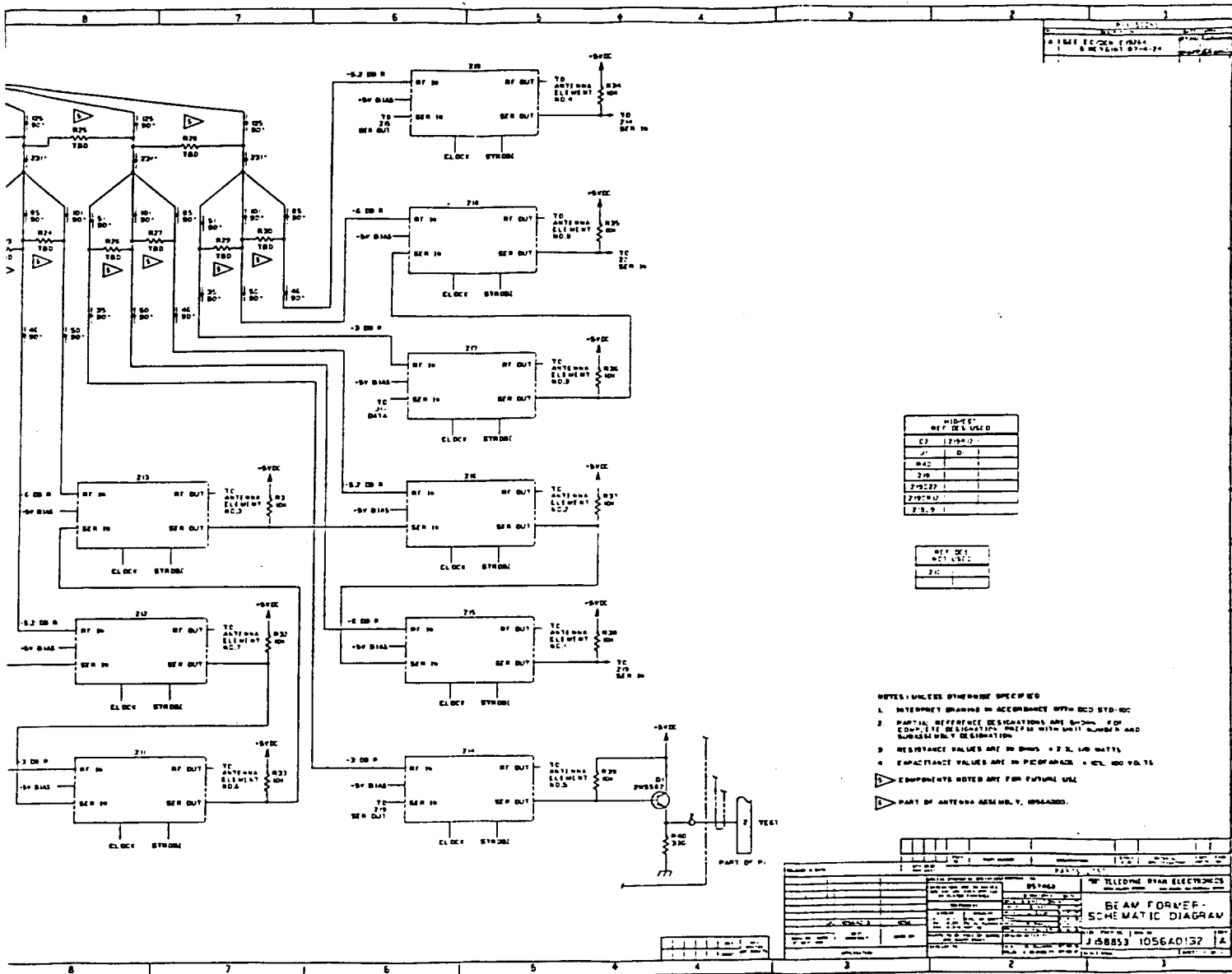




ORIGINAL PAGE IS  
OF POOR QUALITY

FOLDOUT FRAME





- NOTES: UNLESS OTHERWISE SPECIFIED
1. INTERPRET DRAWING IN ACCORDANCE WITH ESD STD-10C
  2. PARTIAL REFERENCE DESIGNATIONS ARE SHOWN FOR EQUALLY SET DESIGNATION PREFIX WITH UNIT NUMBER AND SUBSEQUENTLY DESIGNATION
  3. RESISTANCE VALUES ARE IN OHMS + 2% UNLESS NOTED
  4. CAPACITANCE VALUES ARE IN PICOFARADS + 1% UNLESS NOTED
- ▲ COMPONENTS NOTED ARE FOR FUTURE USE  
 ▼ PART OF ANTENNA ASSEMBLY, ISSUED.

REV.	DATE	BY	CHKD.	APP.	DESCRIPTION
1					BEAM FORMER SCHEMATIC DIAGRAM

TELETYPE BUREAU ELECTRONICS  
 J158853 1056A0132 A

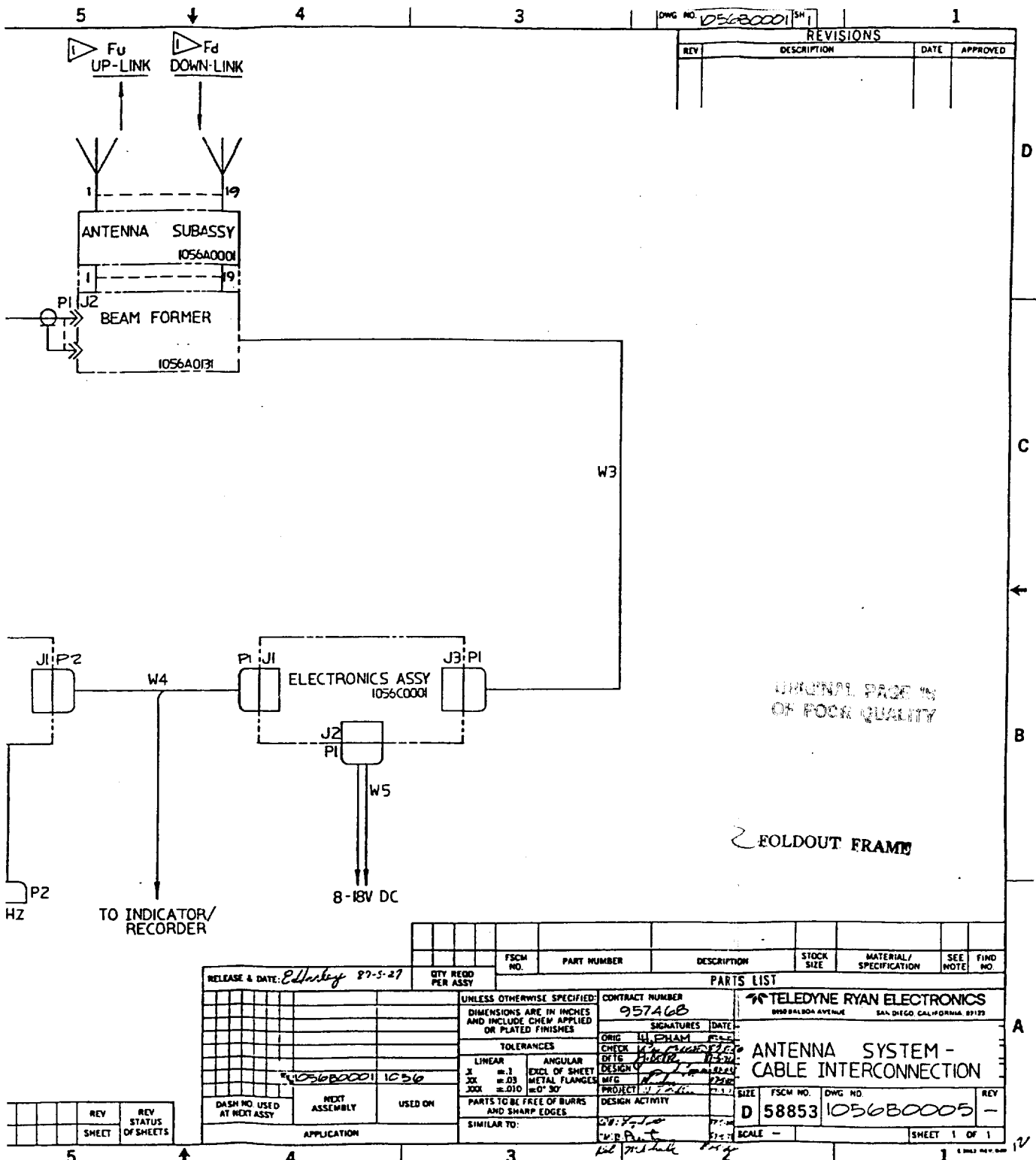
3 FOLDOUT FRAME ORIGINAL PRINTING OF GOOD QUALITY

Figure D-3. TRE Drawing No. 1056A0132. Beamformer Schematic Diagram









REVISIONS			
REV	DESCRIPTION	DATE	APPROVED

ORIGINAL PAGE IN  
OF FOUR QUALITY

FOLDOUT FRAME

REV	REV STATUS OF SHEETS	QTY REQD PER ASSY	FSCM NO.	PART NUMBER	DESCRIPTION	STOCK SIZE	MATERIAL / SPECIFICATION	SEE NOTE	FIND NO.

RELEASE & DATE: <i>Edley 87-5-27</i>	UNLESS OTHERWISE SPECIFIED: DIMENSIONS ARE IN INCHES AND INCLUDE CHAM APPLIED OR PLATED FINISHES	CONTRACT NUMBER <b>957A68</b>	TELEDYNE RYAN ELECTRONICS 8950 BALBOA AVENUE SAN DIEGO, CALIFORNIA 92123
DASH NO USED AT NEXT ASSY	TOLERANCES LINEAR .X = .1 XX = .03 XXX = .010	SIGNATURES (DATE) ORIG: <i>W. B. Pelt</i> CHECK: <i>W. B. Pelt</i> DATE: <i>8/20/87</i> BY: <i>W. B. Pelt</i> PROJECT: <i>1056B</i>	
NEXT ASSEMBLY	EXCL OF SHEET METAL FLANGES NOT 30	DESIGN ACTIVITY	ANTENNA SYSTEM - CABLE INTERCONNECTION
USED ON	PARTS TO BE FREE OF BURRS AND SHARP EDGES	SCALE -	SIZE D FSCM NO. 58853 DWG NO. 1056B0005
APPLICATION	SIMILAR TO:	DATE: <i>8-2-87</i>	REV -

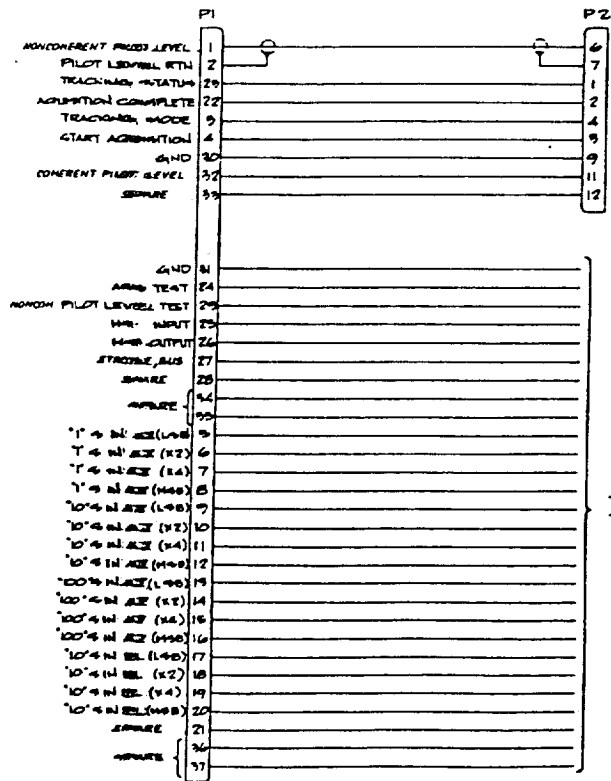
Figure D-4. TRE Drawing No. 1056B0005. Antenna System Cable Interconnection.



NOTES: UNLESS OTHERWISE SPECIFIED

- 1 INTERPRET DRAWING IN ACCORDANCE WITH DD-STD-100
- 2 PERMANENTLY MARK NOMENCLATURE NOTED IN BLACK PER MIL-M-8838, CHARACTERS TO BE VERTICAL GOTHIC OF THE TYPE NOTED.
- 3 PERMANENTLY MARK "W4 58855-103000025" (APPLICABLE W/PIN) PER MIL-M-8838, CHARACTERS SHALL BE VERTICAL GOTHIC, .09 HIGH, LOCATED APPROXIMATELY WHERE SHOWN.
- 4 MARK ON PIN 4, WITH .09 HIGH CHARACTERS, "W4 P1 TO J1 (E.M.M.)"
- 5 MARK ON PIN 4, WITH .09 HIGH CHARACTERS, "W4 P2 TO J1 (R.T.S.)"

ORIGINAL PAGE IS  
OF POOR QUALITY



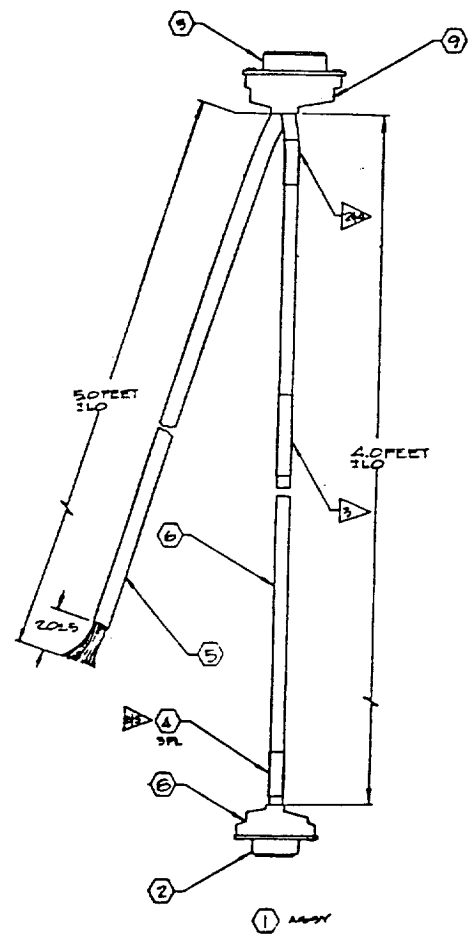
TO CUSTOMER  
TEST CONNECTOR

FOLDOUT FRAME



REVISIONS		DATE	BY
A	SEE COVER & 10211 P. PAGE 07.10.11	11/7/77	J. J. [unclear]

4TD-100  
 ARE  
 OPTIC OF  
 PLUGGABLE (UPPER)  
 AL OPTIC... (DOWN)  
 1 TO J1 (E.M.M.Y.)  
 2 TO J1 (R.T.A.)



ORIGINAL PAGE IS  
 OF POOR QUALITY

Z FOLDOUT FRAME

QTY	DESCRIPTION	UNIT	REVISION	DATE	BY
1	73480 DC 24V-1	FUNCTION SHELL-PLASTIC			
1	73480 DASH 20-1	FUNCTION SHELL-PLASTIC			
AK	M27594-20-1	WIRE-ELEC. UNCL.	2000		
AK	M27594-20-2	WIRE-ELEC. UNCL.	100		
AK	M27594-20-3	WIRE-ELEC. UNCL.	200		
AK	M27594-20-4	WIRE-ELEC. UNCL.	100		
1	M242081-4	CONNECTOR, ELEC.			
1	M242081-2	CONNECTOR, ELEC.			
1		CABLE ASSEMBY			

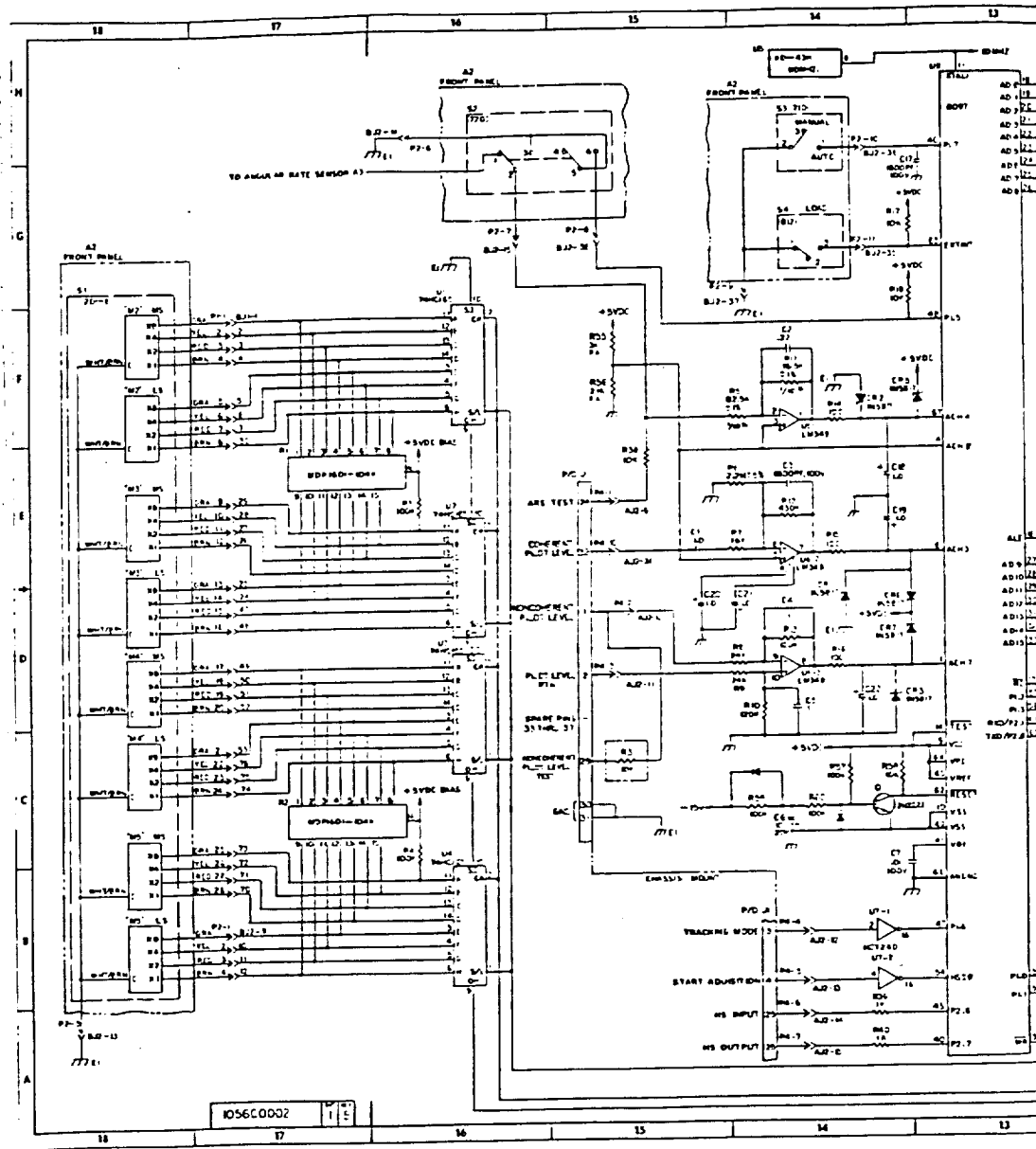
TELETYPE RAN ELECTRONICS  
 CABLE ASSEMBLY,  
 ELECTRONICS ASSEMBLY  
 TEST SET

58853 1056B0025 A

2 1/2 1/2 1/2

Figure D-5. TRE Drawing No. 1056B0025. Cable Assembly, Electronics Assembly/Test Set

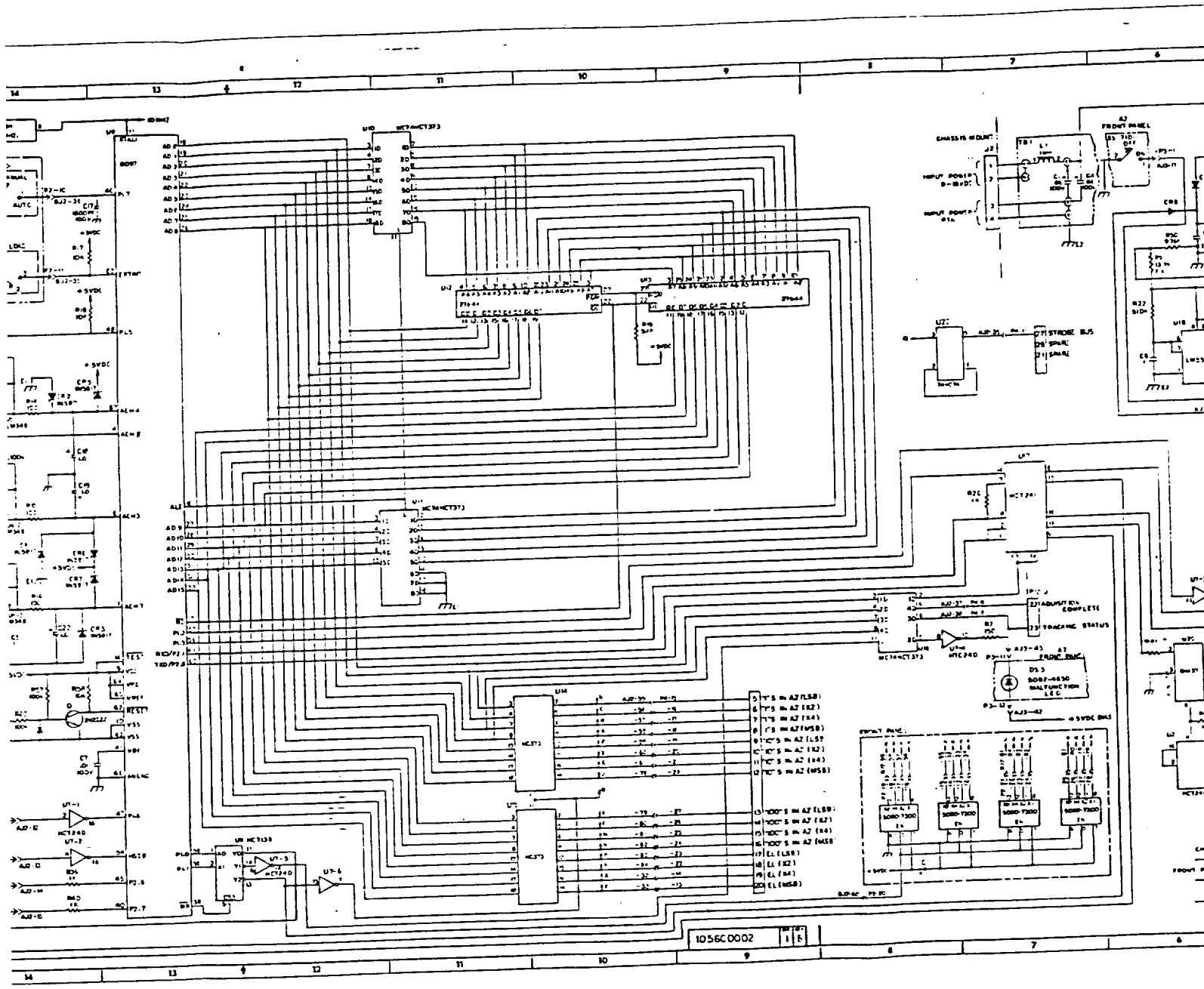




ORIGINAL PAGE IS  
OF POOR QUALITY

FOLDOUT FRAME



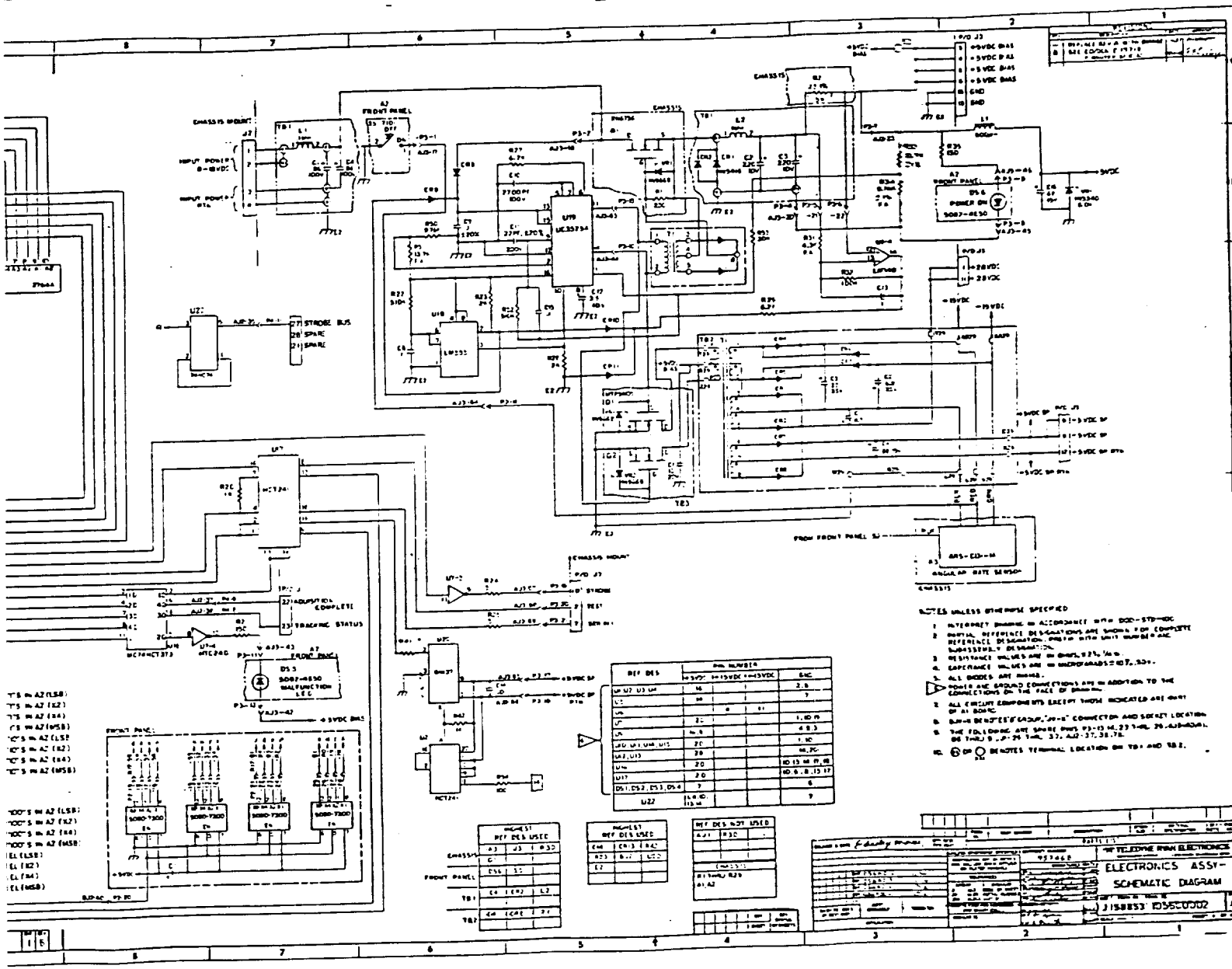


Z FOLDOUT FRAME

ORIGINAL PAGE IS  
OF POOR QUALITY

Figure D-6





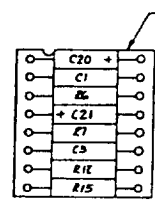
- NOTES UNLESS OTHERWISE SPECIFIED
1. INTERPRET DIMENSIONS IN ACCORDANCE WITH 500-570-000
  2. DIMENSIONAL DIFFERENCES BETWEEN PARTS ARE SHOWN FOR COMPLETE REFERENCE. DIMENSIONS ARE SHOWN WITH UNIT NUMBER AND SUBSTITUTABLE DIMENSIONS.
  3. DIMENSIONAL VALUES ARE IN INCHES, 25.4 MM.
  4. CAPACITANCE VALUES ARE IN MICROFARADS (UF, 10<sup>-6</sup>).
  5. ALL DIMENSIONS ARE IN INCHES.
  6. DIMENSIONS OF GROUND CONNECTIONS ARE IN ADDITION TO THE CONNECTIONS ON THE FACE OF BOARD.
  7. DIMENSIONS OF GROUND CONNECTIONS ARE IN ADDITION TO THE CONNECTIONS ON THE FACE OF BOARD.
  8. THE FOLLOWING ARE SHOWN DIMENSIONS: 1.40, 2.27, 2.54, 3.18, 3.81, 4.45, 5.08, 5.71, 6.35, 6.98, 7.62, 8.25, 8.89, 9.52, 10.16, 10.79, 11.43, 12.06, 12.70, 13.33, 13.97, 14.60, 15.24, 15.87, 16.51, 17.14, 17.78, 18.41, 19.05, 19.68, 20.32, 20.95, 21.59, 22.22, 22.86, 23.50, 24.13, 24.77, 25.40, 26.04, 26.67, 27.31, 27.94, 28.58, 29.22, 29.85, 30.49, 31.12, 31.76, 32.39, 33.03, 33.66, 34.30, 34.93, 35.57, 36.20, 36.84, 37.47, 38.11, 38.74, 39.38, 40.01, 40.65, 41.28, 41.92, 42.55, 43.19, 43.82, 44.46, 45.09, 45.73, 46.36, 47.00, 47.63, 48.27, 48.90, 49.54, 50.17, 50.81, 51.44, 52.08, 52.71, 53.35, 53.98, 54.62, 55.25, 55.89, 56.52, 57.16, 57.79, 58.43, 59.06, 59.70, 60.33, 60.97, 61.60, 62.24, 62.87, 63.51, 64.14, 64.78, 65.41, 66.05, 66.68, 67.32, 67.95, 68.59, 69.22, 69.86, 70.49, 71.13, 71.76, 72.40, 73.03, 73.67, 74.30, 74.94, 75.57, 76.21, 76.84, 77.48, 78.11, 78.75, 79.38, 80.02, 80.65, 81.29, 81.92, 82.56, 83.19, 83.83, 84.46, 85.10, 85.73, 86.37, 87.00, 87.64, 88.27, 88.91, 89.54, 90.18, 90.81, 91.45, 92.08, 92.72, 93.35, 93.99, 94.62, 95.26, 95.89, 96.53, 97.16, 97.80, 98.43, 99.07, 99.70, 100.34, 100.97, 101.61, 102.24, 102.88, 103.51, 104.15, 104.78, 105.42, 106.05, 106.69, 107.32, 107.96, 108.59, 109.23, 109.86, 110.50, 111.13, 111.77, 112.40, 113.04, 113.67, 114.31, 114.94, 115.58, 116.21, 116.85, 117.48, 118.12, 118.75, 119.39, 120.02, 120.66, 121.29, 121.93, 122.56, 123.20, 123.83, 124.47, 125.10, 125.74, 126.37, 127.01, 127.64, 128.28, 128.91, 129.55, 130.18, 130.82, 131.45, 132.09, 132.72, 133.36, 133.99, 134.63, 135.26, 135.90, 136.53, 137.17, 137.80, 138.44, 139.07, 139.71, 140.34, 140.98, 141.61, 142.25, 142.88, 143.52, 144.15, 144.79, 145.42, 146.06, 146.69, 147.33, 147.96, 148.60, 149.23, 149.87, 150.50, 151.14, 151.77, 152.41, 153.04, 153.68, 154.31, 154.95, 155.58, 156.22, 156.85, 157.49, 158.12, 158.76, 159.39, 160.03, 160.66, 161.30, 161.93, 162.57, 163.20, 163.84, 164.47, 165.11, 165.74, 166.38, 167.01, 167.65, 168.28, 168.92, 169.55, 170.19, 170.82, 171.46, 172.09, 172.73, 173.36, 174.00, 174.63, 175.27, 175.90, 176.54, 177.17, 177.81, 178.44, 179.08, 179.71, 180.35, 180.98, 181.62, 182.25, 182.89, 183.52, 184.16, 184.79, 185.43, 186.06, 186.70, 187.33, 187.97, 188.60, 189.24, 189.87, 190.51, 191.14, 191.78, 192.41, 193.05, 193.68, 194.32, 194.95, 195.59, 196.22, 196.86, 197.49, 198.13, 198.76, 199.40, 200.03, 200.67, 201.30, 201.94, 202.57, 203.21, 203.84, 204.48, 205.11, 205.75, 206.38, 207.02, 207.65, 208.29, 208.92, 209.56, 210.19, 210.83, 211.46, 212.10, 212.73, 213.37, 214.00, 214.64, 215.27, 215.91, 216.54, 217.18, 217.81, 218.45, 219.08, 219.72, 220.35, 220.99, 221.62, 222.26, 222.89, 223.53, 224.16, 224.80, 225.43, 226.07, 226.70, 227.34, 227.97, 228.61, 229.24, 229.88, 230.51, 231.15, 231.78, 232.42, 233.05, 233.69, 234.32, 234.96, 235.59, 236.23, 236.86, 237.50, 238.13, 238.77, 239.40, 240.04, 240.67, 241.31, 241.94, 242.58, 243.21, 243.85, 244.48, 245.12, 245.75, 246.39, 247.02, 247.66, 248.29, 248.93, 249.56, 250.20, 250.83, 251.47, 252.10, 252.74, 253.37, 254.01, 254.64, 255.28, 255.91, 256.55, 257.18, 257.82, 258.45, 259.09, 259.72, 260.36, 260.99, 261.63, 262.26, 262.90, 263.53, 264.17, 264.80, 265.44, 266.07, 266.71, 267.34, 267.98, 268.61, 269.25, 269.88, 270.52, 271.15, 271.79, 272.42, 273.06, 273.69, 274.33, 274.96, 275.60, 276.23, 276.87, 277.50, 278.14, 278.77, 279.41, 280.04, 280.68, 281.31, 281.95, 282.58, 283.22, 283.85, 284.49, 285.12, 285.76, 286.39, 287.03, 287.66, 288.30, 288.93, 289.57, 290.20, 290.84, 291.47, 292.11, 292.74, 293.38, 294.01, 294.65, 295.28, 295.92, 296.55, 297.19, 297.82, 298.46, 299.09, 299.73, 300.36, 301.00, 301.63, 302.27, 302.90, 303.54, 304.17, 304.81, 305.44, 306.08, 306.71, 307.35, 307.98, 308.62, 309.25, 309.89, 310.52, 311.16, 311.79, 312.43, 313.06, 313.70, 314.33, 314.97, 315.60, 316.24, 316.87, 317.51, 318.14, 318.78, 319.41, 320.05, 320.68, 321.32, 321.95, 322.59, 323.22, 323.86, 324.49, 325.13, 325.76, 326.40, 327.03, 327.67, 328.30, 328.94, 329.57, 330.21, 330.84, 331.48, 332.11, 332.75, 333.38, 334.02, 334.65, 335.29, 335.92, 336.56, 337.19, 337.83, 338.46, 339.10, 339.73, 340.37, 341.00, 341.64, 342.27, 342.91, 343.54, 344.18, 344.81, 345.45, 346.08, 346.72, 347.35, 347.99, 348.62, 349.26, 349.89, 350.53, 351.16, 351.80, 352.43, 353.07, 353.70, 354.34, 354.97, 355.61, 356.24, 356.88, 357.51, 358.15, 358.78, 359.42, 360.05, 360.69, 361.32, 361.96, 362.59, 363.23, 363.86, 364.50, 365.13, 365.77, 366.40, 367.04, 367.67, 368.31, 368.94, 369.58, 370.21, 370.85, 371.48, 372.12, 372.75, 373.39, 374.02, 374.66, 375.29, 375.93, 376.56, 377.20, 377.83, 378.47, 379.10, 379.74, 380.37, 381.01, 381.64, 382.28, 382.91, 383.55, 384.18, 384.82, 385.45, 386.09, 386.72, 387.36, 387.99, 388.63, 389.26, 389.90, 390.53, 391.17, 391.80, 392.44, 393.07, 393.71, 394.34, 394.98, 395.61, 396.25, 396.88, 397.52, 398.15, 398.79, 399.42, 400.06, 400.69, 401.33, 401.96, 402.60, 403.23, 403.87, 404.50, 405.14, 405.77, 406.41, 407.04, 407.68, 408.31, 408.95, 409.58, 410.22, 410.85, 411.49, 412.12, 412.76, 413.39, 414.03, 414.66, 415.30, 415.93, 416.57, 417.20, 417.84, 418.47, 419.11, 419.74, 420.38, 421.01, 421.65, 422.28, 422.92, 423.55, 424.19, 424.82, 425.46, 426.09, 426.73, 427.36, 428.00, 428.63, 429.27, 429.90, 430.54, 431.17, 431.81, 432.44, 433.08, 433.71, 434.35, 434.98, 435.62, 436.25, 436.89, 437.52, 438.16, 438.79, 439.43, 440.06, 440.70, 441.33, 441.97, 442.60, 443.24, 443.87, 444.51, 445.14, 445.78, 446.41, 447.05, 447.68, 448.32, 448.95, 449.59, 450.22, 450.86, 451.49, 452.13, 452.76, 453.40, 454.03, 454.67, 455.30, 455.94, 456.57, 457.21, 457.84, 458.48, 459.11, 459.75, 460.38, 461.02, 461.65, 462.29, 462.92, 463.56, 464.19, 464.83, 465.46, 466.10, 466.73, 467.37, 468.00, 468.64, 469.27, 469.91, 470.54, 471.18, 471.81, 472.45, 473.08, 473.72, 474.35, 474.99, 475.62, 476.26, 476.89, 477.53, 478.16, 478.80, 479.43, 480.07, 480.70, 481.34, 481.97, 482.61, 483.24, 483.88, 484.51, 485.15, 485.78, 486.42, 487.05, 487.69, 488.32, 488.96, 489.59, 490.23, 490.86, 491.50, 492.13, 492.77, 493.40, 494.04, 494.67, 495.31, 495.94, 496.58, 497.21, 497.85, 498.48, 499.12, 499.75, 500.39, 501.02, 501.66, 502.29, 502.93, 503.56, 504.20, 504.83, 505.47, 506.10, 506.74, 507.37, 508.01, 508.64, 509.28, 509.91, 510.55, 511.18, 511.82, 512.45, 513.09, 513.72, 514.36, 514.99, 515.63, 516.26, 516.90, 517.53, 518.17, 518.80, 519.44, 520.07, 520.71, 521.34, 521.98, 522.61, 523.25, 523.88, 524.52, 525.15, 525.79, 526.42, 527.06, 527.69, 528.33, 528.96, 529.60, 530.23, 530.87, 531.50, 532.14, 532.77, 533.41, 534.04, 534.68, 535.31, 535.95, 536.58, 537.22, 537.85, 538.49, 539.12, 539.76, 540.39, 541.03, 541.66, 542.30, 542.93, 543.57, 544.20, 544.84, 545.47, 546.11, 546.74, 547.38, 548.01, 548.65, 549.28, 549.92, 550.55, 551.19, 551.82, 552.46, 553.09, 553.73, 554.36, 555.00, 555.63, 556.27, 556.90, 557.54, 558.17, 558.81, 559.44, 560.08, 560.71, 561.35, 561.98, 562.62, 563.25, 563.89, 564.52, 565.16, 565.79, 566.43, 567.06, 567.70, 568.33, 568.97, 569.60, 570.24, 570.87, 571.51, 572.14, 572.78, 573.41, 574.05, 574.68, 575.32, 575.95, 576.59, 577.22, 577.86, 578.49, 579.13, 579.76, 580.40, 581.03, 581.67, 582.30, 582.94, 583.57, 584.21, 584.84, 585.48, 586.11, 586.75, 587.38, 588.02, 588.65, 589.29, 589.92, 590.56, 591.19, 591.83, 592.46, 593.10, 593.73, 594.37, 595.00, 595.64, 596.27, 596.91, 597.54, 598.18, 598.81, 599.45, 600.08, 600.72, 601.35, 601.99, 602.62, 603.26, 603.89, 604.53, 605.16, 605.80, 606.43, 607.07, 607.70, 608.34, 608.97, 609.61, 610.24, 610.88, 611.51, 612.15, 612.78, 613.42, 614.05, 614.69, 615.32, 615.96, 616.59, 617.23, 617.86, 618.50, 619.13, 619.77, 620.40, 621.04, 621.67, 622.31, 622.94, 623.58, 624.21, 624.85, 625.48, 626.12, 626.75, 627.39, 628.02, 628.66, 629.29, 629.93, 630.56, 631.20, 631.83, 632.47, 633.10, 633.74, 634.37, 635.01, 635.64, 636.28, 636.91, 637.55, 638.18, 638.82, 639.45, 640.09, 640.72, 641.36, 641.99, 642.63, 643.26, 643.90, 644.53, 645.17, 645.80, 646.44, 647.07, 647.71, 648.34, 648.98, 649.61, 650.25, 650.88, 651.52, 652.15, 652.79, 653.42, 654.06, 654.69, 655.33, 655.96, 656.60, 657.23, 657.87, 658.50, 659.14, 659.77, 660.41, 661.04, 661.68, 662.31, 662.95, 663.58, 664.22, 664.85, 665.49, 666.12, 666.76, 667.39, 668.03, 668.66, 669.30, 669.93, 670.57, 671.20, 671.84, 672.47, 673.11, 673.74, 674.38, 675.01, 675.65, 676.28, 676.92, 677.55, 678.19, 678.82, 679.46, 680.09, 680.73, 681.36, 682.00, 682.63, 683.27, 683.90, 684.54, 685.17, 685.81, 686.44, 687.08, 687.71, 688.35, 688.98, 689.62, 690.25, 690.89, 691.52, 692.16, 692.79, 693.43, 694.06, 694.70, 695.33, 695.97, 696.60, 697.24, 697.87, 698.51, 699.14, 699.78, 700.41, 701.05, 701.68, 702.32, 702.95, 703.59, 704.22, 704.86, 705.49, 706.13, 706.76, 707.40, 708.03, 708.67, 709.30, 709.94, 710.57, 711.21, 711.84, 712.48, 713.11, 713.75, 714.38, 715.02, 715.65, 716.29, 716.92, 717.56, 718.19, 718.83, 719.46, 720.10, 720.73, 721.37, 722.00, 722.64, 723.27, 723.91, 724.54, 725.18, 725.81, 726.45, 727.08, 727.72, 728.35, 728.99, 729.62, 730.26, 730.89, 731.53, 732.16, 732.80, 733.43, 734.07, 734.70, 735.34, 735.97, 736.61, 737.24, 737.88, 738.51, 739.15, 739.78, 740.42, 741.05, 741.69, 742.32, 742.96, 743.59, 744.23, 744.86, 745.50, 746.13, 746.77, 747.40, 748.04, 748.67, 749.31, 749.94, 750.58, 751.21, 751.85, 752.48, 753.12, 753.75, 754.39, 755.02, 755.66, 756.29, 756.93, 757.56, 758.20, 758.83, 759.47, 760.10, 760.74, 761.37, 762.01, 762.64, 763.28, 763.91, 764.55, 765.18, 765.82, 766.45, 767.09, 767.72, 768.36, 768.99, 769.63, 770.26, 770.90, 771.53, 772.17, 772.80, 773.44, 774.07, 774.71, 775.34, 775.98, 776.61, 777.25, 777.88, 778.52, 779.15, 779.79, 780.42, 781.06, 781.69, 782.33, 782.96, 783.60, 784.23, 784.87, 785.50, 786.14, 786.77, 787.41, 788.04, 788.68, 789.31, 789.95, 790.58, 791.22, 791.85, 792.49, 793.12, 793.76, 794.39, 795.03, 795.66, 796.30, 796.93, 797.57, 798.20, 798.84, 799.47, 800.11, 800.74, 801.38, 802.01, 802.65, 803.28, 803.92, 804.55, 805.19, 805.82, 806.46, 807.09, 807.73, 808.36, 809.00, 809.63, 810.27, 810.90, 811.54, 812.17, 812.81, 813.44, 814.08, 814.71, 815.35, 815.98, 816.62, 817.25, 817.89, 818.52, 819.16, 819.79, 820.43, 821.06, 821.70, 822.33, 822.97, 823.60, 824.24, 824.87, 825.51, 826.14, 826.78, 827.41, 828.05, 828.68, 829.32, 829.95, 830.59, 831.22, 831.86, 832.49, 833.13, 833.76, 834.40, 835.03, 835.67, 836.30, 836.94, 837.57, 838.21, 838.84, 839.48, 840.11, 840.75, 841.38, 842.02, 842.65, 843.29, 843.92, 844.56, 845.19, 845.83, 846.46, 847.10, 847.73, 848.37, 849.00, 849.64, 850.27, 850.91, 851.54, 852.18, 852.81, 853.45, 854.08, 854.72, 855.35, 855.99, 856.62, 857.26, 857.89, 858.53, 859.16, 859.80, 860.43, 861.07, 861.70, 862.34, 862.97, 863.61, 864.24, 864.88, 865.51, 866.15, 866.78, 867.42, 868.05, 868.69, 869.32, 869.96, 870.59, 871.23, 871.86, 872.50, 873.13, 873.77, 874.40, 875.04, 875.67, 876.31, 876.94, 877.58, 878.21, 878.85, 879.48, 880.12, 880.75, 881.39, 882.02, 882.66, 883.29, 883.93, 884.56, 885.20, 885.83, 886.47, 887.10, 887.74, 888.37, 889.01, 889.64, 890.28, 890.91, 891.55, 892.18, 892.82, 893.45, 894.09, 894.72, 895.36, 895.99, 896.63, 897.26, 897.90, 898.53, 899.17, 899.80, 900.44, 901.07, 901.71, 902.34, 902.98, 903.61, 904.25, 904.88, 905.52, 906.15, 906.79, 907.42, 908.06, 908.69, 909.33, 909.96, 910.60, 911.23, 911.87, 912.50, 913.14, 913.77, 914.41, 915.04, 915.68, 916.31, 916.95, 917.58, 918.22, 918.85, 919.49, 920.12, 920.76, 921.39, 922.03, 922.66, 923.30, 923.93, 924.57, 925.20, 925.84, 926.47, 927.11, 927.74, 928.38, 929.01, 929.65, 930.28, 930.92, 931.55, 932.19, 932.82, 933.46, 934.09, 934.73, 935.36, 936.00, 936.63, 937.27, 937.90, 938.54, 939.17, 939.81, 940.44, 941.08, 941.71, 942.35, 942.98, 943.62, 944.25, 944.89, 945.52, 946.16, 946.79, 947.43, 948.06, 948.70, 949.33, 949.97, 950.60, 951.24, 951.87, 952.51, 953.14, 953.78, 954.41, 955.05, 955.68, 956.32, 956.95, 957.59, 958.22, 958.86, 959.49, 960.13, 960.76, 961.40, 962.03, 962.67, 963.30, 963.94, 964.57, 965.21, 965.84, 966.48, 967.11, 967.75, 968.38, 969.02, 969.65, 970.29



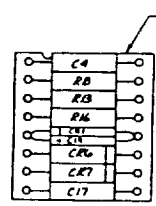
NOTES: UNLESS OTHERWISE SPECIFIED:

1. INTERPRET DRAWING IN ACCORDANCE WITH MIL-STD-883 - AND
2. ROUTE ALL PINS AND LEADS TO ALL BOARD CONTACTS (BARE LEADS).
3. PERMANENT MARK LABELS DESIGNATION - (APPLICABLE SUFFIX), USUAL, FOR ALL COMPONENTS SHALL BE VERTICAL CENTER, BY PINN LOCATE APPROXIMATE POSITION.
4. PERMANENTLY MARK REF DES J, K & L. MARK FOR REF, CHARACTERISTICS SHOWN BY REFERENCE. ALL MARKS SHALL BE PERMANENT.
5. BOARD SOCKET, PIN 12, TO BOARD, PIN 6, BY WIRE BONDING, PIN 12.
6. BEFORE WIRE BONDING, INSTALL WIRE WELD ID PLATES, PIN 12, PIN 11, SOLDER WITH APPROPRIATE REF DES BY FILE DUMP IN THE BOARD ID PLATE TO CORRELATE WITH COMPONENTS ON BOARD LIST.
7. "E" REF DES ARE FOR WIRE PURPOSES ONLY.
8. SOLDER FOR MIL-STD-883 REQUIREMENT 5 ISLAND, PIN 12.
9. INSTALL WIRE, SOLDERLESS WIRE WELD, PINN, FOR MIL-STD-883.

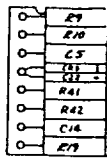
H  
G  
F  
E  
D  
C  
B  
A



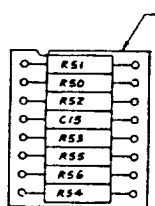
Z3



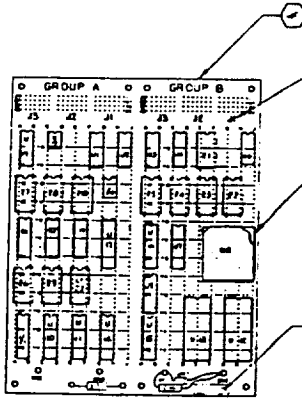
Z4



Z5



Z10



USE ONLY BOARD OF HIGH QUALITY

EOLDOUT FRAME

ASSY

6 7 6







NOTES: UNLESS OTHERWISE SPECIFIED.

1. INTERPRET DRAWING IN ACCORDANCE WITH DDG-STD-400.
2. PERMANENTLY MARK DIMENSIONS UNLESS OTHERWISE APPLICABLE (DIMENSIONS SHOWN IN THIS DRAWING ARE IN INCHES). CHARACTERS SHALL BE VERTICAL, CORNER, 28 HOUR LOCATE APPROPRIATELY WHERE SHOWN.
3. ALPHA-NUMERIC CHARACTERS (FOR IDENTIFICATION) SHOWN ARE INTENDED AS AN ASSEMBLY GUIDE ONLY AND ARE NOT TO BE MARKED BY THE CIRCUIT BOARD.
4. BOND COMPONENT BODIES TO CIRCUIT BOARD WERE ADHESIVE, FM 13.
5. FOR COMPONENT CONNECTIONS, SEE TABLE I.
6. FOR JUMPER CONNECTIONS, SEE TABLE II.
7. REMOVE .062 WIDE SECTION OF COPPER TRACE AS SHOWN.

TABLE I

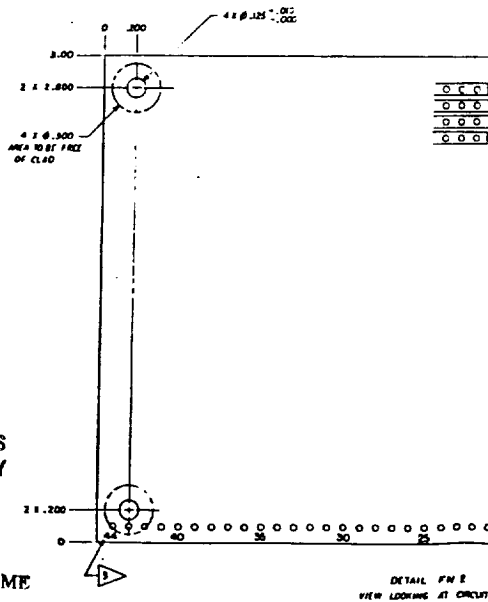
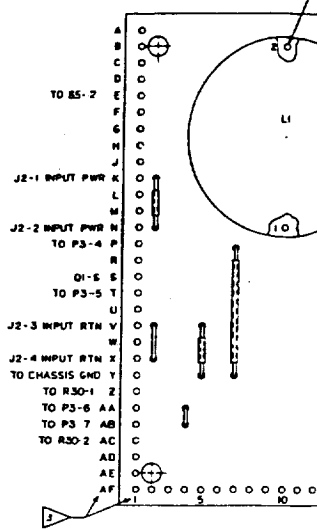
COMPONENT	TO
C1 (+)	B79
C1 (-)	V49
C2 (+)	B37
C2 (-)	V37
C3 (+)	E47
C3 (-)	V42
CR1-K	M34
CR1-A	V34
L1-1	H40
L1-2	H40
L2-1	H28
L2-2	B78

TABLE II

JUMPER	FROM	TO
1	K2	M2
2	V2	E2
3	A4	B4
4	V5	V5
5	P1	V7
6	A45	A45
7	B17	E17
8	H22	S22
9	T25	Z25
10	E39	T39
11	B40	E40

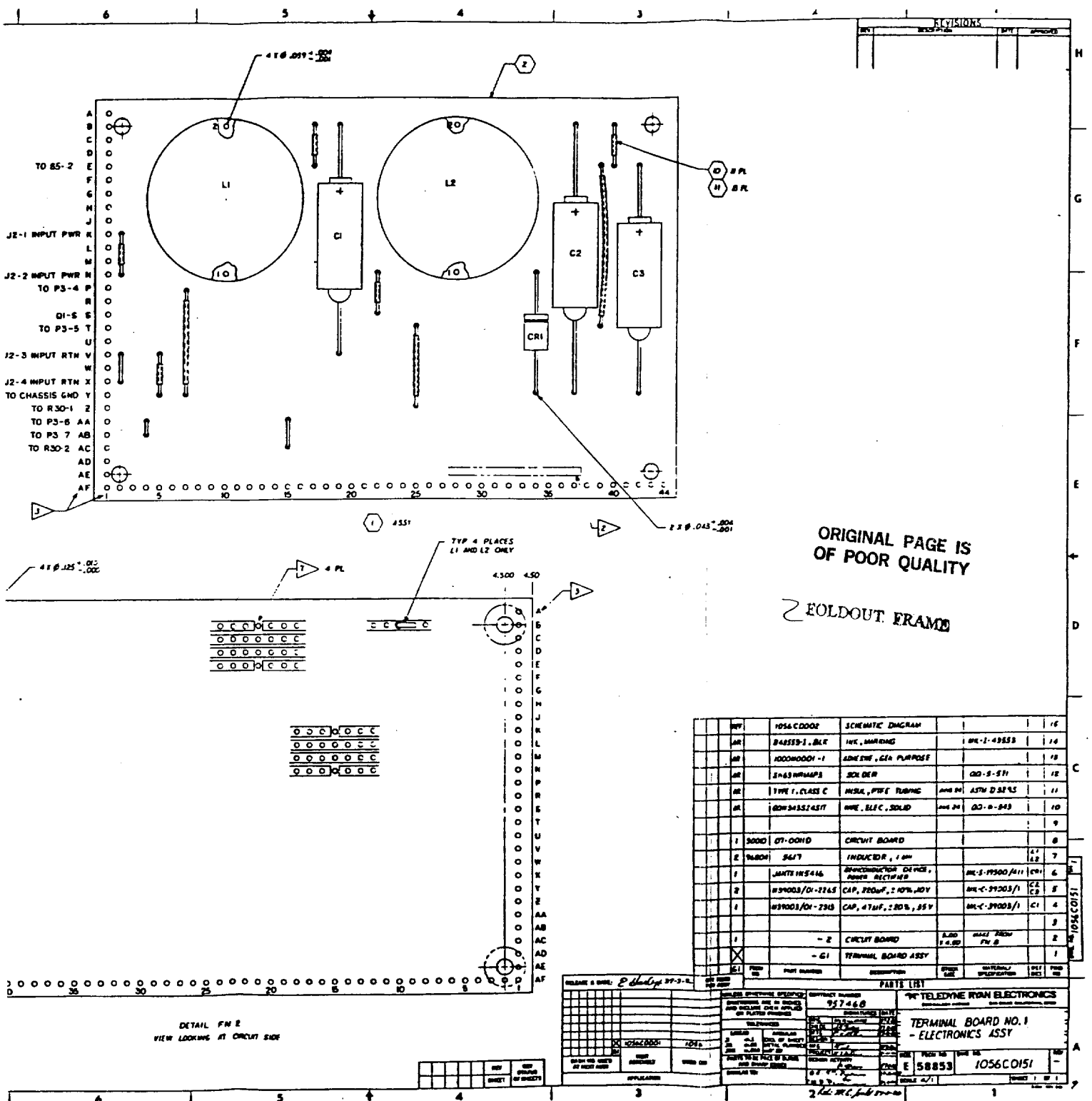
ORIGINAL PAGE IS OF POOR QUALITY

FOLDOUT FRAME



DETAIL FM 8 VIEW LOOKING AT CIRCUIT





ORIGINAL PAGE IS  
OF POOR QUALITY

FOLDOUT FRAME

REV	DESCRIPTION	DATE	BY	CHKD	APPROVED
1	1056C0002 SCHEMATIC DIAGRAM				
2	BASES-1, BLK INK, MARKING				
3	ADHESIVE, GA PURPOSE				
4	SOLDER				
5	INSUL, PTFE TUBING				
6	WIRE, ELEC, SOLID				
7					
8	3000 07-0010 CIRCUIT BOARD				
9	INDUCTOR, 1 OHM				
10	DIODES 1N5416 DIODE/CONDUCTOR DEVICE, POWER RECTIFIER				
11	39003/01-2245 CAP, 220UF, 250V, 50% ADJ				
12	39003/01-230 CAP, 47UF, 250V, 55V				
13	- 2 CIRCUIT BOARD				
14	- G1 TERMINAL BOARD ASSY				

DETAIL FNR  
VIEW LOOKING AT CIRCUIT SIDE

RELEASE & SERIAL: P. 27-3-1		CONTRACT NUMBER: 927460		TELEDYNE IRAN ELECTRONICS	
MATERIAL SPECIFICATIONS		DRAWING NUMBER: 1056C0151		TERMINAL BOARD NO. 1	
MATERIALS		DATE: 10/1/51		ELECTRONICS ASSY	
MATERIALS		DATE: 10/1/51		E 58853 1056C0151	
MATERIALS		DATE: 10/1/51		E 58853 1056C0151	

Figure D-8. TRE Drawing No. 1056C0151. Terminal Board No. 1 - Electronic Assembly



UNLESS OTHERWISE SPECIFIED.

1. INTERPRET DRAWING IN ACCORDANCE WITH DDG-STD-002.
2. UNLESS OTHERWISE SPECIFIED, APPLICABLE DDG-STD-002 SHALL BE USED. DIMENSIONS SHALL BE METRIC. SOME, IF NECESSARY, LOCATE APPROXIMATELY AS SHOWN.
3. ALPHABETIC CHARACTERS FROM IDENTIFICATION AND REFERENCE INDICATORS SHOWN ARE INTENDED AS AN ASSEMBLY CLAD ONLY AND ARE NOT TO BE MARKED ON BOARD.
4. FOR COMPONENT CONNECTIONS SEE TABLE I.
5. FOR JUMPER CONNECTIONS SEE TABLE II.
6. FINISH .030 MET SECTION FROM COPPER CONDUCTOR AS SHOWN.
7. REMOVE .042 MET SECTION FROM COPPER CONDUCTOR AS SHOWN.
8. BOND BOARDS OF ALL COMPONENTS TO CREST BOARD USING ADHESIVE, FM B.

ORIGINAL PAGE IS  
OF POOR QUALITY

TABLE I

COMPONENT	TO
T1-1	L8
T1-2	M9
T1-3	M11
T1-4	L12
T1-5	J12
T1-6	M11
T1-7	M8
T1-8	J8
C1(+)	Y15
C1(-)	L15
C2(+)	L21
C2(-)	AA21
C3(+)	AB24
C3(-)	L24
CR1-K	Y17
CR1-A	M17
CR2-K	Y8
CR2-A	M8
CR3-K	M4
CR3-A	AA4
CR4-K	AB9
CR4-A	M9
CR5-K	AB2
CR5-A	M2
CR6-K	X16
CR6-A	AA16
CR7-K	B15
CR7-A	M15
CR8-K	B4
CR8-A	J4
C4(+)	B24
C4(-)	K24
T1-P1	T8
T1-CT	S10
T1-P2	Z12

TABLE II

JUMPER	FROM	TO
1	L3	X3
2	D5	M5
3	J6	M6
4	D20	K20
5	B26	D26
6	L26	M26
7	V27	AA27
8	G28	L28
9	U28	AB28

FOLDOUT FRAME

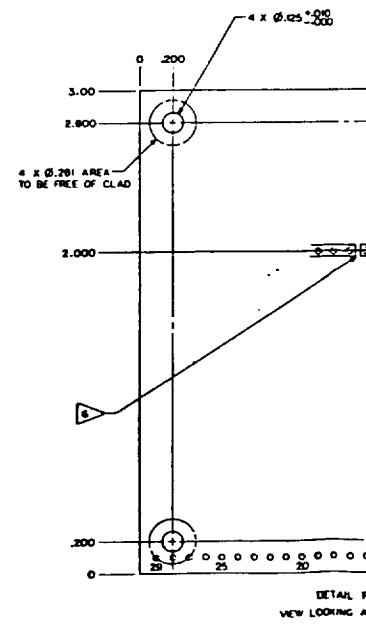
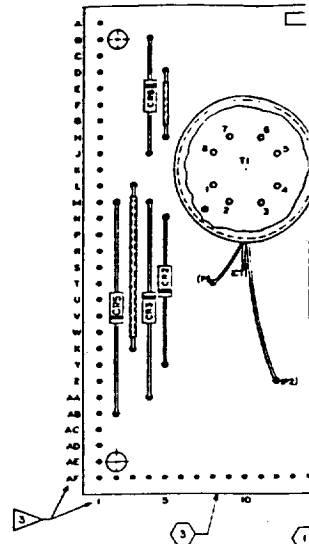
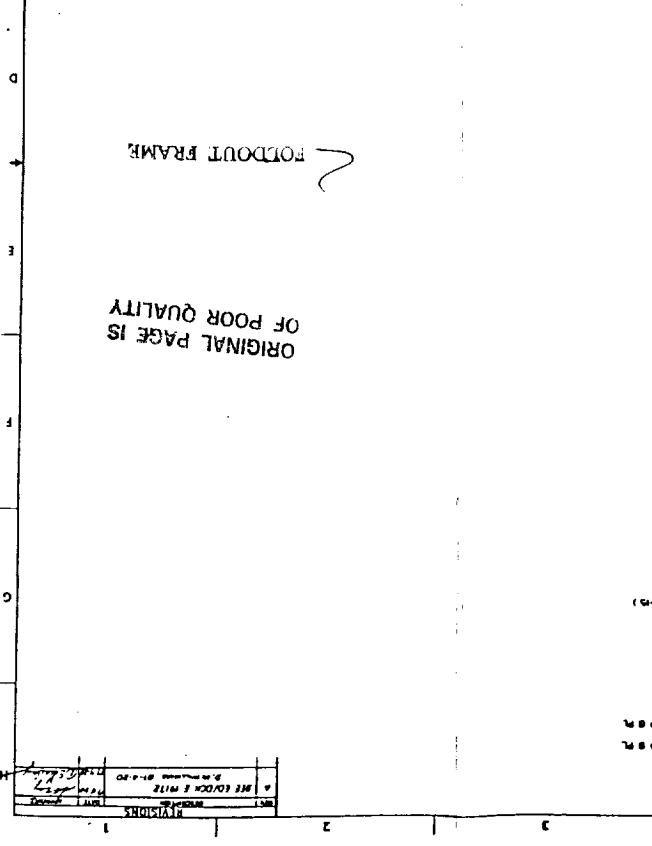
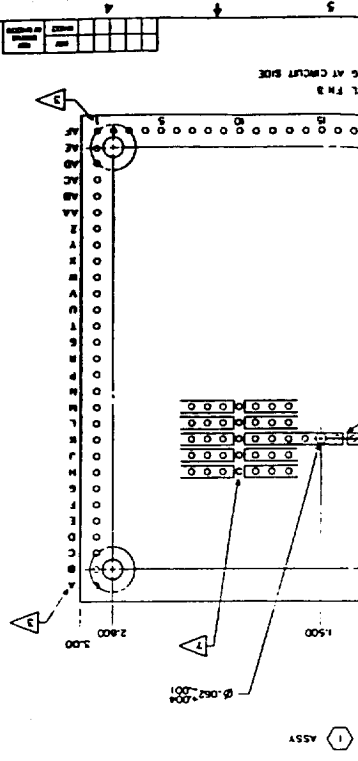




Figure D-9. TRE Drawing No. 1056C0161, Terminal Board No. 2 - Electronic Assembly

D-11

PARTS LIST		REV. NO.		REV. DATE		REV. DESCRIPTION	
1	TERMINAL BOARD ASSY	1	1				
2	CHASSIS BOARD	1	1				
3	CHASSIS BOARD	1	1				
4	CHASSIS BOARD	1	1				
5	CHASSIS BOARD	1	1				
6	CHASSIS BOARD	1	1				
7	CHASSIS BOARD	1	1				
8	CHASSIS BOARD	1	1				
9	CHASSIS BOARD	1	1				
10	CHASSIS BOARD	1	1				
11	CHASSIS BOARD	1	1				
12	CHASSIS BOARD	1	1				
13	CHASSIS BOARD	1	1				
14	CHASSIS BOARD	1	1				
15	CHASSIS BOARD	1	1				
16	CHASSIS BOARD	1	1				



PODDOUT FRAME  
 ORIGINAL PAGE IS  
 OF POOR QUALITY

REV. NO.	REV. DATE	REV. DESCRIPTION
1	1	
2	1	
3	1	
4	1	
5	1	
6	1	
7	1	
8	1	
9	1	
10	1	
11	1	
12	1	
13	1	
14	1	
15	1	
16	1	





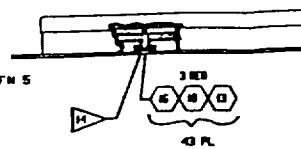






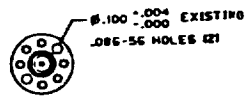
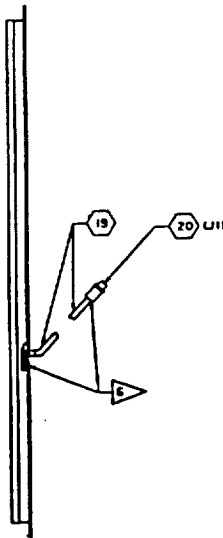
NOTES, UNLESS OTHERWISE SPECIFIED.

1. TORQUE FASTENERS TO  $2.7 \pm .1$  LBF-IN.
2. SOLDER USING FM 28.
3. FRICTION TORQUE FROM SELF-LOCKING DEVICES OR CLOSE FITTING HOLES SHALL BE ADDED TO SPECIFIED TORQUE VALUES.
4. PERMANENTLY MARK 38833 ASSY 105640001 (APPLICABLE SUFFIX) ON FARSIDE USING FM 30. CHARACTERS SHALL BE 12 HIGH VERTICAL GOTHIC. LOCATE APPROXIMATELY WHERE SHOWN.
5. REMOVE PINS MARKED "A" BY UNSOLDERING THEM FROM ARRAY ASSY FM 5 AND BEFORE ASSEMBLY OF FM 5 TO FM 6, 20 PLC.
6. FILL AND SEAL WITH FIND NO 25.
7. FOR WIRING INSTRUCTIONS, SEE TABLE 1 WIRING CHART.



ORIGINAL PAGE IS  
OF POOR QUALITY

DETAIL -10  
SCALE



DETAIL -9 MAKE FROM FIND NO 28  
SCALE 4/1

FOLDOUT FRAME







**APPENDIX E**

**MSAT SYSTEM TEST  
DATA SUMMARY  
(RF SIGNAL)**



## TEST SUMMARY

- Test Conditions
- Acquisition and Track
- Signal Fading
- Intersatellite Isolation
- Amplitude and Phase Deviation
- High Power Test

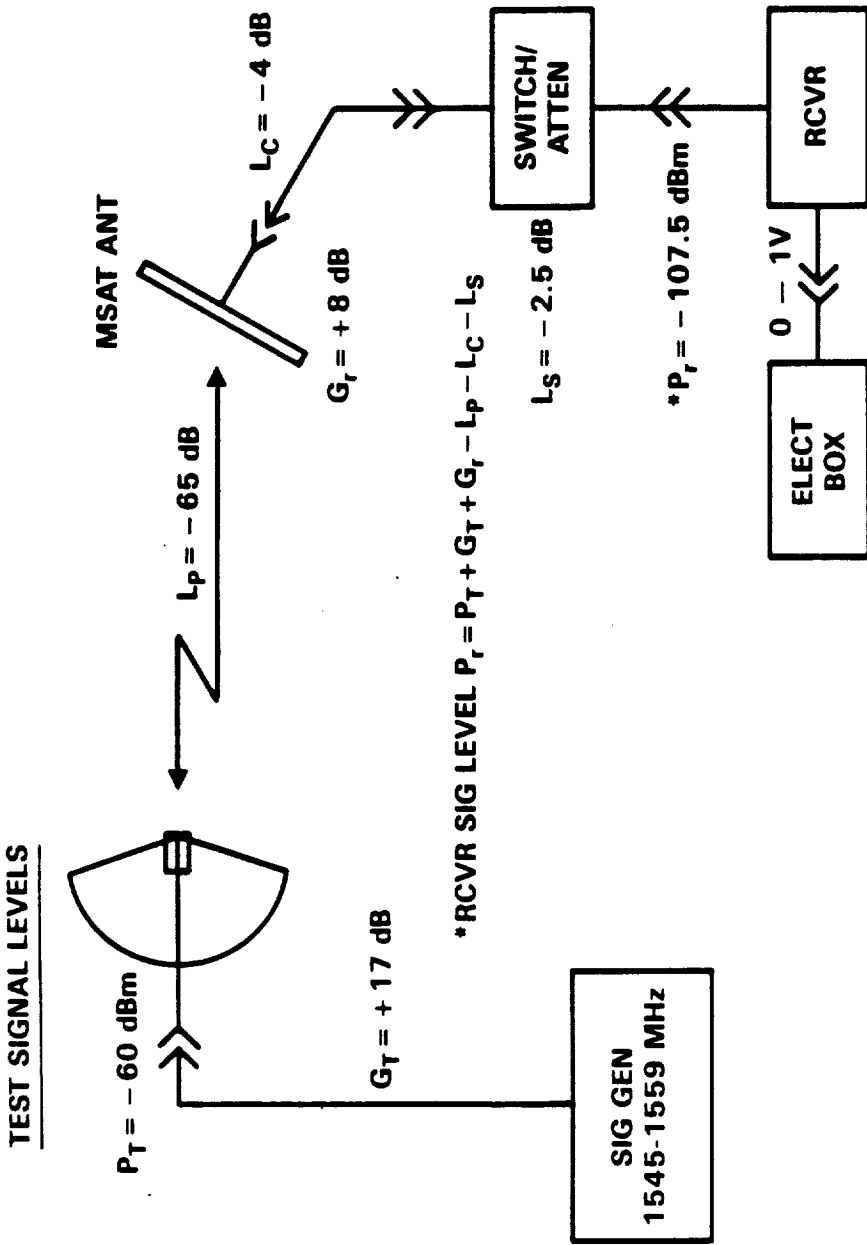


Figure E-1. Acquisition and Tracking

Table E-1. RF Test Data - Acquisition and Track  
 Auto Mode - Beam Steer:  $EL\theta = 30^\circ$ ,  $AZ\phi = 0^\circ$

Table Elev	IF S/N In 3 KHz BW	C/N <sub>0</sub> dB-Hz	ACQ	Track At 8°/MIN
0°	7.5 dB	42.3 dB	Yes	Inter
5°	8.0 dB	42.8 dB	Yes	Yes
10°	12.1 dB	46.8 dB	Yes	Yes
15°	14.0 dB	48.7 dB	Yes	Yes
20°	16.0 dB	50.7 dB	Yes	Yes
25°	21.0 dB	55.7 dB	Yes	Yes
30°	22.0 dB	56.7 dB	Yes	Yes
40°	22.9 dB	57.7 dB	Yes	Yes
50°	22.0 dB	56.7 dB	Yes	Yes
60°	21.3 dB	56.0 dB	Yes	Yes
70°	12.0 dB	46.7 dB	Yes	Yes
80°	6.9 dB	41.6 dB	Yes	Inter

Table E-2. RF Test Data - Signal Fading

Conditions

Beam Steer:  $EL\theta = 30^\circ$ ,  $AZ\phi = 0^\circ$

Table Elev =  $30^\circ$

<u>Δ LEVEL</u>	<u>Track at 8°/Min</u>
-1 dB	Yes
-2 dB	Yes
-3 dB	Yes
-4 dB	Yes
-5 dB	Yes
-6 dB	Yes
5 dB at 40 Hz	Yes

Table E-3. Amplitude and Phase Deviation

Conditions

Dither = 100 Hz

C/N<sub>0</sub> = 70 dB-Hz

Beam Steer: ELθ = 30°, AZφ = 0°

<u>AZ Beam</u>	<u>Δ Phase - PP</u>	<u>Δ AMPL - PP</u>
0°	Not > 10°	Not > 1 dB
45°	Not > 10°	Not > 1 dB
90°	Not > 10°	Not > 1 dB
135°	Not > 10°	Not > 1 dB
180°	Not > 10°	Not > 1 dB

Table E-4. High Power Test

Conditions

$F_o = 1554 \text{ MHz}$

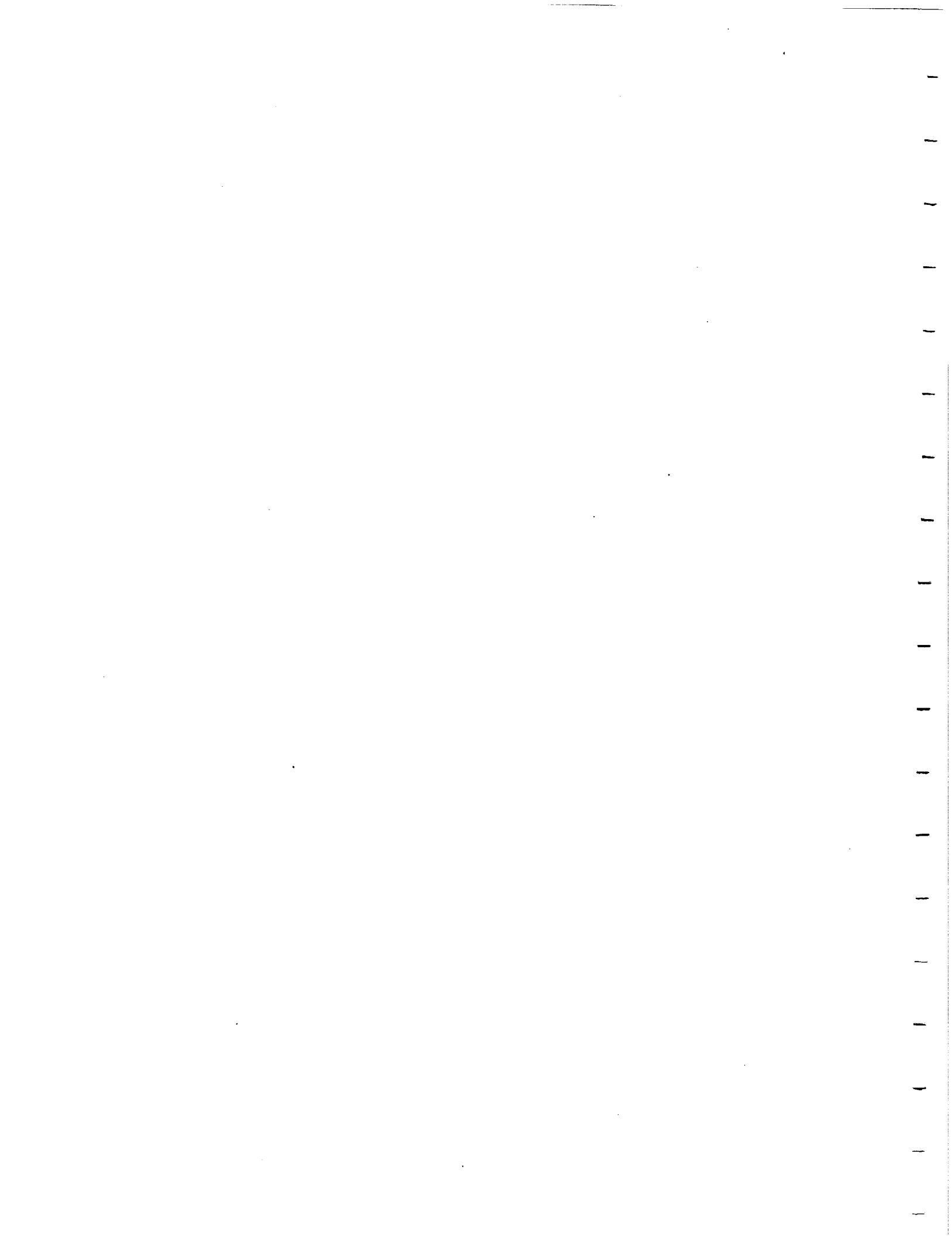
$P_T = 20 \text{ W. to Diplexer (10 W. To ANT)}$

Results

ACQ - Track - Pointing - : No Impairment

**APPENDIX F**

**OPERATING INSTRUCTION MANUAL**  
**FOR**  
**MSAT-X ANTENNA SYSTEM**  
**SIGNAL ACQUISITION & TRACKING**



1.0

INTRODUCTION

This manual describes the installation and operation of the MSAT-X Antenna System with regard to pilot signal and tracking. The system supplied under this contract consists of the following hardware.

<u>Quantity</u>	<u>Item</u>	<u>Part Number</u>
1	Antenna Assy	1056A0001G1
1	Electronics Box Assy	1056C0001G1
1	Test Set, Receiver	1056R0001G1
1	Coaxial Cable, RF	1001-C1001-9001
1	Cable Assy, Interconnect	1056B0025G1
1	Cable Assy, DC Power	1056B0026G1
1	Cable Assy, Signal	1056B0027G1

Both the electronics box and the test set receiver are designed to mount in a standard RTEMA 19" relay rack. While not exactly small, the two units occupy no more than 12 1/4 inches of panel space. As the name implies, the test set receiver is just that, a test set. It is not intended to substitute for the transceiver required of a commercial, operational MSAT system. Its primary purpose is to check the performance of the contractually delivered antenna. A description of the various parts of the MSAT system follows.

1.1

DESCRIPTION

The MSAT-X Antenna System is comprised of the following major components.

1.2

ANTENNA ASSEMBLY

The antenna assembly contains the radiating elements and feed network (consisting of four boards), and a beamforming network consisting of one board, all integrated into one complete unit. The assembly is provided with an SMA female connector for RF I/O. and a 15 pin D - type connector for the beam steering commands. REF Dwgs. 1056A0002 and 1036A0132 in Appendix B of this report.

### 1.3 ELECTRONICS ASSEMBLY

The electronics assembly (Figure F-1) contains all the circuitry required to process the demodulated pilot signal, and to steer the antenna beam in both the automatic and manual mode of operation. A block diagram of the antenna steering control is shown in Figure F-2, and the Schematic Diagram is given in Dwg No. 1056C0002. Switch and display nomenclature is given in Table F-1.

### 1.4 TRANSCEIVER

The transceiver contains all the necessary RF components to simultaneously transmit an up-link carrier signal in the 1646.7 to 1660.5 MHz range, and to receive and demodulate a Down-Link carrier signal in the 1545 to 1559 MHz range.

### 1.5 STATUS PANEL

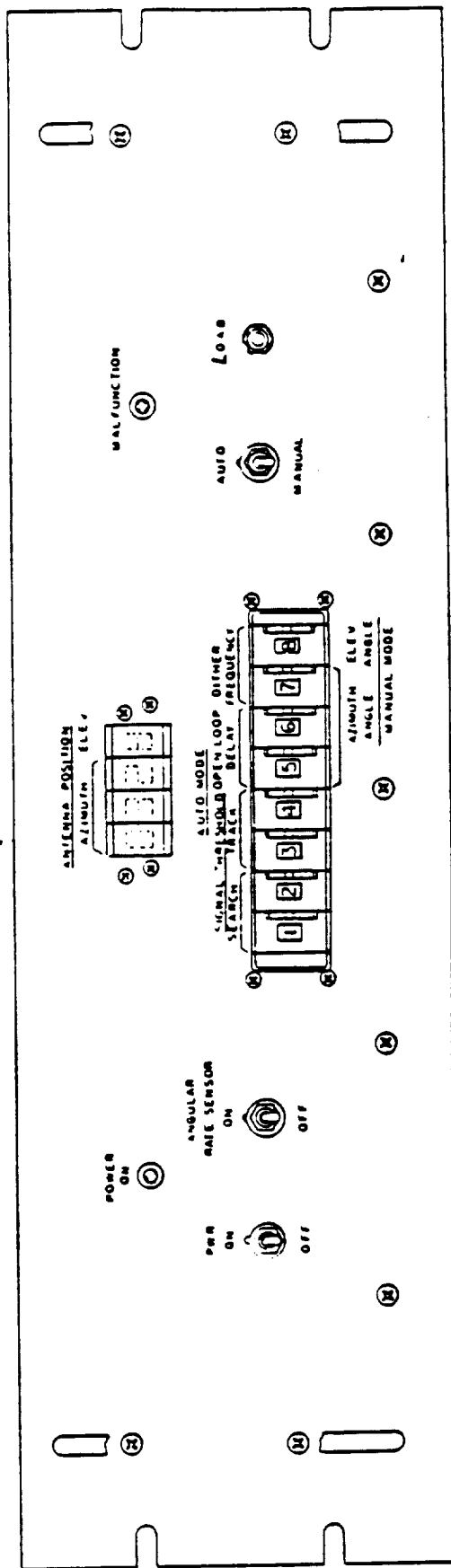
The status panel contains all the circuitry to "Start Acquisition" of the pilot signal, place the system, in either the "Open-Loop" or "Closed-Loop" track mode, and provide an indication of "Track Status" and "Acquisition Complete." The status panel is shown in Figure F-3 and the Schematic Diagram is shown in Dwg No. 1056R0142 (Appendix B). It should be noted that the status panel can be a separate self-contained box, or be incorporated into the transceiver assy or the electronics assembly.

## 2.0 INSTALLATION

Examine the equipment carefully upon its receipt and unpackaging. Any appearance of mishandling or physical damage could indicate potential problems in the check-out and operation of the system. If this were the case, TRE should be contacted immediately.

### 2.1 ANTENNA RANGE INSTALLATION

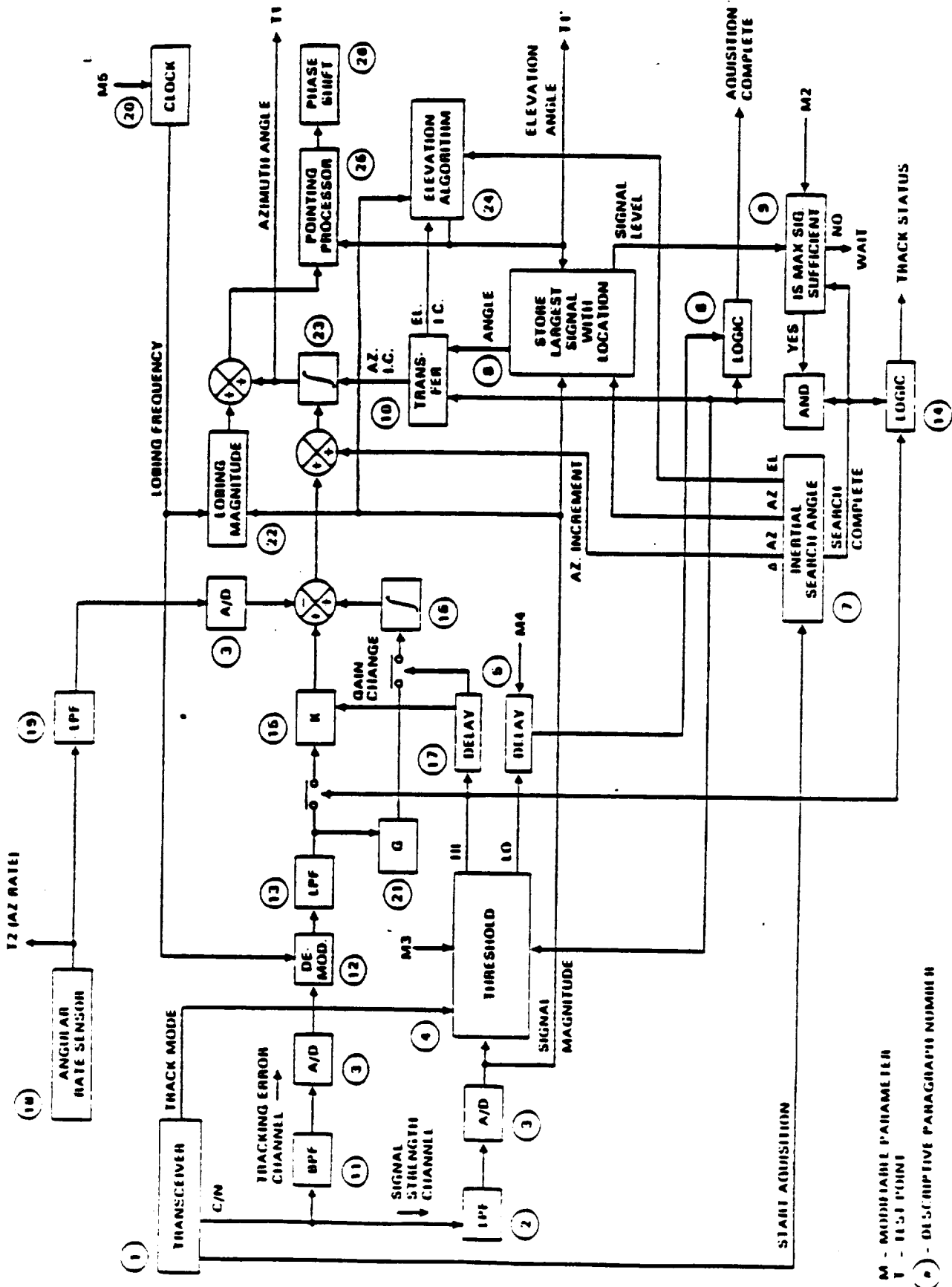
Installing the equipment in a fairly straight-forward operation. For antenna range tests, the customer will probably elect to use a configuration most compatible with his particular range setup. In this case, use Figure F-4 as a cabling guide, setup the equipment and proceed to test. Installing the MSAT-X system in a vehicle is somewhat more involved with the following paragraphs intended to serve as a guide in this respect.



F-4

ORIGINAL PAGE IS  
OF POOR QUALITY

Figure F-1. Electronics Assembly, Front Panel Controls



M - ADJUSTABLE PARAMETER  
 T - TEST POINT  
 ( ) - DESCRIPTIVE PARAGRAPH NUMBER

Figure F-2. MSAT-X Antenna Steering Control

Table F-1. Electronics Assy Switch and Display Nomenclature.

SWITCH NOMENCLATURE

<u>FUNCTION</u>	<u>SETTING</u>	<u>VALUE</u>
Sig Threshold, Search	00 to 99	X0.01 VDC
Sig Threshold, Track	00 to 99	X0.01 VDC
Open Loop Delay	00 to 99	X1 SEC
Dither Frequency	00 to 99	X10 HZ
Azimuth Angle	000 to 360	X1 DEG.
Elevation Angle	0	20 DEG
	1	25 DEG
	2	30 DEG
	3	35 DEG
	4	40 DEG
	5	45 DEG
	6	50 DEG
	7	55 DEG
	8	60 DEG
	9	90 DEG

DISPLAY NOMENCLATURE

<u>DISPLAY</u>	<u>READING</u>	<u>VALUE</u>
Azimuth position	000 to 360	X1 DEG
Elevation position	0 to 90	Same as Elevation Angle.

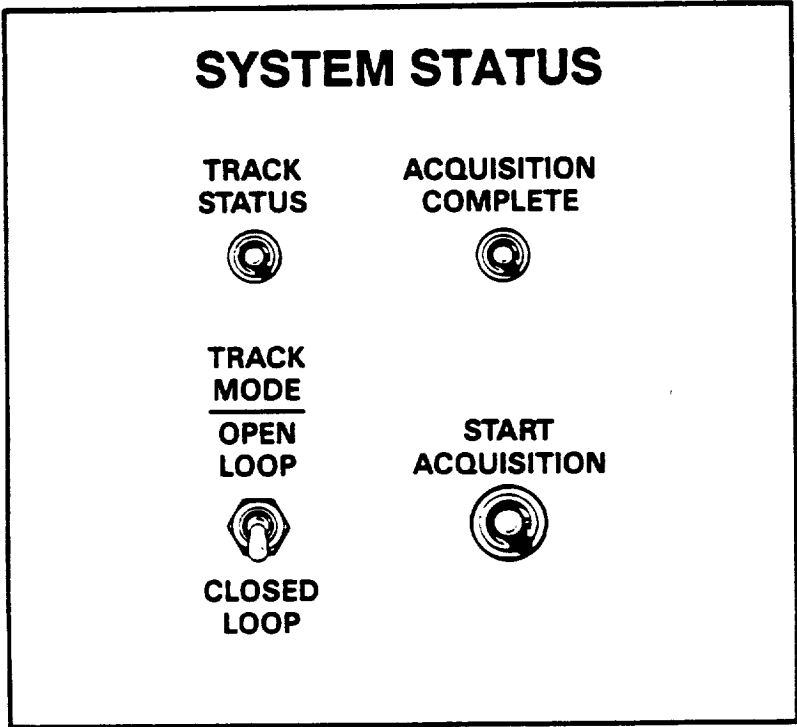


Figure F-3. Status Panel

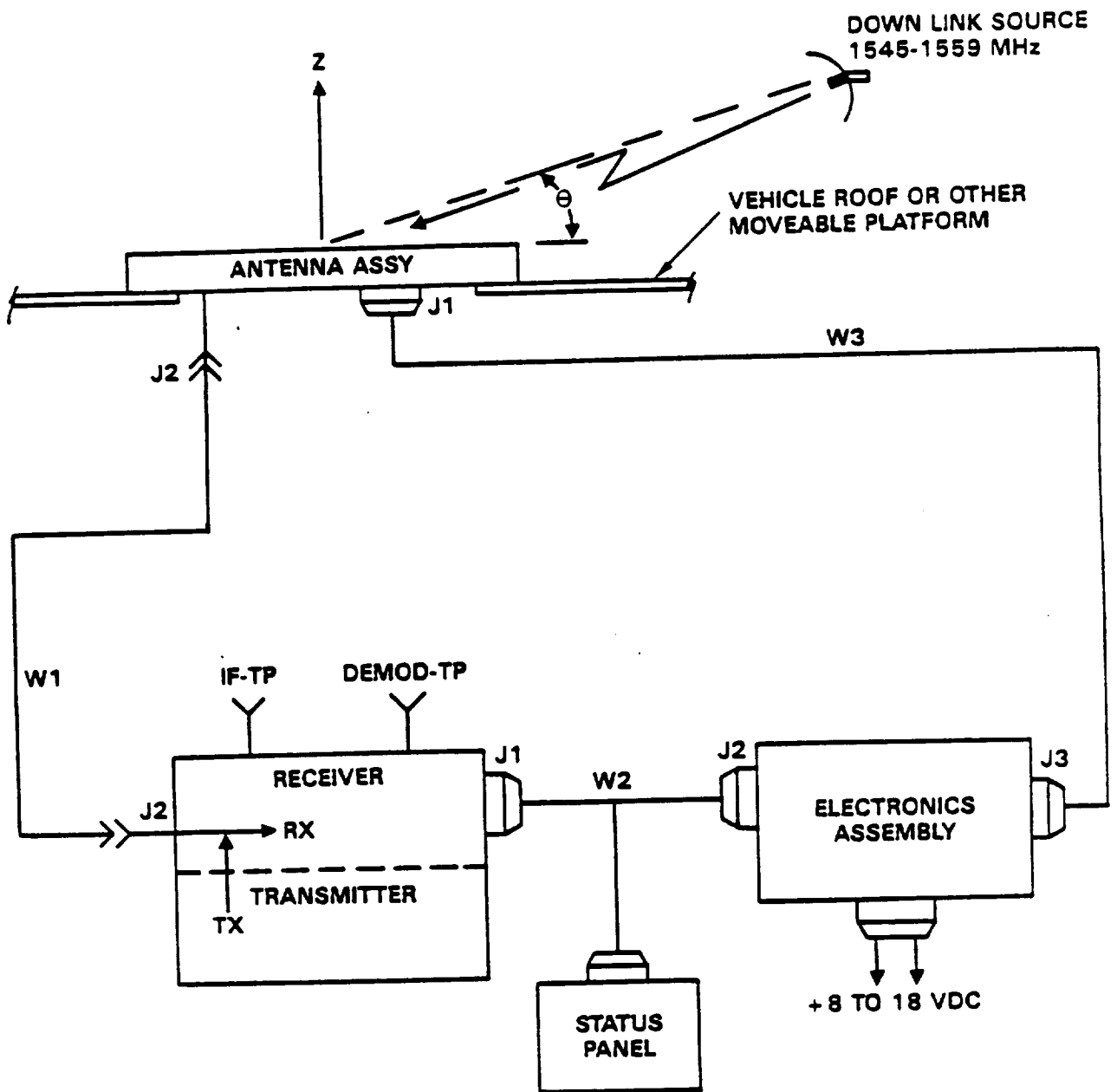


Figure F-4. System Interconnect

## 2.2

### VEHICLE INSTALLATION

For vehicular installation, the electronics box and the test set receiver are bolted in a relay rack (preferably on rack slides) and cabled according to Figure F-4. Care should be taken to ensure that the proper cable is mated with its respective jack or receptacle. The DC power cable must be connected to a fused 10 ampere supply having a voltage range of 8 to 18 volts DC. The test receiver requires a 115 V AC source. This can be supplied by either a small AC generator or a DC/AC inverter of at least 300 watts capacity.

Care should be exercised in handling and installing the antenna. The antenna has a flange mounting ring equipped with 8 1/4" holes equally spaced on a 10.70" radius. The unit is flat and fairly rigid, hence it must be affixed to an adapter conforming to the contour of the mounting surface of the test vehicle. As the antenna itself only weighs 15 pounds, this should allow for the use of a lightweight, yet sturdy mounting ring.

One will note that the RF and power connectors egress from the antenna on the bottom of the unit. Since this is the case, either a hole must be cut in the top of the vehicle to accommodate the cables or they must exit the mounting ring and be routed in the most expeditious manner to the equipment shown in Figure F-4. Once this is accomplished, make sure that the cables are not pinched and that the RF coax has no tight bends. When these requirements are met to the satisfaction of the installer, go ahead and secure the cables. The system is ready to test and use.

## 3.0

### HARDWARE/SOFTWARE INTEGRATION

The following describes the functional relationship between hardware and software. Reference is made to Figure F-2.

## 3.1

### LEGEND:

ARS - Angular Rate Sensor

ACHn - Analog Channel n

TS - Track Status

TM - Track Mode

AC - Acquisition Complete

SA - Start Acquisition

LED's - Position Display

### 3.2 MANUAL ENTRY MODE

3.2.1 With switch closed, manual entry mode is entered and position can be entered, LOADED, and observed at output LED's.

3.2.2 The output PWM (Pulse Width Modulator) can be monitored and verified with a 'scope.

3.2.3 The MAL LED will verify RAM/ROM tests.

Items tested: Serial port, ENTRY and OUTPUT shift registers, Output LED's, MAL LED's, Manual interrupt and load commands, Power supply update routines, and SET POSITION routine.

### 3.3 ACQUISITION MODE

3.3.1 With ACH7 below M2 threshold, TS (Track Status) signal should go high approximately 2.5 seconds after pulsing the SA (Start Acquisition) signal.

3.3.2 With ACH7 above M2 threshold both TS and AC should go high about 2.5 seconds after pulsing SA.

### 3.4 OPEN TRACK MODE

3.4.1 The TM (Track Mode) input signal is held high to maintain OPEN loop tracking. The TS signal should stay high and the AC line should go low after a open loop time-out delay of M4 seconds.

3.4.2 Varying the voltage at ACH4 (ARS) above 2.5 volts should cause the output position to change direction.

3.4.3 Pulsing SA should enter ACQUISITION mode.

### 3.5 CLOSED LOOP TRACK MODE

3.5.1 With the ARS switch open and a constant input frequency at ACHn (pointing error), the frequency at the "LOAD" output should equal Dither Rate M5.

3.5.2 With the ARS switch open, voltages above and below 2.5 volts should cause the output position to change direction.

### 3.6 TIMING AND MEMORY

3.6.1 Memory constraints can be verified by running the previous tests.

3.6.2 Timing of the watch dog and main routines can be verified.

### 4.0 SYSTEM ACQUISITION AND TRACK

#### 4.1 PRELIMINARY SET-UP

4.1.1 Interconnect equipment as shown in Figure F-4.

4.1.2 Verify that the down-link source is transmitting RHCP, and at a frequency within the 1545 MHz to 1559 MHz range.

4.1.3 Verify that the elevation angle  $\theta$ , the angle between the antenna horizontal plane and the down-link source is not less than 20 degrees or greater than 60 degrees.

4.1.4 Verify that the receiver is tuned to the particular frequency being transmitted by the down-link source.

#### 4.2 ACQUISITION

4.2.1 Set switches on electronics assembly as follows (Refer to Table F-1 for Nomenclature):

Power	ON
Angular Rate Sensor	ON
Auto-Manual	AUTO
Search	99
Track	99
Delay	10
Dither	5

Depress the "LOAD" switch to enter the switch settings.

4.2.2 Set "TRACK MODE" switch on status panel to "OPEN LOOP" position, then depress "START ACQUISITION" switch.

4.2.3 After the start acquisition command has been given, the steered beam will begin to scan and search for maximum signal (i.e. signal from Down-Link Source.). Upon acquiring maximum signal, the "ACQUISITION COMPLETE" lamp will light, and in addition the "TRACK STATUS" lamp will light if the track mode switch is in the "OPEN LOOP" position. Acquisition is also indicated by observing the demodulated baseband signal (monitored at "DEMOD TP" jack on receiver) on the 'scope.

Note: Normally, the pilot signal will be acquired in 2 to 3 seconds.

After the start acquisition command has been given, however, if the signal is below the search threshold as set by the search threshold switch on the electronics assembly, the "ACQUISITION COMPLETE" light will not light.

### 4.3 TRACK

4.3.1 Verify that the "AUTO-MANUAL" switch on the electronics assy panel is set to "AUTO" position, and that the "TRACK MODE" switch on the status panel is set to "OPEN-LOOP" position.

4.3.2 Reinitiate the acquisition command by depressing the "START ACQUISITION" switch on the status panel.

4.3.3 After the signal has been acquired and the acquisition complete light comes on, then place the "TRACK MODE" switch on the status panel to the "CLOSED LOOP" position. The "TRACK STATUS" light should go "OFF"

4.3.4 Rotate antenna about Z-Axis at a rate of 10 to 70 degrees per second and verify that the system maintains tracking. This is indicated by the condition that the "ACQUISITION COMPLETE" light is "ON" and the "TRACK STATUS" light is "OFF". Upon losing track, the track mode will revert to open-loop, whereupon the "TRACK STATUS" light will come "ON" and the "ACQUISITION COMPLETE" light will go "OFF".

#### 4.4 SIGNAL LOSS RESPONSE

The tracking system is capable of remaining in the track mode for a signal loss of up to 10 seconds. Verification is as follows.

4.4.1 Place the system in the "CLOSED-LOOP" track mode as describe in paragraph 4.3.1 thru 4.3.3.

4.4.2 Temporarily interrupt the RF signal to the receiver and verify that the system remains in the track mode. Response should be as described in paragraph 4.3.4.

#### 5.0 MANUAL STEERING

The system is capable of steering the beam manually in both azimuth and elevation. The azimuth range is 0 to 360 degrees in increments of 3 degrees. The elevation range is 20 to 90 degrees in increments of 5 degrees from 20 to 60 degrees and one setting for 90 degrees. Reference Table F-1. Verification is as follows.

5.1 Align + y axis of antenna to down-link source, and determine elevation angle  $\theta$ . Reference Dwg No. 1056A0002 and Figure F-4.

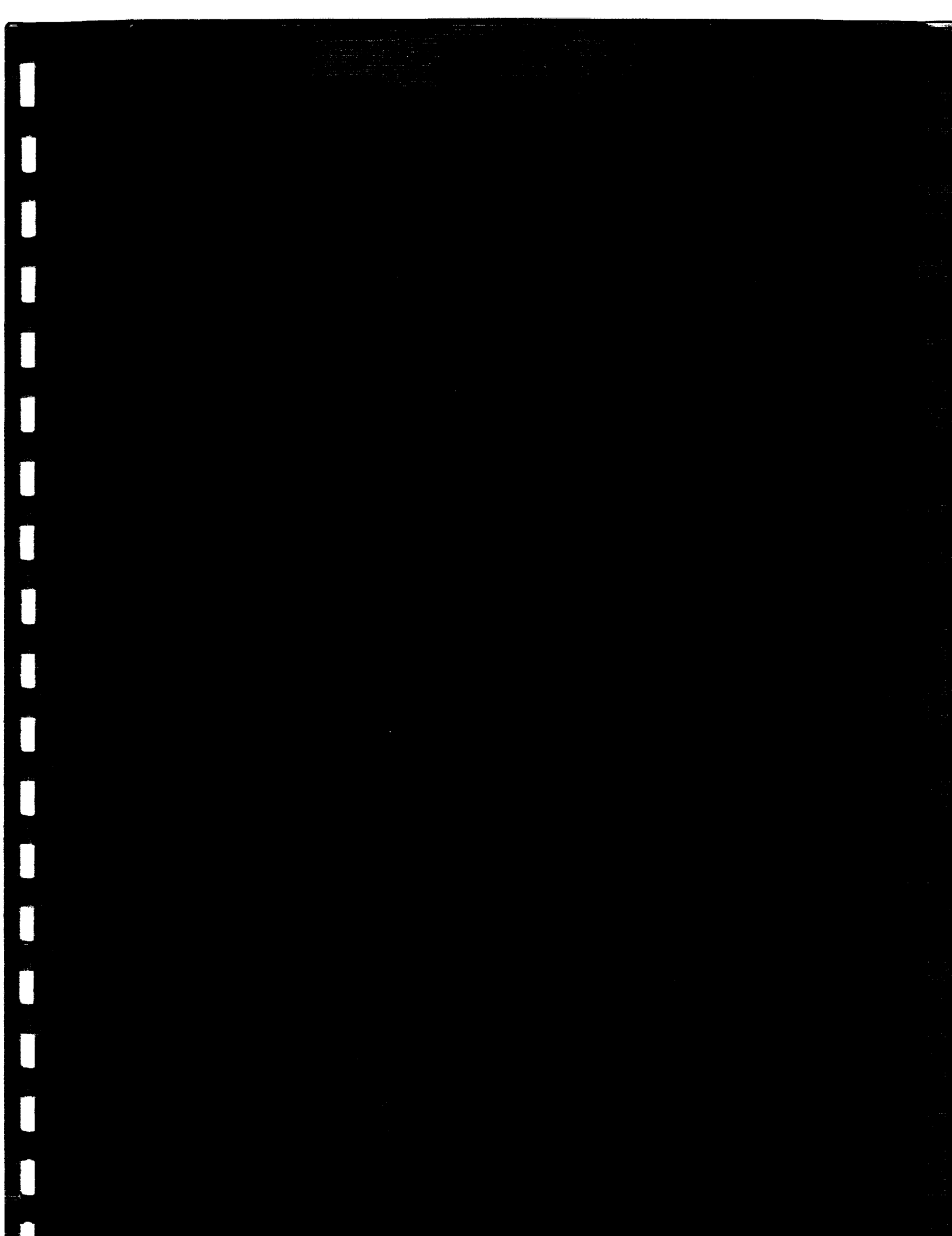
5.2 On electronics assembly, set "AZIMUTH ANGLE" switch to 090, and "ELEV ANGLE" switch to a setting corresponding to the elevation angle  $\theta$  determined in paragraph 5.1.

Note: with reference to Dwg. No. 1056A0002, the + x axis direction corresponds to an azimuth beam angle of 0 degrees. Moving in a counter clockwise direction corresponds to increasing positive angles. Therefore the + y axis direction is an azimuth beam angle of 90 degrees.

5.3 Depress the "LOAD" switch on the electronics assembly to enter switch settings.

5.4 After the switch settings have been entered, the steered beam azimuth and elevation angles will be shown by the "ANTENNA POSITION" display.

5.5 The detected pilot carrier can be monitored at the "DEMOD TP" jack on the receiver. A DC voltage from -0.2V to -0.8V corresponds to a relative signal strength under typical operating conditions.



... ..

... ..

... ..